frontiers | Research Topics

Early origins of lung disease - an interdisciplinary approach

Edited by
Miguel Angel Alejandre Alcazar, Mandy Laube, Sylvia Knapp, Suhas Kallapur, Niki Reynaert, Deb Strickland and Niki Ubags

Published in
Frontiers in Pediatrics
Frontiers in Medicine

FRONTIERS EBOOK COPYRIGHT STATEMENT

The copyright in the text of individual articles in this ebook is the property of their respective authors or their respective institutions or funders. The copyright in graphics and images within each article may be subject to copyright of other parties. In both cases this is subject to a license granted to Frontiers.

The compilation of articles constituting this ebook is the property of Frontiers.

Each article within this ebook, and the ebook itself, are published under the most recent version of the Creative Commons CC-BY licence. The version current at the date of publication of this ebook is CC-BY 4.0. If the CC-BY licence is updated, the licence granted by Frontiers is automatically updated to the new version.

When exercising any right under the CC-BY licence, Frontiers must be attributed as the original publisher of the article or ebook, as applicable.

Authors have the responsibility of ensuring that any graphics or other materials which are the property of others may be included in the CC-BY licence, but this should be checked before relying on the CC-BY licence to reproduce those materials. Any copyright notices relating to those materials must be complied with.

Copyright and source acknowledgement notices may not be removed and must be displayed in any copy, derivative work or partial copy which includes the elements in question.

All copyright, and all rights therein, are protected by national and international copyright laws. The above represents a summary only. For further information please read Frontiers' Conditions for Website Use and Copyright Statement, and the applicable CC-BY licence.

ISSN 1664-8714
ISBN 978-2-88974-904-1
DOI 10.3389/978-2-88974-904-1

About Frontiers

Frontiers is more than just an open access publisher of scholarly articles: it is a pioneering approach to the world of academia, radically improving the way scholarly research is managed. The grand vision of Frontiers is a world where all people have an equal opportunity to seek, share and generate knowledge. Frontiers provides immediate and permanent online open access to all its publications, but this alone is not enough to realize our grand goals.

Frontiers journal series

The Frontiers journal series is a multi-tier and interdisciplinary set of open-access, online journals, promising a paradigm shift from the current review, selection and dissemination processes in academic publishing. All Frontiers journals are driven by researchers for researchers; therefore, they constitute a service to the scholarly community. At the same time, the *Frontiers journal series* operates on a revolutionary invention, the tiered publishing system, initially addressing specific communities of scholars, and gradually climbing up to broader public understanding, thus serving the interests of the lay society, too.

Dedication to quality

Each Frontiers article is a landmark of the highest quality, thanks to genuinely collaborative interactions between authors and review editors, who include some of the world's best academicians. Research must be certified by peers before entering a stream of knowledge that may eventually reach the public - and shape society; therefore, Frontiers only applies the most rigorous and unbiased reviews. Frontiers revolutionizes research publishing by freely delivering the most outstanding research, evaluated with no bias from both the academic and social point of view. By applying the most advanced information technologies, Frontiers is catapulting scholarly publishing into a new generation.

What are Frontiers Research Topics?

Frontiers Research Topics are very popular trademarks of the *Frontiers journals series*: they are collections of at least ten articles, all centered on a particular subject. With their unique mix of varied contributions from Original Research to Review Articles, Frontiers Research Topics unify the most influential researchers, the latest key findings and historical advances in a hot research area.

Find out more on how to host your own Frontiers Research Topic or contribute to one as an author by contacting the Frontiers editorial office: frontiersin.org/about/contact

Early origins of lung disease - an interdisciplinary approach

Topic editors

Miguel Angel Alejandre Alcazar — University Hospital of Cologne, Germany
Mandy Laube — Leipzig University, Germany
Sylvia Knapp — Medical University of Vienna, Austria
Suhas Kallapur — University of California, Los Angeles, United States
Niki Reynaert — Maastricht University, Netherlands
Deb Strickland — University of Western Australia, Australia
Niki Ubags — Centre Hospitalier Universitaire Vaudois, Switzerland

Citation

Alcazar, M. A. A., Laube, M., Knapp, S., Kallapur, S., Reynaert, N., Strickland, D., Ubags, N., eds. (2023). *Early origins of lung disease - an interdisciplinary approach*. Lausanne: Frontiers Media SA. doi: 10.3389/978-2-88974-904-1

Table of contents

frontiers in Pediatrics

ORIGINAL RESEARCH
published: 28 January 2021
doi: 10.3389/fped.2020.619853

Mitochondrial Fission-Mediated Lung Development in Newborn Rats With Hyperoxia-Induced Bronchopulmonary Dysplasia With Pulmonary Hypertension

Yuanyuan Dai[1†], Binyuan Yu[1†], Danyang Ai[2], Lin Yuan[2], Xinye Wang[1], Ran Huo[1], Xiaoqin Fu[1], Shangqin Chen[1] and Chao Chen[1,2*]*

[1] Department of Neonatology, The Second Affiliated Hospital, Yuying Children's Hospital of Wenzhou Medical University, Zhejiang, China, [2] Department of Neonatology, The Children's Hospital of Fudan University, Shanghai, China

OPEN ACCESS

Edited by:
Sylvia Knapp,
Medical University of Vienna, Austria

Reviewed by:
MaryAnn Volpe,
Tufts University School of Medicine, United States
Jonathan Michael Davis,
Tufts University, United States

***Correspondence:**
Chao Chen
chen6010@163.com
Shangqin Chen
chensq5725@163.com

[†] These authors have contributed equally to this work and share first authorship

Specialty section:
This article was submitted to Neonatology, a section of the journal Frontiers in Pediatrics

Received: 21 October 2020
Accepted: 29 December 2020
Published: 28 January 2021

Citation:
Dai Y, Yu B, Ai D, Yuan L, Wang X, Huo R, Fu X, Chen S and Chen C (2021) Mitochondrial Fission-Mediated Lung Development in Newborn Rats With Hyperoxia-Induced Bronchopulmonary Dysplasia With Pulmonary Hypertension. Front. Pediatr. 8:619853. doi: 10.3389/fped.2020.619853

Background: Bronchopulmonary dysplasia (BPD) is the most common chronic respiratory disease in premature infants. Oxygen inhalation and mechanical ventilation are common treatments, which can cause hyperoxia-induced lung injury, but the underlying mechanism is not yet understood. Mitochondrial fission is essential for mitochondrial homeostasis. The objective of this study was to determine whether mitochondrial fission (dynamin-related protein 1, Drp1) is an important mediator of hyperoxia lung injury in rats.

Methods: The animal model of BPD was induced with high oxygen (80–85% O_2). Pulmonary histological changes were observed by hematoxylin-eosin (HE) staining. Pulmonary microvessels were observed by immunofluorescence staining of von Willebrand Factor (vWF). Protein expression levels of Drp1 and p-Drp1 (Ser616) were observed using Western Blot. We used echocardiography to measure pulmonary artery acceleration time (PAT), pulmonary vascular resistance index (PVRi), peak flow velocity of the pulmonary artery (PFVP), pulmonary arteriovenous diameter, and pulmonary vein peak velocity. Mitochondrial division inhibitor-1 (Mdivi-1) was used as an inhibitor of Drp1, and administered through intraperitoneal injection (25 mg/kg).

Results: Pulmonary artery resistance of the hyperoxide-induced neonatal rat model of BPD increased after it entered normoxic convalescence. During the critical stage of alveolar development in neonatal rats exposed to high oxygen levels for an extended period, the expression and phosphorylation of Drp1 increased in lung tissues. When Drp1 expression was inhibited, small pulmonary vessel development improved and PH was relieved.

Conclusion: Our study shows that excessive mitochondrial fission is an important mediator of hyperoxia-induced pulmonary vascular injury, and inhibition of mitochondrial fission may be a useful treatment for hyperoxia-induced related pulmonary diseases.

Keywords: bronchopulmonary dysplasia, pulmonary hypertension, mitochondrial fission, Mdivi-1, Drp1, echocardiography, pulmonary vascular resistance

INTRODUCTION

Bronchopulmonary dysplasia (BPD) is a chronic lung disease that occurs in preterm infants who require respiratory support and oxygen therapy at birth (1). It is caused by a variety of molecular factors such as genetic predisposition, oxygen toxicity, and inflammatory injury, whose complex interactions are still not fully understood; and the prevention and treatment strategies for BPD are still limited (2–4). Impaired intrauterine lung development and post-partum injury can impair angiogenesis and alveolar formation, resulting in simplification of the distal alveoli. These characteristic histological changes of BPD clinically manifest as persistent respiratory diseases, requiring long-term oxygen supplementation (5), and pulmonary hypertension (PH). Approximately 15–25% of BPD cases will develop PH (6). Among severe cases of BPD, the incidence of PH is higher (7). Furthermore, the existence of PH is closely related to adverse outcomes of BPD, and the mortality rate of BPD combined with PH is as high as 48% (8).

It is generally believed that mitochondrial dynamics play a vital role in mitochondrial homeostasis (9). Mitochondrial fission is mediated mainly by dynamin-related protein 1 (Drp1), a GTPase associated with cytoplasmic dynamin-related proteins, which belongs to the dynamin-related family and was the first fission protein discovered (10). When activated, cytoplasmic Drp1 is transported to the mitochondrial outer membrane, where GTPase is hydrolyzed and polymerized (9). Accumulating data also suggest that Drp1 is a key molecule in mitochondrial dynamics that controls mitochondrial fusion and fission (11), and abnormal expression of it may lead to abnormal changes in chronic lung diseases such as PH and lung cancer (12, 13). Besides, post-translational modification of Drp1, such as phosphorylation at Ser616, is an important mechanism for modulating mitochondrial fission (14). Recent studies have found that hypoxia can lead to mitochondrial fission of pulmonary artery smooth muscle (15), but the changes in pulmonary vascular mitochondrial dynamics induced by excessive oxygen have not been studied.

Echocardiography is a common method of PH examination in adults and children (16). Echocardiography can show direct signs of PH due to increased tricuspid regurgitation. However, the tricuspid regurgitation velocity used in adult pulmonary artery pressure estimations cannot be used in children, particularly infants, because it is difficult to obtain a good and clear image, and this measurement may not have good agreement with the data measured using a cardiac catheter (17). Therefore, indirect signs, such as changes in right ventricular function and changes in pulmonary artery acceleration time, are indispensable.

In this study, we hypothesized that hyperoxia would induce mitochondrial fission and thus impact lung development, resulting in the occurrence of BPD combined with PH. We found that after excessive oxygen stimulation, alveolar simplification, PH, and p-Drp1 mitochondrial translocation increased mitochondrial fission. Mdivi-1 is a Drp1 inhibitor that decreases mitochondrial fragmentation (18). Our results also suggest that inhibition of mitochondrial fission may be a useful treatment strategy for hyperoxia-associated pulmonary endothelial injury and related diseases.

MATERIALS AND METHODS

Hyperoxia-Induced Lung Injury

All animal experiments were performed in accordance with the policies and guidelines of the Laboratory Animal Ethics Committee of Wenzhou Medical University. A total of 10 pregnant Sprague Dawley rats were purchased from the Experimental Animal Center of Wenzhou Medical University. The dams were maintained in humidity- and temperature-controlled rooms on a 12:12-h light-dark cycle and were allowed food and water *ad libitum*. On the final day of pregnancy, the dams delivered naturally (120 pups). Seventy-two pups from six pregnant rats were pooled, randomized, and returned to the nursing dams and then divided into two groups: the control ($n = 36$) and hyperoxia ($n = 36$) groups. The hyperoxia group of pups was exposed to 80–85% oxygen in a sealed Plexiglass box for 14 days, while the control group was maintained in room air (21% oxygen). Over the 14 days, the nursing dams were exchanged between the two groups every 24 h to avoid oxygen toxicity. The oxygen level of the Plexiglass box was monitored continuously using an oxygen analyzer.

The pups from the other four pregnant rats (48 pups) were experimentally divided into four groups: control + vehicle ($n = 12$), control + Mdivi-1 ($n = 12$), hyperoxia + vehicle ($n = 12$), and hyperoxia + Mdivi-1 ($n = 12$). Mdivi-1 (25 mg/kg) was given to the pups on days 7–14 by intraperitoneal injection. The pups in the control + vehicle and hyperoxia + vehicle groups were injected with the same volume of vehicle (corn oil, Sohrab Biotechnology, Beijing, China).

Lung Histology and Morphometric Analyses

After 14 days, all hyperoxia groups (hyperoxia alone, hyperoxia + vehicle, and hyperoxia + Mdivi-1) were maintained in room air. Sixty pups in total from the control and hyperoxia groups were sacrificed on days 3, 7, 14, 21, and 28 by injection of 1% pentobarbital. The left lungs were removed and fixed in 4% paraformaldehyde for 48 h. The sections were then embedded into paraffin and sliced into 4-μm sections for hematoxylin-eosin (HE) staining (Sohrab Biotechnology, Beijing, China). At the same time, the right lungs were stored at −80°C for western blot.

The radial alveolar count (RAC, the number of alveoli contained in the terminal respiratory unit), which reflects the degree of alveolation, and Mean alveolar diameter (MAD) was the average alveolar diameter (19). And they were important indicators for the evaluation of non-development. Briefly, six lung sections were taken for HE staining on days 3, 7, 14, 21, and 28 from the control and hyperoxia groups, five fields were randomly selected for imaging under a 100x magnification lens, and the number of alveoli passing from the center of the respiratory bronchioles to the nearest interpleural line were counted as the RAC. The MAD was measured by Image-Pro Plus 6.0 software (Media Cybernetics, Rockville, MD, USA).

Immunofluorescence

On day 14, the lung tissue sections from 24 rats [control + vehicle ($n = 6$), control + Mdivi-1($n = 6$), hyperoxia + vehicle ($n = 6$), and hyperoxia + Mdivi-1 ($n = 6$)] were dried overnight at 37°C and then hydrated in xylene and an ethanol gradient series. The sections were then heated in a microwave in 10 mM citric acid buffer (pH 6.0) for 20 min for antigen retrieval. The sections were then incubated in 5% bovine serum albumin at 37°C for 1 h. The sections were incubated at 4°C overnight with a rabbit polyclonal anti-vWF (AF3000; 1:200 dilution; Affinity Biosciences. OH. USA), while the negative control group was incubated with phosphate-buffered saline. The sections were then incubated with Alexa Fluor-594 sheep anti-rabbit IgG (AB150076; diluted 1:500; Abcam) at room temperature for 4 h and subsequently with 4′,6-diamidino-2-phenylindole (DAPI). Dual immunophotography images were acquired using a scanning microscope (C1; Nikon, Tokyo, Japan).

Western Blotting

Protein was extracted from frozen lung tissue samples from 36 rats in the control and hyperoxia groups on days 3, 7, and 14, and mixed with the loading buffer. Equal amounts of protein were separated by 10% sodium dodecyl sulfate-polyacrylamide gel electrophoresis at 100 V for 3 h and transferred to polyacrylamide difluoride membranes at 100 V for 50 min. Membranes were then blocked in 5% skimmed milk for 3 h at room temperature (20–25°C). Membranes were then incubated with rabbit monoclonal anti-Drp1 (ab184247; 1:500 dilution; Abcam, Cambridge, UK) or rabbit Phospho-Drp1 (Ser616) Antibody (#3455; 1:1,000 dilution; Cell Signaling Technology, Boston, USA) and gently shaken at 4°C overnight. The next day, the membranes were incubated with horseradish peroxidase-conjugated goat anti-rabbit or anti-mouse secondary antibody (1:5,000 dilution; Cell Signaling Technology, Boston, USA) for 2 h after being washed three times in Tris-buffered saline and tween-20, and developed using enhanced chemiluminescence reagents (Thermo Scientific Pierce; Thermo Fisher Scientific, Waltham, MA, USA). Densitometry values of each sample were calculated by Image Lab 5.0 software (Bio-Rad, Hercules, CA, USA) for all bands and standardized relative to β-actin.

Echocardiographic Imaging

On days 14, 21, 28, and 42, six pups from the control and hyperoxia groups and 24 rats from other four groups on days 21 and 28 were prepared for ultrasonic imaging. The rats were anesthetized with isoflurane using a small animal respiratory anesthesia machine (R620-S1, RWD life science, Shenzhen, China). After full chest hair removal, the rats received continuous isoflurane anesthesia, were fixed in the supine position on the examination table, and connected with electrocardiogram electrodes. Their chests were coated with coupling agent.

The probe was slightly adjusted upwards to obtain a minor axial view of the aorta, and the probe was slightly tilted cephalically to obtain a major axial view of the pulmonary artery. The left atrial pulmonary vein junction was located, and the Doppler sampling point was placed at the junction to measure the pulmonary vein flow velocity.

To measure the hemodynamics of the pulmonary arteries and veins, the short-axis view of the aortic valve was obtained first, and the pulmonary artery was identified using a color Doppler instrument. The diameter of the pulmonary artery was measured at the attachment point of the pulmonary valve. The pulsed Doppler gate was placed at the proximal end of the pulmonary valve at an incident angle $<20°$ to maximize laminar flow. Pulmonary acceleration time (PAT), pulmonary ejection time (PET), and peak flow velocity of the pulmonary artery (PFVP) were measured. PAT was measured as the time from the beginning of systolic blood flow to the peak flow rate, while PET was measured as the time from the beginning of systolic blood flow to the completion of pulmonary blood flow. The pulmonary vascular resistance index (PVRi) was calculated as the ratio of PET to PAT. Similarly, the size of the left atrial pulmonary vein junction was measured as the value of the pulmonary vein diameter, and the peak velocity of the pulmonary vein was measured according to the pulmonary vein flow velocity curve. To measure right ventricular load, short-axis views of the right and left ventricles were obtained at the level of the distal mitral valve.

Right and left ventricular diastolic area (RVEDA and LVEDA, respectively) were measured by manual endocardial boundary tracing. The ratio between RVEDA and LVEDA (RVEDA/LVEDA) was calculated as the measurement index of the right ventricular load (20).

Statistical Analysis

The experiments were performed in triplicate and repeated at least three times. The data are presented as the mean ± SD or SEM and were analyzed using one-way analysis of variance (ANOVA) followed by Tukey's *post-hoc* test (equal variance) or Dunnett T3's *post-hoc* test (unequal variance) for multiple comparisons. Correlation analyses were performed using Spearman's rank correlation. Statistical analysis was carried out using SPSS Statistics 19.0 (SPSS Inc., Chicago, USA) or GraphPad 6.0 (GraphPad Software, San Diego, USA). Values of $P < 0.05$ were considered statistically significant.

RESULTS

Hyperoxia Stunts Alveolar Development, Which Is Restored After Recovery in Room Air

Hyperoxia causes substantial morphological simplification in the lung tissue, including a visible decrease in alveolar numbers and increase in alveolar size. These negative changes in the hyperoxia group can be quantified by the decrease in RAC and MAD, an important indicator of lung development. Significant histological differences between the hyperoxia and control groups were found in day 3, 7, 14, 21, and 28 (**Figure 1A**). This result indicated that chronic exposure to hyperoxia interrupts alveolar

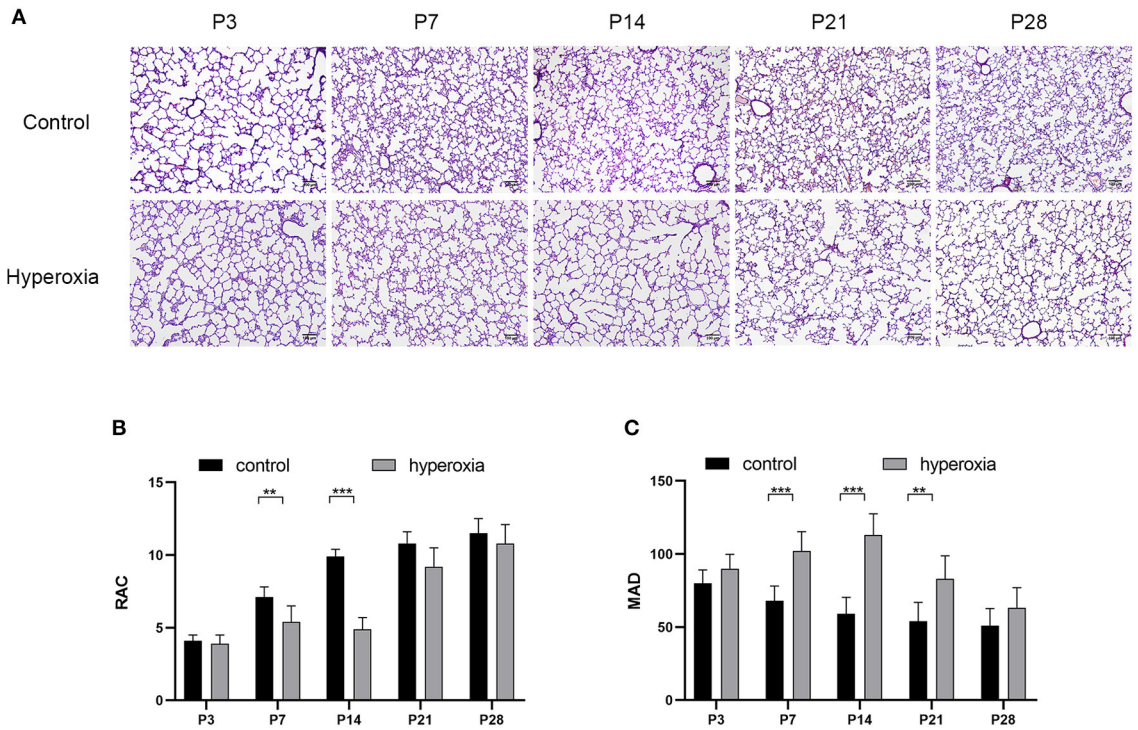

FIGURE 1 | Morphological changes in rat lungs after hyperoxia. Newborn pups (P0) were exposed to 21% O_2 (control) or 80–85% O_2 (hyperoxia) for 14 days. **(A)** Hematoxylin and eosin staining of rat lungs exposed to hyperoxia or control group on day 3, 7, 14, 21, and 28. Scale bar: 100 μm. **(B)** Compared with the controls, the radial alveolar counts (RACs) of hyperoxia group were significantly reduced on five periods. **(C)** The Mean alveolar diameter (MAD) of hyperoxia group were significantly increased on five periods. $n = 6$ per group. Data are shown as mean ± SD; $^{**}P < 0.01$, $^{***}P < 0.001$.

formation, as evidenced by a decrease in alveolar numbers and increase in alveolar diameter. On day 7 (**Figure 1B**), the RAC number of control group was higher than hyperoxia group ($P < 0.01$), and on day 14 this number in control group was much higher than in hyperoxia group ($P < 0.001$). However, these developmental abnormalities in the hyperoxia group were reversed after recovery in room air for 14 days. As for the MAD (**Figure 1C**), the MAD value of control group was significantly lower than hyperoxia group on day 7 ($P < 0.001$), on day 14 ($P < 0.001$), and on day 21 ($P < 0.01$).

Hyperoxia Causes Drp1 Overexpression in Newborn Rat Lungs

To investigate whether hyperoxia altered the expression of Drp1 in rat lung tissues, we examined the levels of Drp1 and p-Drp1 over time by western blotting (**Figure 2A**). On the third day of hyperoxia (**Figure 2B**), the expression of Drp1 in the hyperoxia group was higher than that in the control group ($P < 0.05$). On the seventh day of hyperoxia, the levels of Drp1 ($P < 0.05$) and p-Drp1 (Ser616) ($P < 0.001$) in the hyperoxia group were both significantly elevated (**Figures 2B,C**), although the ratios of p-Drp1 (Ser616)/Drp1 were not different between the two groups, suggesting that the elevated p-Drp1 (Ser616) levels increased concomitantly with Drp1 levels (**Figure 2D**). After 14 days of hyperoxia, Drp1 levels in the hyperoxia group were still high ($P < 0.01$). Furthermore, the ratio of p-Drp1 (Ser616) to Drp1 ($P < 0.001$) was significantly increased compared to the controls, indicating that the phosphorylation of Drp1 at Ser616 (**Figure 2C**) was actively upregulated ($P < 0.001$).

Pharmacological Inhibition of Drp1 With Mdivi-1 During Hyperoxia Mitigates Pulmonary Vascular Complications

Mdivi-1 is a specific inhibitor of Drp1. Based on the results that DRP1 started to increase in the hyperoxia group on P7 and the high level persisted until P14, the Drp1 inhibitor, mdivi-1, was injected intraperitoneally daily from days 7 to 14 to investigate whether mdivi-1 had protective effects on chronic hyperoxia-induced lung injury. To evaluate vascular development, vWF-positive small blood vessels were visualized using immunofluorescence staining and counted (**Figure 3**). We found that long-term hyperoxia significantly decreased the number of pulmonary small blood vessels at day 14 ($P < 0.001$), whereas mdivi-1 treatment in the hyperoxia group (**Figure 3B**) partially rescued this decrease at day 14 ($P < 0.001$), indicating that mdivi-1 can alleviate hyperoxia-induced obstruction of pulmonary vascular development. To evaluate the long-term effects on

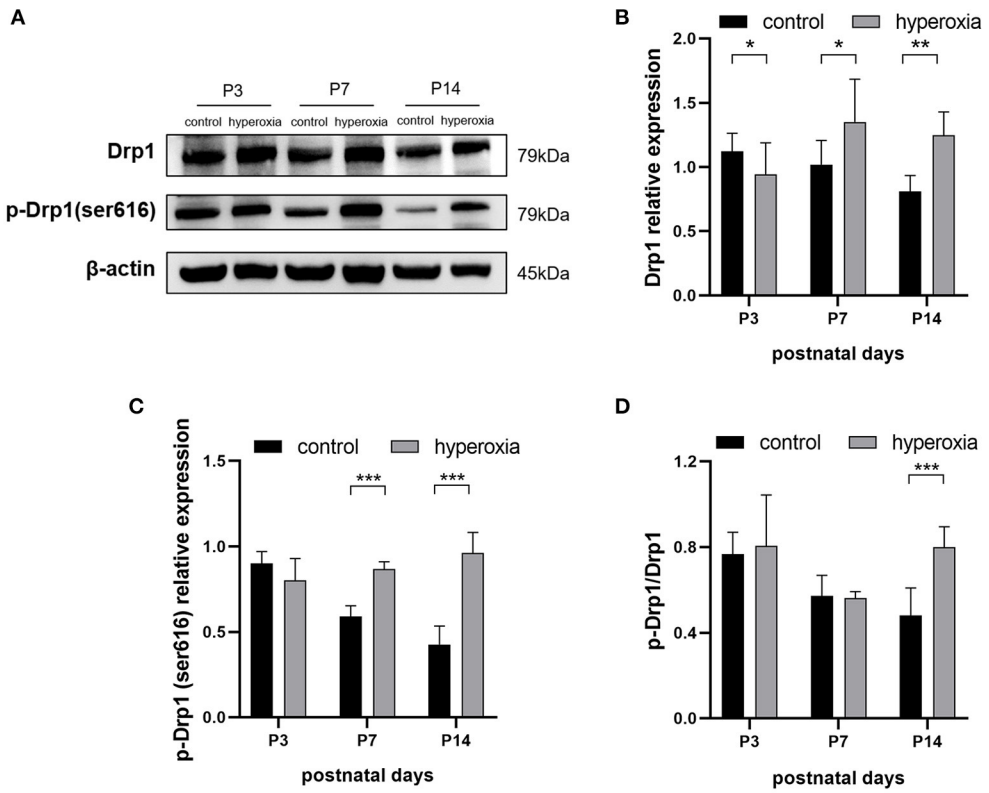

FIGURE 2 | The levels of DRP1 and p-DRP1 (Ser616) in total lung tissues are detected by Western blotting. **(A)** Representative Western blot images of DRP1 and p-DRP1 (Ser616) in lung tissues from controls or from hyperoxia group on day 3, 7, or 14. **(B,C)** Protein levels of DRP1 **(B)** or p-DRP1 (Ser616) **(C)** in arbitrary units (AU) normalized to β-actin levels. **(D)** The ratios of p-DRP1 (Ser616)/DRP1 was calculated based on Western blot results. β-actin was the loading control. $n = 6$ animals/group; Values are expressed as means ± SD; $^{*}P < 0.05$, $^{**}P < 0.01$, $^{***}P < 0.001$.

blood vessels, ultrasonic echocardiogram monitoring revealed that the pulmonary vascular resistance index (**Figure 3C**) of the hyperoxia + mdivi-1 group was significantly lower than that of the hyperoxia + vehicle group on P21 ($P < 0.05$). The peak pulmonary flow velocity was measured on P28 (**Figure 3D**). The results showed that the pulmonary artery peak flow velocity decreased after administration of mdivi-1, indicating an improvement in pulmonary artery pressure. In addition, the heart tissue was weighed and Fulton index was calculated on P28. The Fulton index of the hyperoxia + vehicle group was significantly higher than that of the control + vehicle group (**Figure 3E**), indicating that the right ventricle was hypertrophic. Compared to the hyperoxia + vehicle group, the Fulton index of the hyperoxia + mdivi-1 group was lower, suggesting that right ventricular hypertrophy had improved (**Figure 3E**).

Recovery in Room Air Leaves Hyperoxia-Exposed Rats With Abnormal Pulmonary Hemodynamics Until Adolescence

Although the alveolar developmental obstruction caused by hyperoxia had no significant difference in lung morphology between the control and hyperoxia groups after 7 days of normal oxygen recovery, the pulmonary vessels showed significant abnormalities in the hyperoxia group during the recovery period. We performed continuous pulmonary vascular-related cardiac ultrasonography on rats released from the hypertoxic environment on post-natal day 14, P21, P28, and P42 (**Figure 4**). After measuring indexes from the Doppler ultrasound trace of the pulmonary artery (**Figures 4A,B**), the results showed that the PAT (**Figure 4C**) reflecting the pulmonary circulation resistance was markedly shortened on day 14 ($P < 0.05$), day 21 ($P < 0.01$), and day 28 ($P < 0.001$). The other two indicators: PVRi and peak pulmonary flow velocity were significantly increased (**Figures 4D,E**). PVRi were significantly increased on day 21 ($P < 0.001$) and day 28 ($P < 0.001$) in the hyperoxia group compared to the control group. and the peak pulmonary flow velocity were increased on day 21 ($P < 0.001$), day 28 ($P < 0.001$), and day 42 ($P < 0.05$). In addition, cardiac ultrasound-related features of the pulmonary veins were also detected. After hyperoxia, the diameter of the pulmonary vein (**Figure 4F**) decreased on day 21 ($P < 0.05$), whereas the diameter of the pulmonary artery (**Figure 4G**) was not significantly changed at day 21. In order to observe the effect of this pulmonary hemodynamic abnormality on the heart, particularly on the right ventricular load, we acquired a short-axis image of the

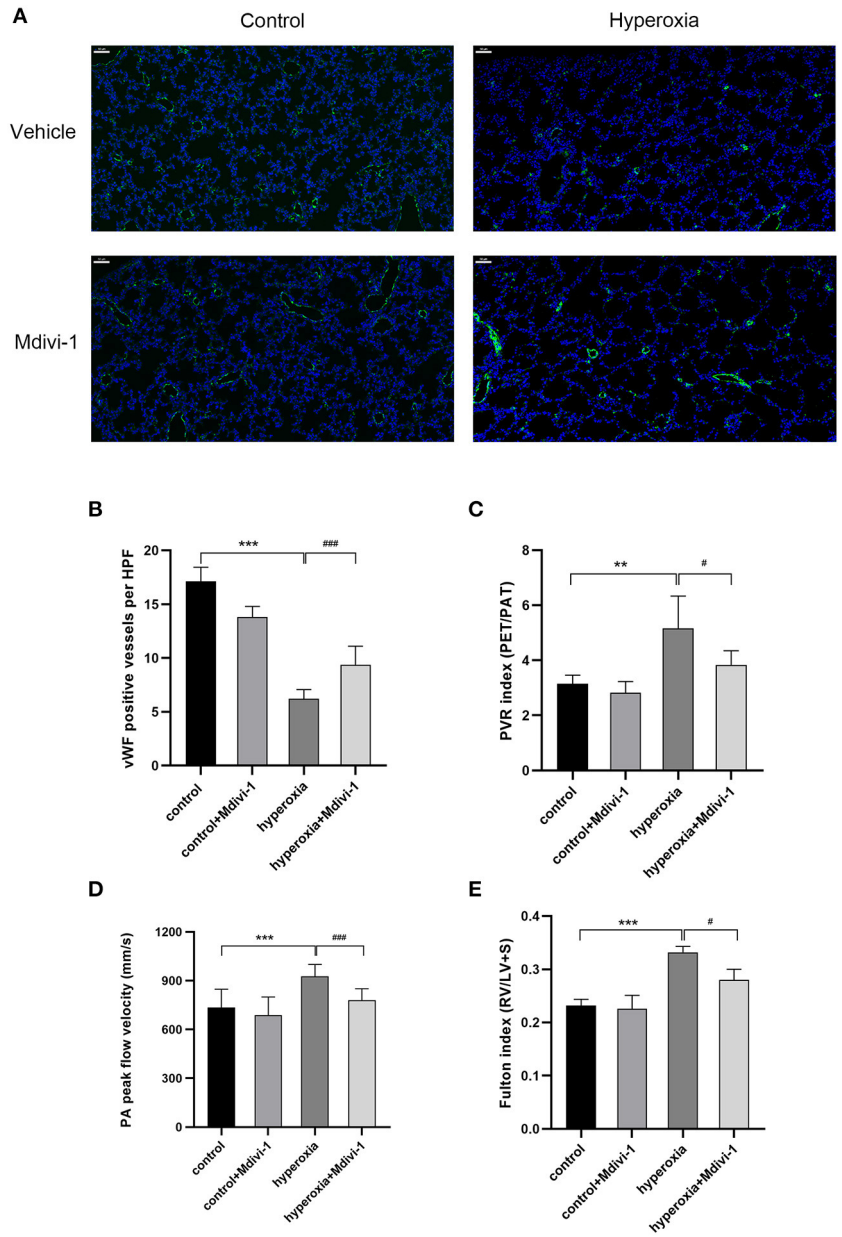

FIGURE 3 | The beneficial effect of Mdivi-1 on pulmonary vasculature after chronic hyperoxia-induced lung injury. DRP1 inhibitor Mdivi-1 was injected intraperitoneally daily to the rats from day 7 to 14. **(A)** Representative images of immunofluorescence staining. Green fluorescence represented vWF expression. Scale bar = 50 μm. **(B)** vWF-positive vessels whose diameters were < 50 μm were calculated accordingly. **(C)** The pulmonary vascular resistance index (PVRi) measured on day 21. **(D)** The peak pulmonary flow velocity was measured on P28 **(E)** the Fulton's index was measured on day 28. $n = 6$ animals/group; Values are presented as mean ± SD. $^{**}P < 0.01$, $^{***}P < 0.001$, hyperoxia vs. control; $^{\#}P < 0.05$, $^{\#\#\#}P < 0.001$, hyperoxia+Mdivi-1 vs. hyperoxia.

end-diastolic ventricle at the mitral valve level, and outlined the cross-sections of the right and left ventricular cavities. The area ratio (RVEDA/LVEDA) is a measurement of the right ventricular load. We found that the area ratio was higher in the hyperoxia group on day 14 ($P < 0.05$) and on day 21 ($P < 0.01$), suggesting that the right ventricle was dilated, and this trend continued for 7 days (up to day 21) in the hyperoxia group (**Figure 4H**). A representative two-dimensional echocardiography image of the left and right ventricular dimensions on day 21 demonstrated right ventricular dilation in the hyperoxia group compared to the control group, indicative of diastolic right ventricle dysfunction (**Figures 4I,J**).

DISCUSSION

In this study, we attempted to explore the relationship between BPD and mitochondrial fission induced by hyperoxia. To simulate severe BPD in rodent models, we

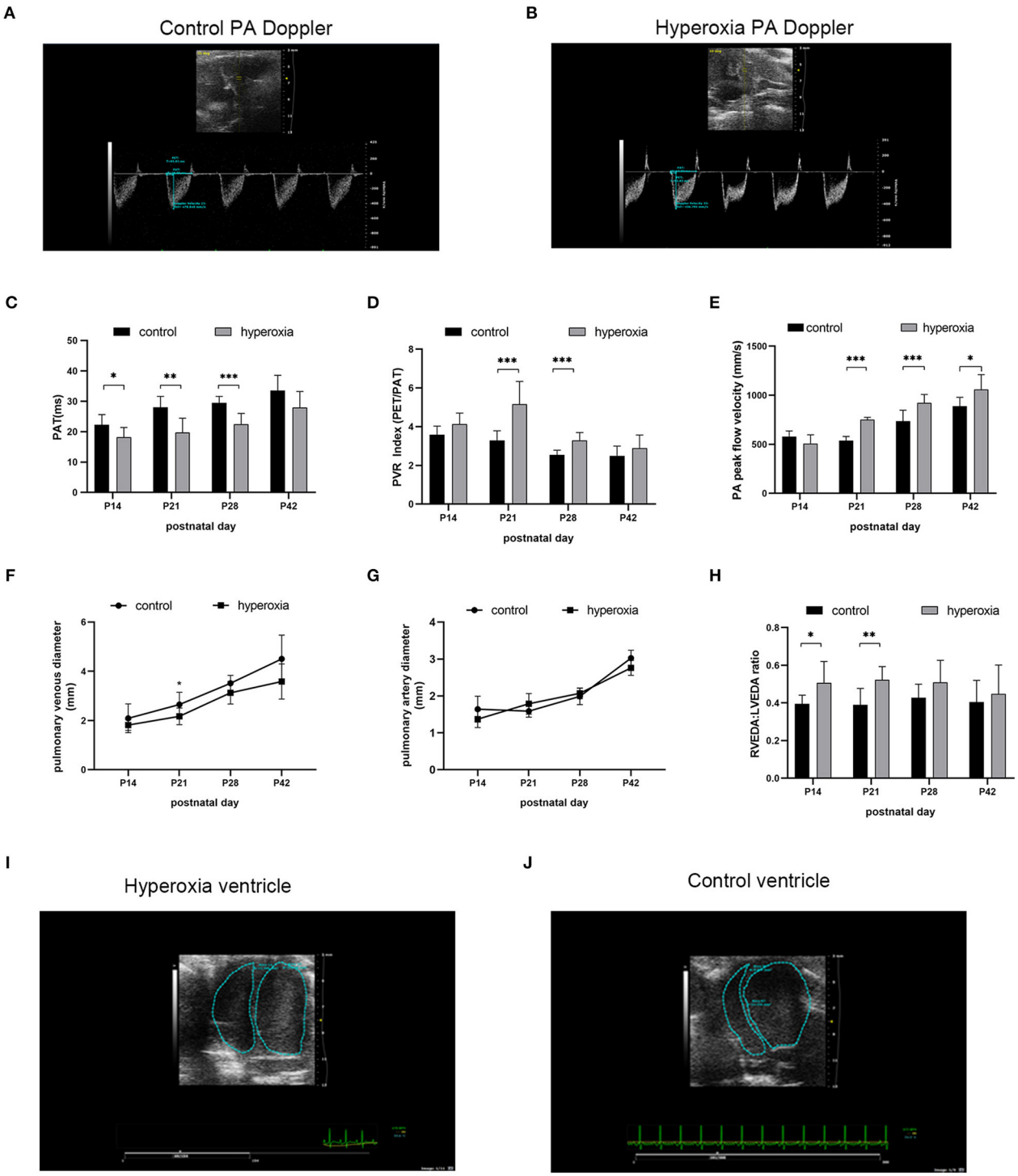

FIGURE 4 | Abnormal pulmonary hemodynamics after hyperoxia. Newborn (P0) pups were exposed to 21% O_2 (control) or 80–85% O_2 (hyperoxia) for 14 days and returned to air to receive echocardiography detection on post-natal day 14, 21, 28, and 42. **(A)** Representative Doppler ultrasound images of the pulmonary artery (PA) on day 21 after exposure to either normoxia or hyperoxia for 14 days from birth. **(B)** Representative 2-dimensional echocardiography images of left and right ventricular dimensions on day 21 was shown by comparing the difference between exposure to normoxia and hyperoxia for 14 days after birth. **(C–H)** Echocardiography and pulse-wave Doppler-derived indexes of pulmonary acceleration time (PAT) **(C)**, pulmonary vascular resistance (PVR) index **(D)**, peak flow velocity of pulmonary artery **(E)**, pulmonary venous diameter **(F)**, pulmonary artery diameter **(G)**, and right ventricular end-diastolic area (RVEDA)-to-left ventricular end-diastolic area ratio (LVEDA) **(H)** were analyzed and compared between hyperoxia group and control group on P14, P21, P28, and P42. **(I,J)** Representative two-dimensional echocardiography images of the left and right ventricular dimensions on control and hyperoxia group on day 21. $n = 6$ animals/group; Values are expressed as means ± SD; $^{*}P < 0.05$, $^{**}P < 0.01$, $^{***}P < 0.001$, compared with hyperoxia and control group.

first exposed rats to 80–85% oxygen for a long period (14 days). The results showed that the lung morphology was seriously damaged and alveolar structure was simplified, which was consistent with the pathology of BPD. Protein expression of Drp1/p-Drp1 in the hyperoxia group was significantly higher compared to in the control group. We then applied the Drp1 inhibitor, Mdivi-1, and found an improvement in the reduction of pulmonary microvasculature under hyperoxia. Finally, we discussed whether hyperoxia-induced BPD would have adverse effects on pulmonary circulation function and followed up with echocardiography.

In recent years, many studies have shown that mitochondrial dysfunction plays an important role in BPD and PH (21). Mitochondrial dynamics are essential for maintaining mitochondrial integrity and regulating apoptosis (22). Drp1 is a mitochondrial outer membrane protein that mediates fission of mitochondria and controls mitochondrial morphology (23). The latest research shows that by inducing overexpression of hypoxia inducible factor-1, hypoxia stimuli can promote the expression of Drp1 to regulate mitochondrial dynamics in pulmonary vascular remodeling (24). In this study Drp1 changes were investigated after hyperoxia exposure in newborn rats to further our understanding of the relationship between hyperoxia and Drp1. We found that Drp1 reached its peak on day 7 in the hyperoxia group and maintained this level until day 14. These results showed that Drp1 protein expression could be enhanced by hyperoxia. Many studies have suggested that abnormally high expression of Drp1 in the lungs is an indicator of poor prognosis, particularly in chronic malignant diseases (25, 26). Drp1 has been regarded as an attractive therapeutic target.

Mitochondrial oxidative stress is a component of general oxidative stress, and excessive reactive oxygen species would lead to increased mitochondrial fission (27). Studies have found that particulate matter ($PM_{2.5}$) can lead to oxidative stress in lung epithelial cells, increasing mitochondrial fission, resulting in cell apoptosis (28), and Drp1 and oxidative stress are essential mediators in cigarette smoke-induced pulmonary endothelial Injury (29). Combined with our findings, we speculated that lung injury caused by hyperoxia in newborn rats would increase mitochondrial fission, namely the expression of Drp1, due to oxidative stress. In addition, experiments have confirmed the relationship between hypoxia and Drp1, studies were not only involved in animal models about Lung Ischemia-reperfusion Injury (30) and lung vascular ischemic/hypoxic injury (31), but also in others like hepatocellular carcinoma cells in hypoxia (32), and Hypoxia-Reoxygenation Injury of Cardiomyocytes (33). Although hypoxia or hyperoxia can trigger similar pathological responses, such as oxidative stress and inflammation, these underlying mechanisms need to be further studied at the cellular level.

Mdivi-1, a specific inhibitor of DRP1 (34) is reported to be effective in suppressing the pulmonary artery smooth muscle cells in lungs with PH (35). Because of the changes in Drp1 after hyper oxygen in this study, the rats were injected intraperitoneally with Mdivi-1 (25 mg/kg) from days 7 to 14 to explore whether inhibition of Drp1 has protective effects on hyperoxia-induced lung injury. It was found that long-term hyperoxia severely hindered the development of small pulmonary vessels, and after mdivi-1 administration, the number of small pulmonary vessels significantly increased. These results indicate that Mdivi-1 can relieve hyperoxia-induced obstruction of pulmonary microvascular development. From the perspective of the long-term effects on blood vessels, ultrasonic monitoring results showed that the PVR and PFVP measured during the recovery period were lower after the administration of Mdivi-1, suggesting improvements in pulmonary artery pressure. In addition, the heart tissue was weighed on 28 days after birth to calculate the Fulton index the results showed that the right ventricular hypertrophy index in the hyperoxia group was significantly higher than that in the control group, suggesting right ventricular hypertrophy.

To investigate whether this BPD model would have an adverse effect on pulmonary circulation function, follow-up detection was carried out by echocardiography in rats at 14, 21, 28, and 42 days after birth. It was demonstrated that PAT in the hyperoxia group was shortened, while the PVRi and PFVP increased significantly compared to the control group. These parameters all reflected higher pulmonary pressure after exposure to hyperoxia for 2 weeks. In addition, by measuring the area ratio and Fulton index, we found that over-circulation influenced right ventricular structure and function.

It is worth mentioning that in this study, in addition to focusing on the pulmonary artery, cardiac echocardiography indicators related to the pulmonary vein were also detected, and it was found that the pulmonary vein diameter showed signs of narrowing after exposure to hyperoxia, while there was no significant difference in pulmonary artery diameter between the two groups. Pulmonary vein stenosis is a rare problem that is often neglected (36); however, it is a severe and increasingly common complication of preterm infants with BPD (37). Although this study identified the manifestations of pulmonary vein stenosis, it did not elucidate the underlying mechanisms, which require further investigation.

Lastly, there are some limitations present in this study. First, we did not further explore the mechanism between hyperoxia and Drp1. Secondly, we did not carry out in *vitro* experiments, such as on pulmonary epithelial cells and microvascular endothelial cells. Thirdly, this experiment only discussed the development of pulmonary vessels after hyperoxia stimulation, but future studies will focus on the effects of Drp1 and Mdivi-1 on alveolar development.

In conclusion, the present study identified the echocardiographic features of hyperoxia-induced BPD-PH models and confirmed that the expression of Drp1 is increased in hyperoxia-induced lung injury. Treatment with Mdivi-1 during hyperoxia was protective against pulmonary vasculature

development and function. However, further studies are required to determine the precise mechanism of Drp1 in BPD and BPD-PH.

DATA AVAILABILITY STATEMENT

The raw data supporting the conclusions of this article will be made available by the authors, without undue reservation.

ETHICS STATEMENT

The animal study was reviewed and approved by Wenzhou Medicial University.

AUTHOR CONTRIBUTIONS

YD conceived and designed the experiments. YD and BY performed the experiments and wrote the paper. YD, DA, and LY analyzed the data. XW, RH, and XF contributed materials and analysis tools. CC and SC edited and approved final draft. All authors contributed to the article and approved the submitted version.

FUNDING

This work was supported by Wenzhou science and technology project (Y20180092 and Y20180006).

REFERENCES

1. Jobe AH, Bancalari E. Bronchopulmonary dysplasia. *Am J Respir Crit Care Med.* (2001) 163:1723–9. doi: 10.1164/ajrccm.163.7.2011060
2. Baraldi E, Filippone M. Chronic lung disease after premature birth. *N Engl J Med.* (2007) 357:1946–55. doi: 10.1056/NEJMra067279
3. Hilgendorff A, Reiss I, Ehrhardt H, Eickelberg O, Alvira CM. Chronic lung disease in the preterm infant. Lessons learned from animal models. *Am J Respir Cell Mol Biol.* (2014) 50:233–45. doi: 10.1165/rcmb.2013-0014TR
4. McEvoy CT, Jain L, Schmidt B, Abman S, Bancalari E, Aschner JL. Bronchopulmonary dysplasia: NHLBI workshop on the primary prevention of chronic lung diseases. *Ann Am Thorac Soc.* (2014) 11(Suppl. 3):S146–53. doi: 10.1513/AnnalsATS.201312-424LD
5. Smith VC, Zupancic JA, McCormick MC, Croen LA, Greene J, Escobar GJ, et al. Rehospitalization in the first year of life among infants with bronchopulmonary dysplasia. *J Pediatr.* (2004) 144:799–803. doi: 10.1016/j.jpeds.2004.03.026
6. Arjaans S, Zwart EAH, Ploegstra MJ, Bos AF, Kooi EMW, Hillege HL, et al. Identification of gaps in the current knowledge on pulmonary hypertension in extremely preterm infants: a systematic review and meta-analysis. *Paediatr Perinat Epidemiol.* (2018) 32:258–67. doi: 10.1111/ppe.12444
7. Mirza H, Ziegler J, Ford S, Padbury J, Tucker R, Laptook A. Pulmonary hypertension in preterm infants: prevalence and association with bronchopulmonary dysplasia. *J Pediatr.* (2014) 165:909–14.e1. doi: 10.1016/j.jpeds.2014.07.040
8. Khemani E, McElhinney DB, Rhein L, Andrade O, Lacro RV, Thomas KC, et al. Pulmonary artery hypertension in formerly premature infants with bronchopulmonary dysplasia: clinical features and outcomes in the surfactant era. *Pediatrics.* (2007) 120:1260–9. doi: 10.1542/peds.2007-0971
9. Archer SL. Mitochondrial dynamics–mitochondrial fission and fusion in human diseases. *N Engl J Med.* (2013) 369:2236–51. doi: 10.1056/NEJMra1215233
10. Jahani-Asl A, Slack RS. The phosphorylation state of Drp1 determines cell fate. *EMBO Rep.* (2007) 8:912–3. doi: 10.1038/sj.embor.7401077
11. Losón OC, Song Z, Chen H, Chan DC. Fis1, Mff, MiD49, and MiD51 mediate Drp1 recruitment in mitochondrial fission. *Mol Biol Cell.* (2013) 24:659–67. doi: 10.1091/mbc.e12-10-0721
12. Kim YY, Yun SH, Yun J. Downregulation of Drp1, a fission regulator, is associated with human lung and colon cancers. *Acta Biochim Biophys Sin.* (2018) 50:209–15. doi: 10.1093/abbs/gmx137
13. Chiang YY, Chen SL, Hsiao YT, Huang CH, Lin TY, Chiang IP, et al. Nuclear expression of dynamin-related protein 1 in lung adenocarcinomas. *Mod Pathol.* (2009) 22:1139–50. doi: 10.1038/modpathol.2009.83
14. Kim YM, Youn SW, Sudhahar V, Das A, Chandhri R, Cuervo Grajal H, et al. Redox regulation of mitochondrial fission protein Drp1 by protein disulfide isomerase limits endothelial senescence. *Cell Rep.* (2018) 23:3565–78. doi: 10.1016/j.celrep.2018.05.054
15. Liu X, Tan H, Liu X, Wu Q. Correlation between the expression of Drp1 in vascular endothelial cells and inflammatory factors in hypertension rats. *Exp Ther Med.* (2018) 15:3892–98. doi: 10.3892/etm.2018.5899
16. Krishnan U, Feinstein JA, Adatia I, Austin ED, Mullen MP, Hopper RK, et al. Evaluation and management of pulmonary hypertension in children with bronchopulmonary dysplasia. *J Pediatr.* (2017) 188:24–34.e1. doi: 10.1016/j.jpeds.2017.05.029
17. Keller RL. Pulmonary hypertension and pulmonary vasodilators. *Clin Perinatol.* (2016) 43:187–202. doi: 10.1016/j.clp.2015.11.013
18. Cassidy-Stone A, Chipuk JE, Ingerman E, Song C, Yoo C, Kuwana T, et al. Chemical inhibition of the mitochondrial division dynamin reveals its role in Bax/Bak-dependent mitochondrial outer membrane permeabilization. *Dev Cell.* (2008) 14:193–204. doi: 10.1016/j.devcel.2007.11.019
19. Bhaskaran M, Xi D, Wang Y, Huang C, Narasaraju T, Shu W, et al. Identification of microRNAs changed in the neonatal lungs in response to hyperoxia exposure. *Physiol Genomics.* (2012) 44:970–80. doi: 10.1152/physiolgenomics.00145.2011
20. Kantores C, McNamara PJ, Teixeira L, Engelberts D, Murthy P, Kavanagh BP, et al. Therapeutic hypercapnia prevents chronic hypoxia-induced pulmonary hypertension in the newborn rat. *Am J Physiol Lung Cell Mol Physiol.* (2006) 291:L912–22. doi: 10.1152/ajplung.00480.2005
21. Shah D, Das P, Bhandari V. Mitochondrial dysfunction in bronchopulmonary dysplasia. *Am J Respir Crit Care Med.* (2018) 197:1363. doi: 10.1164/rccm.201711-2197LE
22. Suen DF, Norris KL, Youle RJ. Mitochondrial dynamics and apoptosis. *Genes Dev.* (2008) 22:1577–90. doi: 10.1101/gad.1658508
23. Westermann B. Mitochondrial fusion and fission in cell life and death. *Nat Rev Mol Cell Biol.* (2010) 11:872–84. doi: 10.1038/nrm3013
24. Chen X, Yao JM, Fang X, Zhang C, Yang YS, Hu CP, et al. Hypoxia promotes pulmonary vascular remodeling via HIF-1α to regulate mitochondrial dynamics. *J Geriatr Cardiol.* (2019) 16:855–71. doi: 10.11909/j.issn.1671-5411.2019.12.003
25. Zhao J, Zhang J, Yu M, Xie Y, Huang Y, Wolff DW, et al. Mitochondrial dynamics regulates migration and invasion of breast cancer cells. *Oncogene.* (2013) 32:4814–24. doi: 10.1038/onc.2012.494
26. Shen F, Gai J, Xing J, Guan J, Fu L, Li Q. Dynasore suppresses proliferation and induces apoptosis of the non-small-cell lung cancer cell line A549. *Biochem Biophys Res Commun.* (2018) 495:1158–66. doi: 10.1016/j.bbrc.2017.11.109
27. Pradeepkiran JA, Reddy PH. Defective mitophagy in Alzheimer's disease. *Ageing Res Rev.* (2020) 64:101191. doi: 10.1016/j.arr.2020.101191
28. Liu X, Zhao X, Li X, Lv S, Ma R, Qi Y, et al. $PM_{2.5}$ triggered apoptosis in lung epithelial cells through the mitochondrial apoptotic way mediated by a ROS-DRP1-mitochondrial fission axis. *J Hazard Mater.* (2020) 397:122608. doi: 10.1016/j.jhazmat.2020.122608
29. Wang Z, White A, Wang X, Ko J, Choudhary G, Lange T, et al. Mitochondrial fission mediated cigarette smoke-induced pulmonary endothelial injury. *Am J Respir Cell Mol Biol.* (2020) 63:637–51. doi: 10.1165/rcmb.2020-0008OC
30. Lin KC, Yeh JN, Chen YL, Chiang JY, Sung PH, Lee FY, et al. Xenogeneic and allogeneic mesenchymal stem cells effectively protect the lung against

ischemia-reperfusion injury through downregulating the inflammatory, oxidative stress, and autophagic signaling pathways in rat. *Cell Transplant.* (2020) 29:963689720954140. doi: 10.1177/0963689720954140
31. Duan C, Wang L, Zhang J, Xiang X, Wu Y, Zhang Z, et al. Mdivi-1 attenuates oxidative stress and exerts vascular protection in ischemic/hypoxic injury by a mechanism independent of Drp1 GTPase activity. *Redox Biol.* (2020) 37:101706. doi: 10.1016/j.redox.2020.101706
32. Lin XH, Qiu BQ, Ma M, Zhang R, Hsu SJ, Liu HH, et al. Suppressing DRP1-mediated mitochondrial fission and mitophagy increases mitochondrial apoptosis of hepatocellular carcinoma cells in the setting of hypoxia. *Oncogenesis.* (2020) 9:67. doi: 10.1038/s41389-020-00251-5
33. Luo H, Song S, Chen Y, Xu M, Sun L, Meng G, et al. Inhibitor 1 of protein phosphatase 1 regulates Ca^{2+}/calmodulin-dependent protein kinase II to alleviate oxidative stress in hypoxia-reoxygenation injury of cardiomyocytes. *Oxid Med Cell Longev.* (2019) 2019:2193019. doi: 10.1155/2019/2193019
34. Bordt EA, Clerc P, Roelofs BA, Saladino AJ, Tretter L, Adam-Vizi V, et al. The putative Drp1 inhibitor mdivi-1 is a reversible mitochondrial complex I inhibitor that modulates reactive oxygen species. *Dev Cell.* (2017) 40:583–94.e6. doi: 10.1016/j.devcel.2017.02.020
35. Marsboom G, Toth PT, Ryan JJ, Hong Z, Wu X, Fang YH, et al. Dynamin-related protein 1-mediated mitochondrial mitotic fission permits hyperproliferation of vascular smooth muscle cells and offers a novel therapeutic target in pulmonary hypertension. *Circ Res.* (2012) 110:1484–97. doi: 10.1161/CIRCRESAHA.111.263848
36. Mahgoub L, Kaddoura T, Kameny AR, Lopez Ortego P, Vanderlaan RD, Kakadekar A, et al. Pulmonary vein stenosis of ex-premature infants with pulmonary hypertension and bronchopulmonary dysplasia, epidemiology, and survival from a multicenter cohort. *Pediatr Pulmonol.* (2017) 52:1063–70. doi: 10.1002/ppul.23679
37. Nasr VG, Callahan R, Wichner Z, Odegard KC, DiNardo JA. Intraluminal pulmonary vein stenosis in children: a "New" lesion. *Anesth Analg.* (2019) 129:27–40. doi: 10.1213/ANE.0000000000003924

Conflict of Interest: The authors declare that the research was conducted in the absence of any commercial or financial relationships that could be construed as a potential conflict of interest.

Copyright © 2021 Dai, Yu, Ai, Yuan, Wang, Huo, Fu, Chen and Chen. This is an open-access article distributed under the terms of the Creative Commons Attribution License (CC BY). The use, distribution or reproduction in other forums is permitted, provided the original author(s) and the copyright owner(s) are credited and that the original publication in this journal is cited, in accordance with accepted academic practice. No use, distribution or reproduction is permitted which does not comply with these terms.

frontiers in Medicine

ORIGINAL RESEARCH
published: 22 February 2021
doi: 10.3389/fmed.2021.614239

Sequential Exposure to Antenatal Microbial Triggers Attenuates Alveolar Growth and Pulmonary Vascular Development and Impacts Pulmonary Epithelial Stem/Progenitor Cells

*Helene Widowski[1,2,3], Niki L. Reynaert[4,5], Daan R. M. G. Ophelders[1,3], Matthias C. Hütten[6,7], Peter G. J. Nikkels[8], Carmen A. H. Severens-Rijvers[9], Jack P. M. Cleutjens[9,10], Matthew W. Kemp[11], John P. Newnham[11], Masatoshi Saito[11,12], Haruo Usuda[11,12], Matthew S. Payne[11], Alan H. Jobe[11,13], Boris W. Kramer[1,3,14], Tammo Delhaas[2,10] and Tim G. A. M. Wolfs[1,3]**

[1] Department of Pediatrics, Maastricht University Medical Center, Maastricht, Netherlands, [2] Department of BioMedical Engineering, Maastricht University Medical Center, Maastricht, Netherlands, [3] GROW School for Oncology and Developmental Biology, Maastricht University Medical Center, Maastricht, Netherlands, [4] Department of Respiratory Medicine, Maastricht University, Maastricht, Netherlands, [5] NUTRIM School of Nutrition and Translational Research in Metabolism, Maastricht University Medical Center, Maastricht, Netherlands, [6] Neonatology, Pediatrics Department, Faculty of Health, Medicine and Life Sciences, Maastricht University Medical Center, Maastricht, Netherlands, [7] University Children's Hospital Würzburg, University of Würzburg, Würzburg, Germany, [8] Department of Pathology, University Medical Center Utrecht, Utrecht, Netherlands, [9] Department of Pathology, Maastricht University Medical Center, Maastricht, Netherlands, [10] CARIM School for Cardiovascular Diseases, Maastricht University Medical Center, Maastricht, Netherlands, [11] Division of Obstetrics and Gynecology, The University of Western Australia, Crawley, WA, Australia, [12] Tohoku University Centre for Perinatal and Neonatal Medicine, Tohoku University Hospital, Sendai, Japan, [13] Perinatal Institute Cincinnati Children's Hospital Medical Center, Cincinnati, OH, United States, [14] School for Mental Health and Neuroscience, Maastricht University, Maastricht, Netherlands

OPEN ACCESS

Edited by:
Anne Hilgendorff, Ludwig Maximilian University of Munich, Germany

Reviewed by:
Chang-Won Choi, Seoul National University, South Korea
Rose M. Viscardi, University of Maryland, Baltimore, United States

***Correspondence:**
Tim G. A. M. Wolfs
tim.wolfs@maastrichtuniversity.nl

Specialty section:
This article was submitted to Pulmonary Medicine, a section of the journal Frontiers in Medicine

Received: *05 October 2020*
Accepted: *02 February 2021*
Published: *22 February 2021*

Citation:
Widowski H, Reynaert NL, Ophelders DRMG, Hütten MC, Nikkels PGJ, Severens-Rijvers CAH, Cleutjens JPM, Kemp MW, Newnham JP, Saito M, Usuda H, Payne MS, Jobe AH, Kramer BW, Delhaas T and Wolfs TGAM (2021) Sequential Exposure to Antenatal Microbial Triggers Attenuates Alveolar Growth and Pulmonary Vascular Development and Impacts Pulmonary Epithelial Stem/Progenitor Cells. Front. Med. 8:614239. doi: 10.3389/fmed.2021.614239

Perinatal inflammatory stress is strongly associated with adverse pulmonary outcomes after preterm birth. Antenatal infections are an essential perinatal stress factor and contribute to preterm delivery, induction of lung inflammation and injury, pre-disposing preterm infants to bronchopulmonary dysplasia. Considering the polymicrobial nature of antenatal infection, which was reported to result in diverse effects and outcomes in preterm lungs, the aim was to examine the consequences of sequential inflammatory stimuli on endogenous epithelial stem/progenitor cells and vascular maturation, which are crucial drivers of lung development. Therefore, a translational ovine model of antenatal infection/inflammation with consecutive exposures to chronic and acute stimuli was used. Ovine fetuses were exposed intra-amniotically to *Ureaplasma parvum* 42 days (chronic stimulus) and/or to lipopolysaccharide 2 or 7 days (acute stimulus) prior to preterm delivery at 125 days of gestation. Pulmonary inflammation, endogenous epithelial stem cell populations, vascular modulators and morphology were investigated in preterm lungs. Pre-exposure to UP attenuated neutrophil infiltration in 7d LPS-exposed lungs and prevented reduction of SOX-9 expression and increased SP-B expression, which could indicate protective responses induced by re-exposure. Sequential exposures did not

markedly impact stem/progenitors of the proximal airways (P63+ basal cells) compared to single exposure to LPS. In contrast, the alveolar size was increased solely in the UP+7d LPS group. In line, the most pronounced reduction of AEC2 and proliferating cells (Ki67+) was detected in these sequentially UP + 7d LPS-exposed lambs. A similar sensitization effect of UP pre-exposure was reflected by the vessel density and expression of vascular markers VEGFR-2 and Ang-1 that were significantly reduced after UP exposure prior to 2d LPS, when compared to UP and LPS exposure alone. Strikingly, while morphological changes of alveoli and vessels were seen after sequential microbial exposure, improved lung function was observed in UP, 7d LPS, and UP+7d LPS-exposed lambs. In conclusion, although sequential exposures did not markedly further impact epithelial stem/progenitor cell populations, re-exposure to an inflammatory stimulus resulted in disturbed alveolarization and abnormal pulmonary vascular development. Whether these negative effects on lung development can be rescued by the potentially protective responses observed, should be examined at later time points.

Keywords: polymicrobial infection, vascular disturbances, adverse pulmonary outcomes, endogenous pulmonary stem cells, bronchopulmonary dysplasia, preterm birth, antenatal inflammation

INTRODUCTION

Perinatal inflammatory stress, including sepsis and mechanical ventilation are strongly associated with adverse pulmonary outcomes after preterm birth (1, 2). One of the most frequently occurring complications after perinatal insults and preterm birth is bronchopulmonary dysplasia (BPD), a chronic respiratory disorder of the premature infant. BPD results from a demand of respiratory support and supplemental oxygen after preterm birth and histologically manifests as a delay in alveolar growth and an impairment in vascular maturation (3, 4). Antenatal infections are an essential factor of perinatal stress and associated with preterm delivery and induction of lung inflammation and injury, thereby pre-disposing to BPD (5, 6).

Recently, we showed that timing of antenatal infection/inflammation and its duration of determine the extent and location of adverse effects in the preterm lungs (7). More precisely, we reported attenuated levels of endogenous stem/progenitor populations and their potential consequences, including altered surfactant protein expression and reduced alveolar differentiation in the course of antenatal inflammation (7).

Antenatal infection is often of polymicrobial nature, with *Ureaplasma* (UP) species being the most frequently cultivated bacteria in human amniotic fluid samples (8). Conceivably, potential interactions between various consecutive inflammatory stimuli might modulate the inflammatory response and either lead to a milder outcome, including a treatable surfactant deficiency, or more severe adverse pulmonary outcome (BPD) in the preterm infant. This concept is supported by earlier findings in different preterm organ systems, showing that sequentially occurring antenatal inflammatory insults of varying exposure time points and durations, cause either preconditioning or sensitization to a consecutive inflammatory hit (9–11). With respect to the lungs, *in utero* sequential exposure to antenatal bacteria and bacteria-derived endotoxins resulted in increased inflammation, along with exacerbation of vascular disturbances in very preterm ovine lungs (12). Conversely, in fetuses of higher gestational age (GA), Kallapur et al. showed that chronic UP exposure pre-conditioned the immature lungs and thereby led to a decreased pro-inflammatory response to a subsequent endotoxin hit (13). The GA of the fetus and the duration of each antenatal insult have been shown to modulate the responsiveness of the lung tissue to inflammation and determine the extent of developmental changes.

Considering the increasing importance of aberrant vascular development in neonatal lung diseases (14), and recent findings of endogenous epithelial stem/progenitor cells playing a key role in the adverse pulmonary development (7, 15), our aim was to examine the consequences of sequential inflammatory stimuli on inflammatory read outs and on these crucial developmental aspects. For this purpose, we used a translational ovine model of antenatal infection/inflammation with consecutive exposures to a chronic and an acute stimulus. Ovine fetuses were exposed intra-amniotically (IA) to live *Ureaplasma parvum* 42 days (chronic stimulus) and/or to lipopolysaccharide (LPS) 2 or 7 days (acute stimulus) prior to preterm delivery at 124 days of gestational age (dGA). LPS exposure occurred at two different time points, since historical data report increased inflammatory and injurious pattern, upon treatment at respectively, 2 and 7 days before preterm delivery in the preterm ovine lungs (16, 17).

MATERIALS AND METHODS

Study Approval

Animal experiments were approved by the animal ethics committee of the University of Western Australia (Perth, Australia).

Animal Experiments and Tissue Sampling

Procedures of the animal experiments and group allocations were published previously (10) and are presented in **Figure 1**. Study groups included 42 day exposure to UP (UP group), LPS exposure 2 or 7 days prior to preterm delivery (2d LPS, 7d LPS groups) and combined 42 days pre-exposure to UP and LPS exposure 2 or 7 days before preterm delivery at 125d GA (UP + 2d LPS, UP + 7d LPS groups). The 125d of GA in sheep correspond to the human gestation at ∼31 weeks representing a moderate preterm neonate with a developing lung at the interface of the canalicular and saccular phase (18, 19).

Briefly, ultrasound-guided intra-amniotic injections were used to administer live UP serovar 3 strain HPA5 (Concentration: 2×10^5 color-changing units CCU) and/or LPS (Concentration: 10 mg, *Escherichia coli* 055:B5; Sigma-Aldrich, St. Louis, MO) at pre-defined time points to 28 time-mated Merino ewes. Therefore, stock cultures of UP were diluted first in sterile culture medium and further in sterile saline (1:100). Sterile saline was also used for the dissolution of LPS and served as a comparable injection in control animals. After surgical delivery of the fetus, both, the ewe and the fetus were euthanized.

Pulmonary pressure volume assessment was conducted after euthanasia. Hereto, an endotracheal tube was introduced into the trachea and the thoracic cavity was opened to allow expansion of the lungs. The inflation of the lungs was achieved with air to a maximum pressure of 40 cm H_2O. Lung deflation volumes were recorded at decreasing pressures starting at 40 cm H_2O. Lung volumes were corrected for the body weight of the fetus (20).

Lung tissue sampling included inflation-fixation of the right upper lobe (RUL) for 24 h with 10% buffered formalin and snap freezing of the right lower lobe (RLL). The whole left lung was used to obtain bronchial lavage fluid.

Histology and Immunohistochemistry

RUL paraffin-embedded lung sections of 4 μm thickness were used for (immuno)histochemical analysis. Tissue sections were stained with hematoxylin and eosin (H&E) for histological evaluation. In addition, the following cellular markers were visualized: CD45 for hematopoietic cells (1:500, MCA2220GA, Biorad, Hercules, CA), PU.1 for differentiating monocytes (1:400, Santa Cruz Biotechnology, H0503), myeloperoxidase for neutrophils (MPO, 1:500, A-0398, Dako, Santa Clara, CA), tumor protein 63 for basal cells (P63, 1:8000, ab124762, Abcam), keratin 14 for differentiating basal cells (KRT-14, 1:1000, 905301, Biolegend, San Diego, CA), thyroid transcription factor-1 for Club and alveolar epithelial type (AEC) 2 cells (TTF-1, 1:8000, WRAB-1231, Seven Hills Bioreagents, Cincinnati, OH) and Ki67 for proliferation (1:1000, 15580, Abcam, Cambridge, UK) (7, 12, 16, 21). Immunohistochemical protocols were performed as previously published, while the PU.1 protocol was modified for optimal signal emission. Briefly, lung sections were deparaffinized in xylol and decreasing ethanol series. Blocking of endogenous peroxidase activity was achieved by incubating in 0.3% H_2O_2 in 1xPBS for 20 min. For antigen retrieval, lung sections were boiled 5 min in citrate buffer (pH 6.0). To prevent aspecific binding of antibodies, sections were incubated with 5% bovine serum albumin in 1xPBS for 30 min. The primary antibody, PU.1 in 0.1% BSA/1xPBS, was added and incubated over night at 4°C. Next, sections were incubated for 1 h with biotin-labeled secondary Swine-anti-Rabbit antibody (1:200, E0353, Dako) in 0.1% BSA/1xPBS. Vectastain ABC Elite kit (PK-6100, Bio-connect) was used for the enhancement of the anti-body specific signal for 30 min. Tissue visualization was performed with diaminobenzidine staining for 90 s, followed by a counterstaining with hematoxylin for 20 s. Sections were dehydrated and coverslipped.

Immunohistochemical Analyses

Methods for the analyses of immunohistochemical experiments have been published previously (7). Results for P63+, KRT-14+ and TTF-1+ cells were presented as cells per bronchus ring of

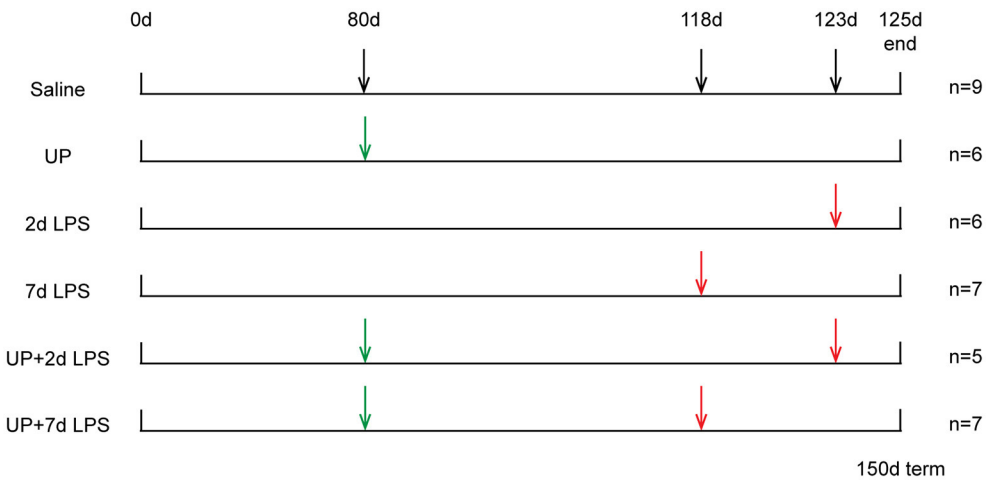

FIGURE 1 | Study design of translational ovine model for antenatal stress. Ultrasound-guided intra-amniotic injections were used for the administration of saline, UP and LPS. Lambs were delivered preterm at 125d GA (150d term).

proximal or distal airways, respectively. TTF-1+ and Ki67+ cells in alveoli were depicted as cells per high power field (HPF).

A magnification of 200x was used for PU.1 quantification and five randomly chosen pictures of alveoli (area of interest) were taken with a light microscope (Leica DM2000, Rijswijk, the Netherlands) and the Leica Application Suite 3.7.0 software (Leica Microsystem, Wetzlar, Germany). Alveolar region included the alveolar walls, alveolar airspaces and perivascular space. Analyses are presented as cells per HPF.

The wall-to-lumen ratio was determined on H&E sections, whereby vessels accompanying terminal bronchioles and an external diameter of $<50\,\mu m$ were investigated at a magnification of 400x. Five randomly chosen vessels were used and the wall-to-lumen ratio was calculated as media wall thickness divided by the radius of the vessel lumen (12).

Mean linear intercepts (MLI) and vessel density were also examined on H&E sections. Hereby, five and 10 images were taken randomly throughout the alveolar region, respectively for the MLI and the vessel quantification. In both cases bronchi and vessels ($>50\,\mu m$ external diameter) were excluded.

For the MLI assessment the ImageJ software (ImageJ 1.52i software, Bethesda, MD, USA) was used and images were superimposed with a $50 \times 50\,\mu m$ transparent grid. On five horizontal lines the intersections of the alveolar wall with the grid lines were counted. The MLI was determined according to the formula $MLI = 2 \times (L_{tot}/L_x)$, whereby, L_{tot} is the total length of all five lines and L_x is the total amount of intersections counted (22). Results are presented as micrometer of alveolar size.

With regard to the vessel quantification, all vessels, which were not accompanying a bronchus and had an external diameter $<50\,\mu m$ were counted (23). Surface area of alveolar tissue was determined with the Leica QWin Pro V3.5.1 software (Leica Microsystem) and results are displayed as vessels per square millimeter.

For all immunohistochemical stainings, as well as lung gas volumes, wall-to-lumen ratio, MLI and vessel quantification, the control values were presented as median and depicted as dotted line in all figures. Additionally, individual control values are provided in the **Supplementary Table 1**.

RNA Extraction and Real-Time PCR

Snap frozen RLL tissue was used for RNA isolation, transcribed and amplified for the following genes (12, 21, 24): interleukin (IL)−6, IL-8, SRY-related HMG-box (SOX)−2, SOX-9, surfactant proteins (SP) -A, -B, -C, -D, aquaporin (Aqp) 5, vascular endothelial growth factor (VEGF) -a, VEGF receptor (VEGFR)−2, Angiopoeitin (Ang)−1, tyrosine-protein kinase receptor (Tie)-2, ribosomal protein S15 (RPS15), Glyceraldehyde 3-phosphate dehydrogenase (GAPDH) and Human 14-3-3 protein zeta/delta (YWHAZ). Due to limited availability of lung tissue, mRNA analysis could not be performed for all animals (some experimental groups miss 1-2 animals). RT-PCR data were converted with the LinReg software and normalized to the Geomean of the housekeeping genes RPS15, GAPDH and YWHAZ. Mean fold changes were calculated with the saline control values set at one. For all RT-PCR results the control values were presented as median and depicted as dotted line in all figures.

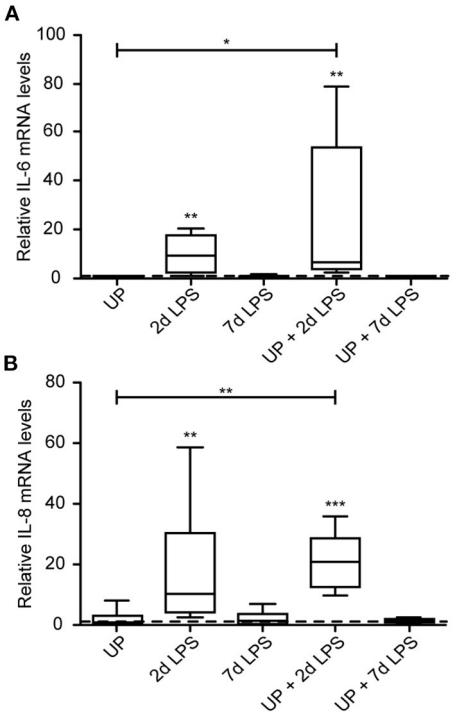

FIGURE 2 | Cytokine and chemokine expression are increased after exposure to 2d LPS and UP + 2d LPS in preterm ovine lung tissue. Fold changes in mRNA levels for IL-6 **(A)** and IL-8 **(B)** are depicted against saline. The median saline value is represented as dotted line. $^*p < 0.05$, $^{**}p < 0.01$, $^{***}p < 0.001$ compared to saline and UP.

Statistical Analysis

A non-parametric analysis of variance (ANOVA) followed by the *post-hoc* analysis Dunn's Multiple Comparison Test and a significance threshold of $p < 0.05$ were used to determine the statistical significance of the results (17). Results are displayed as median and interquartile range (IQR). *P*-values between 0.05 and 0.1 were interpreted as biologically relevant, as described previously (17). Significant changes toward the control groups were presented with asterisks, while differences between the experimental groups were shown with bars and asterisks.

RESULTS

LPS Exposure Increases Pulmonary Inflammation, Which Is Not Further Modulated by Pre-exposure to UP

Single exposure to LPS resulted in increased immune activation when compared to control lambs, which was most pronounced in the 2d LPS-exposed lambs (**Figure 2**). In UP-exposed lambs, signs of increased inflammation were restricted to increased neutrophil infiltration. UP exposure prior to LPS exposure did

not affect the observed increased expression of IL-6 and IL-8 after treatment with LPS alone.

With regard to immune cell infiltration, the increased number of CD45+ immune cells reported in 2d LPS-exposed animals (**Figure 3A**), was also not affected by prior exposure to UP. Further, single and sequential inflammatory insults did not change the numbers of differentiating macrophages in the pulmonary tissue (**Figure 3B**). In addition, pre-exposure to UP did not significantly affect the increased number of neutrophils observed in the 2d LPS groups (**Figure 3C**). However, UP + 7d LPS showed that neutrophil numbers were attenuated to values similar to baseline levels (**Figures 3D–F**).

Pre-exposure to UP Normalizes SOX-9 Expression, but Does Not Impact Stem/Progenitor Cell Responses, After an Initial Insult With LPS

Reduced numbers of endogenous stem/progenitor cell populations of the proximal airways have been reported after intra-amniotic exposure to LPS (7). Here, after sequential insults with UP and LPS no further reduction in P63+ and KRT-14+ cell numbers, as well as SOX-2 mRNA levels, were observed (**Figure 4**).

In distal airways, UP and 7d LPS exposure alone decreased SOX-9 mRNA significantly (**Figure 5A**), while pre-exposure to UP in 7d LPS-exposed animals prevented a decrease in SOX-9 mRNA levels by a 3-fold increase in its expression. Club cell numbers were decreased in UP, 2d and 7d LPS groups, as well as in the UP + 2d LPS and UP + 7d LPS animals (**Figures 5B,D–F**). The number of AEC2 was significantly decreased in UP-infected animals, as well as in UP + 2d LPS and UP + 7d LPS animals compared to control (**Figures 5C,G–I**). Sequential exposure to UP and LPS did not further affect Club cells. In contrast, the most significant reduction in AEC2 numbers was observed in UP + 7d LPS-exposed animals.

Prenatal Inflammation Affects Vascular Growth and Angiogenesis After Single Insults and UP Pre-exposure Sensitizes Vascular Disturbances to a Second Inflammatory Insult, Resulting in a Lower Vascular Density

Vascular remodeling is a common hallmark of BPD and has been found in models of pre- and postnatal inflammation. Here we assessed if single as well as sequential exposure induce vascular changes in preterm ovine lungs.

Vascular development and angiogenesis were influenced by prenatal inflammation as evidenced by a significant drop in mRNA levels of VEGFa after single exposure to UP or LPS (**Figure 6A**). Pre-exposure to UP similarly decreased mRNA levels of VEGFa in the UP + 2d LPS group, whereas the mRNA levels were normalized to control in the combined UP + 7d LPS group. VEGFR-2 mRNA levels were significantly reduced in 7d LPS and UP + 7d LPS-exposed animals (**Figure 6B**).

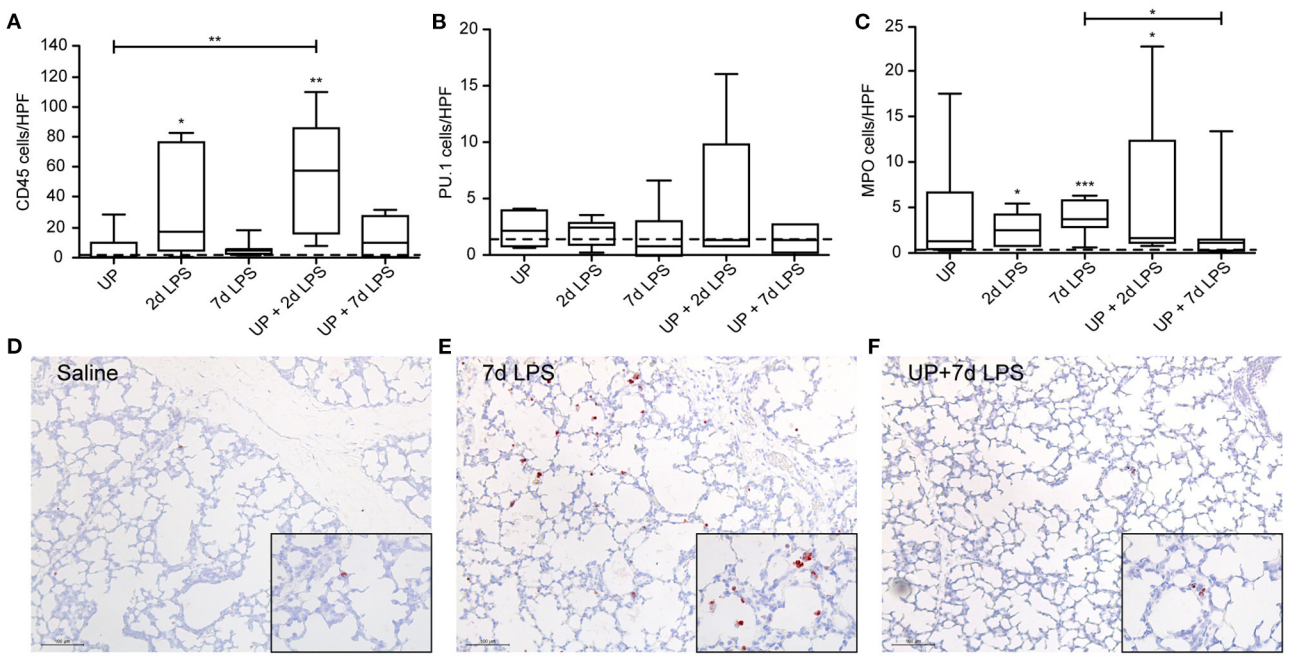

FIGURE 3 | Single and sequential exposure induce immune cell infiltrations in the lung tissue, whereas neutrophil numbers are attenuated after UP + 7d LPS exposure. CD45+ immune cells **(A)**, PU.1+ macrophages **(B)** and MPO+ neutrophils **(C)** were quantified in alveoli and are presented as cells per HPF. The median saline value is represented as dotted line. Representative images are shown for MPO in saline **(D)**, 7d LPS **(E)** and UP + 7d LPS **(F)** groups. Image magnification is 200x, scale bar 100 μm. *$p < 0.05$, **$p < 0.01$, ***$p < 0.001$ compared to saline, UP and 7d LPS.

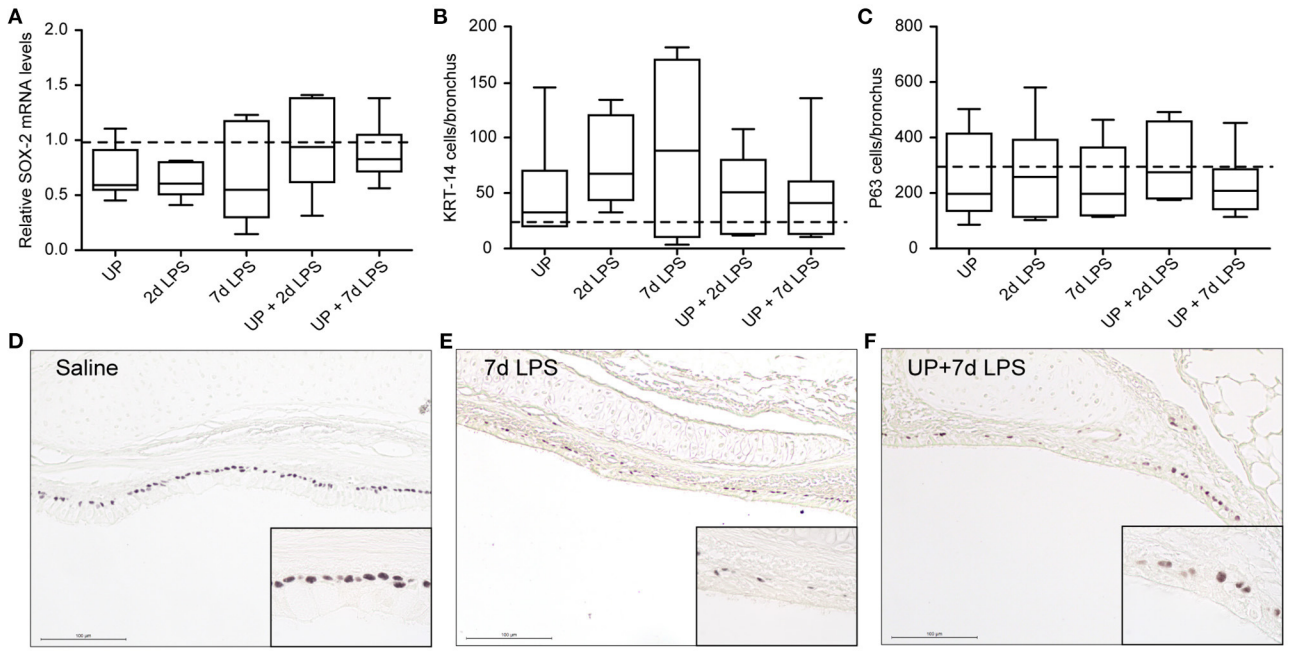

FIGURE 4 | No further changes are observed in basal cells of the proximal airways after single and sequential antenatal inflammation. **(A)** SOX-2 fold changes in mRNA levels are depicted against saline. P63+ **(C)** and KRT-14+ **(B)** basal cells were quantified in proximal airways and are presented as cells per bronchus. The median saline value is represented as dotted line. Representative images are shown for P63 in saline **(D)**, 7d LPS **(E)** and UP + 7d LPS **(F)** groups. Image magnification is 200x, scale bar 100 μm.

Although mRNA levels of VEGFR-2 were unaffected in the 2d LPS group, they were significantly lower in the UP + 2d LPS group compared to control, UP and 2d LPS-exposed animals. Ang-1 mRNA levels were not changed by single exposure to chronic or acute triggers, but showed a significant drop in both sequential exposure groups (**Figure 6C**). Tie-2 mRNA levels were increased in UP and 7d LPS groups and were unaffected after sequential exposure (**Figure 6D**).

These changes on mRNA level of the studied vascular and angiogenic markers prompted us to determine vessel density in the alveolar walls. While UP exposure alone did not alter the density of vessels, 2d LPS exposure decreased the number of vessels significantly by half compared to the control (**Figure 6E**). Pre-exposure to UP before (2 and 7d) LPS attenuated the vascular density even more prominently than LPS exposure alone.

Although changes in vascular and angiogenic markers were detected and the density of vessel reduced after prenatal inflammation, no alterations were measured in the wall-to-lumen ratio of the vessels by single or sequential inflammatory insults (**Figure 6F**).

Developmental Alterations Found in Alveoli Are Most Prominent in UP + 7d LPS Exposed Lambs

Given the AEC2 alterations, we further assessed the alveolar development after sequential antenatal inflammation in terms of proliferation (Ki67) and differentiation (Aqp5) in the alveolar walls (**Figure 7**).

7d LPS and UP + 7d LPS exposure resulted in a significant drop to half of the amount of proliferating cells compared to the control group (**Figure 7A**). AEC1 were significantly decreased by half in the UP + 2d LPS group compared to control levels (**Figure 7B**). Additionally, while 7d LPS exposure decreased Aqp5 mRNA levels, sequential exposure did not result in a significant drop. With regard to the MLI, UP, and LPS exposure alone did not impact alveolar growth, whereas the exposure to UP followed by LPS 7 days before delivery increased the MLI. This result is consistent with the more significant decreased proliferation in the UP + 7d LPS group and the lower number of AEC2 in the same group when compared to single exposure with LPS (**Figure 7C**).

Sequential Exposure to UP and LPS Has Additional Impact on mRNA Levels of Surfactant Proteins Compared to Single Inflammatory Insults, but Does Not Affect Lung Mechanics

As stem/progenitor cell numbers dropped in the distal lung compartments and sensitization of vascular signaling was observed, we further assessed the effects of sequential antenatal insults on functional parameters, including surfactant synthesis and lung mechanics (static lung compliance).

While chronic UP exposure did not alter surfactant mRNA levels, we did see that 2d, 7d LPS groups, as well as pre-exposure with UP + 2d and +7d LPS caused an increase in

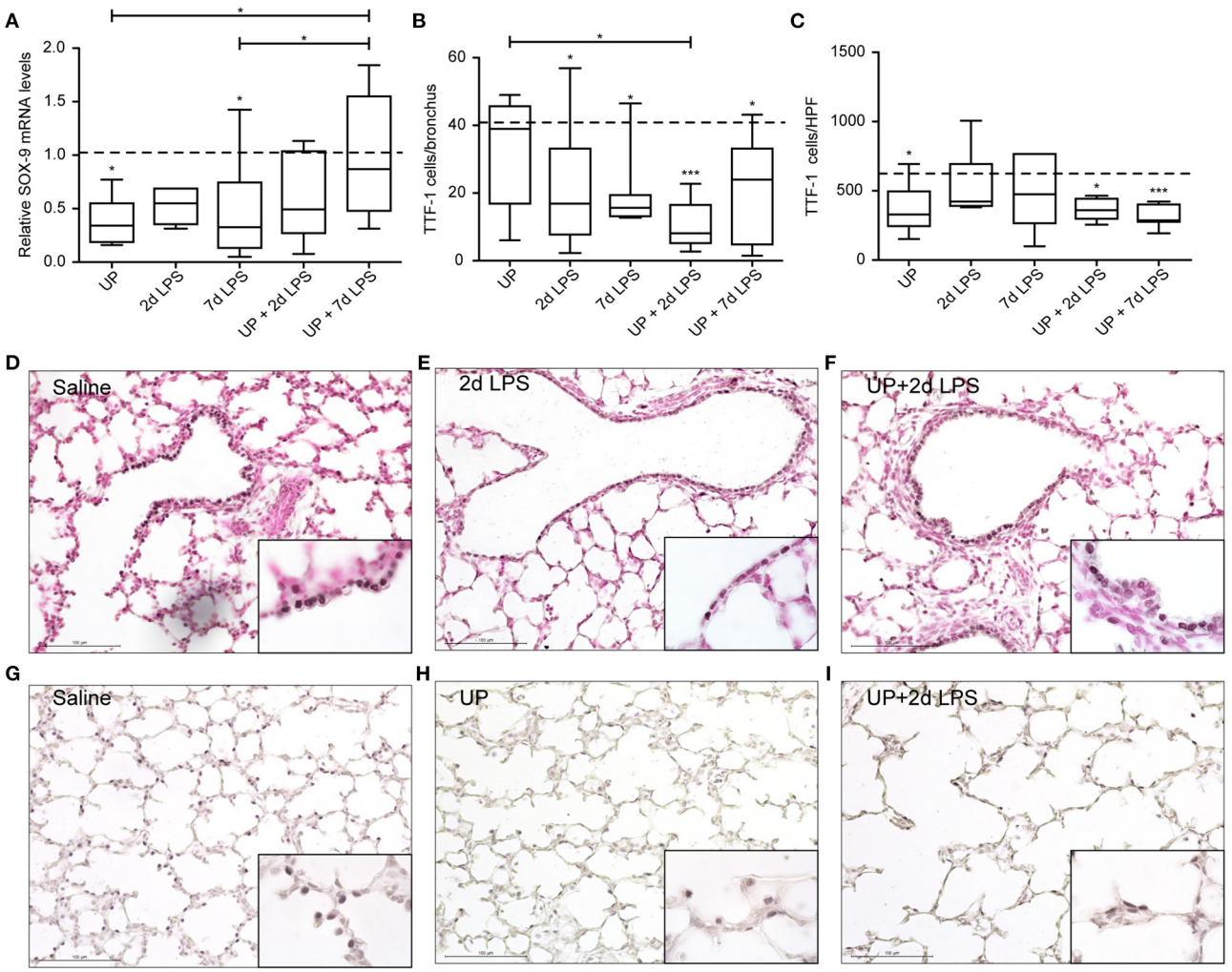

FIGURE 5 | Pre-exposure to UP before the 7d LPS exposure normalizes SOX-9 expression but does not further impact stem/progenitor populations of the distal lung. **(A)** SOX-9 fold changes in mRNA levels are depicted against saline. TTF1+ **(B)** Club cells were quantified in distal airways and presented as cells per bronchus, while TTF-1+ **(C)** AEC2 were counted in alveoli and are presented as cells per HPF. The median saline value is represented as dotted line. Representative images are shown for Club cells in saline **(D)**, 2d LPS **(E)** and UP + 2d LPS **(F)** groups, and for AEC2 in saline **(G)**, UP **(H)** and UP+2d LPS **(I)** animals. Image magnification is 200x, scale bar 100 μm. $*p < 0.05$, $***p < 0.001$ compared to saline, UP and 7d LPS.

mRNA levels of SP-A compared to controls and UP exposure (**Figure 8A**). UP pre-exposure pre-conditioned to 2d and 7d LPS exposure and thereby significantly increased mRNA levels of SP-B, whereas UP, 2d or 7d LPS groups did not result in mRNA changes (**Figure 8B**).

mRNA levels of SP-C were significantly increased in UP + 7d LPS groups, as were mRNA levels for single 7d LPS exposure (**Figure 8C**).

UP + 2d LPS exposure increased mRNA levels for SP-D compared to control and UP alone (**Figure 8D**). In contrast, UP + 7d LPS groups showed normalized SP-D mRNA levels compared to 7d LPS exposure alone.

Lung gas volumes were significantly increased at applied pressures of 0 cmH_2O (data not shown) and 40 cmH_2O in 7d LPS (10-fold) and UP + 7d LPS groups (4-fold) (**Figure 8E**). UP + 2d LPS exposure resulted in significantly lower lung gas volumes compared to UP alone.

DISCUSSION

There is increasing evidence that structural and functional abnormalities of the developing lungs that are provoked during pregnancy by inflammatory triggers, can contribute to postnatal lung pathology (25, 26). However, the mechanisms underlying these antenatal alterations remain largely unknown.

As an essential driver of lung development, endogenous epithelial stem/progenitor cells might play a role in prenatal maldevelopment of the lungs following inflammatory stressors (15, 27). Previously, we demonstrated fewer endogenous stem/progenitor populations as well as potential consequences

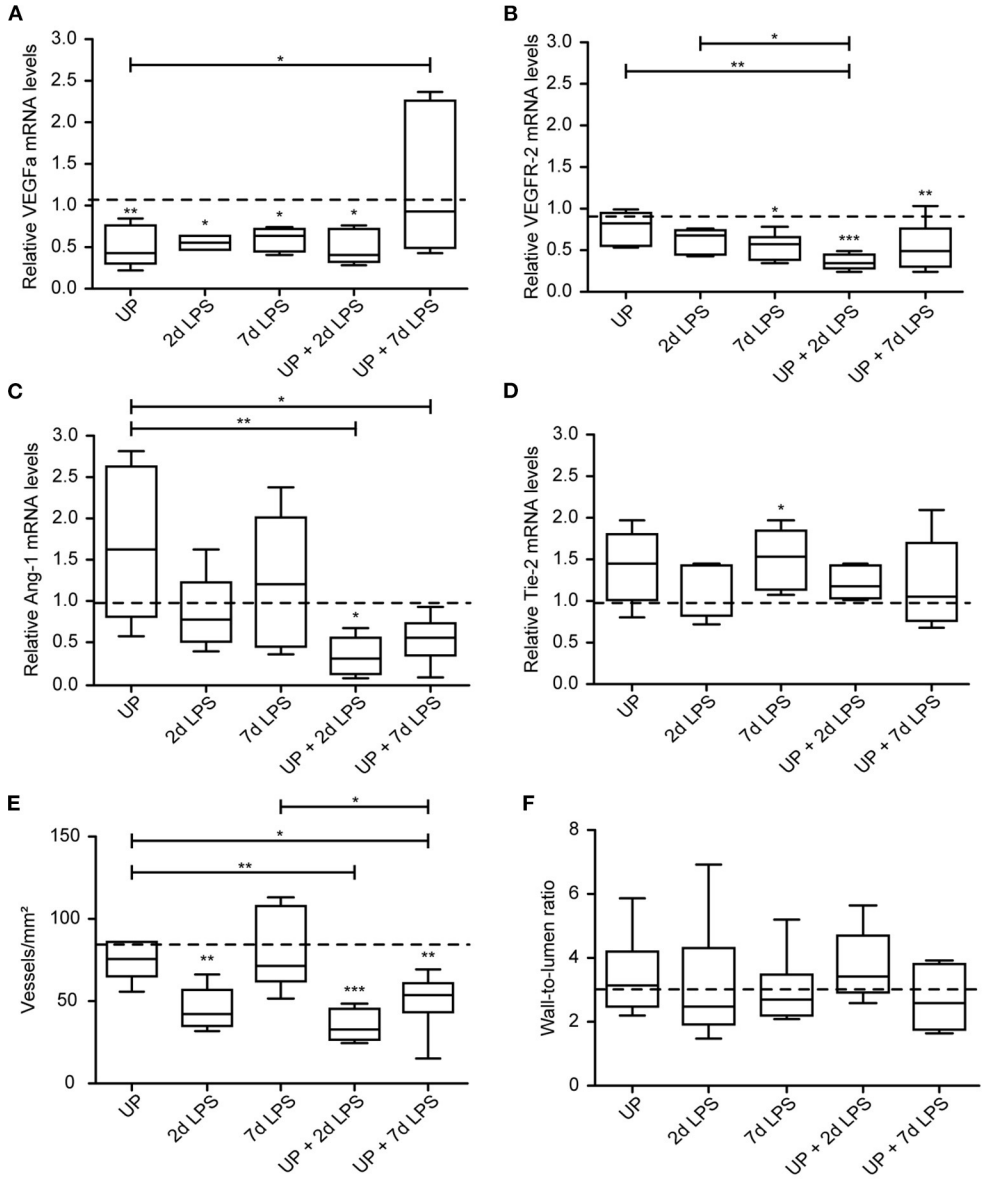

FIGURE 6 | Sequential exposure to UP sensitizes vascular marker VEGFR-2 and Ang-1 to secondary LPS exposure and reduces the vascular density in alveolar tissue. VEGFa **(A)**, VEGFR-2 **(B)**, Ang-1 **(C)** and Tie-2 **(D)** fold changes in mRNA levels are depicted against saline. **(E)** Vascular quantification (for vessels <50 μm diameter) was performed and corrected for surface area of alveolar tissue. **(F)** Wall-to-lumen ratio was measured and calculated from small vessels (<50 μm diameter). The median saline value is represented as dotted line. $^{*}p < 0.05$, $^{**}p < 0.01$, $^{***}p < 0.001$ compared to saline, UP and 2d LPS.

thereof, including reduced alveolar differentiation, in the course of antenatal inflammation. Importantly, distinct stem cell changes in fetal ovine lungs were influenced by the timing and duration of a single chronic or acute inflammatory insult (7).

Clinically, perinatal organ development is frequently affected by multiple and repetitive inflammatory triggers, including infections, hypoxia, sepsis and mechanical ventilation, with serious consequences for the fetus/neonate. Clinical and pre-clinical studies have associated prenatal polymicrobial infections with a diversity of clinical outcomes (28, 29). This diversity in outcomes is difficult to estimate and therefore treatment of preterm infants might start too late to avoid serious postnatal problems. Apart from the microorganisms involved, investigating the effect of multiple inflammatory events during pregnancy is of great importance to understand their influences and impact on prenatal lung development. Prenatal infections, but also different maternal stressors and the event of birth are inevitable incidences that induce inflammation and that the fetus consequently has to cope with (30).

A prerequisite of studying multiple stressors is, to first determine the effects of the single components, which we have reported recently (7). In the current study, we extended our

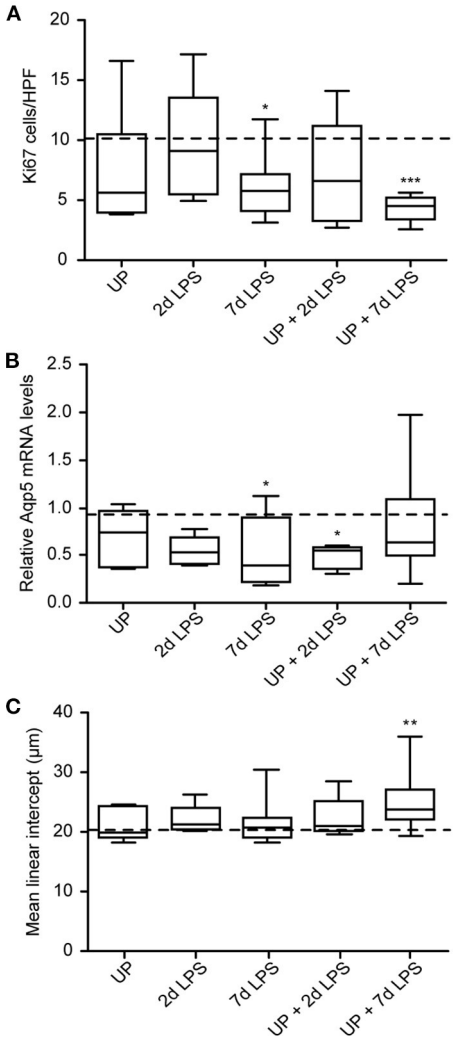

FIGURE 7 | Developmental alveolar alterations are most prominent in UP + 7d LPS exposed lambs. **(A)** Ki67+ cells were quantified in alveoli and shown as cells per HPF. **(B)** Aqp5 fold changes in mRNA levels are depicted against saline. **(C)** The MLI was determined in alveolar tissue and represents the alveolar size in micrometer. The median saline value is represented as dotted line. $^{*}p < 0.05$, $^{**}p < 0.01$, $^{***}p < 0.001$ compared to saline.

previous findings by investigating the effect of multiple sequential insults on important development processes in the preterm lungs and thereby increased the clinical relevance of this pre-clinical model. Moreover, we additionally examined consequences of single and multiple inflammatory events with respect to alveolar morphology and pulmonary vascular development in relation to altered stem/progenitor cell populations, mediators of vascular development and immunological changes.

Our study revealed that the strongest reduction of AEC2 and proliferating cells (Ki67+) was detected in lambs that were sequentially exposed to UP and 7d LPS. In line with this observation, decelerated alveolar growth was exclusively seen in this experimental group, indicated by increased MLI. Importantly, although single exposure to inflammatory stimuli did not result in significant morphological abnormalities, it negatively impacted epithelial stem/progenitor cell populations. These combined findings indicate that single inflammatory hits already negatively affect epithelial stem/progenitor cell populations including their function and numbers, a process that can be further aggravated when sequential inflammatory hits exert their negative effects synergistically. In this study, SOX-9 expression levels in the different experimental groups are of particular interest. SOX-9 expression is restricted to progenitor cells and disappears after proliferation and differentiation into different AEC2 subtypes (31, 32). The acquired single hit exposure data, which showed a reduction of SOX-9 expression in both the UP and LPS group, might potentially be responsible for reduced proliferation and reduced number of TTF-1+ AEC2 in developing alveoli. Of interest, consecutive hits with UP and (7d) LPS prevented a decrease in SOX-9 mRNA, while it caused the most pronounced reduction of TTF-1+ AEC2 and the number of proliferating cells, which was accompanied by an increased MLI. This finding potentially reflects a compensatory function for SOX-9 expression to counteract the reduced number of AEC2 with the pre-exposure to UP. It might be a timing effect that this compensatory function of SOX-9 did not initiate sufficient proliferation and differentiation yet to reverse the reduced number of AEC2. Such protective effects of SOX-9 have previously been observed in an acute lung injury (ALI) model, where SOX-9 was activated in the post-ALI phase and assumed to promote recovery of the damaged lungs (33). This scenario is currently investigated in ongoing postnatal studies. On the other hand, there are multiple transcription factors and developmental pathways involved in the complex process of distal lung development, which themselves potentially attenuated proliferation and growth of alveoli (34, 35). In this study, we also examined the pulmonary vasculature, due to its increasing importance in the development of BPD (36). Sequential inflammatory exposures negatively affected the growth and expansion of pulmonary vessels indicating that UP exposure primarily sensitizes animals that were subsequently exposed to 2d LPS. Consistent with this morphological observation, the pro-angiogenic and vascular factors, Ang-1 and VEGFR-2, were reduced by single inflammatory triggers and pre-exposure to UP sensitized these markers to a secondary insult with LPS. Moreover, VEGFa was decreased in all treatment groups, including this UP + 2d LPS group, which is further indicative for impaired vascularization. These current vascular changes after antenatal stress confirm and extend findings in a previous sequential hit study that was conducted at an earlier gestational age (94d GA in lambs, corresponding to extreme preterm infants in the canalicular stage of lung development) (12). These vascular disturbances, comprising decreased VEGFR-2 and Ang-1 mRNA levels after sequential exposure, seemed not affected by the GA of the fetuses, as comparable results were found in 94d and 125d GA fetuses. In addition, in both studies these disturbances were not associated with vascular remodeling in the preterm lungs (7, 12). Clinically, reduced and dysmorphic capillary networks have been reported in various BPD cohorts (37). Combined, the antenatal angiogenic data point toward a disturbed capillary network, which might be at the origin of postnatal

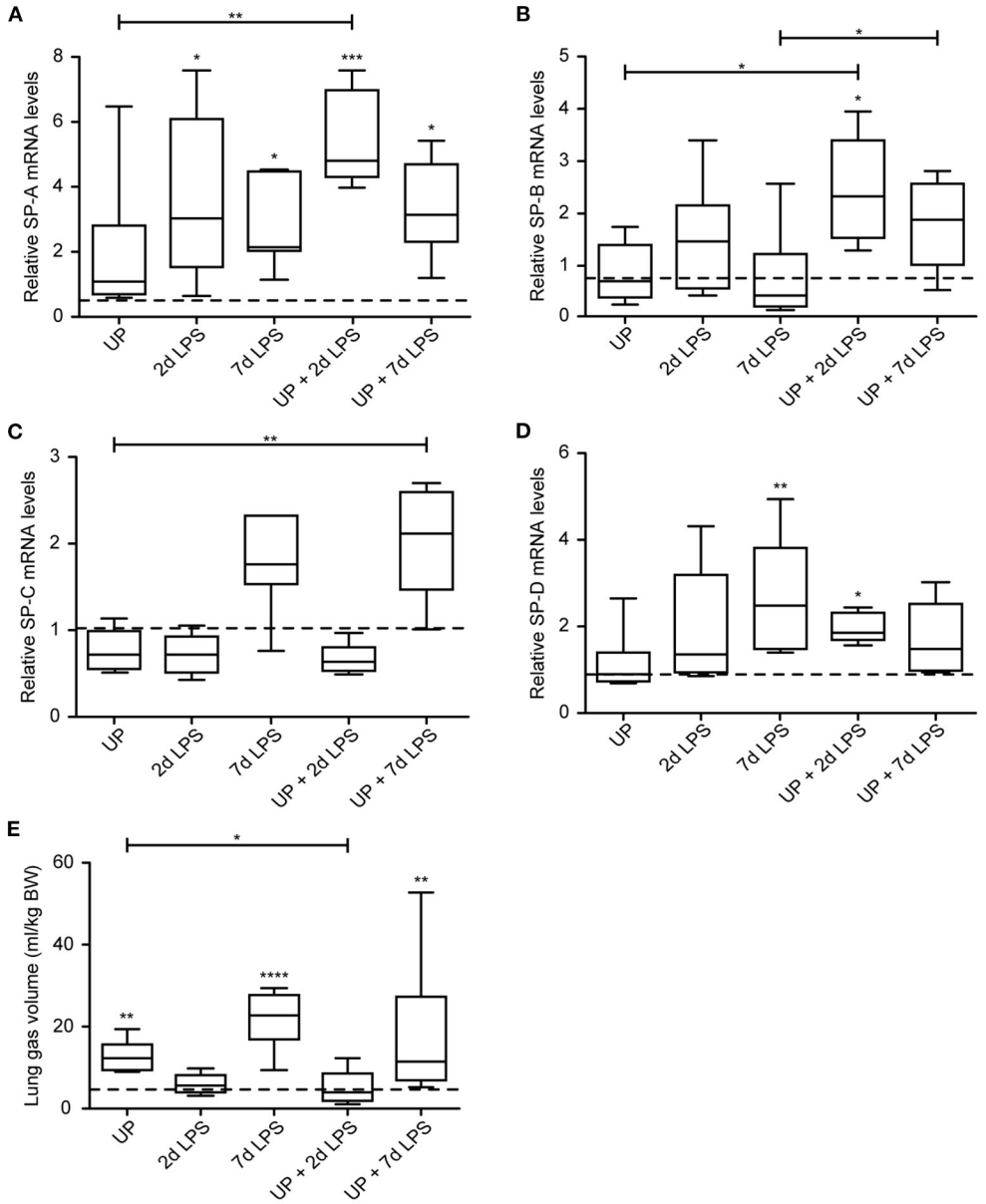

FIGURE 8 | Sequential exposure to UP normalizes SP-B expression after 7d LPS. SP-A **(A)**, SP-B **(B)**, SP-C **(C)** and SP-D **(D)** fold changes in mRNA levels are depicted against saline. **(E)** Lung gas volumes of a pressure of 40 cm H_2O are corrected for the bodyweight of the fetus and shown as ml/kg. The median saline value is represented as dotted line. $^{*}p < 0.05$, $^{**}p < 0.01$, $^{***}p < 0.001$, $^{****}p < 0.0001$ compared to saline, UP and 7d LPS.

adverse vascular development, an aspect that warrants further investigation (36).

In contrast to the attenuated alveolar growth and reduced vasculature, we observed a protective effect of sequential exposure with regard to surfactant synthesis, in particular SP-A and SP-B. Hereby increased SP-A and SP-B expression was found in UP + 2d LPS and UP + 7d LPS exposed animals, respectively, changes that were not as prominent in animals exposed to a single inflammatory trigger.

Our findings on SP-B expression are largely recapitulated by the observed inflammatory changes; Significant inflammatory changes were restricted to the number of neutrophils, which were attenuated in the 7d LPS group when they were pre-exposed to UP. It is tempting to speculate that this immune modulatory effect of UP, which has been described earlier by Kallapur et al. (13), might be involved in the protective effects on SP-B.

The essential role of SP-B in the survival of preterm infants at birth has been emphasized by various clinical studies (38). Chang et al. showed that a deficiency in SP-B through gene polymorphisms increased the risk to develop severe/lethal respiratory distress in preterm neonates (39, 40). Additionally, 75% of preterm infants with need for ventilation have been shown

to have surfactant deficiencies in tracheal aspirates with 80% reduction in SP-B (41, 42). This key role of SP-B is attributed to its important function in the stabilization of the monolayer lipid films of surfactant, as well as in the absorption of lipids to the air/liquid interface (43, 44). Therefore, the increased SP-B mRNA levels, found after sequential insults with UP and LPS, might be an attempt to counteract the inflammation-driven changes, including decreased AEC2 numbers.

Besides this potentially protective effect of SP-B, also the increased expression of SP-A in UP pre-exposed animals (prior to 2d LPS) might indicate a beneficial effect. In the clinical situation and pre-clinical models, a deficiency in SP-A has been associated with an increased risk of BPD development in preterm neonates (24–29 week of GA) and immature baboons that received ventilation (45, 46). Additionally a reduced amount of SP-A mRNA has been reported in premature baboons with a BPD phenotype (47). These findings reveal a strong association between reduced SP-A proteins and BPD development. Through its important role in lung host defense, SP-A has been shown *in vitro* to promote increased ureaplasmacidal phagocytosis of UP isolates (from the BAL of premature infants with BPD) by murine macrophages (RAW 264.7) (48). Moreover, in *in vivo* studies, SP-A deficient mouse strains have been shown to display more excessive pulmonary inflammation after intra-tracheal UP administration compared to wild type controls. In these deficient SP-A mice also the clearance of UP occurred at a later time point (49). Taken together, the increased expression of SP-A after sequential exposure of UP and LPS could be interpreted as a means to eliminate UP from the preterm lungs.

Interestingly, these combined changes of increased SP-B and SP-A expression that suggest a protective effect by prior UP infection, did not overlap with improved lung function that was found to be significant in UP, 7d LPS, and UP + 7d LPS-exposed lambs. Moreover, this improved lung function was paralleled at the studied time points by detrimental alterations of stem/progenitor cells. This apparent lack of uniformity might be caused by a timing effect, but it most likely provides supporting evidence for the concept that perinatal inflammation improves lung function at the expense of inducing peripheral lung abnormalities, including decreased number of large and simplified alveoli, and abnormal pulmonary vascular development, predisposing to adverse postnatal pulmonary outcomes.

Besides the effects of consecutive inflammatory insults on lung development, also other immature organ systems are affected. The impact of multiple insults has been investigated in the preterm brain and gastrointestinal system. In particular, inflammation in the brain was less pronounced in LPS-exposed lambs when they were pre-exposed to UP. Additionally, the protective effect of UP was associated with reduced epigenetic changes (10). Sequential exposure of UP and LPS *in utero* did not amplify injury in the gastrointestinal and the enteric nervous system, that was caused by single exposure to UP or LPS (11). Taken together, these studies reflect the diversity in organ responses and outcomes after exposure to different infectious triggers (50). Additionally, also timing and duration of antenatal inflammatory triggers play a crucial role in the susceptibility of other organs and cells. Close monitoring of antenatal infection and inflammation is necessary for optimal risk classification of postnatal organ outcomes (10).

Regardless, these observed *in utero* alterations in essential cell populations, developmental factors and pulmonary morphology might render the preterm lungs more susceptible to sequential postnatal insults. Previously, it was shown that postnatal hits, including mechanical ventilation and oxygen supplementation, resulted in a decreased differentiation and proliferation potential in isolated lung endogenous stem cells (51). Postnatal cohort studies, using BPD and RDS samples, have also shown that preterm birth combined with common clinical practices, like oxygen supplementation and ventilation, resulted in decreased AEC2 and Club cell numbers, positive for TTF-1 (52, 53). Similarly, vascular abnormalities are a key hallmark of BPD and have been shown to be driven by perinatal insults (14, 36, 37). In a hyperoxia-induced BPD rat model, a lower capillary density was associated with reduced expression of VEGF and VEGFR-2 (54). Reduced and disorganized capillary development has further been reported in baboon models for BPD after interventional series of ventilation and supplemental oxygen (55).

The ovine pre-clinical model, which resembles the human *in utero* situation very closely, enables investigation of developmental disturbances in a prenatal inflammatory setting. The relatively long gestation of sheep, in which developmental stages occur similar as in humans, enables the precise interference in these stages (18, 19). In addition, microbial exposure can be exactly timed and thereby clinical inflammatory settings (chronic and acute) can be mimicked accurately. Another benefit of this study was the use of clinically relevant microorganisms, such as UP. Although LPS is not a living microorganism and specific microorganism-related responses might be missed, this *Escherichia coli*-derived endotoxin is a potent inducer of inflammation and therefore used to mimic clinical situations of acute inflammation. LPS responses are well-defined and accordingly less heterogenicity in responses is detected (56, 57).

Besides the advantages of the model and study, there are also some limitations. In the current study epithelial stem/progenitor populations have been investigated with the use of basic stem cells markers (P63, KRT-14, and TTF-1). However, the observed disturbances might be unique and restricted to a specific subpopulation. Additional examination with more extended techniques, such as cell sorting by FACS and single cell sequencing, would be informative to better define and understand the response of such subpopulations of stem/progenitor cells in the context of prenatal inflammation. Furthermore, considering the observed disturbances in vascular modulators, future investigations should include examination of endothelial stem/progenitor cell alterations. Moreover, fixed time points of intra-amniotic exposure to Ureaplasma or LPS were used, which did not enable us to dissect the effects of prenatal inflammation on extremely, moderate and late preterm organs. Importantly, the postnatal consequences of the observed *in utero* stem/progenitor

cell changes are currently addressed in a postnatal follow up study.

Consistent with previous findings from our group and others, endogenous epithelial stem/progenitor cell populations are attenuated by perinatal inflammatory triggers (7, 58). Additionally, single inflammatory hits during pregnancy are also known to impair vascular growth (59). In the current study, we extended these findings by investigating the effects of sequential antenatal insults on alveolar growth and vascular maturation. We showed that exposure to a single inflammatory trigger already negatively impacts epithelial stem/progenitor cell populations including their function and numbers. This process was further aggravated by re-exposure to an inflammatory stimulus, resulting in disturbed alveolarization and abnormal pulmonary vascular development. The question whether these negative effects on lung development can be rescued by the potentially protective responses observed, will be addressed in an ongoing postnatal study.

Collectively, our data indicate that the type, timing and duration of antenatal stress determine the pulmonary outcome during pregnancy in the context of antenatal infections. Importantly, responses within the lungs can vary between lung compartment and cell types. Unraveling and linking the impact of antenatal and postnatal insults on the preterm lungs is of great importance to expand our understanding of the complex and multifactorial nature of BPD.

DATA AVAILABILITY STATEMENT

The original contributions generated for this study are included in the article/supplementary material, further inquiries can be directed to the corresponding author/s.

ETHICS STATEMENT

The animal study was reviewed and approved by the animal ethics committee of the University of Western Australia.

AUTHOR CONTRIBUTIONS

HW, NR, and TW conceived and designed the research questions. MK, JN, MS, HU, MP, AJ, and BK designed and performed the *in vivo* study. HW conducted experiments, acquired and analyzed data. HW, NR, BK, TD, and TW contributed to the interpretation of results and drafted the manuscript. HW, NR, DO, MH, PN, CS-R, BK, TD, and TW edited and revised the manuscript. HW, NR, DO, MH, PN, CS-R, JC, MK, JN, MS, HU, MP, AJ, BK, TD, and TW read and approved final version of manuscript. All authors contributed to the article and approved the submitted version.

FUNDING

This work was supported by a National Institutes of Health (Bethesda, MD, USA) grant (HD 57869) and by the Dutch Lung Foundation (Longfonds, Grant no. 6.1.16.088 TW, NR, and PN).

ACKNOWLEDGMENTS

We thank Nico Kloosterboer, Lilian Kessels, Kimberly Massy and Anaïs van Leeuwen for their excellent technical assistance.

SUPPLEMENTARY MATERIAL

The Supplementary Material for this article can be found online at: https://www.frontiersin.org/articles/10.3389/fmed.2021.614239/full#supplementary-material

REFERENCES

1. Malleske DT, Chorna O, Maitre NL. Pulmonary sequelae and functional limitations in children and adults with bronchopulmonary dysplasia. *Paediatr Respir Rev.* (2018) 26:55–9. doi: 10.1016/j.prrv.2017.07.002
2. Kallapur SG, Jobe AH. Perinatal events and their influence on lung development and injury. In: *The Newborn Lung*. Elsevier (2019). p. 31–64. doi: 10.1016/B978-0-323-54605-8.00002-7
3. Jobe AH. The new bronchopulmonary dysplasia. *Curr Opin Pediatr.* (2011) 23:167–72. doi: 10.1097/MOP.0b013e3283423e6b
4. Yee M, Domm W, Gelein R, Bentley KL, Kottmann RM, Sime PJ, et al. Alternative progenitor lineages regenerate the adult lung depleted of alveolar epithelial type 2 cells. *Am J Respir Cell Mol Biol.* (2017) 56:453–64. doi: 10.1165/rcmb.2016-0150OC
5. Mandell EW, Abman SH. Fetal vascular origins of bronchopulmonary dysplasia. *J Pediatr.* (2017) 185:7–10 e11. doi: 10.1016/j.jpeds.2017.03.024
6. Taglauer E, Abman SH, Keller RL. Recent advances in antenatal factors predisposing to bronchopulmonary dysplasia. *Semin Perinatol.* (2018) 42:413–24. doi: 10.1053/j.semperi.2018.09.002
7. Widowski H, Ophelders D, van Leeuwen A, Nikkels PGJ, Severens-Rijvers CAH, LaPointe VLS, et al. Chorioamnionitis induces changes in ovine pulmonary endogenous epithelial stem/progenitor cells in utero. *Pediatr Res.* (2020) 1–11. doi: 10.1038/s41390-020-01204-9
8. Yoon BH, Romero R, Lim JH, Shim SS, Hong JS, Shim JY, et al. The clinical significance of detecting Ureaplasma urealyticum by the polymerase chain reaction in the amniotic fluid of patients with preterm labor. *Am J Obstet Gynecol.* (2003) 189:919–24. doi: 10.1067/S0002-9378(03)00839-1
9. Kallapur SG, Presicce P, Rueda CM, Jobe AH, Chougnet CA. Fetal immune response to chorioamnionitis. *Semin Reprod Med.* (2014) 32:56–67. doi: 10.1055/s-0033-1361823
10. Gussenhoven R, Ophelders D, Kemp MW, Payne MS, Spiller OB, Beeton ML, et al. The paradoxical effects of chronic intra-amniotic *Ureaplasma parvum* exposure on ovine fetal brain development. *Dev Neurosci.* (2017) 39:472–86. doi: 10.1159/000479021
11. Heymans C, de Lange IH, Hutten MC, Lenaerts K, de Ruijter NJE, Kessels L, et al. Chronic intra-uterine *Ureaplasma parvum* infection induces injury of the enteric nervous system in ovine fetuses. *Front Immunol.* (2020) 11:189. doi: 10.3389/fimmu.2020.00189
12. Willems MG, Kemp MW, Fast LA, Wagemaker NM, Janssen LE, Newnham JP, et al. Pulmonary vascular changes in extremely preterm sheep after intra-amniotic exposure to *Ureaplasma parvum* and lipopolysaccharide. *PLoS ONE.* (2017) 12:e0180114. doi: 10.1371/journal.pone.0180114
13. Kallapur SG, Kramer BW, Knox CL, Berry CA, Collins JJ, Kemp MW, et al. Chronic fetal exposure to *Ureaplasma parvum* suppresses innate immune responses in sheep. *J Immunol.* (2011) 187:2688–95. doi: 10.4049/jimmunol.1100779

14. Alvira CM. Aberrant pulmonary vascular growth and remodeling in bronchopulmonary dysplasia. *Front Med (Lausanne).* (2016) 3:21. doi: 10.3389/fmed.2016.00021
15. Collins JJ, Thébaud BJBDRPAC, Teratology M. Progenitor cells of the distal lung and their potential role in neonatal lung disease. *Birth Defects Res A Clin Mol Teratol.* (2014) 100:217–26. doi: 10.1002/bdra.23227
16. Collins JJ, Kuypers E, Nitsos I, Jane Pillow J, Polglase GR, Kemp MW, et al. LPS-induced chorioamnionitis and antenatal corticosteroids modulate Shh signaling in the ovine fetal lung. *Am J Physiol Lung Cell Mol Physiol.* (2012) 303:L778–87. doi: 10.1152/ajplung.00280.2011
17. Willems MG, Ophelders DR, Nikiforou M, Jellema RK, Butz A, Delhaas T, et al. Systemic interleukin-2 administration improves lung function and modulates chorioamnionitis-induced pulmonary inflammation in the ovine fetus. *Am J Physiol Lung Cell Mol Physiol.* (2016) 310:L1–7. doi: 10.1152/ajplung.00289.2015
18. Pringle KC. Human fetal lung development and related animal models. *Clin Obstet Gynecol.* (1986) 29:502–13. doi: 10.1097/00003081-198609000-00006
19. Kramer BW. Chorioamnionitis - new ideas from experimental models. *Neonatology.* (2011) 99:320–5. doi: 10.1159/000326620
20. Jobe AH, Newnham JP, Willet KE, Moss TJ, Gore Ervin M, Padbury JF, et al. Endotoxin-induced lung maturation in preterm lambs is not mediated by cortisol. *Am J Respir Crit Care Med.* (2000) 162:1656–61. doi: 10.1164/ajrccm.162.5.2003044
21. Kuypers E, Collins JJ, Kramer BW, Ofman G, Nitsos I, Pillow JJ, et al. Intra-amniotic LPS and antenatal betamethasone: inflammation and maturation in preterm lamb lungs. *Am J Physiol Lung Cell Mol Physiol.* (2012) 302:L380–9. doi: 10.1152/ajplung.00338.2011
22. Tschanz SA, Makanya AN, Haenni B, Burri PH. Effects of neonatal high-dose short-term glucocorticoid treatment on the lung: a morphologic and morphometric study in the rat. *Pediatr Res.* (2003) 53:72–80. doi: 10.1203/00006450-200301000-00014
23. Moreira A, Winter C, Joy J, Winter L, Jones M, Noronha M, et al. Intranasal delivery of human umbilical cord Wharton's jelly mesenchymal stromal cells restores lung alveolarization and vascularization in experimental bronchopulmonary dysplasia. *Stem Cells Transl Med.* (2020) 9:221–34. doi: 10.1002/sctm.18-0273
24. Atik A, Sozo F, Orgeig S, Suri L, Hanita T, Harding R, et al. Long-term pulmonary effects of intrauterine exposure to endotoxin following preterm birth in sheep. *Reprod Sci.* (2012) 19:1352–64. doi: 10.1177/1933719112450327
25. Gras-Le Guen C, Denis C, Franco-Montoya M-L, Jarry A, Delacourt C, Potel G, et al. Antenatal infection in the rabbit impairs post-natal growth and lung alveolarisation. *Eur Respir J.* (2008) 32:1520–8. doi: 10.1183/09031936.00023708
26. Kramer BW, Kallapur S, Newnham J, Jobe AH. Prenatal inflammation and lung development. *Semin Fetal Neonatal Med.* (2009) 14:2–7. doi: 10.1016/j.siny.2008.08.011
27. Leibel S, Post M. Endogenous and exogenous stem/progenitor cells in the lung and their role in the pathogenesis and treatment of pediatric lung disease. *Front Pediatr.* (2016) 4:36. doi: 10.3389/fped.2016.00036
28. Pammi M, Zhong D, Johnson Y, Revell P, Versalovic J. Polymicrobial bloodstream infections in the neonatal intensive care unit are associated with increased mortality: a case-control study. *BMC Infect Dis.* (2014) 14:390. doi: 10.1186/1471-2334-14-390
29. Yoneda N, Yoneda S, Niimi H, Ueno T, Hayashi S, Ito M, et al. Polymicrobial amniotic fluid infection with mycoplasma/ureaplasma and other bacteria induces severe intra-amniotic inflammation associated with poor perinatal prognosis in preterm labor. *Am J Reprod Immunol.* (2016) 75:112–25. doi: 10.1111/aji.12456
30. Mulder EJ, Robles de Medina PG, Huizink AC, Van den Bergh BR, Buitelaar JK, Visser GH. Prenatal maternal stress: effects on pregnancy and the (unborn) child. *Early Hum Dev.* (2002) 70:3–14. doi: 10.1016/S0378-3782(02)00075-0
31. Herriges M, Morrisey EE. Lung development: orchestrating the generation and regeneration of a complex organ. *Development.* (2014) 141:502–13. doi: 10.1242/dev.098186
32. Frank DB, Penkala IJ, Zepp JA, Sivakumar A, Linares-Saldana R, Zacharias WJ, et al. Early lineage specification defines alveolar epithelial ontogeny in the murine lung. *Proc Natl Acad Sci U S A.* (2019) 116:4362–71. doi: 10.1073/pnas.1813952116
33. Li L, Zhang H, Min D, Zhang R, Wu J, Qu H, et al. Sox9 activation is essential for the recovery of lung function after acute lung injury. *Cell Physiol Biochem.* (2015) 37:1113–22. doi: 10.1159/000430236
34. Okubo T, Knoepfler PS, Eisenman RN, Hogan BL. Nmyc plays an essential role during lung development as a dosage-sensitive regulator of progenitor cell proliferation and differentiation. *Development.* (2005) 132:1363–74. doi: 10.1242/dev.01678
35. Rawlins EL, Clark CP, Xue Y, Hogan BL. The Id2+ distal tip lung epithelium contains individual multipotent embryonic progenitor cells. *Development.* (2009) 136:3741–5. doi: 10.1242/dev.037317
36. Thebaud B, Abman SH. Bronchopulmonary dysplasia: where have all the vessels gone? Roles of angiogenic growth factors in chronic lung disease. *Am J Respir Crit Care Med.* (2007) 175:978–85. doi: 10.1164/rccm.200611-1660PP
37. Bhatt AJ, Pryhuber GS, Huyck H, Watkins RH, Metlay LA, Maniscalco WM. Disrupted pulmonary vasculature and decreased vascular endothelial growth factor, Flt-1, and TIE-2 in human infants dying with bronchopulmonary dysplasia. *Am J Respir Crit Care Med.* (2001) 164:1971–80. doi: 10.1164/ajrccm.164.10.2101140
38. Fehrholz M, Hutten M, Kramer BW, Speer CP, Kunzmann S. Amplification of steroid-mediated SP-B expression by physiological levels of caffeine. *Am J Physiol Lung Cell Mol Physiol.* (2014) 306:L101–9. doi: 10.1152/ajplung.00257.2013
39. Nogee LM, Garnier G, Dietz HC, Singer L, Murphy AM, deMello DE, et al. A mutation in the surfactant protein B gene responsible for fatal neonatal respiratory disease in multiple kindreds. *J Clin Invest.* (1994) 93:1860–3. doi: 10.1172/JCI117173
40. Chang HY, Li F, Li FS, Zheng CZ, Lei YZ, Wang J. Genetic polymorphisms of SP-A, SP-B, and SP-D and risk of respiratory distress syndrome in preterm neonates. *Med Sci Monit.* (2016) 22:5091–100. doi: 10.12659/MSM.898553
41. Merrill JD, Ballard RA, Cnaan A, Hibbs AM, Godinez RI, Godinez MH, et al. Dysfunction of pulmonary surfactant in chronically ventilated premature infants. *Pediatr Res.* (2004) 56:918–26. doi: 10.1203/01.PDR.0000145565.45490.D9
42. Ballard PL, Keller RL, Truog WE, Chapin C, Horneman H, Segal MR, et al. Surfactant status and respiratory outcome in premature infants receiving late surfactant treatment. *Pediatr Res.* (2019) 85:305–11. doi: 10.1038/s41390-018-0144-3
43. Veldhuizen EJ, Haagsman HP. Role of pulmonary surfactant components in surface film formation and dynamics. *Biochim Biophys Acta.* (2000) 1467:255–70. doi: 10.1016/S0005-2736(00)00256-X
44. Nkadi PO, Merritt TA, Pillers DA. An overview of pulmonary surfactant in the neonate: genetics, metabolism, and the role of surfactant in health and disease. *Mol Genet Metab.* (2009) 97:95–101. doi: 10.1016/j.ymgme.2009.01.015
45. Hallman M, Merritt TA, Akino T, Bry K. Surfactant protein A, phosphatidylcholine, and surfactant inhibitors in epithelial lining fluid. Correlation with surface activity, severity of respiratory distress syndrome, and outcome in small premature infants. *Am Rev Respir Dis.* (1991) 144:1376–84. doi: 10.1164/ajrccm/144.6.1376
46. Awasthi S, Coalson JJ, Crouch E, Yang F, King RJ. Surfactant proteins A and D in premature baboons with chronic lung injury (Bronchopulmonary dysplasia). Evidence for an inhibition of secretion. *Am J Respir Crit Care Med.* (1999) 160:942–9. doi: 10.1164/ajrccm.160.3.9806061
47. Coalson JJ, King RJ, Yang F, Winter V, Whitsett JA, Delemos RA, et al. SP-A deficiency in primate model of bronchopulmonary dysplasia with infection. *In situ* mRNA and immunostains. *Am J Respir Crit Care Med.* (1995) 151:854–66. doi: 10.1164/ajrccm/151.3_Pt_1.854
48. Okogbule-Wonodi AC, Chesko KL, Famuyide ME, Viscardi RM. Surfactant protein-A enhances ureaplasmacidal activity *in vitro*. *Innate Immun.* (2011) 17:145–51. doi: 10.1177/1753425909360552
49. Famuyide ME, Hasday JD, Carter HC, Chesko KL, He JR, Viscardi RM. Surfactant protein-A limits Ureaplasma-mediated lung inflammation in a murine pneumonia model. *Pediatr Res.* (2009) 66:162–7. doi: 10.1203/PDR.0b013e3181aabd66
50. Gantert M, Been JV, Gavilanes AW, Garnier Y, Zimmermann LJ, Kramer BW. Chorioamnionitis: a multiorgan disease of the fetus? *J Perinatol.* (2010) 30:S21–30. doi: 10.1038/jp.2010.96
51. Moreira AG, Siddiqui SK, Macias R, Johnson-Pais TL, Wilson D, Gelfond JAL, et al. Oxygen and mechanical ventilation impede the functional properties

of resident lung mesenchymal stromal cells. *PLoS ONE.* (2020) 15:e0229521. doi: 10.1371/journal.pone.0229521
52. Stahlman MT, Gray ME, Whitsett JA. Expression of thyroid transcription factor-1 (TTF-1) in fetal and neonatal human lung. *J Histochem Cytochem.* (1996) 44:673–8. doi: 10.1177/44.7.8675988
53. Das I, Das RN, Paul B, Mandal B, Mukherjee S, Chatterjee U. A study of spectrum of pulmonary pathology and expression of thyroid transcription factor-1 during neonatal period. *Indian J Pathol Microbiol.* (2018) 61:334. doi: 10.4103/IJPM.IJPM_650_17
54. Thebaud B, Ladha F, Michelakis ED, Sawicka M, Thurston G, Eaton F, et al. Vascular endothelial growth factor gene therapy increases survival, promotes lung angiogenesis, and prevents alveolar damage in hyperoxia-induced lung injury: evidence that angiogenesis participates in alveolarization. *Circulation.* (2005) 112:2477–86. doi: 10.1161/CIRCULATIONAHA.105.541524
55. Coalson JJ, Winter VT, Siler-Khodr T, Yoder BA. Neonatal chronic lung disease in extremely immature baboons. *Am J Respir Crit Care Med.* (1999) 160:1333–46. doi: 10.1164/ajrccm.160.4.9810071
56. Raetz CR, Whitfield C. Lipopolysaccharide endotoxins. *Annu Rev Biochem.* (2002) 71:635–700. doi: 10.1146/annurev.biochem.71.110601.135414
57. Gilman-Sachs A, Dambaeva S, Salazar Garcia MD, Hussein Y, Kwak-Kim J, Beaman K. Inflammation induced preterm labor and birth. *J Reprod Immunol.* (2018) 129:53–8. doi: 10.1016/j.jri.2018.06.029
58. Möbius MA, Thébaud BJC. Bronchopulmonary dysplasia: where have all the stem cells gone?: origin and (potential) function of resident lung stem cells. *Chest.* (2017) 152:1043–52. doi: 10.1016/j.chest.2017.04.173
59. Kallapur SG, Bachurski CJ, Le Cras TD, Joshi SN, Ikegami M, Jobe AH. Vascular changes after intra-amniotic endotoxin in preterm lamb lungs. *Am J Physiol Lung Cell Mol Physiol.* (2004) 287:L1178–85. doi: 10.1152/ajplung.00049.2004

Conflict of Interest: The authors declare that the research was conducted in the absence of any commercial or financial relationships that could be construed as a potential conflict of interest.

Copyright © 2021 Widowski, Reynaert, Ophelders, Hütten, Nikkels, Severens-Rijvers, Cleutjens, Kemp, Newnham, Saito, Usuda, Payne, Jobe, Kramer, Delhaas and Wolfs. This is an open-access article distributed under the terms of the Creative Commons Attribution License (CC BY). The use, distribution or reproduction in other forums is permitted, provided the original author(s) and the copyright owner(s) are credited and that the original publication in this journal is cited, in accordance with accepted academic practice. No use, distribution or reproduction is permitted which does not comply with these terms.

frontiers in Medicine

BRIEF RESEARCH REPORT
published: 11 March 2021
doi: 10.3389/fmed.2021.642577

Opposing Effects of TGFβ and BMP in the Pulmonary Vasculature in Congenital Diaphragmatic Hernia

*Daphne S. Mous[1], Marjon J. Buscop-van Kempen[1,2], Rene M. H. Wijnen[1], Dick Tibboel[1], Rory E. Morty[3,4] and Robbert J. Rottier[1,2]**

[1] Department of Pediatric Surgery, Erasmus Medical Center – Sophia Children's Hospital, Rotterdam, Netherlands, [2] Department of Cell Biology, Erasmus Medical Center, Rotterdam, Netherlands, [3] Department of Lung Development and Remodelling, Max Planck Institute for Heart and Lung Research, Bad Nauheim, Germany, [4] Department of Internal Medicine (Pulmonology), University of Giessen and Marburg Lung Center (UGMLC), Giessen, Germany

Background: Pulmonary hypertension is the major cause of morbidity and mortality in congenital diaphragmatic hernia (CDH). Mutations in several genes that encode signaling molecules of the transforming growth factor β (TGFβ) and bone morphogenetic protein (BMP) pathways have previously been associated with CDH. Since studies on the activation of these pathways in CDH are scarce, and have yielded inconsistent conclusions, the downstream activity of both pathways was assessed in the nitrofen-CDH rat model.

Methods and Results: Pregnant Sprague-Dawley rats were treated with nitrofen at embryonic day (E) 9.5 to induce CDH in offspring. At E21, lungs were screened for the expression of key factors of both signaling pathways, at both the mRNA transcript and protein levels. Subsequently, paying particular attention to the pulmonary vasculature, increased phosphorylation of SMAD2, and decreased phosphorylation of Smad5 was noted in the muscular walls of small pulmonary vessels, by immunohistochemistry. This was accompanied by increased proliferation of constituent cells of the smooth muscle layer of these vessels.

Conclusions: Increased activation of the TGFβ pathway and decreased activation of the BMP pathway in the pulmonary vasculature of rats with experimentally-induced CDH, suggesting that the deregulated of these important signaling pathways may underlie the development of pulmonary hypertension in CDH.

Keywords: lung, vasculature, BMP, TGF, congenital diagraphma hernia

OPEN ACCESS

Edited by:
Mandy Laube,
Leipzig University, Germany

Reviewed by:
Jan-Hendrik Gosemann,
Hannover Medical School, Germany
Florian Friedmacher,
University Hospital Frankfurt, Germany

***Correspondence:**
Robbert J. Rottier
r.rottier@erasmusmc.nl

Specialty section:
This article was submitted to Pulmonary Medicine, a section of the journal Frontiers in Medicine

Received: *16 December 2020*
Accepted: *22 February 2021*
Published: *11 March 2021*

Citation:
Mous DS, Buscop-van Kempen MJ, Wijnen RMH, Tibboel D, Morty RE and Rottier RJ (2021) Opposing Effects of TGFβ and BMP in the Pulmonary Vasculature in Congenital Diaphragmatic Hernia. Front. Med. 8:642577. doi: 10.3389/fmed.2021.642577

INTRODUCTION

Congenital diaphragmatic hernia (CDH) is a severe developmental anomaly characterized by a diaphragmatic defect. The concomitant pulmonary hypertension (PH) that develops in affected lungs can cause severe problems in the newborn, and is responsible for the high morbidity and mortality in these patients. Although the muscularization of the pulmonary vessels has been demonstrated to be increased in CDH (1), the pathophysiological basis of PH in these patients remains largely unclarified. Mutations in different genes involved in the transforming

growth factor β (TGFβ) and bone morphogenetic protein (BMP) pathways have been described in both adult and pediatric patients with familial, heritable, and idiopathic pulmonary arterial hypertension (PAH). Of these genes, the BMP receptor 2 (BMPR2) is most commonly affected (2).

TGFβ is a negative regulator of airway branching in early lung development. However, TGFβ signaling is also active in the vascular and airway smooth muscle and alveolar and airway epithelium during late lung development. Both up- and down-regulation of TGFβ signaling impairs the alveolarization process (3, 4), depending on the period of study during gestation. Both TGFβ and BMP are documented to influence the proliferation of endothelial and smooth muscle cells, and control apoptosis and extracellular matrix secretion and deposition (5).

Studies on the TGFβ pathway in CDH have not yielded consistent conclusions. Decreased expression of TGFβ1 was found at the mRNA level in the hearts of the nitrofen-exposed rat pups with CDH (6), where increased expression of TGFβ1 in affected lungs was evident by immunohistochemistry (7). In contrast, other studies have reported no perturbations to TGFβ expression and activity—assessed by the phosphorylation of SMAD2/3—in both human samples as well as tissues harvested from the nitrofen-CDH rat model (8). A study performed in pregnant women carrying CDH fetuses revealed decreased TGFβ levels in the amniotic fluid, but no differences in expression of TGFβ in the lungs of these children after birth (9). The expression of both TGFβ receptor (TGFBR) 1 and 2 as well as endoglin, an auxiliary receptor of TGFβ, were found to be decreased in nitrofen-CDH rat pups (10).

In contrast to the TGFβ pathway, conclusions drawn in several reports on components of the BMP pathway in CDH are consistent. Reduced expression of BMPR2 (11, 12) and BMP4 (12, 13) was found in the lungs of different animal models of CDH. Furthermore, the expression of apelin, a target gene of BMPR2 which can have a hypotensive function, is reported to be decreased in nitrofen-CDH rat pups (14); whilst expression of activin receptor-like kinase 1 (ALK1), another receptor of the BMP signaling pathway, was upregulated in the same animal model (15). However, Corbett et al. did not report any differences in downstream signaling of BMPR (16), and did not find any mutations in the BMPR2 gene in CDH patients (17). All findings reported to date addressing the TGFβ and BMP pathways in CDH is summarized in **Supplementary Table 1** and an overview of both pathways is displayed in **Figure 1**.

Investigations conducted to date have focused largely on the expression of receptors in both the TGFβ and BMP pathways, but little is known about the actual activation of these pathways. Therefore, we hypothesized that the analysis of downstream mediators would identify changes in TGFβ and BMP signaling pathways in the lungs of rats in which CDH was induced by nitrofen exposure.

MATERIALS AND METHODS

Animal Model

Pregnant Sprague-Dawley rats received either 100 mg nitrofen dissolved in 1 ml olive oil or just 1 ml olive oil by gavage on gestational age day E9.5. Nitrofen induces CDH in ∼70% of the offspring, while all pups have pulmonary hypertension (18, 19). At embryonic day (E) 21, pups were delivered by cesarean section and euthanized by lethal injection of pentobarbital. Lung tissue of the CDH and control pups were isolated and processed for paraffin embedding (left lobes) or immediately snap frozen (right lobes) for protein and RNA analysis. All animal experiments were approved by an independent animal ethical committee and were conducted according to national guidelines.

Quantitative Real-Time Polymerase Chain Reaction (qPCR)

RNA isolation, cDNA synthesis and subsequent qPCR analysis on right lung lobes was performed as previously (20). The gene-specific primers used are available upon request.

Immunohistochemistry and Immunofluorescence Staining

Immunohistochemistry (IHC) was performed on 5-μm paraffin sections of the left lobe according to standard protocols, using the Envision™ detection system (Dako Cytomatic, Glostrup, Denmark) (20). Primary antibody used for IHC was ZEB2 [1:400, (21)]. Primary antibodies used for IF were smooth muscle actin (α-SMA; MS-113-P1; 1:500, Thermo Scientific, Fremont, CA, USA), phosphorylated SMAD 2 (pSMAD2; 1:250, Cell Signaling, Danvers, MA, USA), phosphorylated SMAD 1/5/8 (pSMAD1/5/8; 1:500, Kerafast, Boston, MA, USA), and KI-67 (1:100, Abcam, Cambridge, UK). Secondary antibodies against mouse (α-SMA) and rabbit (pSMAD2, pSMAD1/5/8, and KI-67) were used. Negative controls were performed by omitting the primary antibody. Antigen retrieval with citric acid buffer (pH 6.0) was used. Negative controls were performed by omitting the primary antibody.

Immunoblotting

Snap-frozen right lung lobes were homogenized on ice in Carin buffer (20 mM Tris pH 8.0, 137 mM NaCl, 10 mM EDTA, 1% NP40, 10% glycerol), containing protease inhibitor Complete (Roche, Basel, Switzerland). Samples were centrifuged at 14,200 r.p.m. for 15 min and protein concentration in the supernatant was measured using the Bradford method. Subsequently 50 μg of protein per lane was loaded onto an SDS-PAGE and transferred to nitrocellulose membranes using wet blotting. Antigens were detected with TGFβ (1:1,000, Abcam), pSMAD2 (1:1,000, Cell Signaling), SMAD2 (1:1,000, Cell Signaling), pSMAD5 (1:1,000, Abcam), SMAD5 (1:1,000, Cell Signaling), and Zeb2 [1:1,000, (21)]. Cofilin (1:400, Abcam) and β-actin (1:1,000, Cell Signaling) were used for loading control.

Statistical Analyses

Data are presented as percentages, means (SD) for normally distributed variables. Univariate analyses were performed using independent samples *t*-tests for normally distributed variables. The analyses were performed using SPSS 21.0 for Windows (Armonk, NY, USA: IBM Corp.). All statistical tests were two-sided and used a significance level of 0.05.

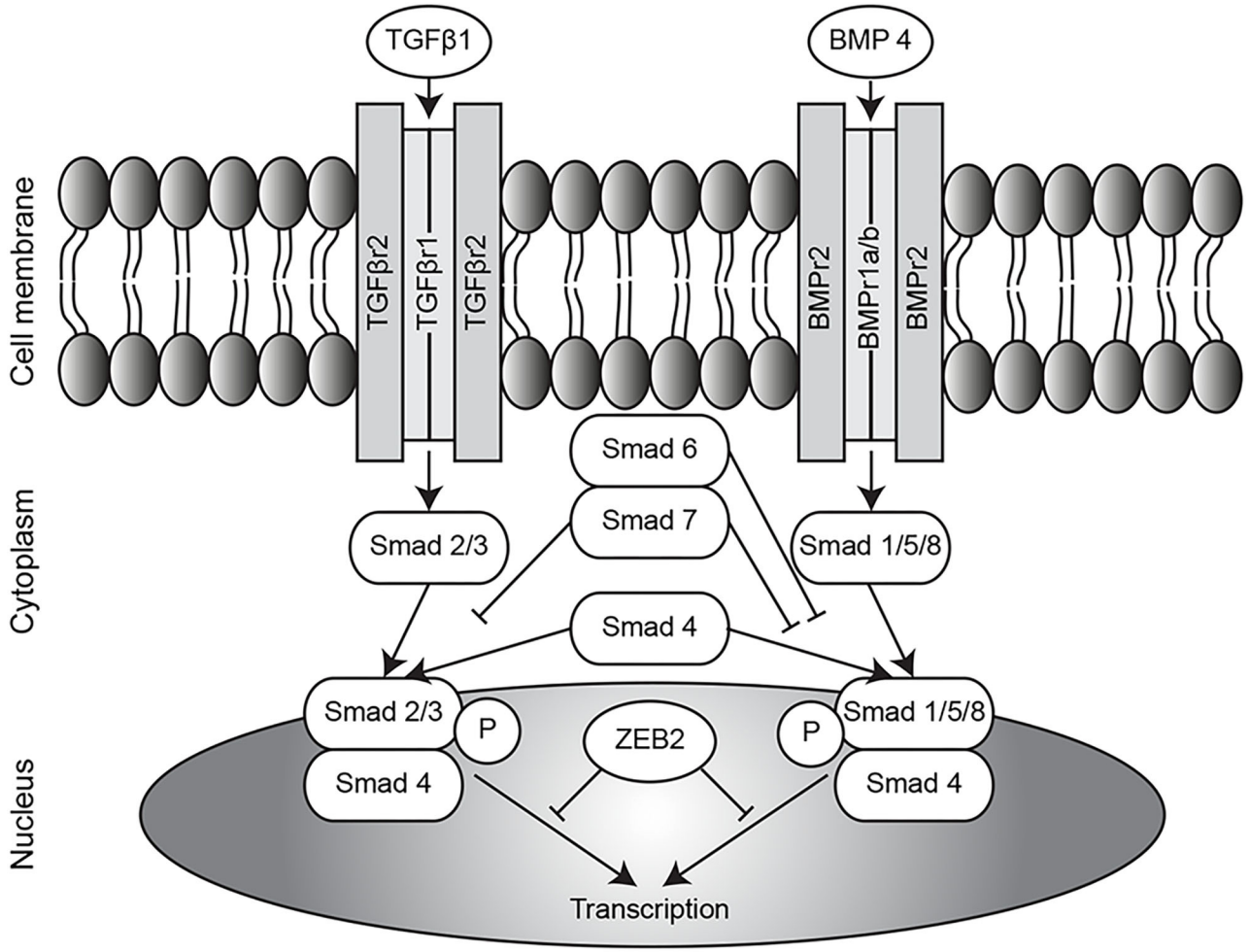

FIGURE 1 | Overview of TGFβ/BMP pathway. Overview of the TGFβ and BMP pathways. TGFβ, transforming growth factor β; BMP, bone morphogenetic protein; ZEB2, zinc finger E-box binding homeobox 2; P, phosphorylation.

RESULTS

TGFβ Activation Is Upregulated in CDH

The expression of key signaling factors in the TGFβ pathway was assessed in whole lung homogenates at the mRNA level, where an increase in the abundance of mRNA transcript encoding both *Tgfbr1* and *Tgfbr2* receptors, but no difference in the abundance of the ligand *Tgfb1* mRNA transcript was noted. The abundance of mRNA transcripts encoding both the receptor-activated SMADs, *Smad2*, and *Smad3*, as well as the co-SMAD, *Smad4*, which together form a signaling complex for translocation into the cell nucleus, was increased in CDH (**Figure 2A**). No differences were found in expression of the TGFβ1 ligand at the protein level (**Figure 2B**). For the activation of the TGFβ pathway, receptor-activated SMADs must be phosphorylated. The degree of phosphorylation of SMAD2 was not different in whole lung homogenates of CDH pups compared to controls (**Figure 2C**). Since the abnormalities in the pulmonary vasculature are key pathological hallmarks of CDH, changes in SMAD phosphorylation were assessed in the small pulmonary vessels (25–50 μm) using immunofluorescence staining. This approach revealed an increased number of smooth muscle actin (SMA)-positive cells in the small vessels of CDH pups expressing phosphorylated SMAD2 (pSMAD2), which points to an increased activation of this pathway in the pulmonary vasculature (**Figure 2D**).

BMP Activation Is Reduced in CDH

In contrast to the TGFβ receptors, a decrease in *Bmpr1b* mRNA transcript abundance was noted in CDH, while no differences in the abundance of the well-studied *Bmpr2* were noted, comparing both groups at mRNA level in whole lung homogenates. Activin receptor-like kinase 1 (*Alk1*), another receptor in the BMP/TGFβ pathway which mediates the signal of *Bmp9* and *Bmp10*, was slightly increased in CDH. *Bmp4*, one of the important ligands in this pathway, and the receptor-activated *Smad1* and *Smad5* showed an increase in CDH (**Figure 3A**). Western blot on whole lung homogenates showed a decreased

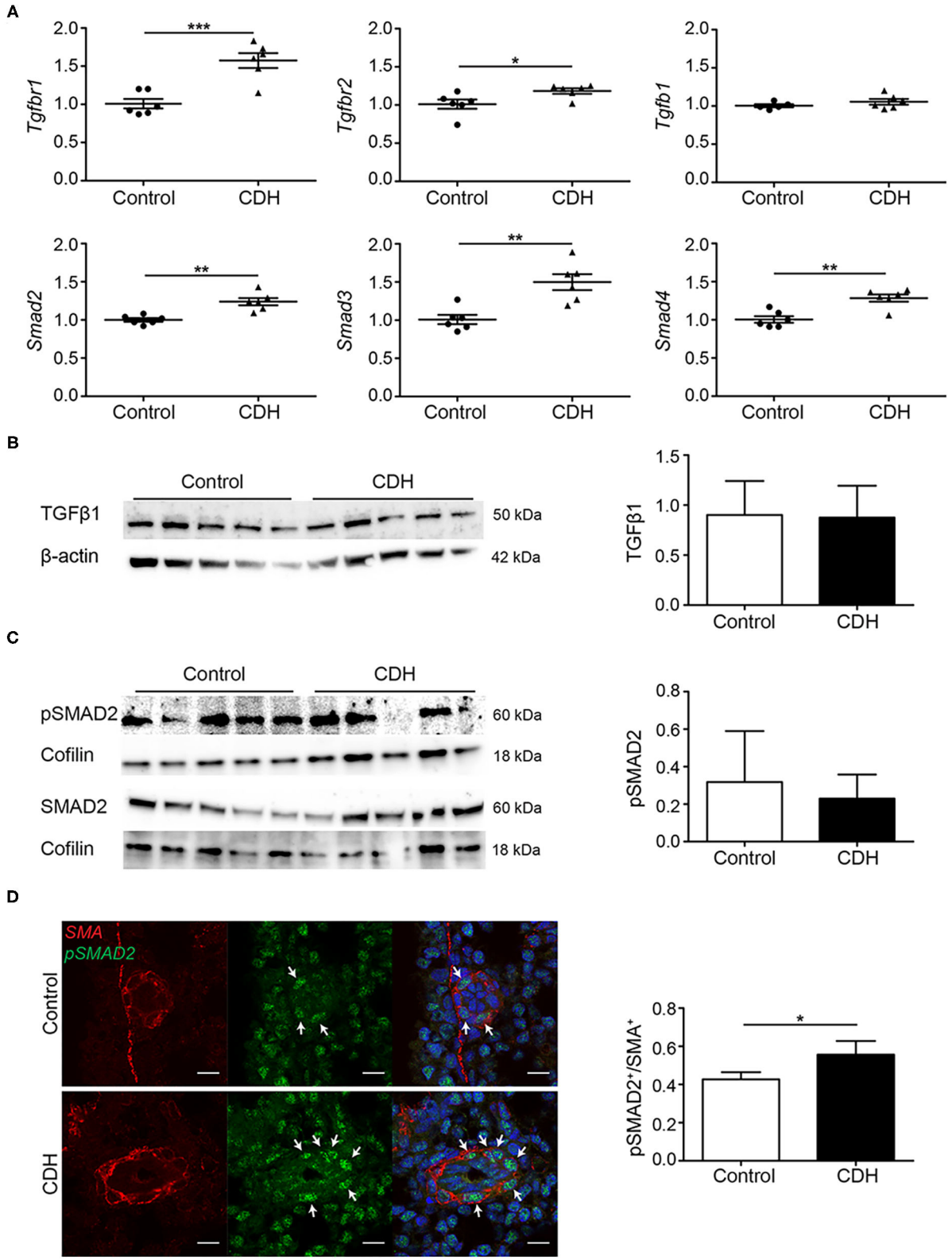

FIGURE 2 | TGFβ activation is upregulated in experimental CDH. **(A)** Quantitative PCR revealed a significant increase in *Tgfbr1* and *Tgfbr2* in CDH ($p < 0.001$ and $p = 0.033$, respectively), but no difference in *Tgfb1* mRNA transcript abundance compared to control. The abundance of *Smad2*, *Smad3*, and *Smad4* mRNA

(Continued)

FIGURE 2 | transcripts were all significantly higher in CDH ($p = 0.001$, $p = 0.002$, and $p = 0.002$, respectively; $n = 6$ for both groups). **(B)** Western blot on whole lung homogenates revealed no differences in TGFβ1 abundance between control and CDH, when normalized to total protein amount using β-actin as a loading control ($n = 5$ for both groups). **(C)** The abundance of pSMAD2 was related to the total SMAD2 protein levels, which was not different between control and CDH in whole lung homogenates, where Cofilin was used as a loading control ($n = 5$ for both groups). **(D)** Representative images of immunofluorescence staining indicate an increase in the ratio of pSMAD2/SMA double-positive cells in small pulmonary vessels in CDH ($p = 0.049$; $n = 3$ samples for both groups). Six vessels per sample were counted. Scale bars represent 10 μm. $^{*}p < 0.05$, $^{**}p < 0.01$, $^{***}p < 0.001$. Error bars represent SD.

expression of SMAD5 in CDH with no differences in relative phosphorylation (**Figure 3B**). However, when focusing on the important pulmonary vasculature, the number of SMA positive cells expressing phosphorylated SMAD1/5/8 was reduced in CDH on immunofluorescence staining, indicating a decreased activation of this pathway in the pulmonary vasculature (**Figure 3C**).

Downstream Effects of TGFβ and BMP Signaling

Both the TGFβ and BMP pathways can be inhibited by the inhibitory SMADs, SMAD6, and SMAD7. These proteins compete with SMAD4 in the formation of heteromeric signaling complexes and can, therefore, prevent transcription of target genes. No differences were noted in the expression of *Smad6* at the mRNA level, but lung *Smad7* transcript abundance was increased in CDH. The lung abundance of mRNA transcripts encoding *Zeb2*, a transcriptional corepressor of the activated pathway, were increases in CDH at the mRNA level (**Figure 4A**). However, no significant differences in protein levels of ZEB2 were noted by western blot analysis of whole lung homogenates (**Figure 4B**), and no changes in the expression of ZEB2 were noted in the small vessels using immunohistochemistry (**Figure 4C**). Since increased activation of the TGFβ pathway can induce proliferation of pulmonary artery smooth muscle cells, the expression of KI-67, a marker for proliferation, was used to identify proliferating cells in the vascular wall. In small pulmonary vessels in CDH, more SMA-positive cells expressed KI-67 (**Figures 4D,E**).

DISCUSSION

In this report, upregulated activation of the TGFβ pathway and downregulated activation of the BMP pathway in small pulmonary vessels in the nitrofen-CDH rat model are demonstrated at the cellular level.

No differences were observed in the ligand TGFβ1 and the degree of phosphorylation of both SMAD2 and SMAD5 at the protein level in whole lung homogenates. Although the total amount of SMAD5 and pSMAD5 was less in whole lung homogenates of CDH pups, no changes were noted in the degree of phosphorylation in total lung extracts. At the cellular level, however, the smooth muscle layer of the small pulmonary vessels of nitrofen-CDH pups revealed increased abundance of pSMAD2 and decreased abundance of pSMAD1/5/8, indicative of more active TGFβ signaling and reduced BMP signaling, respectively. The latter is in line with Makenga and colleagues who reported decreased pSMAD1/5/8 in CDH lung homogenates. Moreover, the differences observed in the small pulmonary arteries in CDH lungs may also reflect the fact that the perivascular cells in CDH lungs are more differentiated compared to perivascular cells in control lungs (22).

Phosphorylation of the receptor-activated SMADs is necessary for the activation of downstream mediators and, therefore, plays an important role in pathway activation. The increased expression of the inhibitory *Smad7* and corepressor *Zeb2* at the mRNA level is in line with SMAD7 being a direct target of ZEB2 and may point to increased production of these inhibitors in order to inhibit the increased activity of the TGFβ pathway (23). The absence of any observed changes in *Smad6*, which only inhibits the BMP pathway, strengthens this idea. However, the expression of ZEB2 at the protein level in whole lung homogenates exhibited a trend toward an increase, and no differences were noted by immunostaining of the pulmonary vessels, indicating a discrepancy between RNA and protein expression. The latter could, in part, explain differences between several reports on TGFβ and BMP signaling in CDH. Moreover, the usage of specific parts of the lung or isolated lung cells may also lead to differences or even opposing results between different reports. Both TGFβ and BMP can regulate proliferation of vascular cells and previous studies have reported increased proliferation of pulmonary artery smooth muscle cells from patients with PAH in response to TGFβ1 (24, 25). The increased proliferation of constituent cells of the smooth muscle layer of small pulmonary vessels was noted in the present study in nitrofen-CDH pup lungs, which might indicate an abnormal response of these cells to the increased TGFβ activity.

TGFβ is a target of retinoic acid (RA) (26), and increased activity of the TGFβ pathway with higher levels of pSMAD2 has been described in RA-deficient foreguts, and in a mouse model with RA deficiency. In that study, lung agenesis was observed both by decreasing RA levels as well as by increasing TGFβ levels, indicating the interaction between both pathways early in development (27). Furthermore, a study in rats with alveolar hypoplasia caused by caloric restriction exhibited improvement of alveolar formation after treatment with RA, accompanied by a decrease in TGFβ activity at postnatal day 21 (28). These findings strengthen the results presented here, about increased TGFβ activity in nitrofen-exposed rats, where nitrofen has been reported to disrupt the retinoid signaling pathway (29). Since a reduction in retinol and retinol binding protein (RBP) has been found in human

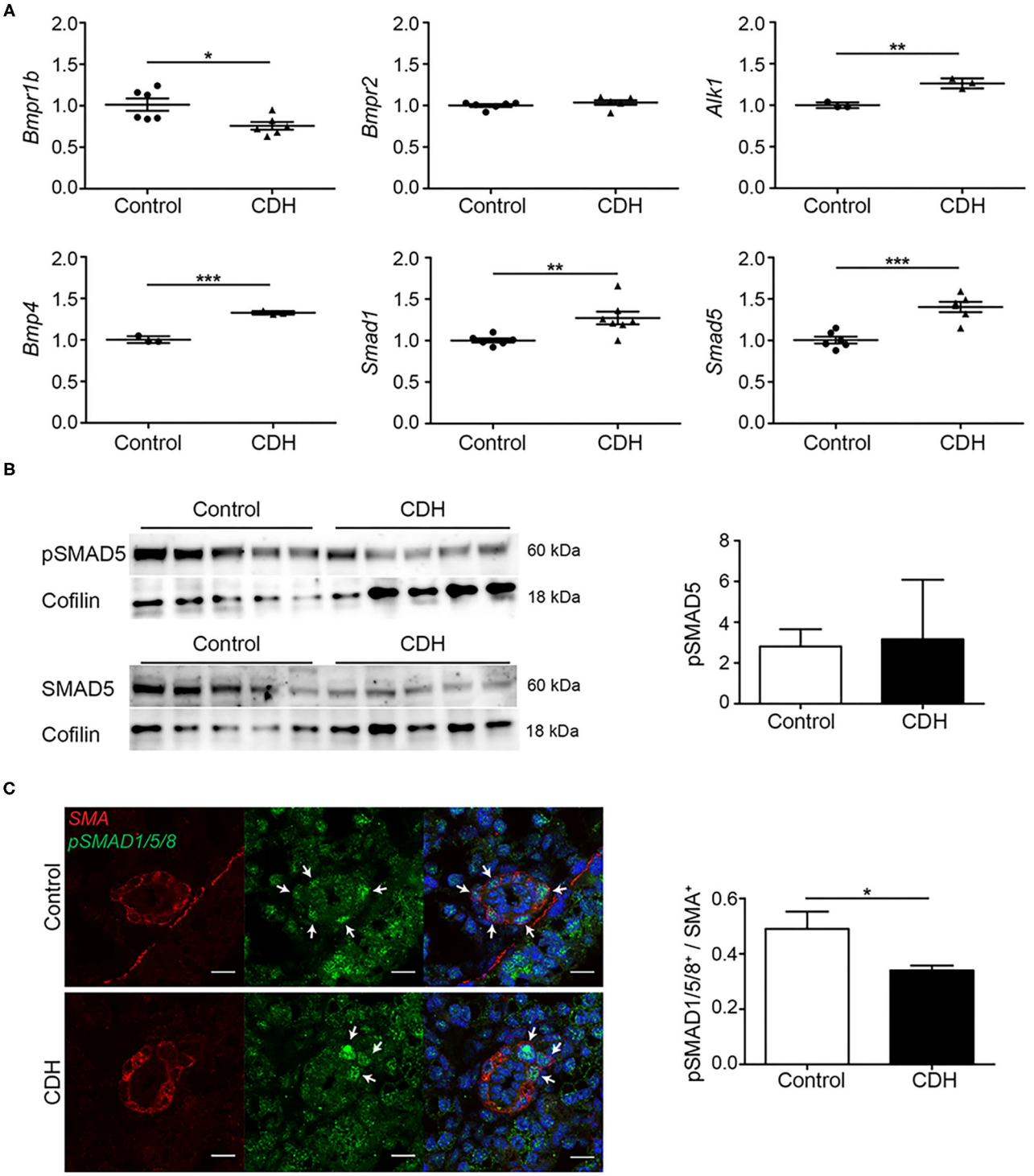

FIGURE 3 | BMP activation is reduced in experimental CDH. **(A)** Quantitative PCR revealed a significantly decreased lung abundance of *Bmpr1b* ($p = 0.016$) but no differences in *Bmpr2*, and increased abundance of *Alk1* ($p = 0.003$) mRNA transcripts in CDH compared to control. The abundance of *Bmp4*, *Smad1*, and *Smad5* mRNA transcripts was significantly higher in CDH [$p < 0.001$, $p = 0.009$, and $p < 0.001$, respectively; $n = 3$ (*Alk1* and *Bmp4*) or 6 (rest) for both groups]. **(B)** The lung abundance of pSMAD5 was related to the total SMAD5 protein abundance, which was not different between control and CDH samples, where Cofilin was used as a loading control ($n = 5$ for both groups). **(C)** Representative images of immunofluorescence staining indicate a decrease in the ratio of pSMAD1/5/8/ SMA double-positive cells in small pulmonary vessels in CDH lungs ($p = 0.016$; $n = 3$ samples for both groups). Six vessels per sample were counted. Scale bars represent 10 μm. $^{*}p < 0.05$, $^{**}p < 0.01$, $^{***}p < 0.001$. Error bars represent SD.

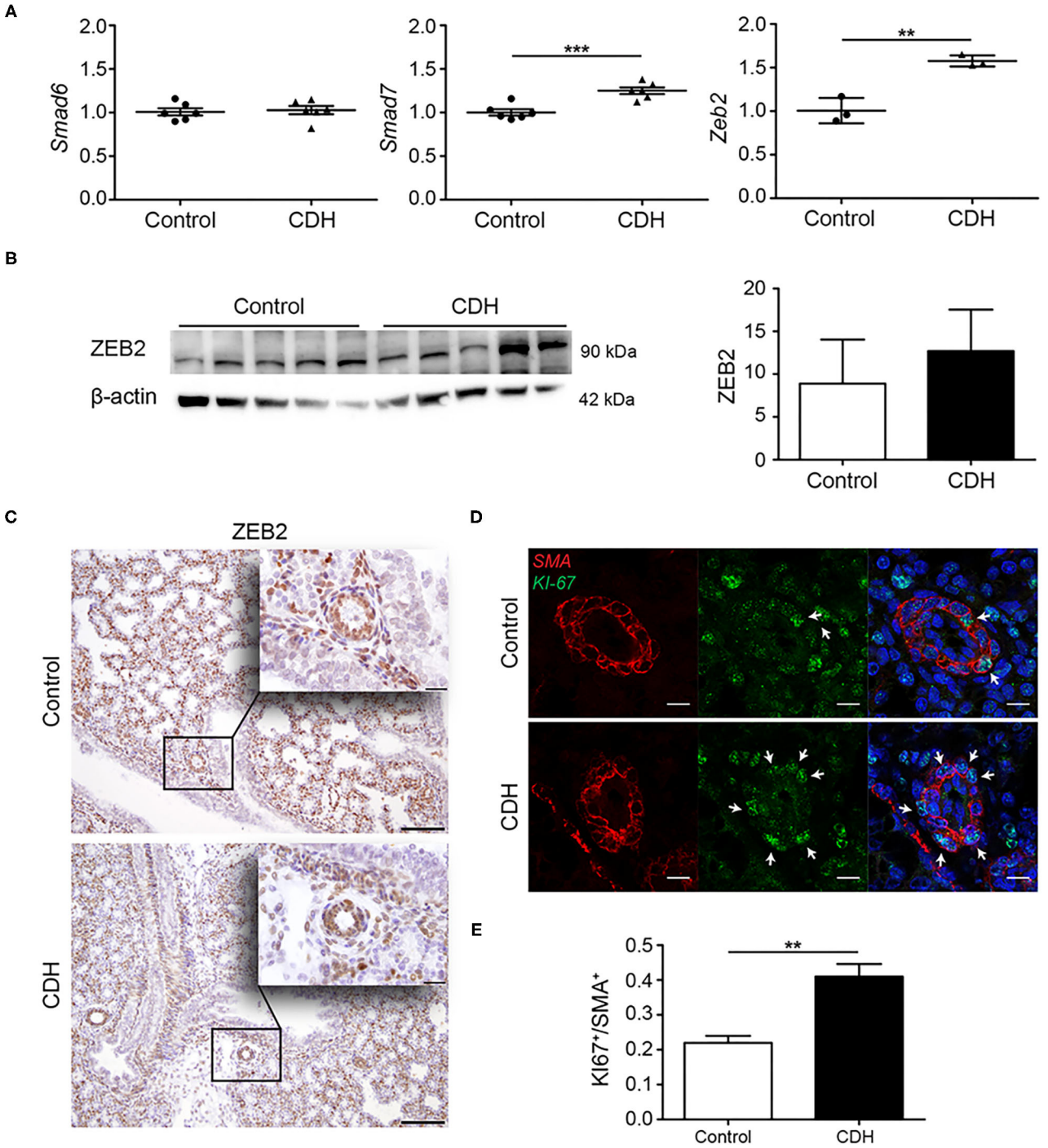

FIGURE 4 | Modulators of TGFβ signaling are upregulated in CDH. **(A)** Quantitative PCR revealed no difference in the abundance of the inhibitory *Smad6* mRNA transcript, but increased abundance of inhibitory *Smad7* and *Zeb2* mRNA transcripts [$p < 0.001$ and $p = 0.003$, respectively; $n = 3$ (*Zeb2*) or 6 (*Smad6*, *Smad7*) per group; y-axis indicated fold-change]. **(B)** Western blot analyses of whole lung homogenates revealed no significant differences in ZEB2 protein abundance comparing CDH and control groups, where β-actin was used as a loading control, and as a reference for quantification ($n = 5$ for both groups). **(C)** Representative images of immunohistochemistry staining show no differences in expression of ZEB2 in the small vessels of all lungs ($n = 3$ samples for both groups). Scale bars represent 100 μm (low power) and 20 μm (high power). $^{**}p < 0.01$, $^{***}p < 0.001$. Error bars represent SD. **(D)** Increased proliferation of the muscular vessel wall in CDH. Representative images of immunofluorescence staining revealed an increase in KI-67/SMA double-positive cells in small pulmonary vessels in CDH ($p = 0.001$; $n = 3$ samples for both groups). **(E)** Quantification of proliferative SMA+ cells. Four vessels per sample were counted. Scale bars represent 10 μm. $^{**}p < 0.01$, $^{***}p < 0.001$. Error bars represent SD.

newborns with CDH (30, 31), and several key components of the RA pathway are affected in human and experimental CDH (32), the increased activity of the TGFβ pathway might play an important role in the development of the lungs in CDH.

Studies available in the literature have reported conflicting trends in expression of different signaling factors in CDH, which might be explained by the differences in the gestation of the animals under study. In the present study, some variability between samples was also noted, suggesting that small differences in gestational age may have an appreciable impact on trends in the expression of signaling molecules under study.

We initially analyzed the TGF-β and BMP pathways in whole lungs, and given our previous report on vascular abnormalities in CDH (22), we focused on the activation of the TGF-β and BMP pathways in the vasculature, using immunofluorescence staining, showing a clearly difference in phosphorylation of SMAD2 and SMAD5.

In conclusion, increased phosphorylation of SMAD2 and decreased phosphorylation of SMAD5 was noted in the in the vessel walls of small pulmonary vessels of nitrofen-CDH pups. These data indicate increased activation of the TGFβ pathway and decreased activation of the BMP pathway in the pulmonary vasculature of these animals at day 21 of gestation, possibly leading to increased proliferation of the muscularized vessel wall. Since the different factors in these pathways are differently expressed during gestation and might differ from the human situation, further research must be conducted at different developmental stages, and most importantly, in material of human patients.

DATA AVAILABILITY STATEMENT

The original contributions presented in the study are included in the article/**Supplementary Material**, further inquiries can be directed to the corresponding authors.

ETHICS STATEMENT

The animal study was reviewed and approved by independent animal ethical committee (EMC).

AUTHOR CONTRIBUTIONS

DT, RM, and RR: conceptualization and writing—original draft. DM, MB-vK, RM, and RR: data curation. DM, MB-vK, and RR: formal analysis and methodology. RM and RR: funding acquisition and supervision. DM and MB-vK: investigation and validation. DT and RW: resources. DM, MB-vK, RW, DT, RM, and RR: writing—review and editing. All authors contributed to the article and approved the submitted version.

FUNDING

RM was supported by the Max Planck Society (MPI-HLR); the German Federal Ministry of Education and Research (DZL-UGMLC) and the German Research Foundation through EXC2026 (390649896), SFB1213 (268555672), KFO309 (284237345), Mo1789/1 (160966624), and Mo1789/4-1 (420759458). RR was supported by the Sophia Medical Research Council, the Dutch Lung Foundation and the Dutch Organization for Scietific Research (NWO).

ACKNOWLEDGMENTS

This manuscript was in part included in the dissertation of DSM, and is archived online at Erasmus University Rotterdam's institutional repository (33).

SUPPLEMENTARY MATERIAL

The Supplementary Material for this article can be found online at: https://www.frontiersin.org/articles/10.3389/fmed.2021.642577/full#supplementary-material

REFERENCES

1. Sluiter I, van der Horst I, van der Voorn P, Boerema-de Munck A, Buscop-van Kempen M, de Krijger R, et al. Premature differentiation of vascular smooth muscle cells in human congenital diaphragmatic hernia. *Exp Mol Pathol.* (2013) 94:195–202. doi: 10.1016/j.yexmp.2012.09.010
2. Ma L, Chung WK. The role of genetics in pulmonary arterial hypertension. *J Pathol.* (2017) 241:273–80. doi: 10.1002/path.4833
3. Alejandre-Alcazar MA, Michiels-Corsten M, Vicencio AG, Reiss I, Ryu J, de Krijger RR, et al. TGF-beta signaling is dynamically regulated during the alveolarization of rodent and human lungs. *Dev Dyn.* (2008) 237:259–69. doi: 10.1002/dvdy.21403
4. Chen H, Sun J, Buckley S, Chen C, Warburton D, Wang XF, et al. Abnormal mouse lung alveolarization caused by Smad3 deficiency is a developmental antecedent of centrilobular emphysema. *Am J Physiol Lung Cell Mol Physiol.* (2005) 288:L683–91. doi: 10.1152/ajplung.00298.2004
5. Eickelberg O, Morty RE. Transforming growth factor beta/bone morphogenic protein signaling in pulmonary arterial hypertension: remodeling revisited. *Trends Cardiovasc Med.* (2007) 17:263–9. doi: 10.1016/j.tcm.2007.09.003
6. Teramoto H, Shinkai M, Puri P. Altered expression of angiotensin II receptor subtypes and transforming growth factor-beta in the heart of nitrofen-induced diaphragmatic hernia in rats. *Pediatr Surg Int.* (2005) 21:148–52. doi: 10.1007/s00383-004-1311-7
7. Xu C, Liu W, Chen Z, Wang Y, Xiong Z, Ji Y. Effect of prenatal tetrandrine administration on transforming growth factor-beta1 level in the lung of nitrofen-induced congenital diaphragmatic hernia rat model. *J Pediatr Surg.* (2009) 44:1611–20. doi: 10.1016/j.jpedsurg.2008.09.021
8. Vuckovic A, Herber-Jonat S, Flemmer AW, Ruehl IM, Votino C, Segers V, et al. Increased TGF-beta: a drawback of tracheal occlusion in human and experimental congenital diaphragmatic hernia? *Am J Physiol Lung Cell Mol Physiol.* (2016) 310:L311–27. doi: 10.1152/ajplung.00122.2015
9. Candilera V, Bouche C, Schleef J, Pederiva F. Lung growth factors in the amniotic fluid of normal pregnancies and with congenital diaphragmatic hernia. *J Matern Fetal Neonatal Med.* (2016) 29:2104–8. doi: 10.3109/14767058.2015.1076387
10. Zimmer J, Takahashi T, Hofmann AD, Puri P. Decreased Endoglin expression in the pulmonary vasculature of nitrofen-induced congenital diaphragmatic hernia rat model. *Pediatr Surg Int.* (2017) 33:263–8. doi: 10.1007/s00383-016-4004-0

11. Gosemann JH, Friedmacher F, Fujiwara N, Alvarez LA, Corcionivoschi N, Puri P. Disruption of the bone morphogenetic protein receptor 2 pathway in nitrofen-induced congenital diaphragmatic hernia. *Birth Defects Res B Dev Reprod Toxicol*. (2013) 98:304–9. doi: 10.1002/bdrb.21065
12. Makanga M, Dewachter C, Maruyama H, Vuckovic A, Rondelet B, Naeije R, et al. Downregulated bone morphogenetic protein signaling in nitrofen-induced congenital diaphragmatic hernia. *Pediatr Surg Int*. (2013) 29:823–34. doi: 10.1007/s00383-013-3340-6
13. Emmerton-Coughlin HM, Martin KK, Chiu JS, Zhao L, Scott LA, Regnault TR, et al. BMP4 and LGL1 are down regulated in an ovine model of congenital diaphragmatic hernia. *Front Surg*. (2014) 1:44. doi: 10.3389/fsurg.2014.00044
14. Hofmann AD, Friedmacher F, Takahashi H, Hunziker M, Gosemann JH, Puri P. Decreased apelin and apelin-receptor expression in the pulmonary vasculature of nitrofen-induced congenital diaphragmatic hernia. *Pediatr Surg Int*. (2014) 30:197–203. doi: 10.1007/s00383-013-3450-1
15. Hofmann AD, Zimmer J, Takahashi T, Gosemann JH, Puri P. The role of activin receptor-like kinase 1 signaling in the pulmonary vasculature of experimental diaphragmatic hernia. *Eur J Pediatr Surg*. (2016) 26:106–11. doi: 10.1055/s-0035-1566105
16. Corbett HJ, Connell MG, Fernig DG, Losty PD, Jesudason EC. ANG-1 TIE-2 and BMPR signalling defects are not seen in the nitrofen model of pulmonary hypertension and congenital diaphragmatic hernia. *PLoS ONE*. (2012) 7:e35364. doi: 10.1371/journal.pone.0035364
17. Chiu JS, Ma L, Wynn J, Krishnan U, Rosenzweig EB, Aspelund G, et al. Mutations in BMPR2 are not present in patients with pulmonary hypertension associated with congenital diaphragmatic hernia. *J Pediatr Surg*. (2017) 52:1747–50. doi: 10.1016/j.jpedsurg.2017.01.007
18. Mous DS, Kool HM, Burgisser PE, Buscop-van Kempen MJ, Nagata K, Boerema-de Munck A, et al. Treatment of rat congenital diaphragmatic hernia with sildenafil and NS-304, selexipag's active compound, at the pseudoglandular stage improves lung vasculature. *Am J Physiol Lung Cell Mol Physiol*. (2018) 315:L276–85. doi: 10.1152/ajplung.00392.2017
19. Mous DS, Kool HM, Buscop-van Kempen MJ, Koning AH, Dzyubachyk O, Wijnen RM, et al. Clinically relevant timing of antenatal sildenafil treatment reduces pulmonary vascular remodeling in congenital diaphragmatic hernia. *Am J Physiol Lung Cell Mol Physiol*. (2016) 311:L734–42. doi: 10.1152/ajplung.00180.2016
20. Rajatapiti P, van der Horst IW, de Rooij JD, Tran MG, Maxwell PH, Tibboel D, et al. Expression of hypoxia-inducible factors in normal human lung development. *Pediatr Dev Pathol*. (2008) 11:193–9. doi: 10.2350/07-04-0257.1
21. Seuntjens E, Nityanandam A, Miquelajauregui A, Debruyn J, Stryjewska A, Goebbels S, et al. Sip1 regulates sequential fate decisions by feedback signaling from postmitotic neurons to progenitors. *Nat Neurosci*. (2009) 12:1373–80. doi: 10.1038/nn.2409
22. Kool HM, Burgisser PE, Edel GG, de Kleer I, Boerema-de Munck A, de Laat I, et al. Inhibition of retinoic acid signaling induces aberrant pericyte coverage and differentiation resulting in vascular defects in congenital diaphragmatic hernia. *Am J Physiol Lung Cell Mol Physiol*. (2019) 317:L317–31. doi: 10.1152/ajplung.00104.2018
23. Weng Q, Chen Y, Wang H, Xu X, Yang B, He Q, et al. Dual-mode modulation of Smad signaling by Smad-interacting protein Sip1 is required for myelination in the central nervous system. *Neuron*. (2012) 73:713–28. doi: 10.1016/j.neuron.2011.12.021
24. Morrell NW, Yang X, Upton PD, Jourdan KB, Morgan N, Sheares KK, et al. Altered growth responses of pulmonary artery smooth muscle cells from patients with primary pulmonary hypertension to transforming growth factor-beta(1) and bone morphogenetic proteins. *Circulation*. (2001) 104:790–5. doi: 10.1161/hc3201.094152
25. Thomas M, Docx C, Holmes AM, Beach S, Duggan N, England K, et al. Activin-like kinase 5 (ALK5) mediates abnormal proliferation of vascular smooth muscle cells from patients with familial pulmonary arterial hypertension and is involved in the progression of experimental pulmonary arterial hypertension induced by monocrotaline. *Am J Pathol*. (2009) 174:380–9. doi: 10.2353/ajpath.2009.080565
26. Balmer JE, Blomhoff R. Gene expression regulation by retinoic acid. *J Lipid Res*. (2002) 43:1773–808. doi: 10.1194/jlr.R100015-JLR200
27. Chen F, Desai TJ, Qian J, Niederreither K, Lu J, Cardoso WV. Inhibition of Tgf beta signaling by endogenous retinoic acid is essential for primary lung bud induction. *Development*. (2007) 134:2969–79. doi: 10.1242/dev.006221
28. Londhe VA, Maisonet TM, Lopez B, Shin BC, Huynh J, Devaskar SU. Retinoic acid rescues alveolar hypoplasia in the calorie-restricted developing rat lung. *Am J Respir Cell Mol Biol*. (2013) 48:179–87. doi: 10.1165/rcmb.2012-0229OC
29. Beurskens N, Klaassens M, Rottier R, de Klein A, Tibboel D. Linking animal models to human congenital diaphragmatic hernia. *Birth Defects Res A Clin Mol Teratol*. (2007) 79:565–72. doi: 10.1002/bdra.20370
30. Beurskens LW, Tibboel D, Lindemans J, Duvekot JJ, Cohen-Overbeek TE, Veenma DC, et al. Retinol status of newborn infants is associated with congenital diaphragmatic hernia. *Pediatrics*. (2010) 126:712–20. doi: 10.1542/peds.2010-0521
31. Major D, Cadenas M, Fournier L, Leclerc S, Lefebvre M, Cloutier R. Retinol status of newborn infants with congenital diaphragmatic hernia. *Pediatr Surg Int*. (1998) 13:547–9. doi: 10.1007/s003830050399
32. Coste K, Beurskens LW, Blanc P, Gallot D, Delabaere A, Blanchon L, et al. Metabolic disturbances of the vitamin A pathway in human diaphragmatic hernia. *Am J Physiol Lung Cell Mol Physiol*. (2015) 308:L147–57. doi: 10.1152/ajplung.00108.2014
33. Mous DS. *Pulmonary Vascular Defects in Congenital Diaphragmatic Hernia: the Quest for Early Factors and Intervention*. Dissertation. Rotterdam: Erasmus University (2017).

Conflict of Interest: The authors declare that the research was conducted in the absence of any commercial or financial relationships that could be construed as a potential conflict of interest.

Copyright © 2021 Mous, Buscop-van Kempen, Wijnen, Tibboel, Morty and Rottier. This is an open-access article distributed under the terms of the Creative Commons Attribution License (CC BY). The use, distribution or reproduction in other forums is permitted, provided the original author(s) and the copyright owner(s) are credited and that the original publication in this journal is cited, in accordance with accepted academic practice. No use, distribution or reproduction is permitted which does not comply with these terms.

frontiers in Pediatrics

ORIGINAL RESEARCH
published: 07 May 2021
doi: 10.3389/fped.2021.625031

Close Association Between Platelet Biogenesis and Alveolarization of the Developing Lung

Xueyu Chen[1], Junyan Zhong[1], Dongshan Han[1], Fang Yao[2], Jie Zhao[2], Gerry. T. M. Wagenaar[3], Chuanzhong Yang[2] and Frans J. Walther[4,5]**

[1] Laboratory of Neonatology, Department of Neonatology, Affiliated Shenzhen Maternity and Child Healthcare Hospital, Southern Medical University, Shenzhen, China, [2] Department of Neonatology, Shenzhen Maternity and Child Healthcare Hospital, The First School of Clinical Medicine, Southern Medical University, Shenzhen, China, [3] Faculty of Science, VU University Amsterdam, Amsterdam, Netherlands, [4] Department of Pediatrics, David Geffen School of Medicine, University of California, Los Angeles, Los Angeles, CA, United States, [5] The Lundquist Institute for Biomedical Innovation at Harbor-UCLA Medical Center, Torrance, CA, United States

Bronchopulmonary dysplasia (BPD) is a neonatal chronic lung disease characterized by an arrest in alveolar and vascular development. BPD is secondary to lung immaturity, ventilator-induced lung injury, and exposure to hyperoxia in extremely premature infants, leading to a lifelong impairment of lung function. Recent studies indicate that the lung plays an important role in platelet biogenesis. However, the dynamic change of platelet production during lung development and BPD pathogenesis remains to be elucidated. We investigated the dynamic change of platelet parameters in extremely premature infants during BPD development, and in newborn rats during their normal development from birth to adulthood. We further studied the effect of hyperoxia exposure on platelet production and concomitant pulmonary maldevelopment in an experimental BPD rat model induced by prolonged exposure to hyperoxia. We detected a physiological increase in platelet count from birth to 36 weeks postmenstrual age in extremely premature infants, but platelet counts in extremely premature infants who developed BPD were persistently lower than gestational age-matched controls. In line with clinical findings, exposure to hyperoxia significantly decreased the platelet count in neonatal rats. Lung morphometry analysis demonstrated that platelet counts stabilized with the completion of lung alveolarization in rats. Our findings indicate a close association between platelet biogenesis and alveolarization in the developing lung. This phenomenon might explain the reduced platelet count in extremely premature infants with BPD.

Keywords: lung development, neonatal lung injury, mean platelet volume, platelet distribution width, hyperoxia, platelet counts

OPEN ACCESS

Edited by:
Niki Reynaert, Maastricht University, Netherlands

Reviewed by:
Birke Benedikter, University of Marburg, Germany
Jennifer J. P. Collins, Erasmus Medical Center, Netherlands

****Correspondence:***
Chuanzhong Yang
yangczgd@163.com
Frans J. Walther
fjwalther@ucla.edu

Specialty section:
This article was submitted to Pediatric Pulmonology, a section of the journal Frontiers in Pediatrics

Received: *02 November 2020*
Accepted: *13 April 2021*
Published: *07 May 2021*

Citation:
Chen X, Zhong J, Han D, Yao F, Zhao J, Wagenaar GTM, Yang C and Walther FJ (2021) Close Association Between Platelet Biogenesis and Alveolarization of the Developing Lung. Front. Pediatr. 9:625031. doi: 10.3389/fped.2021.625031

INTRODUCTION

Bronchopulmonary dysplasia (BPD) is one of the most common complications of prematurity and can lead to chronic lung disease with long-term respiratory insufficiency (1). Despite advances in perinatal care, BPD continues to affect up to 40% of extremely premature infants (2). BPD is histologically characterized by arrested lung development as a result of a complex process in which lung immaturity, ventilator-induced lung injury, and exposure to hyperoxia play major roles (3). There is a growing body of knowledge about the various mechanisms underlying BPD pathogenesis

(4). However, therapeutic approaches based on these mechanisms are far from being effective in clinical practice, indicating that these mechanisms probably do not operate in isolation. As the pathogenesis of lung damage in infants with BPD is not completely understood, other possible causal factors need to be elucidated (5).

Recent studies elegantly unravel the close interplay between platelet biogenesis and lung development. Tsukiji et al. report that platelet-derived CLEC-2 signals activate platelets through spleen tyrosine kinase, inducing the release of TGF-β driving the differentiation of mesothelial cells into alveolar duct myofibroblasts that are critical to primary septum formation and elastogenesis in alveolarization of the lung (6). Rafii et al. demonstrated that activated platelets release stromal-cell-derived factor and stimulate the expression of SDF-1 receptors on pulmonary capillary endothelial cells, subsequently enhancing the proliferation of alveolar epithelial cells and neo-alveolarization (7). The lungs are a major site for platelet biogenesis in humans and rodents and contribute ∼50% of the total platelet production (8–12).

Little is known about the dynamic changes in platelets during the complex process that leads to BPD in extremely premature infants. Besides, the impact of clinical oxygen supplementation exposure on platelet biogenesis is unclear. We hypothesize that platelets play an important role in normal lung development and that disturbed platelet biogenesis might contribute to disrupted lung development and BPD pathogenesis. In this study, we first investigated the dynamic change of platelet parameters in a cohort of extremely premature infants within the time window of BPD development, and in newborn rats during their normal development until young adults. We also used an experimental BPD rat model to evaluate the effect of hyperoxia exposure on platelet production and aberrant pulmonary development.

METHODS AND MATERIALS

Clinical Study

A retrospective study was performed at the Neonatal Intensive Care Unit (NICU) of the Shenzhen Maternity and Child Healthcare Hospital after approval by the Institutional Ethical Committee [SFYLS (2019)-119]. The acquirement of informed consent was waived given that no personal data were explicitly reported. Since premature infants with a younger gestational age have an increased chance to develop BPD, we only included extremely premature infants with a gestational age $\leq$28 weeks and/or a birth weight $\leq$1,000 grams. BPD was diagnosed as a requirement of supplemental oxygen at 36 weeks' postmenstrual age or discharge.

Platelet parameters were collected from complete blood counts (CBC) in the 1st week, 2nd week, 4th week, and 8th week after birth. CBC testing was performed on a Mindray 5390 analyzer (Shenzhen, China), using blood samples obtained from arterial and venipuncture or a central catheter.

Animal Study

All animal procedures in this study were approved by the Institutional Animal Care and Use Committee of Shenzhen Institutes of Advanced Technology of the Chinese Academy of Sciences. Newborn pups from 9 pregnant Wistar rats were randomized into 8 groups: an experimental BPD group ($N = 10$) and 7 control groups (raised in room air, $N = 10$ for each group) sacrificed on postnatal day 3, 6, 10, 20, 30, 60, and at adulthood (day 90). Experimental BPD was induced by hyperoxia exposure as previously reported (13). Briefly, newborn pups were raised in a Plexiglas chamber filled with 95% oxygen for 10 days. Pups were anesthetized at the designated day by intraperitoneal injection of pentobarbital (40 mg/kg). All blood samples were drawn from the abdominal aorta, mixed with EDTA and analyzed using a Mindray 5390 analyzer (Shenzhen, China) to acquire platelet parameters. Lung tissue was fixed *in situ* under constant pressure of 27 cmH_2O for 6 min with formalin as previously reported (13). Hereafter, the thorax was opened, the lungs were removed, fixed additionally in formalin for 24 h, embedded in paraffin and sectioned for hematoxylin and eosin (HE) staining.

Lung Morphometry

Mean linear intercept (MLI) was used to assess lung development status. At least 1,000 alveoli per animal were measured to calculate the MLI. Briefly, 10 non-overlapping photos of lung tissues were made with an Olympus CX43 microscope (Tokyo, Japan) at 200x magnification. Structures, including big vessels and airways, were excluded. The photos were applied for alveolar diameter analysis using a WZCamera S50 software (Shenzhen, China). Alveoli with an area of more than 100 μm^2 were analyzed and simulated to circles for calculation of the absolute alveolar diameter. Two independent researchers blinded to the hyperoxia exposure performed the analysis.

Statistics

Continuous parameters were displayed as mean ± standard deviation or median [interquartile range (IQR)], and analyzed

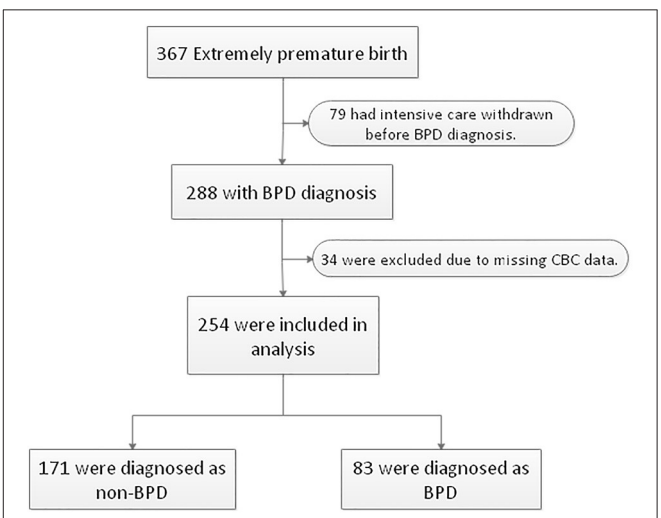

FIGURE 1 | Flowchart of case selection and analysis. Two hundred fifty-four extremely premature infants were enrolled in this study. BPD, bronchopulmonary dysplasia. CBC, complete blood counts.

TABLE 1 | Clinical characteristics of 254 extremely premature infants by BPD status.

	Control ($N = 171$)	BPD ($N = 83$)	$Z/t/\chi^2$	*P*-value
Gestational Age [Wk, M(Q1,Q3)]	27.1 (26.2, 27.6)	26.3 (25.5, 27.2)	−4.01	<0.001
Birth Weight [gr, M(Q1,Q3)]	930 (842, 1,060)	858 (720, 950)	−4.378	<0.001
Sex (male)	91	49	0.765	0.382
Gestational Diabetes Mellitus (GDM)	21	7	0.843	0.359
Gestational Hypertension (GH)	18	7	0.276	0.600
Antenatal steroid	134	66	0.094	0.760
PPROM	56	35	2.375	0.123
Twin	48	28	0.855	0.355
Delivery (C-section)	60	28	0.045	0.832
AS^{1min} [score, M(Q1,Q3)]	8 (5, 9)	6 (5, 8)	−2.049	0.040
AS^{5min} [score, M(Q1,Q3)]	10 (9, 10)	10 (9, 10)	−1.015	0.310
Surfactant	124	76	11.250	0.001
Early onset sepsis (EOS)	75	55	11.959	0.003
Intubation	83	64	21.826	<0.001
Duration of intubation (Days)	0 (0,1)	3.6 (0.8, 22)	−4.417	<0.001
Duration of CPAP (Days)	16 (7, 30)	23 (14, 41)	−3.664	<0.001
Duration of supplemental oxygen (Days)	24 (13, 41)	50 (32, 71)	−6.470	<0.001

CPAP, continuous positive airway pressure. Continuous parameters were displayed as median [interquartile range (IQR)], and analyzed by Mann-Whitney U-test. Categorical variables were displayed with numbers and analyzed by Chi-square test. The statistics were performed using SPSS statistical software version 24.0 (IBM Corporation, NY).

by student *t*-test or Mann-Whitney *U*-test, as appropriate. Categorical variables were displayed with numbers and percentages, and analyzed by Chi-square or Fisher's exact test correspondingly. The patients' data were analyzed using SPSS statistical software version 24.0 (IBM Corporation, NY), and the animals' data were analyzed using GraphPad Prism version 8 software package (San Diego, CA, USA). A $p < 0.05$ was considered statistically significant.

RESULTS

Clinical Characteristics of the Patients

A total of 367 inborn extremely premature infants were admitted to our NICU during the study period. Seventy-nine infants were excluded due to life-support withdrawal before the diagnosis of BPD. Thirty-four infants were excluded due to incomplete CBC data. The remaining 254 extremely premature infants were included in the analysis, of whom 225 (88.6%) were born before 28 weeks and 29 (11.4%) were born after 28 weeks with a birth weight lower than 1,000 grams. The diagnosis of BPD was made in 83 (32.7%) infants (**Figure 1**). The median gestational age was 27.0 (interquartile range: 26.1–27.5) weeks, the median body weight was 910.0 (interquartile range: 807.5, 1013.2) grams. The clinical characteristics of 254 infants by BPD diagnosis were summarized in **Table 1**.

Dynamic Change of Platelet Parameters During BPD Development

A total of 254 extremely premature infants were included in the analysis. BPD was diagnosed in 83 (32.7%) infants. Platelet counts (PLT) continuously increased during the first 8 weeks of postnatal life, while mean platelet volume (MPV) and platelet distribution width (PDW) showed a tendency to decline. However, platelet counts at consecutive time-points of analysis were significantly lower in infants developing BPD compared to infants without BPD (196 ± 85 vs. 231 ± 103 × 10^9/L in the 1st week, 252 ± 112 vs. 293 ± 112 × 10^9/L in the 2nd week, 291 ± 136 vs. 339 ± 136 × 10^9/L in the 4th week, and 308 ± 134 vs. 382 ± 135 × 10^9/L in the 8th week). MPV showed striking changes over the first 2 weeks, with lower values in the 1st week and higher values in the 2nd week in BPD infants compared to infants without BPD (10.39 ± 1.10 vs. 10.85 ± 1.11 fl in the 1st week, 11.27 ± 1.07 vs. 10.97 ± 0.98 fl in the 2nd week. No significant differences in PDW were observed in the two groups (**Figure 2**). In addition, we observed increased PLT and decreased MPV and PDW with advancing postmenstrual age (PMA). BPD infants had lower PLT after PMA of 30–32 weeks than non-BPDs (**Figure 2**).

Rats With Hyperoxia-Induced BPD had Lower Platelet Counts

MLI, an indicator of alveolar size, was significantly higher in rat pups exposed to hyperoxia compared to their age-matched room air (RA) controls (52.1 ± 2.4 vs. 39.5 ± 1.3, $p < 0.001$, **Figures 3D–F**). Similar to our clinical findings shown above, PLT were significantly lower in hyperoxia-induced BPD rats compared to controls raised in room air (642 ± 19 vs. 725 ± 23, $p = 0.0344$). MPV and PDW were significantly higher in experimental BPD pups compared to the controls (8.93 ± 0.35 vs. 7.68 ± 0.17, $p = 0.001$ and 15.81 ± 0.09 vs. 15.43 ± 0.04, $p < 0.001$, respectively, **Figures 3A–C**).

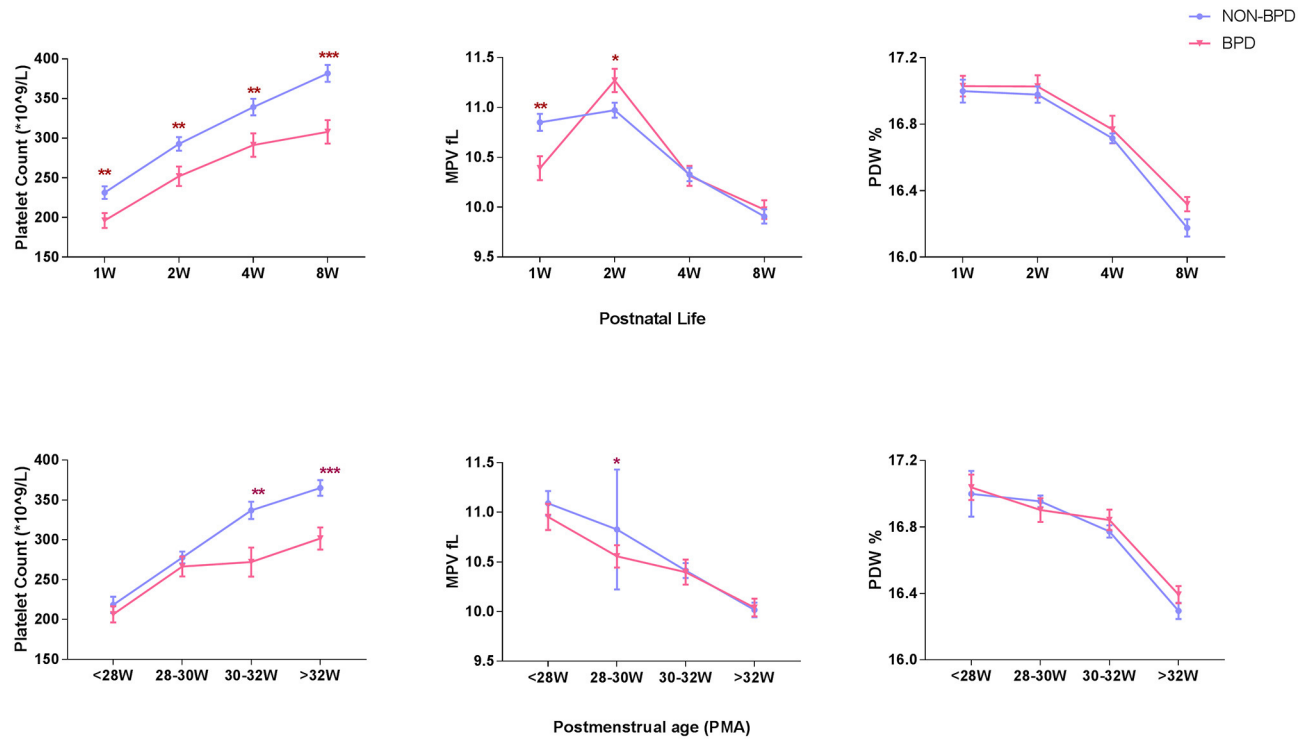

FIGURE 2 | Longitudinal change of platelet parameters defined by postnatal age and postmenstrual age in BPD infants ($N = 83$) and non-BPD infants ($N = 171$). PLT, platelet count, 10^9/L, **(A)**. MPV, mean platelet volume, fL, **(B)**. PDW, platelet distribution width, %, **(C)**. Values are expressed as mean ± SD. $^*p < 0.05$, $^{**}p < 0.01$, $^{***}p < 0.001$, compared with age-matched non-BPDs using the student *t*-test.

Physiological Increase of Platelet Count Synchronized With Alveolarization in Rat Lung

In normal rat development, platelet counts increased from 246 ± 74 × 10^9/L on day 3 to near-adult level of 950 ± 66 × 10^9/L on postnatal day 20 (**Figure 4A**). The MPV and PDW persistently decreased to near-adult levels on postnatal day 20 (**Figures 4B,C**). Alveolarization of rat lung also advanced with age and was complete at around postnatal day 20, as indicated by the stabilization of the MLI (**Figure 4D**) and histology (**Figures 4E–J**).

To better depict the relationship between MLI and platelet parameters, we performed a correlation analysis on MLI and platelet indexes from 3, 6, 9, and 20 days old rats. A significant negative correlation ($r = -0.9959$, $p = 0.0041$) was observed between MLI and PLT. MPV and PDW showed a tendency toward positive correlations with MLI ($p = 0.0643$ and $p = 0.0642$, respectively, **Figure 5**).

DISCUSSION

In this study the dynamic change of longitudinal platelet parameters in premature infants and neonatal rats was investigated. We also evaluated the associations between platelet parameters and lung alveolarization in neonatal rats and found that platelet counts were significantly lower in clinical and experimental BPD. After birth, platelet counts showed a physiological increase in neonatal infants and rat pups while MPV and PDW showed a decrease. Histologically, we confirmed that platelet counts reached stable levels after completion of lung alveolarization in rats (at around postnatal day 20). Correlation analysis demonstrated that platelet counts in rats were significantly associated with the MLI, a marker of alveolar size.

As far as we know, this is the first time to demonstrate an association between platelet index and perinatal lung development. We found a persistent increase in PLT and an overall decrease of MPV and PDW during the first 8 weeks of life of extremely premature infants, which was partly supported by the study from Henry et al., who showed a stepwise increase in platelets during the first 3 months of life in newborn infants (14). Notably, the authors also showed that newborns with advancing gestational age had higher platelet levels at birth (14), suggesting that the platelet parameters are dynamically changing with development during early life. This study also showed a correlation between platelet indexes and lung alveolarization in rats. The lung is an important organ in platelet biogenesis. In humans and rodents around 50% of circulating platelets are generated in the lung (8, 10–12). In the lung, platelets arise in the vascular bed by shedding from megakaryocytes and pro-platelets which embolize in the lungs. Shear stress, turbulence,

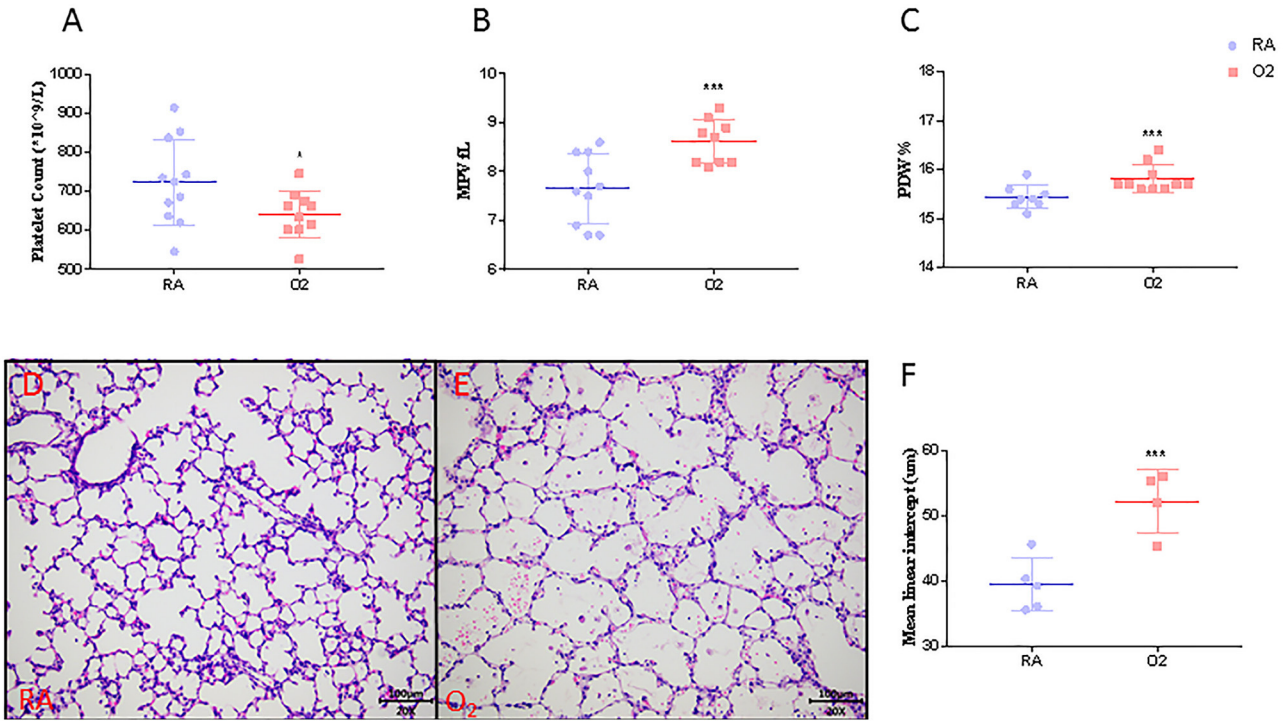

FIGURE 3 | Platelet parameters ($N = 9$–10, **A–C**), mean linear intercept (MLI, $N = 4$–5, **F**) and representative photos of rat pups exposed to room air (RA, **D**) or hyperoxia (O_2, **E**) at postnatal Day 10. Values are expressed as mean ± SD. $^*p < 0.05$, $^{***}p < 0.001$, compared with age-matched RA controls using the student *t*-test. Magnification, 200 x.

and endothelial interaction in the pulmonary vascular bed play an important role in platelet biogenesis by activating shedding from megakaryocytes and pro-platelets (9). During lung development the size of the vascular bed increases, thereby increasing the capacity of platelet synthesis and secretion into the systemic circulation. This explains at least in part the gradual increase in PLT during normal postnatal lung development. Two elegant studies have demonstrated that platelets contribute to embryonic lung development (6) and lung regeneration after pneumonectomy (7), which may explain why the decrease of platelets led to blunted lung development in the current study.

This study showed that platelet counts are significantly lower in infants developing BPD and in rats with experimental BPD induced by hyperoxia. This finding is in line with a study by Okur et al. who reported a lower PLT and PMI in BPD infants during the first week of life (15), but is not supported by Go et al. who report that platelet parameters at birth were not associated with BPD after multivariate analysis (16). This difference might be due to the different timing of these studies. Common pulmonary diseases in adults, including asthma, chronic obstructive pulmonary disease, idiopathic pulmonary fibrosis, and pulmonary hypertension, are not associated with reduced platelet counts (9). This is probably caused by redundancy of the adult pulmonary vascular bed. Only in severe cases of acute respiratory distress syndrome thrombocytopenia was observed, caused by either increased platelet consumption or decreased platelet production (17). PLT largely depend on platelet synthesis and consumption, in which the lung plays an important role. We speculate that in BPD systemic PLT are low because (I) the production of platelets is decreased due to a reduced vascular bed caused by aberrant alveolar and vascular development and lung injury, and (II) increased platelet consumption in the injured lung exposed to hyperoxia.

Previous studies have shown that platelet production may be regulated by oxygen tension. Acute hypoxia in rodents led to a biphasic response with an initial increase, followed by a decrease in platelet counts after 1 week of hypoxia, which may be caused by hypoxia-induced hemoconcentration, platelet activation and vasoconstriction (9, 18, 19). Hyperoxia decreases platelet counts by inhibiting platelet production and enhancing platelet activation for thrombi formation and platelet consumption (20–22). Therefore, there may be a vicious cycle linking platelet production and blunted lung development in the BPD setting (**Figure 6**). However, platelet production and postnatal lung development are both evolving processes, so it is hard to speculate whether decreased platelet biogenesis contributes to BPD, or BPD leads to the reduction of platelets. Well-designed experimental studies are needed to elucidate this interaction.

The study by Henry et al. and our study found a transient increase of MPV in infants during their first 2 weeks of life and then a decrease, which is independent of gestational age at

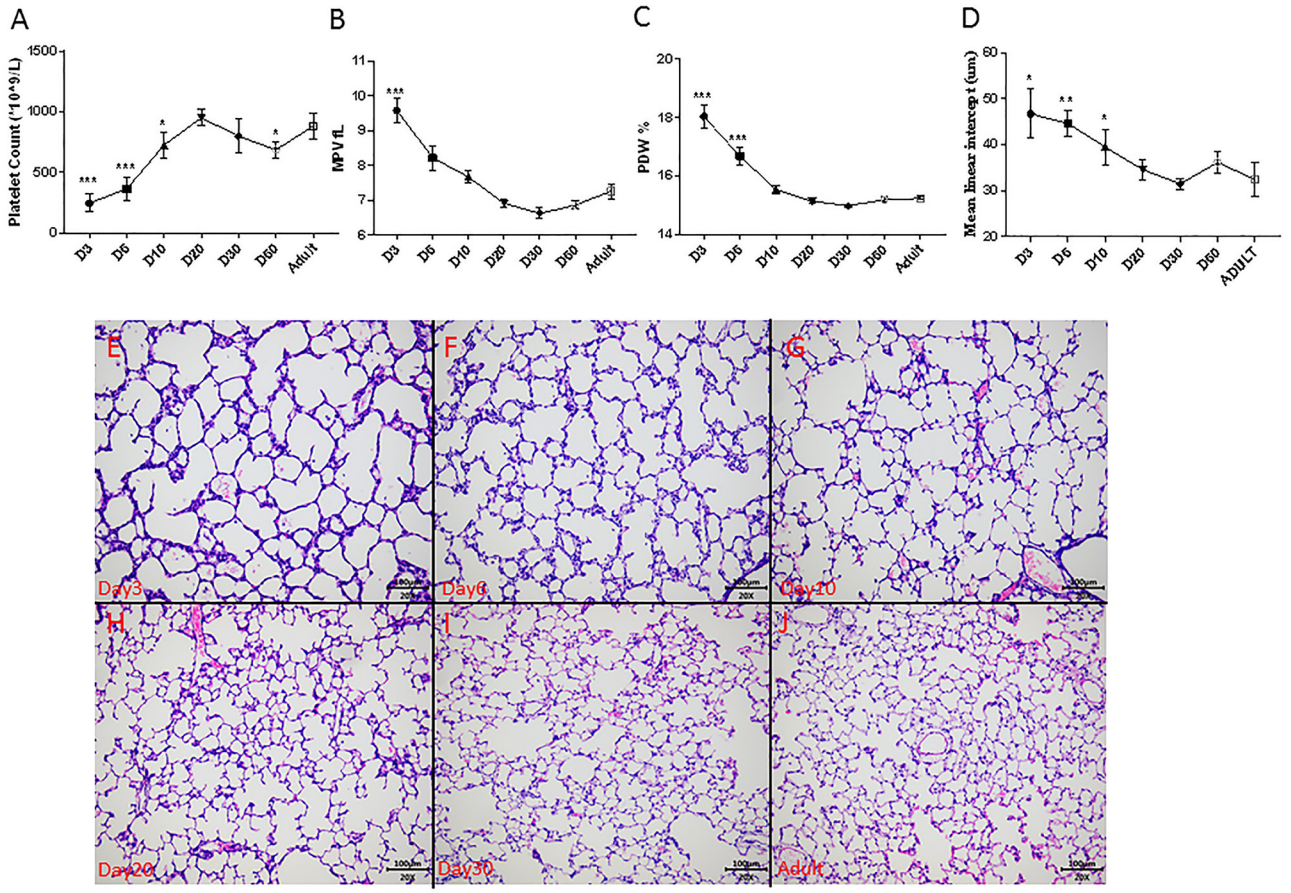

FIGURE 4 | Dynamic change of platelet parameters during lung alveolarization ($N = 8–10$, **A–C**), mean linear intercept (MLI, $N = 3–5$, **D**) and representative photos during rats' development **(E–J)** in normoxia. Values are expressed as mean ± SD. $^{*}p < 0.05$, $^{**}p < 0.01$, $^{***}p < 0.001$, compared with adults using one-way ANOVA. Magnification, 200x.

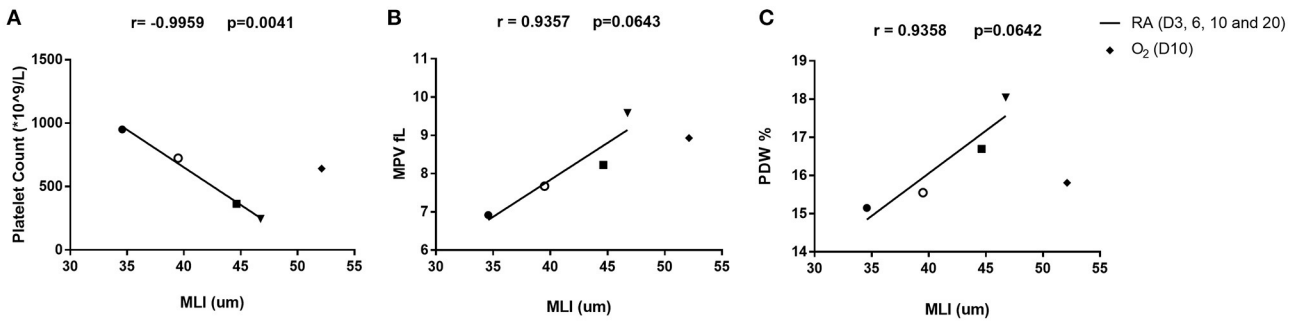

FIGURE 5 | Correlation analysis between platelet parameters and MLI in rats on day 3, 6, 10, and 20 after birth. Correlation between platelet count (PLT) and MLI **(A)**, mean platelet volume (MPV) and MLI **(B)**, platelet distribution width (PDW) and MLI **(C)**. The correlation was analyzed by Pearson correlation using GraphPad Prism version 8. Triangles (▼) indicate 3-day old rats. Squares (■) indicate 6-day old rats. Open circles (○) indicate 10-day old rats and solid circles (●) indicate 20-day old rats. Diamonds (◆) stand for rats exposed to hyperoxia for 10 days in a row. The hyperoxia data were only plotted in the figure but not included in the correlation analysis.

birth (14). However, these findings were inconsistent with the studies from Dani et al. and Cekmez et al. who reported that infants developing BPD had higher MPV levels at 1–3 days of life compared to those without BPD (23, 24). This discrepancy might be attributed to the different time points that platelet parameters were measured. MPV and PDW are both indicators of platelet

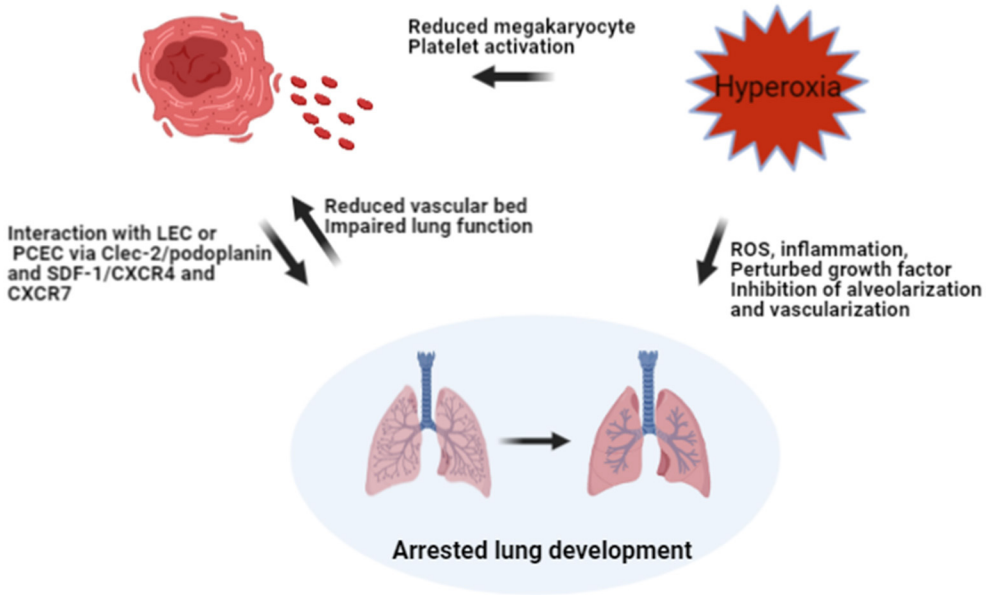

FIGURE 6 | Hypothesis on the interaction between hyperoxia, platelet biogenesis, and lung injury. Hyperoxia may reduce the number of megakaryocytes in the lung and increase platelet consumption by activating platelets, leading to decreased platelet count directly. Hyperoxia may also impair the developing lung by inhibiting alveolarization and vascularization, leading to BPD. The reduction of the vascular bed in BPD, together with impaired lung function might result in reduced shedding of megakaryocytes and pro-platelets trapped in pulmonary capillaries. Meanwhile, reduced PLT may hamper lung development by interacting with LEC and PCEC via ligands and receptors. ROS, reactive oxygen species; LEC, lymphatic endothelial cells; PCEC, pulmonary capillary endothelial cells; Clec-2, C-type lectin-like receptor-2; SDF-1, stromal-cell-derived factor-1; CXCR4 and CXCR7, receptors of SDF-1 on PCEC.

size, indicating platelets are being produced or activated. In the animal experiment, we observed an increase in MPV and PDW in oxygen-exposed rats, which might indicate more platelets are activated in these pups. In BPD infants, we also observed a lower platelet count and a higher MPV at postnatal week 2, which might indicate more platelets are activated in these infants. Besides, we also observed a physiological increase in MPV in these infants, the mechanism under this phenomenon still needs investigation. We speculate that platelet parameters in the first days after birth are prone to be affected by the neonatal transition and medical treatments. Therefore, the analysis of platelet parameters over the clinically defined time window of BPD may provide more reliable evidence.

There are several limitations to this study. The most relevant one is that the direct correlation between impaired platelet formation and arrested lung development was not studied. Besides, we could not evaluate the effect of hyperoxia itself on platelet parameters in extremely premature infants due to the complexity of their clinical condition. Moreover, platelet parameters in rats exposed to hyperoxia were only measured on day 10. It would be interesting to track the interaction between platelet parameters and lung development for a longer period.

In conclusion, clinical and experimental BPD are significantly associated with lower platelet levels. The physiological increase of platelet counts synchronizes with postnatal alveolarization in neonatal rats. Understanding the role of platelets in neonatal lung development may shed new light on BPD prevention in clinics.

DATA AVAILABILITY STATEMENT

The raw data supporting the conclusions of this article will be made available by the authors, without undue reservation.

ETHICS STATEMENT

The studies involving human participants were reviewed and approved by the Institutional Ethical Committee of Shenzhen Maternity and Child Healthcare Hospital. Written informed consent for participation was not provided by the participants' legal guardians/next of kin because: Acquirement of informed consent was waived given that no personal data were explicitly reported. The animal study was reviewed and approved by the Institutional Animal Care and Use Committee of Shenzhen Institutes of Advanced Technology of the Chinese Academy of Sciences.

AUTHOR CONTRIBUTIONS

CY, FW, and XC conceptualized and designed the study and wrote the first draft of the manuscripts. XC, JZho, and FY carried out the clinical data collection. XC and JZha performed the data

analysis. GW, CY, and FW reviewed and revised the manuscripts. All authors read and approved the final manuscript.

FUNDING

This study was supported by Guangdong Basic and Applied Science Committee (2019A1515110614 to XC); Shenzhen Fund for Guangdong Provincial Highlevel Clinical Key Specialties (SZGSP009) and Shenzhen Science and Technology Innovation Committee (JCYJ20190809170219163 to CY).

ACKNOWLEDGMENTS

We kindly acknowledged Chun Chen for her help in data preparation.

REFERENCES

1. Hwang JS, Rehan VK. Recent advances in bronchopulmonary dysplasia: pathophysiology, prevention, and treatment. *Lung.* (2018) 196:129–38. doi: 10.1007/s00408-018-0084-z
2. Stoll BJ, Hansen NI, Bell EF, Walsh MC, Carlo WA, Shankaran S, et al. Trends in care practices, morbidity, and mortality of extremely preterm neonates, 1993-2012. *JAMA.* (2015) 314:1039–51. doi: 10.1097/01.aoa.0000482610.95044.1b
3. Bancalari E, Jain D. Bronchopulmonary dysplasia: 50 years after the original description. *Neonatology.* (2019) 115:384–91. doi: 10.1159/000497422
4. Morty RE. Recent advances in the pathogenesis of BPD. *Semin Perinatol.* (2018) 42:404–12. doi: 10.1053/j.semperi.2018.09.001
5. Naeem A, Ahmed I, Silveyra P. Bronchopulmonary dysplasia: an update on experimental therapeutics. *Europ Med J.* (2019) 4:20–9.
6. Tsukiji N, Inoue O, Morimoto M, Tatsumi N, Nagatomo H, Ueta K, et al. Platelets play an essential role in murine lung development through Clec-2/podoplanin interaction. *Blood.* (2018) 132:1167–79. doi: 10.1182/blood-2017-12-823369
7. Rafii S, Cao Z, Lis R, Siempos, II, Chavez D, et al. Platelet-derived SDF-1 primes the pulmonary capillary vascular niche to drive lung alveolar regeneration. *Nat Cell Biol.* (2015) 17:123–36. doi: 10.1038/ncb3096
8. Lefrancais E, Ortiz-Munoz G, Caudrillier A, Mallavia B, Liu F, Sayah DM, et al. The lung is a site of platelet biogenesis and a reservoir for haematopoietic progenitors. *Nature.* (2017) 544:105–9. doi: 10.1038/nature21706
9. Lefrançais E, Looney MR. Platelet biogenesis in the lung circulation. *Physiology.* (2019) 34:392–401. doi: 10.1152/physiol.00017.2019
10. Kaufman RM, Airo R, Pollack S, Crosby WH. Circulating megakaryocytes and platelet release in the lung. *Blood.* (1965) 26:720–31. doi: 10.1182/blood.V26.6.720.720
11. Levine RF, Eldor A, Shoff PK, Kirwin S, Tenza D, Cramer EM. Circulating megakaryocytes: delivery of large numbers of intact, mature megakaryocytes to the lungs. *Eur J Haematol.* (1993) 51:233–46. doi: 10.1111/j.1600-0609.1993.tb00637.x
12. Pedersen NT. Occurrence of megakaryocytes in various vessels and their retention in the pulmonary capillaries in man. *Scand J Haematol.* (1978) 21:369–75. doi: 10.1111/j.1600-0609.1978.tb00381.x
13. Chen X, Orriols M, Walther FJ, Laghmani EH, Hoogeboom AM, Hogen-Esch ACB, et al. Bone morphogenetic Protein 9 protects against neonatal hyperoxia-induced impairment of alveolarization and pulmonary inflammation. *Front Physiol.* (2017) 8:486. doi: 10.3389/fphys.2017.00486
14. Henry E, Christensen RD. Reference intervals in neonatal hematology. *Clin Perinatol.* (2015) 42:483–97. doi: 10.1016/j.clp.2015.04.005
15. Okur N, Buyuktiryaki M, Uras N, Oncel MY, Ertekin O, Canpolat FE, et al. Platelet mass index in very preterm infants: can it be used as a parameter for neonatal morbidities? *J Matern Fetal Neonatal Med.* (2016) 29:3218–22. doi: 10.3109/14767058.2015.1121475
16. Go H, Ohto H, Nollet KE, Takano S, Kashiwabara N, Chishiki M, et al. Using platelet parameters to anticipate morbidity and mortality among preterm neonates: a retrospective study. *Front Pediatrics.* (2020) 8:90. doi: 10.3389/fped.2020.00090
17. Wei Y, Tejera P, Wang Z, Zhang R, Chen F, Su L, et al. A missense genetic variant in LRRC16A/CARMIL1 improves acute respiratory distress syndrome survival by attenuating platelet count decline. *Am J Respir Critic Care Med.* (2017) 195:1353–61. doi: 10.1164/rccm.201605-0946OC
18. McDonald TP, Cottrell M, Clift R. Effects of short-term hypoxia on platelet counts of mice. *Blood.* (1978) 51:165–75. doi: 10.1182/blood.V51.1.165.bloodjournal511165
19. Jackson CW, Edwards CC. Biphasic thrombopoietic response to severe hypobaric hypoxia. *Br J Haematol.* (1977) 35:233–44. doi: 10.1111/j.1365-2141.1977.tb00580.x
20. Yang J, Yang M, Xu F, Li K, Lee SKM, Ng P-C, et al. Effects of oxygen-induced lung damage on megakaryocytopoiesis and platelet homeostasis in a rat model. *Pediatr Res.* (2003) 54:344–52. doi: 10.1203/01.PDR.0000079186.86219.29
21. Barazzone C, Tacchini-Cottier F, Vesin C, Rochat AF, Piguet PF. Hyperoxia induces platelet activation and lung sequestration: an event dependent on tumor necrosis factor-alpha and CD11a. *Am J Respir Cell Mol Biol.* (1996) 15:107–14. doi: 10.1165/ajrcmb.15.1.8679214
22. Passmore MR, Ki KK, Chan CHH, Lee T, Bouquet M, Wood ES, et al. The effect of hyperoxia on inflammation and platelet responses in an ex vivo extracorporeal membrane oxygenation circuit. *Artif Organs.* (2020) 44:1276–85. doi: 10.1111/aor.13771
23. Dani C, Poggi C, Barp J, Berti E, Fontanelli G. Mean platelet volume and risk of bronchopulmonary dysplasia and intraventricular hemorrhage in extremely preterm infants. *Am J Perinatol.* (2011) 28:551–6. doi: 10.1055/s-0031-1274503
24. Cekmez F, Tanju IA, Canpolat FE, Aydinoz S, Aydemir G, Karademir F, et al. Mean platelet volume in very preterm infants: a predictor of morbidities? *Eur Rev Med Pharmacol Sci.* (2013) 17:134–7.

Conflict of Interest: The authors declare that the research was conducted in the absence of any commercial or financial relationships that could be construed as a potential conflict of interest.

Copyright © 2021 Chen, Zhong, Han, Yao, Zhao, Wagenaar, Yang and Walther. This is an open-access article distributed under the terms of the Creative Commons Attribution License (CC BY). The use, distribution or reproduction in other forums is permitted, provided the original author(s) and the copyright owner(s) are credited and that the original publication in this journal is cited, in accordance with accepted academic practice. No use, distribution or reproduction is permitted which does not comply with these terms.

frontiers in Medicine

REVIEW
published: 07 May 2021
doi: 10.3389/fmed.2021.651552

The Role of Ferroptosis in Acute Respiratory Distress Syndrome

Mengdi Qu†, Hao Zhang†, Zhaoyuan Chen, Xingfeng Sun, Shuainan Zhu, Ke Nan, Wankun Chen* and Changhong Miao**

Department of Anesthesiology, Zhongshan Hospital, Fudan University, Shanghai, China

Ferroptosis is a newly discovered type of regulated cell death that is different from apoptosis, necrosis and autophagy. Ferroptosis is characterized by iron-dependent lipid peroxidation, which induces cell death. Iron, lipid and amino acid metabolism is associated with ferroptosis. Ferroptosis is involved in the pathological development of various diseases, such as neurological diseases and cancer. Recent studies have shown that ferroptosis is also closely related to acute lung injury (ALI)/ acute respiratory distress syndrome (ARDS), suggesting that it can be a novel therapeutic target. This article mainly introduces the metabolic mechanism related to ferroptosis and discusses its role in ALI/ARDS to provide new ideas for the treatment of these diseases.

Keywords: ferroptosis, acute respiratory distress syndrome, metabolism, inflammation, oxidative stress

OPEN ACCESS

Edited by:
Mandy Laube,
Leipzig University, Germany

Reviewed by:
Brent Stockwell,
Columbia University, United States
Claudio Romero Farias Marinho,
University of São Paulo, Brazil

***Correspondence:**
Wankun Chen
chenwank@163.com
Changhong Miao
miaochangh@163.com
Hao Zhang
fuscc_anesthesia@yeah.net

†These authors have contributed equally to this work

Specialty section:
This article was submitted to Pulmonary Medicine, a section of the journal Frontiers in Medicine

Received: *10 January 2021*
Accepted: *12 April 2021*
Published: *07 May 2021*

Citation:
Qu M, Zhang H, Chen Z, Sun X, Zhu S, Nan K, Chen W and Miao C (2021) The Role of Ferroptosis in Acute Respiratory Distress Syndrome. Front. Med. 8:651552. doi: 10.3389/fmed.2021.651552

INTRODUCTION

Ferroptosis, a new form of regulated cell death that can be triggered by erastin or RSL3 [(1S,3R)-RSL3], was first reported in 2012 by Dixon (1). Ferroptosis is characterized by the iron-dependent accumulation of lethal levels of lipid peroxides, while the morphology, biology and genetics are obviously different from those of apoptosis, necrosis, autophagy, and other forms of cell death (1). Amino acid, iron and lipid peroxide metabolism and other metabolic processes are closely related to ferroptosis (2). Studies have shown that ferroptosis, as the main cause of organ damage-related cell death, is involved in many pathological processes, such as neurodegenerative diseases, cancer and ischemia-reperfusion injury (2, 3).

Acute lung injury (ALI), resulting from both direct (e.g., pneumonia) and indirect (e.g., sepsis) pulmonary injuries, refers to pulmonary edema and atelectasis caused by diffuse alveolar-capillary injury and is characterized by refractory hypoxemia and pulmonary infiltration (4). Acute respiratory distress syndrome (ARDS) is a serious form of ALI and is described by the 2012 Berlin unified definition (5). The prevalence of ARDS in intensive care units is 10.4%, and there is a high mortality rate (35–46%) (6) but a lack of effective treatments (7).

In recent years, the role of ferroptosis in ARDS has been gradually revealed, and increasing attention has been given to the importance of regulating ferroptosis in the treatment of ARDS.

MAJOR METABOLIC MECHANISMS OF FERROPTOSIS

Ferroptosis is a form of cell death that is regulated by multiple genes and involves multiple metabolic processes, such as iron homeostasis, amino acid metabolism and lipid peroxidation. The mechanism is very complex as is shown in **Figure 1**, and it will be better explained in the following aspects.

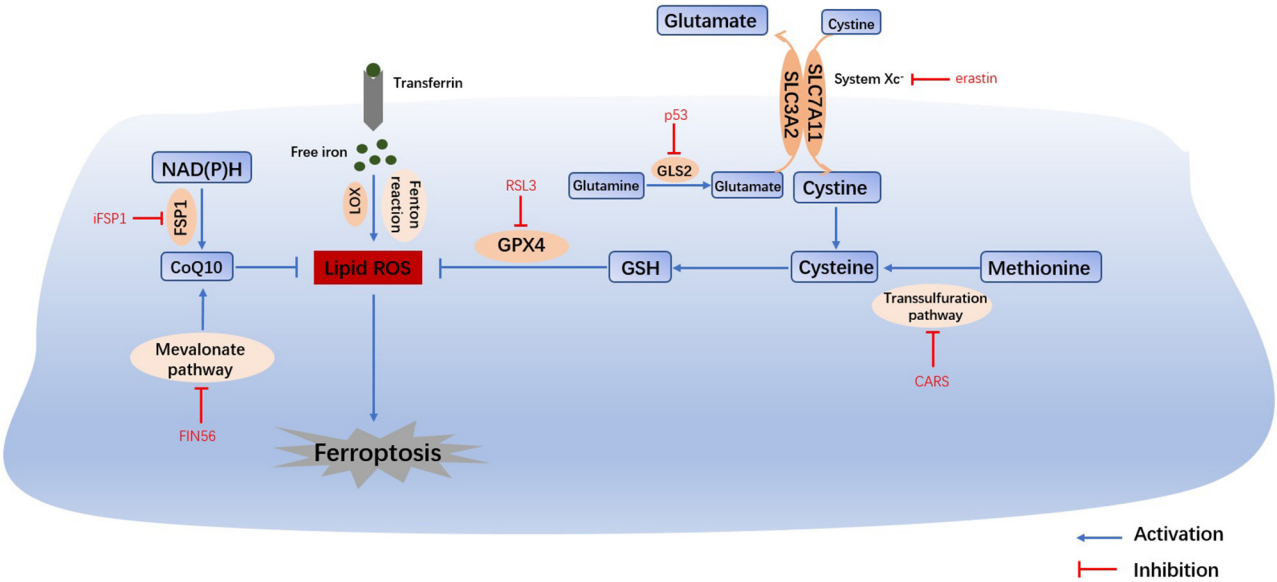

FIGURE 1 | Main mechanisms of ferroptosis. The Fenton reaction, LOX and PUFAs facilitate the generation of lipid ROS. Cysteine can be generated from the uptake of cystine via system Xc- or the transsulfuration pathway. Amino acid metabolism and NAD(P)H, suppresses the synthesis of GSH and CoQ10, thus inhibiting the reduction in lipid ROS. The accumulation of lipid ROS leads to ferroptosis. Therefore, iron homeostasis, lipid peroxidation and amino acid metabolism are the main regulators of ferroptosis. System Xc-, cystine/glutamate transporter; GLS, glutaminase; GSH, glutathione; GPX4, glutathione peroxidase 4; LOX, lipoxygenase; FSP1, ferroptosis suppressor protein 1; CoQ10, coenzyme Q10.

IRON METABOLISM

Iron overload is one of the key events in ferroptosis. Iron is necessary for the accumulation of lipid peroxides, and iron ingestion, storage and transport all affect ferroptosis (2). Iron homeostasis is regulated by a series of iron regulatory proteins (IRPs). Extracellular iron enters the cell through transferrin (TF) and its receptors, and then Fe^{2+} can produce lipid peroxides via the Fenton reaction or the iron-containing enzyme lipoxygenase (LOX) (8). Most intracellular Fe^{2+} is stored in ferritin (FT), and so there is very little free Fe^{2+} (9). The degradation of FT increases the level of intracellular Fe^{2+}, enhances lipid peroxidation, and induces ferroptosis. This process is related to autophagy and is regulated by nuclear receptor coactivator 4 (NCOA4) (8). Iron response element binding protein 2 (IREB2) (1) and other proteins related to iron metabolism (2) (HSPB1, CISD1, etc.) can also increase the sensitivity of cells to ferroptosis.

AMINO ACID METABOLISM

Glutathione (GSH) depletion is another key event in ferroptosis. The cystine/glutamate antiporter System Xc-, which is mainly composed of SLC3A2 (solute carrier family 3 member 2) and SLC7A11 (solute carrier family 7 member 11) (10), is located on the cell membrane and transports extracellular cystine and intracellular glutamate at a ratio of 1:1. Extracellular cystine and intracellular cysteine are essential for the biosynthesis of GSH. Cystine ultimately generates GSH through a series of enzymatic reactions, and GSH is the essential substrate for glutathione peroxide enzyme 4 (GPX4) to degrade phospholipid hydroperoxide (PLOOH) (11). GPX4 is at the intersection of GSH metabolism and lipid peroxidation, both of which are related to ferroptosis. Downregulation of SLC7A11 can also lead to ferroptosis through a decrease in GPX4 activity (12). In addition, methionine can transfer sulfur atoms to serine to generate cysteine through the transsulfuration pathway, which can be upregulated by the knockout of cysteinyl-tRNA synthetase (CARS), thus making cells resistant to ferroptosis (13).

Under physiological conditions, a high level of extracellular glutamate can inhibit the activity of System Xc- and prevent the uptake of cysteine (14). Therefore, glutamate is a natural trigger for ferroptosis and has the same effect as erastin and other System Xc- inhibitors (8). In addition, glutamine is abundant in tissue and plasma and can be converted into glutamate by glutaminase (GLS1 and GLS2) catalysis. Glutaminolysis is necessary for the tricarboxylic acid cycle and lipid biosynthesis, and α-ketoglutarate, as the product of decomposition, is involved in ferroptosis (15). Therefore, when glutamine is deficient or its decomposition is inhibited, reactive oxygen species (ROS) accumulation, lipid peroxidation and ferroptosis are also inhibited. Furthermore, GLS2, as a target gene of the tumor suppressor p53, is closely related to ferroptosis (16). In summary, the metabolism of amino acids (especially glutamate and cystine) plays an important role in the pathological process of ferroptosis.

LIPID METABOLISM

The most prominent feature of ferroptosis is plasma membrane damage caused by the production of iron-dependent lipid peroxides (lipid ROS) (8). ROS include products of oxygen reduction, such as O^{2-}, H_2O_2 and ·OH. Oxygen homeostasis is crucial to normal cellular functions, and the abnormal accumulation of ROS is harmful to the body (3). During ferroptosis, the reduction reaction mediated by GPX4 and ferroptosis suppressor protein 1 (FSP1, formerly known as mitochondrial apoptosis inducing factor 2, AIFM2) is inhibited, and the oxidation reaction catalyzed by Fe^{2+} and a series of iron-dependent enzymes (mainly LOX) is enhanced, inducing the accumulation of polyunsaturated fatty acids (PUFAs) (8). Then, lipid peroxidation drove by PUFAs increases the permeability of the cell membrane and makes the cell more sensitive to oxidation, which eventually leads to ferroptosis (17, 18). The inhibition of lipid peroxidation and the consumption of PUFAs can inhibit ferroptosis (2).

THE FSP1-NAD(P)H PATHWAY

Bersuker and Doll found that FSP1 and GPX4 had a strong synergistic effect (19, 20). In the FSP1-NAD(P)H pathway, coenzyme Q10 (CoQ10) can reduce lipid peroxidation by inhibiting the accumulation of free radicals, and FSP1 catalyzes the production of CoQ10 through NAD(P)H. iFSP1, an inhibitor of FSP1, can induce ferroptosis in cells that overexpress FSP1 (20). In conclusion, the FSP1-CoQ10-NAD(P)H pathway cooperates with GPX4 and GSH to inhibit lipid peroxidation and ferroptosis. Moreover, CoQ10 can also be generated by the mevalonate (MVA) pathway. FIN56 can not only accelerate the degradation of GPX4 but also consume CoQ10 by affecting the MVA pathway, ultimately leading to excessive lipid peroxide accumulation and ferroptosis (21).

PATHOGENESIS OF ARDS

Pathological Mechanism of ARDS

The most common cause of ARDS is bacterial or viral pneumonia, while sepsis, severe trauma and gastric reflux and aspiration are also common factors (22). The inflammatory response is activated by infection, trauma, or damage to the lung. Moderate inflammation is conducive to the clearance of pathogens, but excessive inflammation may lead to alveolar damage and increased permeability of the pulmonary capillary endothelium and alveolar epithelium, after which protein-rich fluid exudes from the alveolar cavity, leading to pulmonary edema (22). Therefore, ARDS is the pulmonary manifestation of systemic inflammatory response syndrome (SIRS) (23), which involves various inflammatory cells (macrophages, neutrophils, vascular endothelial cells, and platelets), and the inflammatory mediators and cytokines released by these cells indirectly mediate inflammation in the lung.

The levels of proinflammatory cytokines (IL-1β, IL-8, TNFα, TGFβ1, etc.) are very high in the pulmonary edema fluid in ARDS patients, and cytokines can activate the innate immune system. Activated neutrophils can produce toxic substances such as ROS and proteases, leading to pulmonary endothelial and alveolar epithelial damage and even necrosiss (24). Necrosis and the accumulation of edema fluid, in turn, trigger more severe inflammation and immune responses. Many clinical trials have evaluated the potential effect of anti-inflammatory therapy to treat ARDS (25–27). In summary, excessive inflammation and increased permeability of the pulmonary capillary endothelium and alveolar epithelium lead to alveolar damage, which is the main pathological mechanism of ARDS.

Iron Overload

Various cell types in the lung, including epithelial cells and macrophages, can produce iron metabolism-related proteins to regulate iron homeostasis and protect lung tissue from oxidative stress (28). Iron metabolism disorders are closely related to lung tissue damage in ARDS patients (29, 30); that is, too much iron can generate ROS and cytotoxicity through the Fenton reaction. Many clinical studies have shown that the severity of ARDS is associated with the levels of iron and iron-related proteins (31). One study indicated that iron in blood products leads to an increase in iron in blood recipients, which promotes the occurrence of blood transfusion-related ALI (32). Elevated levels of Fe^{2+} and iron regulators, such as TF and FT, can be detected in the bronchoalveolar lavage fluid (BALF) of ARDS patients (28, 29, 33–35). In an oleic acid-induced ALI model in mice, iron overload was detected in the lung tissue (36). Moreover, supplementing mice with iron in advance exacerbates damage to the lung (12). A recent study also showed that increased apoptosis in mice with iron overload exacerbated ALI. However, this effect was quite transient and did not affect the degree of inflammation or speed of recovery in ALI (37). Ferroptosis is an iron-dependent process, and iron overload is the driving factor of it. In ARDS, iron overload leads to ferroptosis, which aggravates lung injury. In other words, the cells appear to be overloaded with iron due to ferroptosis and the disease becomes increasingly worse. Therefore, we have enough reason to believe that ferroptosis plays a crucial role in ARDS. And whether iron overload actually causes lung injury or is just a byproduct of ferroptosis remains to be confirmed.

Oxidative Stress

Exhaled breath analysis is expected to be clinically used for the early diagnosis and prediction of ARDS, and most candidate markers are related to oxidative stress (38). Oxidative stress causes damage to the barriers of the pulmonary epithelium and endothelium, and neutrophils accumulate in large quantities in the alveolar fluid, producing proinflammatory cytokines and ROS. Moreover, ROS can further increase the level of cytokines, exacerbating tissue damage and edema. Therefore, oxidative stress plays an important role in the pathogenesis of ARDS (39, 40). ROS are known as important mediators of ARDS (41–44), and enzymes related to the production of ROS (xanthine oxidase (XOR) (45), endothelial nitric oxide synthase (eNOS) (46), cytochrome P450 (CYP) (7), and NADPH oxidase (NOX) (47)) have been reported to be involved in ARDS. The level of malondialdehyde (MDA), a product of lipid peroxidation, is

increased in the ALI mouse model (36, 48). In fact, MDA is commonly regarded as a marker of ferroptosis. Increases in both neutrophils and ROS can be detected in ARDS patients (49).

GSH is the most important antioxidant in the airway epithelium and exerts antioxidant effects through the removal of ROS (50) and the repair of cellular damage (51), thus helping to alleviate inflammation (52). Decreased GSH and increased oxidized GSH (GSSG) were observed in both ALI patients and animal models (12, 36, 42). A lack of GSH in alveolar fluid made ARDS patients more susceptible to lung injury (49). Moreover, ROS and GSH metabolism is the main feature of ferroptosis. Whether these metabolic processes are also involved in the pathogenesis of ARDS by regulating ferroptosis needs to be investigated. Inhibition of ferroptosis can inhibit the production of these peroxides, thus reducing the severity of ARDS, which is a potential therapeutic strategy.

Role of Ferroptosis in ARDS

Indicators related to ferroptosis were detected in ALI animal models, including increased Fe^{2+}, ROS, MDA and decreased GSH. And inhibitors of ferroptosis have the potential to alleviate lung damage. These results show that ferroptosis is indeed associated with ARDS. However, the specific mechanism by which ferroptosis affects the onset of ARDS is still unclear.

As a clinically common respiratory disease, the main pathogenic mechanism of ARDS is the apoptosis of alveolar epithelial cells and pulmonary microvascular endothelial cells and the polarization of alveolar macrophages. Then, a large amount of ROS and inflammatory factors trigger an imbalance between the oxidation and antioxidant systems, and the "cytokine storm" leads to the disturbance in the local microenvironment of the lungs, resulting in a series of inflammatory reactions (53). Unlike apoptosis, ferroptosis is associated with a consistent release of damage-associated molecular patterns (DAMPs) and inflammatory cytokines, which promote a series of inflammatory responses. Therefore, ferroptosis is considered an immunogenic form of cell death (54). Inflammatory cytokines further promote ferroptosis and other forms of cell death, thus forming a self-amplifying loop that mutually promotes organ damage (55). Ferroptosis plays a key role in ALI in mice, and ferroptosis inducers can exacerbate pulmonary edema and alveolar inflammation, accompanied by high levels of cytokines (IL-1β, IL-6, and TNF-α), while these effects can be reversed by ferroptosis inhibitors (12, 41, 48). In the latest study (36), ARDS animal model was prepared by injecting oleic acid into the tail vein of mice. The results showed that the pulmonary cells of ARDS group showed mitochondrial shrinkage and rupture of the mitochondrial membrane. In addition, iron overload, GSH depletion and down-regulated expression of ferritin appeared in lung tissues. Similar results were observed in the model of lung ischemia-reperfusion injury (56). The above results suggest that ferroptosis is involved in the pathogenesis of lung injury, which will provide a new theoretical basis for the clinical treatment of ARDS. However, no clinical studies have examined the association of these ferroptosis indicators with severity and prognosis of ARDS.

Ferroptosis is one of the critical mechanisms contributing to sepsis-induced injuries in mice models, including heart, liver, intestine, and the inhibition of ferroptosis via enhancing GPX4 or nuclear factor erythroid 2-related factor 2 (Nrf2) alleviates these injuries (57–60). It contradicts that erastin attenuates the inflammatory response, resulting in inhibition of sepsis development (61). So what is the real role of ferroptosis? We know that sepsis is also an important inducer of ARDS, so it is natural to consider the role of ferroptosis in sepsis-induced lung injury. Furthermore, the lipid peroxidation in ferroptosis drives pyroptosis, indicating a crosstalk between ferroptosis and other forms of cell death in sepsis, and such interactions may also exist in ARDS (62).

Ultimately, ferroptosis causes cellular injury primarily through inflammation and oxidative stress, and the NOD-like receptor protein 3 (NLRP3) inflammasome and Nrf2 are key molecules in these processes (12, 41, 42, 63, 64). Both of them are important regulatory molecule in ARDS and can be used as targets for the treatment of ARDS (65–71). Of course, they could be recognized as mediators of ferroptosis in ARDS, as shown in **Figure 2**. Ferroptosis may promote inflammation and swelling of alveolar epithelial cells via the NLRP3 inflammasome, bringing about ARDS. NLRP3 is a key mediator in the process of pyroptosis, so crosstalk between ferroptosis and pyroptosis may occur in the pathogenesis of ARDS, aggravating lung injury. Further animal experiments and clinical studies are needed to verify these points. The regulation of the NLRP3 inflammasome by inhibiting ferroptosis to thereby alleviate ARDS may also be a new therapeutic strategy.

At the same time, recent studies have shown that Nrf2 inhibits ferroptosis by regulating the expression of SLC7A11 and heme oxygenase-1 (HO-1), thus alleviating lung injury (12, 64). Nrf2 activators can cause a reduction in ROS and prevent GSH depletion and lipid peroxide accumulation. As a result, ferroptosis is inhibited, thereby alleviating ALI and producing the same effect as that of Fer-1 (42). In addition, inhibitor of apoptosis-stimulating protein of p53 (iASPP) could inhibit ferroptosis and ALI by upregulating Nrf2. Furthermore, the levels of a variety of proinflammatory cytokines (TNF-α, IL-1β, and IL-6) were also decreased (41).

In balance, most studies have not directly focused on the relationship between ferroptosis and ARDS. Therefore, the direct relationship between them needs to be explored, together with more treatments targeting ferroptosis.

Ferroptosis Applications in ARDS Therapy

Disorders of iron homeostasis, the depletion of GSH, and oxidative stress are the key points leading to ferroptosis and could be used as targets for the treatment of ARDS (**Figure 3**).

Iron Chelators

Iron chelators (deferoxamine, deferiprone, and deferasirox), especially deferoxamine (DFO), have been approved by the FDA for the treatment of iron overload (72). In various animal models of infection, DFO has immunomodulatory effects to resist pathogens such as bacteria, viruses, and fungi, in addition to chelating iron (73). DFO can reduce the levels

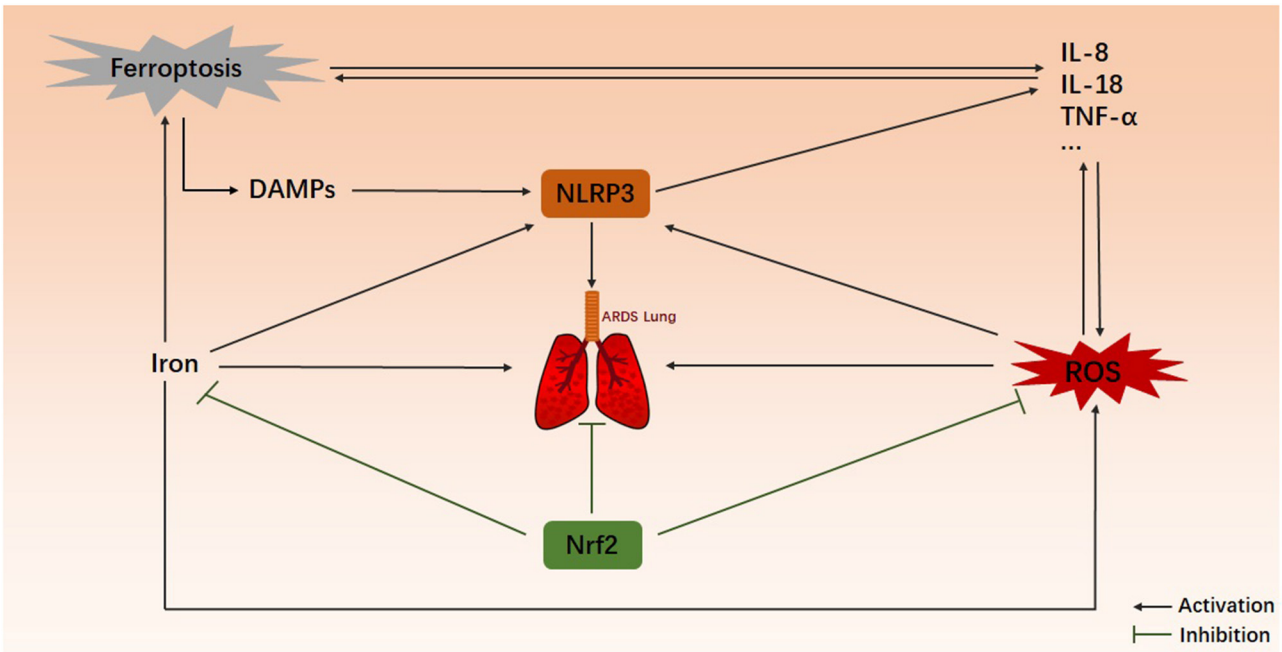

FIGURE 2 | Possible relationship between ferroptosis and ARDS. Here is an ARDS lung. DAMPs, ROS, and iron overload contribute to ARDS, and they can activate the NLRP3 inflammasome, which promotes the maturation and secretion of inflammatory factors, forming a self-amplifying loop with ferroptosis. Nrf2 inhibits the generation of ROS and iron to negatively regulate ferroptosis. However, the direct link between ferroptosis and ARDS is unclear. DAMPs, damage-associated molecular patterns; ROS, reactive oxygen species; NLRP3, NOD-like receptor protein 3; Nrf2, nuclear factor erythroid 2-related factor 2.

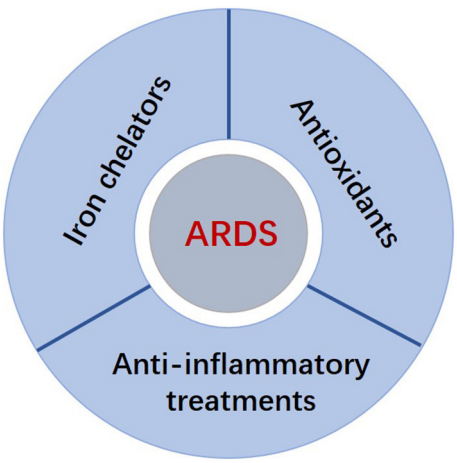

FIGURE 3 | Treatments for ARDS. Therapeutic targets for ARDS associated with ferroptosis, such as iron chelators, antioxidants and anti-inflammatory treatments.

of inflammatory cytokines and ROS *in vitro*, exerting anti-inflammatory effects (74). DFO inhalation was shown to improve pulmonary fibrosis and prevent a decline in pulmonary function in mice (75). Simultaneous perfusion of DFO and FT could attenuate leakage syndrome in isolated mouse lungs (76). In summary, iron chelators may also be effective in treating ARDS, and the mechanism may be related to the suppression of ferroptosis.

Antioxidants

Antioxidants can reduce the severity of ARDS (7). Several kinds of drugs decrease the levels of lipid peroxidation and ROS, attenuate inflammation and oxidative stress, and ultimately alleviate ARDS in mice and improve gas exchange (77–80). GSH supplementation could significantly alleviate mitochondrial dysfunction and oxidative damage in the LPS-induced ALI model (81). Animal experiments and clinical studies have shown that regulating the level of GSH (82) via N-acetylcysteine (NAC) could promote the production of GSH and alleviate ALI (7). NAC treatment resulted in increased pulmonary compliance and reduced pulmonary edema (83). In New York, two patients with ARDS caused by COVID-19 showed significant relief of dyspnea after oral and intravenous GSH supplementation, demonstrating that this is indeed a new treatment strategy for ARDS (52). Given the importance of GSH in ferroptosis, it is also worth investigating whether GSH plays a role in the treatment of ARDS by inhibiting ferroptosis.

Anti-inflammatory Treatments

Inhibiting inflammation is an important treatment strategy for ARDS. Combined inhibition of ferroptosis and inflammation has been reported to treat a variety of diseases, such as stroke, myocardial infarction, and

pancreatitis (54, 55). In ALI mouse models, ferroptosis inhibitors reduced inflammatory cytokines and pulmonary edema to treat ALI (41, 48). The exact mechanism of ferroptosis and inflammation needs to be confirmed by additional experiments, and ways to modulate inflammation by controlling ferroptosis also need to be further explored. These studies will provide new strategies for the clinical treatment of ARDS.

Perspective

Ferroptosis is a newly discovered form of cell death, and ferroptosis regulators provide new therapeutic directions for many refractory diseases (84). Ferroptosis is an abnormal metabolic process involving iron, lipids and amino acids, and the metabolism of these substances plays a key role in cell proliferation and differentiation. Ferroptosis is characterized by metabolic imbalances and disturbances in redox homeostasis, in which the metabolic process is not independent, but a part of a complex metabolic network. The results of animal experiments and clinical trials preliminarily show that a variety of diseases and pathological processes are closely related to ferroptosis, and intervention in ferroptosis can effectively delay the progression of the disease and improve clinical symptoms to a certain extent. However, research on ferroptosis is still in its infancy. Studies on ferroptosis and lung cancer have made some progress, and ferroptosis inducers as new adjuvants based on traditional treatments have shown their effectiveness. The development of new ferroptosis inducers and the application of multiple forms of combined treatment strategies may be expected to provide new ideas for the treatment of lung cancer.

Recent studies have shown that ferroptosis is closely related to ALI/ARDS, making it a potential target for the treatment of ALI/ARDS. The current studies are based on animal models, while there is a lack of clinical studies. In this context, it is worth noting that the precise role of ferroptosis in the development of ALI/ARDS, and the pharmacological inhibition of ferroptosis, but not necroptosis or apoptosis, protects lung tissues from injury, which remains to be fully elucidated. Considering that ferroptosis was proposed as a brand new concept, there are still large gaps that need to be filled. Clinically, whether the key molecules of ferroptosis can be used as biomarkers to predict the severity of ARDS are needed to investigate. Also, it is necessary to prove whether ferroptosis is the core mode of cell death in ARDS and their crosstalk mechanism.

AUTHOR CONTRIBUTIONS

MQ and HZ: conception and design. All authors: manuscript writing and Final approval of manuscript.

FUNDING

This research was supported by the National Key Research and Development Program of China (NO. 2020YFC2008400, 2020YFC2008403), National Natural Science Foundation of China (NO. 81873948, 81871591), Clinical Research Plan of SHDC (NO. SHDC2020CR4064, SHDC2020CR1005A, SHDC12018105), Key Technology and Development Program of Shanghai (NO.17411963400), Talent Program of Fudan University (JIF159607), Shanghai Sailing Program (21YF1406800).

REFERENCES

1. Dixon SJ, Lemberg KM, Lamprecht MR, Skouta R, Zaitsev EM, Gleason CE, et al. Ferroptosis: an iron-dependent form of nonapoptotic cell death. *Cell.* (2012) 149:1060–72. doi: 10.1016/j.cell.2012.03.042
2. Stockwell BR, Friedmann Angeli JP, Bayir H, Bush AI, Conrad M, Dixon SJ, et al. Ferroptosis: a regulated cell death nexus linking metabolism, redox biology, and disease. *Cell.* (2017) 171:273–85. doi: 10.1016/j.cell.2017.09.021
3. Gao M, Jiang X. To eat or not to eat-the metabolic flavor of ferroptosis. *Curr Opin Cell Biol.* (2018) 51:58–64. doi: 10.1016/j.ceb.2017.11.001
4. Sweeney RM, McAuley DF Acute respiratory distress syndrome. *Lancet.* (2016) 388:2416–30. doi: 10.1016/S0140-6736(16)00578-X
5. Ferguson ND, Fan E, Camporota L, Antonelli M, Anzueto A, Beale R, et al. The Berlin definition of ARDS: an expanded rationale, justification, and supplementary material. *Intensive Care Med.* (2012) 38:1573–82. doi: 10.1007/s00134-012-2682-1
6. Bellani G, Laffey JG, Pham T, Fan E, Brochard L, Esteban A, et al. Epidemiology, patterns of care, and mortality for patients with acute respiratory distress syndrome in intensive care units in 50 countries. *JAMA.* (2016) 315:788–800. doi: 10.1001/jama.2016.0291
7. Kellner M, Noonepalle S, Lu Q, Srivastava A, Zemskov E, Black SM. ROS signaling in the pathogenesis of Acute Lung Injury (ALI) and Acute Respiratory Distress Syndrome (ARDS). *Adv Exp Med Biol.* (2017) 967:105–37. doi: 10.1007/978-3-319-63245-2_8
8. Ye Z, Liu W, Zhuo Q, Hu Q, Liu M, Sun Q, et al. Ferroptosis: Final destination for cancer? *Cell Prolif.* (2020) 53, e12761. doi: 10.1111/cpr.12761
9. Nakamura, T, Naguro I, Ichijo H. Iron homeostasis and iron-regulated ROS in cell death, senescence and human diseases. *Biochim Biophys Acta Gen Subj.* (2019) 1863:1398–409. doi: 10.1016/j.bbagen.2019.06.010
10. Dixon SJ, Patel DN, Welsch M, Skouta R, Lee ED, Hayano M, et al. Pharmacological inhibition of cystine-glutamate exchange induces endoplasmic reticulum stress and ferroptosis. *Elife.* (2014) 3:e02523. doi: 10.7554/eLife.02523.018
11. Ingold I, Berndt C, Schmitt S, Doll S, Poschmann G, Buday K, et al. Selenium Utilization by GPX4 is required to prevent hydroperoxide-induced ferroptosis. *Cell.* (2018) 172:409–22. doi: 10.1016/j.cell.2017.11.048
12. Dong H, Qiang Z, Chai D, Peng, J, Xia Y, Hu R, et al. Nrf2 inhibits ferroptosis and protects against acute lung injury due to intestinal ischemia reperfusion via regulating SLC7A11 and HO-1. *Aging (Albany NY).* (2020) 12:12943–59. doi: 10.18632/aging.103378
13. Hayano M, Yang WS, Corn CK, Pagano NC, Stockwell BR. Loss of cysteinyl-tRNA synthetase (CARS) induces the transsulfuration pathway and inhibits ferroptosis induced by cystine deprivation. *Cell Death Differ.* (2016) 23:270–8. doi: 10.1038/cdd.2015.93
14. Murphy TH, Miyamoto M, Sastre A, Schnaar RL, Coyle JT. Glutamate toxicity in a neuronal cell line involves inhibition of cystine transport leading to oxidative stress. *Neuron.* (1989) 2:1547–58. doi: 10.1016/0896-6273(89)90043-3
15. Gao M, Monian P, Quadri N, Ramasamy R, Jiang X. Glutaminolysis and transferrin regulate ferroptosis. *Mol Cell.* (2015) 59:298–308. doi: 10.1016/j.molcel.2015.06.011
16. Jennis M, Kung CP, Basu S, Budina-Kolomets A, Leu JI, Khaku S, et al. An African-specific polymorphism in the TP53 gene impairs p53 tumor

suppressor function in a mouse model. *Genes Dev.* (2015) 30:918–30. doi: 10.1101/gad.275891.115
17. Feng H, Stockwell BR. Unsolved mysteries: how does lipid peroxidation cause ferroptosis? *PLoS Biol.* (2018) 16:e2006203. doi: 10.1371/journal.pbio.2006203
18. Agmon E, Solon J, Bassereau P, Stockwell BR. Modeling the effects of lipid peroxidation during ferroptosis on membrane properties. *Sci Rep.* (2018) 8:5155. doi: 10.1038/s41598-018-23408-0
19. Bersuker K, Hendricks JM, Li Z, Magtanong L, Ford B, Tang PH, et al. The CoQ oxidoreductase FSP1 acts parallel to GPX4 to inhibit ferroptosis. *Nature.* (2019) 575: 688–92. doi: 10.1038/s41586-019-1705-2
20. Doll S, Freitas FP, Shah R, Aldrovandi M, da Silva MC, Ingold I, et al. FSP1 is a glutathione-independent ferroptosis suppressor. *Nature.* (2019) 575:693–8. doi: 10.1038/s41586-019-1707-0
21. Shimada K, Skouta R, Kaplan A, Yang WS, Hayano M, Dixon SJ, et al. Global survey of cell death mechanisms reveals metabolic regulation of ferroptosis. *Nat Chem Biol.* (2016) 12:497–503. doi: 10.1038/nchembio.2079
22. Huppert LA, Matthay MA, Ware LB. Pathogenesis of acute respiratory distress syndrome. *Semin Respir Crit Care Med.* (2019) 40:31–9. doi: 10.1055/s-0039-1683996
23. Potera RM, Cao M, Jordan LF, Hogg RT, Hook JS, Moreland JG. Alveolar macrophage chemokine secretion mediates neutrophilic lung injury in Nox2-deficient mice. *Inflammation.* (2019) 42:185–98. doi: 10.1007/s10753-018-0883-7
24. Wohlrab P, Kraft F, Tretter V, Ullrich R, Markstaller K, Klein KU. Recent advances in understanding acute respiratory distress syndrome. *F1000Res.* (2018) 7:263. doi: 10.12688/f1000research.11148.1
25. Meduri GU, Headley AS, Golden E, Carson SJ, Umberger RA, Kelso T, et al. Effect of prolonged methylprednisolone therapy in unresolving acute respiratory distress syndrome: a randomized controlled trial. *JAMA.* (1998) 280:159–65. doi: 10.1001/jama.280.2.159
26. Steinberg KP, Hudson LD, Goodman RB, Hough CL, Lanken PN, Hyzy R, et al. Efficacy and safety of corticosteroids for persistent acute respiratory distress syndrome. *N Engl J Med.* (2006) 354:1671–684. doi: 10.1056/NEJMoa051693
27. Mongardon N, Piagnerelli M, Grimaldi D, Perrot B, Lascarrou JB, Investigators, Csg. Impact of late administration of corticosteroids in COVID-19 ARDS. *Intensive Care Med.* (2021) 47:110–2. doi: 10.1007/s00134-020-06311-z
28. Ali MK, Kim RY, Karim R, Mayall JR, Martin KL, Shahandeh A, et al. Role of iron in the pathogenesis of respiratory disease. *Int J Biochem Cell Biol.* (2017) 88:181–95. doi: 10.1016/j.biocel.2017.05.003
29. Quinlan GJ, Evans TW, Gutteridge JM. Iron and the redox status of the lungs. *Free Radic Biol Med.* (2002) 33:1306–13. doi: 10.1016/S0891-5849(02)00903-6
30. Khiroya H, Turner AM. The role of iron in pulmonary pathology. *Multidiscip Respir Med.* (2015) 10:34. doi: 10.1186/s40248-015-0031-2
31. Zhang V, Nemeth E, Kim A. Iron in lung pathology. *Pharmaceuticals (Basel).* (2019) 12:30. doi: 10.3390/ph12010030
32. Jenkins ZA, Hagar W, Bowlus CL, Johansson HE, Harmatz P, Vichinsky EP, et al. Iron homeostasis during transfusional iron overload in beta-thalassemia and sickle cell disease: changes in iron regulatory protein, hepcidin, and ferritin expression. *Pediatr Hematol Oncol.* (2007) 24:237–43. doi: 10.1080/08880010701360700
33. Ghio AJ, Carter JD, Richards JH, Richer LD, Grissom CK, Elstad MR. Iron and iron-related proteins in the lower respiratory tract of patients with acute respiratory distress syndrome. *Crit Care Med.* (2003) 31:395–400. doi: 10.1097/01.CCM.0000050284.35609.97
34. Connelly KG, Moss M, Parsons PE, Moore, EE, Moore FA, Giclas PC, et al. Serum ferritin as a predictor of the acute respiratory distress syndrome. *Am J Respir Crit Care Med.* (1997) 155:21–5. doi: 10.1164/ajrccm.155.1.9001283
35. Sharkey RA, Donnelly SC, Connelly KG, Robertson CE, Haslett C, Repine JE. Initial serum ferritin levels in patients with multiple trauma and the subsequent development of acute respiratory distress syndrome. *Am J Respir Crit Care Med.* (1999) 159(5 Pt 1), 1506–9. doi: 10.1164/ajrccm.159.5.9809027
36. Zhou H, Li F, Niu JY, Zhong WY, Tang MY, Lin D, et al. Ferroptosis was involved in the oleic acid-induced acute lung injury in mice. *Sheng Li Xue Bao.* (2019) 71:689–97. doi: 10.13294/j.aps.2019.0070
37. Zhang V, Ganz T, Nemeth E, Kim A. Iron overload causes a mild and transient increase in acute lung injury. *Physiol Rep.* (2020) 8:e14470. doi: 10.14814/phy2.14470
38. Bos LDJ. Diagnosis of acute respiratory distress syndrome by exhaled breath analysis. *Ann Transl Med.* (2018) 6:33. doi: 10.21037/atm.2018.01.17
39. Lamb NJ, Gutteridge JM, Baker C, Evans TW, Quinlan GJ. Oxidative damage to proteins of bronchoalveolar lavage fluid in patients with acute respiratory distress syndrome: evidence for neutrophil-mediated hydroxylation, nitration, and chlorination. *Crit Care Med.* (1999) 27:1738–44. doi: 10.1097/00003246-199909000-00007
40. Carpenter CT, Price PV, Christman BW. Exhaled breath condensate isoprostanes are elevated in patients with acute lung injury or ARDS. *Chest.* (1998) 114:1653–9. doi: 10.1378/chest.114.6.1653
41. Li Y, Cao Y, Xiao J, Shang J, Tan Q, Ping F, et al. Inhibitor of apoptosis-stimulating protein of p53 inhibits ferroptosis and alleviates intestinal ischemia/reperfusion-induced acute lung injury. *Cell Death Differ.* (2020) 27:2635–50. doi: 10.1038/s41418-020-0528-x
42. Qiu YB, Wan BB, Liu G, Wu YX, Chen D, Lu MD, et al. Nrf2 protects against seawater drowning-induced acute lung injury via inhibiting ferroptosis. *Respir Res.* (2020) 21:232. doi: 10.1186/s12931-020-01500-2
43. Erol N, Saglam L, Saglam YS, Erol HS, Altun S, Aktas MS, et al. The protection potential of antioxidant vitamins against acute respiratory distress syndrome: a rat trial. *Inflammation.* (2019) 42:1585–94. doi: 10.1007/s10753-019-01020-2
44. Li X, Zhuang X, Qiao T. Role of ferroptosis in the process of acute radiation-induced lung injury in mice. *Biochem Biophys Res Commun.* (2019) 519:240–5. doi: 10.1016/j.bbrc.2019.08.165
45. Abdulnour R-EE, Peng X, Finigan JH, Han EJ, Hasan EJ, Birukov KG, et al. Mechanical stress activates xanthine oxidoreductase through MAP kinase-dependent pathways. *Am J Physiol Lung Cell Mol Physiol.* (2006). 291:L345–53. doi: 10.1152/ajplung.00453.2005
46. Gross CM, Rafikov R, Kumar S, Aggarwal S, Ham PB, 3rd, Meadows ML, et al. Endothelial nitric oxide synthase deficient mice are protected from lipopolysaccharide induced acute lung injury. *PLoS ONE.* (2015) 10:e0119918. doi: 10.1371/journal.pone.0119918
47. Sato K, Kadiiska MB, Ghio AJ, Corbett J, Fann YC, Holland SM, et al. *In vivo* lipid-derived free radical formation by NADPH oxidase in acute lung injury induced by lipopolysaccharide: a model for ARDS. *FASEB J.* (2002) 16:1713–20. doi: 10.1096/fj.02-0331com
48. Liu P, Feng Y, Li H, Chen X, Wang G, Xu S, et al. Ferrostatin-1 alleviates lipopolysaccharide-induced acute lung injury via inhibiting ferroptosis. *Cell Mol Biol Lett.* (2020) 25:10. doi: 10.1186/s11658-020-00205-0
49. Pacht ER, Timerman AP, Lykens MG, Merola AJ. Deficiency of alveolar fluid glutathione in patients with sepsis and the adult respiratory distress syndrome. *Chest.* (1991) 100:1397–403. doi: 10.1378/chest.100.5.1397
50. Syrkina O, Jafari B, Hales CA, Quinn DA. Oxidant stress mediates inflammation and apoptosis in ventilator-induced lung injury. *Respirology.* (2008) 13:333–40. doi: 10.1111/j.1440-1843.2008.01279.x
51. Gill SS, Tuteja N. (2010). Reactive oxygen species and antioxidant machinery in abiotic stress tolerance in crop plants. *Plant Physiol Biochem.* 48:909–30. doi: 10.1016/j.plaphy.2010.08.016
52. Horowitz RI, Freeman PR, Bruzzese J. Efficacy of glutathione therapy in relieving dyspnea associated with COVID-19 pneumonia: a report of 2 cases. *Respir Med Case Rep.* (2020) 30:101063. doi: 10.1016/j.rmcr.2020.101063
53. Galluzzi L, Vitale I, Aaronson SA, Abrams JM, Adam D, Agostinis P, et al. Molecular mechanisms of cell death: recommendations of the Nomenclature Committee on Cell Death 2018. *Cell Death Differ.* (2018) 25:486–541. doi: 10.1038/s41418-018-0102-y
54. Sun Y, Chen P, Zhai B, Zhang M, Xiang Y, Fang J, et al. The emerging role of ferroptosis in inflammation. *Biomed Pharmacother.* (2020) 127:110108. doi: 10.1016/j.biopha.2020.110108
55. Linkermann A, Stockwell BR, Krautwald S, Anders HJ. Regulated cell death and inflammation: an auto-amplification loop causes organ failure. *Nat Rev Immunol.* (2014) 14:759–67. doi: 10.1038/nri3743
56. Xu Y, Li X, Cheng Y, Yang M, Wang R. Inhibition of ACSL4 attenuates ferroptotic damage after pulmonary ischemia-reperfusion. *FASEB J.* (2020) 34:16262–75. doi: 10.1096/fj.202001758R

57. Li N, Wang W, Zhou H, Wu Q, Duan M, Liu C, et al. Ferritinophagy-mediated ferroptosis is involved in sepsis-induced cardiac injury. *Free Radic Biol Med.* (2020) 160:303–18. doi: 10.1016/j.freeradbiomed.2020.08.009
58. Li J, Lu K, Sun F, Tan S, Zhang X, Sheng W, et al. Panaxydol attenuates ferroptosis against LPS-induced acute lung injury in mice by Keap1-Nrf2/HO-1 pathway. *J Transl Med.* (2021) 19:96. doi: 10.1186/s12967-021-02745-1
59. Wang C, Yuan W, Hu A, Lin J, Xia Z, Yang CF, et al. Dexmedetomidine alleviated sepsisinduced myocardial ferroptosis and septic heart injury. *Mol Med Rep.* (2020). 22:175–84. doi: 10.3892/mmr.2020.11114
60. Wei S, Bi J, Yang L, Zhang J, Wan Y, Chen X, et al. Serum irisin levels are decreased in patients with sepsis, and exogenous irisin suppresses ferroptosis in the liver of septic mice. *Clin Transl Med.* (2020) 10:e173. doi: 10.1002/ctm2.173
61. Oh BM, Lee SJ, Park GL, Hwang YS, Lim J, Park ES, et al. Erastin inhibits septic shock and inflammatory gene expression via suppression of the NF-kappaB pathway. *J Clin Med.* (2019) 8:2210. doi: 10.3390/jcm8122210
62. Kang R, Zeng L, Zhu S, Xie Y, Liu J, Wen Q, et al. Lipid peroxidation drives gasdermin D-mediated pyroptosis in lethal polymicrobial sepsis. *Cell Host Microbe.* (2018) 24:97–108. e104. doi: 10.1016/j.chom.2018.05.009
63. Lee S, Suh GY, Ryter SW, Choi AM. Regulation and function of the nucleotide binding domain leucine-rich repeat-containing receptor, pyrin domain-containing-3 inflammasome in lung disease. *Am J Respir Cell Mol Biol.* (2016) 54:151–60. doi: 10.1165/rcmb.2015-0231TR
64. Qiang Z, Dong H, Xia Y, Chai D, Hu R, Jiang H. Nrf2 and STAT3 alleviates ferroptosis-mediated IIR-ALI by regulating SLC7A11. *Oxid Med Cell Longev.* (2020) 2020:5146982. doi: 10.1155/2020/5146982
65. Zhong WJ, Duan JX, Liu T, Yang HH, Guan XX, Zhang CY, et al. Activation of NLRP3 inflammasome up-regulates TREM-1 expression in murine macrophages via HMGB1 and IL-18. *Int Immunopharmacol.* (2020) 89(Pt A):107045. doi: 10.1016/j.intimp.2020.107045
66. Li D, Ren W, Jiang Z, Zhu L. Regulation of the NLRP3 inflammasome and macrophage pyroptosis by the p38 MAPK signaling pathway in a mouse model of acute lung injury. *Mol Med Rep.* 18:4399–409. doi: 10.3892/mmr.2018.9427
67. He DK, Xu N, Shao YR, Shen J. NLRP3 gene silencing ameliorates phosgene-induced acute lung injury in rats by inhibiting NLRP3 inflammasome and proinflammatory factors, but not anti-inflammatory factors. *J Toxicol Sci.* (2020) 45:625–37. doi: 10.2131/jts.45.625
68. Yang H, Lv H, Li H, Ci X, Peng L. Oridonin protects LPS-induced acute lung injury by modulating Nrf2-mediated oxidative stress and Nrf2-independent NLRP3 and NF-kappaB pathways. *Cell Commun Signal.* (2019) 17:62. doi: 10.1186/s12964-019-0366-y
69. Lv H, Liu Q, Wen Z, Feng H, Deng X, Ci X. Xanthohumol ameliorates lipopolysaccharide (LPS)-induced acute lung injury via induction of AMPK/GSK3beta-Nrf2 signal axis. *Redox Biol.* (2017) 12:311–24. doi: 10.1016/j.redox.2017.03.001
70. Lei J, Wei Y, Song P, Li Y, Zhang T, Feng Q, et al. Cordycepin inhibits LPS-induced acute lung injury by inhibiting inflammation and oxidative stress. *Eur J Pharmacol.* (2018) 818:110–4. doi: 10.1016/j.ejphar.2017.10.029
71. Rojo de la Vega M, Dodson M, Gross C, Mansour HM, Lantz RC, Chapman E, et al. Role of Nrf2 and autophagy in acute lung injury. *Curr Pharmacol Rep.* (2016) 2:91–101. doi: 10.1007/s40495-016-0053-2
72. Crisponi G, Nurchi VM, Lachowicz JI. Iron chelation for iron overload in Thalassemia. *Met Ions Life Sci.* (2019) 19:9. doi: 10.1515/9783110527872-009
73. Williams A, Meyer D. Desferrioxamine as immunomodulatory agent during microorganism infection. *Curr Pharm Des.* (2009) 15:1261–8. doi: 10.2174/138161209787846801
74. Ramezanpour M, Smith JLP, Ooi ML, Gouzos M, Psaltis AJ, Wormald PJ, et al. Deferiprone has anti-inflammatory properties and reduces fibroblast migration *in vitro*. *Sci Rep.* (2019) 9:2378. doi: 10.1038/s41598-019-38902-2
75. Ogger PP, Byrne AJ. Lung fibrosis enters the iron age(dagger). *J Pathol.* (2020) 252:1–3. doi: 10.1002/path.5489
76. Hybertson BM, Connelly KG, Buser RT, Repine JE. Ferritin and desferrioxamine attenuate xanthine oxidase-dependent leak in isolated perfused rat lungs. *Inflammation.* (2002) 26:153–9. doi: 10.1023/A:1016511611435
77. Ni YL, Shen HT, Su CH, Chen WY, Huang-Liu R, Chen CJ, et al. Nerolidol suppresses the inflammatory response during lipopolysaccharide-induced acute lung injury via the modulation of antioxidant enzymes and the AMPK/Nrf-2/HO-1 pathway. *Oxid Med Cell Longev.* (2019) 2019:9605980. doi: 10.1155/2019/9605980
78. Zhang Y, Yu W, Han D, Meng J, Wang H, Cao G. L-lysine ameliorates sepsis-induced acute lung injury in a lipopolysaccharide-induced mouse model. *Biomed Pharmacother.* (2019) 118:109307. doi: 10.1016/j.biopha.2019.109307
79. Vazquez-Medina JP, Tao JQ, Patel P, Bannitz-Fernandes R, Dodia C, Sorokina EM, et al. Genetic inactivation of the phospholipase A2 activity of peroxiredoxin 6 in mice protects against LPS-induced acute lung injury. *Am J Physiol Lung Cell Mol Physiol.* (2019) 316:L656–68. doi: 10.1152/ajplung.00344.2018
80. Ma X, Liu X, Feng J, Zhang D, Huang L, Li D, et al. Fraxin alleviates LPS-induced ARDS by downregulating inflammatory responses and oxidative damages and reducing pulmonary vascular permeability. *Inflammation.* (2019) 42:1901–12. doi: 10.1007/s10753-019-01052-8
81. Aggarwal S, Dimitropoulou C, Lu Q, Black SM, Sharma S. Glutathione supplementation attenuates lipopolysaccharide-induced mitochondrial dysfunction and apoptosis in a mouse model of acute lung injury. *Front Physiol.* (2012) 3:161. doi: 10.3389/fphys.2012.00161
82. Qian M, Lou Y, Wang Y, Zhang M, Jiang Q, Mo Y, et al. PICK1 deficiency exacerbates sepsis-associated acute lung injury and impairs glutathione synthesis via reduction of xCT. *Free Radic Biol Med.* (2018) 118:23–34. doi: 10.1016/j.freeradbiomed.2018.02.028
83. Bernard GR. Potential of N-acetylcysteine as treatment for the adult respiratory distress syndrome. *Eur Respir J Suppl.* (1990) 11:496s−8.
84. Conrad M, Lorenz SM, Proneth B. Targeting ferroptosis: new hope for as-yet-incurable diseases. *Trends Mol Med.* (2020) 27:113–22. doi: 10.1016/j.molmed.2020.08.010

Conflict of Interest: The authors declare that the research was conducted in the absence of any commercial or financial relationships that could be construed as a potential conflict of interest.

Copyright © 2021 Qu, Zhang, Chen, Sun, Zhu, Nan, Chen and Miao. This is an open-access article distributed under the terms of the Creative Commons Attribution License (CC BY). The use, distribution or reproduction in other forums is permitted, provided the original author(s) and the copyright owner(s) are credited and that the original publication in this journal is cited, in accordance with accepted academic practice. No use, distribution or reproduction is permitted which does not comply with these terms.

frontiers in Medicine

ORIGINAL RESEARCH
published: 31 May 2021
doi: 10.3389/fmed.2021.674324

Intrauterine Growth Restriction Promotes Postnatal Airway Hyperresponsiveness Independent of Allergic Disease

Jack O. Kalotas[1], *Carolyn J. Wang*[1], *Peter B. Noble*[1] *and Kimberley C. W. Wang*[1,2]*

[1] School of Human Sciences, The University of Western Australia, Crawley, WA, Australia, [2] Telethon Kids Institute, The University of Western Australia, Nedlands, WA, Australia

Introduction: Intrauterine growth restriction (IUGR) is associated with asthma. Murine models of IUGR have altered airway responsiveness in the absence of any inflammatory exposure. Given that a primary feature of asthma is airway inflammation, IUGR-affected individuals may develop more substantial respiratory impairment if subsequently exposed to an allergen. This study used a maternal hypoxia-induced mouse model of IUGR to determine the combined effects of IUGR and allergy on airway responsiveness.

Methods: Pregnant BALB/c mice were housed under hypoxic conditions (10.5% O_2) from gestational day (GD) 11-GD 17.5 (IUGR group; term = GD 21). Following hypoxic exposure, mice were returned to a normoxic environment (21% O_2). A second group of pregnant mice were housed under normoxic conditions throughout pregnancy (Control). All offspring were sensitized to ovalbumin (OVA) and assigned to one of four treatment groups: Control – normoxic and saline challenge; IUGR – hypoxic and saline challenge; Allergy – normoxic and OVA challenge; and IUGR + Allergy – hypoxic and OVA challenge. At 8 weeks of age, and 24 h post-aerosol challenge, mice were tracheostomised for methacholine challenge and assessment of lung mechanics by the forced oscillation technique, and lungs subsequently fixed for morphometry.

Results: IUGR offspring were lighter than Control at birth and in adulthood. Both Allergy and IUGR independently increased airway resistance after methacholine challenge. The IUGR group also exhibited an exaggerated increase in tissue damping and elastance after methacholine challenge compared with Control. However, there was no incremental effect on airway responsiveness in the combined IUGR + Allergy group. There was no impact of IUGR or Allergy on airway structure and no effect of sex on any outcome.

Conclusion: IUGR and aeroallergen independently increased bronchoconstrictor response, but when combined the pathophysiology was not worsened. Findings suggest that an association between IUGR and asthma is mediated by baseline airway responsiveness rather than susceptibility to allergen.

Keywords: airway hyperresponsiveness, allergy, intrauterine growth restriction, asthma, lung function

OPEN ACCESS

Edited by:
Miguel Angel Alejandre Alcazar, University Hospital of Cologne, Germany

Reviewed by:
Erin Kristin Zinkhan, The University of Utah, United States
Kurt H. Albertine, The University of Utah, United States

***Correspondence:**
Kimberley C. W. Wang
kimberley.wang@uwa.edu.au

Specialty section:
This article was submitted to Pulmonary Medicine, a section of the journal Frontiers in Medicine

Received: *01 March 2021*
Accepted: *07 May 2021*
Published: *31 May 2021*

Citation:
Kalotas JO, Wang CJ, Noble PB and Wang KCW (2021) Intrauterine Growth Restriction Promotes Postnatal Airway Hyperresponsiveness Independent of Allergic Disease. Front. Med. 8:674324. doi: 10.3389/fmed.2021.674324

INTRODUCTION

Asthma is an obstructive airway disease that affects patient quality of life, manifesting as episodes of breathing difficulties. Airway hyperresponsiveness (AHR), a major functional impairment in asthma, results in disproportionate airway narrowing that produces airflow limitation (1). There are numerous potential causes of AHR. A relationship between AHR and allergy has been established; inflammation, orchestrated by T-helper 2 (Th2) cells, results in the release of bronchoactive mediators including histamine, leukotriene B4, prostaglandin D2 and cytokines along with the recruitment of immune cells (2, 3) which mediate excessive airway constriction. "Airway remodeling" that is either independent or co-dependent on inflammation (4), is also associated with AHR. Airway remodeling is a change in the structure (mass, thickness, or volume) of the airway wall (5), exerting a multitude of effects, including increased airway smooth muscle (ASM) force production (1), and reduced and more variable airway caliber (1, 6), all of which at least contribute to the onset of AHR.

The above changes to airway structure-function in asthma have conventionally been attributed to environmental exposures (e.g., allergic stimuli) accumulated through postnatal life. An alternative proposal is that airway abnormalities are the result of a developmental disorder and we particularly note the association between intrauterine growth restriction (IUGR) and asthma (7). After establishing a mouse model of hypoxia-induced IUGR, we demonstrated airway hyperresponsiveness in female offspring and hyporesponsiveness in males (8). Functional changes after IUGR were not associated with airway remodeling (8, 9), rather our data implicated a shift in inflammatory phenotype; an increase in macrophages in the bronchial alveolar lavage (BAL) fluid from both male and female offspring with males also demonstrating an increase in interleukin (IL)-2, IL-13, and eotaxin (10). Importantly, this shift in inflammatory phenotype was the result of a prenatal disruption that persisted into adult life and occurred without exposure to typical environmental triggers (10). Together these observations suggest that developmental changes in airway responsiveness that occur concomitantly with inflammation will alter the susceptibility to environmental influences and subsequent airway disease.

The present study was therefore principally focused on the evolution of AHR in asthma, which as discussed is impacted by structural and inflammatory pathologies and potentially developmental programming. We specifically examined the interaction between IUGR and allergy and hypothesized that persistent biological changes after IUGR worsens the response to allergy and this manifests as more severe bronchoconstriction to contractile stimulation i.e., AHR. To address this study hypothesis, we used our established mouse model of IUGR and exposed both male and female offspring to ovalbumin (OVA) sensitization and challenge.

MATERIALS AND METHODS

Maternal Hypoxia-Induced IUGR Mouse Model

This study was approved by The University of Western Australia Animal Ethics Committee (approval number RA/3/100/1570). All animals were housed in the Pre-Clinical Facility at The University of Western Australia on a 15:9 light:dark cycle. Thirty pregnant BALB/c mice (gestational day "GD" 7) were obtained from the Animal Resources Center (Murdoch, WA, Australia). Mice were exposed to 10.5% O_2 from GD 11 to GD 17.5 (hypoxic conditions; IUGR group) (8–12) which corresponds to the pseudoglandular-canalicular stage in fetal mouse lung development, and therefore peak airway development. At GD 17.5, the pregnant mice were removed from the hypoxic chamber and returned to normoxic conditions (21% O_2) for the remainder of the pregnancy. Another group of pregnant mice remained under normoxic conditions throughout the entire duration of pregnancy (Control group). Only litter sizes of $\leq$6 pups were included in the study since larger litters reduce body weight independently of maternal hypoxia and compromises milk availability to pups. Offspring were weaned and sexed at 3 weeks of age, with access to standard chow and water *ad libitum*. Weights of offspring were recorded at birth and before lung function assessment (8 weeks of age). A subset of offspring was used to determine the effects of IUGR on diaphragm function and structure in postnatal life (11).

Allergy Sensitization Protocol

An established mouse allergy protocol from our lab was used in this study (13). At 5 and 7 weeks of age, all IUGR and Control offspring received 0.2 mL intra-peritoneal (i.p.) injection containing 5 mg.mL^{-1} of OVA (Sigma, St. Louis, MO, U.S.A.) suspended in 50 mL of alum (Alu-gel-S, Serva, Heidelberg, Germany). At 8 weeks of age, half of the Control and IUGR offspring received 1% OVA aerosol (MPC aerosol medication nebulizer, Braintree Scientific, Inc., MA, U.S.A), whilst remaining offspring received a saline aerosol. This resulted in four experimental groups: Control (males, $n = 8$; females, $n = 10$), normal mice with saline aerosol; Allergy (males, $n = 8$; females, $n = 10$), normal mice with OVA aerosol; IUGR (males, $n = 8$; females, $n = 9$), IUGR mice with saline aerosol; and IUGR + Allergy (males, $n = 7$; females, $n = 8$), IUGR mice with OVA aerosol (**Figure 1**).

Lung Function Assessment

Twenty-four h after the aerosol challenge, offspring were anesthetized by i.p. injection of ketamine (0.4 mg.g^{-1} body weight) and xylazine (0.02 mg.g^{-1} body weight). Once under anesthesia, each mouse was tracheostomised, transferred to a FlexiVent system (FX module 1, flexiWare version 7.5, SCIREQ, Montreal, QC, Canada) and then ventilated at 250 breaths.min^{-1} (8, 13). Lung volume history was standardized *via* three slow inflation-deflation manoeuvers up to 20 cmH_2O transrespiratory pressure.

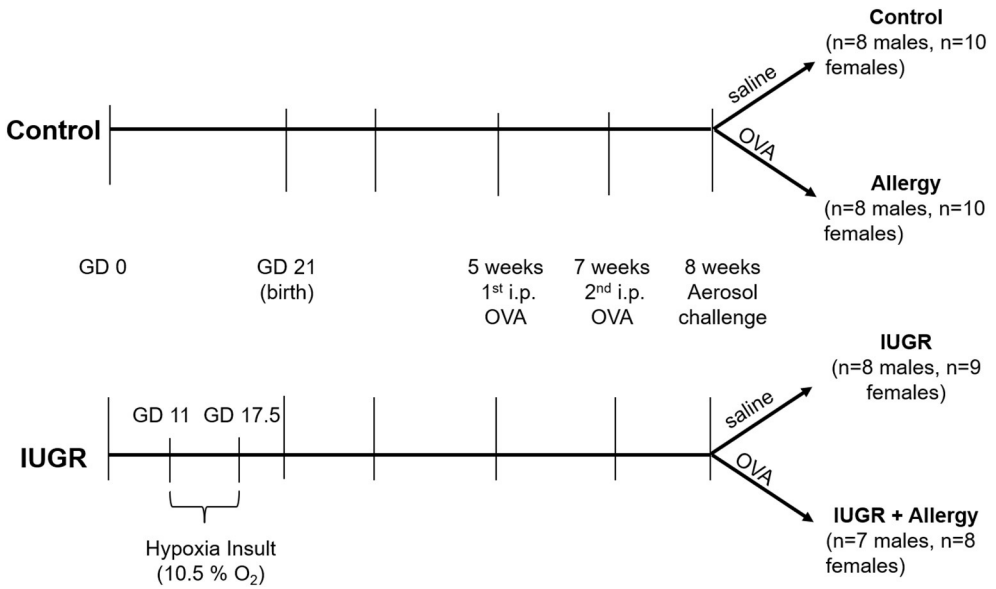

FIGURE 1 | Protocol for IUGR and allergy induction in mice. The superimposition of a maternal hypoxia-induced IUGR model and a well-established allergen protocol, produced 4 experimental groups; Control, Allergy, IUGR and IUGR + Allergy. GD, gestational day; OVA, ovalbumin; i.p., intra-peritoneal; IUGR, intrauterine growth restriction.

Respiratory impedance was measured by forced oscillation technique (FOT). Outcomes of airway resistance (R_{aw}), tissue damping (G), and tissue elastance (H) were derived from impedance using a constant phase model. Once the mouse was stabilized on the ventilator, FOT measurements were recorded once a min for 5 min to establish baseline respiratory mechanics. Mice were then challenged with 10 s aerosols of saline, followed by increasing doses of methacholine (MCh; β-methacholine chloride, Sigma-Aldrich, St. Louis, U.S.A; 0.1 $mg.mL^{-1}$ to 30 $mg.mL^{-1}$) *via* the Aeroneb ultrasonic nebuliser (SCIREQ). After each challenge, measurements were again recorded every min for 5 min. Peak responses were used for analysis. After final MCh response was measured, 0.1 mL atropine (600 μg/mL) was delivered *via* i.p injection, to reverse airway constriction. Ten min after atropine administration, mice were euthanized with an overdose of ketamine and xylazine (13).

ELISA Assay

Following euthanasia, blood serum was collected *via* centrifugation of cardiac puncture samples to determine levels of OVA-specific immunoglobulin E (IgE), according to manufacturer's protocol (BioLegend, Inc.) (13).

Histology and Morphological Analysis

The analysis was only performed in IUGR mice (IUGR compared with IUGR + Allergy groups) since previous study have shown no effect of acute OVA exposure on airway dimensions (13). Lungs were inflation-fixed *in situ* at a transrespiratory pressure of 10 cmH_2O in 4% formaldehyde (8, 13). The left lung was embedded in paraffin wax and two 5 μm transverse sections were stained with Masson's Trichrome. The first section was acquired just below the transition from extra- to intraparenchymal bronchus [middle region in (14), and the second section marginally deeper into the lung toward the lower region in (14)] (14, 15). All airways within each section were measured. The perimeter of the basement membrane (P_{bm}) and areas of the ASM, inner and outer airway wall were measured by Stereo Investigator software (version 10.42.1, MBF Bioscience, United States of America). Airway measurements were averaged within each animal i.e., a case mean was calculated.

Data Analysis and Statistics

Data were normalized where necessary, to ensure assumptions of parametric tests were satisfied. An unpaired *t*-test was performed to assess differences in birth weight (unsexed) between IUGR and Control offspring. Body weights of offspring at 8 weeks of age were analyzed using a two-way ANOVA, examining the effects of sex and *in utero* treatment.

Lung function data were analyzed using two-way ANOVA, examining the effects of sex in three separate analyses; IUGR effect (Control compared with IUGR group), confirming the effect of IUGR on bronchoconstrictor response in saline exposed offspring only; Allergy effect (Control compared with Allergy group), confirming the effects of allergy on bronchoconstrictor response in Control offspring only; combined effect of IUGR and Allergy (IUGR compared with IUGR + Allergy group), examining the effects of allergy on bronchoconstrictor response in IUGR offspring. Outcomes (R_{aw}, G and H) were compared before and after methacholine challenge, and delta change in response to methacholine (e.g., Δ R_{aw}, G and H calculated from the difference between 30 $mg.mL^{-1}$ MCh and saline).

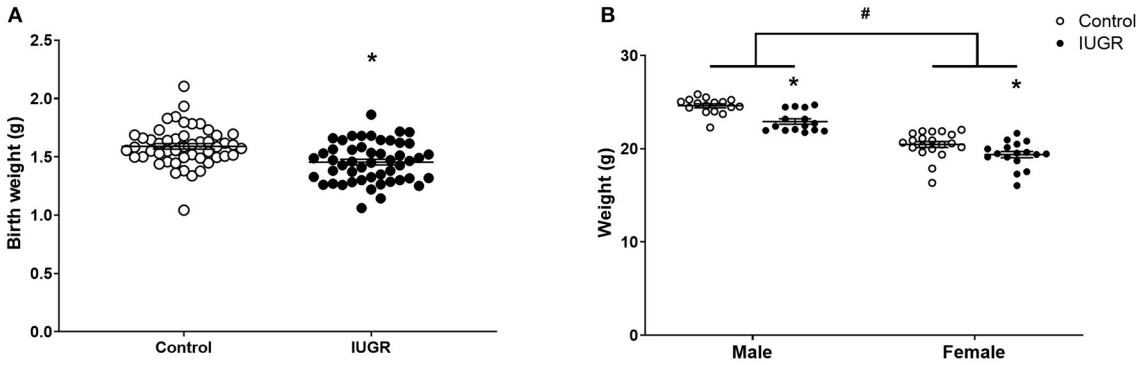

FIGURE 2 | Offspring body weights. Body weights of Control ($n = 50$) and IUGR ($n = 50$) offspring at birth **(A)** and at 8 weeks of age (Control male, $n = 16$; IUGR male, $n = 15$; Control female, $n = 20$; IUGR female, $n = 17$; **B**). Sample size of birth weight is larger than experimental sample size as the birth weight of all pups in each litter was recorded. Data are mean ± SEM. *Significant treatment effect ($P < 0.05$). #Significant sex effect ($P < 0.05$). IUGR, intrauterine growth restriction.

Data for OVA IgE levels were analyzed by separate two-way ANOVAs; Control compared with IUGR groups for male and female mice; Control compared with Allergy groups for male and female mice; IUGR compared with IUGR + Allergy groups for male and female mice. Airway dimensions were also analyzed by two-way ANOVA; IUGR and IUGR + Allergy groups for male and female mice. P-value < 0.05 was considered statistically significant. Graphical and statistical analysis were conducted using PRISM (version 7, GraphPad Software, La Jolla, CA, U.S.A) and SigmaPlot (version 13, Systat Software, Inc., San Jose, CA, U.S.A).

RESULTS

Offspring Growth Outcomes

The IUGR offspring were lighter than Control offspring at birth ($P = 0.0001$, unsexed; **Figure 2A**). The IUGR offspring remained lighter in adulthood (8 weeks; $P < 0.0001$; **Figure 2B**) and at this age, males were heavier than females ($P < 0.0001$; **Figure 2B**). There was no effect of OVA exposure on body weight at 8 weeks of age (saline, 21.81 ± 1.79 g; OVA, 21.94 ± 2.05 g; $P = 0.701$).

Airway Resistance, Tissue Damping, and Elastance

IUGR Effect

To determine the effect of IUGR on bronchoconstrictor response, data were compared in mice exposed only to saline aerosol (i.e., Control and IUGR groups). Before MCh challenge, there was no difference in R_{aw} between Control or IUGR groups ($P = 0.118$) and male or female ($P = 0.275$) mice (**Figure 3A**). After MCh challenge, R_{aw} ($P = 0.018$; **Figure 3B**) and Δ R_{aw} ($P = 0.005$; **Figure 3C**) of IUGR mice were greater than Control. There was no difference in R_{aw} between males and females after MCh challenge ($P = 0.249$).

Before MCh challenge, G ($P = 0.205$; **Supplementary Figure 1A**) and H ($P = 0.205$; **Supplementary Figure 2A**) were similar between IUGR and Control groups. After MCh challenge, G ($P = 0.025$; **Supplementary Figure 1B**) and H ($P = 0.025$; **Supplementary Figure 2B**) of the IUGR group were greater than the Control group. There was no difference in Δ G ($P = 0.053$; **Supplementary Figure 1C**) but a greater Δ H in the IUGR mice compared with Control mice ($P = 0.007$; **Supplementary Figure 2C**). Sex did not affect G (before MCh, $P = 0.431$; after MCh, $P = 0.429$) or H (before MCh, $P = 0.542$; after MCh, $P = 0.976$).

Allergy Effect

Data were compared in Control and Allergy groups to examine OVA effect on R_{aw}. Before MCh challenge, there was no difference in R_{aw} between Control or Allergy groups ($P = 0.671$) or between males and females ($P = 0.109$; **Figure 4A**). Airway resistance ($P = 0.006$; **Figure 4B**) and Δ R_{aw} ($P = 0.004$; **Figure 4C**) of the Allergy group was greater than Control group after MCh challenge. Male mice also exhibited a greater Δ R_{aw} compared with females ($P = 0.016$).

Tissue damping of Allergy and Control groups were similar before ($P = 0.622$) and after ($P = 0.21$) MCh challenge (**Supplementary Figures 3A,B**). Tissue elastance was also similar between Allergy and Control groups before ($P = 0.837$) and after ($P = 0.065$) MCh challenge (**Supplementary Figures 4A,B**). Sex had no effect on G (before MCh, $P = 0.758$; after MCh, $P = 0.608$) or H (before MCh, $P = 0.787$; after MCh, $P = 0.89$).

Combined Effect of IUGR and Allergy

To determine the combined effect of IUGR and Allergy on bronchoconstrictor response, data were compared in IUGR mice that were exposed to either saline or OVA aerosol (i.e., IUGR and IUGR + Allergy groups). There was no difference in R_{aw} of IUGR mice exposed to either saline or OVA, both before ($P = 0.345$; **Figure 5A**) and after ($P = 0.149$; **Figure 5B**) MCh challenge, and Δ R_{aw} ($P = 0.153$; **Figure 5C**). There was also no difference between sexes, before ($P = 0.841$) or after ($P = 0.670$) MCh challenge in R_{aw}.

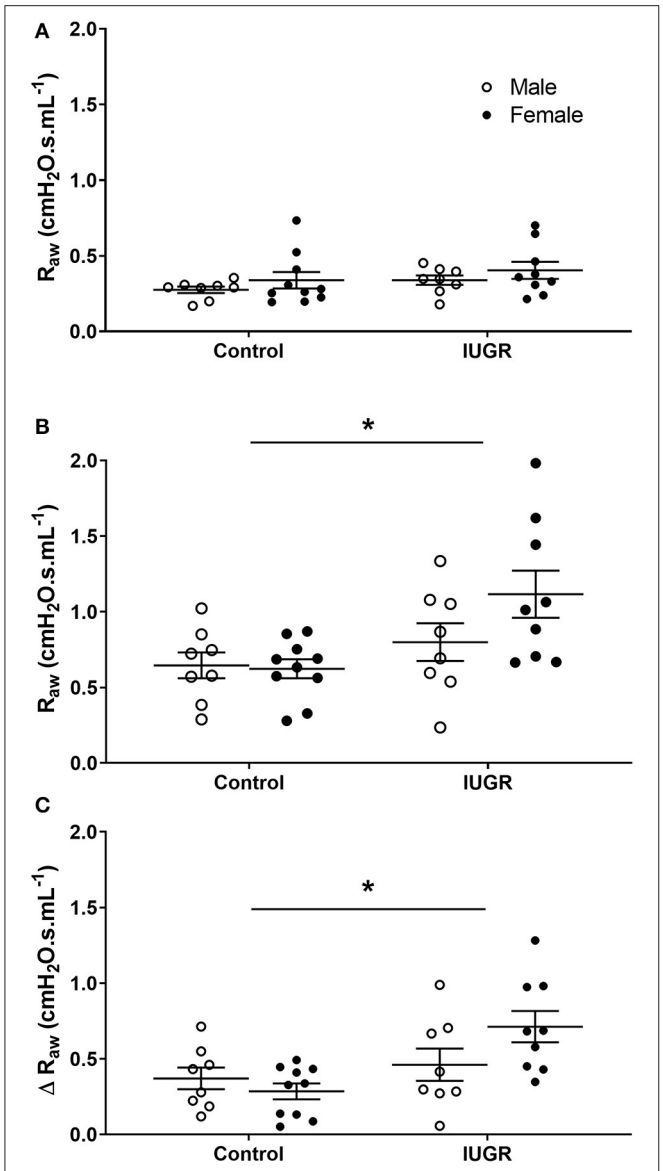

FIGURE 3 | Changes in R_{aw} in Control and IUGR groups. Airway resistance in Control male ($n = 8$) and female ($n = 10$), and IUGR male ($n = 8$) and female ($n = 9$) offspring before **(A)** and after **(B)** MCh challenge, and Δ R_{aw} **(C)**. Data are mean ± SEM. *Significantly different from Control ($P < 0.05$). Males, open circles; Females, closed circles; R_{aw}, airway resistance; IUGR, intrauterine growth restriction; MCh, methacholine; Δ, net change after MCh challenge.

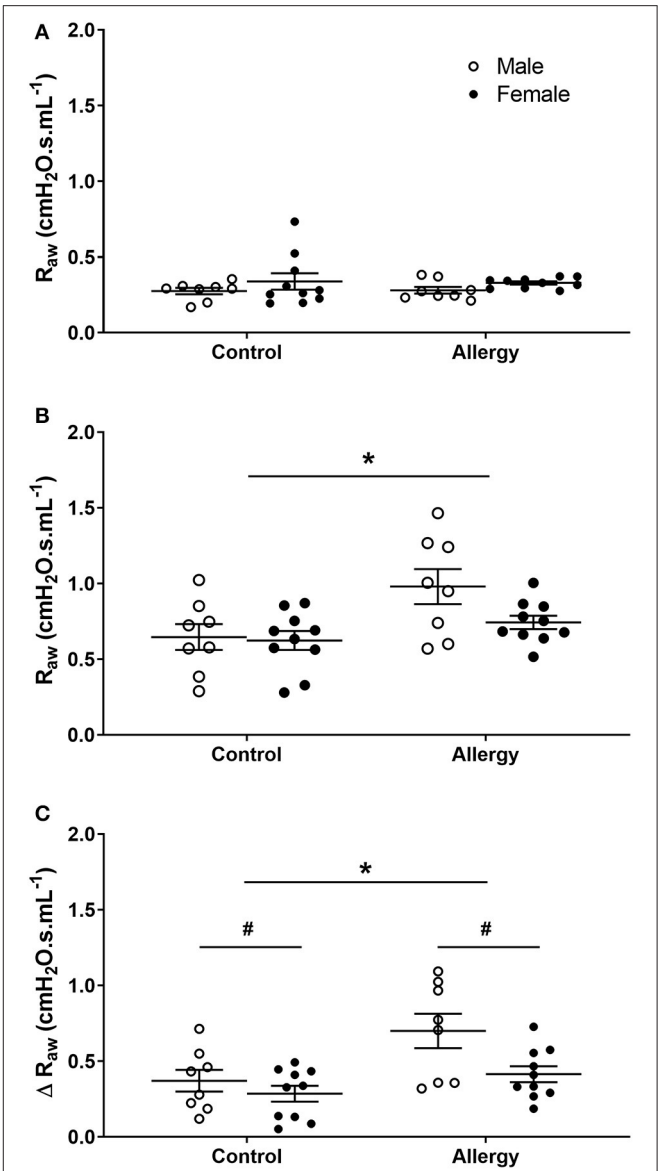

FIGURE 4 | Changes in R_{aw} in Control and Allergy groups. Airway resistance in Control male ($n = 8$) and female ($n = 10$), and Allergy male ($n = 8$) and female ($n = 10$) offspring before **(A)**, and after **(B)** MCh challenge, and Δ R_{aw} **(C)**. Data are mean ± SEM. *Significantly different from Control ($P < 0.05$). #Significantly different from males ($P < 0.05$). Males, open circles; Females, closed circles; R_{aw}, airway resistance; MCh, methacholine; Δ, net change after MCh challenge.

Tissue damping of the IUGR + Allergy group was similar to the IUGR group before ($P = 0.345$) and after ($P = 0.149$) MCh challenge (**Supplementary Figures 5A,B**). Tissue elastance of the IUGR + Allergy group was also similar to the IUGR group, both before ($P = 0.578$) and after ($P = 0.225$) MCh (**Supplementary Figures 6A,B**). There was no sex effect on G (before MCh, $P = 0.62$; after MCh, $P = 0.395$) or H (before MCh, $P = 0.682$; after MCh, $P = 0.932$).

OVA IgE Levels

Female offspring had higher OVA IgE levels than the male offspring in the IUGR group ($P = 0.009$; **Table 1**). There were no other differences between groups ($P > 0.05$).

Airway Morphometry of IUGR Offspring

Airway dimensions are provided in **Table 2** and representative images are shown in **Figure 6**. There were no differences in any of the airway wall parameters measured between IUGR and IUGR + Allergy groups ($P > 0.05$).

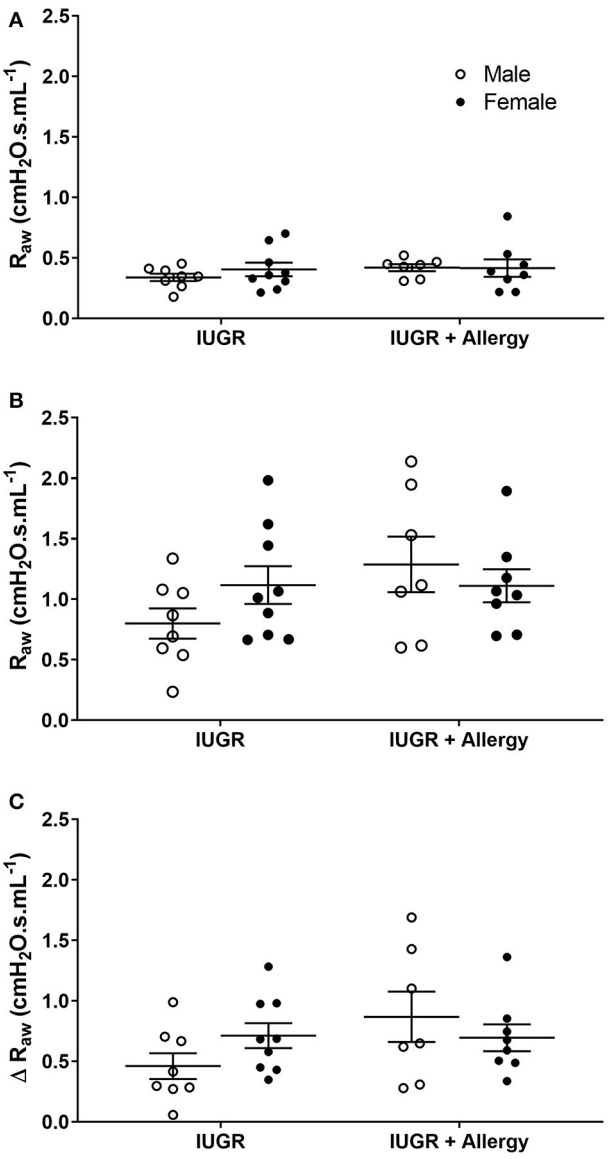

FIGURE 5 | Changes in R_{aw} in IUGR and IUGR + Allergy groups. Airway resistance in IUGR male ($n = 8$) and female ($n = 9$), and IUGR + Allergy male ($n = 7$) and female ($n = 8$) offspring before **(A)** and after **(B)** MCh challenge, and Δ R_{aw} **(C)**. Data are mean ± SEM. Males, open circles; Females, closed circles; R_{aw}, airway resistance; IUGR, intrauterine growth restriction; MCh, methacholine; Δ, net change after MCh challenge.

DISCUSSION

Intrauterine growth restriction and low birth weight are associated with the development of asthma in childhood and adult life (7, 16, 17). Sex and age-dependent changes in AHR within IUGR mice have been documented (8), aligning well with human population studies that show differences in the prevalence of asthma between males and females in early life and adulthood (18–20). Allergy is a major risk factor for asthma (21) and may differentially impact individuals that were growth-restricted *in utero*. The present study used an established mouse model of maternal hypoxia-induced IUGR (8–12) to examine changes in airway responsiveness in IUGR offspring that were subsequently sensitized and challenged with an allergic stimulus i.e., OVA. Findings were unexpected in that the independent effects of IUGR and allergy in promoting AHR did not enhance bronchoconstriction when both abnormalities were combined.

The animal model of IUGR used in this study is robust; the reduction in body weight (at birth and 8 weeks of age) is comparable to that observed previously (8–12), affecting both male and female offspring (10, 11). An acute allergy exposure protocol was preferred as this produces an inflammatory-mediated increase in airway responsiveness (13, 22), without altering body weight (13, 23). Airway responsiveness was assessed from changes in resistance measured using FOT which showed an exaggerated response to MCh after OVA, consistent with AHR. An exaggerated increase in H was also observed, as has been previously documented (13, 22), although G was unchanged. Tissue damping response is at times affected by OVA (22), varying with aerosol deposition patterns (24).

The IUGR and OVA protocols have revealed several interesting biological phenomena, the first of which is apparent after pure sensitization, even prior to bronchial challenge. As discussed, IUGR offspring in the absence of sensitization exhibit sex-dependent changes in airway responsiveness (8). While adult female offspring are hyperresponsive after IUGR (8), males are hyporesponsive, an effect that may well be explained by reduced contractile capacity of the ASM layer (9). We here now observe that after OVA sensitization, male and female mice are both hyperresponsive, in that males switched from a hypo- to hyperresponsive phenotype, manifested by an exaggerated increase in resistance, damping and elastance. Why allergic sensitization modifies airway responsiveness in male offspring is unclear. It has been previously shown that IgE response to house dust mite and OVA sensitization in male and female placentally restricted lambs is increased compared with Control lambs (25), but the OVA-specific IgE levels were comparable between our male and female Control and IUGR mice. One possibility is that a normal response to OVA interacts with a primed basal immunity, previously documented in the offspring of male IUGR mice, specifically elevated IL-13 in BAL fluid (10). Interleukin-13 is produced by natural killer cells after OVA sensitization and is strongly correlated with the Th2-induced allergic cascade and exaggerated bronchoconstrictor response (26).

The primary aim of the study was to examine how a prenatal insult (IUGR) interacts with a common risk factor for asthma i.e., aeroallergen. It seemed reasonable to hypothesize that if IUGR and aeroallergen independently increase airway responsiveness, then combined the respiratory abnormality would worsen. Indeed, aeroallergen exaggerates bronchoconstriction in a mouse model of ASM thickening caused by localized expression of a growth factor (13). Results showed no additional effect (additive or synergistic) of IUGR and allergy on airway responsiveness. Previous studies examining the relationship between atopy and low birth weight report an attenuated allergic response in IUGR individuals (27–29), including a

TABLE 1 | OVA IgE levels.

	Male		Female		Male		Female	
	Control ($n = 8$)	**Allergy ($n = 8$)**	**Control ($n = 10$)**	**Allergy ($n = 10$)**	**IUGR ($n = 8$)**	**IUGR + Allergy ($n = 7$)**	**IUGR ($n = 9$)**	**IUGR + Allergy ($n = 8$)**
OVA IgE (ng/mL)	7.50 ± 2.27	4.87 ± 0.95	6.16 ± 1.13	5.67 ± 0.88	4.98 ± 1.49	3.07 ± 0.65	8.73 ± 1.82	8.33 ± 3.00[#]

Data are mean ± SEM.
[#]Indicates a significant effect of sex within treatment groups. IgE, immunoglobulin E; IUGR, intrauterine growth restriction; OVA, ovalbumin.

TABLE 2 | Airway dimensions in the IUGR offspring.

	Male		Female	
Structure	**IUGR ($n = 6$)**	**IUGR + Allergy ($n = 7$)**	**IUGR ($n = 9$)**	**IUGR + Allergy ($n = 8$)**
P_{bm} (μm)	1352.38 ± 129.28	1349.12 ± 79.64	1359.06 ± 214.62	1306.91 ± 81.53
Total airway wall ($\sqrt{}$area/P_{bm})	0.147 ± 0.009	0.154 ± 0.005	0.150 ± 0.004	0.155 ± 0.007
Outer airway wall ($\sqrt{}$area/P_{bm})	0.069 ± 0.004	0.068 ± 0.002	0.067 ± 0.002	0.069 ± 0.003
Inner airway wall ($\sqrt{}$area/P_{bm})	0.129 ± 0.008	0.137 ± 0.004	0.134 ± 0.003	0.139 ± 0.006
Epithelium ($\sqrt{}$area/P_{bm})	0.111 ± 0.006	0.119 ± 0.004	0.121 ± 0.004	0.121 ± 0.005
ASM ($\sqrt{}$area/P_{bm})	0.056 ± 0.01	0.058 ± 0.002	0.056 ± 0.002	0.056 ± 0.003

Data are mean ± SEM. The sample size of IUGR male is reduced to 6 as two samples were damaged during tissue collection. ASM, airway smooth muscle; IUGR, intrauterine growth restriction; P_{bm}, perimeter of the basement membrane.

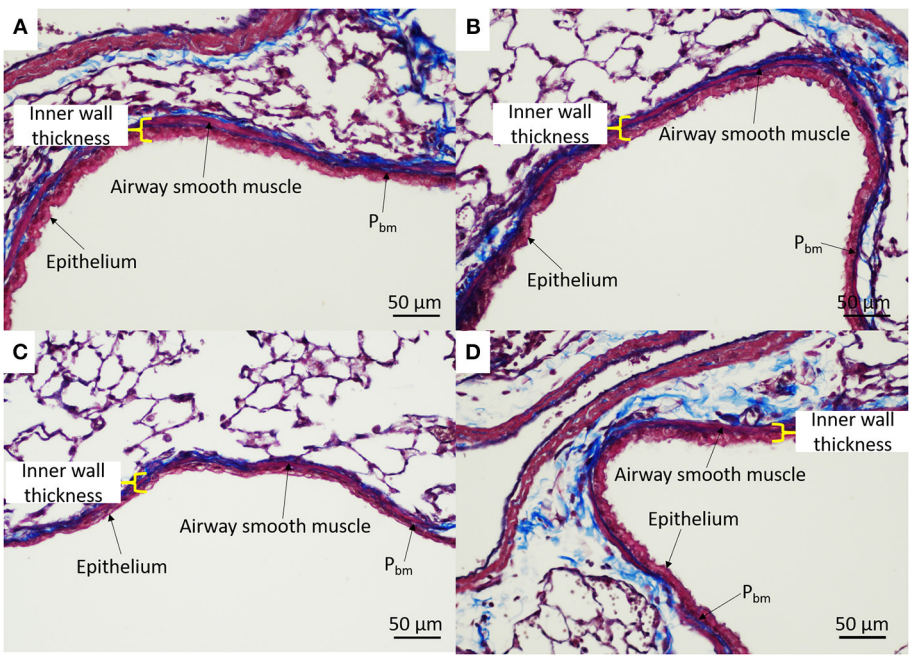

FIGURE 6 | Representative airway histology. IUGR male **(A)**, IUGR + Allergy male **(B)**, IUGR female **(C)**, IUGR + Allergy female **(D)** offspring. P_{bm}, perimeter of the basement membrane.

reduced incidence of atopic dermatitis and food allergies (29). The relationship between low birth weight and asthma in childhood and adult life (7, 16, 17) may therefore reflect innate changes in airway responsiveness rather than a tendency to allergic disease.

We have previously reported no change in postnatal airway morphology after IUGR (8, 12) or acute exposure to OVA (13), including P_{bm} and the thickness of ASM and epithelial layers, and total airway wall thickness. In this study, we investigated whether the effects of IUGR and allergy interact to produce

airway remodeling. Airway wall structure after IUGR was not affected by subsequent exposure to OVA. These data suggest that the increased bronchoconstrictor response observed in IUGR and OVA-induced allergic mice is independent of any change to airway wall structure.

A commonality between changes elicited by IUGR and OVA is airway inflammation; the former leading to increased lung macrophages at 2 and 8 weeks in mice (10) and in adult rats (30). The effects of macrophages are varied in asthma, exerting regulation through phagocytic, anti- and pro-inflammatory activities (31). It is conceivable that macrophage infiltration after IUGR favors excessive bronchoconstriction; macrophages are developed *in utero* and self-maintained throughout life *via* proliferation (32), and are activated by IL-13 (33) which appears in greater concentrations in IUGR male offspring (10). In patients with chronic obstructive pulmonary disease, a treatment-driven reduction in AHR was independently associated with a reduction in sputum macrophages as well as lymphocytes (34). At the same time, if anti-proliferative effects of macrophages dominate, an additional effect of IUGR could be to resist further abnormality following exposure to aeroallergen. Future research on how IUGR alters macrophage behavior is therefore warranted.

Other studies have also queried potential interactions between IUGR and allergen exposure. Landgraf et al. (35) used a gestational maternal undernutrition rat model of IUGR and reported an increase in airway responsiveness after OVA sensitization and challenge. However, in the study by Landgraf et al., IUGR alone did not appear to increase bronchoconstrictor response, although the method of assessing constriction from changes in perfusion pressure of excised lungs is quite indirect and may lack sensitivity (35). Two other studies which also used a maternal undernutrition-induced IUGR model in mice and rats demonstrate increased lung inflammation in IUGR offspring following OVA sensitization and challenge (36, 37). Differences in model parameters likely contribute to these disparate findings, including the method used to induce IUGR (hypoxia or undernutrition), duration of exposure and species. Despite these differences, animal models of IUGR seem to consistently report changes in airway biology that are of relevance to asthma.

We acknowledge that there are differences in mouse lung anatomy compared with human (38) which to some extent reduces the model's relevance to disease. However, the data generated allows us to form hypotheses on how prenatal and postnatal disorders interact and reveals new avenues for therapy. Airway responsiveness is modified by numerous exposures that do not necessarily share the same underlining mechanism. Given that airway biology can be modified by such a diverse range of factors, this could explain why not all treatments have the same efficacy on a given asthmatic patient. In addition to postnatal preventative measures for asthma, the prenatal window of susceptibility needs further consideration.

In summary, results indicate that while sensitized IUGR offspring are hyperresponsive to an inhaled bronchoconstrictor agonist, aeroallergen does not cause further functional disruption. These findings suggest that innate changes in bronchial reactivity are more likely to explain associations between IUGR and asthma, rather than an allergen driven inflammatory response within the lungs.

DATA AVAILABILITY STATEMENT

The original contributions presented in the study are included in the article/**Supplementary Material**, further inquiries can be directed to the corresponding author.

ETHICS STATEMENT

The animal study was reviewed and approved by The University of Western Australia Animal Ethics Committee (approval number RA/3/100/1570).

AUTHOR CONTRIBUTIONS

KW and PN: conceived and designed the experiments. JK, CW, and KW: performed the experiments. All authors analyzed the data, drafted and helped critically revise, read and approve the manuscript.

FUNDING

This project was funded by the National Health and Medical Research Council (NHMRC) of Australia Project Grant 1120128 (KW). KW was supported by a NHMRC Early Career Research Fellowship (1090888), Thoracic Society of Australia and New Zealand/National Asthma Council-Asthma and Airways Career Development Fellowship and a Western Australian Department of Health—New Independent Researcher Infrastructure Support. PN was supported by a Western Australian Department of Health—Medical and Health Research Infrastructure Fund. CW was supported by an Australian Government Research Training Program Scholarship at The University of Western Australia.

ACKNOWLEDGMENTS

We would like to thank Maddison R. Francis for her assistance in animal handling and monitoring, and Luke J. Berry for his assistance in performing the ELISA assay.

SUPPLEMENTARY MATERIAL

The Supplementary Material for this article can be found online at: https://www.frontiersin.org/articles/10.3389/fmed.2021.674324/full#supplementary-material

REFERENCES

1. Chapman DG, Irvin CG. Mechanisms of airway hyperresponsiveness in asthma: the past, present and yet to come. *Clin Exp Allergy.* (2015) 45:706–19. doi: 10.1111/cea.12506
2. Holgate ST, Peters-Golden M, Panettieri RA, Henderson WR. Roles of cysteinyl leukotrienes in airway inflammation, smooth muscle function, and remodeling. *J Allergy Clin Immunol.* (2003) 111:18–36. doi: 10.1067/mai.2003.25
3. Bradding P, Walls AF, Holgate ST. The role of the mast cell in the pathophysiology of asthma. *J Allergy Clin Immunol.* (2006) 117:1277–84. doi: 10.1016/j.jaci.2006.02.039
4. Elliot JG, Noble PB, Mauad T, Bai TR, Abramson MJ, McKay KO, et al. Inflammation-dependent and independent airway remodelling in asthma. *Respirology.* (2018) 23:1138–45. doi: 10.1111/resp.13360
5. Fehrenbach H, Wagner C, Wegmann M. Airway remodeling in asthma: what really matters. *Cell Tissue Res.* (2017) 367:551–69. doi: 10.1007/s00441-016-2566-8
6. Dame Carroll JR, Magnussen JS, Berend N, Salome CM, King GG. Greater parallel heterogeneity of airway narrowing and airway closure in asthma measured by high-resolution CT. *Thorax.* (2015) 70:1163–70. doi: 10.1136/thoraxjnl-2014-206387
7. Källén B, Finnström O, Nygren KG, Otterblad Olausson P. Association between preterm birth and intrauterine growth retardation and child asthma. *Eur Respir J.* (2013) 41:671–6. doi: 10.1183/09031936.00041912
8. Wang KCW, Larcombe AN, Berry LJ, Morton JS, Davidge ST, James AL, et al. Foetal growth restriction in mice modifies postnatal airway responsiveness in an age and sex-dependent manner. *Clin Sci.* (2018) 132:273–84. doi: 10.1042/CS20171554
9. Noble PB, Kowlessur D, Larcombe AN, Donovan GM, Wang KCW. Mechanical abnormalities of the airway wall in adult mice after intrauterine growth restriction. *Front Physiol.* (2019) 10:1073. doi: 10.3389/fphys.2019.01073
10. Looi K, Kicic A, Noble PB, Wang KCW. Intrauterine growth restriction predisposes to airway inflammation without disruption of epithelial integrity in postnatal male mice. *J Dev Orig Health Dis.* (2021) 12:496–504. doi: 10.1017/S2040174420000744
11. Francis MR, Pinniger GJ, Noble PB, Wang KCW. Intrauterine growth restriction affects diaphragm function in adult female and male mice. *Pediatr Pulmonol.* (2020) 55:229–35. doi: 10.1002/ppul.24519
12. Wang KCW, Noble PB. Foetal growth restriction and asthma: airway smooth muscle thickness rather than just lung size? *Respirology.* (2020) 25:889–91. doi: 10.1111/resp.13851
13. Wang KCW, Le Cras TD, Larcombe AN, Zosky GR, Elliot JG, James AL, et al. Independent and combined effects of airway remodelling and allergy on airway responsiveness. *Clin Sci (Lond).* (2018) 132:327–38. doi: 10.1042/CS20171386
14. Sato S, Bartolák-Suki E, Parameswaran H, Hamakawa H, Suki B. Scale dependence of structure-function relationship in the emphysematous mouse lung. *Front Physiol.* (2015) 6:146. doi: 10.3389/fphys.2015.00146
15. Donovan GM, Wang KCW, Shamsuddin D, Mann TS, Henry PJ, Larcombe AN, et al. Pharmacological ablation of the airway smooth muscle layer-mathematical predictions of functional improvement in asthma. *Physiol Rep.* (2020) 8:e14451. doi: 10.14814/phy2.14451
16. Mu M, Ye S, Bai MJ, Liu GL, Tong Y, Wang SF, et al. Birth weight and subsequent risk of asthma: a systematic review and meta-analysis. *Heart Lung Circ.* (2014) 23:511–9. doi: 10.1016/j.hlc.2013.11.018
17. Xu XF, Li YJ, Sheng YJ, Liu JL, Tang LF, Chen ZM. Effect of low birth weight on childhood asthma: a meta-analysis. *BMC Pediatr.* (2014) 14:275. doi: 10.1186/1471-2431-14-275
18. de Marco R, Locatelli F, Sunyer J, Burney P. Differences in incidence of reported asthma related to age in men and women. A retrospective analysis of the data of the European Respiratory Health Survey. *Am J Respir Crit Care Med.* (2000) 162:68–74. doi: 10.1164/ajrccm.162.1.9907008
19. Ernst P, Ghezzo H, Becklake MR. Risk factors for bronchial hyperresponsiveness in late childhood and early adolescence. *Eur Respir J.* (2002) 20:635–9. doi: 10.1183/09031936.02.00962002
20. Manfreda J, Sears MR, Becklake MR, Chan-Yeung M, Dimich-Ward H, Siersted HC, et al. Geographic and gender variability in the prevalence of bronchial responsiveness in Canada. *Chest.* (2004) 125:1657–64. doi: 10.1378/chest.125.5.1657
21. Nelson HS. The importance of allergens in the development of asthma and the persistence of symptoms. *J Allergy Clin Immunol.* (2000) 105(6 Pt 2):S628–32. doi: 10.1067/mai.2000.106154
22. Zosky GR, Larcombe AN, White OJ, Burchell JT, Janosi TZ, Hantos Z, et al. Ovalbumin-sensitized mice are good models for airway hyperresponsiveness but not acute physiological responses to allergen inhalation. *Clin Exp Allergy.* (2008) 38:829–38. doi: 10.1111/j.1365-2222.2007.02884.x
23. Kim DI, Song MK, Lee K. Comparison of asthma phenotypes in OVA-induced mice challenged *via* inhaled and intranasal routes. *BMC Pulm Med.* (2019) 19:241. doi: 10.1186/s12890-019-1001-9
24. Zosky GR, von Garnier C, Stumbles PA, Holt PG, Sly PD, Turner DJ. The pattern of methacholine responsiveness in mice is dependent on antigen challenge dose. *Respir Res.* (2004) 5:15. doi: 10.1186/1465-9921-5-15
25. Wooldridge AL, Bischof RJ, Meeusen EN, Liu H, Heinemann GK, Hunter DS, et al. Placental restriction of fetal growth reduces cutaneous responses to antigen after sensitization in sheep. *Am J Physiol Regul Integr Comp Physiol.* (2014) 306:441–6. doi: 10.1152/ajpregu.00432.2013
26. Chen Z, Wang L. Ovalbumin induces natural killer cells to secrete Th2 cytokines IL-5 and IL-13 in a mouse model of asthma. *Mol Med Rep.* (2019) 19:3210–6. doi: 10.3892/mmr.2019.9966
27. Grieger JA, Clifton VL, Tuck AR, Wooldridge AL, Robertson SA, Gatford KL. In utero programming of allergic susceptibility. *Int Arch Allergy Immunol.* (2016) 169:80–92. doi: 10.1159/000443961
28. Lundholm C, Ortqvist AK, Lichtenstein P, Cnattingius S, Almqvist C. Impaired fetal growth decreases the risk of childhood atopic eczema: a Swedish twin study. *Clin Exp Allergy.* (2010) 40:1044–53. doi: 10.1111/j.1365-2222.2010.03519.x
29. Wooldridge AL, McMillan M, Kaur M, Giles LC, Marshall HS, Gatford KL. Relationship between birth weight or fetal growth rate and postnatal allergy: a systematic review. *J Allergy Clin Immunol.* (2019) 144:1703–13. doi: 10.1016/j.jaci.2019.08.032
30. Wang KCW, Morton JS, Davidge ST, Larcombe AN, James AL, Donovan GM, et al. Increased heterogeneity of airway calibre in adult rats after hypoxia-induced intrauterine growth restriction. *Respirology.* (2017) 22:1329–35. doi: 10.1111/resp.13071
31. van der Veen TA, de Groot LES, Melgert BN. The different faces of the macrophage in asthma. *Curr Opin Pulm Med.* (2020) 26:62–8. doi: 10.1097/MCP.0000000000000647
32. Guilliams M, De Kleer I, Henri S, Post S, Vanhoutte L, De Prijck S, et al. Alveolar macrophages develop from fetal monocytes that differentiate into long-lived cells in the first week of life *via* GM-CSF. *J Exp Med.* (2013) 210:1977–92. doi: 10.1084/jem.20131199
33. Martinez-Nunez RT, Louafi F, Sanchez-Elsner T. The interleukin 13 (IL-13) pathway in human macrophages is modulated by microRNA-155 *via* direct targeting of interleukin 13 receptor alpha1 (IL13Ralpha1). *J Biol Chem.* (2011) 286:1786–94. doi: 10.1074/jbc.M110.169367
34. van den Berge M, Vonk JM, Gosman M, Lapperre TS, Snoeck-Stroband JB, Sterk PJ, et al. Clinical and inflammatory determinants of bronchial hyperresponsiveness in COPD. *Eur Respir J.* (2012) 40:1098–105. doi: 10.1183/09031936.00169711
35. Landgraf MA, Landgraf RG, Jancar S, Fortes ZB. Influence of age on the development of immunological lung response in intrauterine undernourishment. *Nutrition.* (2008) 24:262–9. doi: 10.1016/j.nut.2007.12.005
36. Xing Y, Wei H, Xiao X, Chen Z, Liu H, Tong X, et al. Methylated Vnn1 at promoter regions induces asthma occurrence *via* the PI3K/Akt/NFκB-mediated inflammation in IUGR mice. *Biol Open.* (2020) 9:bio049106. doi: 10.1242/bio.049106
37. Xu XF, Hu QY, Liang LF, Wu L, Gu WZ, Tang LL, et al. Epigenetics of hyper-responsiveness to allergen challenge following intrauterine growth retardation rat. *Respir Res.* (2014) 15:137. doi: 10.1186/s12931-014-0137-7

38. Irvin CG, Bates JH. Measuring the lung function in the mouse: the challenge of size. *Respir Res.* (2003) 4:4. doi: 10.1186/rr199

Conflict of Interest: The authors declare that the research was conducted in the absence of any commercial or financial relationships that could be construed as a potential conflict of interest.

Copyright © 2021 Kalotas, Wang, Noble and Wang. This is an open-access article distributed under the terms of the Creative Commons Attribution License (CC BY). The use, distribution or reproduction in other forums is permitted, provided the original author(s) and the copyright owner(s) are credited and that the original publication in this journal is cited, in accordance with accepted academic practice. No use, distribution or reproduction is permitted which does not comply with these terms.

frontiers in Medicine

REVIEW
published: 15 June 2021
doi: 10.3389/fmed.2021.667315

Perinatal Nutritional and Metabolic Pathways: Early Origins of Chronic Lung Diseases

Celien Kuiper-Makris[1†], Jaco Selle[1†], Eva Nüsken[2], Jörg Dötsch[2] and Miguel A. Alejandre Alcazar[1,3,4,5]*

[1] Department of Pediatric and Adolescent Medicine, Translational Experimental Pediatrics—Experimental Pulmonology, Faculty of Medicine and University Hospital Cologne, University of Cologne, Cologne, Germany, [2] Department of Pediatric and Adolescent Medicine, Faculty of Medicine and University Hospital Cologne, University of Cologne, Cologne, Germany, [3] Center for Molecular Medicine Cologne (CMMC), Faculty of Medicine and University Hospital Cologne, University of Cologne, Cologne, Germany, [4] Excellence Cluster on Stress Responses in Aging-associated Diseases (CECAD), Faculty of Medicine and University Hospital Cologne, University of Cologne, Cologne, Germany, [5] Member of the German Centre for Lung Research (DZL), Institute for Lung Health, University of Giessen and Marburg Lung Centre (UGMLC), Gießen, Germany

Lung development is not completed at birth, but expands beyond infancy, rendering the lung highly susceptible to injury. Exposure to various influences during a critical window of organ growth can interfere with the finely-tuned process of development and induce pathological processes with aberrant alveolarization and long-term structural and functional sequelae. This concept of developmental origins of chronic disease has been coined as perinatal programming. Some adverse perinatal factors, including prematurity along with respiratory support, are well-recognized to induce bronchopulmonary dysplasia (BPD), a neonatal chronic lung disease that is characterized by arrest of alveolar and microvascular formation as well as lung matrix remodeling. While the pathogenesis of various experimental models focus on oxygen toxicity, mechanical ventilation and inflammation, the role of nutrition before and after birth remain poorly investigated. There is accumulating clinical and experimental evidence that intrauterine growth restriction (IUGR) as a consequence of limited nutritive supply due to placental insufficiency or maternal malnutrition is a major risk factor for BPD and impaired lung function later in life. In contrast, a surplus of nutrition with perinatal maternal obesity, accelerated postnatal weight gain and early childhood obesity is associated with wheezing and adverse clinical course of chronic lung diseases, such as asthma. While the link between perinatal nutrition and lung health has been described, the underlying mechanisms remain poorly understood. There are initial data showing that inflammatory and nutrient sensing processes are involved in programming of alveolarization, pulmonary angiogenesis, and composition of extracellular matrix. Here, we provide a comprehensive overview of the current knowledge regarding the impact of perinatal metabolism and nutrition on the lung and beyond the cardiopulmonary system as well as possible mechanisms determining the individual susceptibility to CLD early in life. We aim to emphasize the importance of unraveling the mechanisms of perinatal metabolic programming to develop novel preventive and therapeutic avenues.

Keywords: lung development and pulmonary diseases, perinatal nutrition, maternal obesity, intrauterine growth restriction, chronic lung disease, bronchopulmonary dysplasia (BPD)

OPEN ACCESS

Edited by:
Hsiao-Chi Chuang,
Taipei Medical University, Taiwan

Reviewed by:
Robbert J. Rottier,
Erasmus Medical Center, Netherlands
Daan Ophelders,
Maastricht University, Netherlands

****Correspondence:***
Miguel A. Alejandre Alcazar
miguel.alejandre-alcazar@uk-koeln.de

[†]These authors share first authorship

Specialty section:
This article was submitted to Pulmonary Medicine, a section of the journal Frontiers in Medicine

Received: *12 February 2021*
Accepted: *12 May 2021*
Published: *15 June 2021*

Citation:
Kuiper-Makris C, Selle J, Nüsken E, Dötsch J and Alejandre Alcazar MA (2021) Perinatal Nutritional and Metabolic Pathways: Early Origins of Chronic Lung Diseases. Front. Med. 8:667315. doi: 10.3389/fmed.2021.667315

INTRODUCTION

Chronic lung diseases (CLD) such as asthma, chronic obstructive pulmonary disease (COPD) and pulmonary arterial hypertension (PAH) have a major impact on global health, with COPD being the third leading cause of death worldwide (WHO Global Health Estimates, 2020). CLDs do not only have an enormous impact on the patient's quality of life, but also on health care costs (e.g., an average of $4147 per COPD patient per year) (1, 2). While the pathology of adult lung diseases and the influence of environmental factors such as smoking have been extensively studied, the mechanisms determining the individual susceptibility to CLD early in life remain elusive. This review will provide insights in the current knowledge on how perinatal nutritional and metabolic conditions adversely affect lung development and contribute to the origin of CLDs.

Maternal obesity and intrauterine growth restriction (IUGR) represent alterations of the antenatal, perinatal and postnatal nutritional and metabolic status with adverse consequences for the fetus and newborn. (1) First, both maternal obesity and IUGR increase the risk of pregnancy complications and prematurity of the offspring. Epidemiological studies have shown that not only the risk of pregnancy complications for overweight and obese mothers is higher; it is also associated with an early pregnancy loss, congenital malformations, premature birth and stillbirth (3). In addition, the offspring has an increased risk of being either macrosome or IUGR, both introducing their own risk of comorbidity. IUGR is diagnosed in 5–10% of all pregnancies, characterized as a rate of fetal growth less than the growth potential that is appropriate for the gestational age, and well–recognized as an additional risk factor for prematurity (4, 5). (2) Second, fetal and postnatal nutritional supply as well as maternal weight and metabolism can adversely affect the long-term health of the child. This is referred to as *perinatal or metabolic programming* (6, 7). This concept was initially coined by Barker as the *fetal origins* hypothesis, also known as *fetal programming*. Barker et al. proposed that the developing fetus adapts its growth rate and metabolism as a response to variations in the supply of nutrients (and oxygen), which may lead to permanent changes of organs' structure and physiology in the newborn (8). Over the past two decades, the developmental origins of health and disease have gained increasing scientific interest. There has been an enormous effort and an accumulation of studies devoted to elucidating the underlying mechanisms of perinatal (metabolic) programming of diseases as well as its prevention and therapy. (3) Lastly, maternal obesity and IUGR are associated with long-term alterations of lung function and lung structure. For example, clinical reports showed a positive linear trend between birth weight, adjusted for maternal factors, and lung function in adulthood (9). Furthermore, children that were exposed to maternal obesity during pregnancy or gestational diabetes mellitus (GDM) have an increased risk of developing asthma in childhood (10–12). These findings indicate the significant impact of body weight, nutrition, and metabolism during critical phases of pregnancy and the early postnatal period on the lung development and later pulmonary function of a child (13).

In addition to the adverse nutritive and metabolic influences, the time of exposure is of great importance with regard to the resulting lung pathology. There are different critical windows of lung development with diverse developmental biological processes. The lung develops in five stages, with the last (alveolarization) starting shortly before birth and continuing beyond infancy (14). The window and the nature of exposure to adverse influences render not only the prenatal, but also postnatal lung development highly susceptible to injury and CLDs (15). This basic principle of timing emphasizes the far-reaching complex consequences of antenatal, perinatal and postnatal nutrition. Here, we provide an overview of the impact and mechanisms of nutritive surplus with metabolic disorder (maternal obesity) as well as nutritive deprivation (e.g., IUGR) on the child's lung health (schematic representation in **Figure 1**).

THE IMPACT OF PERINATAL NUTRITIVE SURPLUS ON THE ORIGINS OF CHRONIC LUNG DISEASE

Obesity and overweight result from an imbalance of energy consumption and energy intake, causing fat accumulation in adipose tissue (16). The origin of obesity is multifactorial and comprises a complex interaction of genetic and life style factors (17, 18). It is widely accepted that each individual has a certain level of predisposition for obesity due to genetic and epigenetic adaptations along with modifying environmental factors that can in part contribute to familiar obesity (17). Two central endocrine pathways in obesity are those of insulin and leptin. Insulin is a critical regulator of adipocyte biology that promotes the uptake of glucose and fatty acids and stimulates lipogenesis while inhibiting lipolysis (19). In obesity, the glucose transport and adipocyte metabolism are decreased despite high circulating levels of insulin, also known as insulin resistance (20). Leptin is produced by adipose tissue and acts as a regulator of appetite and energy expenditure (21). Obesity is associated with high levels of circulating leptin combined with leptin resistance (22). Leptin and insulin directly interact with each other and in addition, leptin influences insulin sensitivity through the regulation of glucose metabolism (23). Interestingly, targeting the energy balance to favor weight loss might induce compensatory behavioral and metabolic actions that favor the maintenance of bodyweight (24). This is one of the explanations for the further increasing numbers of obesity, despite multiple broad scale attempts on lifestyle and dietary interventions. Instead, obesity has grown into a worldwide pandemic. Surveys conducted by the WHO in 2008 showed that around 1.5 billion adults worldwide suffer from overweight, which corresponds to a body mass index (BMI) of over 25. Of far greater concern are the ∼200 million men and 300 million women with a BMI of more than 30, therefore considered to be obese (25). It is alarming that the prevalence of overweight and obesity is not only increasing dramatically among adults, but also children (26).

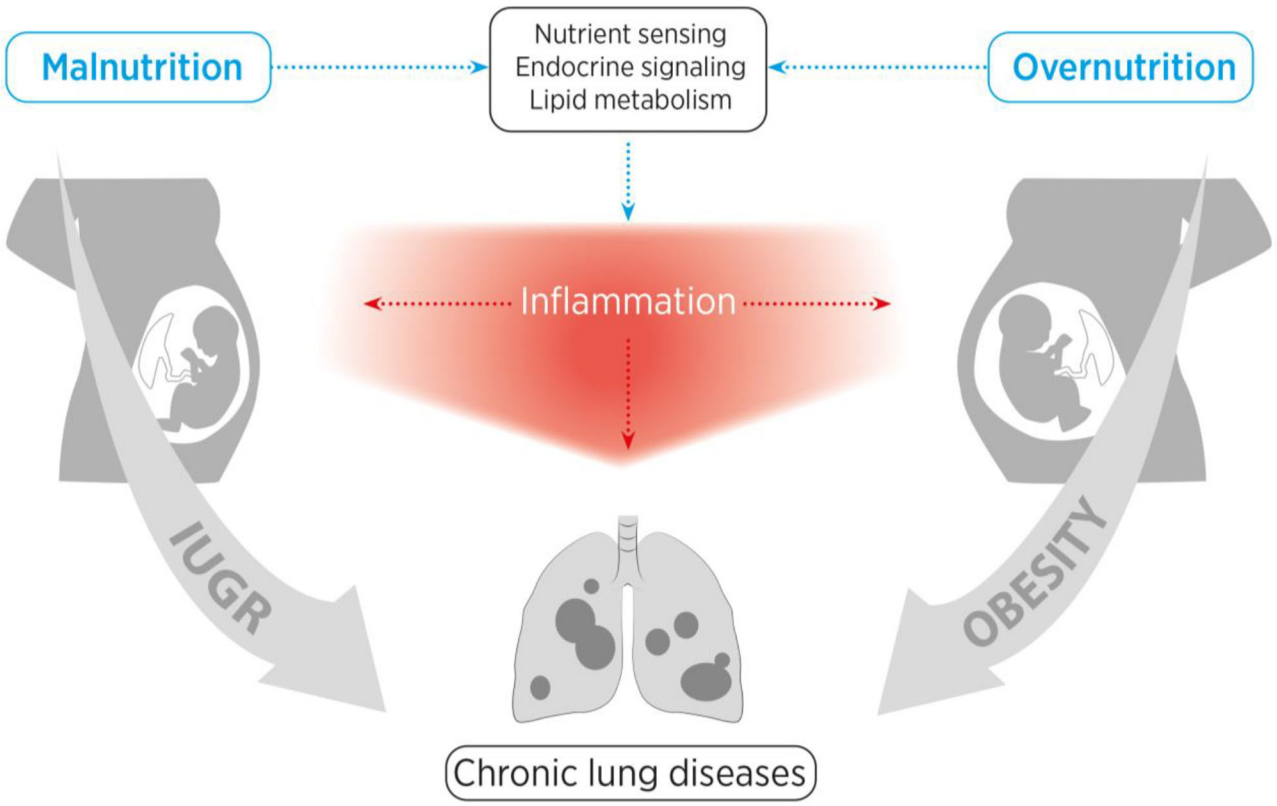

FIGURE 1 | Schematic representation of the structure of this review. We aim to provide a comprehensive overview of the influences of maternal obesity, early childhood obesity and intrauterine growth restriction (IUGR) on nutrient sensing as well as endocrine and inflammatory pathways, and how these adverse perinatal effects contribute to the early origins of chronic lung diseases.

Linking Maternal to Childhood Obesity: a Transgenerational Vicious Circle

Early childhood obesity has been proposed as a strong predictor of overweight in early adulthood (27). It has also been reported that maternal obesity and GDM can cause early-onset childhood obesity, which is associated with a higher prevalence of overweight or obesity in adulthood (28). In the USA, 17% of children are already considered obese (26, 29). Studies show that 1 to 2-year-old overweight children are more likely to be obese in their teenage and middle age years, and are prone to develop early-onset metabolic syndrome (30–33). Metabolic syndrome is characterized by obesity, type 2 diabetes, cardiovascular diseases, dyslipidemia and hypertension. As the prevalence of obesity amongst young adults continues to rise, the number of overweight/obese pregnant women is also steadily increasing. Interestingly, there is accumulating evidence of a transgenerational effect of obesity that adversely affects child health throughout life (34, 35). Specifically, maternal BMI shows a significant correlation with high offspring's birth weight and children's overweight (30, 36, 37). Thus, children of overweight mothers are at high risk of developing overweight later in life and tend to suffer from overweight-associated diseases (38). These findings are supported by experimental studies that show higher tendency for obesity and impaired insulin response in offspring of obese dams (39–41).

These transgenerational effects can be attributed, in part, to epigenetic changes in the offspring of obese mothers. The DNA is hypomethylated at the start of embryonic development, therefore, the developing embryo is particularly sensitive to epigenetic changes (e.g., DNA methylation, histone modification and microRNA expression) in response to the intrauterine environment (42). For example, maternal high-fat diet before, during and after pregnancy has been shown to alter miRNA expression and to induce a chronic dysregulation of insulin-like growth factor 2 (IGF-2) signaling in a mouse model (43). Such changes are not only detectable in adult mice (42), but also in human fetal umbilical cord blood (44). In addition, there are multiple reports of modified DNA methylation on sites of importance for metabolic processes after dysglycemia and/or high-fat diet during pregnancy (45–47).

In addition to metabolic consequences, the rising incidence of early childhood obesity is particularly concerning because of the association with respiratory symptoms and diseases in youth. One of the most common respiratory symptoms in childhood is wheezing, with ∼30% of all children suffering from it (48). The risk of recurrent wheezing is especially high in

children of obese mothers (49, 50). Obese children experience exertional dyspnea and often suffer from obstructive sleep apnea syndrome (OSAS) as well as obesity hypoventilation syndrome (OHS) (51, 52). In case of an emergency, obese children show dyspnea related to sedation and post-operative care (53). Furthermore, persistent asthma is strongly associated with high BMI throughout childhood (54–56), which manifests in a 92% higher prevalence of asthma in adult obese patients (57). In addition, the functional parameters of lung function such as respiratory muscle strength and endurance, airway resistance, lung volume and function or gas exchange are negatively influenced by obesity (58–60). Collectively, these studies indicate an adverse clinical course of respiratory diseases in children of obese mothers and after childhood obesity. In the following, we will discuss possible causes for the association between maternal obesity and child lung health.

Molecular Insights Into the Mechanical Effects of Obesity on Lung Function

Mechanical and physical influences on the lung play a significant role in the overall health of obese children and adults. Obese persons, including children, experience a lung restrictive syndrome, which goes along with increased overall body volume causing a narrowing of the upper airway and a reduced full inflation due to neck fat and an inadequate thoracic expansion, respectively (61). Accordingly, obese children suffer from obstructive sleep apnea hypoventilation syndrome (OSAHS) which is associated with hypoxemia, hypoventilation, sleep interruptions and chronic fatigue (62). Therefore, OSAHS has a drastic effect on oxygen supply and can induce hypoxia-associated changes in gene expression through the transcription factor hypoxia-inducible factor (HIF) (63). Under normoxia, prolyl hydroxylases (PHDs) hydroxylate proline residues on HIF-α subunits leading to subsequent proteasomal degradation through ubiquitination. In contrast, hypoxia reduces the O_2-dependent hydroxylation of HIF-α subunits by PHDs, resulting in nuclear HIF-α accumulation (64). In a murine model, the effects of hypoxia-mediated HIF activity have been reported to be involved in the pathogenesis of pulmonary arterial hypertension (PAH), in part by upregulating the vasoconstrictor endothelin-1 (65, 66). Deficiency of HIF-2α, however, partly protected from the increase in endothelin and PAH (65, 66). In addition, stabilization of HIF-α induces alveolar epithelial type 2 cell (ATII) apoptosis and subsequent fibrotic lung diseases (67). In contrast, the use of PHD inhibitors *in vivo* to stabilize HIF-α improved lung growth and function in a model of prematurity (68, 69).

It has been shown that HIF-1α in part sustains the Warburg effect (70, 71). The Warburg effect describes a condition in which the cells obtain their energy mainly through glycolysis with subsequent excretion of lactate. This alternative metabolic state for energy production is used by cancer cells, but also by healthy cells under hypoxia (*anaerobic glycolysis*). As described above, obesity-associated mechanical forces can lead to an activation of HIF, a mediator of hypoxia. HIF can cause a shift toward glycolysis rather than oxidative phosphorylation, in order to meet the energy demands under hypoxic conditions (70). Interestingly, studies suggested a Warburg effect inversion, a condition in which cancer cells exposed to an adiposity environment increase energy production by aerobic respiration as well as gluconeogenesis (72). The authors suggest that the cells do not consume glucose in glycolysis, but produce glucose through gluconeogenesis. Moreover, it has been described that during hypoxia, mitochondria increase the production of reactive oxygen species (ROS) at complex III (73), leading to inhibition of PHD activity and subsequent stabilization of HIF-α (74, 75). The shift toward glycolysis by the Warburg effect and the increased production of ROS, both induced and maintained by hypoxia, resemble mitochondrial dysfunction (76, 77). Increasing evidence points toward a central role for mitochondrial dysfunction in the development of cancer as well as CLDs including asthma, COPD and PAH (71, 76, 77). Furthermore, recent studies have indicated that the hypoxia-induced increase of ROS in acute lung injury contributes to pulmonary fibrosis by triggering an epithelial-mesenchymal transition (EMT) (78, 79) *via* the stabilization of HIF-1α in several cell types, including alveolar epithelial cells (80).

These findings highlight the effect of obesity on oxygen sensing and energy metabolism as well as the subsequent consequences for the development of CLDs. HIF, as a central player in oxygen sensing, might serve as a potential therapeutic approach to target the rising incidences of obesity-related diseases. For example, preclinical data show that blocking HIF with digoxin in a mouse model prevented or slowed down the progression of PAH (81, 82). These promising findings demonstrate that not only preventing obesity itself, but also targeting specific metabolic processes might offer new preventive strategies for CLDs.

Cell Homeostasis and Inflammatory Response Under Obese Conditions

Obesity represents a state of *low-grade chronic inflammation*. The numbers of inflammatory cells such as $CD8^+$, $CD4^+$ and $CD68^+$ cells are significantly elevated in adipose tissue (83, 84). These immune cells along with adipocytes release a wide range of inflammatory factors including leptin, tumor necrosis factor-alpha (TNF-α) (85), interleukin 6 (IL-6), and IL-8 (86), C-reactive protein, monocyte chemoattractant protein-1 (MCP-1), and Plasminogen activator inhibitor-1 (PAI-1) (87–89). Exposure of the lung to these pro-inflammatory cytokines can occur in three different ways at different time points during lung development: (1) through transplacental transport from the obese mother to the fetus; (2) through breast milk of the obese mother during lactation; and (3) through the child's own adipose tissue as a result of (early) postnatal obesity. For example, maternal high-fat diet in a murine model during lactation [postnatal day 1 (P1) to P21] induced an early-onset obesity in the offspring with elevated inflammatory cytokines, such as IL-4, IL-6, IL-13, IL-17A, and TNF-α. The early inflammatory response was related to increased airway hyperreactivity, similar to asthma (90). The adverse effect of IL-6 on the lung was further supported by a study that showed that elevated IL-6 could in part account for the development of emphysema through IL-6

trans-signaling-mediated apoptosis of ATII. Blocking IL-6/gp130 signaling, however, prevented features of lung emphysema (91, 92). Furthermore, elevated IL-6 levels contribute to PAH (93). For example, IL-6 induces a downstream activation of Stat3, which in turn causes a phosphorylation of the transcription factor forkhead box O (FoxO) 1. Phosphorylation of FoxO1 leads to its cytoplasmatic sequestration, subsequent inactivation and ultimately to a hyperproliferation of bronchial smooth muscle cells (SMC) (93, 94). In addition to IL-6, TNF-α is also a notable adipocytokine that is elevated under obese conditions (95). TNF-α modulates the effects of G-protein coupled receptor (GPCR)-induced hyperreactivity in cultured murine airway SMCs and increases contractility (96). By this mechanism, TNF-α may be contributing to SMC responsiveness and the development of asthma. Consequently, the anti-inflammatory adiponectin reduces TNF-α-induced nuclear factor κ B (NFκB) signaling. Thus, the obesity-related decrease in adiponectin further contributes to a dysregulated TNF-α signaling (97). Due to its potential impact on the development of asthma, TNF-α is under intense investigation as a therapeutic target (98–100). Another important functional aspect of TNF-α is the ability to contribute to insulin resistance by inhibiting tyrosine phosphorylation of insulin receptor substrate-1 (IRS-1) (95). Similarly, PAI-1 is produced and secreted by adipocytes and elevated in obesity serum levels (89). In a mouse model of airway hyperresponsiveness, PAI-1 was involved in airway remodeling after LPS-induced lung injury (101). Chronically elevated levels of PAI-1 affect the extracellular matrix turnover and contribute to collagen deposition in the airways (102). Moreover, dysfunction of the adipose tissue after perinatal obesity can further contribute to the maintenance of *low-grade chronic inflammation*. For example, a recent study indicated that maternal obesity induces metabolic programming of adipocytes in the offspring with lifelong dysfunctional adipose tissue and obesity (103). Collectively, obesity represents a state of *low-grade chronic inflammation* exposing the developing lung to pro-inflammatory cytokines which could adversely affect lung growth as a first "hit" and increase susceptibility for CLDs in later life.

Nutrient Sensing and Leptin Signaling as a Mechanism of Perinatal Obesity

Under physiological conditions, leptin is integrated in the complex mechanisms of airway and bronchial maturation. A recent study highlighted the importance of physiological non-obese levels of leptin in lung maturation through the upregulation of the expression and the secretion of surfactant protein A (*Sftpa*) in ATII (104, 105). Similarly, leptin promoted maturation of lung structure and contributed to postnatal lung remodeling and enlargement of the alveolar surface area *via* the induction of the genes *Col1a1*, *Col3a1*, *Col6a3*, *Mmp2*, *Tieg1*, and *Stat1* (106). A lack of leptin signaling in *ob/ob* mice (induced by leptin deficiency) resulted in a significant reduction of alveolar surface, indicating a critical role of leptin in postnatal lung growth (106). These contradictory observations may be due to effects of high circulating concentrations of glucose and insulin during pregnancy in obese mothers, which might potentially overrule the beneficial effect of leptin on lung development (107). In addition, long-term exposure to leptin before birth could affect the expression of pulmonary leptin receptors, disturbing leptin-signaling, leading to defective lung maturation and respiratory function at birth (108, 109).

Leptin has a central role in the immune response as well. Leptin was linked to asthma in adults as well as in children; the severity of asthma was correlated to serum leptin levels in a meta-analysis of 13 studies (110–113). High leptin levels increased the T-helper cell type 2 (Th2)-type immune response in airways *via* a leptin-mediated and XBP1 (X-box binding protein 1) s-dependent activation of mTOR (mechanistic target of rapamycin) as well as MAPK (mitogen-activated protein kinase) signaling (114). A shift toward the Th2-type immune response in airways is characteristic for the pathogenesis of asthma, thus providing a relevant link between obesity-induced high circulating leptin levels and the development of asthma (114, 115). Adiponectin acts as an anti-inflammatory agent, counteracting leptin (88, 89). Circulating adiponectin levels are known to be reduced in obesity, possibly further contributing to the pathogenesis of obesity-associated asthma (116).

There have been several attempts to alter the high leptin and low adiponectin levels in order to restore the metabolic balance. For example, pharmacological elevation of adiponectin levels in obese mice protected from hyperglycemia, glucose intolerance, and insulin resistance (117) as well as increasing insulin sensitivity (118). However, to date, the effect of adiponectin supplementation on pulmonary development and function remains elusive. In diabetes, thiazolidinedione (TZD) is possibly the most extensively characterized regulator of adiponectin expression. TZDs, such as pioglitazone and rosiglitazone increase adiponectin expression through the activation of peroxisome proliferator-activated receptor gamma (PPARγ) (119, 120). Since it is already a well-established therapeutic intervention for diabetes, targeting adiponectin might be a new promising therapeutic approach for the prevention of long-term consequences of obesity such as pulmonary remodeling and reduced lung function.

Lipid Metabolism and Perinatal Obesity

Obesity is characterized by a dysregulation of the energy and lipid metabolism. Lipoproteins are responsible for the transport of fatty acids, cholesterol and phospholipids. Therefore, the lipoproteins in obese patients show a change in circulating protein levels (121). For example, apolipoprotein E (ApoE), which is part of the low-density lipoprotein (LDL), is elevated in the obese and contributes to fat mass accumulation (122). LDL/ApoE is internalized into cells by its receptor, the low-density lipoprotein receptors (LDLRs), and is the main source of cholesterol and phospholipids efflux out of cells. In the lung, ApoE is produced by lung macrophages and acts on ciliated airway epithelial cells, where it can modulate airway hyperreactivity, mucin gene expression, and goblet cell hyperplasia (121). Thereby, it is involved in reducing the susceptibility to airway hyperresponsiveness (121, 123). In line with this, genetic modified mice with an ApoE deletion show reduced alveologenesis and abnormal pulmonary function

with increased airway resistance as well as high dynamic and static compliance (124). PPARγ is a nuclear receptor and considered one of the master regulators of adipogenesis, showing a high expression pattern in adipose tissue and in the lung (125–127). PPARγ is essential for normal lung development *via* the induction of alveolar epithelial-mesenchymal paracrine signaling (128, 129). Murine studies with genetically deactivated PPARγ demonstrated a spontaneous development of PAH. Here, PPARγ has an anti-proliferative effect on smooth muscle cell proliferation, which might give the opportunity to use PPARγ agonists in treating PAH (130, 131). Moreover, unsaturated fatty acids and several eicosanoids are regulators of PPARγ and induce expression of genes encoding lipoprotein lipase, CD36, phosphoenolpyruvate carboxykinase, aquaporin 7 and adiponectin (132). This is of particular interest since the western style diet has high concentrations of poly-unsaturated fatty acids (133). In this context of western style diet and a higher rate of obese individuals in industrial western countries, elevated fatty acid levels in obesity may be important regulators and modulators of normal and aberrant lung development.

Glucose Metabolism and Hyperinsulemia

Obesity is intimately linked to insulin resistance, accompanied by elevated circulating insulin concentrations. The transduction of insulin signaling is in part mediated through the downstream phosphatidylinositol 3-kinase (PI3K)/protein kinase B (AKT) and mTOR pathways (134–137). The mTOR cascade is integral in orchestrating the complex mechanism of lung development, balancing nutrient and energy supply in the early stages of embryogenesis and fine-tuning tissue growth during organogenesis. An elaborated and comprehensive article by Land et al. provides a broad overview of the role of mTOR in lung development (138). High levels of insulin from diabetic mothers have the potential to inhibit the *Sftpa* gene expression in lung epithelial cells and thereby delay the fetuses' lung development. This insulin-induced inhibition acts *via* the rapamycin-sensitive PI3K signaling pathway and not *via* mitogen-activated protein kinase (MAPK) (139). This notion is further supported by the fact that inhibition of PI3K can contribute to insulin resistance and diabetes (140). Moreover, Ikeda and colleagues demonstrated that insulin reduces vascular endothelial growth factor (VEGF) expression and the transcriptional activity of HIF-2 on the VEGF promoter in an AKT-mTOR-dependent manner in cultured lung epithelial cells. They further demonstrated that activation of the AKT-mTOR pathway in mice reduced alveolar capillarization, stressing the importance of this pathway in lung epithelium and in the development of infant respiratory distress syndrome (RDS) (141). Interestingly, moderate physical activity of obese mothers can rescue maternal and the offsprings' insulin sensitivity, overall improving the metabolic, as well as potential pulmonary outcome in the obese mother as well as her offspring (142).

Insulin does not only affect the alveolar epithelial cells, but also increases the expression of genes related to the contractile phenotype of airway SMC through a Rho kinase- and PI3K-dependent mechanism (143). Apart from these direct effects on pulmonary cells, insulin is involved in the modulation of the immune response and thereby in the pathogenesis of asthma. For example, in mast cells, insulin induces PI3K-dependent signaling, which could contribute to allergic bronchoconstriction (144). On the other hand, Viardot and colleagues demonstrated that insulin influences T cell differentiation promoting a shift toward a Th2-type response. They state, that this effect may contribute to insulin's anti-inflammatory role in chronic inflammation associated with obesity and type 2 diabetes (145). Insulin further exhibits anti-inflammatory properties in acute Th1-type inflammation, where insulin diminishes acute lung injury and reduces levels of inflammatory cytokines (146). Taken together, insulin plays an important role in physiological lung development, supporting alveolarization. In obese patients, however, elevated insulin levels interfere with lung development and maturation, while facilitating a pro-asthmatic immune environment, which could affect the outcome of CLDs in later life.

Collectively, these studies show that perinatal obesity resulting from maternal and early childhood obesity may determine individual susceptibility for CLDs later in life. In addition to mechanical factors due to increased body mass, adipose tissue dysfunction and its consequences play a particularly important role. *Low-grade chronic inflammation* with increased levels of adipocytokines, impaired insulin signaling, and altered lipid metabolism can be important in metabolic programming of CLDs. In the future, further elucidation of the fat-lung axis is imperative for a better understanding of metabolic mechanisms in the development of CLDs and to develop new preventive and therapeutic approaches.

THE IMPACT OF PERINATAL NUTRITIVE DEFICIENCY ON THE ORIGINS OF CHRONIC LUNG DISEASE

Nutrient Deprivation and Lung Development: the Role of Intrauterine Growth Restriction

Intrauterine growth restriction (IUGR) was first described as "dysmaturity" and indicates an abnormally low birth weight for the gestational age. Classically, IUGR was defined as a birthweight below 2,500 g (147). More recently, it has been characterized as "not reaching the biologically based potential," often due to reduced perfusion or malnutrition *in utero* (148–150). IUGR and "small for gestational age" (SGA, birthweight of-2 SD/mean) are often used interchangeably; however, SGA neither excludes nor proves IUGR but serves as an easily quantifiable proxy for IUGR. Pathological intrauterine circumstances induce IUGR, resulting in an infant with low birth weight, often followed by a period of rapid postnatal weight gain, also called "catch-up growth." Catch-up growth is associated with altered nutrient supply, and overlaps with the final stages of pulmonary alveolarization and vascular maturation (151, 152). Moreover, infants with catch-up growth after IUGR have a higher risk to become overweight or obese and to develop metabolic disorders later in life (4, 153). These clinical findings have been supported by experimental models of IUGR (154–157).

The etiology of IUGR can be divided in (1) *fetal origins*, such as genetic abnormalities (e.g., chromosomal abnormalities), (2) *maternal factors* (e.g., vascular diseases, persistent hypoxia or undernutrition, and toxins), and (3) *placental etiologies* (e.g., placental insufficiency, inflammation) (158). It is thought that 40% of birth weight is ascribable to genetic factors and that the remaining 60% is due to fetal environmental exposures (159). Several historical events have caused a surge of IUGR cases in a defined birth cohort, which has provided deeper insight into the clinical sequelae of IUGR. The latest temporary surge of IUGR caused by maternal malnutrition in Europe was caused by the Second World War. Investigations of the Dutch Famine Birth Cohort (Amsterdam, 1944-1946) have shown that low birth weight infants often have a lower FEV1 and FVC, but not FEV1/FVC ratios, indicative of restrictive lung alterations (160, 161). Other cohorts, however, including an Indian study demonstrate an association of small head circumference (indicative of early gestational growth restriction) with reduced FEV1/FVC ratios (162, 163). These data show the diverse impact of intrauterine nutrient deprivation on lung health that could be in part accounted to the window of injury or the type of nutrient restriction (e.g., protein, vitamins). Overall, these observational and experimental studies highlight that being born IUGR represents a pathologic condition with far-reaching consequences for the child's health and disease, especially regarding metabolism and the lung.

The Interplay Between IUGR and Obesity

Maternal obesity and GDM are often associated with macrosomic offspring (164). However, in uncontrolled or badly controlled GDM, diabetic vasculopathy and nephropathy may lead to placental insufficiency-induced IUGR (165, 166). In addition, experimental data have shown that overnutrition of pregnant sheep causes IUGR in the fetus, likely due to major restriction in placental growth and relative hypoglycemia and fetal hypoinsulinemia during late pregnancy (167). This might be partly related to fetal hypoxia, in turn inducing fetal catecholamine expression and reducing circulating insulin concentrations (168). On the contrary, IUGR induces metabolic changes to the growing fetus that cause a risk for developing obesity, diabetes and metabolic syndrome later in life (4, 153). These changes are passed onto the next generation; female IUGR rat offspring exhibit symptoms of gestational diabetes, and their offspring has increased fasting glucose and insulin levels despite having a normal birth weight when compared to controls (169). These transgenerational changes might be attributed to epigenetic changes, not only affecting the IUGR offspring, but also the second generation by direct exposition of the offspring germ-line to the IUGR environment (170, 171). More specifically, the increased risk for childhood and adult obesity in IUGR offspring could be in part due to *programming* of the adipocytes toward lipogenesis and proliferation (172, 173). Moreover, the combination of IUGR (induced by surgical bilateral artery ligation) with maternal obesity increased hepatic cholesterol accumulation and LDLR expression when compared to non-IUGR controls (156). These data further support the notion that maternal obesity along with IUGR provides an additional risk for metabolic complications.

The Adverse Effects of IUGR on Pulmonary Structure and Function

IUGR causes structural changes to the lung. Multiple animal studies have shown that IUGR impairs alveolar formation and lung growth, leading to reduced lung function (155, 174–179). In addition, a recent study from our group has demonstrated that IUGR also negatively influences angiogenesis and extracellular matrix formation (157). The intimate link between angiogenesis and alveologenesis has been shown in various animal studies, where alveolar formation was reduced after blocking angiogenesis (180–182). Conversely, the positive influence of angiogenesis on alveolar growth and regeneration is of great therapeutic importance (181, 183). Structural alveolar and vascular changes during lung development could account for the functional alterations that were reported after IUGR in epidemiological studies: several cohort studies have shown that school-children born IUGR have a significantly lower FEV1 and airway resistance as well as a higher susceptibility to airway infections, independent of catch-up growth (184–189). Moreover, in long-term follow-up studies it was shown that a low birthweight decreases lung function in adulthood, with a reduction of lung capacity and elasticity, resembling a COPD phenotype (9, 190). In summary, there is compelling epidemiological and experimental evidence that IUGR determines lung structure and function and could thereby predispose for CLDs.

Endocrine Effects of IUGR and Catch-Up Growth Resemble those of Obesity

Children born SGA have an increased risk of reduced embryonic β-cell growth, glucose intolerance, insulin resistance, type II diabetes and obesity in childhood as well as later in life (191–197). The effect of IUGR on the regulation of insulin levels has been extensively studied, as insulin is not only important for euglycemia in the fetus but also serves as a major fetal (pulmonary-) growth factor (159). The stable glucose flow over the placenta during healthy pregnancy causes fetal insulin secretion that regulates normal adipose tissue development and deposition (198). As stated before, IUGR fetus can exhibit hypoglycemia and hypoinsulinemia due to inhibition of endocrine signaling by catecholamines (168). In addition, the pancreatic function can be decreased after IUGR, resulting in lower levels of intrauterine insulin secretion as well (199). In contrast, reports on postnatal insulin levels in IUGR newborns are contradictive, they might be slightly lower or equal to healthy controls (200, 201). Thus, IUGR causes a deregulation of intrauterine insulin levels, an important mediator in adipose tissue development and fat deposition.

The phase of catch-up growth after IUGR appears to be a strong determinant of future (lung) health. A key fetal adaptation to nutrient deprivation is the intrauterine upregulation of the insulin receptor under hypoinsulinemic circumstances in fetal skeletal muscle (202). After birth and under nutrient

surplus, this upregulated receptor is activated by an abundance of glucose and insulin, inducing accelerated body growth (202, 203). The closely related insulin-like growth factor 1 (IGF-1) is induced by growth hormone (GH)/somatropin and is an essential regulator of body growth. The inhibition of the GH/IGF-1 axis has been shown to dysregulate alveologenesis, mainly through disruption of the physiological deposition of the extracellular matrix (204). Work by our group has shown that inhibition of the GH/IGF-1 axis by IUGR was associated with an arrest of lung development; in contrast, catch-up growth caused a significant increase of GH/IGF-1 expression (174). Interestingly, recent work demonstrated that postnatal treatment with recombinant human IGF-1 improves lung growth and structure in a model for bronchopulmonary dysplasia (BPD) (205). In conclusion, there is a postnatal reactive upregulation of both the insulin receptor and the insulin-signaling (including IGF-1) pathway after IUGR, resulting in an initially increased insulin sensitivity during postnatal catch-up growth (4). However, school-aged and adolescent children with accelerated weight gain and catch-up growth after IUGR show increased levels of insulin and reduced insulin sensitivity, indicating the long-lasting effects of prenatal metabolic programming (206, 207).

In addition to the dysregulation of prenatal and postnatal insulin signaling, leptin has been identified to be dysregulated after IUGR as well. Animal studies have shown that IUGR rat pups rapidly develop leptin resistance during their catch-up growth, thereby stimulating weight gain through hyperphagia (208–210). An important molecular link between nutrient status, insulin/leptin signaling and metabolic outcome is the mTOR pathway, controlling cell growth in response to its environment (e.g., stress, oxygen, nutrient status) through protein synthesis as well as lipid, nucleotide, and glucose metabolism (211, 212). A study from our group has shown that nutrient sensing *via* the mTOR signaling pathway is dysregulated in lungs from a rat model of nutrient deprivation-induced IUGR (157). Recent reports demonstrated that the mTOR signaling pathway is also altered in the placenta of humans and in experimental IUGR studies, enforcing adaptive mechanisms from both the maternal nutrient supply and the fetus's energy demands (213, 214). These studies suggest that both the placenta and the fetus react to nutrient availability by regulating this key nutrient sensor. The mTOR pathway is postnatally essential for pancreatic β-cell and islet maturation (215). Furthermore, mTOR is a potent mediator of endocrine responses, translating signals from leptin and insulin to a negative feedback for insulin (216). Interestingly, studies demonstrate that mTOR is involved in lung development as well, by regulating cell growth for proper organ development (211, 212) and by interfering with essential developmental signaling pathways, such as pulmonary angiogenesis (VEGF) and extracellular matrix deposition (bone morphogenetic protein, BMP) (217, 218). Collectively, these data highlight the eminent impact of intrauterine nutrient deprivation on endocrine function. Of note are the converging similarities between IUGR and obesity with regard to the endocrine system and the long-term metabolic and pulmonary sequelae.

IUGR Causes Transgenerational Metabolic Programing

Epidemiological studies as well as animal studies have shown transgenerational effects of IUGR on metabolic function (219–221). In part, these effects can be attributed to epigenetic programming (222, 223). For example, Fu et al. as well as Tosh et al. described histone modification along the IGF-1 gene and subsequently altered mRNA expression of IGF-1 in a rat model for IUGR induced by placental insufficiency or maternal malnutrition, respectively (224, 225). In addition, Tosh et al. showed that the restriction of early postnatal nutrient intake partly prevents these epigenetic changes (224). Park et al. observed consistent epigenetic adaptations related to differential binding of dinucleotide methyl transferase 1 and 3a together with changes in histone acetylation and methylation in the promoter region of the *Pdx1* homeobox gene in a rat model of IUGR (226). Recent studies by Gonzalez-Rodriguez et al., demonstrated the genetic imprinting of H19/IGF2 in second-generation IUGR offspring. This genetic imprinting was associated with altered H19 and IGF2 expression, which is in turn related to an increased risk for obesity and associated metabolic diseases (220, 227). Interestingly, this effect is reversible with postnatal essential nutrient supplementation (220, 228). These studies highlight the influence of perinatal nutrition in the development but also the primary prevention of metabolic diseases, including their secondary pulmonary complications as described in the previous chapter. In summary, these data indicate the great potential of perinatal nutrition and metabolism as a preventive and therapeutic target for metabolic health and CLDs.

Chronic Inflammation in IUGR-Associated CLD

One of the vital connections between the metabolic consequences of intrauterine nutrient deprivation and altered lung development is chronic inflammation. Chronic inflammation has been associated with (1) IUGR (229–232), (2) obesity, type 2 diabetes and metabolic syndrome (233–235) as well as (3) CLDs (236–239). IUGR, followed by catch-up growth, shows similar endocrine dysregulation and activation of inflammatory mechanisms as obesity. For example, both obesity and IUGR exhibit similar levels of leptin and insulin resistance in response to their prenatal nutritional status and postnatal accelerated weight gain (191–197). A possible shift of the Th2 immune response might be another link between CLDs and metabolic changes, e.g., elevated leptin (240) and insulin (206, 207) levels after IUGR. Interestingly, a study in IUGR mice has shown that the Th2 shift and consequent recruitment of macrophages cause inflammation in the pancreatic β-cell islets, causing type 2 diabetes (230). To date, there is no conclusive evidence whether IUGR-associated chronic inflammation is causative for or a consequence of metabolic distress, but the reports support an intimate link between both conditions.

A clinical study on the cord blood of 20 SGA neonates showed that IUGR causes a low-grade inflammatory response: infants born IUGR had significantly increased levels of inflammatory markers IL-6, TNF-α, CRP and thrombopoetin

(232). Moreover, animal studies have demonstrated IUGR-associated systemic inflammation in various organs: adult (uteroplacental) IUGR rats exhibited increased pancreatic β-cell inflammation, increasing the risk of diabetes (230, 241); a sheep model for hypothermia-induced IUGR showed a decrease of NF-κB as key regulator of immune-responses (231); and finally, a recent study in IUGR lambs demonstrated increased inflammatory markers and expression of inflammatory as well as pro-apoptotic genes in liver tissue (229). Along with these reports, prior work from our group has shown that IUGR causes dysregulation of key developmental signaling pathways such as NPY(neuropeptide Y)/PKC(protein kinase C), IL-6/AMPKα and TGFβ (transforming growth factor β) signaling as well as the associated inflammatory response (178, 179, 242).

A highly relevant comorbidity for IUGR infants is prematurity. About 30–50% of all extremely premature infants display symptoms of IUGR (243, 244). The causes of prematurity are multifactorial, but there is a strong correlation with maternal obesity. A meta-analysis of 84 clinical studies has shown a significantly increased risk of (induced) preterm labor in overweight and obese pregnancies (245). In addition, the risk of neonatal respiratory complications after premature birth is higher in obese *vs.* non-obese pregnancies (246, 247).

Premature birth and perinatal inflammatory responses have been intimately linked to pathological processes (248). The lungs of preterm infants are often in the late-saccular to early-alveolar phase at birth and require respiratory support (249). Mechanical ventilation, continuous positive airway pressure (CPAP) or oxygen supplementation are necessary treatments, but cause inflammation, acute lung injury and lead to a neonatal CLD, also known as BPD (250–254). Lungs of infants with BPD are characterized by vascular and alveolar hypoplasia (255). As stated previously, IUGR alone adversely affects lung microvascular and alveolar formation. Interestingly, the combination of IUGR with the immature lung in premature infants increases the risk for the clinical manifestation of BPD (i.e., prolonged need of oxygen supplementation >36 weeks of gestation) (251, 256). These reports indicate that IUGR might be an initial "hit" to the organism, raising susceptibility to CLDs such as BPD.

In conclusion, similar to perinatal obesity and GDM, IUGR leads to acute as well as long-term functional and structural changes in the lung. A distinction must be made between an intrauterine and a postnatal phase in the process of perinatal programming caused by IUGR. While the intrauterine phase is characterized by nutritional deprivation, the postnatal phase is usually characterized by a catch-up growth. With regard to the pathomechanisms, metabolic signaling pathways, inflammation, and nutrient-sensing processes play an essential role, ultimately controlling alveolar and vascular formation and lung growth. However, the different phases of injury in IUGR also provide windows of opportunity for preventive strategies, therapeutic interventions and reprogramming in the future (**Figure 2**).

THE MICROBIOME AS A LINK BETWEEN NUTRITION AND LUNG HEALTH: OPPORTUNITY FOR INTERVENTION

As stated before, obesity represents a state of *low-grade chronic systemic inflammation*, as illustrated by the increased amount of circulating inflammatory cells (83, 84) as well as elevated expression levels of inflammatory factors (85–88). External influences on the lung health such as airway pollution and cigarette smoking have been extensively studied in the last decade. Recently however, another field of interest has gained momentum: the gut-lung microbiome. This represents an extremely important link between nutrition, chronic inflammation and pulmonary health. In the following, we will detail the role of the microbiome in the early origins of CLDs.

The infant's microbiome is predominantly established during and shortly after birth, where it is exposed to the maternal and environmental microbiome (257). The introduction of solid foods into the children's diet is the next essential step in the microbiome development. Western diet (rich in meat and fat) has been linked to decreased bacterial gut richness, whereas a diet-based on fruits and vegetables is associated with increased bacterial richness (258, 259). The human microbiome is closely related to the nutritional status and chronic inflammatory processes of the individual (260, 261). Studies have shown that it is possible to predict if an individual is lean or obese based on a classification of the gut microbiome with an accuracy of over 90% (262). In humans for example, the abundance of bacteria of the taxa *Christensenella* is negatively correlated with BMI; in contrast, in *in vivo* experiments feeding mice *Christensenella* bacteria induces weight loss (263). Another human study revealed that the gut microbiome can influence leptin concentrations, indicating that the microbiome might regulate appetite (264). Interestingly, it has been shown that the same dietary ingredients have different effects on the blood glucose levels in humans, which is thought to be mediated by the microbiome as well (265). In addition, new studies have shown that the fecal transplantation of lean to obese patients improves insulin sensitivity (266).

The microbiome alters the immune system and future immune response. For example, it has been shown that the yeast *Candida Albicans* in particular has a prominent effect on the TNF-α response of the host; and the palmitoleic acid metabolism of bacteria has been associated with lower systemic responses (267). An overall decrease of bacterial richness is linked to a variety of diseases including obesity, coronary vascular disease, metabolic syndrome insulin resistance, dyslipidemia, and inflammatory disorders (268, 269). When the development of the infants' microbiome is perturbed by the use of antibiotics it can lead to the development of obesity or asthma in later life (270). These examples highlight the mutual relationship between the immune system and the microbiome, creating a finely tuned balance (271). As a result, an imbalance between both creates a lifelong signature of the infants' microbiome (272).

The gut microbiome has been extensively studied, but the lung microbiome has only recently gained interest with the

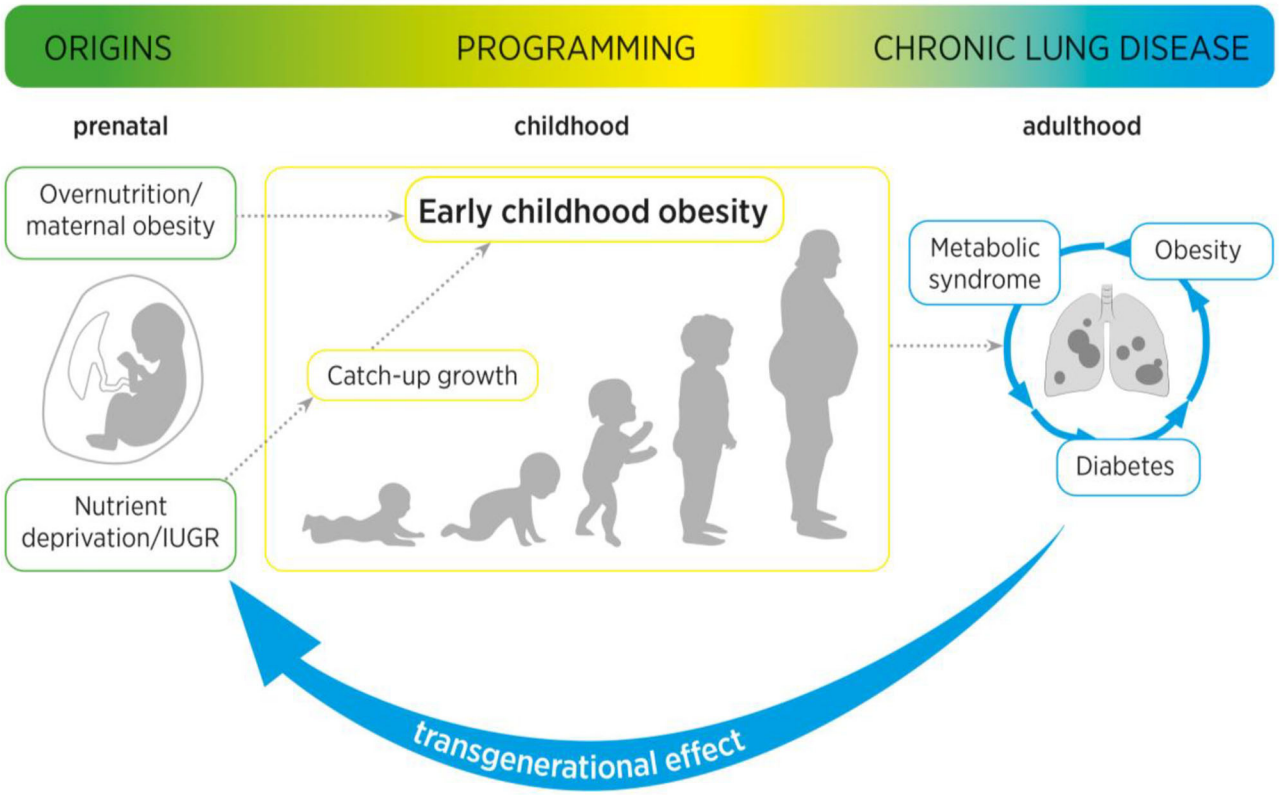

FIGURE 2 | Maternal obesity as well as intrauterine growth restriction (IUGR) increase the risk of (catch-up growth mediated) early childhood obesity. Maternal and early childhood obesity are associated with long-term adverse metabolic effects, including type 2 diabetes mellitus and metabolic syndrome. These pathological metabolic processes are not only intimately linked to an increased risk for pulmonary diseases, but can cause a transgenerational effect from mother to child, to second-generation offspring.

first reports of altered microbiome in asthma (273). The lung microbiome has a strong influence on the susceptibility to a wide array of chronic lung diseases, including COPD, asthma, Idiopathic Pulmonary Fibrosis (IPF) as well as altering the prognosis of cystic fibrosis (CF) (274). In healthy individuals, the lung microbiome is well-regulated by the environment (high clearance, low immigration and low nutrient availability). However, processes that favor alterations of the microbiome and inflammation include the increased production of mucus, creating a moist and warm bacterial niche, increased vascular permeability which increases the nutrient availability and selective growth promotion as well as selective clearance due to the altered immune response to airway colonization (275, 276). These factors promote the bacterial colonization of the airways as well as the selective overgrowth of certain well-adapted species, thereby creating a shift of the microbiome from healthy to diseased and inducing the "dysbiosis-inflammation cycle" as introduced by Dickson et al. (275–278). Thus, a perpetual cycle of microbial changes, possibly due to initial nutritional changes before and early after birth, along with inflammation has a significant impact on the development and prognosis of CLDs.

To date, the gut-lung axis remains elusive, especially with regard to clinical interventions. Nonetheless, several initial successes have been reported in the recent years. For example, stimulation of the gut microbiome with a high-fiber diet in COPD patients has been shown to increase the production of anti-inflammatory short chain fatty acids (SCFAs). These anti-inflammatory factors might reduce chronic inflammation of the lungs, prevent or decrease lung remodeling and therefore improve the lung health of COPD patients (279). Meanwhile, the Canadian Healthy Infant Longitudinal Development (CHILD) Study revealed that bacterial genera *Lachnospira*, *Veillonella*, *Faecalibacterium*, and *Rothia* are significantly reduced in infants at risk for asthma. Inoculation with these four bacteria reduced airway inflammation in a mouse model, possibly lowering the risk for asthma (280). These studies highlight the promising benefits of dietary changes or adjustment of the gut microbiome for the improvement of lung health.

The virome, including the genes of pathogenic viruses, resident viruses and bacteriophages, is of interest for CLDs as well (281, 282). Viral infection is the predominant reason for acute respiratory infections and the exacerbation of CLDs such as asthma, COPD and CF (283, 284). Next generation

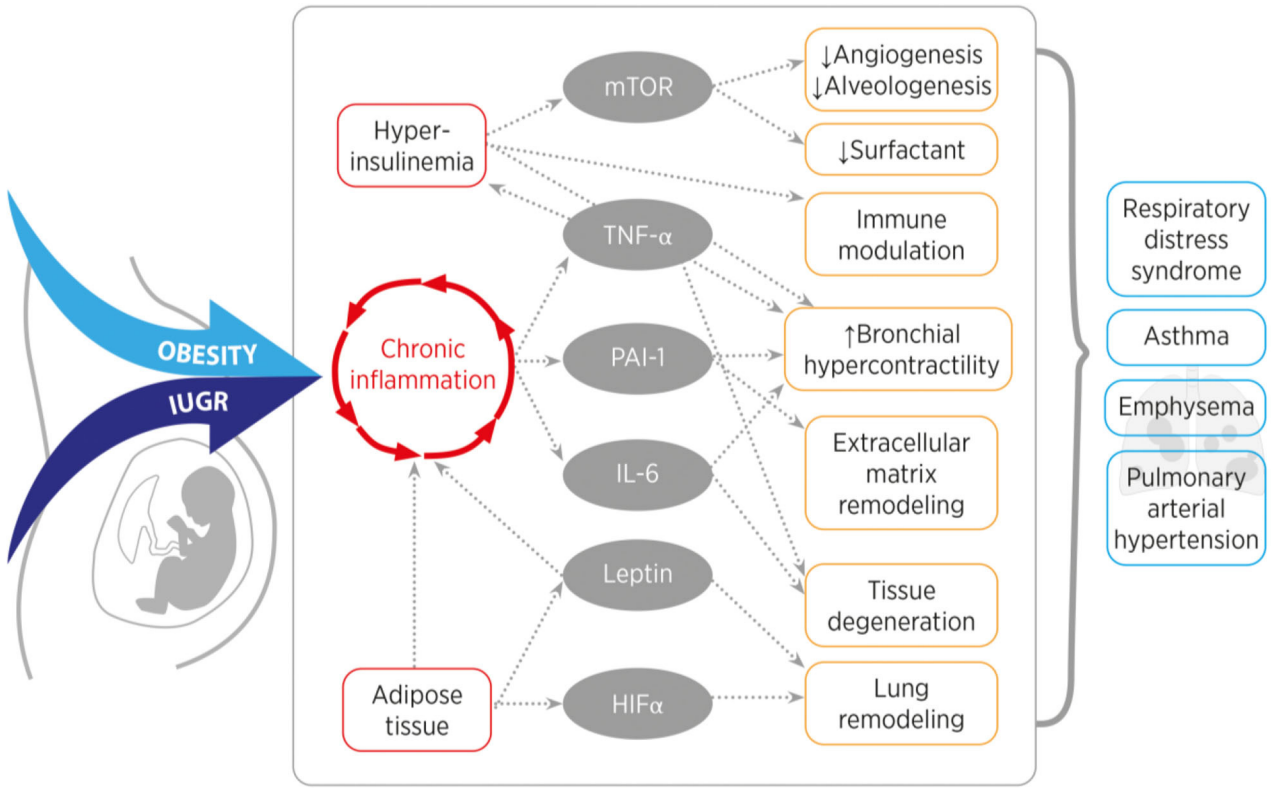

FIGURE 3 | Overview of the converging inflammatory signaling and nutrient sensing pathways of obesity and intrauterine growth restriction (IUGR). Obesity or IUGR lead to chronic inflammation and hyperinsulinemia, which induces mTOR, TNF-α, PAI-1, IL-6, Leptin, and HIF-α signaling. In the lung, these signaling molecules cause for example tissue remodeling, reduce alveolarization and induce smooth muscle cell hyperreactivity. These features are characteristics for a higher susceptibility to develop a chronic lung disease in later life. [mTOR (mechanistic target of rapamycin), TNF-α (tumor necrosis factor alpha), PAI-1 (plasminogen activator inhibitor-1), IL-6 (interleukin-6), HIF-α (hypoxia inducible hypoxia-inducible factor alpha)].

sequencing has made it possible to assess the viral DNA or RNA load in respiratory samples (285, 286). Obesity influences the virome of the host; it has been reported that increased viral RNA abundance is closely correlated to an increase of fat mass and hyperglycemia in mice (287). In line with this finding, obese patients show a higher susceptibility to dengue fever (288). Moreover, the adenovirus Ad-36 interferes with adipocyte differentiation, leptin production and glucose metabolism (289). Special interest is drawn to the fact that viral presence in the gut influences the host's immune response (290) by interfering with the host's microbiome and immune-modulatory actions (e.g., through the TNF-α pathway) (267, 291). This crosstalk between the bacterial microbiome and virome and their immune-modulating properties have also been reported in the lung (277, 292).

In conclusion, nutritional changes can directly and indirectly influence the intestinal and pulmonary microbiome (including the virome), modulating the immune response and increasing inflammation, and ultimately the risk of severe CLD. Targeting the microbiome might offer new preventive and therapeutic avenues for CLDs early in life.

SYSTEMIC CONSEQUENCES OF FETAL PROGRAMMING

Maternal obesity, maternal malnutrition or fetal nutrient deficiency through placental insufficiency naturally not only affect the lung, but all other organs as well. The organ-specific susceptibility to metabolic influences varies, and the "window of exposure" plays a crucial role. In other words, the timeframe during which organ development and/or -function is especially vulnerable differs from organ to organ. While a lot of research has been performed with traditional technologies, the ever-growing possibilities of bioinformatics will improve the longitudinal integration of transcriptomic, proteomic and lipidomic data with clinical parameters. These analyses will help to increase the understanding of the complex interaction of internal and external variables during development, resulting in a healthy individual or one with programmed disease. While the strength of animal models lies in the possibility to elucidate molecular mechanisms, it will be a challenge for clinicians to identify individuals at risk. Harmonization and standardization of cohorts like in the LifeCycle-Project (293) improves the epidemiological basis to translate hypotheses on the early origins of disease from animal models in to the human context and to confirm their clinical

TABLE 1 | Overview of the signaling molecules and pathways involved in the perinatal nutritional and metabolic origins of chronic lung diseases.

Disease	Regulator	Obesity	IUGR	Effector	Outcome and reference	
Pulmonary arterial hypertension (PAH)	HIF-α ↓	✓		Endothelin-1 ↑	Vascular remodeling (65, 66)	
	IL-6 ↑	✓	✓	Stat3 ↑ FoxO1 ↓	SMC proliferation (92, 93, 178)	
	PPARγ ↓	✓			Reduced SMC proliferation (130, 131)	Protective
	mTOR ↓		✓	VEGF ↓ BMP ↓	Reduced angiogenesis Altered ECM disposition (157, 218)	
COPD and emphysema	IL-6 ↑	✓	✓		ATII apoptosis (91, 232)	
	Leptin			Sftpa ↑	ATII maturation (104, 105)	Protective
	↑	✓	✓	Col1a1, Col3a1, Col6a3, Mmp2, Tieg1, Stat1 ↑	Enlarged alveoli (106, 157)	
Respiratory distress syndrome (RDS)	Insulin ↑	✓	✓	VEGF ↓ HIF-2 ↓ mTOR ↑	Reduced angiogenesis (141)	
		✓	✓	PI3K ↑ Sftpa ↓	Increased alveolar surface tension (139)	
			✓	GH/IGF-1 ↓ ↑	Reduced alveologenesis Lung- and bodygrowth (174, 204)	Protective
	PPARγ				Promotes Lung maturation (128, 129)	Protective
	Leptin ↓	✓	✓	Leptin resistance ↑ mTOR ↓	Reduced alveolar surface (173, 210, 213, 214)	
Asthma	TNF-α ↑	✓	✓	G-proteins ↑	Hyperreactivity in SMC (96, 232)	
	Adiponectin ↓	✓		NF-κB ↑	Enhanced TNF-α activity (97)	
	PAI-1 ↑	✓			Collagen, fibrin deposition (89)	
	Insulin ↑	✓	✓	Th2 shift	Enhanced immune response (145)	
		✓	✓	PI3K-signaling ↑	Contractile SMC phenotype (143)	
	Leptin ↑	✓	✓	mTOR ↑ MAPK ↑	Hyperreactivity (114)	

relevance. In this context, research on biomarkers is of high relevance to improve the diagnostic options in early detection of aberrant organ development. Candidates have been studied in clinical situations of known organ damage, e.g., BDP (294, 295) and neonatal kidney injury (296–298) and will have to be tested in the context of metabolic programming. Importantly, the goal is not to label an individual organ function as pathological beyond classical criteria but to identify individuals who are at risk to develop disease later in life in order to provide targeted prevention strategies.

Looking at molecular mechanisms, it is important to note that early metabolic origins of disease are based on a complex encounter of small-scale dysregulations rather than one single dysregulated pathway. Interestingly, apparently distinct causes of nutritional programming can cause similar molecular alterations. As discussed in detail for the lung, both IUGR (299) and maternal obesity-associated (300) models seem to induce inflammation in other organs as well. Briefly summarized, it is demonstrated that neuroinflammation is an important mechanism contributing to neurocognitive impairment after IUGR and maternal obesity (301, 302) and the window of vulnerability extends well-beyond birth (303, 304). Circulating inflammatory proteins were even tested as biomarkers for later cognitive impairment in preterm infants (305). Experimental studies have also linked perinatal inflammation to adverse kidney development (306, 307) and cardiac dysfunction (308). Taken together, these studies highlight the need to consider inter-organ communication as an important contributor to health and disease.

CONCLUSION

The mission of this article was to provide a comprehensive review of the impact of perinatal nutrition and metabolism on lung development and early origins of CLD. The current literature provides compelling evidence that maternal obesity, early childhood obesity and IUGR are intimately linked to increased risk for lung disease. These perinatal nutritional alterations of the fetus and infant converge in similar metabolic, endocrine, nutrient sensing and inflammatory signaling pathways. Key regulators are insulin and leptin, and their respective downstream signaling cascades. Both hormones are essential for physiological growth and development

during pregnancy; in contrast, interruption of the concerted interaction and balance of hormones, cytokines and growth factors during a critical window of development can disrupt developmental processes and adversely affect child (lung) health throughout life. For example, maternal obesity and early childhood obesity cause hyperinsulinemia and hyperleptinemia combined with insulin- and leptin-insensitivity. On the other hand, IUGR is characterized by a transient prenatal downregulation of insulin- and leptin signaling, followed by a postnatal upregulation during catch-up growth resulting in the same pathology as obesity. These two endocrine factors subsequently cause a cascade of pro-inflammatory programing with the release of (adipo-) cytokines and can contribute to metabolic and pulmonary disease (**Figure 3**, **Table 1**). These pulmonary sequelae span from aberrant alveolarization and angiogenesis to remodeling of the extracellular matrix and ultimately reducing lung function. While the present review primarily focused on the lung, other organs are affected as well, highlighting the importance of inter-organ communication. Beyond the metabolo-inflammatory stress response after perinatal nutritional alterations, smoking, air pollution as well as a consecutive dysbiosis of the intestinal and pulmonary microbiome contribute to the susceptibility and early origins of CLDs such as COPD, PAH and Asthma.

Both obesity-related comorbidities and CLDs are a relevant socioeconomic and individual burden. The alarmingly increasing rates of overweight and obese adults, pregnant women, and children emphasize the need to investigate and decipher the crosstalk between nutrition metabolism and the early origins of CLDs. Elucidation of the metabolo-pulmonary axis with subsequent identification of novel targets will provide new avenues to prevent metabolic programming and the early origins of CLDs.

AUTHOR CONTRIBUTIONS

CK-M, JS, EN, and MA conceived, designed, and drafted the manuscript. CK-M, JS, EN, JD, and MA edited and revised the manuscript and approved the final version of the manuscript. All authors contributed to the article and approved the submitted version.

FUNDING

This work was supported by Deutsche Forschungsgemeinschaft AL1632/2-1 (MA), the Marga and Walter Boll Stiftung, the Stiftung Oskar-Helene Heim, and by the Center for Molecular Medicine Cologne, faculty of medicine and university hospital Cologne, Germany (CMMC; MA).

ACKNOWLEDGMENTS

We greatly thank Mrs. Petra Kleinwächter (MedizinFoto Köln, University Hospital Cologne, University of Cologne) for her extraordinary support in graphical design and preparing the illustrations.

REFERENCES

1. May SM, Li JT. Burden of chronic obstructive pulmonary disease: healthcare costs and beyond. *Allergy Asthma Proc.* (2015) 36:4–10. doi: 10.2500/aap.2015.36.3812
2. Maleki-Yazdi MR, Kelly SM, Lam SY, Marin M, Barbeau M, Walker V. The burden of illness in patients with moderate to severe chronic obstructive pulmonary disease in Canada. *Can Respir J.* (2012) 19:319–24. doi: 10.1155/2012/328460
3. Poston L, Caleyachetty R, Cnattingius S, Corvalan C, Uauy R, Herring S, et al. Preconceptional and maternal obesity: epidemiology and health consequences. *Lancet Diabetes Endocrinol.* (2016) 4:1025–36. doi: 10.1016/S2213-8587(16)30217-0
4. Longo S, Bollani L, Decembrino L, Di Comite A, Angelini M, Stronati M. Short-term and long-term sequelae in intrauterine growth retardation (IUGR). *J Matern Fetal Neonatal Med.* (2013) 26:222–5. doi: 10.3109/14767058.2012.715006
5. Nardozza LM, Caetano AC, Zamarian AC, Mazzola JB, Silva CP, Marcal VM, et al. Fetal growth restriction: current knowledge. *Arch Gynecol Obstet.* (2017) 295:1061–77. doi: 10.1007/s00404-017-4341-9
6. Lucas A. Programming by early nutrition in man. *Ciba Found Symp.* (1991) 156:38–50.
7. Plagemann A. Perinatal programming and functional teratogenesis: impact on body weight regulation and obesity. *Physiol Behav.* (2005) 86:661–8. doi: 10.1016/j.physbeh.2005.08.065
8. Barker DJ. Intrauterine programming of adult disease. *Mol Med Today.* (1995) 1:418–23. doi: 10.1016/S1357-4310(95)90793-9
9. Edwards CA, Osman LM, Godden DJ, Campbell DM, Douglas JG. Relationship between birth weight and adult lung function: controlling for maternal factors. *Thorax.* (2003) 58:1061–5. doi: 10.1136/thorax.58.12.1061
10. Harpsoe MC, Basit S, Bager P, Wohlfahrt J, Benn CS, Nohr EA, et al. Maternal obesity, gestational weight gain, and risk of asthma and atopic disease in offspring: a study within the Danish national birth cohort. *J Allergy Clin Immunol.* (2013) 131:1033–40. doi: 10.1016/j.jaci.2012.09.008
11. Haataja P, Korhonen P, Ojala R, Hirvonen M, Paassilta M, Gissler M, et al. Asthma and atopic dermatitis in children born moderately and late preterm. *Eur J Pediatr.* (2016) 175:799–808. doi: 10.1007/s00431-016-2708-8
12. Aspberg S, Dahlquist G, Kahan T, Kallen B. Confirmed association between neonatal phototherapy or neonatal icterus and risk of childhood asthma. *Pediatr Allergy Immunol.* (2010) 21:e733–9. doi: 10.1111/j.1399-3038.2010.01038.x
13. Dyer JS, Rosenfeld CR. Metabolic imprinting by prenatal, perinatal, and postnatal overnutrition: a review. *Semin Reprod Med.* (2011) 29:266–76. doi: 10.1055/s-0031-1275521
14. Schittny JC. Development of the lung. *Cell Tissue Res.* (2017) 367:427–44. doi: 10.1007/s00441-016-2545-0
15. Burri PH. Structural aspects of postnatal lung development - alveolar formation and growth. *Biol Neonate.* (2006) 89:313–22. doi: 10.1159/000092868
16. Chooi YC, Ding C, Magkos F. The epidemiology of obesity. *Metabolism.* (2019) 92:6–10. doi: 10.1016/j.metabol.2018.09.005
17. Albuquerque D, Stice E, Rodriguez-Lopez R, Manco L, Nobrega C. Current review of genetics of human obesity: from molecular mechanisms to an evolutionary perspective. *Mol Genet Genomics.* (2015) 290:1191–221. doi: 10.1007/s00438-015-1015-9
18. Hopkins M, Blundell JE. Energy balance, body composition, sedentariness and appetite regulation: pathways to obesity. *Clin Sci.* (2016) 130:1615–28. doi: 10.1042/CS20160006
19. Kahn BB, Flier JS. Obesity and insulin resistance. *J Clin Invest.* (2000) 106:473–81. doi: 10.1172/JCI10842

20. Reaven GM. Pathophysiology of insulin resistance in human disease. *Physiol Rev.* (1995) 75:473–86. doi: 10.1152/physrev.1995.75.3.473
21. Schwartz MW, Woods SC, Porte D Jr, Seeley RJ, Baskin DG. Central nervous system control of food intake. *Nature.* (2000) 404:661–71. doi: 10.1038/35007534
22. El-Haschimi K, Pierroz DD, Hileman SM, Bjorbaek C, Flier JS. Two defects contribute to hypothalamic leptin resistance in mice with diet-induced obesity. *J Clin Invest.* (2000) 105:1827–32. doi: 10.1172/JCI9842
23. Kamohara S, Burcelin R, Halaas JL, Friedman JM, Charron MJ. Acute stimulation of glucose metabolism in mice by leptin treatment. *Nature.* (1997) 389:374–7. doi: 10.1038/38717
24. King NA, Caudwell P, Hopkins M, Byrne NM, Colley R, Hills AP, et al. Metabolic and behavioral compensatory responses to exercise interventions: barriers to weight loss. *Obesity.* (2007) 15:1373–83. doi: 10.1038/oby.2007.164
25. Ng M, Fleming T, Robinson M, Thomson B, Graetz N, Margono C, et al. Global, regional, and national prevalence of overweight and obesity in children and adults during 1980-2013: a systematic analysis for the Global burden of disease study 2013. *Lancet.* (2014) 384:766–81. doi: 10.1016/S0140-6736(14)60460-8
26. Ogden CL, Carroll MD, Fryar CD, Flegal KM. Prevalence of obesity among adults and youth: United States, 2011-2014. *NCHS Data Brief.* (2015) 219:1–8.
27. Venn AJ, Thomson RJ, Schmidt MD, Cleland VJ, Curry BA, Gennat HC, et al. Overweight and obesity from childhood to adulthood: a follow-up of participants in the 1985 Australian schools health and fitness survey. *Med J Aust.* (2007) 186:458–60. doi: 10.5694/j.1326-5377.2007.tb01436.x
28. Santangeli L, Sattar N, Huda SS. Impact of maternal obesity on perinatal and childhood outcomes. *Best Pract Res Clin Obstet Gynaecol.* (2015) 29:438–48. doi: 10.1016/j.bpobgyn.2014.10.009
29. Flegal KM, Carroll MD, Kit BK, Ogden CL. Prevalence of obesity and trends in the distribution of body mass index among US adults, 1999-2010. *JAMA.* (2012) 307:491–7. doi: 10.1001/jama.2012.39
30. Knight B, Shields BM, Hill A, Powell RJ, Wright D, Hattersley AT. The impact of maternal glycemia and obesity on early postnatal growth in a nondiabetic Caucasian population. *Diabetes Care.* (2007) 30:777–83. doi: 10.2337/dc06-1849
31. Cheng CW, Rifai A, Ka SM, Shui HA, Lin YF, Lee WH, et al. Calcium-binding proteins annexin A2 and S100A6 are sensors of tubular injury and recovery in acute renal failure. *Kidney Int.* (2005) 68:2694–703. doi: 10.1111/j.1523-1755.2005.00740.x
32. Parsons TJ, Power C, Manor O. Fetal and early life growth and body mass index from birth to early adulthood in 1958 British cohort: longitudinal study. *BMJ.* (2001) 323:1331–5. doi: 10.1136/bmj.323.7325.1331
33. Reilly MP, Rader DJ. The metabolic syndrome: more than the sum of its parts? *Circulation.* (2003) 108:1546–51. doi: 10.1161/01.CIR.0000088846.10655.E0
34. Han JC, Lawlor DA, Kimm SY. Childhood obesity. *Lancet.* (2010) 375:1737–48. doi: 10.1016/S0140-6736(10)60171-7
35. Godfrey KM, Reynolds RM, Prescott SL, Nyirenda M, Jaddoe VW, Eriksson JG, et al. Influence of maternal obesity on the long-term health of offspring. *Lancet Diabetes Endocrinol.* (2017) 5:53–64. doi: 10.1016/S2213-8587(16)30107-3
36. Ehrenberg HM, Mercer BM, Catalano PM. The influence of obesity and diabetes on the prevalence of macrosomia. *Am J Obstet Gynecol.* (2004) 191:964–8. doi: 10.1016/j.ajog.2004.05.052
37. Patel MS, Srinivasan M, Laychock SG. Metabolic programming: role of nutrition in the immediate postnatal life. *J Inherit Metab Dis.* (2009) 32:218–28. doi: 10.1007/s10545-008-1033-4
38. Eising JB, Uiterwaal CS, van der Ent CK. Maternal body mass index, neonatal lung function and respiratory symptoms in childhood. *Eur Respir J.* (2015) 46:1342–9. doi: 10.1183/13993003.00784-2014
39. Aalinkeel R, Srinivasan M, Song F, Patel MS. Programming into adulthood of islet adaptations induced by early nutritional intervention in the rat. *Am J Physiol Endocrinol Metab.* (2001) 281:E640–8. doi: 10.1152/ajpendo.2001.281.3.E640
40. Vadlamudi S, Hiremagalur BK, Tao L, Kalhan SC, Kalaria RN, Kaung HL, et al. Long-term effects on pancreatic function of feeding a HC formula to rats during the preweaning period. *Am J Physiol.* (1993) 265:E565–71. doi: 10.1152/ajpendo.1993.265.4.E565
41. Srinivasan M, Dodds C, Ghanim H, Gao T, Ross PJ, Browne RW, et al. Maternal obesity and fetal programming: effects of a high-carbohydrate nutritional modification in the immediate postnatal life of female rats. *Am J Physiol Endocrinol Metab.* (2008) 295:E895–903. doi: 10.1152/ajpendo.90460.2008
42. Bird A. DNA methylation patterns and epigenetic memory. *Genes Dev.* (2002) 16:6–21. doi: 10.1101/gad.947102
43. Zhang J, Zhang F, Didelot X, Bruce KD, Cagampang FR, Vatish M, et al. Maternal high fat diet during pregnancy and lactation alters hepatic expression of insulin like growth factor-2 and key microRNAs in the adult offspring. *BMC Genomics.* (2009) 10:478. doi: 10.1186/1471-2164-10-478
44. Jing J, Wang Y, Quan Y, Wang Z, Liu Y, Ding Z. Maternal obesity alters C19MC microRNAs expression profile in fetal umbilical cord blood. *Nutr Metab.* (2020) 17:52. doi: 10.1186/s12986-020-00475-7
45. Antoun E, Kitaba NT, Titcombe P, Dalrymple KV, Garratt ES, Barton SJ, et al. Maternal dysglycaemia, changes in the infant's epigenome modified with a diet and physical activity intervention in pregnancy: Secondary analysis of a randomised control trial. *PLoS Med.* (2020) 17:e1003229. doi: 10.1371/journal.pmed.1003229
46. Finer S, Mathews C, Lowe R, Smart M, Hillman S, Foo L, et al. Maternal gestational diabetes is associated with genome-wide DNA methylation variation in placenta and cord blood of exposed offspring. *Hum Mol Genet.* (2015) 24:3021–9. doi: 10.1093/hmg/ddv013
47. Moody L, Wang H, Jung PM, Chen H, Pan YX. Maternal and post-weaning high-fat diets produce distinct DNA methylation patterns in hepatic metabolic pathways within specific genomic contexts. *Int J Mol Sci.* (2019) 20:3229. doi: 10.3390/ijms20133229
48. Martinez FD, Wright AL, Taussig LM, Holberg CJ, Halonen M, Morgan WJ. Asthma and wheezing in the first six years of life. The group health medical associates. *N Engl J Med.* (1995) 332:133–8. doi: 10.1056/NEJM199501193320301
49. Zugna D, Galassi C, Annesi-Maesano I, Baiz N, Barros H, Basterrechea M, et al. Maternal complications in pregnancy and wheezing in early childhood: a pooled analysis of 14 birth cohorts. *Int J Epidemiol.* (2015) 44:199–208. doi: 10.1093/ije/dyu260
50. Kumar R, Story RE, Pongracic JA, Hong X, Arguelles L, Wang G, et al. Maternal pre-pregnancy obesity and recurrent wheezing in early childhood. *Pediatr Allergy Immunol Pulmonol.* (2010) 23:183–90. doi: 10.1089/ped.2010.0032
51. Arens R, Muzumdar H. Childhood obesity and obstructive sleep apnea syndrome. *J Appl Physiol.* (2010) 108:436–44. doi: 10.1152/japplphysiol.00689.2009
52. Rosen CL. Clinical features of obstructive sleep apnea hypoventilation syndrome in otherwise healthy children. *Pediatr Pulmonol.* (1999) 27:403–9. doi: 10.1002/(SICI)1099-0496(199906)27:6<403::AID-PPUL7>3.0.CO;2-811
53. Adams JP, Murphy PG. Obesity in anaesthesia and intensive care. *Br J Anaesth.* (2000) 85:91–108. doi: 10.1093/bja/85.1.91
54. Ekstrom S, Magnusson J, Kull I, Andersson N, Bottai M, Besharat Pour M, et al. Body mass index development and asthma throughout childhood. *Am J Epidemiol.* (2017) 186:255–63. doi: 10.1093/aje/kwx081
55. Black MH, Smith N, Porter AH, Jacobsen SJ, Koebnick C. Higher prevalence of obesity among children with asthma. *Obesity.* (2012) 20:1041–7. doi: 10.1038/oby.2012.5
56. Porter M, Wegienka G, Havstad S, Nageotte CG, Johnson CC, Ownby DR, et al. Relationship between childhood body mass index and young adult asthma. *Ann Allergy Asthma Immunol.* (2012) 109:408–11. e401. doi: 10.1016/j.anai.2012.09.009
57. Beuther DA, Sutherland ER. Overweight, obesity, and incident asthma: a meta-analysis of prospective epidemiologic studies. *Am J Respir Crit Care Med.* (2007) 175:661–6. doi: 10.1164/rccm.200611-1717OC
58. Koenig SM. Pulmonary complications of obesity. *Am J Med Sci.* (2001) 321:249–79. doi: 10.1097/00000441-200104000-00006
59. Lazarus R, Colditz G, Berkey CS, Speizer FE. Effects of body fat on ventilatory function in children and adolescents: cross-sectional findings from a random

population sample of school children. *Pediatr Pulmonol.* (1997) 24:187–94. doi: 10.1002/(SICI)1099-0496(199709)24:3<187::AID-PPUL4>3.0.CO;2-K
60. Li AM, Chan D, Wong E, Yin J, Nelson EA, Fok TF. The effects of obesity on pulmonary function. *Arch Dis Child.* (2003) 88:361–3. doi: 10.1136/adc.88.4.361
61. Watson RA, Pride NB, Thomas EL, Fitzpatrick J, Durighel G, McCarthy J, et al. Reduction of total lung capacity in obese men: comparison of total intrathoracic and gas volumes. *J Appl Physiol.* (2010) 108:1605–12. doi: 10.1152/japplphysiol.01267.2009
62. Gislason T, Benediktsdottir B. Snoring, apneic episodes, and nocturnal hypoxemia among children 6 months to 6 years old. An epidemiologic study of lower limit of prevalence. *Chest.* (1995) 107:963–6. doi: 10.1378/chest.107.4.963
63. Semenza GL, Wang GL. A nuclear factor induced by hypoxia via de novo protein synthesis binds to the human erythropoietin gene enhancer at a site required for transcriptional activation. *Mol Cell Biol.* (1992) 12:5447–54. doi: 10.1128/MCB.12.12.5447
64. Ivan M, Kondo K, Yang H, Kim W, Valiando J, Ohh M, et al. HIFalpha targeted for VHL-mediated destruction by proline hydroxylation: implications for O2 sensing. *Science.* (2001) 292:464–8. doi: 10.1126/science.1059817
65. Brusselmans K, Compernolle V, Tjwa M, Wiesener MS, Maxwell PH, Collen D, et al. Heterozygous deficiency of hypoxia-inducible factor-2alpha protects mice against pulmonary hypertension and right ventricular dysfunction during prolonged hypoxia. *J Clin Invest.* (2003) 111:1519–27. doi: 10.1172/JCI15496
66. Yu AY, Shimoda LA, Iyer NV, Huso DL, Sun X, McWilliams R, et al. Impaired physiological responses to chronic hypoxia in mice partially deficient for hypoxia-inducible factor 1alpha. *J Clin Invest.* (1999) 103:691–6. doi: 10.1172/JCI5912
67. Krick S, Eul BG, Hanze J, Savai R, Grimminger F, Seeger W, et al. Role of hypoxia-inducible factor-1alpha in hypoxia-induced apoptosis of primary alveolar epithelial type II cells. *Am J Respir Cell Mol Biol.* (2005) 32:395–403. doi: 10.1165/rcmb.2004-0314OC
68. Asikainen TM, Waleh NS, Schneider BK, Clyman RI, White CW. Enhancement of angiogenic effectors through hypoxia-inducible factor in preterm primate lung *in vivo*. *Am J Physiol Lung Cell Mol Physiol.* (2006) 291:L588–95. doi: 10.1152/ajplung.00098.2006
69. Asikainen TM, Chang LY, Coalson JJ, Schneider BK, Waleh NS, Ikegami M, et al. Improved lung growth and function through hypoxia-inducible factor in primate chronic lung disease of prematurity. *FASEB J.* (2006) 20:1698–700. doi: 10.1096/fj.06-5887fje
70. Levine AJ, Puzio-Kuter AM. The control of the metabolic switch in cancers by oncogenes and tumor suppressor genes. *Science.* (2010) 330:1340–4. doi: 10.1126/science.1193494
71. Burns JS, Manda G. Metabolic pathways of the warburg effect in health and disease: perspectives of choice, chain or chance. *Int J Mol Sci.* (2017) 18:2755. doi: 10.3390/ijms18122755
72. Luis C, Duarte F, Faria I, Jarak I, Oliveira PF, Alves MG, et al. Warburg effect inversion: adiposity shifts central primary metabolism in MCF-7 breast cancer cells. *Life Sci.* (2019) 223:38–46. doi: 10.1016/j.lfs.2019.03.016
73. Chandel NS, McClintock DS, Feliciano CE, Wood TM, Melendez JA, Rodriguez AM, et al. Reactive oxygen species generated at mitochondrial complex III stabilize hypoxia-inducible factor-1alpha during hypoxia: a mechanism of O2 sensing. *J Biol Chem.* (2000) 275:25130–8. doi: 10.1074/jbc.M001914200
74. Semenza GL. Targeting HIF-1 for cancer therapy. *Nat Rev Cancer.* (2003) 3:721–32. doi: 10.1038/nrc1187
75. Ivan M, Haberberger T, Gervasi DC, Michelson KS, Gunzler V, Kondo K, et al. Biochemical purification and pharmacological inhibition of a mammalian prolyl hydroxylase acting on hypoxia-inducible factor. *Proc Natl Acad Sci USA.* (2002) 99:13459–64. doi: 10.1073/pnas.192342099
76. Prakash YS, Pabelick CM, Sieck GC. Mitochondrial dysfunction in airway disease. *Chest.* (2017) 152:618–26. doi: 10.1016/j.chest.2017.03.020
77. Rowlands DJ. Mitochondria dysfunction: A novel therapeutic target in pathological lung remodeling or bystander? *Pharmacol Ther.* (2016) 166:96–105. doi: 10.1016/j.pharmthera.2016.06.019
78. Kim KK, Kugler MC, Wolters PJ, Robillard L, Galvez MG, Brumwell AN, et al. Alveolar epithelial cell mesenchymal transition develops in vivo during pulmonary fibrosis and is regulated by the extracellular matrix. *Proc Natl Acad Sci USA.* (2006) 103:13180–5. doi: 10.1073/pnas.0605669103
79. Zhou G, Dada LA, Wu M, Kelly A, Trejo H, Zhou Q, et al. Hypoxia-induced alveolar epithelial-mesenchymal transition requires mitochondrial ROS and hypoxia-inducible factor 1. *Am J Physiol Lung Cell Mol Physiol.* (2009) 297:L1120–30. doi: 10.1152/ajplung.00007.2009
80. Schroedl C, McClintock DS, Budinger GR, Chandel NS. Hypoxic but not anoxic stabilization of HIF-1alpha requires mitochondrial reactive oxygen species. *Am J Physiol Lung Cell Mol Physiol.* (2002) 283:L922–31. doi: 10.1152/ajplung.00014.2002
81. Zhang H, Qian DZ, Tan YS, Lee K, Gao P, Ren YR, et al. Digoxin and other cardiac glycosides inhibit HIF-1alpha synthesis and block tumor growth. *Proc Natl Acad Sci USA.* (2008) 105:19579–86. doi: 10.1073/pnas.0809763105
82. Abud EM, Maylor J, Undem C, Punjabi A, Zaiman AL, Myers AC, et al. Digoxin inhibits development of hypoxic pulmonary hypertension in mice. *Proc Natl Acad Sci USA.* (2012) 109:1239–44. doi: 10.1073/pnas.1120385109
83. Weisberg SP, McCann D, Desai M, Rosenbaum M, Leibel RL, Ferrante AW. Obesity is associated with macrophage accumulation in adipose tissue. *J Clin Invest.* (2003) 112:1796–808. doi: 10.1172/JCI200319246
84. Travers RL, Motta AC, Betts JA, Bouloumie A, Thompson D. The impact of adiposity on adipose tissue-resident lymphocyte activation in humans. *Int J Obes.* (2015) 39:762–9. doi: 10.1038/ijo.2014.195
85. Bullo M, Garcia-Lorda P, Salas-Salvado J. Plasma soluble tumor necrosis factor alpha receptors and leptin levels in normal-weight and obese women: effect of adiposity and diabetes. *Eur J Endocrinol.* (2002) 146:325–31. doi: 10.1530/eje.0.1460325
86. Bastard JP, Jardel C, Bruckert E, Blondy P, Capeau J, Laville M, et al. Elevated levels of interleukin 6 are reduced in serum and subcutaneous adipose tissue of obese women after weight loss. *J Clin Endocrinol Metab.* (2000) 85:3338–42. doi: 10.1210/jcem.85.9.6839
87. Roth CL, Kratz M, Ralston MM, Reinehr T. Changes in adipose-derived inflammatory cytokines and chemokines after successful lifestyle intervention in obese children. *Metabolism.* (2011) 60:445–52. doi: 10.1016/j.metabol.2010.03.023
88. Rajala MW, Scherer PE. Minireview: the adipocyte–at the crossroads of energy homeostasis, inflammation, and atherosclerosis. *Endocrinology.* (2003) 144:3765–73. doi: 10.1210/en.2003-0580
89. Nawrocki AR, Scherer PE. The delicate balance between fat and muscle: adipokines in metabolic disease and musculoskeletal inflammation. *Curr Opin Pharmacol.* (2004) 4:281–9. doi: 10.1016/j.coph.2004.03.003
90. Dinger K, Kasper P, Hucklenbruch-Rother E, Vohlen C, Jobst E, Janoschek R, et al. Early-onset obesity dysregulates pulmonary adipocytokine/insulin signaling and induces asthma-like disease in mice. *Sci Rep.* (2016) 6:24168. doi: 10.1038/srep24168
91. Ruwanpura SM, McLeod L, Dousha LF, Seow HJ, Alhayyani S, Tate MD, et al. Therapeutic targeting of the IL-6 trans-signaling/mechanistic target of rapamycin complex 1 axis in pulmonary emphysema. *Am J Respir Crit Care Med.* (2016) 194:1494–505. doi: 10.1164/rccm.201512-2368OC
92. Jones SA, Scheller J, Rose-John S. Therapeutic strategies for the clinical blockade of IL-6/gp130 signaling. *J Clin Invest.* (2011) 121:3375–83. doi: 10.1172/JCI57158
93. Savai R, Al-Tamari HM, Sedding D, Kojonazarov B, Muecke C, Teske R, et al. Pro-proliferative and inflammatory signaling converge on FoxO1 transcription factor in pulmonary hypertension. *Nat Med.* (2014) 20:1289–300. doi: 10.1038/nm.3695
94. Tamura Y, Phan C, Tu L, Le Hiress M, Thuillet R, Jutant EM, et al. Ectopic upregulation of membrane-bound IL6R drives vascular remodeling in pulmonary arterial hypertension. *J Clin Invest.* (2018) 128:1956–70. doi: 10.1172/JCI96462
95. Hotamisligil GS. Inflammatory pathways and insulin action. *Int J Obes Relat Metab Disord.* (2003) 27(Suppl. 3):S53–5. doi: 10.1038/sj.ijo.0802502
96. Chen H, Tliba O, Van Besien CR, Panettieri RA, Jr Amrani Y. TNF-[alpha] modulates murine tracheal rings responsiveness to G-protein-coupled receptor agonists and KCl. *J Appl Physiol.* (2003) 95:864–72. doi: 10.1152/japplphysiol.00140.2003

97. Ouchi N, Kihara S, Funahashi T, Matsuzawa Y, Walsh K. Obesity, adiponectin and vascular inflammatory disease. *Curr Opin Lipidol.* (2003) 14:561–6. doi: 10.1097/00041433-200312000-00003
98. Kim J, Remick DG. Tumor necrosis factor inhibitors for the treatment of asthma. *Curr Allergy Asthma Rep.* (2007) 7:151–6. doi: 10.1007/s11882-007-0013-3
99. Desai D, Brightling C. TNF-alpha antagonism in severe asthma? *Recent Pat Inflamm Allergy Drug Discov.* (2010) 4:193–200. doi: 10.2174/187221310793564218
100. Antoniu SA, Mihaltan F, Ulmeanu R. Anti-TNF-alpha therapies in chronic obstructive pulmonary diseases. *Expert Opin Investig Drugs.* (2008) 17:1203–11. doi: 10.1517/13543784.17.8.1203
101. Savov JD, Brass DM, Berman KG, McElvania E, Schwartz DA. Fibrinolysis in LPS-induced chronic airway disease. *Am J Physiol Lung Cell Mol Physiol.* (2003) 285:L940–8. doi: 10.1152/ajplung.00102.2003
102. Oh CK, Ariue B, Alban RF, Shaw B, Cho SH. PAI-1 promotes extracellular matrix deposition in the airways of a murine asthma model. *Biochem Biophys Res Commun.* (2002) 294:1155–60. doi: 10.1016/S0006-291X(02)00577-6
103. Litzenburger T, Huber EK, Dinger K, Wilke R, Vohlen C, Selle J, et al. Maternal high-fat diet induces long-term obesity with sex-dependent metabolic programming of adipocyte differentiation, hypertrophy and dysfunction in the offspring. *Clin Sci.* (2020) 134:921–39. doi: 10.1042/CS20191229
104. Chen H, Zhang JP, Huang H, Wang ZH, Cheng R, Cai WB. Leptin promotes fetal lung maturity and upregulates SP-A expression in pulmonary alveoli type-II epithelial cells involving TTF-1 activation. *PLoS ONE.* (2013) 8:e69297. doi: 10.1371/journal.pone.0069297
105. Kirwin SM, Bhandari V, Dimatteo D, Barone C, Johnson L, Paul S, et al. Leptin enhances lung maturity in the fetal rat. *Pediatr Res.* (2006) 60:200–4. doi: 10.1203/01.pdr.0000227478.29271.52
106. Huang K, Rabold R, Abston E, Schofield B, Misra V, Galdzicka E, et al. Effects of leptin deficiency on postnatal lung development in mice. *J Appl Physiol.* (2008) 105:249–59. doi: 10.1152/japplphysiol.00052.2007
107. Lock M, McGillick EV, Orgeig S, McMillen IC, Morrison JL. Regulation of fetal lung development in response to maternal overnutrition. *Clin Exp Pharmacol Physiol.* (2013) 40:803–16. doi: 10.1111/1440-1681.12166
108. Myers MG, Cowley MA, Munzberg H. Mechanisms of leptin action and leptin resistance. *Annu Rev Physiol.* (2008) 70:537–56. doi: 10.1146/annurev.physiol.70.113006.100707
109. Halaas JL, Boozer C, Blair-West J, Fidahusein N, Denton DA, Friedman JM. Physiological response to long-term peripheral and central leptin infusion in lean and obese mice. *Proc Natl Acad Sci USA.* (1997) 94:8878–83. doi: 10.1073/pnas.94.16.8878
110. Zhang L, Yin Y, Zhang H, Zhong W, Zhang J. Association of asthma diagnosis with leptin and adiponectin: a systematic review and meta-analysis. *J Investig Med.* (2017) 65:57–64. doi: 10.1136/jim-2016-000127
111. Guler N, Kirerleri E, Ones U, Tamay Z, Salmayenli N, Darendeliler F. Leptin: does it have any role in childhood asthma? *J Allergy Clin Immunol.* (2004) 114:254–9. doi: 10.1016/j.jaci.2004.03.053
112. Gurkan F, Atamer Y, Ece A, Kocyigit Y, Tuzun H, Mete N. Serum leptin levels in asthmatic children treated with an inhaled corticosteroid. *Ann Allergy Asthma Immunol.* (2004) 93:277–80. doi: 10.1016/S1081-1206(10)61501-3
113. Tanju A, Cekmez F, Aydinoz S, Karademir F, Suleymanoglu S, Gocmen I. Association between clinical severity of childhood asthma and serum leptin levels. *Indian J Pediatr.* (2011) 78:291–5. doi: 10.1007/s12098-010-0281-0
114. Zheng H, Wu D, Wu X, Zhang X, Zhou Q, Luo Y, et al. Leptin promotes allergic airway inflammation through targeting the unfolded protein response pathway. *Sci Rep.* (2018) 8:8905. doi: 10.1038/s41598-018-27278-4
115. Maffei M, Halaas J, Ravussin E, Pratley RE, Lee GH, Zhang Y, et al. Leptin levels in human and rodent: measurement of plasma leptin and ob RNA in obese and weight-reduced subjects. *Nat Med.* (1995) 1:1155–61. doi: 10.1038/nm1195-1155
116. Shore SA, Fredberg JJ. Obesity, smooth muscle, and airway hyperresponsiveness. *J Allergy Clin Immunol.* (2005) 115:925–7. doi: 10.1016/j.jaci.2005.01.064
117. Xu A, Wang H, Hoo RL, Sweeney G, Vanhoutte PM, Wang Y, et al. Selective elevation of adiponectin production by the natural compounds derived from a medicinal herb alleviates insulin resistance and glucose intolerance in obese mice. *Endocrinology.* (2009) 150:625–33. doi: 10.1210/en.2008-0999
118. Combs TP, Pajvani UB, Berg AH, Lin Y, Jelicks LA, Laplante M, et al. A transgenic mouse with a deletion in the collagenous domain of adiponectin displays elevated circulating adiponectin and improved insulin sensitivity. *Endocrinology.* (2004) 145:367–83. doi: 10.1210/en.2003-1068
119. Riera-Guardia N, Rothenbacher D. The effect of thiazolidinediones on adiponectin serum level: a meta-analysis. *Diabetes Obes Metab.* (2008) 10:367–75. doi: 10.1111/j.1463-1326.2007.00755.x
120. Amin RH, Mathews ST, Camp HS, Ding L, Leff T. Selective activation of PPARgamma in skeletal muscle induces endogenous production of adiponectin and protects mice from diet-induced insulin resistance. *Am J Physiol Endocrinol Metab.* (2010) 298:E28–37. doi: 10.1152/ajpendo.00446.2009
121. Yao X, Remaley AT, Levine SJ. New kids on the block: the emerging role of apolipoproteins in the pathogenesis and treatment of asthma. *Chest.* (2011) 140:1048–54. doi: 10.1378/chest.11-0158
122. Gao J, Katagiri H, Ishigaki Y, Yamada T, Ogihara T, Imai J, et al. Involvement of apolipoprotein E in excess fat accumulation and insulin resistance. *Diabetes.* (2007) 56:24–33. doi: 10.2337/db06-0144
123. Yao X, Gordon EM, Figueroa DM, Barochia AV, Levine SJ. Emerging roles of Apolipoprotein E and Apolipoprotein A-I in the pathogenesis and treatment of lung disease. *Am J Respir Cell Mol Biol.* (2016) 55:159–69. doi: 10.1165/rcmb.2016-0060TR
124. Massaro D, Massaro GD. Apoetm1Unc mice have impaired alveologenesis, low lung function, and rapid loss of lung function. *Am J Physiol Lung Cell Mol Physiol.* (2008) 294:L991–7. doi: 10.1152/ajplung.00013.2008
125. Chen H, Jackson S, Doro M, McGowan S. Perinatal expression of genes that may participate in lipid metabolism by lipid-laden lung fibroblasts. *J Lipid Res.* (1998) 39:2483–92. doi: 10.1016/S0022-2275(20)33329-0
126. Tontonoz P, Hu E, Spiegelman BM. Regulation of adipocyte gene expression and differentiation by peroxisome proliferator activated receptor gamma. *Curr Opin Genet Dev.* (1995) 5:571–6. doi: 10.1016/0959-437X(95)80025-5
127. Lazar MA. PPAR gamma, 10 years later. *Biochimie.* (2005) 87:9–13. doi: 10.1016/j.biochi.2004.10.021
128. Simon DM, Arikan MC, Srisuma S, Bhattacharya S, Tsai LW, Ingenito EP, et al. Epithelial cell PPAR[gamma] contributes to normal lung maturation. *FASEB J.* (2006) 20:1507–9. doi: 10.1096/fj.05-5410fje
129. Torday JS, Torres E, Rehan VK. The role of fibroblast transdifferentiation in lung epithelial cell proliferation, differentiation, and repair *in vitro*. *Pediatr Pathol Mol Med.* (2003) 22:189–207. doi: 10.1080/pdp.22.3.189.207
130. Hansmann G, de Jesus Perez VA, Alastalo TP, Alvira CM, Guignabert C, Bekker JM, et al. An antiproliferative BMP-2/PPARgamma/apoE axis in human and murine SMCs and its role in pulmonary hypertension. *J Clin Invest.* (2008) 118:1846–57. doi: 10.1172/JCI32503
131. Rabinovitch M. PPARgamma and the pathobiology of pulmonary arterial hypertension. *Adv Exp Med Biol.* (2010) 661:447–58. doi: 10.1007/978-1-60761-500-2_29
132. Koutnikova H, Cock TA, Watanabe M, Houten SM, Champy MF, Dierich A, et al. Compensation by the muscle limits the metabolic consequences of lipodystrophy in PPAR gamma hypomorphic mice. *Proc Natl Acad Sci USA.* (2003) 100:14457–62. doi: 10.1073/pnas.2336090100
133. Ailhaud G, Massiera F, Weill P, Legrand P, Alessandri JM, Guesnet P. Temporal changes in dietary fats: role of n-6 polyunsaturated fatty acids in excessive adipose tissue development and relationship to obesity. *Prog Lipid Res.* (2006) 45:203–36. doi: 10.1016/j.plipres.2006.01.003
134. Kanai F, Ito K, Todaka M, Hayashi H, Kamohara S, Ishii K, et al. Insulin-stimulated GLUT4 translocation is relevant to the phosphorylation of IRS-1 and the activity of PI3-kinase. *Biochem Biophys Res Commun.* (1993) 195:762–8. doi: 10.1006/bbrc.1993.2111
135. Czech MP, Corvera S. Signaling mechanisms that regulate glucose transport. *J Biol Chem.* (1999) 274:1865–8. doi: 10.1074/jbc.274.4.1865
136. Courtneidge SA, Heber A. An 81 kd protein complexed with middle T antigen and pp60c-src: a possible phosphatidylinositol kinase. *Cell.* (1987) 50:1031–7. doi: 10.1016/0092-8674(87)90169-3
137. Dibble CC, Manning BD. Signal integration by mTORC1 coordinates nutrient input with biosynthetic output. *Nat Cell Biol.* (2013) 15:555–64. doi: 10.1038/ncb2763

138. Land SC, Scott CL, Walker D. mTOR signalling, embryogenesis and the control of lung development. *Semin Cell Dev Biol.* (2014) 36:68–78. doi: 10.1016/j.semcdb.2014.09.023
139. Miakotina OL, Goss KL, Snyder JM. Insulin utilizes the PI 3-kinase pathway to inhibit SP-A gene expression in lung epithelial cells. *Respir Res.* (2002) 3:27. doi: 10.1186/rr191
140. Maffei A, Lembo G, Carnevale D. PI3Kinases in diabetes mellitus and its related complications. *Int J Mol Sci.* (2018) 19:4098. doi: 10.3390/ijms19124098
141. Ikeda H, Shiojima I, Oka T, Yoshida M, Maemura K, Walsh K, et al. Increased Akt-mTOR signaling in lung epithelium is associated with respiratory distress syndrome in mice. *Mol Cell Biol.* (2011) 31:1054–65. doi: 10.1128/MCB.00732-10
142. Fernandez-Twinn DS, Gascoin G, Musial B, Carr S, Duque-Guimaraes D, Blackmore HL, et al. Exercise rescues obese mothers' insulin sensitivity, placental hypoxia and male offspring insulin sensitivity. *Sci Rep.* (2017) 7:44650. doi: 10.1038/srep44650
143. Schaafsma D, McNeill KD, Stelmack GL, Gosens R, Baarsma HA, Dekkers BG, et al. Insulin increases the expression of contractile phenotypic markers in airway smooth muscle. *Am J Physiol Cell Physiol.* (2007) 293:C429–39. doi: 10.1152/ajpcell.00502.2006
144. Lessmann E, Grochowy G, Weingarten L, Giesemann T, Aktories K, Leitges M, et al. Insulin and insulin-like growth factor-1 promote mast cell survival via activation of the phosphatidylinositol-3-kinase pathway. *Exp Hematol.* (2006) 34:1532–41. doi: 10.1016/j.exphem.2006.05.022
145. Viardot A, Grey ST, Mackay F, Chisholm D. Potential antiinflammatory role of insulin via the preferential polarization of effector T cells toward a T helper 2 phenotype. *Endocrinology.* (2007) 148:346–53. doi: 10.1210/en.2006-0686
146. Shapiro H, Kagan I, Shalita-Chesner M, Singer J, Singer P. Inhaled aerosolized insulin: a "topical" anti-inflammatory treatment for acute lung injury and respiratory distress syndrome? *Inflammation.* (2010) 33:315–9. doi: 10.1007/s10753-010-9187-2
147. Wigglesworth JS. Foetal growth retardation. *Br Med Bull.* (1966) 22:13–5. doi: 10.1093/oxfordjournals.bmb.a070429
148. Kesavan K, Devaskar SU. Intrauterine growth restriction: postnatal monitoring and outcomes. *Pediatr Clin North Am.* (2019) 66:403–23. doi: 10.1016/j.pcl.2018.12.009
149. Gordijn SJ, Beune IM, Ganzevoort W. Building consensus and standards in fetal growth restriction studies. *Best Pract Res Clin Obstet Gynaecol.* (2018) 49:117–26. doi: 10.1016/j.bpobgyn.2018.02.002
150. Beune IM, Bloomfield FH, Ganzevoort W, Embleton ND, Rozance PJ, van Wassenaer-Leemhuis AG, et al. Consensus based definition of growth restriction in the newborn. *J Pediatr.* (2018) 196:71–6. e71. doi: 10.1016/j.jpeds.2017.12.059
151. Ong KK, Ahmed ML, Emmett PM, Preece MA, Dunger DB. Association between postnatal catch-up growth and obesity in childhood: prospective cohort study. *BMJ.* (2000) 320:967–71. doi: 10.1136/bmj.320.7240.967
152. Healy MJ, Lockhart RD, Mackenzie JD, Tanner JM, Whitehouse RH. Aberdeen growth study. I. The prediction of adult body measurements from measurements taken each year from birth to 5 years. *Arch Dis Child.* (1956) 31:372–81. doi: 10.1136/adc.31.159.372
153. Ravelli GP, Stein ZA, Susser MW. Obesity in young men after famine exposure *in utero* and early infancy. *N Engl J Med.* (1976) 295:349–53. doi: 10.1056/NEJM197608122950701
154. Rozance PJ, Seedorf GJ, Brown A, Roe G, O'Meara MC, Gien J, et al. Intrauterine growth restriction decreases pulmonary alveolar and vessel growth and causes pulmonary artery endothelial cell dysfunction in vitro in fetal sheep. *Am J Physiol Lung Cell Mol Physiol.* (2011) 301:L860–71. doi: 10.1152/ajplung.00197.2011
155. Joss-Moore L, Carroll T, Yang Y, Fitzhugh M, Metcalfe D, Oman J, et al. Intrauterine growth restriction transiently delays alveolar formation and disrupts retinoic acid receptor expression in the lung of female rat pups. *Pediatr Res.* (2013) 73:612–20. doi: 10.1038/pr.2013.38
156. Zinkhan EK, Zalla JM, Carpenter JR, Yu B, Yu X, Chan G, et al. Intrauterine growth restriction combined with a maternal high-fat diet increases hepatic cholesterol and low-density lipoprotein receptor activity in rats. *Physiol Rep.* (2016) 4:e12862. doi: 10.14814/phy2.12862
157. Kuiper-Makris C, Zanetti D, Vohlen C, Fahle L, Muller M, Odenthal M, et al. Mendelian randomization and experimental IUGR reveal the adverse effect of low birth weight on lung structure and function. *Sci Rep.* (2020) 10:22395. doi: 10.1038/s41598-020-79245-7
158. Brodsky D, Christou H. Current concepts in intrauterine growth restriction. *J Intensive Care Med.* (2004) 19:307–19. doi: 10.1177/0885066604269663
159. Devaskar SU, Chu A. Intrauterine growth restriction: hungry for an answer. *Physiology.* (2016) 31:131–46. doi: 10.1152/physiol.00033.2015
160. Lumey LH, Stein AD. Offspring birth weights after maternal intrauterine undernutrition: a comparison within sibships. *Am J Epidemiol.* (1997) 146:810–9. doi: 10.1093/oxfordjournals.aje.a009198
161. Lopuhaa CE, Roseboom TJ, Osmond C, Barker DJ, Ravelli AC, Bleker OP, et al. Atopy, lung function, and obstructive airways disease after prenatal exposure to famine. *Thorax.* (2000) 55:555–61. doi: 10.1136/thorax.55.7.555
162. Stein CE, Kumaran K, Fall CH, Shaheen SO, Osmond C, Barker DJ. Relation of fetal growth to adult lung function in south India. *Thorax.* (1997) 52:895–9. doi: 10.1136/thx.52.10.895
163. Lawlor DA, Ebrahim S, Davey Smith G. Association of birth weight with adult lung function: findings from the British Women's Heart and Health Study and a meta-analysis. *Thorax.* (2005) 60:851–8. doi: 10.1136/thx.2005.042408
164. Baeten JM, Bukusi EA, Lambe M. Pregnancy complications and outcomes among overweight and obese nulliparous women. *Am J Public Health.* (2001) 91:436–40. doi: 10.2105/AJPH.91.3.436
165. Hayes EK, Lechowicz A, Petrik JJ, Storozhuk Y, Paez-Parent S, Dai Q, et al. Adverse fetal and neonatal outcomes associated with a life-long high fat diet: role of altered development of the placental vasculature. *PLoS ONE.* (2012) 7:e33370. doi: 10.1371/journal.pone.0033370
166. Gutaj P, Wender-Ozegowska E, Iciek R, Zawiejska A, Pietryga M, Brazert J. Maternal serum placental growth factor and fetal SGA in pregnancy complicated by type 1 diabetes mellitus. *J Perinat Med.* (2014) 42:629–33. doi: 10.1515/jpm-2013-0227
167. Wallace JM, Bourke DA, Aitken RP, Palmer RM, Da Silva P, Cruickshank MA. Relationship between nutritionally-mediated placental growth restriction and fetal growth, body composition and endocrine status during late gestation in adolescent sheep. *Placenta.* (2000) 21:100–8. doi: 10.1053/plac.1999.0440
168. Limesand SW, Rozance PJ. Fetal adaptations in insulin secretion result from high catecholamines during placental insufficiency. *J Physiol.* (2017) 595:5103–13. doi: 10.1113/JP273324
169. Thamotharan M, Garg M, Oak S, Rogers LM, Pan G, Sangiorgi F, et al. Transgenerational inheritance of the insulin-resistant phenotype in embryo-transferred intrauterine growth-restricted adult female rat offspring. *Am J Physiol Endocrinol Metab.* (2007) 292:E1270–9. doi: 10.1152/ajpendo.00462.2006
170. Skinner MK. What is an epigenetic transgenerational phenotype? F3 or F2. *Reprod Toxicol.* (2008) 25:2–6. doi: 10.1016/j.reprotox.2007.09.001
171. Horsthemke B. A critical view on transgenerational epigenetic inheritance in humans. *Nat Commun.* (2018) 9:2973. doi: 10.1038/s41467-018-05445-5
172. Meng R, Lv J, Yu C, Guo Y, Bian Z, Yang L, et al. Prenatal famine exposure, adulthood obesity patterns and risk of type 2 diabetes. *Int J Epidemiol.* (2018) 47:399–408. doi: 10.1093/ije/dyx228
173. Desai M, Ross MG. Fetal programming of adipose tissue: effects of intrauterine growth restriction and maternal obesity/high-fat diet. *Semin Reprod Med.* (2011) 29:237–45. doi: 10.1055/s-0031-1275517
174. Nawabi J, Vohlen C, Dinger K, Thangaratnarajah C, Klaudt C, Lopez Garcia E, et al. Novel functional role of GH/IGF-I in neonatal lung myofibroblasts and in rat lung growth after intrauterine growth restriction. *Am J Physiol Lung Cell Mol Physiol.* (2018) 315:L623–37. doi: 10.1152/ajplung.00413.2017
175. Khazaee R, McCaig LA, Yamashita C, Hardy DB, Veldhuizen RAW. Maternal protein restriction during perinatal life affects lung mechanics and the surfactant system during early postnatal life in female rats. *PLoS ONE.* (2019) 14:e0215611. doi: 10.1371/journal.pone.0215611
176. Joss-Moore LA, Wang Y, Baack ML, Yao J, Norris AW, Yu X, et al. IUGR decreases PPARgamma and SETD8 Expression in neonatal rat lung and these

effects are ameliorated by maternal DHA supplementation. *Early Hum Dev.* (2010) 86:785–91. doi: 10.1016/j.earlhumdev.2010.08.026
177. Dravet-Gounot P, Morin C, Jacques S, Dumont F, Ely-Marius F, Vaiman D, et al. Lung microRNA deregulation associated with impaired alveolarization in rats after intrauterine growth restriction. *PLoS ONE.* (2017) 12:e0190445. doi: 10.1371/journal.pone.0190445
178. Alejandre Alcazar MA, Ostreicher I, Appel S, Rother E, Vohlen C, Plank C, et al. Developmental regulation of inflammatory cytokine-mediated Stat3 signaling: the missing link between intrauterine growth restriction and pulmonary dysfunction? *J Mol Med.* (2012) 90:945–57. doi: 10.1007/s00109-012-0860-9
179. Alejandre Alcazar MA, Morty RE, Lendzian L, Vohlen C, Oestreicher I, Plank C, et al. Inhibition of TGF-beta signaling and decreased apoptosis in IUGR-associated lung disease in rats. *PLoS ONE.* (2011) 6:e26371. doi: 10.1371/journal.pone.0026371
180. Thebaud B, Abman SH. Bronchopulmonary dysplasia: where have all the vessels gone? Roles of angiogenic growth factors in chronic lung disease. *Am J Respir Crit Care Med.* (2007) 175:978–85. doi: 10.1164/rccm.200611-1660PP
181. Tang JR, Markham NE, Lin YJ, McMurtry IF, Maxey A, Kinsella JP, et al. Inhaled nitric oxide attenuates pulmonary hypertension and improves lung growth in infant rats after neonatal treatment with a VEGF receptor inhibitor. *Am J Physiol Lung Cell Mol Physiol.* (2004) 287:L344–51. doi: 10.1152/ajplung.00291.2003
182. Jakkula M, Le Cras TD, Gebb S, Hirth KP, Tuder RM, Voelkel NF, et al. Inhibition of angiogenesis decreases alveolarization in the developing rat lung. *Am J Physiol Lung Cell Mol Physiol.* (2000) 279:L600–7. doi: 10.1152/ajplung.2000.279.3.L600
183. Yun EJ, Lorizio W, Seedorf G, Abman SH, Vu TH. VEGF and endothelium-derived retinoic acid regulate lung vascular and alveolar development. *Am J Physiol Lung Cell Mol Physiol.* (2016) 310:L287–98. doi: 10.1152/ajplung.00229.2015
184. Svanes C, Omenaas E, Heuch JM, Irgens LM, Gulsvik A. Birth characteristics and asthma symptoms in young adults: results from a population-based cohort study in Norway. *Eur Respir J.* (1998) 12:1366–70. doi: 10.1183/09031936.98.12061366
185. Rona RJ, Gulliford MC, Chinn S. Effects of prematurity and intrauterine growth on respiratory health and lung function in childhood. *BMJ.* (1993) 306:817–20. doi: 10.1136/bmj.306.6881.817
186. Greenough A, Yuksel B, Cheeseman P. Effect of in utero growth retardation on lung function at follow-up of prematurely born infants. *Eur Respir J.* (2004) 24:731–3. doi: 10.1183/09031936.04.00060304
187. Ronkainen E, Dunder T, Kaukola T, Marttila R, Hallman M. Intrauterine growth restriction predicts lower lung function at school age in children born very preterm. *Arch Dis Child Fetal Neonatal Ed.* (2016) 101:F412–7. doi: 10.1136/archdischild-2015-308922
188. Kotecha SJ, Watkins WJ, Heron J, Henderson J, Dunstan FD, Kotecha S. Spirometric lung function in school-age children: effect of intrauterine growth retardation and catch-up growth. *Am J Respir Crit Care Med.* (2010) 181:969–74. doi: 10.1164/rccm.200906-0897OC
189. He B, Kwok MK, Au Yeung SL, Lin SL, Leung JYY, Hui LL, et al. Birth weight and prematurity with lung function at ∼17.5 years: "Children of 1997" birth cohort. *Sci Rep.* (2020) 10:341. doi: 10.1038/s41598-019-56086-7
190. Cai Y, Shaheen SO, Hardy R, Kuh D, Hansell AL. Birth weight, early childhood growth and lung function in middle to early old age: 1946 British birth cohort. *Thorax.* (2016) 71:916–22. doi: 10.1136/thoraxjnl-2014-206457
191. Simmons RA, Templeton LJ, Gertz SJ. Intrauterine growth retardation leads to the development of type 2 diabetes in the rat. *Diabetes.* (2001) 50:2279–86. doi: 10.2337/diabetes.50.10.2279
192. Ravelli AC, van Der Meulen JH, Osmond C, Barker DJ, Bleker OP. Obesity at the age of 50 y in men and women exposed to famine prenatally. *Am J Clin Nutr.* (1999) 70:811–6. doi: 10.1093/ajcn/70.5.811
193. Newsome CA, Shiell AW, Fall CH, Phillips DI, Shier R, Law CM. Is birth weight related to later glucose and insulin metabolism?–A systematic review. *Diabet Med.* (2003) 20:339–48. doi: 10.1046/j.1464-5491.2003.00871.x
194. Mohan R, Baumann D, Alejandro EU. Fetal undernutrition, placental insufficiency, and pancreatic beta-cell development programming *in utero*. *Am J Physiol Regul Integr Comp Physiol.* (2018) 315:R867–78. doi: 10.1152/ajpregu.00072.2018
195. Laitinen J, Pietilainen K, Wadsworth M, Sovio U, Jarvelin MR. Predictors of abdominal obesity among 31-y-old men and women born in Northern Finland in 1966. *Eur J Clin Nutr.* (2004) 58:180–90. doi: 10.1038/sj.ejcn.1601765
196. Crume TL, Scherzinger A, Stamm E, McDuffie R, Bischoff KJ, Hamman RF, et al. The long-term impact of intrauterine growth restriction in a diverse US. cohort of children: the EPOCH study. *Obesity.* (2014) 22:608–15. doi: 10.1002/oby.20565
197. Barker DJ, Hales CN, Fall CH, Osmond C, Phipps K, Clark PM. Type 2 (non-insulin-dependent) diabetes mellitus, hypertension and hyperlipidaemia (syndrome X): relation to reduced fetal growth. *Diabetologia.* (1993) 36:62–7. doi: 10.1007/BF00399095
198. Illsley NP, Baumann MU. Human placental glucose transport in fetoplacental growth and metabolism. *Biochim Biophys Acta Mol Basis Dis.* (2020) 1866:165359. doi: 10.1016/j.bbadis.2018.12.010
199. Boehmer BH, Limesand SW, Rozance PJ. The impact of IUGR on pancreatic islet development and beta-cell function. *J Endocrinol.* (2017) 235:R63–76. doi: 10.1530/JOE-17-0076
200. Yada KK, Gupta R, Gupta A, Gupta M. Insulin levels in low birth weight neonates. *Indian J Med Res.* (2003) 118:197–203.
201. Wolf HJ, Ebenbichler CF, Huter O, Bodner J, Lechleitner M, Foger B, et al. Fetal leptin and insulin levels only correlate inlarge-for-gestational age infants. *Eur J Endocrinol.* (2000) 142:623–9. doi: 10.1530/eje.0.1420623
202. Muhlhausler BS, Duffield JA, Ozanne SE, Pilgrim C, Turner N, Morrison JL, et al. The transition from fetal growth restriction to accelerated postnatal growth: a potential role for insulin signalling in skeletal muscle. *J Physiol.* (2009) 587:4199–211. doi: 10.1113/jphysiol.2009.173161
203. Dunlop K, Cedrone M, Staples JF, Regnault TR. Altered fetal skeletal muscle nutrient metabolism following an adverse *in utero* environment and the modulation of later life insulin sensitivity. *Nutrients.* (2015) 7:1202–16. doi: 10.3390/nu7021202
204. Beyea JA, Sawicki G, Olson DM, List E, Kopchick JJ, Harvey S. Growth hormone (GH) receptor knockout mice reveal actions of GH in lung development. *Proteomics.* (2006) 6:341–8. doi: 10.1002/pmic.200500168
205. Seedorf G, Kim C, Wallace B, Mandell EW, Nowlin T, Shepherd D, et al. rhIGF-1/BP3 preserves lung growth and prevents pulmonary hypertension in experimental bronchopulmonary dysplasia. *Am J Respir Crit Care Med.* (2020) 201:1120–34. doi: 10.1164/rccm.201910-1975OC
206. Invitti C, Gilardini L, Mazzilli G, Sartorio A, Viberti GC, Ong KK, et al. Insulin sensitivity and secretion in normal children related to size at birth, postnatal growth, and plasma insulin-like growth factor-I levels. *Diabetologia.* (2004) 47:1064–70. doi: 10.1007/s00125-004-1565-6
207. Ibanez L, Potau N, Marcos MV, de Zegher F. Exaggerated adrenarche and hyperinsulinism in adolescent girls born small for gestational age. *J Clin Endocrinol Metab.* (1999) 84:4739–41. doi: 10.1210/jc.84.12.4739
208. Gurugubelli Krishna R, Vishnu Bhat B. Molecular mechanisms of intrauterine growth restriction. *J Matern Fetal Neonatal Med.* (2018) 31:2634–40. doi: 10.1080/14767058.2017.1347922
209. Desai M, Gayle D, Han G, Ross MG. Programmed hyperphagia due to reduced anorexigenic mechanisms in intrauterine growth-restricted offspring. *Reprod Sci.* (2007) 14:329–37. doi: 10.1177/1933719107303983
210. Coupe B, Grit I, Hulin P, Randuineau G, Parnet P. Postnatal growth after intrauterine growth restriction alters central leptin signal and energy homeostasis. *PLoS ONE.* (2012) 7:e30616. doi: 10.1371/journal.pone.0030616
211. Saxton RA, Sabatini DM. mTOR signaling in growth, metabolism, and disease. *Cell.* (2017) 169:361–71. doi: 10.1016/j.cell.2017.03.035
212. Kim J, Guan KL. mTOR as a central hub of nutrient signalling and cell growth. *Nat Cell Biol.* (2019) 21:63–71. doi: 10.1038/s41556-018-0205-1
213. Ganguly A, Collis L, Devaskar SU. Placental glucose and amino acid transport in calorie-restricted wild-type and Glut3 null heterozygous mice. *Endocrinology.* (2012) 153:3995–4007. doi: 10.1210/en.2011-1973
214. Brett KE, Ferraro ZM, Yockell-Lelievre J, Gruslin A, Adamo KB. Maternal-fetal nutrient transport in pregnancy pathologies: the role of the placenta. *Int J Mol Sci.* (2014) 15:16153–85. doi: 10.3390/ijms150916153
215. Sinagoga KL, Stone WJ, Schiesser JV, Schweitzer JI, Sampson L, Zheng Y, et al. Distinct roles for the mTOR pathway in postnatal morphogenesis,

maturation and function of pancreatic islets. *Development*. (2017) 144:2402–14. doi: 10.1242/dev.146316
216. Hu F, Xu Y, Liu F. Hypothalamic roles of mTOR complex I: integration of nutrient and hormone signals to regulate energy homeostasis. *Am J Physiol Endocrinol Metab.* (2016) 310:E994–1002. doi: 10.1152/ajpendo.00121.2016
217. Zhong H, Chiles K, Feldser D, Laughner E, Hanrahan C, Georgescu MM, et al. Modulation of hypoxia-inducible factor 1alpha expression by the epidermal growth factor/phosphatidylinositol 3-kinase/PTEN/AKT/FRAP pathway in human prostate cancer cells: implications for tumor angiogenesis and therapeutics. *Cancer Res.* (2000) 60:1541–5. doi: 10.1002/cyto.990020515
218. Wahdan-Alaswad RS, Song K, Krebs TL, Shola DT, Gomez JA, Matsuyama S, et al. Insulin-like growth factor I suppresses bone morphogenetic protein signaling in prostate cancer cells by activating mTOR signaling. *Cancer Res.* (2010) 70:9106–17. doi: 10.1158/0008-5472.CAN-10-1119
219. Pinheiro AR, Salvucci ID, Aguila MB, Mandarim-de-Lacerda CA. Protein restriction during gestation and/or lactation causes adverse transgenerational effects on biometry and glucose metabolism in F1 and F2 progenies of rats. *Clin Sci.* (2008) 114:381–92. doi: 10.1042/CS20070302
220. Gonzalez-Rodriguez P, Cantu J, O'Neil D, Seferovic MD, Goodspeed DM, Suter MA, et al. Alterations in expression of imprinted genes from the H19/IGF2 loci in a multigenerational model of intrauterine growth restriction (IUGR). *Am J Obstet Gynecol.* (2016) 214:625. doi: 10.1016/j.ajog.2016.01.194
221. Berends LM, Ozanne SE. Early determinants of type-2 diabetes. *Best Pract Res Clin Endocrinol Metab.* (2012) 26:569–80. doi: 10.1016/j.beem.2012.03.002
222. Aiken CE, Ozanne SE. Transgenerational developmental programming. *Hum Reprod Update.* (2014) 20:63–75. doi: 10.1093/humupd/dmt043
223. Joss-Moore LA, Lane RH, Albertine KH. Epigenetic contributions to the developmental origins of adult lung disease. *Biochem Cell Biol.* (2015) 93:119–27. doi: 10.1139/bcb-2014-0093
224. Tosh DN, Fu Q, Callaway CW, McKnight RA, McMillen IC, Ross MG, et al. Epigenetics of programmed obesity: alteration in IUGR rat hepatic IGF1 mRNA expression and histone structure in rapid vs. delayed postnatal catch-up growth. *Am J Physiol Gastrointest Liver Physiol.* (2010) 299:G1023–9. doi: 10.1152/ajpgi.00052.2010
225. Fu Q, Yu X, Callaway CW, Lane RH, McKnight RA. Epigenetics: intrauterine growth retardation (IUGR) modifies the histone code along the rat hepatic IGF-1 gene. *FASEB J.* (2009) 23:2438–49. doi: 10.1096/fj.08-124768
226. Park JH, Stoffers DA, Nicholls RD, Simmons RA. Development of type 2 diabetes following intrauterine growth retardation in rats is associated with progressive epigenetic silencing of Pdx1. *J Clin Invest.* (2008) 118:2316–24. doi: 10.1172/JCI33655
227. Deodati A, Inzaghi E, Liguori A, Puglianiello A, Germani D, Brufani C, et al. IGF2 methylation is associated with lipid profile in obese children. *Horm Res Paediatr.* (2013) 79:361–7. doi: 10.1159/000351707
228. Goodspeed D, Seferovic MD, Holland W, McKnight RA, Summers SA, Branch DW, et al. Essential nutrient supplementation prevents heritable metabolic disease in multigenerational intrauterine growth-restricted rats. *FASEB J.* (2015) 29:807–19. doi: 10.1096/fj.14-259614
229. Zhang H, Fan Y, Elsabagh M, Guo S, Wang M, Jiang H. Dietary supplementation of L-Arginine and N-carbamylglutamate attenuated the hepatic inflammatory response and apoptosis in suckling lambs with intrauterine growth retardation. *Mediators Inflamm.* (2020) 2020:2453537. doi: 10.1155/2020/2453537
230. Jaeckle Santos LJ, Li C, Doulias PT, Ischiropoulos H, Worthen GS, Simmons RA. Neutralizing Th2 inflammation in neonatal islets prevents beta-cell failure in adult IUGR rats. *Diabetes.* (2014) 63:1672–84. doi: 10.2337/db13-1226
231. Dodson RB, Powers KN, Gien J, Rozance PJ, Seedorf G, Astling D, et al. Intrauterine growth restriction decreases NF-kappaB signaling in fetal pulmonary artery endothelial cells of fetal sheep. *Am J Physiol Lung Cell Mol Physiol.* (2018) 315:L348–59. doi: 10.1152/ajplung.00052.2018
232. Amarilyo G, Oren A, Mimouni FB, Ochshorn Y, Deutsch V, Mandel D. Increased cord serum inflammatory markers in small-for-gestational-age neonates. *J Perinatol.* (2011) 31:30–2. doi: 10.1038/jp.2010.53
233. Fresno M, Alvarez R, Cuesta N. Toll-like receptors, inflammation, metabolism and obesity. *Arch Physiol Biochem.* (2011) 117:151–64. doi: 10.3109/13813455.2011.562514
234. Bhargava P, Lee CH. Role and function of macrophages in the metabolic syndrome. *Biochem J.* (2012) 442:253–262. doi: 10.1042/BJ20111708
235. Bastard JP, Maachi M, Lagathu C, Kim MJ, Caron M, Vidal H, et al. Recent advances in the relationship between obesity, inflammation, and insulin resistance. *Eur Cytokine Netw.* (2006) 17:4–12.
236. Vieira Braga FA, Kar G, Berg M, Carpaij OA, Polanski K, Simon LM, et al. A cellular census of human lungs identifies novel cell states in health and in asthma. *Nat Med.* (2019) 25:1153–63. doi: 10.1038/s41591-019-0468-5
237. Speer CP. Chorioamnionitis, postnatal factors and proinflammatory response in the pathogenetic sequence of bronchopulmonary dysplasia. *Neonatology.* (2009) 95:353–61. doi: 10.1159/000209301
238. Ramakrishna L, de Vries VC, Curotto de Lafaille MA. Cross-roads in the lung: immune cells and tissue interactions as determinants of allergic asthma. *Immunol Res.* (2012) 53:213–28. doi: 10.1007/s12026-012-8296-4
239. Bhat TA, Panzica L, Kalathil SG, Thanavala Y. Immune dysfunction in patients with chronic obstructive pulmonary disease. *Ann Am Thorac Soc.* (2015) 12(Suppl. 2):S169–75. doi: 10.1513/AnnalsATS.201503-126AW
240. Kyriakakou M, Malamitsi-Puchner A, Militsi H, Boutsikou T, Margeli A, Hassiakos D, et al. Leptin and adiponectin concentrations in intrauterine growth restricted and appropriate for gestational age fetuses, neonates, and their mothers. *Eur J Endocrinol.* (2008) 158:343–8. doi: 10.1530/EJE-07-0692
241. Rashid CS, Lien YC, Bansal A, Jaeckle-Santos LJ, Li C, Won KJ, et al. Transcriptomic analysis reveals novel mechanisms mediating islet dysfunction in the intrauterine growth-restricted rat. *Endocrinology.* (2018) 159:1035–49. doi: 10.1210/en.2017-00888
242. Thangaratnarajah C, Dinger K, Vohlen C, Klaudt C, Nawabi J, Lopez Garcia E, et al. Novel role of NPY in neuroimmune interaction and lung growth after intrauterine growth restriction. *Am J Physiol Lung Cell Mol Physiol.* (2017) 313:L491–506. doi: 10.1152/ajplung.00432.2016
243. Rosenberg A. The IUGR newborn. *Semin Perinatol.* (2008) 32:219–24. doi: 10.1053/j.semperi.2007.11.003
244. Regev RH, Reichman B. Prematurity and intrauterine growth retardation–double jeopardy? *Clin Perinatol.* (2004) 31:453–73. doi: 10.1016/j.clp.2004.04.017
245. McDonald SD, Han Z, Mulla S, Beyene J, Knowledge Synthesis G. Overweight and obesity in mothers and risk of preterm birth and low birth weight infants: systematic review and meta-analyses. *BMJ.* (2010) 341:c3428. doi: 10.1136/bmj.c3428
246. Lynch TA, Malshe A, Colihan S, Meyers J, Li D, Holloman C, et al. Impact of maternal obesity on perinatal outcomes in preterm prelabor rupture of membranes >/=34 weeks. *Am J Perinatol.* (2020) 37:467–74. doi: 10.1055/s-0039-1698833
247. Vincent S, Czuzoj-Shulman N, Spence AR, Abenhaim HA. Effect of pre-pregnancy body mass index on respiratory-related neonatal outcomes in women undergoing elective cesarean prior to 39 weeks. *J Perinat Med.* (2018) 46:905–12. doi: 10.1515/jpm-2017-0384
248. Goldenberg RL, Culhane JF. Prepregnancy health status and the risk of preterm delivery. *Arch Pediatr Adolesc Med.* (2005) 159:89–90. doi: 10.1001/archpedi.159.1.89
249. Smith LJ, McKay KO, van Asperen PP, Selvadurai H, Fitzgerald DA. Normal development of the lung and premature birth. *Paediatr Respir Rev.* (2010) 11:135–42. doi: 10.1016/j.prrv.2009.12.006
250. Kumar VH, Lakshminrusimha S, Kishkurno S, Paturi BS, Gugino SF, Nielsen L, et al. Neonatal hyperoxia increases airway reactivity and inflammation in adult mice. *Pediatr Pulmonol.* (2016) 51:1131–41. doi: 10.1002/ppul.23430
251. Jobe AH. The new bronchopulmonary dysplasia. *Curr Opin Pediatr.* (2011) 23:167–72. doi: 10.1097/MOP.0b013e3283423e6b
252. Dumpa V, Bhandari V. Surfactant, steroids and non-invasive ventilation in the prevention of BPD. *Semin Perinatol.* (2018) 42:444–52. doi: 10.1053/j.semperi.2018.09.006
253. Collins JJP, Tibboel D, de Kleer IM, Reiss IKM, Rottier RJ. The future of bronchopulmonary dysplasia: emerging pathophysiological concepts and potential new avenues of treatment. *Front Med (Lausanne).* (2017) 4:61. doi: 10.3389/fmed.2017.00061

254. Bustani P, Kotecha S. Role of cytokines in hyperoxia mediated inflammation in the developing lung. *Front Biosci.* (2003) 8:s694–704. doi: 10.2741/1113
255. Hwang JS, Rehan VK. Recent advances in bronchopulmonary dysplasia: pathophysiology, prevention, and treatment. *Lung.* (2018) 196:129–38. doi: 10.1007/s00408-018-0084-z
256. Garite TJ, Clark R, Thorp JA. Intrauterine growth restriction increases morbidity and mortality among premature neonates. *Am J Obstet Gynecol.* (2004) 191:481–7. doi: 10.1016/j.ajog.2004.01.036
257. Koenig JE, Spor A, Scalfone N, Fricker AD, Stombaugh J, Knight R, et al. Succession of microbial consortia in the developing infant gut microbiome. *Proc Natl Acad Sci USA.* (2011) 108(Suppl. 1):4578–85. doi: 10.1073/pnas.1000081107
258. Hehemann JH, Correc G, Barbeyron T, Helbert W, Czjzek M, Michel G. Transfer of carbohydrate-active enzymes from marine bacteria to Japanese gut microbiota. *Nature.* (2010) 464:908–912. doi: 10.1038/nature08937
259. Craig WJ. Health effects of vegan diets. *Am J Clin Nutr.* (2009) 89:1627S−33S. doi: 10.3945/ajcn.2009.26736N
260. Wu GD, Chen J, Hoffmann C, Bittinger K, Chen YY, Keilbaugh SA, et al. Linking long-term dietary patterns with gut microbial enterotypes. *Science.* (2011) 334:105–8. doi: 10.1126/science.1208344
261. Levy M, Kolodziejczyk AA, Thaiss CA, Elinav E. Dysbiosis and the immune system. *Nat Rev Immunol.* (2017) 17:219–32. doi: 10.1038/nri.2017.7
262. Knights D, Parfrey LW, Zaneveld J, Lozupone C, Knight R. Human-associated microbial signatures: examining their predictive value. *Cell Host Microbe.* (2011) 10:292–6. doi: 10.1016/j.chom.2011.09.003
263. Goodrich JK, Waters JL, Poole AC, Sutter JL, Koren O, Blekhman R, et al. Human genetics shape the gut microbiome. *Cell.* (2014) 159:789–99. doi: 10.1016/j.cell.2014.09.053
264. Zhang C, Yin A, Li H, Wang R, Wu G, Shen J, et al. Dietary modulation of gut microbiota contributes to alleviation of both genetic and simple obesity in children. *EBioMedicine.* (2015) 2:968–84. doi: 10.1016/j.ebiom.2015.07.007
265. Zeevi D, Korem T, Zmora N, Israeli D, Rothschild D, Weinberger A, et al. Personalized nutrition by prediction of glycemic responses. *Cell.* (2015) 163:1079–94. doi: 10.1016/j.cell.2015.11.001
266. Vrieze A, Van Nood E, Holleman F, Salojarvi J, Kootte RS, Bartelsman JF, et al. Transfer of intestinal microbiota from lean donors increases insulin sensitivity in individuals with metabolic syndrome. *Gastroenterology.* (2012) 143:913–6.e917. doi: 10.1053/j.gastro.2012.06.031
267. Schirmer M, Smeekens SP, Vlamakis H, Jaeger M, Oosting M, Franzosa EA, et al. Linking the human gut microbiome to inflammatory cytokine production capacity. *Cell.* (2016) 167:1897. doi: 10.1016/j.cell.2016.10.020
268. Le Chatelier E, Nielsen T, Qin J, Prifti E, Hildebrand F, Falony G, et al. Richness of human gut microbiome correlates with metabolic markers. *Nature.* (2013) 500:541–6. doi: 10.1038/nature12506
269. Cotillard A, Kennedy SP, Kong LC, Prifti E, Pons N, Le Chatelier E, et al. Dietary intervention impact on gut microbial gene richness. *Nature.* (2013) 500:585–8. doi: 10.1038/nature12480
270. Trasande L, Blustein J, Liu M, Corwin E, Cox LM, Blaser MJ. Infant antibiotic exposures and early-life body mass. *Int J Obes.* (2013) 37:16–23. doi: 10.1038/ijo.2012.132
271. Karczewski J, Poniedzialek B, Adamski Z, Rzymski P. The effects of the microbiota on the host immune system. *Autoimmunity.* (2014) 47:494–504. doi: 10.3109/08916934.2014.938322
272. Maynard CL, Elson CO, Hatton RD, Weaver CT. Reciprocal interactions of the intestinal microbiota and immune system. *Nature.* (2012) 489:231–41. doi: 10.1038/nature11551
273. Hilty M, Burke C, Pedro H, Cardenas P, Bush A, Bossley C, et al. Disordered microbial communities in asthmatic airways. *PLoS ONE.* (2010) 5:e8578. doi: 10.1371/journal.pone.0008578
274. O'Dwyer DN, Dickson RP, Moore BB. The lung microbiome, immunity, and the pathogenesis of chronic lung disease. *J Immunol.* (2016) 196:4839–47. doi: 10.4049/jimmunol.1600279
275. Siwicka-Gieroba D, Czarko-Wicha K. Lung microbiome - a modern knowledge. *Cent Eur J Immunol.* (2020) 45:342–5. doi: 10.5114/ceji.2020.101266
276. Dickson RP, Martinez FJ, Huffnagle GB. The role of the microbiome in exacerbations of chronic lung diseases. *Lancet.* (2014) 384:691–702. doi: 10.1016/S0140-6736(14)61136-3
277. Sencio V, Machado MG, Trottein F. The lung-gut axis during viral respiratory infections: the impact of gut dysbiosis on secondary disease outcomes. *Mucosal Immunol.* (2021) 14:296–304. doi: 10.1038/s41385-020-00361-8
278. Dickson RP, Erb-Downward JR, Huffnagle GB. The role of the bacterial microbiome in lung disease. *Expert Rev Respir Med.* (2013) 7:245–57. doi: 10.1586/ers.13.24
279. Vaughan A, Frazer ZA, Hansbro PM, Yang IA. COPD and the gut-lung axis: the therapeutic potential of fibre. *J Thorac Dis.* (2019) 11:S2173–80. doi: 10.21037/jtd.2019.10.40
280. Arrieta MC, Stiemsma LT, Dimitriu PA, Thorson L, Russell S, Yurist-Doutsch S, et al. Early infancy microbial and metabolic alterations affect risk of childhood asthma. *Sci Transl Med.* (2015) 7:307ra152. doi: 10.1126/scitranslmed.aab2271
281. Virgin HW, Wherry EJ, Ahmed R. Redefining chronic viral infection. *Cell.* (2009) 138:30–50. doi: 10.1016/j.cell.2009.06.036
282. Duerkop BA, Hooper LV. Resident viruses and their interactions with the immune system. *Nat Immunol.* (2013) 14:654–9. doi: 10.1038/ni.2614
283. Hewitt R, Farne H, Ritchie A, Luke E, Johnston SL, Mallia P. The role of viral infections in exacerbations of chronic obstructive pulmonary disease and asthma. *Ther Adv Respir Dis.* (2016) 10:158–74. doi: 10.1177/1753465815618113
284. Billard L, Le Berre R, Pilorge L, Payan C, Hery-Arnaud G, Vallet S. Viruses in cystic fibrosis patients' airways. *Crit Rev Microbiol.* (2017) 43:690–708. doi: 10.1080/1040841X.2017.1297763
285. van Boheemen S, van Rijn AL, Pappas N, Carbo EC, Vorderman RHP, Sidorov I, et al. retrospective validation of a metagenomic sequencing protocol for combined detection of RNA and DNA viruses using respiratory samples from pediatric patients. *J Mol Diagn.* (2020) 22:196–207. doi: 10.1016/j.jmoldx.2019.10.007
286. Prachayangprecha S, Schapendonk CM, Koopmans MP, Osterhaus AD, Schurch AC, Pas SD, et al. Exploring the potential of next-generation sequencing in detection of respiratory viruses. *J Clin Microbiol.* (2014) 52:3722–30. doi: 10.1128/JCM.01641-14
287. Yadav H, Jain S, Nagpal R, Marotta F. Increased fecal viral content associated with obesity in mice. *World J Diabetes.* (2016) 7:316–20. doi: 10.4239/wjd.v7.i15.316
288. Tan VPK, Ngim CF, Lee EZ, Ramadas A, Pong LY, Ng JI, et al. The association between obesity and dengue virus (DENV) infection in hospitalised patients. *PLoS ONE.* (2018) 13:e0200698. doi: 10.1371/journal.pone.0200698
289. Vangipuram SD, Yu M, Tian J, Stanhope KL, Pasarica M, Havel PJ, et al. Adipogenic human adenovirus-36 reduces leptin expression and secretion and increases glucose uptake by fat cells. *Int J Obes.* (2007) 31:87–96. doi: 10.1038/sj.ijo.0803366
290. Mukhopadhya I, Segal JP, Carding SR, Hart AL, Hold GL. The gut virome: the 'missing link' between gut bacteria and host immunity? *Therap Adv Gastroenterol.* (2019) 12:1756284819836620. doi: 10.1177/1756284819836620
291. Tian Y, Jennings J, Gong Y, Sang Y. Viral infections and interferons in the development of obesity. *Biomolecules.* (2019) 9:726. doi: 10.3390/biom9110726
292. Russell CD, Unger SA, Walton M, Schwarze J. The human immune response to respiratory syncytial virus infection. *Clin Microbiol Rev.* (2017) 30:481–502. doi: 10.1128/CMR.00090-16
293. Jaddoe VWV, Felix JF, Andersen AN, Charles MA, Chatzi L, Corpeleijn E, et al. The LifeCycle project-EU child cohort network: a federated analysis infrastructure and harmonized data of more than 250,000 children and parents. *Eur J Epidemiol.* (2020) 35:709–24. doi: 10.1007/s10654-020-00662-z
294. Piersigilli F, Lam TT, Vernocchi P, Quagliariello A, Putignani L, Aghai ZH, et al. Identification of new biomarkers of bronchopulmonary dysplasia using metabolomics. *Metabolomics.* (2019) 15:20. doi: 10.1007/s11306-019-1482-9
295. Sahni M, Yeboah B, Das P, Shah D, Ponnalagu D, Singh H, et al. Novel biomarkers of bronchopulmonary dysplasia and bronchopulmonary dysplasia-associated pulmonary hypertension. *J Perinatol.* (2020) 40:1634–43. doi: 10.1038/s41372-020-00788-8

296. Askenazi DJ, Koralkar R, Patil N, Halloran B, Ambalavanan N, Griffin R. Acute kidney injury urine biomarkers in very low-birth-weight infants. *Clin J Am Soc Nephrol.* (2016) 11:1527–35. doi: 10.2215/CJN.13381215
297. Baumert M, Surmiak P, Wiecek A, Walencka Z. Serum NGAL and copeptin levels as predictors of acute kidney injury in asphyxiated neonates. *Clin Exp Nephrol.* (2017) 21:658–64. doi: 10.1007/s10157-016-1320-6
298. Jung YH, Han D, Shin SH, Kim EK, Kim HS. Proteomic identification of early urinary-biomarkers of acute kidney injury in preterm infants. *Sci Rep.* (2020) 10:4057. doi: 10.1038/s41598-020-60890-x
299. Watanabe IKM, Jara ZP, Volpini RA, Franco MDC, Jung FF, Casarini DE. Up-regulation of renal renin-angiotensin system and inflammatory mechanisms in the prenatal programming by low-protein diet: beneficial effect of the post-weaning losartan treatment. *J Dev Origins Health Dis.* (2018) 9:530–5. doi: 10.1017/S2040174418000296
300. Flynn ER, Alexander BT, Lee J, Hutchens ZM, Jr Maric-Bilkan C. High-fat/fructose feeding during prenatal and postnatal development in female rats increases susceptibility to renal and metabolic injury later in life. *Am J Physiol Regul Integr Comp Physiol.* (2013) 304:R278–85. doi: 10.1152/ajpregu.00433.2012
301. Wixey JA, Chand KK, Colditz PB, Bjorkman ST. Review: neuroinflammation in intrauterine growth restriction. *Placenta.* (2017) 54:117–24. doi: 10.1016/j.placenta.2016.11.012
302. Bangma JT, Hartwell H, Santos HP, O'Shea TM, Fry RC. Placental programming, perinatal inflammation, and neurodevelopment impairment among those born extremely preterm. *Pediatr Res.* (2021) 89:326–35. doi: 10.1038/s41390-020-01236-1
303. Leviton A, Fichorova RN, O'Shea TM, Kuban K, Paneth N, Dammann O, et al. Two-hit model of brain damage in the very preterm newborn: small for gestational age and postnatal systemic inflammation. *Pediatr Res.* (2013) 73:362–70. doi: 10.1038/pr.2012.188
304. Leviton A, Allred EN, Fichorova RN, Kuban KC, Michael O'Shea T, Dammann O. Systemic inflammation on postnatal days 21 and 28 and indicators of brain dysfunction 2years later among children born before the 28th week of gestation. *Early Hum Dev.* (2016) 93:25–32. doi: 10.1016/j.earlhumdev.2015.11.004
305. Kuban KC, Joseph RM, O'Shea TM, Heeren T, Fichorova RN, Douglass L, et al. Circulating inflammatory-associated proteins in the first month of life and cognitive impairment at age 10 years in children born extremely preterm. *J Pediatr.* (2017) 180:116–23.e111. doi: 10.1016/j.jpeds.2016.09.054
306. Guo W, Guan X, Pan X, Sun X, Wang F, Ji Y, et al. Post-natal inhibition of NF-kappaB activation prevents renal damage caused by prenatal LPS exposure. *PLoS ONE.* (2016) 11:e0153434. doi: 10.1371/journal.pone.0153434
307. Nüsken E, Fink G, Lechner F, Voggel J, Wohlfarth M, Sprenger L, et al. Altered molecular signatures during kidney development after intrauterine growth restriction of different origins. *J Mol Med.* (2020) 98:395–407. doi: 10.1007/s00109-020-01875-1
308. Rounioja S, Rasanen J, Glumoff V, Ojaniemi M, Makikallio K, Hallman M. Intra-amniotic lipopolysaccharide leads to fetal cardiac dysfunction. A mouse model for fetal inflammatory response. *Cardiovasc Res.* (2003) 60:156–64. doi: 10.1016/S0008-6363(03)00338-9

Conflict of Interest: The authors declare that the research was conducted in the absence of any commercial or financial relationships that could be construed as a potential conflict of interest.

Copyright © 2021 Kuiper-Makris, Selle, Nüsken, Dötsch and Alejandre Alcazar. This is an open-access article distributed under the terms of the Creative Commons Attribution License (CC BY). The use, distribution or reproduction in other forums is permitted, provided the original author(s) and the copyright owner(s) are credited and that the original publication in this journal is cited, in accordance with accepted academic practice. No use, distribution or reproduction is permitted which does not comply with these terms.

frontiers in Medicine

MINI REVIEW
published: 16 June 2021
doi: 10.3389/fmed.2021.662262

Early Life Microbial Exposure and Immunity Training Effects on Asthma Development and Progression

*Andressa Daronco Cereta[1], Vinícius Rosa Oliveira[2,3], Ivan Peres Costa[4], Letícia Lopes Guimarães[1], João Pedro Ribeiro Afonso[5], Adriano Luís Fonseca[5], Alan Robson Trigueiro de Sousa[5], Guilherme Augusto Moreira Silva[5], Diego A. C. P. G. Mello[5], Luis Vicente Franco de Oliveira[5] and Renata Kelly da Palma[1,2,6]**

[1] School of Veterinary Medicine and Animal Sciences, University of São Paulo, São Paulo, Brazil, [2] Department of Physical Therapy, EUSES University School, University of Barcelona-University of Girona (UB-UdG), Barcelona, Spain, [3] Research Group on Methodology, Methods, Models and Outcomes of Health and Social Sciences (M_3O), University of VIC-Central University of Catalonia, Vic, Spain, [4] Master's and Doctoral Programs in Rehabilitation Sciences, Nove de Julho University, São Paulo, Brazil, [5] Human Movement and Rehabilitation, Post Graduation Program Medical School, University Center of Anápolis-UniEVANGELICA, Anápolis, Brazil, [6] Institute for Bioengineering of Catalonia, Barcelona, Spain

Asthma is the most common inflammatory disease affecting the lungs, which can be caused by intrauterine or postnatal insults depending on the exposure to environmental factors. During early life, the exposure to different risk factors can influence the microbiome leading to undesired changes to the immune system. The modulations of the immunity, caused by dysbiosis during development, can increase the susceptibility to allergic diseases. On the other hand, immune training approaches during pregnancy can prevent allergic inflammatory diseases of the airways. In this review, we focus on evidence of risk factors in early life that can alter the development of lung immunity associated with dysbiosis, that leads to asthma and affect childhood and adult life. Furthermore, we discuss new ideas for potential prevention strategies that can be applied during pregnancy and postnatal period.

Keywords: asthma, lung microbiome, dysbiosis, early life immunity, prevention strategies

OPEN ACCESS

Edited by:
Jennifer J.P. Collins, Erasmus Medical Center, Netherlands

Reviewed by:
Hermelijn Helene Smits, Leiden University, Netherlands
Marc Hershenson, University of Michigan, United States

***Correspondence:**
Renata Kelly da Palma
rekellyp@hotmail.com

Specialty section:
This article was submitted to Pulmonary Medicine, a section of the journal Frontiers in Medicine

Received: *31 January 2021*
Accepted: *20 May 2021*
Published: *16 June 2021*

Citation:
Cereta AD, Oliveira VR, Costa IP, Guimarães LL, Afonso JPR, Fonseca AL, Sousa ARTd, Silva GAM, Mello DACPG, Oliveira LVF and da Palma RK (2021) Early Life Microbial Exposure and Immunity Training Effects on Asthma Development and Progression. Front. Med. 8:662262. doi: 10.3389/fmed.2021.662262

INTRODUCTION

Asthma is the most common heterogeneous inflammatory lung disease appearing generally in childhood. Adults are also affected, and more than 339 million people of all ages are living with asthma worldwide. Over 80% of asthma-related deaths occur in low-and lower-middle income countries (1). The pathophysiology of asthma is complex including phenotypes (visible properties) and Endotypes (mechanisms). Regarding phenotypes, the most common are allergic, in early onset, mild, or moderate-to-severe remodeled asthma or non-allergic with late-onset eosinophilic asthma or non-eosinophilic asthma (2). In addition, several factors such environmental, genetic polymorphisms, epigenetic regulations, aberrant immune maturation during pregnancy, and other factors in early life can contribute to the development of asthma. Regarding these factors we can find respiratory infections (mainly the viral ones), the exposure to airborne environment agents (tobacco smoke, pollutants), and most recently comes to light the important role in microbiome imbalance (3).

In this sense, there is not a unique cause or major determinant risk factor that contributes to the development of asthma. Apparently, the combination of several factors in early life

and inflammatory response due to it in a period of rapid growth and development of the lung causes structural and immune impairments that leading to asthma (4). Therefore, the key for developing prevention and strategies treatment in asthma is trying to understand the early-life exposures. In this review, we focus on evidence of risk factors in early life that can alter the development of lung immunity associated with dysbiosis, that leads to asthma and affect childhood and adult life.

EVENTS IN EARLY LIFE AND DYSBIOSIS IN ASTHMA

As above mentioned, asthma is developed due to several risk factors and can be linked with prenatal or early life events, causing it to appear specially in childhood. During early life, asthma can be associated with factors (**Figure 1**) such as delivery by cesarean section, antibiotics usage during the neonatal period, maternal low fiber diet, formula feeding, pollution and the variety of microbes due to environmental exposure (5). Therefore, perturbations on microbial composition (dysbiosis) can consequently alter immune development in mucosal tissues and lead to an increased susceptibility to asthma. Alterations in the microbiome in asthma are due to an association between changes in diversity and composition of lung microbiota along with modifications of functional genes (6). Besides that of the lung, nasal and bronchial microbiomes, asthmatic children also have alterations in the gut microbiome (7). Instances of crosstalk between gut and lung, called the "gut-lung" axis, have been demonstrated. For example, several studies have demonstrated that gut microbiome modulate Tregs in immune function by producing local and systemic mediators which impact on asthma development mediated by gut-lung axis (5, 8, 9).

In the recent years there were many advances in gene sequencing technology, expanding the knowledge on lung and gut microbiome, and on the significant role of the interactions between these two niches in the development and incidence of chronic airway disease. The airways are composed by a resident microbiota that develops after birth and interacts with different body sites, such as the gut, and its composition changes in health and disease (10).

Previous studies have suggested a strong correlation between mode of delivery and asthma incidence (11, 12). At the time of birth, maternal bacterial population is transferred to the baby. Stokholm et al. (13) demonstrated that vaginal delivery was associated with neonatal colonization of the intestinal tract by *Escherichia coli* at age 1 week while colonization by *Citrobacter freundii, Clostridium species, Enterobacter cloacae, Enterococcus faecalis, Klebsiella oxytoca, Klebsiella pneumoniae*, and *Staphylococcus aureus* were associated with cesarean section. However, at age 1 year this gut microbial perturbations were not apparent. Therefore, the same group conducted a cohort prospectively study with 700 children to investigate a risk of developing asthma in the first 6 years of life (14). Children who retained a cesarean gut microbial profile at age 1 year were more susceptible to developing asthma by age 6. On the other hand, Boker et al. (15) demonstrated no association between the mode of delivery and asthma incidence. However, this study has some limitations regarding sample size and information about exposition of the neonatal to maternal microflora due to premature rupture of membranes. Therefore, further research should be addressed to answer the questions regarding mode of delivery and asthma incidence.

In addition to mode of delivery, the antibiotics usage during the pregnancy seems alter both the maternal and neonatal microbiomes which may lead to subsequent allergy diseases in childhood (16, 17). Moreover, evidence suggesting that maternal antibiotic usage before and after pregnancy can increase the childhood asthma's risk (18). Furthermore, it should be noted that child exposed to antibiotics in the first days of life can reduced abundance and diversity of *Bifidobacterium* species (18) and increase the abundancy of *Enterobacteriaceae* species (19), which may induce the development of asthma. Therefore, it is important to raise the question about the contributions of antibiotics and infection on microbiome disturbance during and after pregnancy, further studies regarding this topic should be address.

The microbiota colonization of the child may be promoted by maternal gut microbiota *in utero*, after delivery and finally through breastfeeding. Maternal nutrition seems to play an important role on gut microbiota composition alterations in the child. Mother who intake a high-fat diet alters the child microbiome during pregnancy and lactation. The high-fat diet induces increase in *Enterococcus* and decreases *Bacteroides* in the third trimester of pregnancy, aside from decrease *Bacteroides* at delivery (20). Moreover, obese breastfeeding mothers has showed *Bacteroides* decreases in breast milk (21) which can induce a risk of asthma development in the early life (22).

On the other hand, human milk from mother who intake adequate nutrition, induces a general health benefits for the child and the World Health Organization recommends breastfeeding for at least 6 months after birth. Le Doare et al. (23) suggested that human milk can provide nutrition for the microbiome and prevent pathogenic bacterial adhesion. However, in nowadays some mothers has been replaced the breastfeeding and/or supplemented with cow's milk formula. In this sense, several studies have been demonstrated that the food sensitization in the early life may be associated with an increased risk of asthma (24) which can be mediated by an inflammatory immune response driven by Th2 cells. Liang et al. (25) demonstrated that neonatal fed by breast milk had an increase in *Bifidobacterium* and *Lactobacillus* and less viruses in stool samples in compared to those fed with cow's milk, which suggest that breastfeeding can be a potential protection against asthma. A Randomized Clinical Trial with a total of 312 newborns in 6 years follow-up, demonstrated that the cow's formula milk should be avoiding in the first 3 days of life especially in neonatal with higher levels of total Immunoglobulin-E (IgE) that can presents food sensitization

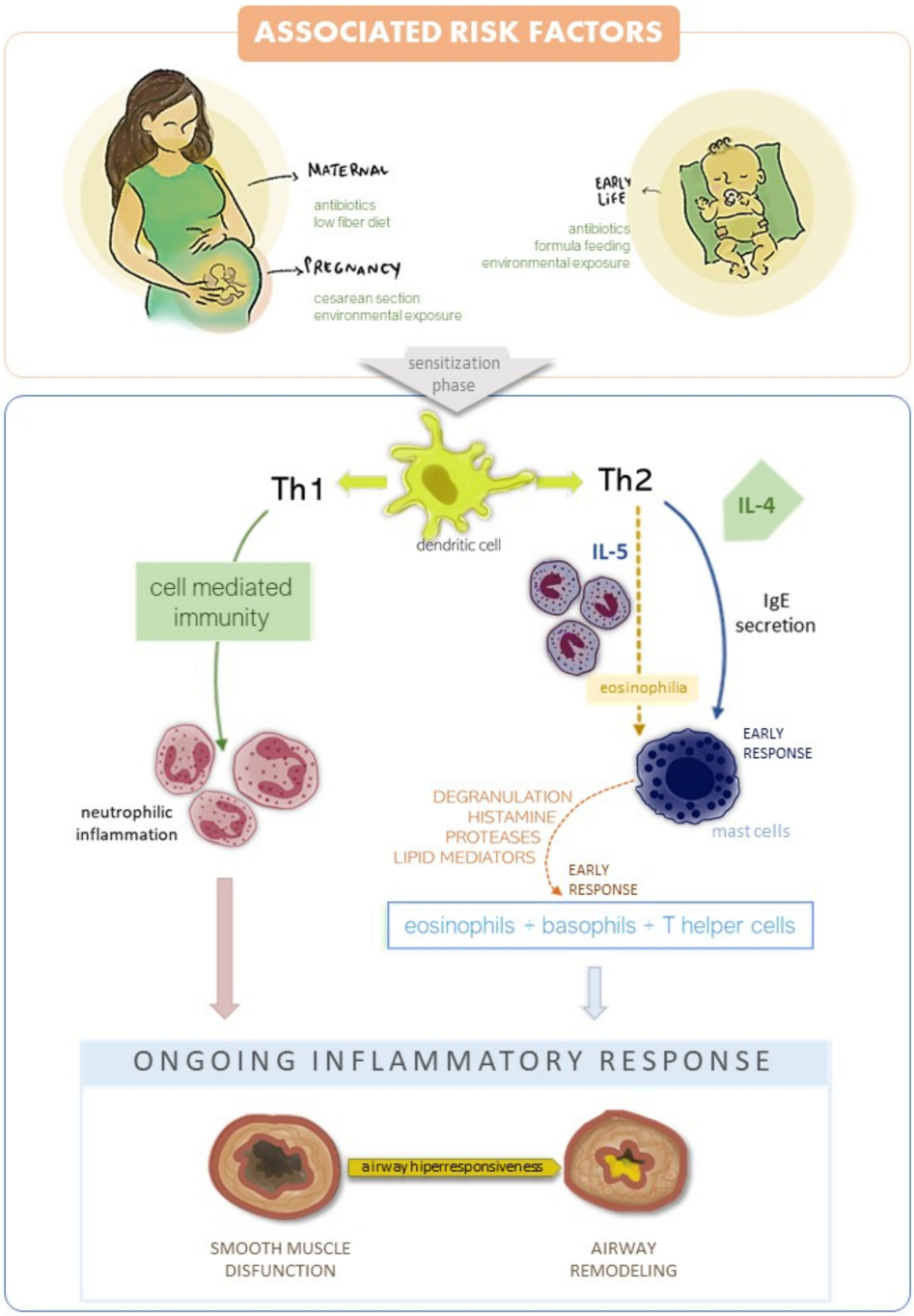

FIGURE 1 | Associated risk factors and asthma development. There are two inflammatory responses in asthma: Th1 and Th2 mediated. Th2 is the most common and leads to an early response by IgE production, presence of eosinophilia and mast cell recruitment. Late response in Th2 mediated asthma recruits' eosinophils, basophils and T helper cells to the mucosa leads to inflammatory response. Th1 mediate cell immunity in asthma, with neutrophilic inflammation affecting the epithelial layer. Both Th1 and Th2 cause airway hyper responsiveness, smooth muscle disfunction and airway remodeling.

in the early life (26). On the "Prevention strategies and immune training" section, we can observer that as earlier we introduce the allergic food the child can development a protective allergic effect.

Apart from food, the pollution and smoking exposure can be a risk for allergic sensitization and enhancement the probability of allergic asthma. Zheng et al. (27) collected fecal samples from 21 children in clean and smog days. Air pollution alters the intestinal

microbiome in asthmatic children, increasing *Bacteroidetes* and decreasing *Firmicutes*, these changes can be associated with asthma development. Besides air pollution, tobacco smoke exposure *in utero* and after birth may be associated with a risk of respiratory symptoms in childhood (28).

Children of mothers who smoked during their entire pregnancy present with a higher abundance of *Enterobacteriaceae* (29) at birth and increased abundance of *Bacteroides* and *Staphylococcus* at 6 months of age (30).

Therefore, we can suggest that the gut microbiota presents an important role in asthma development, probably due to the transfer of metabolites and immunomodulatory signals to the lung by gut-lung axis. Although are evidence regarding this connection, the appropriate pathway is not well-elucidated. Previous study demonstrated that gut dysbiosis can increase the allergic lung inflammation through both dendritic cells and T cells (31). Further studies should be address in this field. However, knowing the factor risks which induce a gut dysbiosis and may developed asthma, we can trace potential prevention strategies that can be applied during pregnancy and postnatal period.

PREVENTION STRATEGIES AND IMMUNE TRAINING

Pinning down strategies for asthma prevention in pregnancy and childhood has attracted great interest lately. The identification of potentially modifiable environmental and host risk factors for asthma development appears to be the cornerstone for the paradigm shift from disease treatment toward primary asthma prevention (32). Childhood asthma risk can be dampened by an appropriate maternal asthma control. The latter includes components such as monthly monitoring of lung function, patient education on inhaler technique, avoidance of environmental triggers (e.g., cigarette smoking, pollen, air pollution), and pharmacological treatment of comorbid conditions (e.g., depression, rhinitis, gastroesophageal reflux) (33).

The capacity of immune training the fetus by maternal environment provides possibilities for prevention of asthma after birth. Management of microbial dysbiosis could be a potential target for this training. Maternal diet and nutritional supplementation can shape immune *in utero* regarding to the airway's response later in life. Evidence suggests that a mother who intake high-fiber diet during pregnancy, leads to changes in the microbiota, enhancing T-regulatory cell numbers and function (34). Moreover, recent randomized clinical trials showed positive results on asthma prevention in offspring derived from adequate levels of vitamin D, antioxidants and fish oil intake during pregnancy (35–38).

In the postnatal period, prevention measures include the control of severe neonatal respiratory infections (e.g., respiratory syncytial virus and human rhinovirus), incentive for breastfeeding and enhancing other microbial exposure through the "farm effect," as endorsed by the hygiene hypothesis (39, 40). Beyond that, after the LEAP study (41), the old-fashioned avoidance allergenic foods strategy from the diets of infants began to be replaced by the tolerance strategy toward early exposure to allergens. This remarkable study demonstrated that early exposure to allergen can increase the levels of allergic-specific IgG and IgG4 which may induce an absence allergic reaction. Afterward, Pitt et al. (42) demonstrated a reduced risk of allergic sensitization following exposure through breast-feeding. In this sense, as early allergic foods are introduced its possible to training the immune system against allergic sensitization and it can be a strategy for asthma prevention.

Furthermore, supplementation with probiotic and vitamin could be a good strategy for immune training. Administration of probiotic—*Lactobacillus rhamnosus*- on postnatal period, showed a reduced risk of childhood asthma (43) probably because the probiotics can modulate the levels of short chain fatty acid and alters the microbiome composition. On the other side, the role of vitamin D on asthma management relies on its effects on immune cell function (44), corticosteroid responsiveness mediated by pathways involving IL-10 (45), IL-17 (46), oxidative stress (47), and airway remodeling (48). Results from observational studies are still mixed and limited, with more studies showing a beneficial effect for supplementation with vitamin D (49).

Prevention strategies involved in the translation of the environmental exposures elucidated in epidemiological studies mainly focus on asthma protective environmental microbial exposures associated with rural lifestyle activities. This led to some preclinical studies with bacterial lysates (ongoing clinical trial NCT02148796) and metabolites, dietary derivatives and helminthic compounds in order to prevent the disease development (50).

Moreover, The Finnish Allergy prevention program (51) describe practical advices regarding early life exposure: (i) Support breastfeeding, with solid foods from 4–6 months, (ii) do not avoid exposure to environmental allergens (foods, pets), (iii) do not smoke, (iv) probiotic bacteria in fermented food or other preparations and (v) Antibiotics should be taken only if is really necessary. All this simple practical approach can shape the immune system during early life and prevent asthma.

CONCLUSIONS

The changes in microbiome composition due to diseases is called *dysbiosis*. Understanding its roles and the immune responses due to this imbalance in asthma are promising both to comprehend the disease pathophysiology and to elaborate preventive strategies. Dietary interventions are considered safe and promising to boost the immune system and attenuate asthma symptomatology in children. Nevertheless, tackling asthma prevention is challenging because of the existing knowledge gap on the immune pathways that predispose some infants to develop asthma and not others.

It seems that the beneficial effects resulting from prevention approaches are due to the combination of them, instead of just one strategy. However, further research is needed on observational studies and clinical trials on the effects of using different combined strategies vs. a sole intervention for asthma prevention.

AUTHOR CONTRIBUTIONS

LG, JA, AF, AS, GS, DM, and LO conceived the design and concepts. RP, AC, VO, and IC wrote the manuscript. All authors contributed to the editing and revision of the manuscript and approved the submission.

REFERENCES

1. World Health Organization. *Chronic Respiratory Disease: Asthma*. (2020). Available online at: http:// www.who.int/news-room/q-a-detail/chronic-respiratory-diseases-asthma (accessed December 05, 2020).
2. Kaur R, Chupp G. Phenotypes and endotypes of adult asthma: moving toward precision medicine. *J Allergy Clin Immunol.* (2019) 144:1–12. doi: 10.1016/j.jaci.2019.05.031
3. Mims JW. Asthma: definitions and pathophysiology. *Int Forum Allergy Rhinol.* (2015) 5(Suppl. 1):S2–6. doi: 10.1002/alr.21609
4. Decrue F, Gorlanova O, Usemann J, Frey U. Lung functional development and asthma trajectories. *Semin Immunopathol.* (2020) 42:17–27. doi: 10.1007/s00281-020-00784-2
5. Gollwitzer ES, Marsland BJ. Impact of early-life exposures on immune maturation and susceptibility to disease. *Trends Immunol.* (2015) 36:684–96. doi: 10.1016/j.it.2015.09.009
6. Huang C, Yu Y, Du W, Liu Y, Dai R, Tang W, et al. Fungal and bacterial microbiome dysbiosis and imbalance of trans-kingdom network in asthma. *Clin Transl Allergy.* (2020) 10:42. doi: 10.1186/s13601-020-00345-8
7. Stokholm J, Blaser MJ, Thorsen J, Rasmussen MA, Waage J, Vinding RK, et al. Maturation of the gut microbiome and risk of asthma in childhood. *Nat Commun.* (2018) 9:141. doi: 10.1038/s41467-017-02573-2
8. Trompette A, Gollwitzer ES, Yadava K, Sichelstiel AK, Sprenger N, Ngom-Bru C, et al. Gut microbiota metabolism of dietary fiber influences allergic airway disease and hematopoiesis. *Nat Med.* (2014) 20:159–66. doi: 10.1038/nm.3444
9. Frati F, Salvatori C, Incorvaia C, Bellucci A, Di Cara G, Marcucci F, et al. The role of the microbiome in asthma: the gut−lung axis. *Int J Mol Sci.* (2018) 20:123. doi: 10.3390/ijms20010123
10. Santacroce L, Charitos IA, Ballini A, Inchingolo F, Luperto P, De Nitto E, et al. The human respiratory system and its microbiome at a glimpse. *Biology.* (2020) 9:318. doi: 10.3390/biology9100318
11. Black M, Bhattacharya S, Philip S, Norman JE, McLernon DJ. Planned cesarean delivery at term and adverse outcomes in childhood health. *JAMA.* (2015) 314:2271–9. doi: 10.1001/jama.2015.16176
12. van Berkel AC, den Dekker HT, Jaddoe VW, Reiss IK, Gaillard R, Hofman A, et al. Mode of delivery and childhood fractional exhaled nitric oxide, interrupter resistance and asthma: the Generation R study. *Pediatr Allergy Immunol.* (2015) 26:330–6. doi: 10.1111/pai.12385
13. Stokholm J, Thorsen J, Chawes BL, Schjørring S, Krogfelt KA, Bønnelykke K, et al. Cesarean section changes neonatal gut colonization. *J Allergy Clin Immunol.* (2016) 138:881–9.e2. doi: 10.1016/j.jaci.2016.01.028
14. Stokholm J, Thorsen J, Blaser MJ, Rasmussen MA, Hjelmsø M, Shah S, et al. Delivery mode and gut microbial changes correlate with an increased risk of childhood asthma. *Sci Transl Med.* (2020) 12:eaax9929. doi: 10.1126/scitranslmed.aax9929
15. Boker F, Alzahrani A, Alsaeed A, Alzhrani M, Albar R. Cesarean section and development of childhood bronchial asthma: is there a risk? *J Med Sci.* (2019) 7:347–51. doi: 10.3889/oamjms.2019.085
16. Meropol SB, Edwards A. Development of the infant intestinal microbiome: a bird's eye view of a complex process. *Birth Defects Res.* (2015) 105:228–39. doi: 10.1002/bdrc.21114
17. Baron R, Taye M, der Vaart IB, Ujčič-Voortman J, Szajewska H, Seidell JC, et al. The relationship of prenatal antibiotic exposure and infant antibiotic administration with childhood allergies: a systematic review. *BMC Pediatr.* (2020) 20:312. doi: 10.1186/s12887-020-02042-8
18. Uzan-Yulzari A, Turta O, Belogolovski A, Ziv O, Kunz C, Perschbacher S, et al. Neonatal antibiotic exposure impairs child growth during the first six years of life by perturbing intestinal microbial colonization. *Nat Commun.* (2021) 12:443. doi: 10.1038/s41467-020-20495-4
19. Greenwood C, Morrow AL, Lagomarcino AJ, Altaye M, Taft DH, Yu, et al. Early empiric antibiotic use in preterm infants is associated with lower bacterial diversity and higher relative abundance of Enterobacter. *J Pediatr.* (2014) 165:23–9. doi: 10.1016/j.jpeds.2014.01.010
20. Chu DM, Antony KM, Ma J, Prince AL, Showalter L, Moller M, et al. The early infant gut microbiome varies in association with a maternal high-fat diet. *Genome Med.* (2016) 8:77. doi: 10.1186/s13073-016-0330-z
21. Williams JE, Carrothers JM, Lackey KA, Beatty NF, York MA, Brooker SL, et al. Human milk microbial community structure is relatively stable and related to variations in macronutrient and micronutrient intakes in healthy lactating women. *J Nutr.* (2017) 147:1739–48. doi: 10.3945/jn.117.248864
22. Mesa MD, Loureiro B, Iglesia I, Fernandez Gonzalez S, Llurba Olivé E, García Algar O, et al. The evolving microbiome from pregnancy to early infancy: a comprehensive review. *Nutrients.* (2020) 12:133. doi: 10.3390/nu12010133
23. Le Doare K, Holder B, Bassett A, Pannaraj PS. Mother's milk: a purposeful contribution to the development of the infant microbiota and immunity. *Front Immunol.* (2018) 9:361. doi: 10.3389/fimmu.2018.00361
24. Alduraywish SA, Lodge CJ, Campbell B, Allen KJ, Erbas B, Lowe AJ, et al. The march from early life food sensitization to allergic disease: a systematic review and meta-analyses of birth cohort studies. *Allergy.* (2016) 71:77–89. doi: 10.1111/all.12784
25. Liang G, Zhao C, Zhang H, Mattei L, Sherrill-Mix S, Bittinger K, et al. The stepwise assembly of the neonatal virome is modulated by breastfeeding. *Nature.* (2020) 581:470–4. doi: 10.1038/s41586-020-2192-1
26. Tachimoto H, Imanari E, Mezawa H, Okuyama M, Urashima T, Hirano D, et al. Effect of avoiding cow's milk formula at birth on prevention of asthma or recurrent wheeze among young children: extended follow-up from the ABC randomized clinical trial. *JAMA Netw Open.* (2020) 3:e2018534. doi: 10.1001/jamanetworkopen.2020.18534
27. Zheng P, Zhang B, Zhang K, Lv X, Wang Q, Bai X. The impact of air pollution on intestinal microbiome of asthmatic children: a panel study. *BioMed Res Int.* (2020) 2020:5753427. doi: 10.1155/2020/5753427
28. Vardavas CI, Hohmann C, Patelarou E, Martinez D, Henderson AJ, Granell R, et al. The independent role of prenatal and postnatal exposure to active and passive smoking on the development of early wheeze in children. *Eur Respir J.* (2016) 48:115–24. doi: 10.1183/13993003.01016-2015
29. Gosalbes MJ, Llop S, Vallès Y, Moya A, Ballester F, Francino MP. Meconium microbiota types dominated by lactic acid or enteric bacteria are differentially associated with maternal eczema and respiratory problems in infants. *Clin Exp Allergy.* (2013) 43:198–211. doi: 10.1111/cea.12063
30. Levin AM, Sitarik AR, Havstad SL, Fujimura KE, Wegienka G, Cassidy-Bushrow AE, et al. Joint effects of pregnancy, sociocultural, and environmental factors on early life gut microbiome structure and diversity. *Sci Rep.* (2016) 6:31775. doi: 10.1038/srep31775
31. Cait A, Hughes MR, Antignano F, Cait J, Dimitriu PA, Maas KR, et al. Microbiome-driven allergic lung inflammation is ameliorated by short-chain fatty acids. *Mucosal Immunol.* (2018) 11:785–95. doi: 10.1038/mi.2017.75
32. Polk BI, Bacharier LB. Potential strategies and targets for the prevention of pediatric asthma. *Immunol Allergy Clin North Am.* (2019) 39:151–62. doi: 10.1016/j.iac.2018.12.010
33. Bonham CA, Patterson KC, Strek ME. Asthma outcomes and management during pregnancy. *Chest.* (2018) 153:515–27. doi: 10.1016/j.chest.2017.08.029
34. Thorburn AN, McKenzie CI, Shen S, Stanley D, Macia L, Mason LJ, et al. Evidence that asthma is a developmental origin disease influenced by maternal diet and bacterial metabolites. *Nat Commun.* (2015) 6:7320. doi: 10.1038/ncomms8320

35. Bisgaard H, Stokholm J, Chawes BL, Vissing NH, Bjarnadóttir E, Schoos AM, et al. Fish oil-derived fatty acids in pregnancy and wheeze and asthma in offspring. *N Eng J Med.* (2016) 375:2530–9. doi: 10.1056/NEJMoa1503734
36. Hansen S, Strøm M, Maslova E, Dahl R, Hoffmann HJ, Rytter D, et al. Fish oil supplementation during pregnancy and allergic respiratory disease in the adult offspring. *J Allergy Clin Immunol.* (2017) 139:104–11.e4. doi: 10.1016/j.jaci.2016.02.042
37. Litonjua AA, Carey VJ, Laranjo N, Harshfield BJ, McElrath TF, O'Connor GT, et al. Effect of prenatal supplementation with vitamin D on asthma or recurrent wheezing in offspring by age 3 years: the VDAART randomized clinical trial. *JAMA.* (2016) 315:362–70. doi: 10.1001/jama.2015.18589
38. Wolsk HM, Harshfield BJ, Laranjo N, Carey VJ, O'Connor G, Sandel M, et al. Vitamin D supplementation in pregnancy, prenatal 25(OH)D levels, race, and subsequent asthma or recurrent wheeze in offspring: secondary analyses from the Vitamin D antenatal asthma reduction trial. *J Allergy Clin Immunol.* (2017) 140:1423–9.e5. doi: 10.1016/j.jaci.2017.01.013
39. Chung KF. Airway microbial dysbiosis in asthmatic patients: a target for prevention and treatment? *J Allergy Clin Immunol.* (2017) 139:1071–81. doi: 10.1016/j.jaci.2017.02.004
40. Gur M, Hakim F, Bentur L. Better understanding of childhood asthma, towards primary prevention - are we there yet? *Consideration of pertinent literature. F1000Res.* (2017) 6:2152. doi: 10.12688/f1000research.11601.1
41. Du Toit G, Roberts G, Sayre PH, Bahnson HT, Radulovic S, Santos AF, et al. Randomized trial of peanut consumption in infants at risk for peanut allergy. *N Eng J Med.* (2015) 372:803–13. doi: 10.1056/NEJMoa1414850
42. Pitt TJ, Becker AB, Chan-Yeung M, Chan ES, Watson W, Chooniedass R, et al. Reduced risk of peanut sensitization following exposure through breast-feeding and early peanut introduction. *J Allergy Clin Immunol.* (2018) 141:620–25.e1. doi: 10.1016/j.jaci.2017.06.024
43. Du X, Wang L, Wu S, Yuan L, Tang S, Xiang Y, et al. Efficacy of probiotic supplementary therapy for asthma, allergic rhinitis, and wheeze: a meta-analysis of randomized controlled trials. *Allergy Asthma Proc.* (2019) 40:250–60. doi: 10.2500/aap.2019.40.4227
44. Pfeffer PE, Hawrylowicz CM. Vitamin D in asthma: mechanisms of action and considerations for clinical trials. *Chest.* (2018) 153:1229–39. doi: 10.1016/j.chest.2017.09.005
45. Xystrakis E, Kusumakar S, Boswell S, Peek E, Urry Z, Richards DF, et al. Reversing the defective induction of IL-10-secreting regulatory T cells in glucocorticoid-resistant asthma patients. *J Clin Invest.* (2006) 116:146–55. doi: 10.1172/JCI21759
46. Chambers ES, Nanzer AM, Pfeffer PE, Richards DF, Timms PM, Martineau AR, et al. Distinct endotypes of steroid-resistant asthma characterized by IL-17A(high) and IFN-γ(high) immunophenotypes: potential benefits of calcitriol. *J Allergy Clin Immunol.* (2015) 136:628–37.e4. doi: 10.1016/j.jaci.2015.01.026
47. Lan N, Luo G, Yang X, Cheng Y, Zhang Y, Wang X, et al. 25-Hydroxyvitamin D3-deficiency enhances oxidative stress and corticosteroid resistance in severe asthma exacerbation. *PLoS ONE.* (2014) 9:e111599. doi: 10.1371/journal.pone.0111599
48. Gupta A, Sjoukes A, Richards D, Banya W, Hawrylowicz C, Bush A, et al. Relationship between serum vitamin D, disease severity, and airway remodeling in children with asthma. *Am J Respir Crit Care Med.* (2011) 184:1342–9. doi: 10.1164/rccm.201107-1239OC
49. Litonjua AA. Vitamin D and childhood asthma: causation and contribution to disease activity. *Curr Opin Allergy Clin Immunol.* (2019) 19:126–31. doi: 10.1097/ACI.0000000000000509
50. von Mutius E, Smits HH. Primary prevention of asthma: from risk and protective factors to targeted strategies for prevention. *Lancet.* (2020) 396:854–66. doi: 10.1016/S0140-6736(20)31861-4
51. Haahtela T, Valovirta E, Bousquet J, Mäkelä M, Allergy Programme Steering Group. The Finnish Allergy Programme 2008-2018 works. *Eur Respir J.* (2017) 49:1700470. doi: 10.1183/13993003.00470-2017

Conflict of Interest: The authors declare that the research was conducted in the absence of any commercial or financial relationships that could be construed as a potential conflict of interest.

Copyright © 2021 Cereta, Oliveira, Costa, Guimarães, Afonso, Fonseca, Sousa, Silva, Mello, Oliveira and da Palma. This is an open-access article distributed under the terms of the Creative Commons Attribution License (CC BY). The use, distribution or reproduction in other forums is permitted, provided the original author(s) and the copyright owner(s) are credited and that the original publication in this journal is cited, in accordance with accepted academic practice. No use, distribution or reproduction is permitted which does not comply with these terms.

frontiers in Pediatrics

ORIGINAL RESEARCH
published: 12 August 2021
doi: 10.3389/fped.2021.621381

Etiologies of Hospitalized Acute Bronchiolitis in Children 2 Years of Age and Younger: A 3 Years' Study During a *Pertussis* Epidemic

Sainan Chen[1†], *Yuqing Wang*[1*], *Anrong Li*[1], *Wujun Jiang*[1†], *Qiuyan Xu*[2], *Min Wu*[1], *Zhengrong Chen*[1], *Chuangli Hao*[1], *Xunjun Shao*[1] *and Jun Xu*[1]

[1] *Department of Respiratory Medicine, Children's Hospital of Soochow University, Suzhou, China,* [2] *Department of Pediatrics, Affiliated Suzhou Science and Technology Town Hospital of Nanjing Medical University, Suzhou, China*

Objective: In recent years, the incidence of *Bordetella pertussis* infection in infants and young children has been increasing. Multiple studies have suggested that *B. pertussis* may be one of the pathogens of bronchiolitis in infants and young children. However, the prevalence and clinic characteristic of *B. pertussis* in bronchiolitis is controversial. This prospective descriptive study evaluated the prevalence and clinical manifestations of infants and young children hospitalized for bronchiolitis with *B. pertussis.*

Methods: Children hospitalized with bronchiolitis were eligible for a prospective study for 36 months from January 1, 2017, to December 31, 2019. Besides *B. pertussis*, 10 common respiratory viruses and *Mycoplasma pneumoniae* (MP) were confirmed by laboratory tests. Medical records of patients were reviewed for demographic, clinical characteristics, and laboratory examination.

Results: A total of 1,092 patients with bronchiolitis were admitted. *B. pertussis* was detected in 78/1,092 (7.1%) patients. Of the 78 patients with *B. pertussis* bronchiolitis, coinfections occurred in 45 (57.7%) patients, most frequently with human rhinovirus (28/78, 35.9%), followed by MP (9/78, 11.4%), and human bocavirus (6/78, 7.7%). The peak incidence of *B. pertussis* infection was in May. A high leukocyte count could help distinguish *B. pertussis*–associated acute bronchiolitis from other acute bronchiolitis etiologies. After excluding coinfections, children with *B. pertussis*–only bronchiolitis exhibited a milder clinical presentation than those with RSV-only infection; also, children with MP-only and other pathogen infections revealed similar severity. The morbidity of *B. pertussis* was common (31/78, 39.7%) in infants with bronchiolitis under 3 months.

Conclusion: In summary, *B. pertussis* is one of the pathogens in children with bronchiolitis, and coinfection of *B. pertussis* with other viruses is common in bronchiolitis. *B. pertussis* should be considered when patients hospitalized with bronchiolitis present a longer course and have an elevated leukocyte count. Patients with *B. pertussis*–associated bronchiolitis present a milder clinical presentation.

Keywords: *Bordetella pertussis*, bronchiolitis, coinfection, immunization, disease progression, high leukocyte count

OPEN ACCESS

Edited by:
Mandy Laube,
Leipzig University, Germany

Reviewed by:
Carla Bellinghausen,
Goethe University Frankfurt, Germany
Sompong Vongpunsawad,
Chulalongkorn University, Thailand

***Correspondence:**
Yuqing Wang
wang_yu_qing@126.com

[†] *These authors have contributed equally to this work*

Specialty section:
This article was submitted to Pediatric Pulmonology, a section of the journal Frontiers in Pediatrics

Received: *26 October 2020*
Accepted: *29 June 2021*
Published: *12 August 2021*

Citation:
Chen S, Wang Y, Li A, Jiang W, Xu Q, Wu M, Chen Z, Hao C, Shao X and Xu J (2021) Etiologies of Hospitalized Acute Bronchiolitis in Children 2 Years of Age and Younger: A 3 Years' Study During a Pertussis Epidemic. Front. Pediatr. 9:621381. doi: 10.3389/fped.2021.621381

INTRODUCTION

Pertussis, caused by the bacterium *Bordetella pertussis*, is a highly contagious respiratory disease and one of the leading causes of death from infectious diseases in children. *B. pertussis*, a Gram-negative bacterium that was first described by Bordet and Gengou in 1906 (1), has recently reemerged as a major public health threat. The World Health Organization reported 141,074 confirmed pertussis cases worldwide in 2018 (2). Approximately 160,700 deaths were reported worldwide in 2014 from pertussis in children <5 years of age (3).

Bronchiolitis is the most common acute respiratory disease in infants and young children, and one of the most common causes of hospital admission (4, 5). A total of 40–80% of infection is caused by respiratory syncytial virus (RSV), followed by human rhinovirus (HRV), adenovirus (ADV), parainfluenza virus, human bocavirus (hBoV), and human metapneumovirus (hMPV) (6, 7).

In recent years, several studies suggested that *B. pertussis* is a possible pathogen causing bronchiolitis in infants and young children hospitalized for lower respiratory tract infections (8–10). However, studies reporting the prevalence and clinical characteristics of *B. pertussis* bronchiolitis are rare. This study aimed to assess the epidemiological features and clinical characteristics of *B. pertussis* infection and evaluate its impact on infants and young children hospitalized with acute bronchiolitis.

MATERIALS AND METHODS

Patients and Definitions

This prospective descriptive study was conducted on children presenting with acute bronchiolitis who were admitted to the Department of Respiratory Medicine in the Children's Hospital of Soochow University between January 1, 2017, and December 31, 2019. Acute bronchiolitis was characterized by age ≤2, cough, tachypnea, retraction, and expiratory wheezes, often accompanied by rales (11). *B. pertussis* was confirmed by polymerase chain reaction (PCR) assays (12). Patients requiring oxygen supply were considered with severe conditions. The exclusion criteria were as follows: (1) patients with incomplete clinical data; (2) patients with bronchopulmonary dysplasia, heredity metabolic diseases, neurological disorders, congenital heart disease, and immunodeficiency; and (3) patients with evidence suggesting that wheezing was caused by tuberculosis and non-infectious factors such as bronchial foreign bodies.

The study was approved by the ethics committees of Children's Hospital Soochow University (Approval No. 2016026). Informed consent was obtained from the parents of all children enrolled in this study.

Determination of Vaccination Status

Vaccination history was obtained by querying the "Suzhou Children's Vaccination Inquiry and Evaluation Platform." A diphtheria, tetanus, and acellular pertussis combination vaccine was administered as a primary series at 3, 4, and 5 months, followed by a booster dose at 24 months in China. The vaccination status was regarded as ever-vaccinated if one to three doses were received.

TABLE 1 | Gene primer sequence and product length detected by real-time PCR.

Gene name	Primer sequence products	Length
IS481	5′GATTCAATAGGTTGTATGCATGGTT3′	145
	5′TGGACCATTTCGAGTCGACG3′	
PtxA-pr	5′CCAACGCGCATGCGTGCAGATTCGTC3′	191
	5′CCCTCTGCGTTTGATGGTGCCTATTTTA3′	

Data Collection

Data regarding demographic, clinical, and laboratory characteristics were documented. Demographic and clinical characteristics included age, gender, length of hospital stay, and requirement of supplemental oxygen. Laboratory specimens were obtained including blood and nasopharyngeal aspirates (NPAs). NPAs were obtained during the first 24 h of hospitalization, using a sterile plastic catheter briefly inserted into the lower pharynx *via* the nasal cavity. The blood samples were taken immediately after hospitalization. The laboratory data of leukocyte count, percentages of lymphocytes and neutrophils, and detection of common viruses were collected.

PCR Detection of *B. pertussis*

B. pertussis DNA was detected in NPAs by real-time PCR assays. The primer sequence was synthesized by Shanghai Sangon Biotech Company. The pertussis PtxA-pr and IS481 gene sequences were used as specific primers (**Table 1**). The RT-PCR assay result was considered negative if the cycle threshold (CT) was ≥40. Specimens that tested positive by PCR for both insertion sequence IS481 (CT < 40) and ptxS1 (CT < 40) were considered positive for *B. pertussis*. If a specimen was PtxA-pr target negative with an IS481 assay CT <35, it was also considered positive for *B. pertussis*.

Respiratory Pathogens

Direct immunofluorescence was used to detect RSV; ADV; influenza virus A (IV-A) and B (IV-B); and parainfluenza virus 1 (PIV I), 2 (PIV II), and 3 (PIV III) using a D^3 Ultra Respiratory Virus Screening and LD Kit (Diagnostic Hybrids, Athens, OH, USA). A positive result was defined as over five inclusion bodies analyzed under a fluorescence microscope. *Mycoplasma pneumoniae* (MP), HRV, HMPV, and HBoV were detected by a PCR (nucleic acid amplification fluorescent reagent kit, Ann Gene Co., Guangdong, China) according to the manufacturer's instructions.

Statistical Analyses

Statistical analyses were conducted using SPSS 26.0 (IBM, SPSS, Chicago, IL, USA).

Data were shown as mean ± standard deviation and median and interquartile range. Quantitative variables among the three age groups were compared using one-way analysis of variance or the Kruskal–Wallis test when appropriate. Frequency

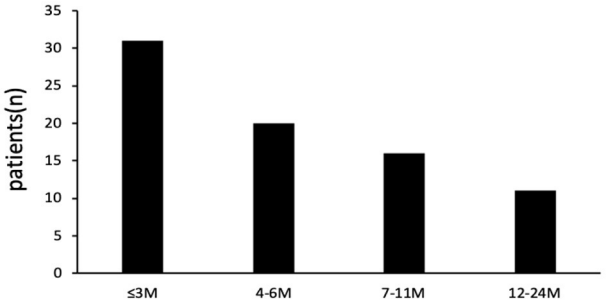

FIGURE 1 | Distribution of *B. pertussis* infection in infants and young children stratified by age.

distribution was compared by the chi-square test. A p value <0.05 was considered as a significant difference.

RESULTS

Demographic Characteristics

Of the total 1,092 patients admitted for bronchiolitis, one or more respiratory pathogens including virus and MP were detected in 1,057 of 1,092 patients (a positive rate of 96.8%) and *B. pertussis* was identified in 78 patients (7.1%, based on positive results by PCR). Of the 78 cases of bronchiolitis with *B. pertussis* infection, 47 (60.3%) were male and 31 (39.7%) were female. The male-to-female ratio was 1.52:1. The median age was 6.45 ± 4.94 months. The age distribution of patients is shown in **Figure 1**; 31 (39.7%) patients were aged ≤3 months, 20 (25.6%) patients were aged 4–6 months, 16 (20.5%) patients were aged 7–11 months, and 11 (14.1%) patients were aged ≥12 months.

Seasonality of *B. pertussis* Infection

The monthly distribution of *B. pertussis* infection is shown in **Figures 2A,B**. Bronchiolitis could occur throughout the year, and the peak incidence was in winter. The most common pathogen of bronchiolitis was RSV (534/1092, 48.9%), and the peak incidence was in December. MP was detected in 159/1,092 (14.6%) children with bronchiolitis, and the peak incidence was in September. Differing from the above two pathogens, the peak incidence of *B. pertussis* infection was in May, with a total of 10 (19.2%, 10/52) patients reported, and no patients were infected in October and December.

Coinfection Status

Overall, one or more respiratory pathogens including virus and MP were detected in 1,057 of 1,092 patients. The most commonly detected pathogens in patients with bronchiolitis were as follows: RSV (48.9%), HRV (25.9%), HMPV (13.0%), MP (14.6%), HBoV (12.1%), *B. pertussis* (7.1%), PIV III (7.0%), ADV (1.1%), and PIV I (1.1%).

Of the 78 *B. pertussis*–infected patients, *B. pertussis* was the sole pathogen detected in 33 (42.3%) patients. The remaining 45 patients (57.7%) were coinfected with other respiratory pathogens, most frequently with HRV ($n = 28$, 35.9%), followed by MP ($n = 9$, 11.4%), HBoV ($n = 6$, 7.7%), PIV III ($n = 4$, 5.1%), RSV ($n = 3$, 3.9%), IV-A ($n = 3$, 3.9%), and HMPV ($n = 2$, 2.6%) (**Figure 3**).

Clinical Features of *B. pertussis*–Only Infection Compared With Infections With Other Pathogens

In the present study, 33 patients with *B. pertussis*–only infection, 438 patients with RSV-only infection, 87 patients with MP-only infection, and 534 patients infected with other pathogens were analyzed. In unadjusted comparisons, children with *B. pertussis*–only infection were similar to children with RSV-only infection in age, but the number of children with age ≤ 3 months who were only infected with pertussis was less than that of children with RSV-only infection (**Table 2**). Children with *B. pertussis*–only infection were significantly more likely to have vomiting (36.4%), cyanosis (12.1%), leukocyte count $>15 \times 10^9$ (57.6%), longer duration of symptoms before admission (media day, 14.0), and longer hospital stay (media day, 9.0) compared with those with RSV-only infection (17.8%, 2.7%, 7.5%, media 5.0, and 8.0 days, respectively; $p < 0.05$ for all comparisons). Patients with *B. pertussis*–only infection requiring supplement oxygen were fewer than patients with RSV-only infection (6.1 vs. 34.9%; $p < 0.05$).

In unadjusted comparisons, among 120 patients with *B. pertussis* and MP infections excluding co-detection with other pathogen types, children with *B. pertussis*–only infection were younger than children with MP-only infection (median 3.9 vs. 5.8 months, respectively) (**Table 2**). Children with *B. pertussis*–only infection were significantly more likely to have dyspnea (6.1%), rhinorrhea (15%), vomiting (15%), cyanosis (4%), and leukocyte count $>15 \times 10^9$/L (57.6%) compared with those with MP-only infection (0.0, 24.1, 10.3, 0.0, and 6.9%, respectively; $p < 0.05$ for all comparisons). Children with *B. pertussis*–only infection had a higher number of leukocyte and higher percentage of lymphocyte compared with children with MP-only infection. Children with *B. pertussis*–only infection had a longer duration of hospital stay (median 9.0 days) than those with MP-only infection (median 8.0 days); however, no significant difference was observed in the duration of symptoms before admission.

B. pertussis Infection and Results of Laboratory Examination in Different Age Groups

B. pertussis–positive patients were divided into three age groups to assess the difference among different age groups (**Table 3**). A total of 31 patients aged ≤3 months, 36 patients aged 4–11 months, and 11 patients aged ≥12 months were analyzed. Patients aged ≤3 months had a longer duration of hospital stay than others ($p < 0.05$). The common clinic characteristics among the 78 confirmed patients were paroxysmal cough 92.3% (72/78), whoops 15.5% (12/78), post-tussive vomiting 38.5% (30/78), and cyanosis 12.8% (10/78). Patients with cyanosis aged ≤3 months were more compared with older ones ($p < 0.05$); the others exhibited no difference among three age groups ($p > 0.05$). Patients aged ≤3 months requiring supplemental oxygen were more compared

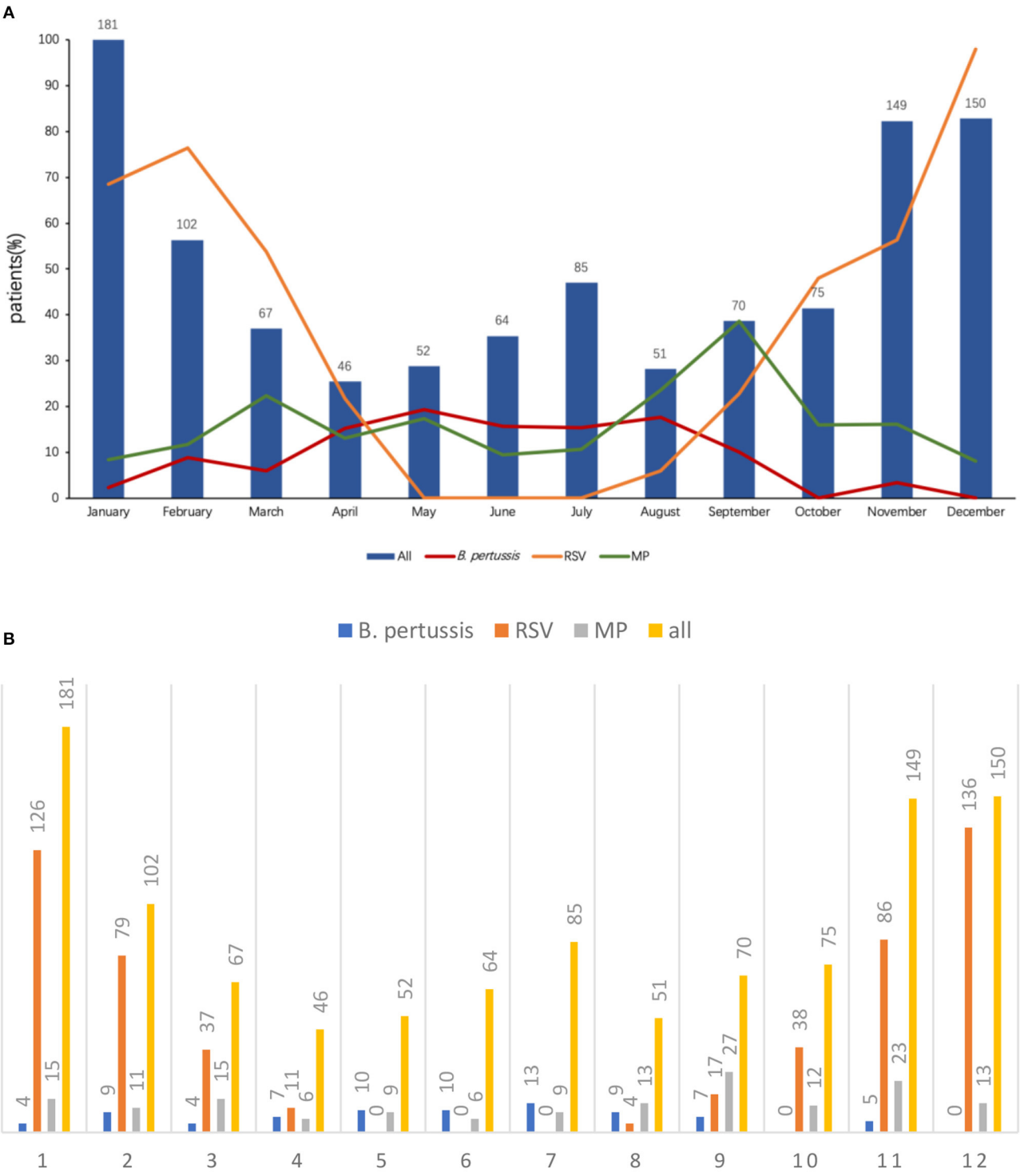

FIGURE 2 | (A) Distribution of *B. pertussis* and other pathogen infection by month. **(B)** Distribution of *B. pertussis* and other pathogen infection by month.

with older ones ($p < 0.05$). The gender ratio exhibited no significant difference among the three groups ($p < 0.05$). Coinfection among the three age groups was also compared, which showed no difference ($p > 0.05$). Although, patients aged ≥12 months had a higher number of leukocytes, and higher percentages of neutrophils and lymphocytes, no

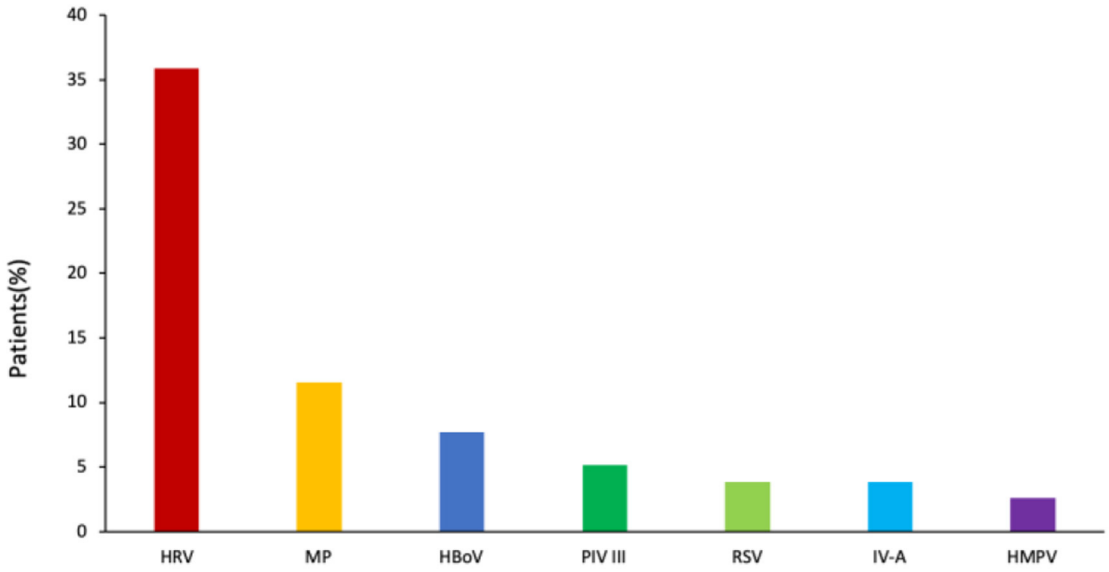

FIGURE 3 | Distribution of pathogen coinfections associated with *B. pertussis* infection.

significant difference was observed among the three groups ($p > 0.05$).

Clinical Features of *B. pertussis*–Only Infection Compared With Coinfection

Patients with *B. pertussis*–only infection were younger and had a high incidence of paroxysmal cough compared with patients with coinfection ($p < 0.05$). However, patients with coinfection had an increased demand for oxygen and showed more crackles in lungs ($p < 0.05$) (**Table 4**).

DISCUSSION

In recent years, an increasing incidence of pertussis has been reported in infants and young children (13). Several studies suggested that *B. pertussis* is a possible pathogen causing bronchiolitis in infants (8–10). Several investigators demonstrated that *B. pertussis* is a common pathogen of bronchiolitis (14, 15). A study conducted in Turkey identified 44 (25.6%) of the 172 infants with *B. pertussis* hospitalized for acute bronchiolitis (15). Another study showed *B. pertussis* involvement in 12 of 142 (8.5%) infants hospitalized for bronchiolitis in Finland (9). Yet other studies identified that *B. pertussis* was an uncommon pathogen in bronchiolitis (16). Pedro A. Piedra and his colleges found only four of 2,027 children admitted to the hospital as *B. pertussis* positive using PCR in the USA (10). Similarly, Walsh et al. found *B. Pertussis* infection in three of 488 patients (0.6%) in the emergency department (17). The present study found that 7.1% of infants and young children hospitalized with acute bronchiolitis had a positive *B. pertussis* test, which demonstrated that *B. pertussis* was a common pathogen in bronchiolitis. The variation in the prevalence of *B. pertussis* in children hospitalized with bronchiolitis among the studies might be due to the difference in climates, recruit criteria, and vaccination. According to the finding of this study, the peak incidence of *B. pertussis* infection was from May to July, with a total of 33 (50.15%) patients, which has not been reported before.

Studies reported that *B. pertussis* coinfection with other respiratory viruses was common in children hospitalized for bronchiolitis; the incidence rate was 36–67% (9, 14, 15, 18). However, the present study reported that 45 (57.7%) patients with *B. pertussis* were coinfected with other respiratory viruses, which was in agreement with previous studies. Some studies (6, 15, 19) suggested that coinfection with RSV was the most common in young children hospitalized for bronchiolitis with *B. pertussis* infection. However, in the present study, the most common coinfection respiratory viruses in children with *B. pertussis* hospitalized for bronchiolitis were HRV (35.9%), followed by MP (11.4%), and HBoV (7.7%); these differences in coinfection might be due to the heterogeneity of social demography and differences in study methods and periods.

Symptom duration before admission and hospital stay were more common in *B. pertussis*–only infection than in RSV-only infection ($p < 0.05$). It indicated that patients with *B. pertussis*–associated bronchiolitis often presented a longer course, which was consistent with the clinical symptoms of *B. pertussis* infection (20) and could help distinguish *B. pertussis*–associated acute bronchiolitis from other acute bronchiolitis etiologies. The present study compared *B. pertussis*–only infection with RSV-only infection in children with bronchiolitis. Children with *B. pertussis*–only infection requiring supplement oxygen

TABLE 2 | Select characteristics of hospitalized children with *B. pertussis*-only infection compared with RSV-only, MP-only, and other pathogens infection ($n = 1,092$).

	***B. pertussis*–only infection ($n = 33$)**	**RSV-only infection ($n = 438$)**	***MP*-only infection ($n = 87$)**	**Other pathogens infection ($n = 534$)**	***p*-value**
Gender (male/female)	21/12	321/117	54/33	374/160	0.148
Median age, months	3.9 (2.5, 5.0)	2.8 (2.0, 4.9)	5.8 (3.0, 13.0)**	6.8 (3.7, 12.0)*	**<0.001**
Age group					
≤3 months	17 (51.5%)	300 (68.5%)**	30 (34.5%)	152 (28.5%)*	**<0.001**
4–6 months	10 (30.3%)	78 (17.8%)	18 (20.7%)	124 (23.2%)	0.107
7–11 months	4 (12.1%)	39 (8.9%)	12 (13.8%)	120 (22.5%)	**<0.001**
12–24 months	2 (6.1%)	21 (4.8%)	27 (31.0%)*	138 (25.8%)	**<0.001**
Duration of symptoms before admission (days)	14.0 (7.0, 15.0)	5.0 (4.0, 8.0)**	9.0 (5.0, 17.0)	10.0 (5.0, 15.0)	**0.001**
Duration of symptoms before admission group					
<7d *n* (%)	3 (9.1%)	285 (65.1%)*	30 (34.5%)*	200 (37.5%)*	**<0.001**
7–14d *n* (%)	12 (36.4%)	72 (16.4%)*	30 (34.5%)**	139 (26.0%)	**<0.001**
≥14d *n* (%)	17 (51.5%)	81 (18.5%)*	27 (31.0%)	195 (36.5%)	**<0.001**
Clinic presentation					
Cough	33 (100.0%)	430 (98.2%)	84 (96.6%)	529 (99.1%)	0.236
Dyspnea	2 (6.1%)	18 (4.1%)	0 (0.0%)**	54 (10.1%)	**<0.001**
Rhinorrhea	15 (45.5%)	195 (44.5%)	21 (24.1%)**	218 (40.8%)	**0.005**
Vomiting	12 (36.4%)	78 (17.8%)**	9 (10.3%)*	117 (21.9%)	**0.005**
Cyanosis *n* (%)	4 (12.1%)	12 (2.7%)*	0 (0.0%)*	36 (6.7%)	**<0.001**
O_2 requirement [*n* (%)]	2 (6.1%)	153 (34.9%)*	12 (13.8%)	100 (18.7%)	**<0.001**
Crackles *n* (%)	14 (42.4%)	291 (66.4%)*	54 (62.1%)	292 (54.7%)	**<0.001**
Laboratory findings					
Leukocyte count (× 109/L)	16.8 ± 6.7	9.0 ± 4.0*	9.5 ± 3.7*	11.3 ± 5.9*	**<0.001**
Leukocyte count >15 × 10^9	19 (57.6%)	33 (7.5%)*	6 (6.9%)*	106 (19.9%)*	**<0.001**
Lymphocyte count (%)	42.5 ± 28.6	60.8 ± 13.4*	48.2 ± 18.4	53.3 ± 24.4	**0.006**
Neutrophil count (%)	21.4 ± 21.7	32.9 ± 44.1	44.4 ± 18.6**	40.0 ± 21.0	**<0.001**
Hospital stay (day)	9.0 (7.0, 12.0)	8.0 (7.0, 9.3)**	8.0 (7.0, 9.0)**	8.0 (7.0, 10.0)	**0.011**

*B. pertussis–only infection: detection of B. pertussis without coinfection with any other virus or MP; RSV-only: detection of RSV without coinfection with any other virus or B. pertussis; MP-only: detection of RSV without coinfection with any other virus or B. pertussis; other pathogens: pathogens excluding B. pertussis–only, RSV-only, and MP-only infection. Data are expressed as % of positive cases, mean (quartile), unless otherwise stated. $p < 0.05$ considered statistically significant, listed in bold text, and represents p values for comparisons across all groups. Asterisks indicate statistical significance ($p < 0.05$) in bivariate comparison (B. pertussis–only vs. RSV-only, MP-only, and other pathogens infection. **$p < 0.008$, *$p < 0.05$).*

were fewer than children with RSV-only infection, indicating that the former had a milder clinical presentation compared with the latter. This study also compared *B. pertussis*–only infection with MP-only infection and infections with other pathogens in children and revealed similar severity among these pathogens. This is a novel report explaining such associations. Several other studies (9, 14, 15, 18, 20–22) assessed the influence of *B. pertussis* on acute bronchiolitis, but they could not exclude the possibility of other respiratory pathogens contributing to the illness. In the present study, the leukocyte count was higher in patients with *B. pertussis*–only bronchiolitis infection than that in patients with RSV-only infection, MP-only infection, and infections with other pathogens ($p < 0.008$ for all comparisons), which could also help distinguish *B. pertussis*–associated acute bronchiolitis from other acute bronchiolitis etiologies. One study showed that the leukocyte count $> 60 \times 10^9$/L was associated with death in children with *B. pertussis* infection (23). Another study demonstrated that the leukocyte count $> 100 \times 10^9$/L was an independent risk factor of death in children with pertussis (24). However, no patent died of *B. pertussis* infection in the present study, which might be because the vast majority of infants and young children with mild-to-moderate bronchiolitis were considered, and severe bronchiolitis in the PICU setting was ignored.

Pertussis is a vaccine-preventable respiratory disease. *B. pertussis* could affect all individuals, but the highest morbidity and mortality rates were among newborns and unvaccinated or incompletely vaccinated young infants (21, 25, 26). In the present study, the morbidity of *B. pertussis* was common (31/78, 39.7%) in infants with bronchiolitis who had been unvaccinated (infants ≤3 months). The unvaccinated infants were associated with a longer hospital stay and more likely to require supplemental oxygen. Studies suggested that early identification and treatment of *B. pertussis* could shorten the duration of paroxysmal cough (27, 28),

TABLE 3 | Clinical characteristics and results of laboratory examination among the different age groups with *B. pertussis* infection.

	≤3 months (*n* = 31)	4-11 months (*n* = 36)	≥12 months (*n* = 11)	*p*-value
Clinical characteristics				
Hospital stay (day)	12.5 ± 6.69	9.91 ± 3.41	9 ± 1.56	0.049
Requirement for supplemental oxygen *n* (%)	10 (32.3%)	2 (5.6%)	1 (9.1%)	0.011
Paroxysmal cough *n* (%)	30 (96.8%)	33 (91.7%)	9 (81.8%)	0.237
Whoops *n* (%)	3 (9.7%)	9 (25.0%)	0 (0.0%)	0.076
Post-tussive vomiting *n* (%)	13 (41.9%)	12 (33.3%)	5 (45.5%)	0.694
Cyanosis *n* (%)	8 (25.8%)	2 (5.6%)	0 (0.0%)	0.030
Low oxygen saturation *n* (%)[a]	3 (9.7%)	2 (5.6%)	1 (9.1%)	0.728
Crackles *n* (%)	18 (58.1%)	27 (75.0%)	4 (36.5%)	0.051
Laboratory results				
Leukocyte count (× 109/L)	15.83 ± 6.58	17.72 ± 8.39	14.25 ± 5.52	0.356
Lymphocyte (%)	38.57 ± 28.89	51.42 ± 26.63	35.77 ± 25.29	0.102
Neutrophil (%)	22.31 ± 22.73	20.15 ± 14.76	24.70 ± 18.31	0.723

TABLE 4 | Comparison between *B. pertussis*–only infection and coinfection.

	B. pertussis–only infection (*n* = 33)	*B. pertussis* and virus coinfection (*n* = 45)	*p*-value
Gender (male) *n* (%)	21 (63.6%)	25 (55.6%)	0.473
Age ≤3 months *n* (%)	17 (51.5%)	12 (26.7%)	0.025
Vaccination	22 (66.7%)	27 (60.0%)	0.547
Oxygen *n* (%)	2 (6.1%)	11 (24.4%)	0.031
Paroxysmal cough *n* (%)	33 (100%)	39 (86.7%)	0.036
Whoops *n* (%)	6 (18.2%)	6 (13.3%)	0.558
Post-tussive vomiting *n* (%)	12 (36.4%)	18 (40%)	0.744
Cyanosis *n* (%)	4 (12.1%)	6 (13.3%)	0.874
Low oxygen saturation *n* (%)[a]	2 (6.1%)	4 (8.9%)	0.643
Crackles *n* (%)	14 (42.4%)	35 (77.8%)	0.001

B. pertussis–only infection: detection of B. pertussis without coinfection with any other virus or MP.
[a]*Low oxygen saturation is less than 92%.*

and antibiotics against pertussis could limit the severity of disease if started in the catarrhal phase (27, 29). In addition, several systematic reviews confirmed the safety and effectiveness of maternal pertussis vaccination during pregnancy (30–32). Therefore, it is important to early recognize and initiate treatment.

This study had potential limitations. It enrolled only inpatients hospitalized with *B. pertussis* infection, but more patients with *B. pertussis* infection were treated in the outpatient department. Therefore, patients with more severe symptoms might have been overrepresented, and the prevalence of *B. pe*rtussis in children with bronchiolitis-associated hospitalization might be affected.

In summary, *B. pertussis* is one of the pathogens in children with bronchiolitis, and coinfection of *B. pertussis* with other viruses is common in bronchiolitis. *B. pertussis* should be considered when patients hospitalized with bronchiolitis present a longer course and have an elevated leukocyte count. Patients with *B. pertussis*–associated bronchiolitis present a milder clinical presentation.

DATA AVAILABILITY STATEMENT

The raw data supporting the conclusions of this article will be made available by the authors, without undue reservation.

ETHICS STATEMENT

The studies involving human participants were reviewed and approved by Ethics committees of Children's Hospital Soochow University (Approval No.: 2016026). Written informed consent to participate in this study was provided by the participants' legal guardian/next of kin.

AUTHOR CONTRIBUTIONS

WJ and SC wrote the main manuscript text. CH and YW designed the study and revised the manuscript. ZC and MW carried out the initial analyses. XS and JX performed the microbiological detection. AL and QX performed the data collection. All authors read and approved the final manuscript.

REFERENCES

1. Bordet J, Gengou O. Le microbe de la coqueluche. *Ann. I'Institut Pasteur.* (1906) 20:731–741.
2. World Health Organization. *Immunization Vaccines and Biologicals: Pertussis* 2018 (2019). Available online at: https://www.who.int/immunization/monitoring_surveillance/burden/vpd/surveillance_type/passive/pertussis/en/.
3. Yeung K, Duclos P, Nelson E, Hutubessy R, Hutubessy RCW. An update of the global burden of pertussis in children younger than 5 years: a modelling study. *Lancet Infect Dis*. (2017) 17:974–80. doi: 10.1016/S1473-3099(17)30390-0
4. Carroll KN, Gebretsadik T, Griffin MR, Wu P, Dupont WD, Mitchel EF, et al. Increasing burden and risk factors for bronchiolitis-related medical visits in infants enrolled in a state health care insurance plan. *Pediatrics.* (2008) 122:58–64. doi: 10.1542/peds.2007-2087
5. Hasegawa K, Tsugawa Y, Brown D, Mansbach JM, Camargo CA. Trends in bronchiolitis hospitalizations in the United States, 2000-2009. *Pediatrics.* (2013) 132:28–36. doi: 10.1542/peds.2012-3877
6. Robledo-Aceves M, Moreno-Peregrina M, Velarde-Rivera F, Ascencio-Esparza E, Preciado-Figueroa FM, Caniza MA, et al. Risk factors for severe bronchiolitis caused by respiratory virus infections among Mexican children in an emergency department. *Medicine.* (2018) 97:e0057. doi: 10.1097/MD.0000000000010057
7. Cui D, Feng L, Chen Y, Lai S, Zhang Z, Yu F, et al. Clinical and epidemiologic characteristics of hospitalized patients with laboratory-confirmed respiratory syncytial virus infection in eastern China between 2009 and 2013: a retrospective study. *PLoS ONE.* (2016) 11:e0165437. doi: 10.1371/journal.pone.0165437
8. Heininger U, Burckhardt MA. Bordetella pertussis and concomitant viral respiratory tract infections are rare in children with cough illness. *Pediatr Infect Dis J.* (2011) 30:640–4. doi: 10.1097/INF.0b013e3182152d28
9. Nuolivirta K, Koponen P, He Q, Halkosalo A, Korppi M, Vesikari T, et al. Bordetella pertussis infection is common in nonvaccinated infants admitted for bronchiolitis. *Pediatr Infect Dis J*. (2010) 29:1013–5. doi: 10.1097/INF.0b013e3181f537c6
10. Piedra PA, Mansbach JM, Jewell AM, Thakar SD, Camargo CA. Bordetella pertussis is an uncommon pathogen in children hospitalized with bronchiolitis during the winter season. *Pediatr Infect Dis J.* (2015) 34:566–70. doi: 10.1097/INF.0000000000000596
11. Ralston SL, Lieberthal AS, Meissner HC, Alverson BK, Baley JE, Gadomski AM, et al. Clinical practice guideline: the diagnosis, management, and prevention of bronchiolitis. *Pediatrics.* (2014) 134:e1474–502. doi: 10.1542/peds.2014-2742
12. Cherry JD, Tan T, von König Carl-Heinz W, Forsyth KD, Usa T, David G, et al. Clinical definitions of pertussis: summary of a global pertussis initiative roundtable meeting, February 2011. *Clin Infect Dis.* (2012) 54:1756–64. doi: 10.1093/cid/cis302
13. Wood N, Mcintyre P. Pertussis: review of epidemiology, diagnosis, management and prevention. *Paediatr Respir Rev.* (2008) 9:201–11; quiz 211–2. doi: 10.1016/j.prrv.2008.05.010
14. Raya BA, Bamberger E, Kassis I, Kugelman A, Srugo I, Miron, et al. Bordetella pertussis infection attenuates clinical course of acute bronchiolitis. *Pediatr Infect Dis J.* (2013) 32:619–21. doi: 10.1097/INF.0b013e3182877973
15. Gökçe S, Kurugöl Z, Söhret Aydemir S, Çiçek C, Aslan A, Koturoglu G. Bordetella pertussis infection in hospitalized infants with acute bronchiolitis. *Indian J Pediatr*. (2018) 85:189–93. doi: 10.1007/s12098-017-2480-4
16. Efendiyeva E, Kara TT, Erat T, Yahi A, Ifti E. The incidence and clinical effects of Bordetella pertussis in children hospitalized with acute bronchiolitis. *Turk J Pediatr*. (2020) 62:726–33. doi: 10.24953/turkjped.2020.05.003
17. Walsh P, Overmeyer C, Kimmel L, Feola M, Adelson ME. Prevalence of Bordetella pertussis and Bordetella parapertussis in Samples Submitted for RSV screening. *West J Emerg Med.* (2008) 9:135–40.
18. Greenberg D, Bamberger E, Ben-Shimol S, Gershtein R, Srugo, I. Pertussis is under diagnosed in infants hospitalized withlower respiratory tract infection in the pediatric intensive care unit. *Med Sci Monit.* (2007) 13:CR475–480.
19. Sun H, Ji Y, Ji W, Hao C, Yan Y, Chen Z. Impact of RSV coinfection on human bocavirus in children with acute respiratory infections. *J Trop Pediatr.* (2019) 65:342–51. doi: 10.1093/tropej/fmy057
20. Melvin JA, Scheller EV, Miller JF, Cotter PA. Bordetella pertussis pathogenesis: current and future challenges. *Nat Rev Microbiol.* (2014) 12:274–88. doi: 10.1038/nrmicro3235
21. Somerville RL, Grant CC, Grimwood K, Murdoch D, Graham D, Jackson P, et al. Infants hospitalised with pertussis: estimating the true disease burden. *J Paediatr Child Health.* (2007) 43:617–22. doi: 10.1111/j.1440-1754.2007.01154.x
22. Jiang W, Wu M, Chen S, Li A, Xu J, Wang Y, et al. Share virus coinfection is a predictor of radiologically confirmed pneumonia in children with bordetella pertussis infection. *Infect Dis Ther.* (2020) 10:335–46. doi: 10.1007/s40121-020-00376-5
23. Paddock C, Sanden G, Cherry J, Langston C, Tatti K, Wu KH, et al. Pathology and pathogenesis of fatal bordetella pertussis infection in infants. *Clin Infect Dis.* (2008) 47:328–38. doi: 10.1086/589753
24. Pierce C, Klein N, Peters M. Is leukocytosis a predictor of mortality in severe pertussis infection? *Intens Care Med.* (2014) 26:1512–4. doi: 10.1007/s001340000587
25. Tanaka M, Vitek CR, Brain Pascual F, Bisgard KM, Tate JE, Murphy TV. Trends in pertussis among infants in the United States, 1980-1999. *JAMA.* (2003) 290:2968–75. doi: 10.1001/jama.290.22.2968
26. Masseria C, Martin CK, Krishnarajah G, Becker LK, Buikema A, Tan TQ, et al. Incidence and burden of pertussis among infants less than 1 year of age. *Pediatr Infect Dis J.* (2017) 36:e54–61. doi: 10.1097/INF.0000000000001440
27. Carlsson R, Segebaden KV, Bergstrom J, Kling A, Nilsson, L. Surveillance of infant pertussis in Sweden 1998-2012: severity of disease in relation to the national vaccination programme. *Euro Surveill.* (2015) 20:21032. doi: 10.2807/1560-7917.ES2015.20.6.21032
28. Tiwari TS BA, Clark TA. First pertussis vaccine dose and prevention of infant mortality. *Pediatrics.* (2015) 135:990–9. doi: 10.1542/peds.2014-2291
29. Bergquist SO, Brenander S, Dahnsjö H, Sundelöf B. Erythromycin in the treatment of pertussis- a study of bacteriologic and clinical effects. *Pediatr Infect Dis J.* (1987) 6:458–61. doi: 10.1097/00006454-198705000-00009
30. Switzer C, D'Heilly C, Macina D. Immunological and clinical benefits of maternal immunization against pertussis: a systematic review. *Infect Dis Ther*. (2019) 8:499–541. doi: 10.1007/s40121-019-00264-7
31. Heilly CD, Switzer C, Macina D. Safety of maternal immunization against pertussis: a systematic review. *Infect Dis Ther*. (2019) 8:543–68. doi: 10.1007/s40121-019-00265-6
32. Ashish A, Sanjeev S, Kolhapure S, Kandeil W, Pai R, Singhal T. Neonatal pertussis, an under-recognized health burden and rationale for maternal immunization: a systematic review of south and South-East Asian Countries. *Infect Dis Ther.* (2019) 8:139–53. doi: 10.1007/s40121-019-0245-2

Conflict of Interest: The authors declare that the research was conducted in the absence of any commercial or financial relationships that could be construed as a potential conflict of interest.

Publisher's Note: All claims expressed in this article are solely those of the authors and do not necessarily represent those of their affiliated organizations, or those of the publisher, the editors and the reviewers. Any product that may be evaluated in this article, or claim that may be made by its manufacturer, is not guaranteed or endorsed by the publisher.

Copyright © 2021 Chen, Wang, Li, Jiang, Xu, Wu, Chen, Hao, Shao and Xu. This is an open-access article distributed under the terms of the Creative Commons Attribution License (CC BY). The use, distribution or reproduction in other forums is permitted, provided the original author(s) and the copyright owner(s) are credited and that the original publication in this journal is cited, in accordance with accepted academic practice. No use, distribution or reproduction is permitted which does not comply with these terms.

frontiers in Pediatrics

ORIGINAL RESEARCH
published: 30 August 2021
doi: 10.3389/fped.2021.689699

An Experimental Model of Bronchopulmonary Dysplasia Features Long-Term Retinal and Pulmonary Defects but Not Sustained Lung Inflammation

Lakshanie C. Wickramasinghe[1], *Peter van Wijngaarden*[2,3], *Chad Johnson*[4], *Evelyn Tsantikos*[1] *and Margaret L. Hibbs*[1]*

[1] Leukocyte Signalling Laboratory, Department of Immunology and Pathology, Central Clinical School, Monash University, Melbourne, VIC, Australia, [2] Department of Surgery - Ophthalmology, University of Melbourne, Melbourne, VIC, Australia, [3] Centre for Eye Research Australia, Royal Victorian Eye and Ear Hospital, East Melbourne, VIC, Australia, [4] Monash Micro Imaging, Alfred Research Alliance, Monash University, Melbourne, VIC, Australia

OPEN ACCESS

Edited by:
Niki Ubags,
Centre Hospitalier Universitaire Vaudois (CHUV), Switzerland

Reviewed by:
Manuel Sanchez-Solis,
University of Murcia, Spain
Dilip Shah,
Cooper University Hospital, United States
Andrew Dylag,
University of Rochester, United States

***Correspondence:**
Margaret L. Hibbs
margaret.hibbs@monash.edu

Specialty section:
This article was submitted to Pediatric Pulmonology, a section of the journal Frontiers in Pediatrics

Received: 01 April 2021
Accepted: 06 August 2021
Published: 30 August 2021

Citation:
Wickramasinghe LC, van Wijngaarden P, Johnson C, Tsantikos E and Hibbs ML (2021) An Experimental Model of Bronchopulmonary Dysplasia Features Long-Term Retinal and Pulmonary Defects but Not Sustained Lung Inflammation. Front. Pediatr. 9:689699. doi: 10.3389/fped.2021.689699

Bronchopulmonary dysplasia (BPD) is a severe lung disease that affects preterm infants receiving oxygen therapy. No standardized, clinically-relevant BPD model exists, hampering efforts to understand and treat this disease. This study aimed to evaluate and confirm a candidate model of acute and chronic BPD, based on exposure of neonatal mice to a high oxygen environment during key lung developmental stages affected in preterm infants with BPD. Neonatal C57BL/6 mouse pups were exposed to 75% oxygen from postnatal day (PN)-1 for 5, 8, or 14 days, and their lungs were examined at PN14 and PN40. While all mice showed some degree of lung damage, mice exposed to hyperoxia for 8 or 14 days exhibited the greatest septal wall thickening and airspace enlargement. Furthermore, when assessed at PN40, mice exposed for 8 or 14 days to supplemental oxygen exhibited augmented septal wall thickness and emphysema, with the severity increased with the longer exposure, which translated into a decline in respiratory function at PN80 in the 14-day model. In addition to this, mice exposed to hyperoxia for 8 days showed significant expansion of alveolar epithelial type II cells as well as the greatest fibrosis when assessed at PN40 suggesting a healing response, which was not seen in mice exposed to high oxygen for a longer period. While evidence of lung inflammation was apparent at PN14, chronic inflammation was absent from all three models. Finally, exposure to high oxygen for 14 days also induced concurrent outer retinal degeneration. This study shows that early postnatal exposure to high oxygen generates hallmark acute and chronic pathologies in mice that highlights its use as a translational model of BPD.

Keywords: bronchopulmonary dysplasia, lung development, inflammation, animal model, supplemental oxygen, chronic obstructive pulmonary disease, retinopathy of prematurity, choroidal thinning

INTRODUCTION

Bronchopulmonary dysplasia (BPD) is the most common respiratory disorder affecting premature infants provided long-term oxygen therapy and respiratory support (1). Advancements in neonatal care have improved the survival of severely premature infants born earlier in gestation; however, the incidence of BPD has remained unchanged over the last decade (2). Surfactant therapy and corticosteroid treatments, in concert with less invasive respiratory support, have helped transform the lung phenotype observed in "old BPD" from extensive parenchymal fibrosis, interstitial edema and severe inflammation to a milder lung pathology observed in infants born today (3). The lung phenotype observed in infants that come into the neonatal intensive care unit (NICU) nowadays is characterized by impaired alveolar and vascular development and mild inflammation and fibrosis. Of greatest concern, is the capacity of this disease to progress into severe lung complications by adulthood, including reduced exercise capacity (4), childhood and adolescent asthma (5), and in serious cases, the development of chronic obstructive pulmonary disease (COPD) (6, 7).

Numerous high oxygen schemes have been used to model BPD in rodents. These models have contributed to our understanding of mechanisms responsible for the development of this condition, such as the role of oxidative stress and inflammation (8), and they have replicated some of the histological aberrations that occur within the human neonatal lung following the routine use of supplemental oxygen in the clinical setting (9). However, despite these findings, no single experimental model is used consistently. Previous models have used varying concentrations and durations of oxygen exposure. In most cases, there is no rationale for why a particular model was selected over others and whether concurrent changes in other tissues occur and disease persists into adulthood. Therefore, having a standardized experimental protocol of oxygen-induced BPD would limit the variability in data output between studies and most importantly, minimize discrepancies when trialing potential therapeutic candidates (10–12).

In previous studies, supraphysiological levels of oxygen (85–100%) have been administered over a long period of time (13, 14). Such high concentrations have been shown to increase the susceptibility to respiratory infections when recovering in room air (13). In addition, some mouse strains, such as FVB/N, are more susceptible to oxygen toxicity than others and therefore, sublethal oxygen concentrations can result in exaggerated lung pathology or in severe cases, death of mice in the litter (14). Even with the use of lower oxygen concentrations (40–65%), the length of oxygen exposure can also generate varying degrees of lung damage (15, 16). For instance, the use of oxygen concentrations as low as 40% administered over 7 days in the postnatal period has been shown to trigger a reduction in the total number of alveoli and an increase in respiratory resistance (15). Similarly, an oxygen concentration of 65% delivered over 1 month has also been shown to impair alveolar structure (16). In a 2015 review, it was noted that in a 30-month period alone, there were 41 publications that used different strategies to model BPD, highlighting the need to establish a model that would provide consistency and standardization across neonatal respiratory research studies (12). More recently, a comprehensive multi-model study tested oxygen concentrations of 40, 60, and 80% over 14 days, as well as a 24 h oscillating exposure that ranged from 85 to 40% (15). This study found that the use of 85% oxygen for 7 or 14 days from birth caused the most lung damage, inducing septal wall thickness and alveolar enlargement (15), which are two key features of "new" BPD. However, lung inflammation and fibrosis were not examined in this study, with the extent of both being an important distinguishing feature between the "old" form of BPD and "new" BPD. In addition, the long-term consequence of early life oxygen-induced injury in the adult period was not investigated, which is an essential component of any BPD model to aid in the understanding of the deleterious effect of oxygen therapy on long-term sequelae in the lung. Another important consideration is the capacity of a BPD model to induce concurrent retinal damage, given that in a clinical setting, retinopathy of prematurity (ROP) frequently presents as a co-morbidity of BPD (17). Therefore, an oxygen protocol modeling BPD that could also incite the development of other neonatal diseases that affect a preterm infant could enhance the clinical relevance of the model, as well as its pre-clinical utility.

The appearance of the alveolar deformities associated with BPD is largely connected with the interruption to normal lung development (8). This is almost certainly due to the fact that the majority of premature babies are born during the final two stages of lung organogenesis—the saccular and alveolar stages—the time at which they receive oxygen therapy. The saccular stage prepares the lung for life outside of the womb, with the formation of primitive alveoli called saccules and production of surfactants in cuboidal alveolar cells (18–20). Simultaneously, microvascular maturation in the parenchyma leads to the thinning of the double capillary layer into a single layer, necessary to meet the respiratory requirements of the growing fetus (18, 21, 22). In the final alveolar stage of organogenesis, the saccules undergo rapid subdivision (secondary septation) into smaller gas-exchange units called alveoli, expanding the gas-exchange surface area (23, 24). In mice, the saccular stage of lung development occurs in the first 5 days after birth, which is ordinarily complete in full-term infants (25). Thus, the fact that the last two lung developmental stages occur post-birth in mice renders mice an excellent experimental tool for BPD studies.

The purpose of this study was to validate whether acute high oxygen exposure received during key periods of lung development would lead to long-term pulmonary changes. Given that the aforementioned multi-model study only assessed lung damage at day 14, in this study, we have focused on evaluating different parameters of lung pathology that may arise in adulthood, and unlike other multi-model studies, the assessment of outer retinal changes as a common co-morbidity of BPD were also prioritized in this study. Herein, we demonstrate that prolonged oxygen exposure in early neonatal life leads to sustained alveolar deterioration in adulthood, as well as defects in retinal tissue, and therefore is a suitable model for early and later life studies of BPD and research into the long-term impact of oxygen toxicity to the eye.

MATERIALS AND METHODS

Experimental Models

C57BL/6 mice were used for this study and were purchased from Alfred Animal Services at the Alfred Research Alliance. Neonatal mice together with their dam, in litter sizes of 6–7 pups (to control for maternal nutrition), were exposed to 75% oxygen within 12 h of birth (defined as PN1) up to PN5, PN8, or PN14, and were cycled with 21% oxygen (room air) for 3 h per day to prevent oxygen toxicity to the dam (17). Following exposure, the mice were returned to room air and lungs were analyzed on PN14, PN40, and PN80. Neonatal pups and dams housed under room air conditions in the same experimental room, served as age-matched controls. All experiments were performed in accordance with National Health and Medical Research Council of Australia (NH&MRC) guidelines for animal experimentation, with ethics approval granted from the Alfred Research Alliance Animal Ethics Committee (experimental approval number: E/1746/2017/M).

Lung Histology and Immunohistochemistry

On PN14, PN40, and PN80, postmortem lungs were inflation-fixed with 10% neutral buffered formalin at 25 cm water pressure, embedded in paraffin and sectioned by microtome at 5 μm thickness prior to staining. Lung sections were stained with Hematoxylin and Eosin (H&E) or Picrosirius Red (PR). H&E stained sections were imaged using an Olympus BX-51 bright field microscope equipped with a DP-70 color camera and 10x and 40x objectives (Olympus Corporation, Tokyo, Japan). Quantitation of alveolar airspace diameter and septal wall thickness was determined using the mean linear intercept method and alveolar septal wall thickness technique, as previously described (17). Investigators were blinded to experimental groups. PR-stained sections were scanned using the Aperio ScanScope CS (Leica Biosystems, Wetzlar, Germany) whole slide scanner at 8x and 4x magnification. Images were uploaded into ImageJ Analysis software (1.37 (NIH, Bethesda, MD; http://imagej.nih.gov/ij) and analyzed using a published script (17) with minor modifications as follows. The script used a pre-defined color threshold (set by eye) to isolate the PR signal and created a binarized image, which was measured for area. A similar method was then used to threshold the background of the tissue, in order for the total tissue area within the image to be calculated. These results were used to calculate the % PR-stained area within the tissue.

For immunohistochemistry, deparaffinized sections underwent antigen-retrieval with DAKO Target Retrieval Solution (DAKO Corp, CA, USA). Sections were blocked for 30 min with 5% BSA and incubated for 3 h at room temperature with 1:500 dilution of anti-mouse CD45 (rabbit IgG, catalog; ab10558, Abcam, Cam, UK) to stain all immune cells. Control sections had primary antibody substituted with PBS. Staining was revealed by incubation with 1:500 HRP-conjugated secondary antibody (goat anti-rabbit IgG H+L, catalog; ab205718, Abcam, Cam, UK) for 1 h and color development with diaminobenzidine chromogen solution (Agilent, CA, USA). Slides were counterstained with hematoxylin. Cells expressing CD45 were labeled brown, while negative cells were stained blue. Four randomly selected microscopic fields (40x) of lung tissue per mouse were used to calculate the percentage of CD45 positive cells/total cells as described (17). On separate lung sections, type II alveolar epithelial cells (AEC-II) were detected by staining for Pro-SPC using a previously described method (26). AEC-II's were labeled with anti-mouse Pro-SPC (rabbit IgG, 1:500, catalog ab90716: Abcam, Cam, UK), followed by red fluorescent secondary antibody (AF568 donkey anti-rabbit IgG (H+L), 1:1,000, catalog ab175693; Abcam, Cam, UK). Control sections had secondary antibody only incubated to test for non-specific binding. Stained cells were imaged using a Nikon A1r inverted confocal microscope (Nikon Corporation, Tokyo, Japan). Two large scanned images at 20x magnification were taken at two randomly selected lung sites and analyzed using a bespoke ImageJ script (**Supplementary Table 1**). Briefly, quantitation of AEC-II numbers was conducted with the aid of a DAPI nuclear stain as well as the overall background fluorescence to segment a field of individual cells and create regions of interest (ROIs) for each fluorescent marker. These ROIs were then used to determine if each cell was positive for a specific color based on a user defined pixel intensity threshold for each channel set up at the start of the script.

Lung Function Assessment

At PN80, mice were anesthetized by intraperitoneal injection of 125 mg/kg of Ketamine and 10 mg/kg Xylazine (Centravet, FR). Following confirmation of deep anesthesia, mice underwent tracheostomy and a 19G cannula was inserted before being connected to an animal ventilator (Flexivent, SCIREQ, CA). Mice were mechanically ventilated (150 breaths/min, tidal volume 10 ml/kg) and a positive end-expiratory pressure (PEEP) was set at 3 cm H_2O. The flexiware software (v8.0.4) was used to perform respiratory system mechanics, as previously detailed (27). A negative pressure-driven forced expiratory (NPFE) maneuver was performed to generate the flow-volume loop used to calculate the forced expired volume over 0.1 s (FEV0.1) and forced vital capacity (FVC), which were used to determine the ratio between FEV0.1/FVC as a clinical measure of lung performance. Three independent measurements were taken for all perturbations for each mouse and the average was calculated.

Eye Histology

Paraffin-embedded eyes were sectioned at 3 μm thickness and every 20th section was stained with H&E. Four photomicrographs (x10) of each cross-section were captured across the full circumference of the eye and the average diameter (in μm) per section for each eye was determined to obtain choroidal thickness as previously described (17). Investigators were masked to the experimental groups.

Statistical Analysis

Values are presented as median ± IQR. Results from individual models were compared to the room air controls using the non-parametric unpaired *T*-test (Mann-Whitney) in GraphPad Prism software (version 4.03, SD, USA); $P < 0.05$ was considered

statistically significant. Unmarked bars on figures indicate that no significance was achieved.

RESULTS

Body Weight Gain Is Affected in Mice Exposed to High Oxygen for Longer Periods

To define the best experimental model that most closely recapitulates BPD, we trialed three oxygen exposure protocols (**Supplementary Figures 1A–C**). For each of these, we used a moderate oxygen concentration of 75%, as we have previously reported that this concentration is sufficient to elicit both early and long-term damage in the neonatal lung and eye (17). Oxygen exposure in neonatal pups for 5 days had no effect on body weight gain at PN14 or PN40 as their weight was comparable to that of age-matched room air control mice (**Supplementary Figures 1D,E**). Conversely, neonatal mouse pups exposed to oxygen for 8 days had reduced body weight gain at PN14, which had normalized by PN40 (**Supplementary Figures 1D,E**). However, mice exposed to high oxygen for 14 days had reduced body weight gain at both PN14 and PN40 compared to mice exposed to high oxygen for shorter periods and age-matched room air controls, suggesting a more profound impact (**Supplementary Figures 1D,E**).

Prolonged Oxygen Exposure Leads to BPD-Like Damage in Neonatal Mice

In mice, the bulk of alveolarization in the lung is complete by PN14 (28), forming a suitable time-point for assessment of the major structural changes to the alveoli. We used two primary measurements, alveolar septal wall thickness and airspace size, to evaluate the structural damage induced in oxygen-exposed mouse lungs. Mice reared in room air from the day of birth, up to and including PN14, had normal alveolar structure, as shown by typical alveolar septal wall thickness and airspace diameter (**Figures 1A–C**). Exposure to 75% oxygen for the first 5 days of life (PN1-5) had minimal effect on the visual appearance of the lung. Morphometric measurement revealed a possible thickening of the septal wall compared to room air controls; however, this was not significant and there was no difference in airspace size between the oxygen-exposed and room air groups (**Figures 1A–C**). Extending the duration of oxygen exposure to 8 days (PN1-8) induced a change in parenchymal architecture, demonstrated by an increase in alveolar septal wall thickening and alveolar diameter (**Figures 1A–C**). Lengthening the oxygen exposure further to 14 days (PN1-14) gave rise to lungs with severe alveolar deformities, showing a marked increase in septal wall thickening and exaggerated alveolar size compared to room air controls. The airspace diameter in this group showed even greater enlargement compared to mice exposed to oxygen for 8 days (**Figures 1A–C**).

Prolonged Neonatal Oxygen Exposure Leads to the Development of Emphysema in Young Adult Mice

It is now well-appreciated that preterm infants diagnosed with BPD have an increased susceptibility to other lung diseases in later life, including COPD (6, 7). To examine the longer-term impact of neonatal oxygen exposure, the lungs of mice administered 75% oxygen for the first 5, 8, or 14 days of life, were examined at PN40. Mice that had been exposed from birth to 75% oxygen for 8 days (PN1-8), but not 5 days (PN1-5), showed modest yet significant increases in septal wall thickness and airspace size compared to age-matched room air controls at PN40 (**Figures 1D–F**). Interestingly, in the PN1-8 model, both the septal wall thickness and airspace size at PN40 were somewhat reduced compared to measurements at PN14, suggesting possible healing (**Figures 1C–F**). However, mice that had been exposed for their first 14 days of life to 75% oxygen demonstrated pronounced structural alternations in lung parenchyma, including a variable but highly significant increase in septal wall thickness and airspace diameter compared to mice exposed to oxygen for 8 days (**Figures 1D–F**). This finding demonstrates the capacity of the PN1-14 oxygen model to generate structural changes consistent with emphysema in adulthood (29).

Oxygen Exposure Did Not Induce Severe Parenchymal Fibrosis in Neonatal and Adult Lung

A phenotype of "old" BPD is the presence of extensive parenchymal fibrosis, however this trait is significantly milder in the lungs of infants with newly diagnosed BPD due to the changes in respiratory care implemented in the NICU over the last few decades (3, 30). Thus, contemporary experimental models should not feature severe parenchymal fibrosis. To determine the prevalence of fibrosis, the lungs of mice at PN14 were stained with Picrosirius Red (PR), a histological stain that renders collagen fibers red. Minimal collagen staining was observed in the extracellular matrix of the lungs of all mice at PN14, except mice exposed to 75% oxygen for 14 days (**Figures 2A,B**). While there was a significant increase in parenchymal fibrosis in mice exposed to high oxygen for 14 days, on average, only 1.94% of the lung tissue in this model was positive for PR (**Figures 2A,B**). When fibrosis was assessed at day 40, only mice exposed to 8 days of high oxygen demonstrated a significant increase in the proportion of lung tissue positive for PR compared to room air control mice, although changes were mild (**Figures 2C,D**). Thus, the concentration and window of oxygen exposure did not lead to the development of extensive fibrosis resembling old BPD in any of the three models tested in neonatal and adult life.

Eight Days of Oxygen Exposure in Neonatal Mice Stimulates Mild Expansion of Type II Alveolar Epithelial Cells in Adulthood

Hyperoxia has been associated with impaired AEC development, promoting an enlarged and simplified lung structure that is commonly observed in BPD (26, 31). To determine if the high

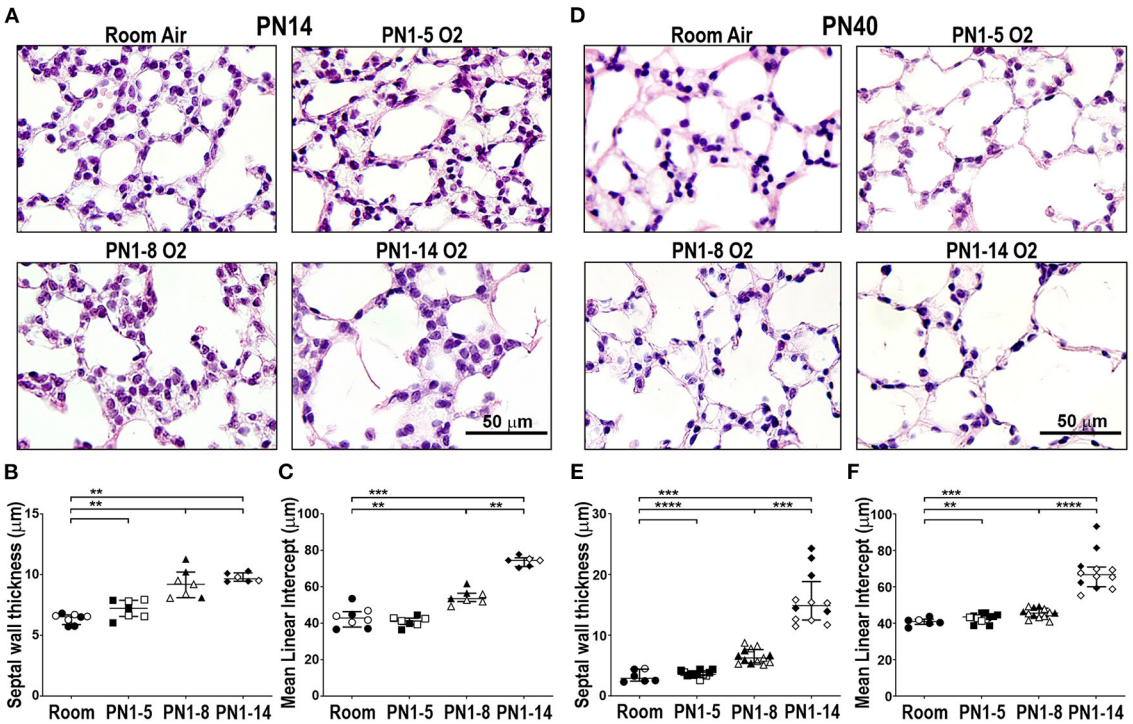

FIGURE 1 | Prolonged supplemental oxygen induces severe lung damage in neonatal mice that persists into young adulthood. C57BL/6 mice were housed in room air or treated from the day of birth with 75% O_2 for 5, 8, or 14 days, then analyzed at PN14 **(A–C)** or PN40 **(D–F)**. **(A)** Representative photomicrographs of H&E-stained lung cross-sections at PN14. **(B)** Median alveolar septal wall thickness of mice in **(A)**. **(C)** Alveolar airspace size by mean linear intercept length (μm) of mice in **(A)**. **(D)** Representative photomicrographs of H&E-stained lung cross-sections at PN40. **(E)** Median alveolar septal wall thickness of mice in **(D)**. **(F)** Alveolar airspace size by mean linear intercept length (μm) of mice in **(D)**. Images in **(A)** and **(D)** were taken using a 40x objective using an Olympus BX-51 bright field microscope. Scale bar = 50 μm. For **(B,C,E,F)**, data is median (μm) ± IQR. $^{**}P < 0.01$, $^{***}P < 0.001$, $^{****}P < 0.0001$ by Mann-Whitney *U*-test (2-tailed). n ≥ 6 mice per group, with 1–2 L used to analyze each oxygen group in **(A–C)**, and 2–3 L used to analyze each oxygen group in **(D–F)**. Gender is represented by closed (male) and open symbols (female). PN, postnatal.

oxygen insult utilized in the three different models induced changes in the proportions of type II AECs in the lung parenchyma of adult mice, immunostaining of Pro-SPC was performed. At PN40, proportions of AEC-II in the lungs of mice exposed to high oxygen for 5 or 14 days were comparable with those in room air control mice, however surprisingly, there was a mild expansion of AEC-II in the lungs of mice exposed to 75% oxygen for 8 days (**Figures 3A,B**).

Neonatal Oxygen Exposure Induces Alveolar Inflammation in Early BPD

In order to investigate the effect of high oxygen exposure on lung inflammation in the neonate, immunohistochemical staining for CD45-expressing leukocytes was performed. In the normal developing lung at PN14, ∼20% of the cells present were CD45+ leukocytes, which were mostly found within the alveolar walls, around small vessels and occasionally also in the airspaces (**Figures 4A,B**). In all high oxygen-exposed models there was a variable increase in leukocytes in the lung, ∼10–15% more than in the room air control mice, which was significant in the PN1-5 and PN1-14 models (**Figures 4A,B**). Thus, an increase in lung inflammation is a feature of high oxygen exposure of neonatal mice.

Alveolar Inflammation Is Not a Feature of Adult Mice Exposed to an Oxygen Insult in Infancy

To determine if the high oxygen insult utilized in the three different models led to sustained inflammation in the lung parenchyma, immunostaining was performed on lung sections from 40-day-old mice. At PN40, proportions of CD45+ leukocytes in all high oxygen exposure models were comparable with the room air control mice (**Figures 4C,D**) indicating that lung inflammation observed at the early time period had resolved by adulthood.

Prolonged Oxygen Exposure Leads to Choroidal Thinning in Adulthood

The neonatal retina is highly susceptible to changes in oxygen tensions and it is a prominent co-morbidity of BPD. Survivors of this eye condition exhibit thinning of the outer retina (choroid). To evaluate the impact of neonatal high oxygen exposure on the thickness of the outer retina, H&E-stained eye sections from

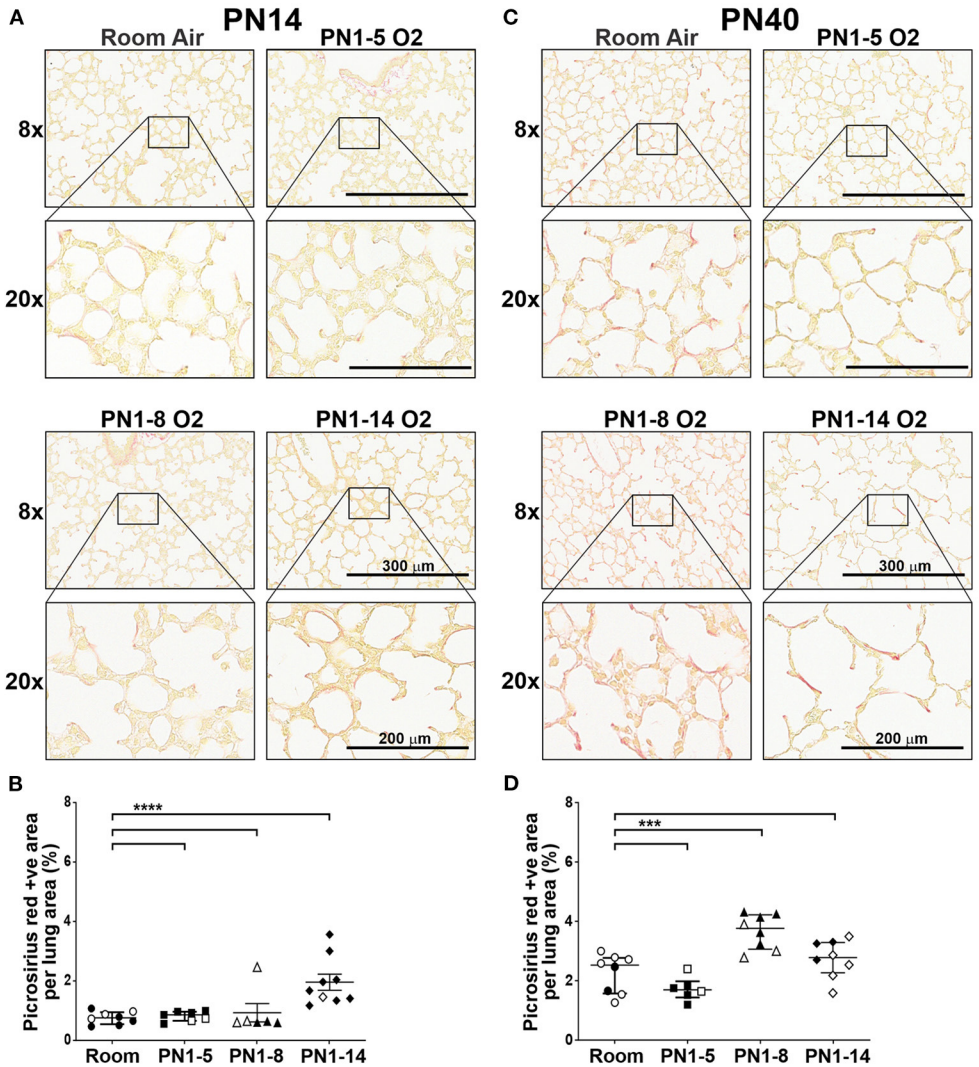

FIGURE 2 | Extensive fibrosis is not a feature of the lungs of neonatal or young adult mice exposed to prolonged supplemental oxygen in early life. C57BL/6 mice were housed in room air or treated from the day of birth with 75% O_2 for 5, 8, or 14 days, then analyzed at PN14 **(A,B)** or PN40 **(C,D)**. **(A)** Representative images of PR-stained cross-sections of lungs at PN14. **(B)** Proportion of lung tissue of the mice in **(A)** stained with PR. **(C)** Representative images of PR-stained cross-sections of lungs at PN40. **(D)** Proportion of lung tissue of the mice in **(C)** stained with PR. For **(A,C)**, images were taken with 8x and 20x objectives using Aperio ScanScope CS; scale bar = 300 and 200 μm, respectively. For **(B,D)**, data is presented as median (μm) ± IQR. $^{***}P < 0.001$, $^{****}P < 0.0001$ by Mann-Whitney *U*-test (2-tailed). $n \geq 6$ mice per group, with 2–3 L used to analyze each oxygen group in **(A,B)**, and 1–3 L used to analyze each oxygen group in **(C,D)**. Gender is represented by closed (male) and open symbols (female). PN, postnatal.

40-day-old mice were examined. At PN40, there was a trending decrease in choroidal thickness in mice exposed to high oxygen for 5 ($p = 0.0513$) and 8 days ($p = 0.0728$) but it was significantly decreased in mice exposed to high oxygen for 14 days compared to room air control mice (**Figures 5A,B**). These results indicate that extended oxygen exposure in early infancy was sufficient to induce concurrent outer retinal changes in adulthood.

Lung Function Is Impaired in Mature Adult Mice Exposed to Hyperoxia in Infancy

A vital question arising from the above data is whether the structural deterioration observed in mice exposed to prolonged hyperoxia worsens structurally and functionally with age. At PN80, mature adult C57BL/6 mice that had been exposed from day of birth to 14 days of hyperoxia showed progressive alveolar hypoplasia, with larger and simplified alveoli, as indicated by increase in alveolar diameter, compared to those reared solely in room air conditions (**Figures 6A,B**). In patients with COPD, persistent airflow limitation is a clinical indicator of disease progression (32, 33). A significant increase in FEV0.1 and FVC was observed at PN80 in C57BL/6 mice that had received an oxygen insult during the first 14 days of neonatal development compared to room air control counterparts (**Figures 6C,D**). The ratio between FEV0.1/FVC, which is a clinical measure of COPD

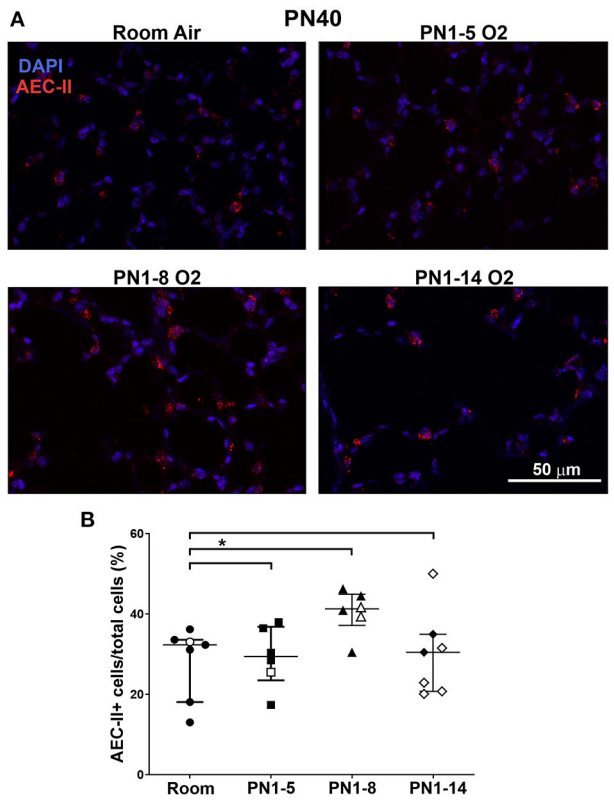

FIGURE 3 | Neonatal oxygen promotes mild AEC-II expansion in adulthood. **(A)** Representative immunofluorescent images of lungs from room air control mice or mice exposed to 75% oxygen for the indicated times. Staining was undertaken at PN40 with anti-Pro-SPC (red) to depict AEC-II. DAPI-stained nuclei appear blue. Scale bar = 50 μm. Images were taken with 20x glycerol objective using a Nikon A1r inverted confocal microscope, zoom setting 2. **(B)** Quantitation of proportions of AEC-II+ cells indicated as AEC-II+/total lung cells. Data is presented as median ± IQR. *$P < 0.05$ by Mann-Whitney *U*-test (2-tailed). $n \geq 6$ mice per group, with 2–4 L used in the analysis of each oxygen group. Gender is represented by closed (male) and open symbols (female). PN, postnatal.

in humans at FEV at 1 s, was significantly decreased (< 0.9) in oxygen exposed mice at PN80 (**Figure 6E**). These findings indicate that prolonged oxygen exposure in early infancy that induces BPD can progress into pulmonary function decline resembling COPD in adulthood.

DISCUSSION

There is an unresolved need for effective preventative and reparative treatments that can overcome the long-term respiratory burden faced by preterm infants that develop BPD. Over many years, the use of animal models has proven to be valuable for uncovering new disease mechanisms and new targets for therapy in a variety of human diseases. In BPD, a standardized experimental model is not used routinely and instead, many studies have used varying concentrations of oxygen, different lengths of oxygen exposures, contrasting initiation times, and additionally, insults to the mouse dam to promote an inflammatory environment, which only occurs in a small proportion of very low birth weight infants. Here, we investigated the long-term effect of 75% oxygen delivered at various developmental windows of lung organogenesis in the neonate, to best replicate the timing of injury in premature infants at risk of developing BPD and to assess the long-term repercussions of this early-life oxygen exposure on the lung but also to ocular structures such as the choroid. Importantly, all three models evaluated were initiated within 12 h of birth of the mouse.

Our findings show that two of the three models tested induced damage to the alveolar compartment in neonatal and adult mice, increasing in severity as the window of oxygen exposure lengthened. While both the PN1-8 and PN1-14 models yielded lung disease characteristics common to infants affected by BPD, the PN1-14 model yielded more exaggerated lung disease traits, particularly alveolar airspace enlargement at PN14 and PN40. At PN80, the PN1-14 model led to worsened emphysema, which was associated with a decline in respiratory mechanics, an important characteristic that is often overlooked. Therefore, our research supports that the delivery of 75% oxygen to mouse pups for 14 days is the optimal model for standardized use in BPD research, to investigate the early and long-term effects of neonatal hyperoxia.

In other hyperoxia models, prolonged exposure to high oxygen (85–100%) for 14 days or longer has been reported to result in the development of extensive fibrosis in the lung parenchyma (21, 34–36). This feature was prevalent in the early form of human BPD, that was encountered in the past (21). However, since the introduction of surfactant therapy, antenatal corticosteroids and advanced neonatal oxygen management, the BPD phenotype observed today no longer features severe pulmonary fibrosis (37). Thus, to accurately model contemporary BPD, it is important to understand whether mice delivered a high oxygen insult develop excessive parenchymal fibrosis, which is a feature that is not regularly considered in other studies. Despite a slight but significant increase in PR staining in the lung of mice exposed to high oxygen for 14 days, none of the models exhibited marked fibrosis in the extracellular matrix of the alveoli at the 14-day assessment timepoint. Interestingly, all mice showed mild increases in fibrosis between day 14 and 40, which likely reflects developmental remodeling of the extracellular matrix during lung alveolarization. However, mice that had been exposed to high oxygen for the first 8 days of life exhibited a significant increase in lung fibrosis at day 40 compared to room air controls that was not seen in the other models. While the reason for this is unknown, it is interesting that these mice were also the only group to show a significant increase in AEC-II numbers at day 40. This collectively implies a healing response, which is also suggested by a reduction in the thickness of septal walls and airspace size at PN40 compared to that seen at PN14. These features were not seen in mice given a prolonged oxygen insult, which may suggest that their lungs have become too damaged. Thus, we confirm that it is suitable to use a high

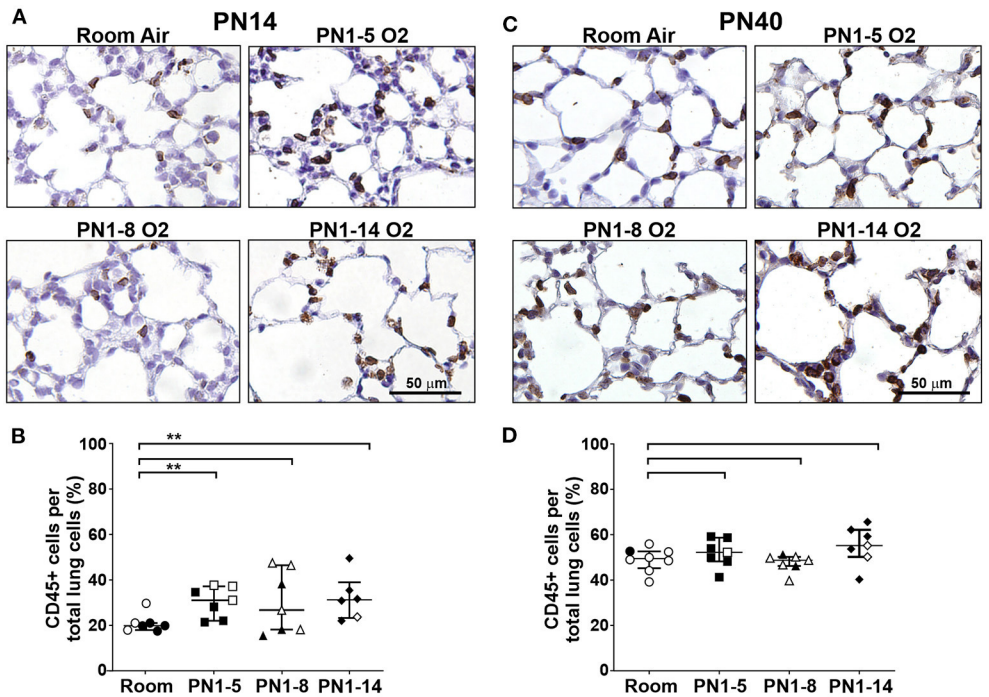

FIGURE 4 | Inflammation is present in the lungs of neonatal mice exposed at birth to supplemental oxygen but is moderated in young adult mice. C57BL/6 mice were housed in room air or treated from the day of birth with 75% O_2 for 5, 8, or 14 days, then their lungs were analyzed at PN14 **(A,B)** or PN40 **(C,D)** by staining with the pan-leukocyte cell surface marker CD45. **(A)** Representative images of lung paraffin sections stained at PN14, and **(B)** quantitation of the proportion of CD45+ immune cells per total alveolar cells. **(C)** Representative images of lung paraffin sections stained at PN40, and **(D)** quantitation of the proportion of CD45+ immune cells per total alveolar cells. In **(A,C)**, sections were counter-stained with hematoxylin and CD45+ cells are indicated by brown staining; scale bar = 50 μm. Note that lungs were not perfused or flushed prior to fixation and extraction. Images were taken with 40x objective using an Olympus BX-51 bright field microscope. Data in **(B,D)** is presented as median ± IQR. $^{**}P < 0.01$ by Mann-Whitney *U*-test (2-tailed). $n \geq 6$ mice per group, with 1–2 L used for analysis of each oxygen group in **(A,B)**, and 2–3 L used for analysis of each oxygen group in **(C,D)**. Gender is represented by closed (male) and open symbols (female). PN, postnatal.

oxygen concentration of 75% for up to 14 days in C57BL/6 mice to emulate the form of BPD that prevails in the neonatal clinic today.

Targeting oxygen exposure within the critical window of lung development in experimental models is an important consideration to maintain clinical relevance to human BPD. Importantly, the saccular and alveolar stages of lung development appear to be most impacted during oxygen administration in preterm infants in NICUs (38). The mouse represents an excellent system to model BPD, as the saccular stage of lung development, which is generally complete in full-term infants, occurs predominantly in the first 5 days of postnatal life of the mouse. In the first model tested, oxygen exposure was limited to this important developmental stage. This scheme did not induce major structural changes in the neonatal or adult lung, despite a hint of septal wall thickening at day 14. Previous studies have reported that this short window of exposure during the saccular stage of lung development was sufficient to elicit severe alveolar damage in 8–9-week-old adult mice (13, 39). This difference likely relates to the lower concentration of oxygen used in our model but may also be due to the housing environment or the assessment timepoint, since we examined mice at 40 days of age (13, 39). Thus, it is possible that lung defects may manifest later on if the damage progresses at a slower rate. In a study exposing neonatal pups to 40, 60, and 100% oxygen from PN1-4, only 100% oxygen led to lung dysmorphogenesis in C57BL/6 mice; however, outbred CD1 mice exhibited lung development changes in response to 60% oxygen as well (40), indicating that genetic background contributes to the response of the lungs to an oxygen insult. In the second model we tested, mice were exposed to high oxygen for 8 days, which encompasses the saccular stage and the start of the alveolar phase of lung development. Interestingly, this slightly longer insult led to the development of enlarged and simplified airspaces at both assessment timepoints, albeit lung damage at PN40 was moderate. There was also an expansion of AEC-II cells observed in the lungs of this model at PN40, which was not apparent in the PN1-5 and PN1-14 protocols at this timepoint. This was an unexpected finding as fewer AEC-II cells have previously been observed in adult mice recovering from neonatal oxygen exposure (41). However, in that study, newborn mice were exposed to 100% oxygen, which is a severe oxygen insult compared to the 75% oxygen concentration used in this study and one that is unlikely to be utilized in the NICU. Nevertheless, oxygen concentration and timing could influence the degree of activation/inhibition of different cell populations in the lung (41).

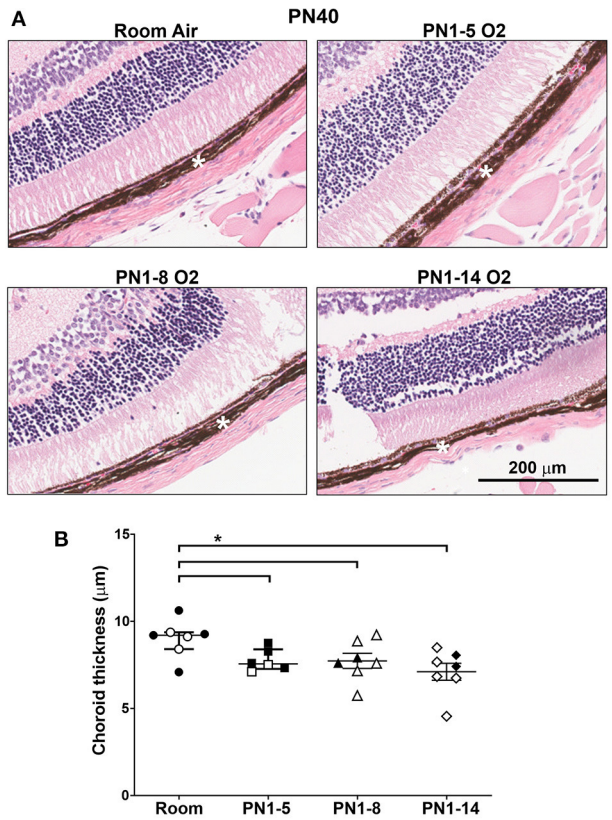

FIGURE 5 | Choroidal thinning in young adult mice exposed to prolonged oxygen in infancy. **(A)** Representative H&E photomicrographs of sections depicting choroid (white asterisk) at PN40 comparing C57BL/6 room air control mice and the indicated oxygen-exposed mice. Images were taken with 10x objective using Aperio ScanScope CS. Scale bar = 200 μm. **(B)** Quantitation of choroidal thickness (asterisk) of eye sections shown in **(A)**. All data are presented as median ± IQR and assessed using Mann-Whitney *U*-test (2-tailed); $^*P < 0.05$. $n \geq 6$ mice per group, with 2 L used in the analysis of each oxygen group. Gender is represented by closed (male) and open symbols (female). PN, postnatal. The retinas were obtained from the same mice used to assess lung pathology in other figures. Outliers were removed using a ROUTS outlier test.

As expected, 14 days of high oxygen exposure generated the greatest degree of alveolar dysmorphogenesis in the neonatal lung, which manifested as severe pulmonary emphysema in the young and mature adult. The impact of this structural deterioration on lung mechanics was evident by the impaired respiratory function in mature adults exposed to this oxygen scheme. Taken together, these findings indicate that prolonged high oxygen exposure during the two final lung developmental stages in mice promotes lung injury that approximates that seen in preterm infants with BPD, and may even capture those infants that go onto to develop COPD in later life. This model will therefore also be useful to unravel mechanisms that underpin chronic lung conditions that have origins in early life. The ability of the 14-day exposure regime to generate long-term lung damage and functional decline within a relatively short time frame compared to current models in use (42, 43), also provides a unique advantage when trialing potential therapeutic interventions for BPD. For example, the efficacy of a select intervention to ameliorate or attenuate long-term damage can be determined in mice within 40 days of birth, making testing of therapeutics easily achievable. Another important consideration is the emerging influence of the lung and gut microbiome on the development of BPD. Given that selective pressures such as moisture, pH and nutrition can shape the local microbial niche (44), mice housed in different animal facilities are subsequently exposed to diverse environmental conditions. Therefore, these factors may also influence the severity of lung pathology generated in oxygen-exposed mice and could also account for the discrepancies observed between different research groups using the same oxygen models.

Inflammation is also recognized to contribute to the deterioration of the alveolar structure in the neonatal lung following a high oxygen insult (45). Airway sections obtained from preterm infants with BPD often show elevated levels of pro-inflammatory chemokines and cytokines, and can occur early in neonatal life before the presentation of clinical symptoms (46, 47). However, infants with BPD have demonstrated increased susceptibility to COPD, respiratory viral infections and asthma in later life compared to their non-BPD counterparts, which may involve the dysregulation of immune pathways in the lung during neonatal hyperoxia exposure (13). In a previous study, exposure to hyperoxia during the first 12 days of neonatal life led to persistent inflammation in the lungs of adult mice, implicating chronic inflammation in the lung of BPD survivors (48). To determine whether oxygen exposure at varying developmental windows would influence the immune profile in the adult lung, immunohistochemical staining for CD45+ leukocytes was conducted on lung tissue. All mice showed an increase in leukocytes in lung between day 14 and 40, which likely reflects the maturation of the immune system, which undergoes rapid development during the early postnatal period; however, alveolar inflammation at day 40 was not a feature of any of the three high oxygen regimes trialed in this study. This suggests that the structural changes apparent in adulthood are most likely the consequences of oxygen exposure during critical lung stages in infancy (49). Concurrently, there may also be changes occurring in other tissue components external to inflammation, such as modifications to extracellular matrix proteins (50).

A common clinical co-morbidity of infants diagnosed with BPD is ROP (51). The retinal vasculature is sensitive to the changes in oxygen tension and extreme hyperoxia/hypoxia can hinder the normal growth of the blood vessels in the retina which can lead to poor vision in later life (52). Adult survivors of ROP have been reported to exhibit late-onset vitreoretinal complications (53) and retinal detachment (54). In addition, a thinner choroid has been associated with reduced vision in individuals with a history of ROP, and has been speculated to be primary to the long-term changes in the inner retinal layers (55). Therefore, the degree of choroidal thinning was assessed across all three oxygen models and presents a unique aspect of this study. While only the 14-day exposure model showed a significant reduction in choroidal thickness, the other

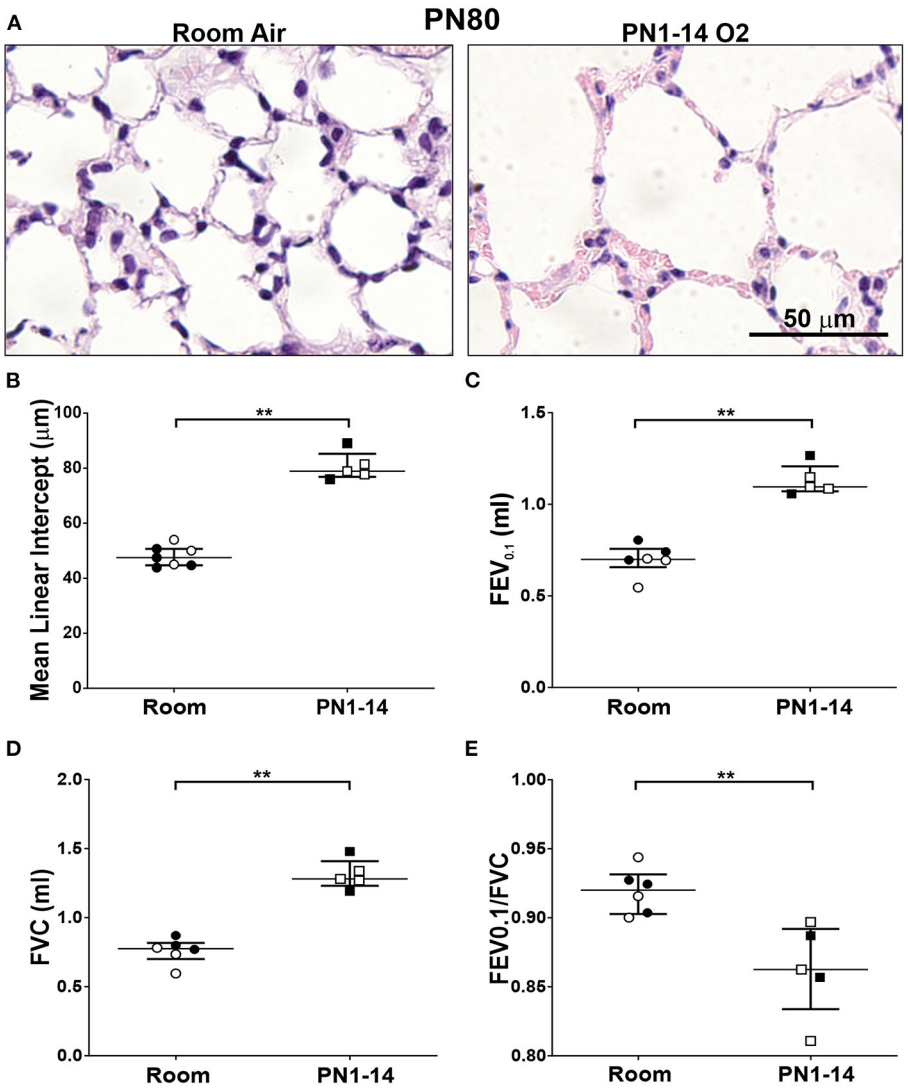

FIGURE 6 | Decline in lung function in mature adult mice exposed to prolonged supplemental oxygen in infancy. **(A)** Representative photomicrographs of H&E-stained lung cross-sections at PN80 comparing C57BL/6 room air control mice and PN1-14 oxygen-exposed mice. Images were taken with a 40x objective using an Olympus BX-51 bright field microscope. Scale bar = 50 μm. **(B)** Quantitation of airspace diameter (MLI) of lung sections shown in **(A)**. Assessment of **(C)** FEV0.1, **(D)** FVC, and **(E)** FEV0.1/FVC ratio by negative pressure-driven forced expiration using the Flexivent. All data are presented as median ± IQR and assessed using Mann-Whitney *U*-test (2-tailed); $^{**}P < 0.01$. $n = 5$–6 mice per group from 1 litter. Gender is represented by closed (male) and open symbols (female). PN, postnatal.

two models displayed trending degrees of vascular thinning. This demonstrates that an extended period of high oxygen exposure in neonatal life can also provoke long-term damage in organs outside of the lung and evaluation of other tissues implicated in BPD could enhance the clinical relevance and translatability of this model. However, the timing of the oxygen exposure soon after birth in the 14-day model employed in this study is considerably different to that used in the established model of ROP, known as the oxygen-induced retinopathy model. Due to differences in retinal development between mouse and man, high oxygen exposure in the oxygen-induced retinopathy model commences on postnatal day seven to mimic the vascular developmental stage in preterm infants (56). Therefore, the specific molecular changes underlying the vascular damage in the retina may be grossly different between the two oxygen schemes and should be considered closely before use in ocular research.

In the absence of a cure for BPD, there is a need to identify the mechanisms underlying this debilitating condition. Accordingly, the development of a benchmark model of BPD will allow for greater comparison of results amongst research groups and advances in the understanding of the disease. The current study describes a model of oxygen-induced BPD, comprised of a 14-day exposure to 75% oxygen, initiated within 12 h of birth, which was associated with features of contemporary BPD in neonatal mice. Moreover, the model was associated with the impaired development of alveoli in adult mice that resembled COPD encountered by adult survivors of BPD alongside outer retinal decay, which is a distinguishing feature of this model.

These findings provide a distinct advantage, suggesting that this model could be a key translational tool for the trialing of new treatments which may advance therapeutic strategies to improve the care and long-term outcome for vulnerable premature infants. We advocate that the standardized PN1-14 model described herein may facilitate studies into the early life impact of high oxygen-exposure but also expedite investigations into the lifelong effect of oxygen insults received during the neonatal period.

DATA AVAILABILITY STATEMENT

The raw data supporting the conclusions of this article will be made available by the authors, without undue reservation.

ETHICS STATEMENT

The animal study was reviewed and approved by Alfred Research Alliance Animal Ethics Committee (experimental approval number: E/1746/2017/M).

AUTHOR CONTRIBUTIONS

MH and LW conceived the study, designed research, and analyzed data. LW performed experiments. PW supplied an integral piece of equipment, provided critical intellectual content, and important manuscript revisions. CJ contributed a new analytic tool. ET provided valuable insight and made important intellectual contributions. LW and MH wrote the paper. All authors provided editorial comments and gave final approval for publication.

FUNDING

LW was supported by a scholarship from the Australia Government administered by Monash University, and the research work was supported by a NH&MRC project grant to ET and MH (APP1141208). The Center for Eye Research Australia receives Operational Infrastructure Support from the Victorian Government.

ACKNOWLEDGMENTS

The authors acknowledge the dedicated assistance of animal technicians for animal breeding and husbandry, and the Monash Histology Platform for support with histological studies. We are grateful to Ms. Suhashi M. Wickramasinghe (BSc, BOcc Therapy Hons) for comments on the manuscript.

SUPPLEMENTARY MATERIAL

The Supplementary Material for this article can be found online at: https://www.frontiersin.org/articles/10.3389/fped.2021.689699/full#supplementary-material

Supplementary Figure 1 | Oxygen exposure models trialed in this study. Within 12 h of birth, neonatal C57BL/6 mice were exposed to **(A)** 75% O2 for 5 [PN1-5], **(B)** 8 [PN1-8], or **(C)** 14 days [PN1-14] with a daily 3-h period in room air (not shown in figure). Cohorts of mice were analyzed at PN14 or PN40, and for the PN1-14 model at PN80 (red arrows) alongside room air control mice. Body weights of room air control mice and oxygen-exposed mice at **(D)** PN14 or **(E)** PN40. $^{**}P < 0.01$ and $^{***}P < 0.001$ by Mann-Whitney *U*-test (2-tailed). $n \geq 6$ mice per group, with 1–2 L used in the analysis of each oxygen group. Gender is represented by closed symbols (male) and open symbols (female). PN, postnatal.

Supplementary Table 1 | Custom imageJ script used for the quantitation of fluorescence positive cells.

REFERENCES

1. Baraldi E, Filippone M. Chronic lung disease after premature birth. *N Engl J Med.* (2007) 357:1946–55. doi: 10.1056/NEJMra067279
2. Stoll B, Hansen N, Bell E, Walsh MC, Carlo WA, Shankaran S, et al. Human Development Neonatal Research NetworkTrends in care practices, morbidity, and mortality of extremely preterm neonates, 1993-2012. *JAMA.* (2015) 314:1039–51. doi: 10.1001/jama.2015.10244
3. Husain AN, Siddiqui NH, Stocker JT. Pathology of arrested acinar development in postsurfactant bronchopulmonary dysplasia. *Hum Pathol.* (1998) 29:710–7. doi: 10.1016/S0046-8177(98)90280-5
4. Smith LJ, van Asperen PP, McKay KO, Selvadurai H, Fitzgerald DA. Reduced exercise capacity in children born very preterm. *Pediatrics.* (2008) 122:e287–93. doi: 10.1542/peds.2007-3657
5. Tarazona SP, Galan PS, Alguacil EB, Diego JA. Bronchopulmonary dysplasia as a risk factor for asthma in school children and adolescents: a systematic review. *Allergol Immunopathol.* (2018) 46:87–98. doi: 10.1016/j.aller.2017.02.004
6. Hilgendorff A, O'Reilly MA. Bronchopulmonary dysplasia early changes leading to long-term consequences. *Front Med.* (2015) 2:2. doi: 10.3389/fmed.2015.00002
7. Islam JY, Keller RL, Aschner JL, Hartert TV, Moore PE. Understanding the short-and long-term respiratory outcomes of prematurity and bronchopulmonary dysplasia. *Am J Respir Crit Care Med.* (2015) 192:134–56. doi: 10.1164/rccm.201412-2142PP
8. Hilgendorff A, Reiss I, Ehrhardt H, Eickelberg O, Alvira CM. Chronic lung disease in the preterm infant. lessons learned from animal models. *Am J Respir Cell Mol Biol.* (2014) 50:233–45. doi: 10.1165/rcmb.2013-0014TR
9. Buczynski BW, Maduekwe ET, O'Reilly MA. The role of hyperoxia in the pathogenesis of experimental BPD. *Semin Perinatol.* (2013) 37:69–78. doi: 10.1053/j.semperi.2013.01.002
10. Dayanim S, Lopez B, Maisonet TM, Grewal S, Londhe VA. Caffeine induces alveolar apoptosis in the hyperoxia-exposed developing mouse lung. *Pediatr Res.* (2014) 75:395–402. doi: 10.1038/pr.2013.233
11. Weichelt U, Cay R, Schmitz T, Strauss E, Sifringer M, Bührer C, et al. Prevention of hyperoxia-mediated pulmonary inflammation in neonatal rats by caffeine. *Europ Respir J.* (2013) 41:966–73. doi: 10.1183/09031936.00012412
12. Silva DM, Nardiello C, Pozarska A, Morty RE. Recent advances in the mechanisms of lung alveolarization and the pathogenesis of bronchopulmonary dysplasia. *Am J Physiol Lung Cell Mol Physiol.* (2015) 309:L1239–L72. doi: 10.1152/ajplung.00268.2015
13. O'Reilly MA, Yee M, Buczynski BW, Vitiello PF, Keng PC, Welle SL, et al. Neonatal oxygen increases sensitivity to influenza A virus infection in adult mice by suppressing epithelial expression of Ear1. *Am J Pathol.* (2012) 181:441–51. doi: 10.1016/j.ajpath.2012.05.005
14. Warner BB, Stuart LA, Papes RA, Wispé JR. Functional and pathological effects of prolonged hyperoxia in neonatal mice. *Am J Physiol Lung*

Cell Mol Physiol. (1998) 275:L110–L7. doi: 10.1152/ajplung.1998.275.1.L110
15. Nardiello C, MiŽíková I, Silva DM, Ruiz-Camp J, Mayer K, Vadász I, et al. Standardisation of oxygen exposure in the development of mouse models for bronchopulmonary dysplasia. *Dis Model Mech.* (2017) 10:185–96. doi: 10.1242/dmm.027086
16. Dauger S, Ferkdadji L, Saumon G, Vardon G, Peuchmaur M, Gaultier C, et al. Neonatal exposure to 65% oxygen durably impairs lung architecture and breathing pattern in adult mice. *Chest.* (2003) 123:530–8. doi: 10.1378/chest.123.2.530
17. Wickramasinghe LC, Lau M, Deliyanti D, Gottschalk TA, van Wijngaarden P, Talia D, et al. Lung and eye disease develop concurrently in supplemental oxygen-exposed neonatal mice. *Am J Pathol.* (2020) 190:1801–12. doi: 10.1016/j.ajpath.2020.05.016
18. Schittny JC. Development of the lung. *Cell Tissue Res.* (2017) 367:427–44. doi: 10.1007/s00441-016-2545-0
19. Kresch MJ, Christian C, Wu F, Hussain N. Ontogeny of apoptosis during lung development. *Pediatr Res.* (1998) 43:426–31. doi: 10.1203/00006450-199803000-00020
20. Solaligue DES, Rodríguez-Castillo JA, Ahlbrecht K, Morty RE. Recent advances in our understanding of the mechanisms of late lung development and bronchopulmonary dysplasia. *Am J Physiol Lung Cell Mol Physiol.* (2017) 313:L1101–53. doi: 10.1152/ajplung.00343.2017
21. Baker CD, Alvira CM. Disrupted lung development and bronchopulmonary dysplasia: opportunities for lung repair and regeneration. *Curr Opin Pediatr.* (2014) 26:306. doi: 10.1097/MOP.0000000000000095
22. Mund SI, Stampanoni M, Schittny JC. Developmental alveolarization of the mouse lung. *Dev Dynam.* (2008) 237:2108–16. doi: 10.1002/dvdy.21633
23. Branchfield K, Li R, Lungova V, Verheyden JM, McCulley D, Sun X. A three-dimensional study of alveologenesis in mouse lung. *Dev Biol.* (2016) 409:429–41. doi: 10.1016/j.ydbio.2015.11.017
24. Gouveia L, Betsholtz C, Andrae J. Expression analysis of platelet-derived growth factor receptor alpha and its ligands in the developing mouse lung. *Physiol Rep.* (2017) 5:e13092. doi: 10.14814/phy2.13092
25. Domm W, Misra RS, O'Reilly MA. Affect of early life oxygen exposure on proper lung development and response to respiratory viral infections. *Front Med.* (2015) 2:55. doi: 10.3389/fmed.2015.00055
26. Hou A, Fu J, Yang H, Zhu Y, Pan Y, Xu S, et al. Hyperoxia stimulates the transdifferentiation of type II alveolar epithelial cells in newborn rats. *Am J Physiol Lung Cell Mol Physiol.* (2015) 308:L861–L72. doi: 10.1152/ajplung.00099.2014
27. Nicola T, Hagood JS, James ML, MacEwen MW, Williams TA, Hewitt MM, et al. Loss of Thy-1 inhibits alveolar development in the newborn mouse lung. *Am J Physiol Lung Cell Mol Physiol.* (2009) 296:L738–L50. doi: 10.1152/ajplung.90603.2008
28. Pozarska A, Rodríguez-Castillo JA, Surate Solaligue DE, Ntokou A, Rath P, MiŽíková I, et al. Stereological monitoring of mouse lung alveolarization from the early postnatal period to adulthood. *Am J Physiol Lung Cell Mol Physiol.* (2017) 312:L882–L95. doi: 10.1152/ajplung.00492.2016
29. Vlahovic G, Russell ML, Mercer RR, Crapo JD. Cellular and connective tissue changes in alveolar septal walls in emphysema. *Am J Respir Crit Care Med.* (1999) 160:2086–92. doi: 10.1164/ajrccm.160.6.9706031
30. Walkup LL, Tkach JA, Higano NS, Thomen RP, Fain SB, Merhar SL, et al. Quantitative magnetic resonance imaging of bronchopulmonary dysplasia in the neonatal intensive care unit environment. *Am J Respir Crit Care Med.* (2015) 192:1215–22. doi: 10.1164/rccm.201503-0552OC
31. Yee M, Buczynski BW, O'Reilly MA. Neonatal hyperoxia stimulates the expansion of alveolar epithelial type II cells. *Am J Respir Cell Mol Biol.* (2014) 50:757–66. doi: 10.1165/rcmb.2013-0207OC
32. Papandrinopoulou D, Tzouda V, Tsoukalas G. Lung compliance and chronic obstructive pulmonary disease. *Pulm Med.* (2012) 2012:542769. doi: 10.1155/2012/542769
33. Mikamo M, Shirai T, Mori K, Shishido Y, Akita T, Morita S, et al. Predictors of expiratory flow limitation measured by forced oscillation technique in COPD. *BMC Pulm Med.* (2014) 14:23. doi: 10.1186/1471-2466-14-23
34. Velten M, Heyob KM, Rogers LK, Welty SE. Deficits in lung alveolarization and function after systemic maternal inflammation and neonatal hyperoxia exposure. *J Appl Physiol.* (2010) 108:1347–56. doi: 10.1152/japplphysiol.01392.2009
35. Deakins KM. Bronchopulmonary dysplasia. *Respir Care.* (2009) 54:1252–62.
36. Balany J, Bhandari V. Understanding the impact of infection, inflammation, and their persistence in the pathogenesis of bronchopulmonary dysplasia. *Front Med.* (2015) 2:90. doi: 10.3389/fmed.2015.00090
37. Bland RD. Neonatal chronic lung disease in the post-surfactant era. *Neonatology.* (2005) 88:181–91. doi: 10.1159/000087581
38. Bourbon J, Boucherat O, Chailley-Heu B, Delacourt C. Control mechanisms of lung alveolar development and their disorders in bronchopulmonary dysplasia. *Pediatr Res.* (2005) 57:38–46. doi: 10.1203/01.PDR.0000159630.35883.BE
39. Yee M, Chess PR, McGrath-Morrow SA, Wang Z, Gelein R, Zhou R, et al. Neonatal oxygen adversely affects lung function in adult mice without altering surfactant composition or activity. *Am J Physiol Lung Cell Mol Physiol.* (2009) 297:L641–9. doi: 10.1152/ajplung.00023.2009
40. Leary S, Das P, Ponnalagu D, Singh H, Bhandari V. Genetic strain and sex differences in a hyperoxia-induced mouse model of varying severity of bronchopulmonary dysplasia. *Am J Pathol.* (2019) 189:999–1014. doi: 10.1016/j.ajpath.2019.01.014
41. Yee M, Vitiello PF, Roper JM, Staversky RJ, Wright TW, McGrath-Morrow SA, et al. Type II epithelial cells are critical target for hyperoxia-mediated impairment of postnatal lung development. *Am J Physiol Lung Cell Mol Physiol.* (2006) 291:L1101–L11. doi: 10.1152/ajplung.00126.2006
42. Woyda K, Koebrich S, Reiss I, Rudloff S, Pullamsetti S, Rühlmann A, et al. Inhibition of phosphodiesterase 4 enhances lung alveolarisation in neonatal mice exposed to hyperoxia. *European Respir J.* (2009) 33:861–70. doi: 10.1183/09031936.00109008
43. Tibboel J, Joza S, Reiss I, de Jongste JC, Post M. Amelioration of hyperoxia-induced lung injury using a sphingolipid-based intervention. *Europ Respir J.* (2013) 42:776–84. doi: 10.1183/09031936.00092212
44. Willis KA, Stewart JD, Ambalavanan N. Recent advances in understanding the ecology of the lung microbiota and deciphering the gut-lung axis. *Am J Physiol Lung Cell Mol Physiol.* (2020) 319:L710–L6. doi: 10.1152/ajplung.00360.2020
45. Speer C. Pulmonary inflammation and bronchopulmonary dysplasia. *J Perinatol.* (2006) 26:S57–62. doi: 10.1038/sj.jp.7211476
46. Kotecha S. Cytokines in chronic lung disease of prematurity. *Eur J Pediatr.* (1996) 155:S14–17. doi: 10.1007/BF01958074
47. Hjort MR, Brenyo AJ, Finkelstein JN, Frampton MW, LoMonaco MB, Stewart JC, et al. Alveolar epithelial cell-macrophage interactions affect oxygen-stimulated interleukin-8 release. *Inflammation.* (2003) 27:137–45. doi: 10.1023/A:1023817811850
48. Kumar VH, Lakshminrusimha S, Kishkurno S, Paturi BS, Gugino SF, Nielsen L, et al. Neonatal hyperoxia increases airway reactivity and inflammation in adult mice. *Pediatr Pulmonol.* (2016) 51:1131–41. doi: 10.1002/ppul.23430
49. Kumar VH, Wang H, Kishkurno S, Paturi BS, Nielsen L, Ryan RM. Long-term effects of neonatal hyperoxia in adult mice. *Anat Rec.* (2018) 301:717–26. doi: 10.1002/ar.23766
50. Kindermann A, Binder L, Baier J, Gündel B, Simm A, Haase R, et al. Severe but not moderate hyperoxia of newborn mice causes an emphysematous lung phenotype in adulthood without persisting oxidative stress and inflammation. *BMC Pulm Med.* (2019) 19:1–12. doi: 10.1186/s12890-019-0993-5
51. Kachurina D, Sadykova AZ, Tyan E, Tulebaeva ZS, Pirmakhanova A. The bronchopulmonary dysplasia in infants with retinopathy of prematurity. *Iran J Pediatr.* (2014) 24:S1.
52. Flynn JT, Bancalari E, Snyder ES, Goldberg RN, Feuer W, Cassady J, et al. A cohort study of transcutaneous oxygen tension and the incidence and severity of retinopathy of prematurity. *N Engl J Med.* (1992) 326:1050–4. doi: 10.1056/NEJM199204163261603
53. Tufail A, Singh A, Haynes R, Dodd C, McLeod D, Charteris D. Late onset vitreoretinal complications of regressed retinopathy of prematurity. *Br J Ophthalmol.* (2004) 88:243–6. doi: 10.1136/bjo.2003.022962

54. Terasaki H, Hirose T. Late-onset retinal detachment associated with regressed retinopathy of prematurity. *Jpn J Ophthalmol.* (2003) 47:492–7. doi: 10.1016/S0021-5155(03)00088-1
55. Wu W-C, Shih C-P, Wang N-K, Lien R, Chen Y-P, Chao A-N, et al. Choroidal thickness in patients with a history of retinopathy of prematurity. *JAMA Ophthalmol.* (2013) 131:1451–8. doi: 10.1001/jamaophthalmol.2013.5052
56. Smith LEH, Wesolowski E, McLellan A, Kostyk SK, D'Amato RJ, Sullivan R, et al., editors. Oxygen-induced retinopathy in the mouse. *Invest Ophthalmol Vis Sci*. (1994) 35:101–11.

Conflict of Interest: The authors declare that the research was conducted in the absence of any commercial or financial relationships that could be construed as a potential conflict of interest.

Publisher's Note: All claims expressed in this article are solely those of the authors and do not necessarily represent those of their affiliated organizations, or those of the publisher, the editors and the reviewers. Any product that may be evaluated in this article, or claim that may be made by its manufacturer, is not guaranteed or endorsed by the publisher.

Copyright © 2021 Wickramasinghe, van Wijngaarden, Johnson, Tsantikos and Hibbs. This is an open-access article distributed under the terms of the Creative Commons Attribution License (CC BY). The use, distribution or reproduction in other forums is permitted, provided the original author(s) and the copyright owner(s) are credited and that the original publication in this journal is cited, in accordance with accepted academic practice. No use, distribution or reproduction is permitted which does not comply with these terms.

frontiers in Medicine

ORIGINAL RESEARCH
published: 06 September 2021
doi: 10.3389/fmed.2021.678438

Development and Functional Characterization of Fetal Lung Organoids

Mandy Laube[1]*, *Soeren Pietsch*[1], *Thomas Pannicke*[1], *Ulrich H. Thome*[1] and *Claire Fabian*[2]

[1] Division of Neonatology, Department of Paediatrics, Center for Paediatric Research Leipzig, University of Leipzig, Leipzig, Germany, [2] Department of Vaccines and Infection Models, Fraunhofer Institute for Cell Therapy and Immunology, Leipzig, Germany

Preterm infants frequently suffer from pulmonary complications due to a physiological and structural lung immaturity resulting in significant morbidity and mortality. Novel *in vitro* and *in vivo* models are required to study the underlying mechanisms of late lung maturation and to facilitate the development of new therapeutic strategies. Organoids recapitulate essential aspects of structural organization and possibly organ function, and can be used to model developmental and disease processes. We aimed at generating fetal lung organoids (LOs) and to functionally characterize this *in vitro* model in comparison to primary lung epithelial cells and lung explants *ex vivo*. LOs were generated with alveolar and endothelial cells from fetal rat lung tissue, using a Matrigel-gradient and air-liquid-interface culture conditions. Immunocytochemical analysis showed that the LOs consisted of polarized epithelial cell adhesion molecule (EpCAM)-positive cells with the apical membrane compartment facing the organoid lumen. Expression of the alveolar type 2 cell marker, RT2-70, and the Club cell marker, CC-10, were observed. Na^+ transporter and surfactant protein mRNA expression were detected in the LOs. First time patch clamp analyses demonstrated the presence of several ion channels with specific electrophysiological properties, comparable to vital lung slices. Furthermore, the responsiveness of LOs to glucocorticoids was demonstrated. Finally, maturation of LOs induced by mesenchymal stem cells confirmed the convenience of the model to test and establish novel therapeutic strategies. The results showed that fetal LOs replicate key biological lung functions essential for lung maturation and therefore constitute a suitable *in vitro* model system to study lung development and related diseases.

Keywords: lung, 3D culture, organoids, patch clamp, fetal development, model system

OPEN ACCESS

Edited by:
Constance Barazzone-Argiroffo, University of Geneva, Switzerland

Reviewed by:
Michael Adam O'Reilly, University of Rochester, United States
Marc Chanson, Université de Genève, Switzerland

***Correspondence:**
Mandy Laube
mandy.laube@medizin.uni-leipzig.de

Specialty section:
This article was submitted to Pulmonary Medicine, a section of the journal Frontiers in Medicine

Received: *09 March 2021*
Accepted: *16 August 2021*
Published: *06 September 2021*

Citation:
Laube M, Pietsch S, Pannicke T, Thome UH and Fabian C (2021) Development and Functional Characterization of Fetal Lung Organoids. Front. Med. 8:678438. doi: 10.3389/fmed.2021.678438

INTRODUCTION

The study of fetal lung development is a challenging task. Any model system needs to reflect the biological properties such as morphology and function, while also being reproducible and, if possible, broadly accessible. Although many basic properties like cell morphology or protein localization can be modeled using classic 2-dimensional (2D) cell culture with cell lines or primary cells, their reflection of biological functions is often limited. The situation is further complicated by the highly complex nature of the pulmonary system with uniquely specialized cells. The lung is the central organ of the respiratory system, providing barrier function to facilitate oxygen delivery

and carbon dioxide elimination. Severe clinical consequences can arise from a disruption of fetal lung development. Especially in preterm infants, pulmonary complications are common due to a physiological and structural lung immaturity leading to significant morbidity and mortality. Impaired perinatal transition from the liquid-filled to air-breathing lungs can result in respiratory distress syndrome (RDS), and possibly subsequent development of bronchopulmonary dysplasia (BPD). The pathology of BPD is based on an arrested lung development, including a reduced alveolar surface area and alveolar number, as well as impaired functions down to a cellular level. Functional disturbances of RDS mainly arise from a lack of differentiated alveolar type 2 (ATII) cells that are involved in surfactant synthesis and pulmonary fluid homeostasis. Alveolar fluid clearance (AFC) enables perinatal lung transition to air breathing that is accomplished by active Na^+ transport across the alveolar epithelium driven by epithelial Na^+ channels (ENaC). Importantly, ENaC expression is reduced in the preterm lungs (1), compromising AFC. These pathognomonic features must be reflected in model systems of fetal lung development. Animal models improved the understanding of lung development as well as the pathogenic mechanisms leading to RDS and BDP. Rats are a widely used animal model to reproduce the histopathology of human preterm infants with BPD. Exposing newborn rats to hyperoxia induces lung structural and functional impairment, accompanied by high levels of pulmonary inflammation (2). Thereby the critical relationship between oxygen toxicity and mechanical ventilation with lung injury and BPD development was demonstrated. However, rodent models are mainly used as endpoint models in which tissue damage and functional alterations are determined after sacrifice, preventing analysis of the disease course. Furthermore, newborn rodents are viable at birth and do not exhibit lung immaturity, which is of central importance in human BPD. Besides, respiratory distress in preterm infants is multifactorial, including congenital infection, growth restriction and placental dysfunction, and most preterm infants were exposed to clinical interventions like antenatal corticosteroids. This is not reflected in most animal models possibly leading to different responses to pathogenic challenges as well as therapeutic strategies. Therefore, novel model systems are required to study the underlying mechanisms of late lung maturation and to facilitate the development of novel therapeutic approaches. Moreover, any *in vitro* and *in vivo* model should replicate key features of lung development and maturation, and allow for a qualitative, quantitative, and most importantly, functional analysis. Immortalized lung cell lines were commonly used to determine gene expression and signaling pathways, but due to their immortalized nature, their differentiation capacity is limited. Instead, primary fetal distal lung epithelial (FDLE) cells represent a widely studied *in vitro* model due to their ability to differentiate into polarized and functional epithelia (3). FDLE cells are derived from fetal rat pups 24–48 h prior to birth. Studies showed that fetal rat pups born 24 h prior to term birth experience respiratory distress due to structural and functional lung immaturity (4). Na^+ transport as well as the expression and secretion of surfactant proteins were studied in FDLE cells before. Furthermore, FDLE cells enable analysis of sex-specific differences between male and female cells (5), and can be used for co-culture with other primary lung cell types. On the other hand, FDLE cells are limited in their lifetime and offer only a short time window for experiments of 2–3 days.

Lung organoids (LOs) offer the chance to bridge the gap between conventional *in vitro* and *in vivo* models. Organoids are self-organizing 3D structures that can be grown from stem cells or defined tissue-specific progenitor cells (6). They supposedly recapitulate the organs' structural organization, with multiple specialized cells, and function, although actual organ-like function has yet to be determined. The first 3D lung cell cultures, called organoids or "mass cultures," were generated using a crude cell mix derived from digested fetal lung tissue. This cell suspension consisted of epithelial, endothelial, mesenchymal and hematopoietic cells (7). By culturing the cell suspension at the air-liquid-interface (ALI) on a floating membrane filter, differentiation into mature ATII cells as well as connective tissue formation was achieved (7). This demonstrated the ability of fetal lung cells to self-organize in co-culture with other cells types and that ALI culture represents an important differentiation signal. However, lack of 3D growth limited the use of these early organoid cultures. The absence of a supporting structure, like hydrogels or a scaffold, resulted in a wide-stretched, multilayered and heterogeneous cell aggregation instead of the sophisticated 3D structures seen today. In addition, culture time was limited to a few days before mesenchymal cells overgrew and destroyed the epithelial cell structures. The culture of fetal and adult ATII cells on basement membrane extracts from Engelbreth-Holm-Swarm (EHS) tumor tissue (also known as matrix gel or Matrigel™) led to the establishment of organotypic cell cultures. ATII cell culture on polystyrol resulted in a loss of lamellar bodies, induced cell flattening and cell proliferation, while culture with EHS gels prevented the loss of lamellar bodies and the cells retained their cuboidal morphology (8, 9). These studies showed the importance of the biophysical environment, including the extracellular matrix (ECM) as well as the interface to air, to generate relevant *in vitro* lung models. The use of isolated and defined cell populations and the co-culture of lung epithelial cells with other lung-derived cell types like endothelial cells (10), mesenchymal stem cells (11), and fibroblasts (12), led to the development of self-organizing LOs reflecting morphological and cellular compositions of bronchial and alveolar tissue.

Our study focused on the generation of a biological relevant model system of fetal lung development that can be easily reproduced by other scientists. Furthermore, functional analyses demonstrated the opportunities this model offers for a variety of studies, including gene expression and patch clamp analyses. Fetal LOs were generated using FDLE and lung endothelial cells from fetal rat lungs. This allows a concise validation of the advantages and limitations of LOs as a model system for fetal lung development in comparison to the existing *in vitro* and *in vivo* studies done with rats.

MATERIALS AND METHODS

Cell Isolation

Sprague-Dawley rats (RGD Cat# 70508, RRID:RGD_70508) were obtained from the Medical Experimental Center (MEZ) of Leipzig University. Animals were kept in rooms with a 12 h

light-dark cycle, constant temperature (22°C) and humidity (55%). Food and water were supplied *ad libitum*. At gestational day E20-21 (term E22) pregnant rats were anesthetized by CO_2 inhalation and euthanized by Pentobarbital injection. All experimental procedures were approved by the institutional review board (Landesdirektion Leipzig, permit number: T23/15). Fetal lungs were mechanically dissociated with razor blades. The resulting cell suspension was enzymatically digested with trypsin (0.125%, Fisher Scientific, Schwerte, Germany) and DNase (0.4 mg/mL, CellSystems, Troisdorf, Germany) in Hanks' Balanced Salt solution (HBSS, Fisher Scientific) for 10 min at 37°C, followed by MEM containing collagenase (0.1%, CellSystems) and DNase for 15 min at 37°C. FDLE cells, a model of fetal ATII cells, were isolated by plating the crude lung cell mix twice for 1.5 h to remove adjacent lung fibroblasts followed by differential centrifugation (3, 13). The supernatant contained FDLE cells with >95% purity (3). For the isolation of $CD31^+$ endothelial cells, fetal lungs were digested using the multi tissue dissociation kit II according to the manufacturer's recommendations, followed by Magnetic Activated Cell Sorting (MACS, GentleMACS Octo) using $CD31^+$ beads (all by Miltenyi Biotech, Bergisch Gladbach, Germany). The obtained cell mix was strained with a 70 µm filter (Miltenyi). Resuspension and all subsequent labeling and washing steps were done using 0.5% BSA/OptiMEM (Fisher Scientific). The cells were incubated with an anti-CD31-PE antibody (1:50, #REA396, Miltenyi) for 10 min at 4°C, followed by incubation with anti-PE magnetic beads (20 µl/10^7 cells) for 15 min at 4°C. Up to 10^8 cells were loaded on a LS Column (Miltenyi), inserted in a QuadroMACS™ Separator (Miltenyi) and passed twice over the same column to enrich $CD31^+$ cells. To obtain a homogenous $CD31^+$ cell population, two rounds of subsequent antibody-mediated cell sorting were required. The first step enriched the $CD31^+$ cells to ∼60–80% and the second step led to a purity of >90%. Enrichment was controlled by flow cytometry (BDAccuri, BD biosciences, San Jose, CA, USA). $CD31^+$ cells were cultured on gelatin-coated flasks with Endothelial Cell Growth Supplement (ECGS) medium containing DMEM (high glucose, GlutaMAX™, Fisher Scientific), 20% FCS (Biochrom, Berlin, Germany), 15 mM HEPES (Merck, Darmstadt, Germany), Heparin (100 µg/mL, Merck), ECGS (50 µg/mL, Corning, Corning, NY, USA), penicillin (100 units/mL, Fisher Scientific), streptomycin (100 µg/mL, Fisher Scientific), and amphotericin B (0.25 µg/mL, Fisher Scientific). After ∼2 weeks in culture, confluent $CD31^+$ cells were used for LO generation up to passage 3 (**Supplementary Figure 1**). Subculture was done using TripLE™ Express (Fisher Scientific). A tube formation assay was done to determine the ability of $CD31^+$ cells to form tube-like structures to verify their endothelial cell character. The tube formation assay was done by plating $CD31^+$ cells at 5×10^4 cells on a Matrigel-coated well of a 24-well-plate in ECGS medium. Cell morphology was analyzed after 22 h (**Supplementary Figure 1**).

3D Culture

Transparent permeable transwell inserts (ThinCert, #662610, surface area 33.6 mm^2, Greiner Bio-One, Frickenhausen, Germany) were first coated with growth-factor reduced (GFR) Matrigel (3 mg/mL, #356230, Corning) at 37°C. Matrigel GFR was dissolved in ice-cold LO medium (LO-Med) consisting of DMEM/F12 (#31330095, Fisher Scientific), 10% FCS, 1% insulin-transferrin-selenium-ethanolamine (ITS-X, #51500056, Fisher Scientific), 1 mM HEPES (#A1069,0250, AppliChem, Darmstadt, Germany), penicillin (100 units/mL), streptomycin (100 µg/mL) and amphotericin B (0.25 µg/mL). Freshly isolated FDLE cells (1.5×10^5 per well) were mixed with $CD31^+$ cells (0.375×10^5 per well), constituting an epithelial to endothelial cell ratio of 1:0.25. The defined cell mix was combined with Matrigel GFR (0.4 mg/mL in LO-Med) and transferred to the coated inserts. The lower compartment of the transwell insert was filled with LO-Med, while the upper compartment containing the cells in Matrigel was not submerged in medium enabling air-liquid interface (ALI) conditions. LOs were cultured at 37°C with medium exchange every 2 days. Live cell imaging was done using a microscope (CKX41, Olympus, Hamburg, Germany) with a temperature controller (ibidi, Graefelfing, Germany) and a CO_2 controller (The Brick Gas Mixer, Life Imaging Services, Basel, Switzerland) during the first day of FDLE and $CD31^+$ co-culture under submerged culture conditions to determine their initial self-organization. To analyze the effect of specific stimulating agents LO-Med was supplemented with dexamethasone (100 nM, Merck). Furthermore, the effect of mesenchymal stem cell-conditioned medium (MSC-CM) on LOs was determined after the organoids reached 15 days *in vitro* (div). The organoids were further cultured for 4 additional days in MSC-CM or the corresponding medium used for the culture of MSCs, which consisted of DMEM (low glucose, GlutaMAX™, Fisher Scientific) and 2% FCS. To subculture LOs or obtain them for further analyses, cell recovery solution (#354253, Corning) was used. To this end, all inserts were incubated on ice for ∼2 h with ice cold cell recovery solution. Subsequently, the cell recovery solution was replaced by sterile 10% BSA (#8076.2, Carl Roth, Karlsruhe, Germany) in PBS. The digested Matrigel solution was centrifuged at 300 × g for 5 min, sedimented LOs were resuspended, washed twice in PBS and used for patch clamp analyses or fixed with 2% formaldehyde (#11586711, Fisher Scientific) in PBS for 20 min at room temperature followed by embedding in Tissue-Tek™ O.C.T. (#4583, Weckert, Kitzingen, Germany) for immunofluorescence staining. LO compactness was defined as the cellular area in proportion to the whole organoid area using Image J version 1.53c (ImageJ, RRID:SCR_003070) as published before (14). Compactness, also known as solidity, includes the packing density and the intercellular space cavities thereby indicating internal cellularity and external branching.

Immunofluorescence

Characterization of LOs was carried out with immunofluorescence staining of cryotome sections (5 µm). LO slices were washed with PBS and then treated with 5% BSA/PBS containing 0.5% Triton-X 100 (Merck) for 1 h at room temperature. Afterwards, the slices were incubated at 4°C overnight with the respective primary antibody, diluted in 5% BSA/PBS. LO slices were incubated with rabbit-anti-epithelial

cell adhesion molecule (EpCAM) primary antibody (1:50; # ab71916, Abcam, Cambridge, UK, RRID:AB_1603782), mouse-anti-RT1-40 (1:150, #TB-11ART1-40, Terrace Biotech, San Francisco, CA, USA) for staining of ATI cells (15), rabbit-anti-aquaporin 5 (Aqp 5, 1:100, #178615, Merck, RRID:AB_211472), mouse-anti-RT2-70 (1:150, #TB-44ART2-70, Terrace Biotech) to detect ATII cells (16), rabbit-anti-Club cell secretary protein (CC-10, 1:100, #ab40873, Abcam, RRID:AB_778766), and rabbit-anti-Ki-67 (1:500, #9129, Cell Signaling Technology, Danvers, MA, USA, RRID:AB_2687446). Control slices were treated with 5% BSA/PBS without the primary antibody. The secondary antibody NL-493 (1:200; R&D Systems, Boston, USA, RRID:AB_663764) was used for primary rabbit IgG antibodies and NL-637 (1:200; R&D Systems, RRID:AB_663771) was used for primary mouse IgG antibodies. Nuclei were stained with DAPI (1 μg/ml, #D8417-1MG, Merck). For Live-Dead staining LOs were resuspended in fresh LO-Med containing 2 mg/mL Matrigel and plated on a glass bottom dish (#81218-200, ibidi). After 3 days, LO-Med was replaced by a solution containing Calcein-AM (5 μM, #sc-203865, Santa Cruz) and propidium iodide (PI, 1 μg/mL, #CN74.1, Carl Roth). Staining of actin filaments was performed with FITC-labeled phalloidin (2.5 μg/mL, #P1951, Merck, RRID:AB_2315148). All sections were covered with ProLong™ Glass Antifade Mountant (#P36980, Fischer Scientific). For image capturing a confocal laser-scanning microscope (LSM710, Laser: Diode 405, Argon 488, Helium-Neon 543; Objective: Plan- Apochromat 20 x, Zeiss, Goettingen, Germany) was used. Area and fluorescence calculation were done with Image J. Calculation of cell numbers was done by manual counting. Depending on the used antibodies, either whole positively stained cells (EpCAM) or in case of apical markers, cells with an adjacent positive staining (RT2-70), were counted as positive.

Gene Expression Analyses

RNA isolation was done at 15 div using the Purelink RNA Mini Kit (Fisher Scientific) according to the manufacturer's instructions. Reverse transcription was carried out using the Maxima H Minus First Strand cDNA Synthesis Kit with dsDNase (Fisher Scientific). Real-time quantitative PCR (RT-qPCR) was done in the CFX 96 Real-Time PCR Detection System (Bio-Rad, Munich, Germany) using the SYBR Select Master Mix (Fisher Scientific) and gene-specific primers listed in **Table 1**. A serial dilution of target-specific plasmid DNA was used for absolute quantification. Molecule concentrations were then normalized to a reference gene encoding for the mitochondrial ribosomal protein S18a (*Mrps18a*). Constant expression of *Mrps18a* was confirmed against other common reference genes. Using the relative standard curve method mRNA levels were calculated and expressed as relative fold change of the respective control. Melting curves and gel electrophoresis of PCR products were routinely performed to control the specificity of the PCR reaction.

Patch Clamp Analyses

Patch clamp studies were performed at 15 div. LOs were transferred to the recording chamber in a bath on the stage of a microscope (BX61WI, Olympus), which was filled with a solution containing (mM): 135 KCl, 2 $MgCl_2$, 6 NaCl, 5.5 Glucose, 10 HEPES (pH 7.4). Cell attached currents were recorded with an EPC10 patch clamp amplifier (Heka Elektronik, Lambrecht, Germany). A standard personal computer running Patchmaster software (Heka, Patchmaster, RRID:SCR_000034) controlled the EPC10 and stored the current tracings. Patch pipettes were pulled from borosilicate capillaries with 1.5 mm outer diameter and 0.86 mm inner diameter (Science Products, #GB150-8P) using a P2000 laser puller (Sutter, Novato, CA). The pipettes were filled with a solution containing (mM): 140 NaCl, 5 KCl, 1 $MgCl_2$, 1.8 $CaCl_2$, 5.5 Glucose, 10 HEPES (pH 7.4), resulting in a tip resistance between 4 and 6 MΩ. ATII cells were identified using Lysotracker (1 μM, LysoTracker Green DND-26, Fisher Scientific), which selectively accumulates in their lamellar bodies (18). After forming a gigaohm seal, currents were recorded at membrane potentials between −100 and +100 mV in 10 mV increments, filtered at 2 kHz and sampled at 10 kHz. Cell attached recordings were analyzed with Fitmaster software (Heka, Fitmaster, RRID:SCR_016233). Voltages are given as the negative of the patch pipette potential, which represents the shift of the patch potential from the resting potential. Negative potentials represent hyperpolarization, and positive potentials represent depolarization of the cell membrane away from the resting potential. Highly selective cation (HSC) channels and non-selective cation (NSC) channels were identified by characteristic channel kinetics and the current-voltage relationship for the channel.

Ussing Chamber Measurements

Ussing chamber measurements of FDLE cells were performed 4 days after cell isolation, as previously reported (5). Only monolayers with a transepithelial resistance (R_{te}) exceeding 300 $\Omega \cdot cm^2$ were included in the analyses. Electrophysiological solutions consisted of: 145 mM Na^+, 5 mM K^+, 1.2 mM Ca^{2+}, 1.2 mM Mg^{2+}, 125 mM Cl^-, 25 mM HCO_3^-, 3.3 mM $H_2PO_4^-$, and 0.8 mM HPO_4^{2-} (pH 7.4). For the basolateral solution, 10 mM glucose was used, while 10 mM mannitol was used in the apical solution. During measurements, the solutions were continuously bubbled with carbogen (5% CO_2 and 95% O_2). Equivalent short-circuit currents (I_{SC}) were determined every 20 s by measuring transepithelial voltage (V_{te}) and R_{te} with a transepithelial current clamp (Physiologic instruments, San Diego, CA) and calculating the quotient $I_{SC} = V_{te}/R_{te}$. After the I_{SC} reached a stable plateau (I_{base}), amiloride (10 μM, # A7410, Sigma-Aldrich) was applied to the apical chamber to assess the amiloride-sensitive ΔI_{SC} (ΔI_{amil}). The current reduction induced by amiloride (ΔI_{amil}) was used as a measure of ENaC activity. Amiloride was dissolved in water.

Isolation of Human Mesenchymal Stem Cells

The study was approved by the ethical board of the medical faculty of Leipzig University. The umbilical cord tissue was collected after delivery from human newborns whose mothers granted informed consent. MSC isolation and characterization are described elsewhere (19). MSC-CM was produced by

TABLE 1 | Primer sequences.

Gene	Primer (forward, 5′-3′)	Primer (reverse, 5′-3′)
α-ENaC NM_031548.2	TTCTGGGCGGTGCTGTGGCT	GCGTCTGCTCCGTGATGCGG
β-ENaC NM_012648.1	TGCAGGCCCAATGCCGAGGT	GGGCTCTGTGCCCTGGCTCT
γ-ENaC NM_017046.1	CACGCCAGCCGTGACCCTTC	CTCGGGACACCACGATGCGG
Na,K-ATPases-α$_1$ NM_012504.1	GGACGAGACAAGTATGAGCCCGC	CATGGAGAAGCCACCGAACAGC
Na,K-ATPases-β$_1$ NM_013113.2	GCGCAGCACTCGCTTTCCCT	GGGCCACACGGTCCTGGTACG
CFTR NM 031506.1	GCCTTCGCTGGTTGCACAGTAGTC	GCTTCTCCAGCACCCAGCACTAGA
Mrps18a NM_198756.2	GCGACCGGCTGGTTATGGCT	GGGCACTGGCCTGAGGGATTAG
Sftpa (17) NM_001270647.1	CCTCTTCTTGACTGTTGTCGCTGG	GCTGAGGACTCCCATTGTTTGCAG
Sftpb (17) NM_138842.1	GGAGCTAATGACCTGTGCCAAGAG	CTGGCCCTGGAAGTAGTCGATAAC
Sftpc (17) NM_017342.2	GATGGAGAGCCCACCGGATTACTC	GAACGATGCCAGTGGAGCCAATAG

incubating the culture medium with MSCs for 72 h, followed by sterile filtration.

Statistical Analyses

Differences between two groups were analyzed with the unpaired *T*-test or the Mann-Whitney test. A probability of $p < 0.05$ was considered significant for all statistical analyses. Statistical analysis was performed with GraphPad Prism software (GraphPad Software, La Jolla, CA, USA, RRID:SCR_002798).

RESULTS

Development of Fetal LOs

The generation of LOs is schematically illustrated in **Figure 1A**. The isolation of $CD31^+$ cells was done by antibody-mediated cell sorting using magnetic beads. This allowed analysis of cells during every step of the isolation process: the initial amount of $CD31^+$ cells in the total lung cell mix, the $CD31^+$ cells bound to the magnetic column as well as the non-bound cells in the flow-through. $CD31^+$ cells represented 5.2 ± 2.6% (Mean ± SD; $n = 16$) of total lung cells. $CD31^+$ cells were cultured for 7–14 days to increase their cell numbers. These $CD31^+$ cells were combined with freshly isolated FDLE cells and used for organoid generation. LO formation was compared between Matrigel-coated permeable inserts covered with cells in Matrigel exposed to air (ALI culture) and Matrigel-containing cell suspension plated at the bottom of a well and overlaid with LO-Med (submerged culture) (**Figure 1B**). The ALI condition resulted in more diverse and complex LO formation of branched and cystic morphology, while the submerged culture condition mainly led to the formation of cystic LOs. In some cystic LOs, differentiated cells with beating cilia within the lumen were observed (data not shown). **Figure 1C** shows examples of the different morphologies observed. Cystic LOs exhibited one lumen and were mainly transparent. Branched morphology consisted of several cysts attached to each other, reminding of budding structures or even more condensed structures with opaque appearance. The discrimination between cystic and branched morphology was done according to published studies (20). Submerged cultures were not investigated further because of the morphology and presence of cilia. Testing different FDLE cell numbers demonstrated that at least 0.5×10^5 cells per well were required for 3D LO formation, otherwise only 2D cell layers were observed. Furthermore, without $CD31^+$ cells no 3D LOs were observed (**Figure 1D**). $CD31^+$ cells began to align themselves in the Matrigel and formed tube-like structures within the first 24 h of culture (**Supplementary Figures 1B,C**). Without $CD31^+$ cells, FDLE cells did not show active migration, but in co-culture cell-cell adhesive interactions between FDLE and $CD31^+$ cells led to initial cell aggregates (**Supplementary Figure 1C**). The 3D assembly was enhanced by direct interaction of FDLE cells with $CD31^+$ cells, while indirect co-culture delayed LO formation by ∼1 week (**Figure 1D**). Different cell ratios were tested (FDLE to $CD31^+$ cells of 1:1, 1:0.5, and 1:0.25). Increasing the number of $CD31^+$ cells decreased LO area and number (**Figures 1E,F**). After 15 days in culture LOs reached mean sizes of 115.34 ± 44.82 μm (Mean ± SEM, $n = 22$). LO size increased during culture reaching a maximum at about 15 div, no further increase of LO size was observed at 43 div (**Figure 1G**). Prolonged LO culture led to overgrowth of a cell layer after ∼1 month that consumed all medium and impaired organoid growth. Thus, splitting of LO cultures was necessary, which enabled further

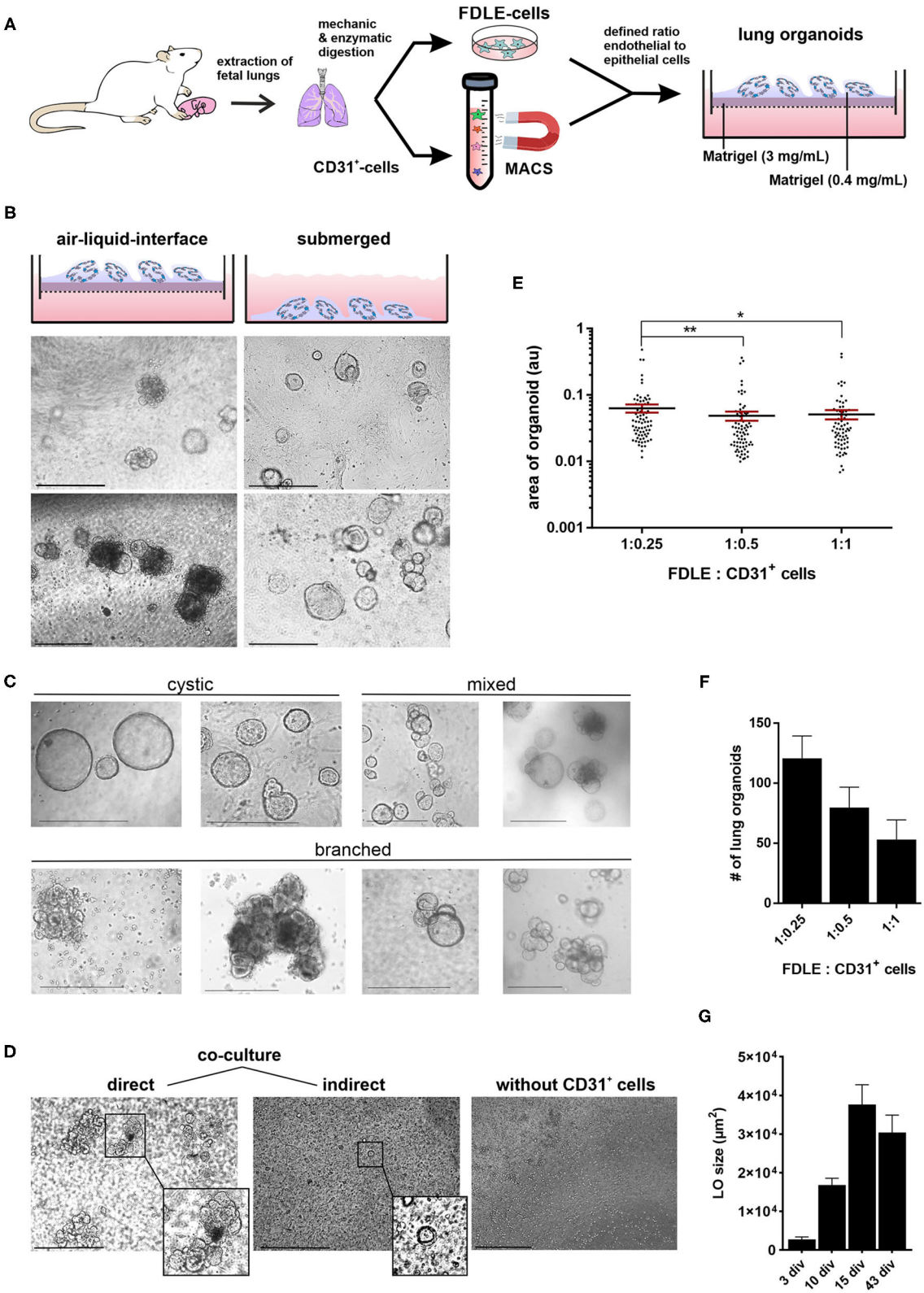

FIGURE 1 | Generation of fetal LOs. **(A)** Schematic illustration of LO generation. CD31+ cells were mixed with freshly isolated FDLE cells and used for LO generation. **(B)** LO formation was compared between ALI culture, in which LOs were cultured on permeable inserts exposed to air, and submerged culture without air exposure. ALI conditions resulted in more divers and complex LOs of branched and cystic morphology, while the submerged culture condition mainly led to the formation

(Continued)

FIGURE 1 | of cystic LOs (pictures were taken at 15 div). **(C)** Exemplary demonstration of different morphologies (cystic, branched or a mixed appearance) observed during LO culture. **(D)** The 3D assembly was enhanced by direct interaction of FDLE cells with $CD31^+$ cells (3 div), while indirect co-culture delayed LO formation (3 div). Furthermore, without $CD31^+$ cells no LO formation was observed (4 div). **(E)** Different cell ratios were tested (FDLE to $CD31^+$ cells of 1:1, 1:0.5, and 1:0.25). Data of LO area are displayed in a scatter dot plot with mean (horizontal line) ± SEM. Increasing the number of $CD31^+$ cells decreased LO area ($n = 70–75$; $^{**}p < 0.01$; $^{*}p < 0.05$ by *T*-test). **(F)** Numbers of LOs are displayed as mean + SEM. Increasing the number of $CD31^+$ cells further decreased LO numbers. **(G)** LO size (μm^2) at 3, 10, 15, and 43 div ($n = 40$). div, days *in vitro*. Scale bar: 500 μm.

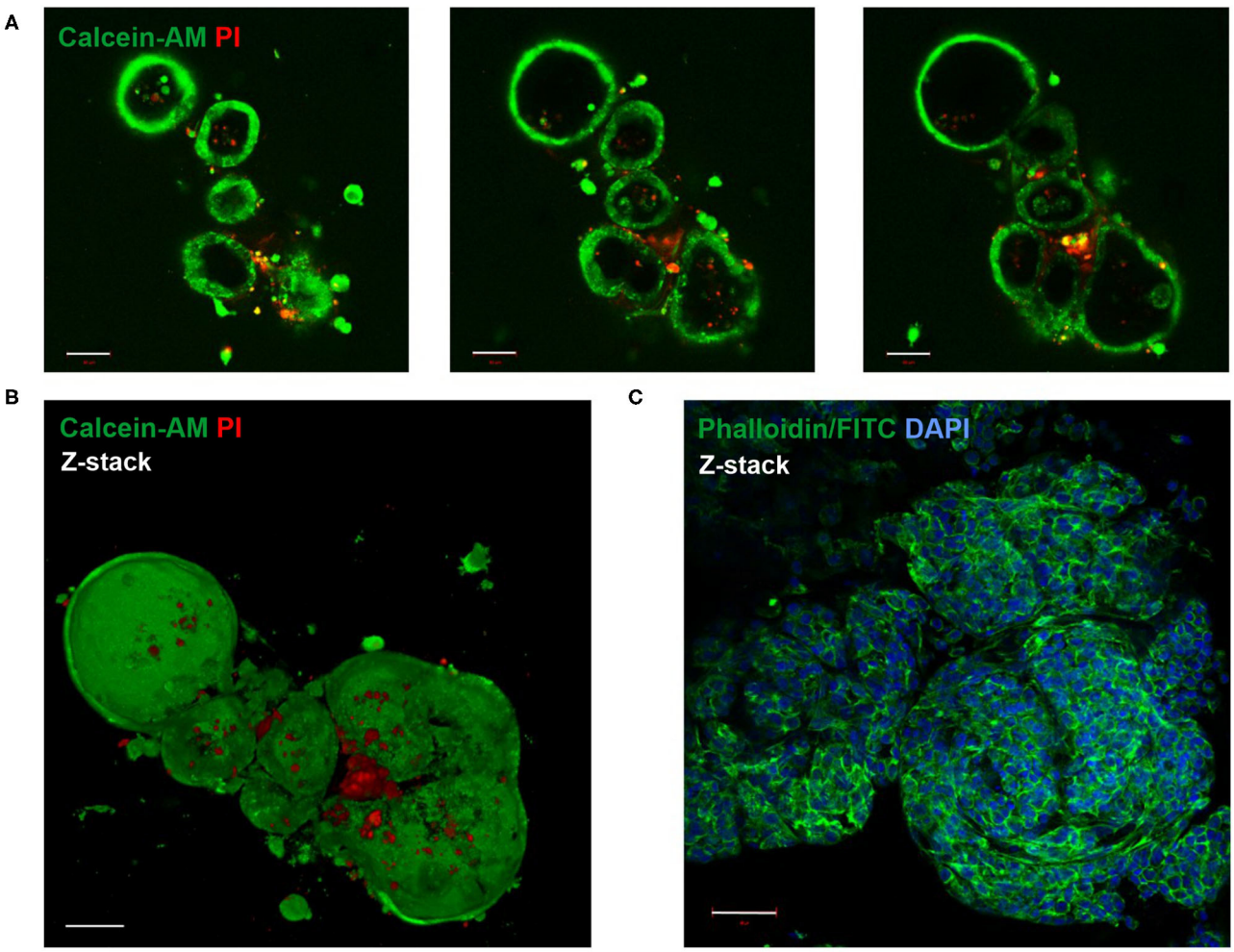

FIGURE 2 | Live-Dead and F-actin staining of fetal LOs. Fluorescence Z-stack serial images were taken by confocal microscopy. The bottom-to-top distance was 58 μm with 1 μm distance intervals between images. **(A)** Live-Dead staining with Calcein-AM (green) that accumulated in living cells and propidium iodide (PI, red) that accumulated in dead cells (23 div). Images of different optical sections through the LOs (11, 22, and 30 μm distance from bottom) demonstrated that the majority of cells were alive. **(B)** Z-stack image of **(A)** showed that dead cells were mainly attached to the LOs, while the LO structures consisted of living cells. **(C)** Z-stack image of F-actin staining that showed the structural organization of the LO (17 div) by phalloidin-FITC fluorescence (green). Nuclei were stained with DAPI (blue). div, days *in vitro*. Scale bar: 50 μm.

subculture, without the need to add additional $CD31^+$ cells. Using fetal adjacent lung fibroblasts or human umbilical vein-derived endothelial cells (HUVECs) instead of $CD31^+$ cells also resulted in the formation of 3D LOs.

Morphological Characterization of Fetal Lung Organoids

Live-Dead staining of passaged LOs showed that the majority of cells within the organoid were alive (**Figures 2A,B**). Staining with phalloidin-FITC was used to visualize the structural organization of filamentous actin (F-actin) with a cobblestone-like epithelial appearance of the LOs (**Figure 2C**). The cellular composition of the LOs consisted only of $EpCAM^+$ cells without direct integration of $CD31^+$ cells. We did not perform an additional staining of $CD31^+$ cells in the lung organoids at 15 div, since our initial experiments testing different medium conditions (data not shown) showed that the culture condition used for lung organoids was not supporting $CD31^+$ cells growth during

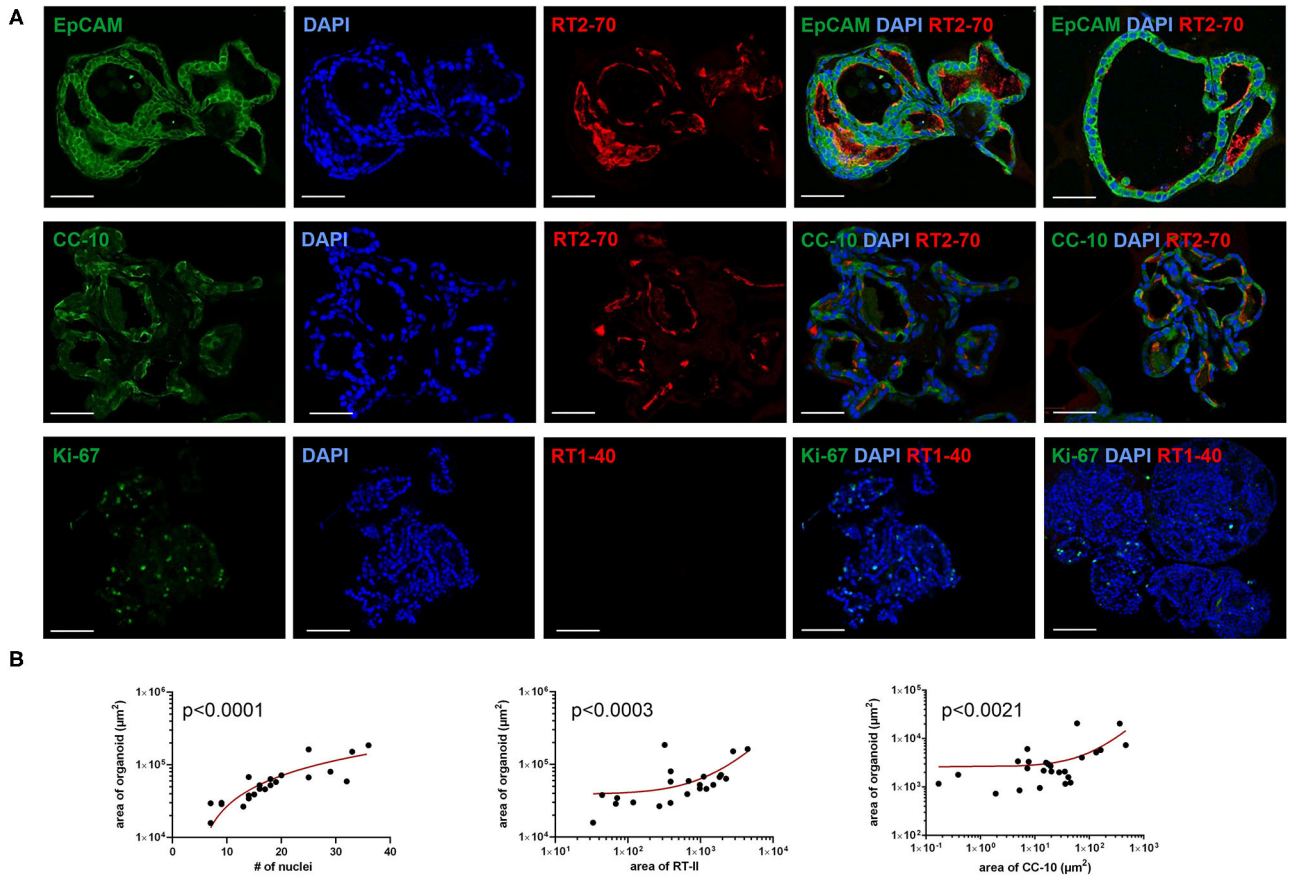

FIGURE 3 | Immunofluorescence characterization of fetal LOs. Fluorescence images of LO slices (15 div) were taken by confocal microscopy. **(A)** Organoids were strongly positive for EpCAM expression. Nuclei were stained with DAPI. Epithelial cells within the LOs polarized with the apical membrane compartment facing the lumen, as shown by the luminal expression of the RT2-70 antigen. Furthermore, expression of the Club cell marker CC-10 was detected. In contrast, the ATI cell marker RT1-40 was rarely observed in the LOs. Ki-67 staining showed that only a small subset of the total cells was actively proliferating. Scale bar: 50 µm. **(B)** The area of LOs positively correlated with the number of nuclei ($n = 21$; $p < 0.0001$). The area of RT2-70$^+$ cells positively correlated with LO area ($n = 21$; $p < 0.0003$). Furthermore, area of CC-10$^+$ expression positively correlated with LO area ($n = 25$; $p < 0.0021$). div, days *in vitro*.

long term culture. LOs were strongly positive for EpCAM expression (**Figure 3A**). Notably, epithelial cells within the LOs polarized with the apical membrane compartment facing the lumen of the organoid, as shown by the luminal expression of the RT2-70 antigen. Furthermore, expression of the Club cell marker CC-10 was detected. In contrast, the ATI cell markers, RT1-40 (T1α or podoplanin) and Aqp5 were not observed in the LOs. Notably, RT1-40 expression was also not detected in fetal rat lung slices (E21), while their pronounced and widespread expression was detected in adult rat lung tissue (**Supplementary Figure 2**). Ki-67 staining showed that only a small subset of the total cells was actively proliferating at 15 div.

The area of LOs positively correlated with the number of nuclei, determined by DAPI staining (Spearman r = 0.89; $p < 0.001$; **Figure 3B**). The positively stained area for ATII cells (RT2-70$^+$) positively correlated with LO area (in µm^2; Spearman r = 0.703; $p < 0.001$; **Figure 3B**), and 1.59 ± 0.37% of the LO area expressed the RT2-70 antigen, independent of organoid size. Furthermore, 1.38 ± 0.30% of total LO area was CC-10$^+$, whose expression also positively correlated with organoid size (Spearman r = 0.619; $p < 0.01$; **Figure 3B**). Notably, the positively stained area (in%) does not reflect the actual cell number.

Functional Characterization of Fetal Lung Organoids

Patch clamp analyses of LOs demonstrated the presence of ion channels of different conductance, open probability and open and closed time. First, ATII cells within the LOs were identified by fluorescence staining after incubation with Lysotracker (**Figure 4A**). Single as well as multiple channel activities were observed at different holding potentials, showing exemplary outward currents as demonstrated by the upward direction

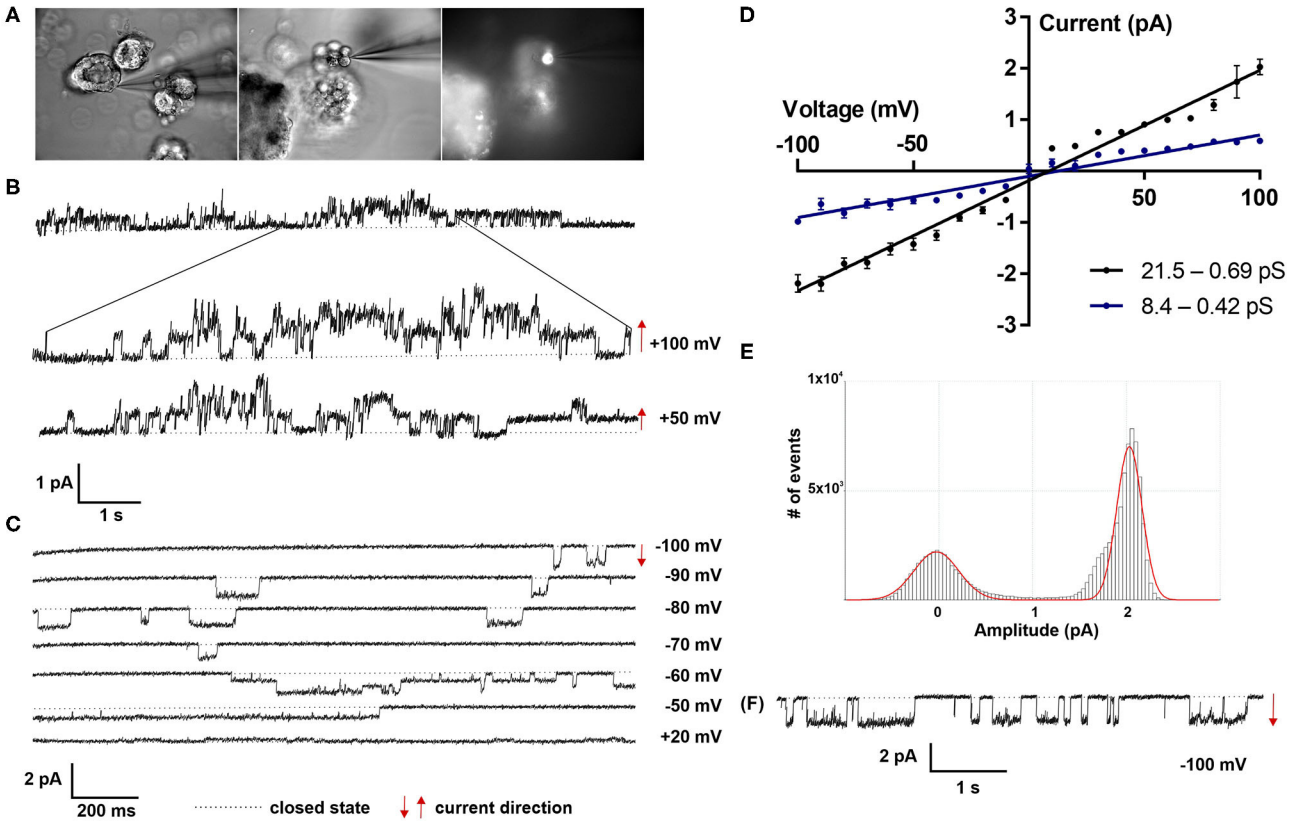

FIGURE 4 | Electrophysiological characterization of fetal LOs. Patch clamp analyses of LOs at 15 div demonstrated the presence of ion channels of different conductance, open probabilities and open and closed times. **(A)** ATII cells within the LOs were identified by fluorescence after incubation with Lysotracker. **(B)** Single as well as multiple channel activities were observed at different holding potentials (+100 and +50 mV), showing exemplary outward currents as demonstrated by the upward direction of openings from the closed state. **(C)** Furthermore, inward currents were observed at different negative holding potentials (−100 to +20 mV) as shown by the downward direction of the openings from the closed state. **(D)** Plotting the current-voltage relationship identified two types of channels: a channel with a conductance of 8.4 ± 0.42 pS (slope ± SE, $n = 18$ cells) and a reversal potential of 11.3 mV ($R^2 = 0.982$), and a second channel with a conductance of 21.5 ± 0.69 pS ($n = 15$ cells) that reversed at 9.2 mV ($R^2 = 0.955$). **(E,F)** Amplitude histogram and current tracing of single channel openings at −100 mV. Closed state is indicated by the dotted line. The arrows indicate the current direction with ↑ outward and ↓ inward currents.

of openings from the closed state (**Figure 4B**). Furthermore, inward currents were observed at different negative holding potentials as shown by the downward direction of the openings from the closed state (**Figure 4C**). Plotting the current-voltage relationship identified two types of channels: a channel with a slope conductance of 8.4 ± 0.42 pS (slope ± SE, $n = 18$ cells) and a reversal potential of 11.3 mV ($R^2 = 0.982$), and a second channel with a conductance of 21.5 ± 0.69 pS ($n = 15$ cells) that reversed at 9.2 mV ($R^2 = 0.955$) (**Figure 4D**). Thus, ATII cells within the LOs displayed functional epithelial Na^+ channels with HSC and NSC channel-like transport properties. **Figures 4E,F**, **5A,B** further show the amplitude histograms of single and multiple channel openings on hyperpolarization. Different open times at different holding potentials are displayed in **Figure 5C**. Finally, high variability of channel kinetics (amplitude, open and closed times) are shown for a recording with voltage steps from −100 to +100 mV and a reversal potential close to 0 (**Figure 5D**). According to the strong rectifying properties of the illustrated recording, with smaller inward currents on hyperpolarization (28.41 pS) and larger outward currents when the patch membrane was depolarized (82.54 pS), an outwardly rectifying Cl^- channel (ORCC) can be assumed.

Reviewing the Effect of Certain Lung-Stimulating Factors

Gene expression analysis of LOs demonstrated the mRNA expression of *ENaC* and the *Na,K-ATPase* as well as surfactant protein (*Sftp*)-A, B, and C, which exhibit essential functions in mature ATII cells. Dexamethasone is known to increase the mRNA expression of Na^+ transporters and surfactant genes *in vitro* and *in vivo*. Thus, LOs were incubated with dexamethasone (100 nM) for 48 h, prior to RNA isolation at 15 div. Dexamethasone significantly increased mRNA expression of the *ENaC subunits* (α, β, γ) and the *Na,K-ATPase subunit-β1* compared to control LOs cultured without dexamethasone (*p*

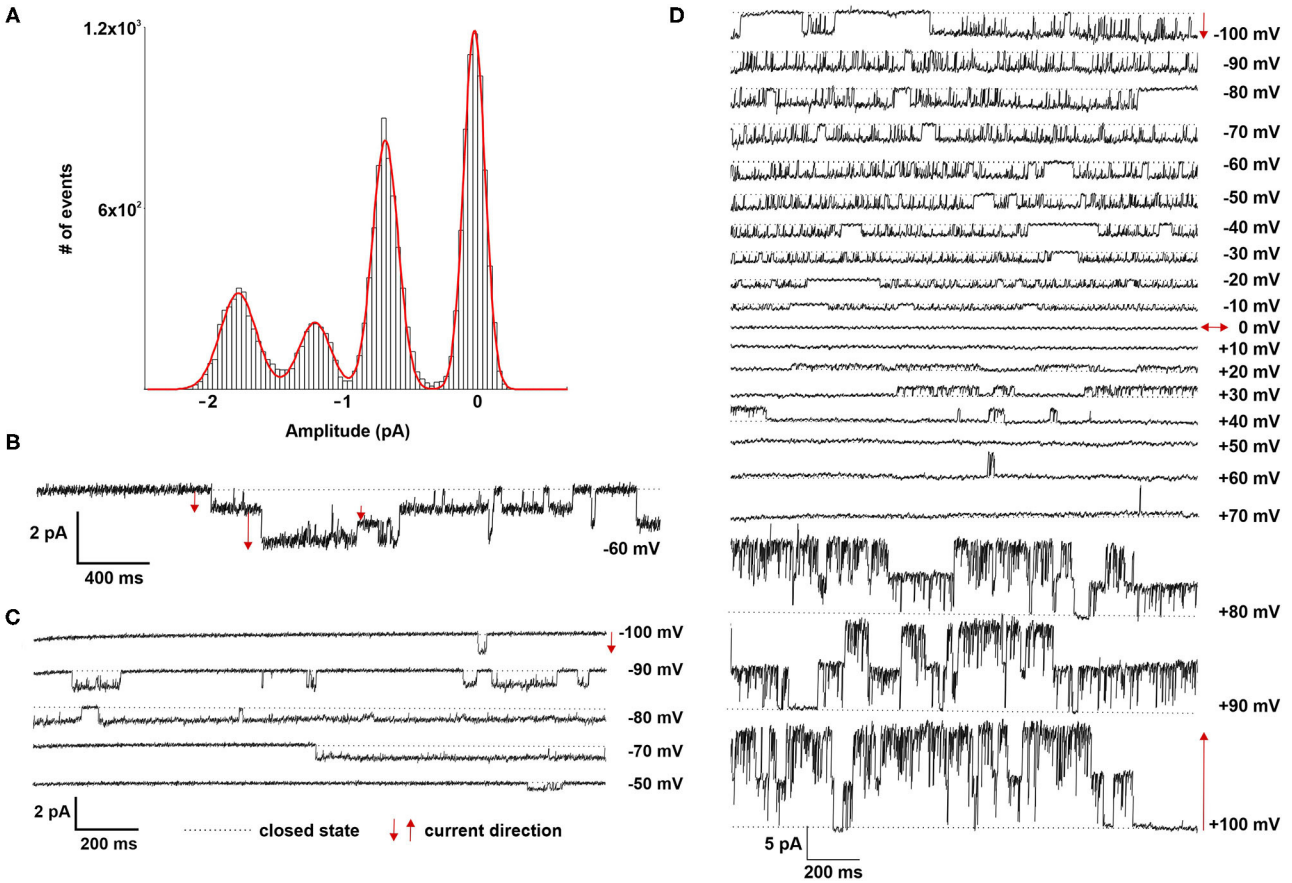

FIGURE 5 | Electrophysiological characterization of fetal LOs. **(A,B)** Amplitude histogram and current tracing of multiple channel openings at −60 mV. **(C)** Different open times at different holding potentials (−100 to −50 mV) are displayed. **(D)** High variability of channel kinetics (amplitude, open and closed times) are shown for a recording with voltage steps from −100 to +100 mV and a reversal potential close to 0. The strong rectifying properties of the illustrated recording, with smaller inward currents on hyperpolarization and larger outward currents when the patch membrane was depolarized, suggests an outwardly rectifying Cl^- channel (ORCC). Closed state is indicated by the dotted line. The arrows indicate the current direction with ↑ outward and ↓ inward currents.

< 0.01, $p < 0.05$; **Figure 6A**). In contrast, mRNA expression of the cystic fibrosis conductance regulator (*CFTR*) was significantly reduced by dexamethasone ($p < 0.05$). Furthermore, the mRNA expression of *Sftpb* (surfactant protein B) and *Sftpc* (surfactant protein C) were significantly increased by dexamethasone in LOs ($p < 0.01$, $p < 0.05$; **Figure 6A**). In agreement, dexamethasone significantly increased mRNA expression of ENaC and the Na,K-ATPase in primary FDLE cells grown on permeable inserts ($p < 0.001$; **Figure 6B**). Furthermore, Na^+ transport was significantly enhanced by dexamethasone as determined in Ussing chambers (**Figure 6C**). Dexamethasone increased I_{base} from 3.67 ± 0.09 μA/cm² (Mean ± SEM) to 4.71 ± 0.13 μA/cm² and the ΔI_{amil} from 2.99 ± 0.08 μA/cm² to 4.06 ± 0.12 μA/cm² ($p < 0.001$; **Figure 6C**). These results show that the fetal LOs mimic the response to dexamethasone seen in primary fetal lung epithelia and that the observed increase of mRNA expression causes an elevated transepithelial Na^+ transport activity. Furthermore, LOs were strongly positive for EpCAM expression (**Figure 7A**). Notably, dexamethasone significantly increased expression of the EpCAM and RT2-70 antigen ($p < 0.01$; **Figure 7B**). Finally, morphology of LOs treated with dexamethasone was not altered compared to control LOs (**Supplementary Figure 3**).

Mesenchymal stem cells (MSCs) have demonstrated therapeutic potential in animal models of neonatal lung disease (21–23) and thus represent a promising future therapeutic approach to alleviate disease burden in preterm infants. In our previous study we determined the paracrine effect of MSCs on lung functional and structural development in FDLE cells and fetal lung explants (19). Herein we aimed at reproducing the reactivity of LOs in comparison to the prior study and to extend the knowledge about cellular effects of MSCs. The LOs (15 div) were cultured with mesenchymal stem cell-conditioned medium (MSC-CM) for 4 days. The respective LO control was incubated with medium used for MSC culture, without MSC conditioning. MSC-CM enhanced lumen formation and thinning of the epithelial layer, in contrast to the denser morphology of control

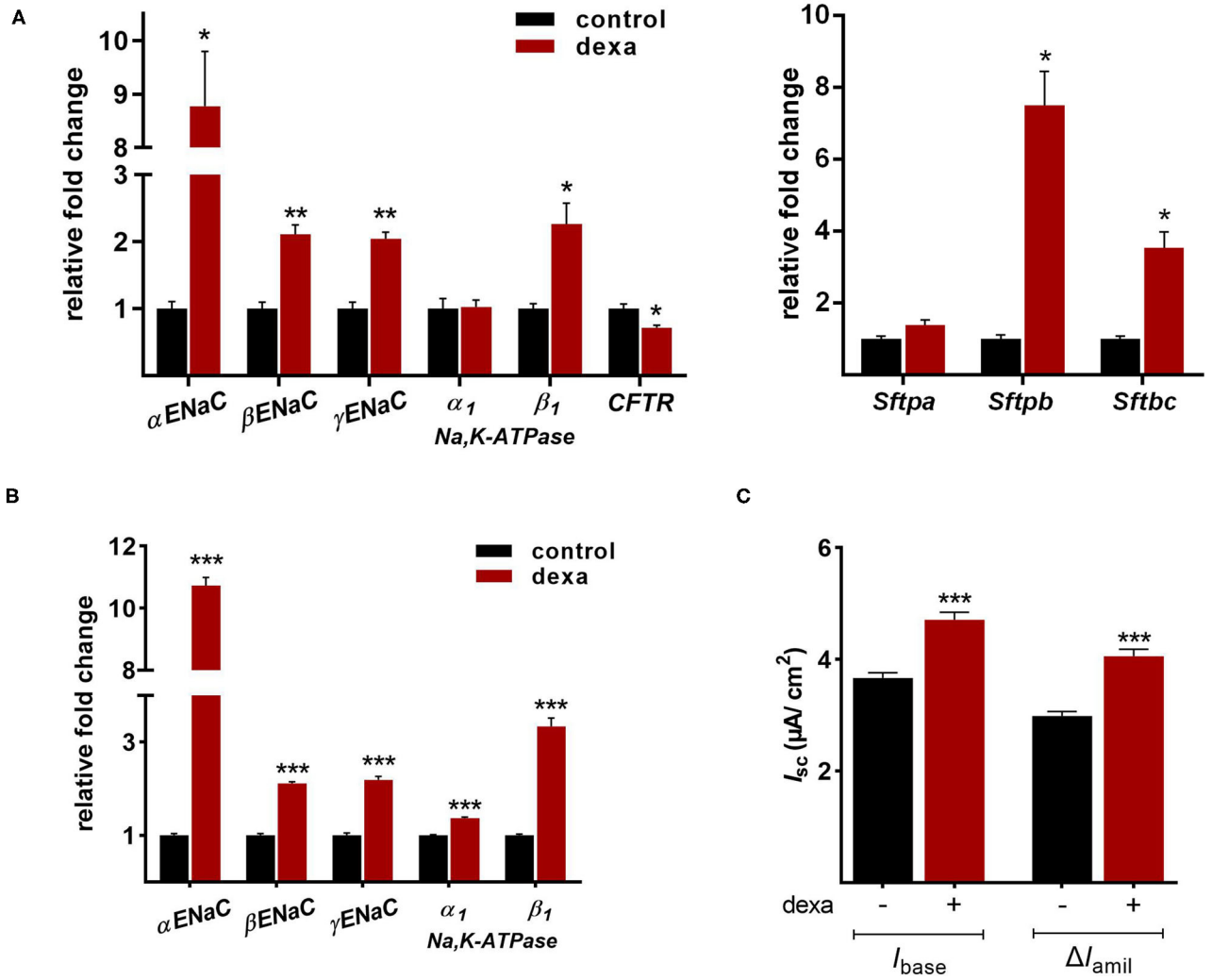

FIGURE 6 | Effects of dexamethasone on fetal LOs compared to FDLE cells. Data are displayed as Mean + SEM. **(A)** Gene expression analysis of LOs (15 div) stimulated with dexamethasone (100 nM) for 48 h. Dexamethasone significantly increased mRNA expression of the *ENaC subunits* (α, β, γ) and the *Na,K-ATPase subunit-β1* compared to control LOs cultured without dexamethasone ($n = 4/5$; $^{**}p < 0.01$; $^{*}p < 0.05$ by *T*-test). mRNA expression of *CFTR* was reduced by dexamethasone ($^{*}p < 0.05$ by *T*-test). Furthermore, the mRNA expression of *Sftpb* and *Sftpc* were significantly increased by dexamethasone ($n = 4$; $^{*}p < 0.05$ by *T*-test). **(B)** FDLE cells were also stimulated with dexamethasone (100 nM) for 48 h. In accordance to LOs, dexamethasone strongly increased the mRNA expression of the Na^+ transporters ($n = 12$; $^{***}p < 0.001$ by *T*-test). **(C)** The increased mRNA expression was accompanied by an enhanced Na^+ transport (I_{base}) and ENaC activity (ΔI_{amil}) in FDLE cells, as determined in Ussing chambers ($n = 78/92$; $^{***}p < 0.001$ by *T*-test). div, days *in vitro*.

LOs (**Figure 8A**). This was quantified by the compactness of the LOs, which is defined as the cellular area in proportion to the whole organoid area. Control LOs displayed a higher compactness compared to LOs treated with MSC-CM ($p < 0.01$; **Figure 8B**). These results show that MSC-CM-treated LOs exhibit a lower cellular packing density and higher intercellular space cavities in contrast to control LOs. Moreover, MSC-CM significantly increased the area of EpCAM and RT2-70 antigen expression, as shown by immunofluorescence and the percentage of RT2-70^+ cell area within the LOs ($p < 0.001$; **Figures 9A,B**). This was accompanied by an elevated RT2-70^+ cell number, which increased from 3.90 ± 3.67% (Mean ± SD) in control LOs to 11.78 ± 6.84% in MSC-CM-treated LOs ($p < 0.001$; **Figure 9B**). While we could not detect T1α using the antibody RT1-40 in LOs at 15 div, staining of LOs treated with MSC-CM showed at least some RT1-40^+ ATI cells (**Figure 9C**). It is open whether this may be due to the four additional days in culture or the change of medium.

DISCUSSION

The study describes the establishment of fetal rat LOs as a relevant *in vitro* model of fetal lung development that allows scientists to replicate and functionally analyze key elements of lung maturation. For the first time, patch clamp

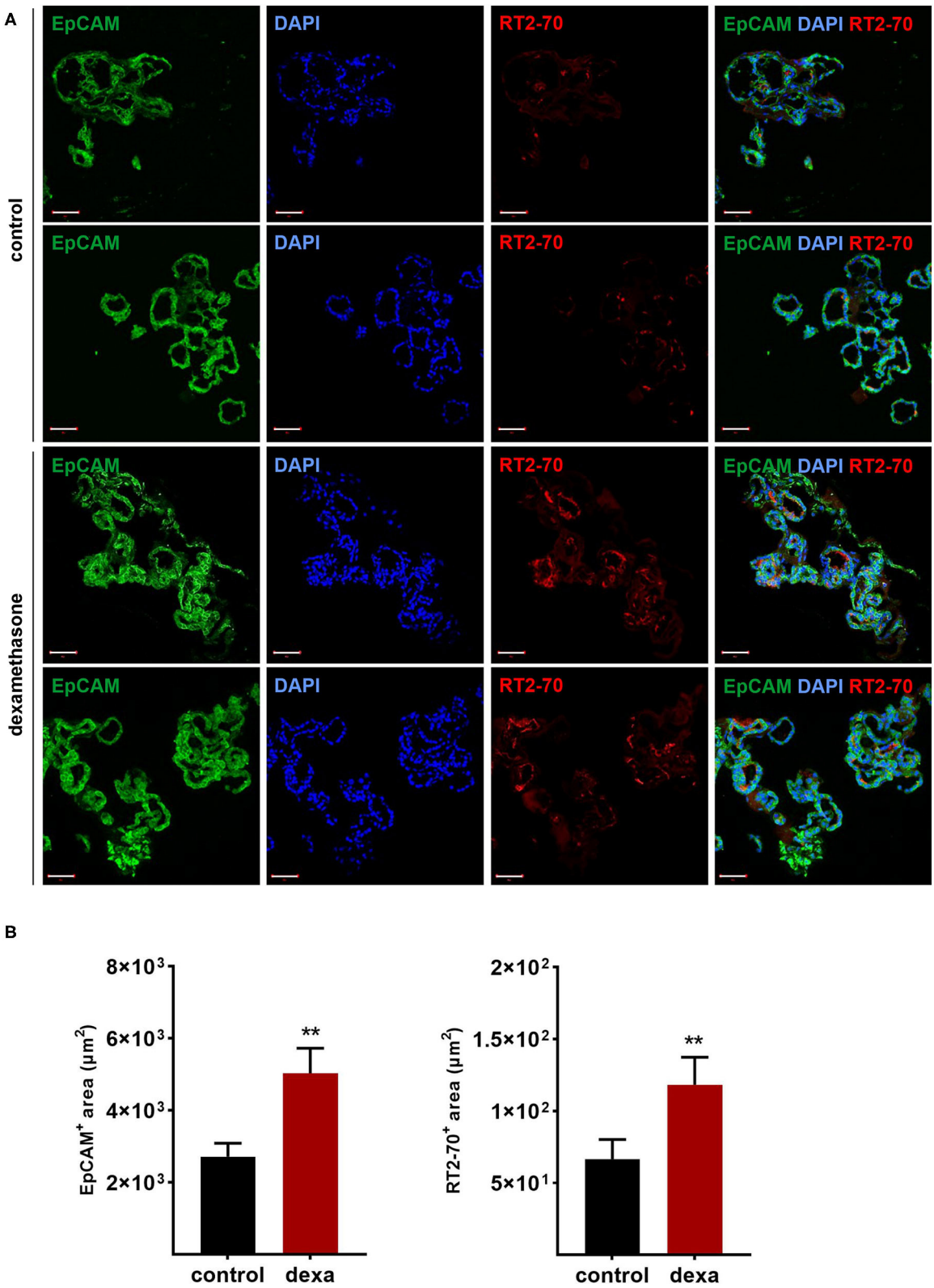

FIGURE 7 | Effects of dexamethasone on fetal LOs. LOs (15 div) were stimulated with dexamethasone (100 nM) for 48 h. Fluorescence images of LO slices were taken by confocal microscopy. **(A)** Organoids were strongly positive for EpCAM expression. Nuclei were stained with DAPI. Some epithelial cells showed luminal expression of the RT2-70 antigen. Scale bar: 50 µm. **(B)** Data are displayed as Mean + SEM. The area of $EpCAM^+$ area and $RT2\text{-}70^+$ area was higher in LOs stimulated with dexamethasone compared to control LOs ($n = 25$; $^{**}p < 0.01$ by Mann-Whitney test). div, days *in vitro*.

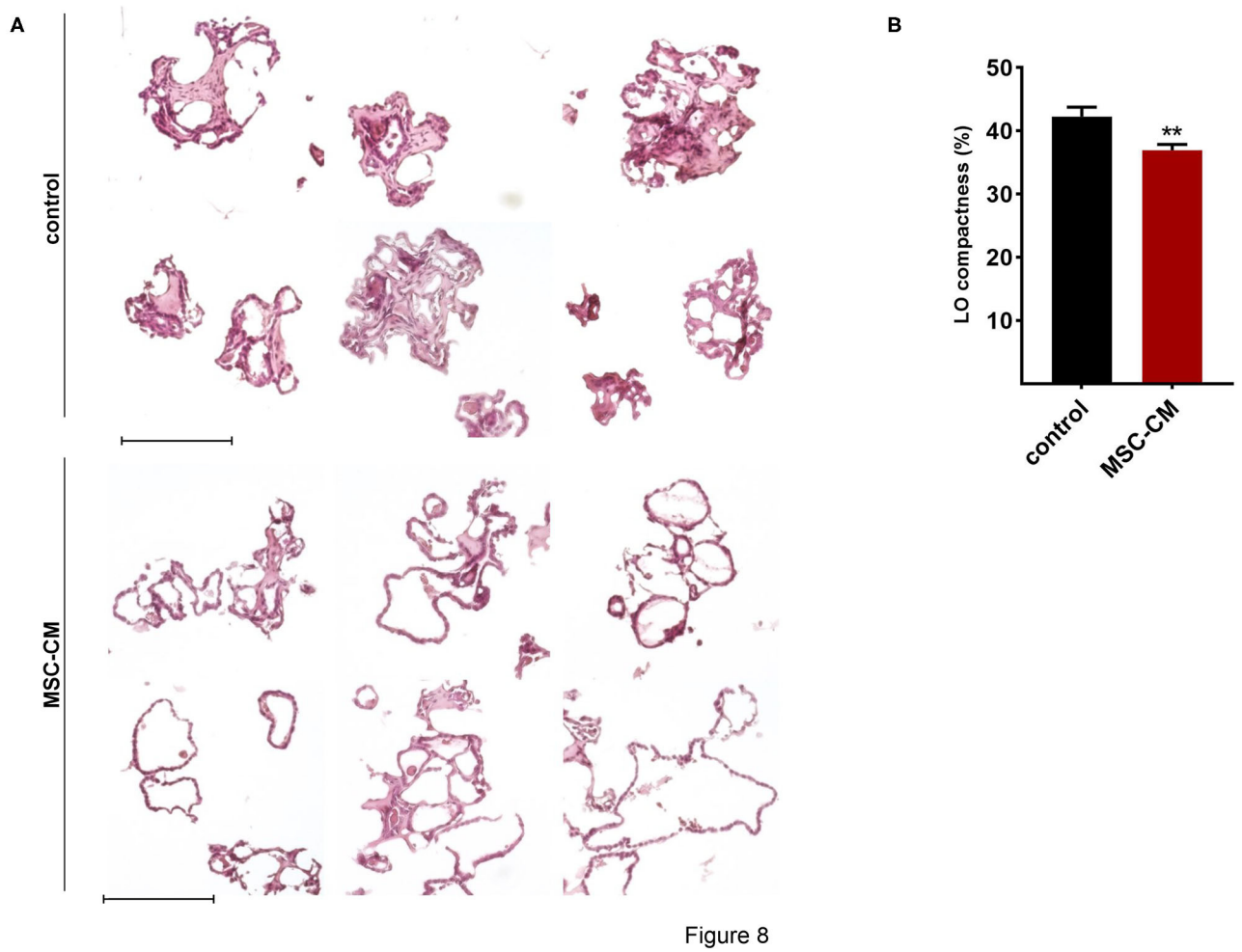

Figure 8

FIGURE 8 | Effects of mesenchymal stem cell-conditioned medium (MSC-CM) on fetal LOs. LOs (15 div) were cultured with MSC-CM for 96 h prior to analysis. **(A)** MSC-CM enhanced lumen formation and thinning of the epithelial layer, in contrast to the denser morphology of control LOs. Scale bar: 200 μm. **(B)** Data are displayed as Mean + SEM. Compactness was higher in control LOs compared to LOs treated with MSC-CM ($n = 56$; $^{**}p < 0.01$ by *T*-test). div, days *in vitro*.

measurement demonstrated single ion channel activity in LOs. The responsiveness of fetal rat LOs to glucocorticoid mimicked the response *in vitro* and *in vivo,* thereby enhancing the relevance of the established model. Furthermore, the response of LOs to MSC-CM demonstrated the convenience of the model to test future therapeutic strategies to enhance maturation of immature lungs.

Even though the first described LOs were created using an undefined cell mix from fetal rat lungs (7), the further development of defined 3D organoid cultures in hydrogels was focusing on mouse and, later, human cells. Defined LOs were successfully generated from mouse and human cells, using primary fetal and adult lung cells as well as pluripotent cells, including embryonic stem cells (ESCs) and induced pluripotent stem cells (iPSCs) (10–12, 24–29). However, the rat is an important animal model and has been widely studied to gain a better understanding of physiological, developmental and pathophysiological mechanisms. Compared to rodent models, the use of human LOs harbors several limitations. Besides the limited availability of fetal lung tissue, its use is highly restricted due to ethical considerations. Similar ethical concerns can be raised for ESCs. ESCs or iPSCs possess great potential to model development and differentiation, but their use is accompanied by the need for a specialized laboratory and technical expertise, the high cost of cell culture, and the long time required for differentiation and production of respective LOs. In contrast, murine LO generation is feasible and can be easily reproduced. Another big obstacle of human fetal lung models and iPSCs is that they cannot be directly compared to the situation *in vivo*, while for rodents a comparison with animal models is possible. This may help to define the possibilities as well as limitations of the different *in vitro* fetal lung models, especially as basis for a future comparison with human fetal lung models. In addition, comparison of *in vivo* validated murine LOs with murine or human LOs from ESCs or iPSCs will show whether LOs from non-lung

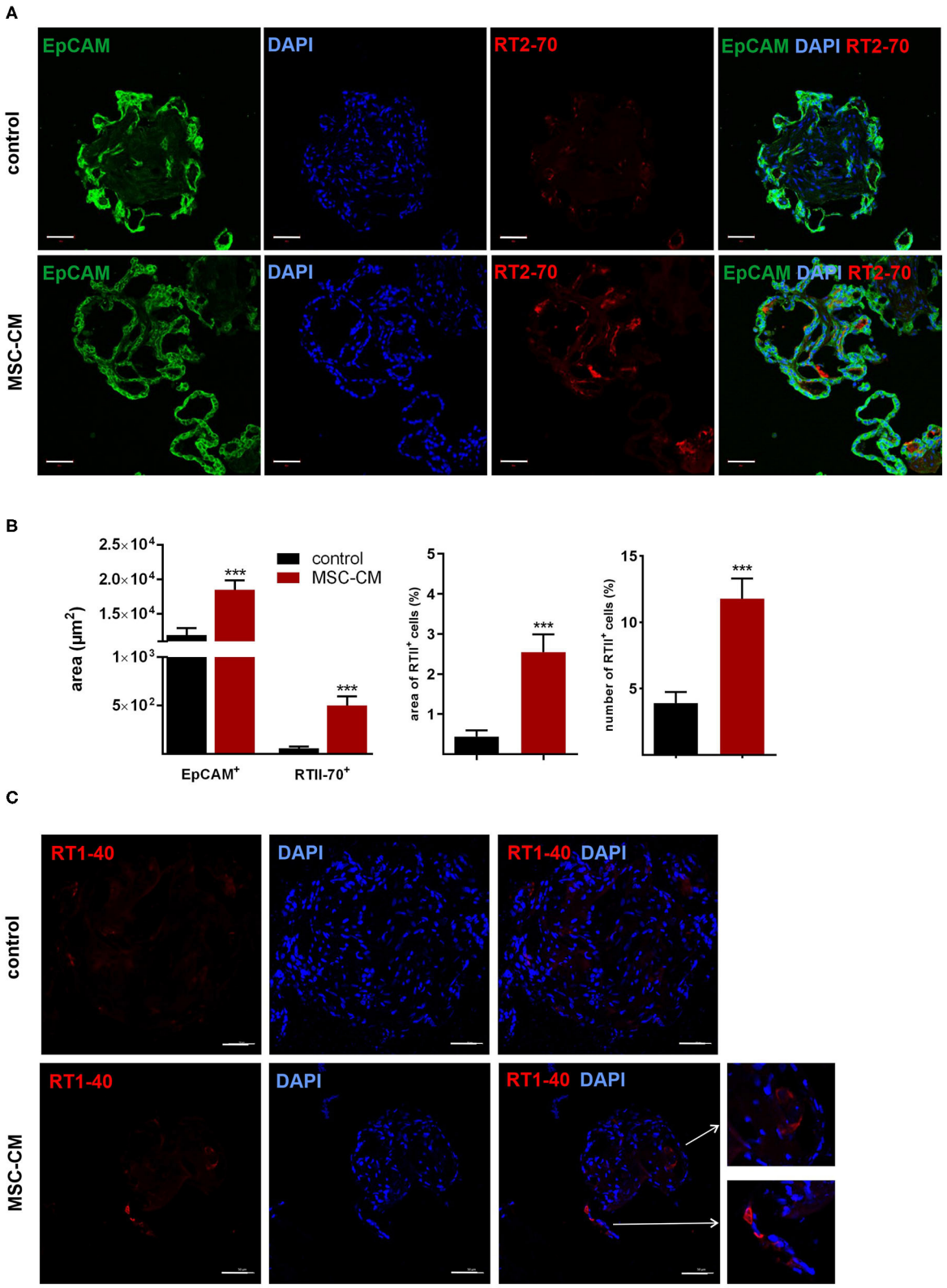

FIGURE 9 | Effects of mesenchymal stem cell-conditioned medium (MSC-CM) on fetal LOs. LOs (15 div) were cultured with MSC-CM for 96 h prior to analysis. Fluorescence images of LO slices were taken by confocal microscopy. **(A)** Organoids were strongly positive for EpCAM expression. Nuclei were stained with DAPI. Some epithelial cells showed luminal expression of the RT2-70 antigen. Scale bar: 50 µm. **(B)** Data are displayed as Mean + SEM. MSC-CM significantly increased

(Continued)

FIGURE 9 | the area of EpCAM and RT2-70 antigen expression, as shown by immunofluorescence and the percentage of RT2-70$^+$ cell area within the LOs ($n = 20$; $^{***}p < 0.001$ by T-test with Welch's correction). Furthermore, RT2-70$^+$ cell numbers were increased by MSC-CM ($n = 20$; $^{***}p < 0.001$ by Mann-Whitney test). **(C)** The ATI cell marker RT1-40 was observed in some individual cells of the MSC-CM-treated LOs. Scale bar: 50 μm. div, days *in vitro*.

sources can reflect essential lung functions and key elements of lung maturation.

Morphological Characterization of Fetal Lung Organoids

During their formation, fetal LOs demonstrated different morphologies of cystic, branched, and mixed appearance. Submerged culture mainly resulted in cystic LOs and cilia activity was observed in some of these cystic LOs. In contrast, ALI culture induced a heterogeneous cystic and branched morphology of LOs. Direct co-culture and interaction between CD31$^+$ and FDLE cells was required for LO formation within 24 h, while indirect co-culture delayed the LO formation and reduced the efficacy. Furthermore, direct co-culture with lung mesenchymal cells like fetal lung fibroblasts as well as human CD31$^+$ cells (HUVEC) could also support LO formation. Endothelial and mesenchymal cells were highly migratory in Matrigel, while FDLE cells did not show active migration. Direct cell-cell contact between endothelial/mesenchymal cells and FDLE cells facilitated initial cell aggregation required for organoid formation. Thus, the effect of helper cells may not be strictly cell-type specific, but rather based on their migratory capacity, and both endothelial and mesenchymal cells can support organoid growth. In addition, paracrine mechanisms might also be involved, since indirect co-culture with helper cells also resulted in, although delayed, LO formation, which is in contrast to FDLE cell-only culture that lacked LO formation. However, a big advantage of endothelial cells is that their proliferation is not supported under LO culture conditions, while mesenchymal cells proliferate and overgrow the whole cell culture. Notably, all cells in the LOs were positive for EpCAM staining, demonstrating that it consisted only of epithelial cells. Since culture conditions involved a rich serum-containing medium in combination with an ECM, CD31$^+$ cells were probably not required as feeder cells, but rather for the 3D assembly of FDLE cells. CD31$^+$ cells were highly migratory and provided early tube-like structures. The culture conditions allowed for formation and long-time persistence of vital LOs, showing only a few dead cells in the periphery. Although, these dead cells were not analyzed, the fact that LOs consisted of EpCAM$^+$ cells only and CD31$^+$ cells were not proliferating, these dead cells could well be leftover CD31$^+$ cells. Concerning the maximal size reached at about 15 div, prior studies demonstrated that the ECM environment (Matrigel in our case) imposes solid stress on the growing organoid. Organoids in a mechanically resistant matrix grow until a growth-inhibitory threshold level of solid stress is attained. This is accompanied by an increase of cellular packing density, decreasing apoptosis with no significant changes in proliferation (30). It is therefore assumed that the maximum LO size depends on the mechanical properties of the ECM used.

Staining of LOs demonstrated the presence of EpCAM$^+$ cells and cells being also positive for RT2-70 or CC-10, which are markers of ATII and Club cells, respectively. The EpCAM$^+$ cells were polarized with the apical side facing the lumen, shown by the apical expression of RT2-70. In contrast to the ATII and Club cell markers, no ATI cells (RT1-40$^+$ = T1α) were observed. T1α is expressed throughout lung morphogenesis although on a low and widespread level. T1α mRNA and protein expression increases during late fetal development and is then restricted to ATI cells in the distal epithelium (31, 32). We assume that the lack of RT1-40 staining in our fetal LOscould be based on an immature differentiation state with low T1α expression. Alveolarization start in rodents at postnatal day 4, while our FDLE cells are isolated at the saccular stage of lung development prior to actual development of alveoli. In our research context this immature LO mimics lung immaturity of fetal infants born prior to the start of alveolarization. We assume that the budding branched luminal structures we observe in the LOs possibly represent sacculi, a precursor which correspond to the later alveolar sacculi. In agreement, fetal rat lung slices of the same gestational age were negative for T1α protein staining, while adult rat lung slices were strongly positive for T1α.

Functional Characterization of Fetal Lung Organoids

Ion channel activity is important for lung growth *in utero* as well as for the perinatal adaptation to air breathing. The analysis of ion channels thus demonstrates a biological function of high physiological relevance with regard to fetal lung maturation. In general, the phenotype of isolated ATII cells under classical culture conditions differs from mature cells *in vivo*. They show differences with regard to cell-cell-communication, expression of tight junctions proteins, barrier function, and general morphology [reviewed by (33)]. Herein we show that fetal LOs represent a physiological model for AFC, as the contributing ion channels can be measured with patch clamp. We demonstrate the presence of ion channels with HSC and NSC channel-like properties in accordance with previous studies of vital lung slices, which showed an average conductance of 8.8 ± 3.2 pS (HSC) and 22.5 ± 6.3 pS (NSC) (34). We observed currents that reverse near 0 mV and exhibit little rectification, which is in contrast to the current-voltage relationship for HSC and NSC channels from ATII cells in primary culture (35). Therein, HSC channels strongly rectify and reverse at high depolarizing potentials, and NSC channels reverse at ∼+40 mV (35). High K^+ concentration in our bathing solution is supposed to depolarize the cell and to establish a resting membrane potential near 0 mV. Thereby the holding potential installed at the pipette should represent the actual patch potential. By their nature NSC channels must reverse at a patch potential of 0 mV, which means that the observed

reversal potential is representative of the membrane potential. Thus, in primary ATII cells the membrane potential is ∼-40 mV, while in our depolarized LOs the membrane potential must be close to 0 mV, equal to the observed reverse potential. The same was reported for vital lung slices, which demonstrated HSC and NSC channels that reverse near 0 mV and HSC channels exhibiting little rectification (35, 36). Possible causes for the differences between cultured primary ATII cells and lung slices have been discussed in detail by the authors (35). It further underlines that LOs more closely represent vital lung tissue in contrast to primary ATII cells, which is important for studying ion transport in alveolar cells. Furthermore, anion channels with properties like ORCC were observed, which possibly contribute to balancing the electroneutrality of Na^+ transport in ATII cells. In our study, we did not aim at thoroughly depicting ion channel activities in fetal LOs, but to demonstrate the biological function and applicability of the model system. According to our observations, fetal LOs constitute a physiological model system to study the single channel activity of the (fetal) alveolar epithelia.

The Stimulating Effects of Dexamethasone and MSCs

After the characterization of LO function, we determined their responsiveness to established lung maturation-inducing hormones. Antenatal glucocorticoids accelerate late-gestation lung maturation in low doses by enhancing surfactant synthesis, increasing the volume density of ATII cells and upregulating AFC (37–39). Mice lacking intracellular glucocorticoid receptors died of respiratory failure shortly after birth (40). Their lung development was retarded, accompanied by a reduction of *ENaC* mRNA levels in total lung RNA (40). Several studies demonstrated the stimulation of *ENaC subunit* expression by glucocorticoids (13, 41). In accordance, dexamethasone strongly increased mRNA expression of all *ENaC subunits* and that of the rate-limiting *Na,K-ATPase* β_1*-subunit* in fetal LO. In contrast, *CFTR* mRNA expression was reduced by dexamethasone as previously shown in FDLE and human bronchial submucosal gland-derived Calu-3 cells (42, 43). Furthermore, dexamethasone stimulated mRNA expression of *Sftpb* and *Sftpc,* confirming the surfactant synthesis-stimulating effect. We complemented the analyses of mRNA expression in LOs with measurements done in our FDLE cell model. The comparison showed a similar increase of *ENaC* and *Na,K-ATPase* mRNA expression induced by dexamethasone. Furthermore, the elevated Na^+ transport and ENaC activity stimulated by dexamethasone was shown in Ussing chamber measurements, demonstrating the relevance of elevated mRNA expression for channel activity. These results confirm the validity of our fetal LO model reproducing the response to glucocorticoids seen *in vitro* and *in vivo.* Furthermore, dexamethasone increased the area of EpCAM and RT2-70 antigen expression, thereby underlining the stimulating effect of glucocorticoids on alveolar differentiation.

Regarding the immature state of lungs from preterm infants, developing and testing new therapeutic strategies is of high clinical relevance. Due to the immunomodulatory and regenerative potential of MSCs, MSC-based cell therapies represent an interesting therapeutic strategy to enhance lung maturation (23). The therapeutic potential of MSCs is mainly attributed to paracrine effects. In accordance, MSC-CM affected LO morphology with an enhanced lumen formation as well as an increased expression of EpCAM and RT2-70. The results showed that up to 15% of the cells expressed the RT2-70 antigen. This is close to the situation *in vivo*, where ATII cells comprise ∼15% of all lung cells, but cover only ∼2–5% of the internal surface area (44). These results suggest an enhanced maturation of LOs induced by MSC-CM, which is in line with a prior study of our group (19). Therein we showed that MSC-CM strongly stimulated functional and structural maturation of fetal lungs. Fetal lung explant growth and branching as well as surfactant protein mRNA expression were enhanced by MSC-CM (19). Furthermore, MSC-CM strongly increased the activity and mRNA expression of *ENaC* and the *Na,K-ATPase* in FDLE cells (19). These effects were at least partially mediated by the PI3-K/AKT (phosphoinositide 3-kinase/protein kinase B) and Rac1 (Ras-related C3 botulinum toxin substrate 1) signaling pathways (19). In agreement, we demonstrated changes in structural maturation in LOs stimulated with MSC-CM, as shown by reduced compactness, increased ATII cell number and area, and first detection of ATI cells. Therefore, results observed in fetal rat lung explants as well as primary FDLE culture were reproduced in fetal LOs, confirming its relevance as a functional *in vitro* model, which can be used to study novel therapeutic developments.

Limitations and Outlook

There are also several limitations of our fetal LOs as an *in vitro* model. An important aspect to consider is the undefined culture condition, which may affect research focused on differentiation and signaling pathways. The culture conditions applied in this study uses FCS and Matrigel, both complex, undefined, and batch-to-batch varying solutions isolated from primary tissue sources of different species, supplying growth factors or basement membrane proteins. Adapting the culture conditions of LOs in the future will possibly enable the generation of more complex co-culture systems to study direct and indirect cellular interactions.

In general, a detailed morphological analysis of fetal rat lung cells and tissues was challenging, since antibodies specific for rat lung tissue are rare. Furthermore, differences in antibody binding between fetal and adult lung tissue were observed and organ specific expression was also seen. Although several studies have shown that the monoclonal antibody RT2-70 is specific for the apical surfaces of rat ATII cells, the respective protein is largely unknown. It is therefore also unknown at which maturational state an ATII cell expresses this unknown protein and whether a lack of expression rules out an ATII cell identity. The target protein is expressed only at the apical membrane compartment, hence only a small area of the cell is stained, but most luminally located cells expressed the RT2-70 antigen. This is in contrast to the EpCAM staining, which can be found on the complete cell surface. Correlating the

area positive for EpCAM to the whole LO area in comparison to the area positive for RT2-70 does not reflect the number of ATII cells and might underestimate the amount of ATII cells in our LOs. Despite these limitations FDLE cells are a physiologically well-characterized *in vitro* model that has been studied with Ussing chambers and patch clamp in addition to mRNA expression analyses. We have determined the effect of glucocorticoids, female and male sex hormones, insulin and many other factors on the maturity of FDLE cells in prior studies (45–49), which enabled us to compare the different *in vitro* fetal lung models and to evaluate if the generated 3D fetal LOs represent a novel *in vitro* model suitable for studies addressing developmental or therapeutic approaches. The FDLE cells are derived from fetal rat pups 24–48 h prior to birth. Studies showed that fetal rat pups born 24 h prior to term birth experience respiratory distress due to structural and functional lung immaturity, reflected in a survival rate of only 6% by 36 h after delivery if the pups were placed in air, which increased to 47% when they were placed in >95% oxygen (4). The authors concluded that the preterm rat is a suitable model for studies of acute and chronic neonatal lung disease, as structural and functional lung immaturity is a major risk factor for pulmonary complications. Due to this and other reports we believe that our model is suitable to study immaturity-associated complications arising from preterm birth.

While the $CD31^+$ cells used in this study were required for an efficient LO formation, their role and interactions seemed to be limited to the first days. It would be interesting to analyze how a combined co-culture of endothelial and mesenchymal cells may further enhance LO differentiation, especially with defined medium and ECM conditions. This could also provide an *in vitro* model to study the effects of inflammation on lung development by either applying proinflammatory stimuli or using a direct or indirect co-culture approach with cells of the innate immune system. Another aspect, which should be considered to enhance LOs as *in vitro* lung model, is the biophysical property of the environment, although this may be more technically challenging to adapt. This includes the defined elastic moduli of hydrogels, the oxygen concentration to present hyperoxia or hypoxia as well as biomechanical stimuli and stress induction by periodical stretching or acute pressure. Despite these limitations and currently unsolved challenges, LOs provide a fast and easy *in vitro* model that allows a faster screening procedure compared to animal models, while also providing a higher biological relevance compared to classical cell culture. LOs will allow for a broad range of manipulation and can be adjusted to the study needs like changing signal pathways using agonists or antagonists, adaption of the physical and chemical properties of the ECM, genetic manipulation of the cells used for LO formation, and/or co-culture with different cell types or pathogens. This could lead to more complex models with multiple and/or sequential impacts to recapitulate fetal and/or newborn lung injuries.

CONCLUSION

In conclusion, LOs generated from FDLE cells represent a fetal lung model that replicates key biological lung functions essential for lung maturation. In detail, the fetal LOs demonstrated the development of fetal lung alveoli, the expression of surfactant proteins, and most importantly the expression and electrophysiological activity of ion channels. For the first time electrophysiological analysis by patch clamp allowed the single cell measurement of ion channel activity in LOs. Furthermore, fetal LOs showed functional responsiveness to glucocorticoids and MSCs. The main goal was to develop an immature LO model to enable the study of maturation and how this can be enhanced to benefit preterm infants in the future. Thus, fetal LOs demonstrated the convenience of the model to test and establish new therapeutic strategies.

DATA AVAILABILITY STATEMENT

The original contributions presented in the study are included in the article/**Supplementary Materials**, further inquiries can be directed to the corresponding author.

ETHICS STATEMENT

The animal study was reviewed and approved by Landesdirektion Leipzig.

AUTHOR CONTRIBUTIONS

ML and CF: conceptualization, formal analysis, funding acquisition, resources, supervision, and writing-original draft. ML, SP, TP, and CF: data curation, investigation, and methodology. ML, SP, and CF: validation. All authors writing-review and editing.

FUNDING

ML and CF were supported by the European Regional Development Fund (EFRE) of the European Community and by funding of the State Saxony (grant numbers 100322373, 100322375, and 100322365).

ACKNOWLEDGMENTS

We wish to thank Jessica Loeffler and Annett Friedrich-Stoeckigt for excellent technical assistance. We acknowledge support from Leipzig University for Open Access Publishing.

SUPPLEMENTARY MATERIAL

The Supplementary Material for this article can be found online at: https://www.frontiersin.org/articles/10.3389/fmed.2021.678438/full#supplementary-material

REFERENCES

1. Barker PM, Gowen CW, Lawson EE, Knowles MR. Decreased sodium ion absorption across nasal epithelium of very premature infants with respiratory distress syndrome. *J Pediatr.* (1997) 130:373–7. doi: 10.1016/S0022-3476(97)70198-7
2. Hilgendorff A, Reiss I, Ehrhardt H, Eickelberg O, Alvira CM. Chronic lung disease in the preterm infant. Lessons learned from animal models. *Am J Respir Cell Mol Biol.* (2014) 50:233–45. doi: 10.1165/rcmb.2013-0014TR
3. Jassal D, Han RN, Caniggia I, Post M, Tanswell AK. Growth of distal fetal rat lung epithelial cells in a defined serum-free medium. *In Vitro Cell Dev Biol.* (1991) 27:625–32. doi: 10.1007/BF02631105
4. Tanswell AK, Wong L, Possmayer F, Freeman BA. The preterm rat: a model for studies of acute and chronic neonatal lung disease. *Pediatr Res.* (1989) 25:525–9. doi: 10.1203/00006450-198905000-00020
5. Kaltofen T, Haase M, Thome UH, Laube M. Male sex is associated with a reduced alveolar epithelial sodium transport. *PLoS ONE.* (2015) 10:e0136178. doi: 10.1371/journal.pone.0136178
6. Lancaster MA, Knoblich JA. Organogenesis in a dish: modeling development and disease using organoid technologies. *Science.* (2014) 345:1247125. doi: 10.1126/science.1247125
7. Zimmermann B, Barrach HJ, Merker HJ, Hinz N. Basement membrane formation and lung cell differentiation *in vitro*. *Eur J Cell Biol.* (1985) 36:66–73.
8. Rannels SR, Yarnell JA, Fisher CS, Fabisiak JP, Rannels DE. Role of laminin in maintenance of type II pneumocyte morphology and function. *Am J Physiol.* (1987) 253(6 Pt 1):C835–45. doi: 10.1152/ajpcell.1987.253.6.C835
9. Paine R, Ben-Ze'ev A, Farmer SR, Brody JS. The pattern of cytokeratin synthesis is a marker of type 2 cell differentiation in adult and maturing fetal lung alveolar cells. *Dev Biol.* (1988) 129:505–15. doi: 10.1016/0012-1606(88)90396-X
10. Lee J-H, Bhang DH, Beede A, Huang TL, Stripp BR, Bloch KD, et al. Lung stem cell differentiation in mice directed by endothelial cells via a BMP4-NFATc1-thrombospondin-1 axis. *Cell.* (2014) 156:440–55. doi: 10.1016/j.cell.2013.12.039
11. McQualter JL, Yuen K, Williams B, Bertoncello I. Evidence of an epithelial stem/progenitor cell hierarchy in the adult mouse lung. *Proc Natl Acad Sci U S A.* (2010) 107:1414–9. doi: 10.1073/pnas.0909207107
12. Barkauskas CE, Cronce MJ, Rackley CR, Bowie EJ, Keene DR, Stripp BR, et al. Type 2 alveolar cells are stem cells in adult lung. *J Clin Invest.* (2013) 123:3025–36. doi: 10.1172/JCI68782
13. Thome UH, Davis IC, Nguyen SV, Shelton BJ, Matalon S. Modulation of sodium transport in fetal alveolar epithelial cells by oxygen and corticosterone. *Am J Physiol Lung Cell Mol Physiol.* (2003) 284:L376–85. doi: 10.1152/ajplung.00218.2002
14. Drakhlis L, Biswanath S, Farr C-M, Lupanow V, Teske J, Ritzenhoff K, et al. Human heart-forming organoids recapitulate early heart and foregut development. *Nat Biotechnol.* (2021) 39:737–46. doi: 10.1038/s41587-021-00815-9
15. Gonzalez RF, Dobbs LG. Isolation and culture of alveolar epithelial Type I and Type II cells from rat lungs. *Methods Mol Biol.* (2013) 945:145–59. doi: 10.1007/978-1-62703-125-7_10
16. Dobbs LG, Pian MS, Maglio M, Dumars S, Allen L. Maintenance of the differentiated type II cell phenotype by culture with an apical air surface. *Am J Physiol.* (1997) 273(2 Pt 1):L347–54. doi: 10.1152/ajplung.1997.273.2.L347
17. Kirwin SM, Bhandari V, Dimatteo D, Barone C, Johnson L, Paul S, et al. Leptin enhances lung maturity in the fetal rat. *Pediatr Res.* (2006) 60:200–4. doi: 10.1203/01.pdr.0000227478.29271.52
18. van der Velden JL, Bertoncello I, McQualter JL. LysoTracker is a marker of differentiated alveolar type II cells. *Respir Res.* (2013) 14:123. doi: 10.1186/1465-9921-14-123
19. Obendorf J, Fabian C, Thome UH, Laube M. Paracrine stimulation of perinatal lung functional and structural maturation by mesenchymal stem cells. *Stem Cell Res Ther.* (2020) 11:525. doi: 10.1186/s13287-020-02028-4
20. Thalheim T, Quaas M, Herberg M, Braumann U, Kerner C, Loeffler M, et al. Linking stem cell function and growth pattern of intestinal organoids. *Dev Biol.* (2018) 433:254–61. doi: 10.1016/j.ydbio.2017.10.013
21. van Haaften T, Byrne R, Bonnet S, Rochefort GY, Akabutu J, Bouchentouf M, et al. Airway delivery of mesenchymal stem cells prevents arrested alveolar growth in neonatal lung injury in rats. *Am J Respir Crit Care Med.* (2009) 180:1131–42. doi: 10.1164/rccm.200902-0179OC
22. Di Bernardo J, Maiden MM, Jiang G, Hershenson MB, Kunisaki SM. Paracrine regulation of fetal lung morphogenesis using human placenta-derived mesenchymal stromal cells. *J Surg Res.* (2014) 190:255–63. doi: 10.1016/j.jss.2014.04.013
23. Laube M, Stolzing A, Thome UH, Fabian C. Therapeutic potential of mesenchymal stem cells for pulmonary complications associated with preterm birth. *Int J Biochem Cell Biol.* (2016) 74:18–32. doi: 10.1016/j.biocel.2016.02.023
24. Dye BR, Hill DR, Ferguson MA, Tsai Y-H, Nagy MS, Dyal R, et al. *In vitro* generation of human pluripotent stem cell derived lung organoids. *Elife.* (2015) 4:e05098. doi: 10.7554/eLife.05098
25. Hegab AE, Arai D, Gao J, Kuroda A, Yasuda H, Ishii M, et al. Mimicking the niche of lung epithelial stem cells and characterization of several effectors of their *in vitro* behavior. *Stem Cell Res.* (2015) 15:109–21. doi: 10.1016/j.scr.2015.05.005
26. Dye BR, Dedhia PH, Miller AJ, Nagy MS, White ES, Shea LD, et al. A bioengineered niche promotes *in vivo* engraftment and maturation of pluripotent stem cell derived human lung organoids. *Elife.* (2016) 5:e19732. doi: 10.7554/eLife.19732
27. Tan Q, Choi KM, Sicard D, Tschumperlin DJ. Human airway organoid engineering as a step toward lung regeneration and disease modeling. *Biomaterials.* (2016) 113:118–32. doi: 10.1016/j.biomaterials.2016.10.046
28. Ng-Blichfeldt J-P, Schrik A, Kortekaas RK, Noordhoek JA, Heijink IH, Hiemstra PS, et al. Retinoic acid signaling balances adult distal lung epithelial progenitor cell growth and differentiation. *EBioMedicine.* (2018) 36:461–74. doi: 10.1016/j.ebiom.2018.09.002
29. McQualter JL, Bertoncello I. Clonal culture of adult mouse lung epithelial stem/progenitor cells. *Methods Mol Biol.* (2015) 1235:231–41. doi: 10.1007/978-1-4939-1785-3_17
30. Helmlinger G, Netti P, Lichtenbeld H, Melder R, Jain R. Solid stress inhibits the growth of multicellular tumor spheroids. *Nat Biotechnol.* (1997) 15:778–83. doi: 10.1038/nbt0897-778
31. Ramirez MI, Millien G, Hinds A, Cao Y, Seldin DC, Williams MC. T1α, a lung type I cell differentiation gene, is required for normal lung cell proliferation and alveolus formation at birth. *Dev Biol.* (2003) 256:62–73. doi: 10.1016/S0012-1606(02)00098-2
32. Nikolić MZ, Caritg O, Jeng Q, Johnson J-A, Sun D, Howell KJ, et al. Human embryonic lung epithelial tips are multipotent progenitors that can be expanded *in vitro* as long-term self-renewing organoids. *Elife.* (2017) 6:e26575. doi: 10.7554/eLife.26575
33. Dobbs LG, Johnson MD. Alveolar epithelial transport in the adult lung. *Respir Physiol Neurobiol.* (2007) 159:283–300. doi: 10.1016/j.resp.2007.06.011
34. Helms MN, Jain L, Self JL, Eaton DC. Redox regulation of epithelial sodium channels examined in alveolar type 1 and 2 cells patch-clamped in lung slice tissue. *J Biol Chem.* (2008) 283:22875–83. doi: 10.1074/jbc.M801363200
35. Trac PT, Thai TL, Linck V, Zou L, Greenlee M, Yue Q, et al. Alveolar nonselective channels are ASIC1a/α-ENaC channels and contribute to AFC. *Am J Physiol Lung Cell Mol Physiol.* (2017) 312:L797–811. doi: 10.1152/ajplung.00379.2016
36. Shlyonsky V, Goolaerts A, Mies F, Naeije R. Electrophysiological characterization of rat type II pneumocytes *in situ*. *Am J Respir Cell Mol Biol.* (2008) 39:36–44. doi: 10.1165/rcmb.2007-0227OC
37. Ballard PL, Ning Y, Polk D, Ikegami M, Jobe AH. Glucocorticoid regulation of surfactant components in immature lambs. *Am J Physiol.* (1997) 273(5 Pt 1):L1048–57. doi: 10.1152/ajplung.1997.273.5.L1048
38. Folkesson HG, Norlin A, Wang Y, Abedinpour P, Matthay MA. Dexamethasone and thyroid hormone pretreatment upregulate alveolar epithelial fluid clearance in adult rats. *J Appl Physiol.* (2000) 88:416–24. doi: 10.1152/jappl.2000.88.2.416
39. Snyder JM, Rodgers HF, O'Brien JA, Mahli N, Magliato SA, Durham PL. Glucocorticoid effects on rabbit fetal lung maturation *in vivo*: an ultrastructural morphometric study. *Anat Rec.* (1992) 232:133–40. doi: 10.1002/ar.1092320115

40. Cole TJ, Blendy JA, Monaghan AP, Krieglstein K, Schmid W, Aguzzi A, et al. Targeted disruption of the glucocorticoid receptor gene blocks adrenergic chromaffin cell development and severely retards lung maturation. *Genes Dev.* (1995) 9:1608–21. doi: 10.1101/gad.9.13.1608
41. Tchepichev S, Ueda J, Canessa C, Rossier BC, O'Brodovich H. Lung epithelial Na channel subunits are differentially regulated during development and by steroids. *Am J Physiol.* (1995) 269(3 Pt 1):C805–12. doi: 10.1152/ajpcell.1995.269.3.C805
42. Prota LFM, Cebotaru L, Cheng J, Wright J, Vij N, Morales MM, et al. Dexamethasone regulates CFTR expression in Calu-3 cells with the involvement of chaperones HSP70 and HSP90. *PLoS ONE.* (2012) 7:e47405. doi: 10.1371/journal.pone.0047405
43. Laube M, Bossmann M, Thome UH. Glucocorticoids distinctively modulate the CFTR channel with possible implications in lung development and transition into extrauterine life. *PLoS ONE.* (2015) 10:e0124833. doi: 10.1371/journal.pone.0124833
44. Dobbs LG. Isolation and culture of alveolar type II cells. *Am J Physiol Lung Cell Mol Physiol.* (1990) 258:L134–7. doi: 10.1152/ajplung.1990.258.4.L134
45. Schmidt C, Klammt J, Thome UH, Laube M. The interaction of glucocorticoids and progesterone distinctively affects epithelial sodium transport. *Lung.* (2014) 192:935–46. doi: 10.1007/s00408-014-9640-3
46. Haase M, Laube M, Thome UH. Sex-specific effects of sex steroids on alveolar epithelial Na+ transport. *Am J Physiol Lung Cell Mol Physiol.* (2017) 312:L405–14. doi: 10.1152/ajplung.00275.2016
47. Laube M, Küppers E, Thome UH. Modulation of sodium transport in alveolar epithelial cells by estradiol and progesterone. *Pediatr Res.* (2011) 69:200–5. doi: 10.1203/PDR.0b013e3182070ec8
48. Laube M, Riedel D, Ackermann B, Haase M, H Thome U. Glucocorticoids equally stimulate epithelial Na+ transport in male and female fetal alveolar cells. *Int J Mol Sci.* (2019) 21:57. doi: 10.3390/ijms21010057
49. Mattes C, Laube M, Thome UH. Rapid elevation of sodium transport through insulin is mediated by AKT in alveolar cells. *Physiol Rep.* (2014) 2:e00269. doi: 10.1002/phy2.269

Conflict of Interest: The authors declare that the research was conducted in the absence of any commercial or financial relationships that could be construed as a potential conflict of interest.

Publisher's Note: All claims expressed in this article are solely those of the authors and do not necessarily represent those of their affiliated organizations, or those of the publisher, the editors and the reviewers. Any product that may be evaluated in this article, or claim that may be made by its manufacturer, is not guaranteed or endorsed by the publisher.

Copyright © 2021 Laube, Pietsch, Pannicke, Thome and Fabian. This is an open-access article distributed under the terms of the Creative Commons Attribution License (CC BY). The use, distribution or reproduction in other forums is permitted, provided the original author(s) and the copyright owner(s) are credited and that the original publication in this journal is cited, in accordance with accepted academic practice. No use, distribution or reproduction is permitted which does not comply with these terms.

frontiers in Pediatrics

ORIGINAL RESEARCH
published: 01 October 2021
doi: 10.3389/fped.2021.667094

Wheezing Characteristics and Predicting Reactivity to Inhaled β2-Agonist in Children for Home Medical Care

Chizu Habukawa[1], Naoto Ohgami[2], Takahiro Arai[3], Haruyuki Makata[4], Tomoki Nishikido[5], Morimitsu Tomikawa[6] and Katsumi Murakami[7]*

[1] Department of Pediatrics, Minami Wakayama Medical Center, Tanabe, Japan, [2] Technology Development HQ, Omron Healthcare Co., Ltd., Muko, Japan, [3] Arai Pediatric Clinic, Yamagata, Japan, [4] Makata Pediatrics and Allergy Clinic, Yamaguchi, Japan, [5] Osaka Women's and Children's Hospital, Izumi, Japan, [6] Odasaga Pediatrics and Allergy, Sagamihara, Japan, [7] Department of Psychosomatic Medicine, Sakai Sakibana Hospital, Sakai, Japan

OPEN ACCESS

Edited by:
Niki Ubags, Centre Hospitalier Universitaire Vaudois, Switzerland

Reviewed by:
Kelechi Benjamin Ugonna, Sheffield Children's Hospital, United Kingdom
Manuel Sanchez-Solis, University of Murcia, Spain

***Correspondence:**
Chizu Habukawa
gd6c-hbkw@asahi-net.or.jp

Specialty section:
This article was submitted to Pediatric Pulmonology, a section of the journal Frontiers in Pediatrics

Received: *12 February 2021*
Accepted: *27 August 2021*
Published: *01 October 2021*

Citation:
Habukawa C, Ohgami N, Arai T, Makata H, Nishikido T, Tomikawa M and Murakami K (2021) Wheezing Characteristics and Predicting Reactivity to Inhaled β2-Agonist in Children for Home Medical Care. Front. Pediatr. 9:667094. doi: 10.3389/fped.2021.667094

Background: Given that wheezing is treated with inhaled β2-agonists, their effect should be reviewed before the condition becomes severe; however, few methods can currently predict reactivity to inhaled β2-agonists. We investigated whether preinhalation wheezing characteristics identified by lung sound analysis can predict reactivity to inhaled β2-agonists.

Methods: In 202 children aged 10–153 months, wheezing was identified by auscultation. Lung sounds were recorded for 30 s in the chest region on the chest wall during tidal breathing. We analyzed the wheezing before and after β2-agonist inhalation. Wheezing was displayed as horizontal bars of intensity defined as a wheeze power band, and the wheezing characteristics (number, frequency, and maximum intensity frequency) were evaluated by lung sound analysis. The participants were divided into two groups: non-disappears (wheezing did not disappear after inhalation) and disappears (wheezing disappeared after inhalation). Wheezing characteristics before β2-agonist inhalation were compared between the two groups.

The characteristics of wheezing were not affected by body size. The number of wheeze power bands of the non-responder group was significantly higher than those of the responder group ($P < 0.001$). The number of wheeze power bands was a predictor of reactivity to inhaled β2-agonists, with a cutoff of 11.1. The 95% confidence intervals of sensitivity, specificity, and positive and negative predictive values were 88.8, 42, 44, and 81.1% ($P < 0.001$), respectively.

Conclusions: The number of preinhalation wheeze power bands shown by lung sound analysis was a useful indicator before treatment. This indicator could be a beneficial index for managing wheezing in young children.

Keywords: wheezing, young children, lung sound analysis, β2-agonists, wheeze analysis

INTRODUCTION

In the medical field, technical innovation has engendered telemedicine and home-based therapy; however, the practical use of these technologies has been limited. For respiratory diseases, lung sounds represent simple physical data, which have no value by themselves and are only clinically important when evaluated by a physician (1–3).

Appropriate judgment of lung sound data by specialists is required, especially when determining the patient's response to treatment, which constitutes important information in telemedicine. Acute exacerbation typically occurs at night and needs to be treated promptly; therefore, caregivers need to cope with the symptoms of this acute exacerbation. For parents, properly managing these exacerbations in young children is challenging, especially in infants. At present, there is no specific tool or criterion for treating these exacerbations.

Wheezing is a typical sign of respiratory exacerbation in individuals of all ages. Wheezing that occurs repeatedly over prolonged periods is an important factor in the diagnosis of bronchial asthma. Some young children with recurrent wheezing do not exhibit asthma (4, 5). Wheezing episodes in young children should initially be treated with inhaled short-acting beta-2 (β2) agonists, regardless of whether a clinical diagnosis of asthma has been made (6). According to international guidelines, initial treatment provided at home should comprise an inhaled β2-agonist, and the effect should be reviewed before the condition becomes severe (6). Physicians usually judge reactivity of inhaled β2-agonist by whether wheezing sounds disappear or do not disappear after inhaling the β2-agonist. Accurately evaluating a child's reactivity to inhaled β2-agonists at home is therefore challenging for parents/caregivers. There are currently few methods for predicting the effects of inhaled β2-agonists on wheezing in young children.

Wheezing is an important physical sign of worsening respiratory conditions that can be auscultated using a stethoscope (7–9). Recent developments in signal processing methods have improved the extraction of physiologically and clinically relevant information from a lung sound analysis (10–12), a noninvasive method that does not require the infant's cooperation and is useful in objectively evaluating wheezing. A number of studies have evaluated the severity of airway obstruction by assessing the particular characteristics of wheezing (13, 14).

However, wheezing characteristics have not yet been adequately analyzed to establish their association with reactivity to inhaled β2-agonists in exacerbations. Our aim is to develop a home medical device to evaluate the wheezing condition. In this study, we investigated (as an objective index) whether preinhalation wheezing characteristics, detected by lung sound analysis, could predict reactivity to inhaled β2-agonists in children, including infants.

MATERIALS AND METHODS

Participants

All participants were outpatients from the Arai Pediatric Clinic, Makata Pediatrics and Allergy Clinic, Osaka Women's and Children's Hospital, Odasada Pediatrics and Allergy, or Minami Wakayama Medical Center in Japan, who were brought to each of these hospitals to treat recurrent wheezing, cough, and dyspnea. All participants had more than 3 episodes of wheezing and were diagnosed with asthma according to the Japanese pediatric guidelines for the treatment and management of asthma (6). The exclusion criteria included the presence of respiratory syncytial virus infection, human metapneumovirus infection, chronic wheezing diseases, laryngomalacia, whooping cough, immunodeficiency, and cardiac and neonatal pulmonary problems. These diagnoses were evaluated by a pediatrician who specializes in childhood respiratory and allergic diseases.

The required number of samples was 41, with an AUC of 0.8, a power of 0.95, and a one-sided test (*R* version 3.4.1 software). The study population comprised 202 pediatric outpatients (median age, 19.9 months; range, 10–153 months; male/female ratio, 107/95). Written informed consent was obtained from the parents or legal guardians of all participants, and the study protocol was approved by the Minami Wakayama Medical Center's ethics committee [approval number 2016–22 (2)].

Study Design

All participants exhibited audible wheezing during tidal breathing, as observed by auscultation. Lung sounds were recorded for 30 s in the upper right anterior chest region at the second intercostal space and at the midclavicular line on the chest wall during tidal breathing. The lung sounds, including wheezing, were identified and independently confirmed by each specialist physician who recorded the wheezing according to previous methods (15). A total of 197 participants, for whom data were available, were examined to evaluate heart rate and oxygen saturation. Information regarding symptom exacerbation, including wheezing, coughing, heavy breathing, reduced activity, shortness of breath, and sleep disturbance was obtained from the parents or legal guardians.

Thereafter, all participants were treated with inhaled β2-agonists (10–30 μg of procaterol and 2.0 ml of saline) (6, 16). The study physicians auscultated and recorded the lung sounds simultaneously 15 min after the β2-agonist inhalation (12, 15). All participants were treated according to the Japanese pediatric guidelines for the treatment and management of asthma (6).

Wheezing was evaluated to identify changes before and after inhalation via auscultation and lung sound analysis. According to the reactivity to the inhaled β2-agonists, the participants were divided into two groups: non-disappear and disappear. Participants whose wheezing disappeared after inhaling β2-agonists were assigned to the disappear group, whereas those whose wheezing did not disappear after inhaling β2-agonists were assigned to the non-disappear group.

We compared the physical signs, including heart rate, oxygen saturation, and participant characteristics between the two groups. The wheezing characteristics before inhaling β2-agonists were compared between the two groups as described below.

Sound Recording and Sound Analysis

Figure 1 shows a block diagram of the equipment employed in the lung sound recordings (17). The sound recording

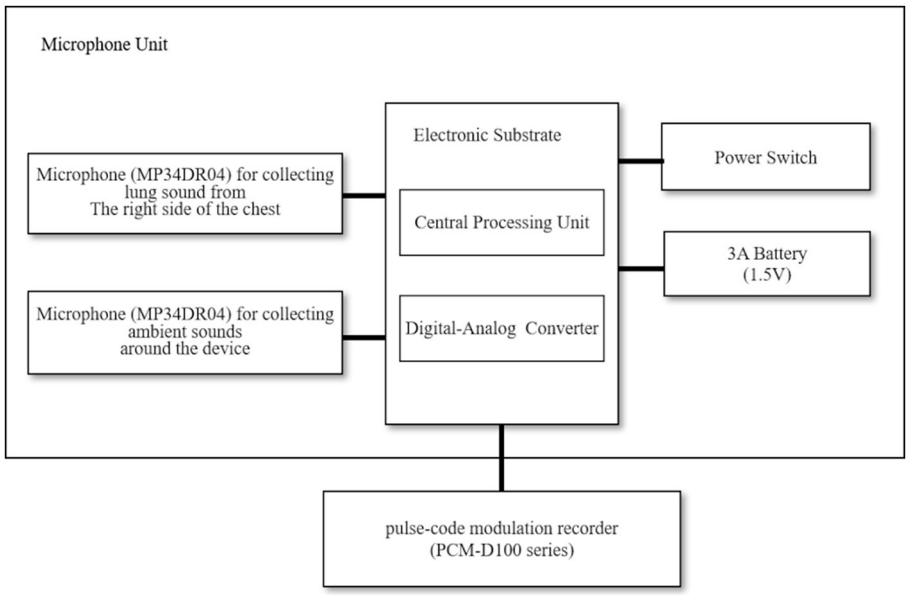

FIGURE 1 | Block diagram showing the equipment used for lung sound recording.

system consisted of a handheld assembled microphone unit (prototype device, Omron Healthcare Corporation, Ltd., Kyoto, Japan) and a pulse-code modulation recorder (PCM-D100 series, Sony Corporation, Tokyo, Japan). Two microphones (MP34DR04, STMicroelectronics, Geneva, Switzerland) were set in the microphone unit; one collected ambient sounds around the device, while the other collected lung sounds from the right side of the chest. We resampled the lung sounds at 44.1-kHz with 16-bit quantization, performing a 4,096-point fast Fourier transformation using sound analysis software (Adobe Audition CC 2018, Adobe Inc., San Jose, CA, United States).

Figure 2 shows a sample of the spectrogram and spectrum of the wheezing sounds (17). Prior to the sound analysis, engineering researchers and two trained physicians evaluated all recordings. The recorded lung sounds were reviewed to discriminate wheezes from other sounds, such as noises generated due to friction between the microphone and the participants' skin. We detected wheezing on the sound spectrograms as defined by the Computerized Respiratory Sound Analysis (CORSA) guidelines. A wheeze is defined as a continuous adventitious musical sound. Acoustically, it is characterized by periodic waveforms with a dominant frequency typically over 100 Hz and lasting over 100 ms (18).

Wheezing Indexes

The lung sound analysis is displayed as horizontal bars of intensity with corresponding sharp peaks of power. The sharp peak of power was defined as a wheeze power band (**Figure 2A**) (17, 19–21). Wheezing was analyzed during both inspiratory and expiratory periods in each recorded file according to the six indexes explained below.

Number of Wheeze Power Bands per 30s

We counted the number of wheeze power bands per 30s in each file (17).

Lowest Frequency of Wheeze Power Bands

We calculated the lowest frequencies of all wheeze power bands as described above (**Figure 2B**) (17).

Highest Frequency of Wheeze Power Bands

We recorded the highest frequency that could be recognized on the spectrogram (**Figure 2B**) (17), as well as the highest frequencies of all wheeze power bands in each file, and calculated the mean frequencies of all wheeze power bands from the individual data.

Maximum Intensity Frequency of Wheeze Power Bands

We recorded the maximum intensity frequency of all wheeze power bands (20, 21) and calculated the mean frequency of the wheeze power bands' maximum intensity for each recorded file (**Figure 2C**) (17).

Statistical Analysis

The correlation coefficients between age, weight, and height with sound variables were determined using Pearson's correlation coefficient.

We performed the statistical analyses using STATFLEX ver. 6.0 (Artec Co., Ltd., Osaka, Japan). The wheezing indexes and participant characteristics are presented as the mean ±

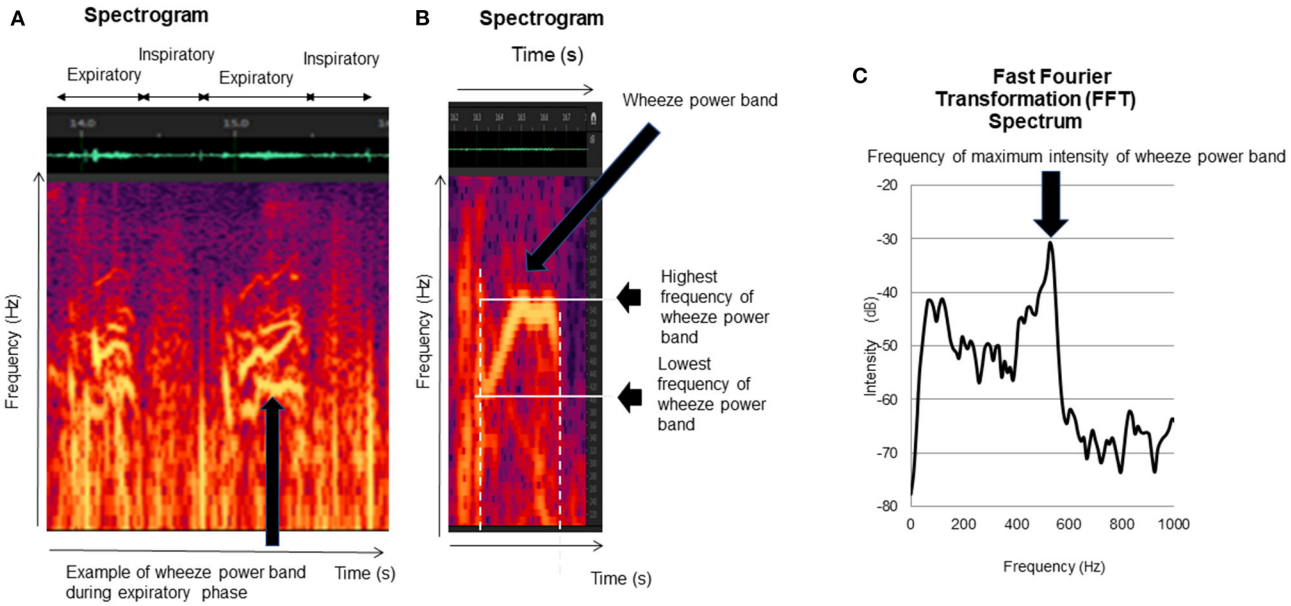

FIGURE 2 | Wheezing indexes. The lung sound analysis displayed wheezes as horizontal bars of intensity with corresponding sharp peaks of power. The sharp peak of power was defined as a wheeze. The following indexes were calculated: (1) duration of wheeze power bands **(B)**, (2) number of wheeze bands per 30s **(B)**, (3) lowest frequency of wheeze power bands **(B)**, (4) highest frequency of wheeze power bands **(B)**, and (5) frequency of maximum intensity of wheeze power bands **(C)**.

standard deviation. We compared the participant characteristics and wheezing indexes between the two groups using an unpaired *t*-test.

We calculated the sensitivity (true-positive rate), specificity (true-negative rate), positive predictive value, negative predictive value, and positive and negative likelihood ratios (the probability of symptom exacerbation according to the wheezing index cutoff value), and we used a receiver operating characteristic curve to describe the relationship between the sensitivity and specificity of the various cutoff values (wheezing index) as reactivity to the inhaled β2-agonists.

We also calculated the area under the curve (AUC) for all possible cutoff values of the highest frequency of the wheeze power bands. $P < 0.05$ were considered statistically significant. The confidence interval of the data analyzed was 95%.

RESULTS

Differences in Participant Characteristics

Table 1 lists the participant characteristics and respiratory statuses of the two groups. Except for heart rate, there were no significant differences between the two groups.

TABLE 1 | Participants' characteristics and respiratory statuses of the two groups.

	Disappear Group ($n = 91$)	Nondisappear Group ($n = 111$)	*P-value*
Age, month (Range)	51.5 ± 41.2 (10∼151)	48.8 ± 34.0 (10∼153)	0.62
Sex (M/F)	43/48	64/47	0.09
Height, cm	98.6 ± 21.8	97.4 ± 18.9	0.70
Weight, kg	16.4 ± 8.2	16.4 ± 8.4	0.87
Food allergy (positive %)	81.0%	93.8%	0.27
House dust and/or Mice allergy (positive %)	87.5%	63.3%	0.18
Total IgE, IU/ml	944.7 ± 815.5	971.8 ± 109.1	0.37
SaO_2, %	98.0 ± 1.4	97.7 ± 1.5	0.30
Heart rate, bpm	107.3 ± 26.1	121.8 ± 17.8	* 0.008
Respiratory rate, /min	31.0 ± 14.1	30.6 ± 10.8	0.86

**P-values of <0.01 was considered statistically significant. Values are presented as mean ± standard deviation. IgE, immunoglobulin E; SaO_2, oxygen saturation.*

Correlations of the Wheezing Indexes With Age, Height, and Weight

All the wheezing indexes were not significantly affected by age, height, and weight (**Table 2**). The respiratory cycle was not significantly correlated with all the wheezing indexes.

Comparison of the Wheeze Power Band Duration

No significant differences were observed in the duration of wheeze power bands between the two groups ($P = 0.09$). The duration of the wheeze power bands in the disappear group was 338.9 ± 202.7 ms, whereas that of the non-disappear group was 398.3 ± 205.9 ms.

TABLE 2 | *P*-values of correlations of the wheezing indexes with age, height, and weight.

	Age (month)	Height(cm)	Weight (kg)	Respiratory Rate(breaths /min)
Number of wheeze power bands per 30 s	0.04	0.04	0.08	0.17
Highest frequency of wheeze power bands (Hz)	0.07	0.03	0.01	0.007
Lowest frequency of wheeze power bands (Hz)	0.18	0.14	0.14	0.04
Maximum intensity frequency of the wheeze power bands (Hz)	0.18	0.13	0.11	0.04

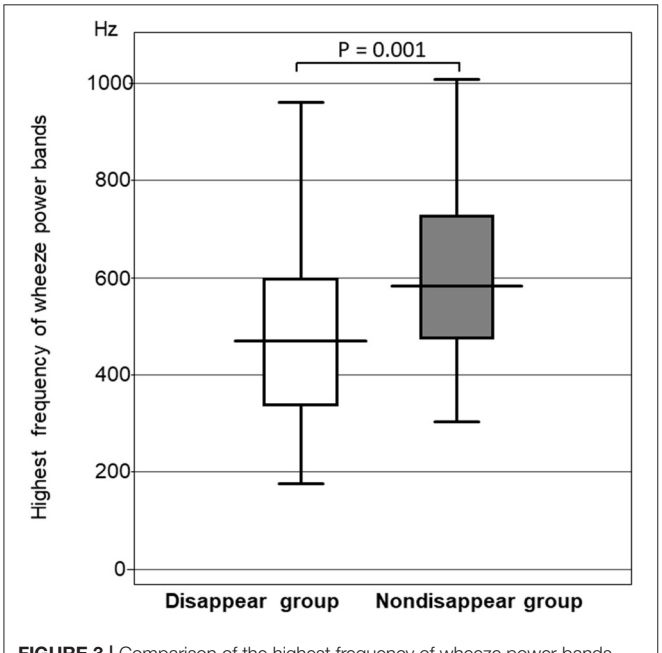

FIGURE 3 | Comparison of the highest frequency of wheeze power bands between the two groups.

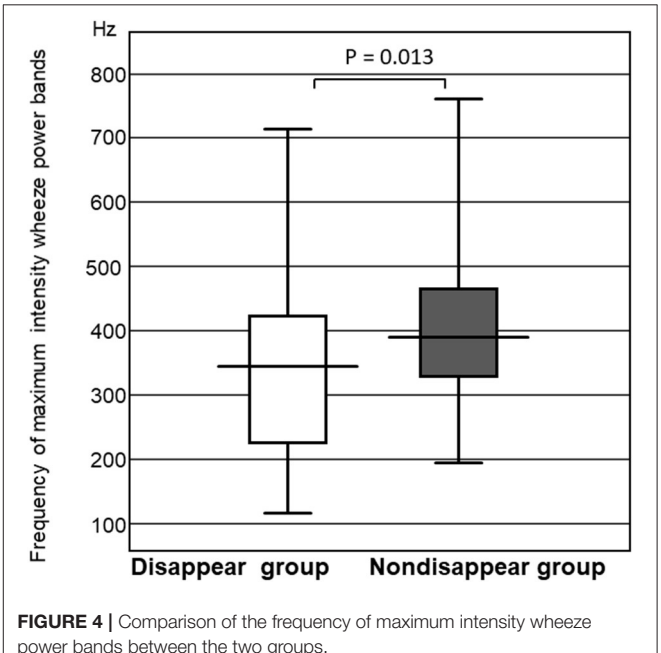

FIGURE 4 | Comparison of the frequency of maximum intensity wheeze power bands between the two groups.

Comparison of the Highest Frequency of the Wheeze Power Bands

The highest frequency of the wheeze power bands was significantly higher in the non-disappear group than in the disappear group ($P = 0.0014$). The highest frequency of the wheeze power bands in the non-disappear group was 592.6 ± 223.4 Hz, whereas that of the disappear group was 460.8 ± 220.1 Hz (**Figure 3**).

Comparison of the Lowest Frequency of the Wheeze Power Bands

No significant differences were observed between the two groups in the lowest frequency of the wheeze power bands ($P = 0.23$). The lowest frequency of the wheeze power bands in the non-disappear group was 235.2 ± 106.8 Hz, whereas that of the disappear group was 210.3 ± 144.6 Hz.

Comparison of the Maximum Intensity Frequency of the Wheeze Power Bands

The frequency of the wheeze power bands was significantly higher in the non-disappear group than that of the disappear group ($P = 0.013$). The maximum intensity frequency of the wheeze power bands in the non-disappear group was 396.1 ± 136.7 Hz, whereas that of the disappear group was 331.3 ± 175.7 Hz (**Figure 4**).

Comparison of the Number of Wheeze Power Bands per 30s

Figure 5 shows that the number of wheeze power bands per 30s for the non-disappear group was larger than that of the disappear group ($P = 0.0001$). The number of wheeze power bands per 30s was 9.8 ± 7.3 for the non-disappear group and 4.1 ± 5.3 for the disappear group.

Receiver Operating Characteristic Curve Analysis in Response to Inhaled β2-Agonists With Respect to the Number of Wheeze Power Bands per 30s

The cutoff value for the number of wheeze power bands per 30 s that could predict a response to the inhaled β2-agonists was 11.1. The 95% confidence intervals of sensitivity, specificity, positive and negative predictive values, and positive and negative likelihood ratios were 88.8, 42, 44, and 81.1%, and 1.53 and 0.27 ($P < 0.001$), respectively, with an AUC of 0.72 ± 0.03 (**Figure 6**).

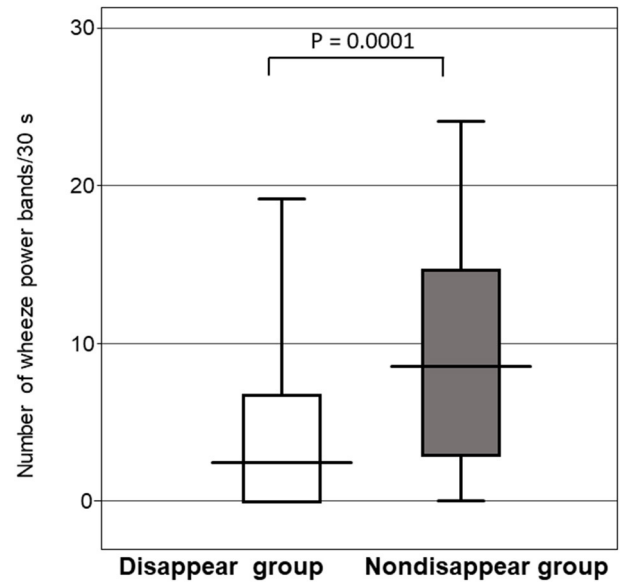

FIGURE 5 | Comparison of the number of wheeze power bands per 30 s between the two groups. Horizontal line indicates the response to the inhaled β2-agonist, and the error bars indicate the standard deviation.

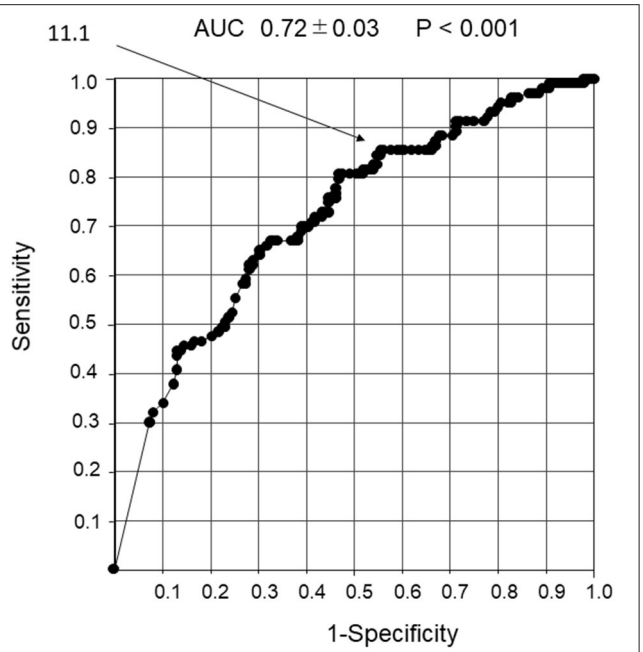

FIGURE 6 | Receiver operator characteristic curve analysis in response to the β2-agonist inhalation with the number of wheeze power bands per 30 s. Detection of non-response to inhaled β2-agonist using the number of wheeze power bands per 30 s. An ROC curve analysis was performed to determine the response to inhaled β2-agonist with the number of wheeze power bands per 30 s. The cutoff value for the number of wheeze power bands per 30 s that could predict reactivity to the inhaled β2-agonist was 11.1.

DISCUSSION

In the present study, the characteristics of preinhalation wheezing could predict reactivity to inhaled β2-agonists. We found that the number of preinhalation wheeze power bands was a predictor of reactivity to inhaled β2-agonists and a useful indicator of prolonged exacerbation risk. None of the wheezing characteristics were affected by height, weight, or age. Noninvasively and objectively predicting the reactivity to inhaled β2-agonists before administering treatment is crucial for managing wheezing in children. Understanding the differences in the characteristics of wheezing can be beneficial for administering treatment and managing children with asthma for remote medical care that children cannot go to hospital when they afraid catch some virus infection using home medical device which we developed (22).

Wheezing is a continuous adventitious lung sound that is superimposed on breathing sounds. According to the definitions in the present CORSA guidelines, the maximum frequency of a wheeze is typically >100 Hz, and its duration is >100 ms (19–21). Baughman and Loudon reported that wheezing was also associated with a peak in the signal and that peak amplitude constituted a criterion for classifying the sound as a wheeze. Wheezing was displayed as horizontal bars of intensity with corresponding sharp peaks of power, known as wheeze power bands (23). Using lung sound analysis, we found that the wheezing of non-disappear group had certain wheeze power band characteristics, such as higher number, higher frequency, and higher frequency at maximum intensity.

Several studies have reported the association between wheezing characteristics and lung function, with one study showing that expiratory wheezing had high respiratory resistance in infants (14).

For the frequency and intensity of wheezing, Shim and Williams found that high frequency, louder, and longer wheezing were associated with a lower peak expiratory flow rate. Loudness and high frequency wheezing are associated with more severe obstruction (24). The degree of bronchospasm (abnormal muscle contraction in the bronchi walls, causing airway obstruction) is related to the frequency of wheezing sound signals, rather than the wheezing intensity (25). Our data correspond with this suggestion.

Based on the number of wheeze power bands, wheezing is divided into two categories according to international guidelines' best-known signs of airway obstruction: monophonic and polyphonic (9). Wheezing is considered monophonic when only one pitch is heard and polyphonic when multiple frequencies are simultaneously perceived. Polyphonic wheezing involves more severe bronchial constriction than monophonic wheezing (3, 17, 18). Wheezing is considered monophonic when there is only a peak intensity of one frequency and polyphonic when numerous peak intensities of varying frequencies are perceived simultaneously by the lung sound analysis. In other words, monophonic wheezes have one

wheeze power band, while polyphonic have multiple wheeze power bands, thereby indicating that polyphonic wheezing involves more severe bronchial constriction that monophonic wheezing (9, 24, 25). The number of wheeze bands in patients with polyphonic wheezing was greater than that of patients with monophonic wheezing. Moreover, patients with more wheeze bands have a greater risk of exacerbation (9, 19–21).

In our study, the non-disappear group had more wheeze power bands than the disappear group. In other words, the patients in the non-disappear group believed that they had a more severe airway obstruction. The study subjects were young children with a mean age of 19.9 months who had bronchial asthma and viral lower respiratory tract infections associated with asthma. In our subjects, the cause of airway obstruction could be a combination of airway inflammation and airway spasm, and the treatment response to bronchodilator inhalation therapy might have been different.

For home treatment, parents use bronchodilator inhalation to prevent exacerbations even when it is difficult to identify whether the wheezing is due to an asthma attack or a viral infection associated with asthma. The cutoff value for wheeze power bands was set to have low specificity but high sensitivity so that parents do not overlook signs of deterioration. Thus, wheeze power bands may be a useful index for avoiding the risk of future deterioration of respiratory status because the therapeutic effect can be predicted before inhalation of bronchodilators regardless of the cause of wheezing.

Gavriely et al. employed a wheeze-detection device for overnight nocturnal monitoring to assess asthma activity in symptomatic school-aged children (26). Although wheezing monitoring is useful for asthma management, it is difficult to record wheezing overnight in young children, particularly in infants, because they cannot endure being attached to a monitor for a long period, and it is difficult for the family to manage and prevent the microphone from becoming dislodged. It is therefore important to perform the examination in young children within a short period. Furthermore, it would be more useful for the family to have knowledge of the characteristics of preinhalation wheezing so they can predict reactivity to inhaled β2-agonists. However, it should be noted that this study had the limitation that the participants with severe airway obstruction did not demonstrate any audible lung sounds (known as "silent chest").

Wheezing characteristics are presumably associated with bronchial obstruction. To date, there have been no reports regarding how the preinhalation characteristics of wheezing can predict reactivity to inhaled β2-agonists. The number of preinhalation wheeze power bands assessed by lung sound analysis was a useful indicator for predicting reactivity to inhaled β2-agonists of airway obstruction in younger children. The study subjects all had mild asthma attacks. As shown in **Table 1**, SaO_2 did not decrease in the non-disappear group, and only heart rate increased as compared with that in the disappear group. However, no significant differences were found in SaO_2 and respiratory rates during the stable respiratory state. The number of power band was a highly sensitive index predictive exacerbation even in mild attacks with increased heart rate and before decreased SaO_2. This information can be obtained before treatment using a noninvasive method and a 30-s assessment. The results could be useful for managing wheezing in young children with mild to moderate attack, by physicians, parents, and legal guardians.

Lung sound analysis can noninvasively detect detailed characteristics of wheezing in young children, including infants. The number of wheeze power bands before inhalation may be a predictor of responsiveness to bronchodilator inhalation, regardless of asthma or virus infection in children, including infants.

In home treatment, even when the cause of wheezing is unclear, either asthma attack or concomitant viral infection, the therapeutic effect of bronchodilator inhalation can be predicted and considered as an index for avoiding the risk of exacerbation.

DATA AVAILABILITY STATEMENT

The raw data supporting the conclusions of this article will be made available by the authors, without undue reservation.

ETHICS STATEMENT

The studies involving human participants were reviewed and approved by Yoshinori Nakamura, Minami Wakayama Medical Center's ethics committee. Written informed consent to participate in this study was provided by the participants' legal guardian/next of kin. Written informed consent was obtained from the individual(s), and minor(s)' legal guardian/next of kin, for the publication of any potentially identifiable images or data included in this article.

AUTHOR CONTRIBUTIONS

CH was the guarantor of the manuscript. CH and KM conceived, designed the study, analyzed, and interpreted the data. CH, TA, HM, TN, and MT collected the data. CH prepared the manuscript. All authors approved the final version of the manuscript. Omron Healthcare Co., Ltd. had no such involvement.

FUNDING

The authors declare that this study received funding from Omron Healthcare Co., Ltd. The funder was not involved in the study design, collection, analysis, interpretation of data, the writing of this article or the decision to submit it for publication.

ACKNOWLEDGMENTS

The authors express their immense gratitude to the children and parents who consented to participate in this study.

REFERENCES

1. Aliverti A. Wearable technology: role in respiratory health and disease. *Breathe.* (2017) 13:e27–36. doi: 10.1183/20734735.008417
2. Zhang J, Ser W, Yu J, Zhang TT. A novel wheeze detection method for wearable monitoring systems. In: *International Symposium on Intelligent Ubiquitous Computing and Education (2009)*. Chengdu: IEEE Computer Society (2009). 331–4. doi: 10.1109/IUCE.2009.66
3. Taplidou SA, Hadjileontiadis LJ, Kitsas IK, Panoulas KI, Penzel T, Gross V, et al. On applying continuous wavelet transform in wheeze analysis. *In: The 26th Annual International Conference of the IEEE Engineering in Medicine and Biology Society*. San Francisco, CA: IEEE (2004) 2:3832–5.
4. McFadden ER, Kiser R, DeGroot WJ. Acute bronchial relations between clinical and physiologic manifestations. *N Engl J Med.* (1973) 288:221–5. doi: 10.1056/NEJM197302012880501
5. Godfrey S, Edwards RHT, Campbell EJM, Armitage P, Oppenheimer EA. Repeatability of physical signs in airway obstruction. *Thorax.* (1969) 24:4–9. doi: 10.1136/thx.24.1.4
6. Arakawa H, Hamasaki Y, Kohno Y, Ebisawa M, Kondo N, Nishima S, et al. Japanese guidelines for childhood asthma 2017. *Allergol Int.* (2017) 66:190–204. doi: 10.1016/j.alit.2016.11.003
7. American Thoracic Society Committee on Pulmonary Nomenclature. *Am Thorac Soc News.* San Francisco, CA: American Thoracic Society Committee on Pulmonary Nomenclature (1977) 3:6.
8. Murphy RL. In defense of the stethoscope. *Respir Care.* (2008) 53:355—69.
9. Forgacs P. The functional basis of pulmonary sounds. *Chest.* (1978) 73:399–405. doi: 10.1378/chest.73.3.399
10. Habukawa C, Murakami K, Endoh M, Horii N, Nagasaka Y. Treatment evaluation using lung sound analysis in asthmatic children. *Respirology.* (2017) 22:1564–9. doi: 10.1111/resp.13109
11. Shimoda T, Obase Y, Nagasaka Y, Nakano H, Kishikawa R, Iwanaga T. Lung sound analysis is useful for monitoring therapy in patients with bronchial asthma. *J Allerg Clin Immunol.* (2017) 27:246–51. doi: 10.18176/jiaci.0132
12. Habukawa C, Murakami K, Endoh M, Yamada M, Horii N, Nagasaka Y. Evaluation of airflow limitation using a new modality of lung sound analysis in asthmatic children. *Allergol Int.* (2015) 64:84–9. doi: 10.1016/j.alit.2014.08.006
13. Pasterkamp H, Brand PL, Everard M, Garcia-Marcos L, Melbye H, Priftis KN. Towards the standardisation of lung sound nomenclature. *Eur Respir J.* (2016) 47:724–32. doi: 10.1183/13993003.01132-2015
14. Fischer HS, Puder LC, Wilitzki S, Usemann J, Bührer C, Godfrey S, et al. Relationship between computerized wheeze detection and lung function parameters in young infants. *Pediatr Pulmonol.* (2016) 51:402–10. doi: 10.1002/ppul.23310
15. Bentur L, Beck R, Berkowitz D, Hasanin J, Berger I, Elias N, et al. Adenosine bronchial provocation with computerized wheeze detection in young infants with prolonged cough: correlation with long-term follow-up. *Chest.* (2004) 126:1060–5. doi: 10.1378/chest.126.4.1060
16. Marques A, Oliveira A, Jacome C. Computerized adventitious respiratory sounds as outcome measures for respiratory therapy: a systemic review. *Respir Care.* (2014) 5:765–76. doi: 10.4187/respcare.02765
17. Habukawa C, Ohgami N, Matsumoto N, Hashino K, Asai K, Sato T, et al. Wheeze sound characteristics are associated with nighttime sleep disturbances in younger children. *Asia Pac Allergy.* (2020) 10:e26. doi: 10.5415/apallergy.2020.10.e26
18. Sovijarvi ARA, Dalmasso F, Vanderschoot J, Malmberg LP, Righini G, Stoneman AAT. Definition of terms for applications of respiratory sounds. *Eur Respir Rev.* (2000) 10:597–610.
19. Sovijärvi ARA, Malmberg LP, Charbonneau G, Vanderschoot J, Dalmasso F, Sacco C, et al. Characteristics of breath sounds and adventitious respiratory sounds. *Eur Respir Rev.* (2000) 10:591–6.
20. Meslier N, Charbonneau G, Racineux JL. Wheezes. *Eur Respir J.* (1995) 8:1942–8. doi: 10.1183/09031936.95.08111942
21. Sovijarvi AR, Vanderschoot J, Earis JE. Standardization of computerized respiratory sound analysis. *Eur Respir Rev.* (2000) 10:585.
22. Chizu Habukawa, Naoto Ohgami, Naoki Matsumoto, Kenji Hashino, Kei Asai, Tetsuya Sato, et al. A wheeze recognition algorithm for practical implementation in children. *PLoS ONE.* (2020) 15:e0240048. doi: 10.1371/journal.pone.0240048
23. Baughman RP, Loudon RG. Lung-sound analysis for continuous evaluation of airflow obstruction in asthma. *Chest.* (1985) 88:364–8. doi: 10.1378/chest.88.3.364
24. Shim CS, Williams MH. Relationship of wheezing to the severity of obstruction in asthma. *Arch Intern Med.* (1983) 143:890—2.
25. Baughman RP, Loudon RG. Quantitation of wheezing in acute asthma. *Chest.* (1984) 86:718–22. doi: 10.1378/chest.86.5.718
26. Bentur L, Beck R, Shinawi M, Naveh T, Gavriely N. Wheeze monitoring in children for assessment of nocturnal asthma and response to therapy. *Eur Respir J.* (2003) 21:621–6. doi: 10.1183/09031936.03.00036302

Conflict of Interest: CH and KM received research grant from the Omron Health Care Corporation. NO is an employee of Omron Healthcare Co., Ltd.

The remaining authors declare that the research was conducted in the absence of any commercial or financial relationships that could be construed as a potential conflict of interest.

Publisher's Note: All claims expressed in this article are solely those of the authors and do not necessarily represent those of their affiliated organizations, or those of the publisher, the editors and the reviewers. Any product that may be evaluated in this article, or claim that may be made by its manufacturer, is not guaranteed or endorsed by the publisher.

Copyright © 2021 Habukawa, Ohgami, Arai, Makata, Nishikido, Tomikawa and Murakami. This is an open-access article distributed under the terms of the Creative Commons Attribution License (CC BY). The use, distribution or reproduction in other forums is permitted, provided the original author(s) and the copyright owner(s) are credited and that the original publication in this journal is cited, in accordance with accepted academic practice. No use, distribution or reproduction is permitted which does not comply with these terms.

frontiers in Pediatrics

ORIGINAL RESEARCH
published: 24 November 2021
doi: 10.3389/fped.2021.670469

The Correlation Between Bronchopulmonary Dysplasia and Platelet Metabolism in Preterm Infants

*Longli Yan, Zhuxiao Ren†, Jianlan Wang†, Xin Xia, Liling Yang, Jiayu Miao, Fang Xu, Weiwei Gao and Jie Yang**

Department of Neonatology, Guangdong Women and Children Hospital, Guangzhou Medical University, Guangzhou, China

OPEN ACCESS

Edited by:
Deb Strickland, University of Western Australia, Australia

Reviewed by:
Hercília Guimarães, University of Porto, Portugal
Christoph Bührer, Charité–Universitätsmedizin Berlin, Germany

***Correspondence:**
Jie Yang
jieyang0830@126.com

†*These authors have contributed equally to this work*

Specialty section:
This article was submitted to Neonatology, a section of the journal Frontiers in Pediatrics

Received: *21 February 2021*
Accepted: *04 October 2021*
Published: *24 November 2021*

Citation:
Yan L, Ren Z, Wang J, Xia X, Yang L, Miao J, Xu F, Gao W and Yang J (2021) The Correlation Between Bronchopulmonary Dysplasia and Platelet Metabolism in Preterm Infants. Front. Pediatr. 9:670469. doi: 10.3389/fped.2021.670469

Background: Platelets play an important role in the formation of pulmonary blood vessels, and thrombocytopenia is common in patients with pulmonary diseases. However, a few studies have reported on the role of platelets in bronchopulmonary dysplasia.

Objective: The objective of the study was to explore the relationship between platelet metabolism and bronchopulmonary dysplasia in premature infants.

Methods: A prospective case-control study was performed in a cohort of premature infants (born with a gestational age < 32 weeks and a birth weight $< 1{,}500$ g) from June 1, 2017 to June 1, 2018. Subjects were stratified into two groups according to the diagnostic of bronchopulmonary dysplasia: with bronchopulmonary dysplasia (BPD group) and without bronchopulmonary dysplasia (control group). Platelet count, circulating megakaryocyte count (MK), platelet-activating markers (CD62P and CD63), and thrombopoietin (TPO) were recorded and compared in two groups 28 days after birth; then serial thrombopoietin levels and concomitant platelet counts were measured in infants with BPD.

Results: A total of 252 premature infants were included in this study. Forty-eight premature infants developed BPD, 48 premature infants without BPD in the control group who were matched against the study infants for gestational age, birth weight, and admission diagnosis at the age of postnatal day 28. Compared with the controls, infants with BPD had significantly lower peripheral platelet count [BPD vs. controls: 180.3 (24.2) $\times$ 10^9/L vs. 345.6 (28.5) $\times$ 10^9/L, $p = 0.001$]. Circulating MK count in the BPD group was significantly more abundant than that in the control group [BPD vs. controls: 30.7 (4.5)/ml vs. 13.3 (2.6)/ml, $p = 0.025$]. The level of CD62p, CD63, and TPO in BPD group was significantly higher than the control group [29.7 (3.1%) vs. 14.5 (2.5%), 15.4 (2.0%) vs. 5.8 (1.7%), 301.4 (25.9) pg/ml vs. 120.4 (14.2) pg/ml, all $p < 0.05$]. Furthermore, the concentration of TPO was negatively correlated with platelet count in BPD group with thrombocytopenia.

Conclusions: Our findings suggest that platelet metabolism is involved in the development of BPD in preterm infants. The possible mechanism might be through increased platelet activation and promoted TPO production by feedback.

Keywords: bronchopulmonary dysplasia, platelet, TPO, megakaryocyte, CD62P, CD63

INTRODUCTION

Bronchopulmonary dysplasia (BPD) is one of the common complications in neonatal intensive care units (NICU) and is considered to be the main cause of death in preterm infants (1). In recent years, with advances in perinatal and neonatal care of preterm infants such as antenatal steroid usage, surfactant therapy, and ventilation strategies, the survival rate of premature infants also increases, resulting in an increasing incidence of BPD. BPD severely influences premature infants by increasing their risk of respiratory infection, asthma, and chronic obstructive pulmonary distress in their later life (2–4).

Currently, alveolar and microvascular arrest is considered as the pathological feature of clinical bronchopulmonary dysplasia (5), the development of alveolar microvascular can promote the formation of alveoli structure; therefore, the role of pulmonary vascular development, especially in pulmonary microvascular development in BPD is getting more and more attention.

The platelet has been recognized as a multifunctional cell, besides hemostasis and thrombosis. The platelet plays an essential role in the formation and development of pulmonary blood vessels, as demonstrated by numerous studies (6, 7). Some clinical retrospective studies (8, 9) found that mean platelet volume might predict the occurrence of BPD, and also, a study (10) has shown that higher platelet count is an independent factor of the development of moderate–severe BPD, and the research (11) found that a higher platelet transfusion threshold can increase the risk of BPD in premature infants. So, we speculate that platelets are involved in the occurrence of BPD, and a few studies have been reported in this regard.

In the present study, we evaluated this hypothesis by comparing peripheral platelet count, circulating MK count, platelet-activating markers, (CD62P and CD63) 28 days after birth in two groups, and the relationship between TPO expression and platelet count in infants with BPD.

MATERIALS AND METHODS

Study Design and Population

This is a prospective study performed at the Neonatal Intensive Care Unit (NICU), Guangdong Women and Children Hospital from June 1, 2017 to June 1, 2018. This study was approved by the ethics committee of Guangdong Women and Children Hospital. Preterm infants cared for in our center were enrolled if they satisfied the following recruitment criteria: (1) gestation <32 weeks, (2) birth weight <1.5 kg, (3) requiring mechanical ventilation for the treatment of respiratory distress syndrome for at least 3 days during the first weeks of life, (4) ventilator and/or oxygen dependent at the time of enrollment, and (5) presence of clinical and radiologic signs of BPD.

Prospectively determined exclusion criteria included the following conditions: (1) congenital abnormalities; (2) infection (bacterial infection confirmed by positive blood culture or viral infection confirmed by serological test or viral culture); (3) evidence of complications of perinatal asphyxia including an Apgar score <3 at 1 or 5 min after birth, evidence of hypoxic–ischemic encephalopathy, acute tubular necrosis, or transient myocardial ischemia; and (4) identifiable hematologic disease.

The infants who were matched against the study infant for gestational age, birth weight, and admission diagnosis were recruited as control group at their age of postnatal day 28.

Definition of Clinical Variables

The diagnosis of BPD in preterm birth was assessed using the consensus definition of the National Institute of Child Health and Human Development (NICHD). Briefly, BPD was defined as the need for supplemental oxygen for more than 28 days and the severity was assessed according to the oxygen concentration required at 36 weeks PMA or discharge (12). Neonatal thrombocytopenia was defined arbitrarily as a platelet count of $<150{,}000\ mm^3$. Neonatal respiratory distress syndrome (NRDS) was defined according to Gomella's Neonatology (13).

Data Collection

The following data were retrieved from the electronic medical record, including maternal disease, gestation, birth weight, gender, Apgar score, NRDS, ventilation mode, blood testing (hemoglobin, white cell count, platelet count, blood gas) using the samples collected within 1 h after birth from the peripheral arterial of the infants.

Measurements

Blood Sampling

In enrolled premature infants at their age of postnatal day 28, during blood sampling for routine laboratory investigation, 1 ml of blood was drawn from the peripheral arterial and placed into an EDTA tube. After mixing gently, 40 μl of whole blood was used as an aliquot for the detection of CD62P and CD63 expressions by flow cytometry. After centrifugation at 400 × *g*, plasma was separated from the blood and preserved at −80°C for TPO level detection. The cell pellet was resuspended in phosphate-buffered saline (PBS) for circulating MK isolation. All samples were processed within 1 h of collection.

Platelet Counts and Circulating Megakaryocyte Counts

Blood platelets were quantified by a Japanese Sysmex KX221 automatic blood cell analyzer. Circulating MK count was

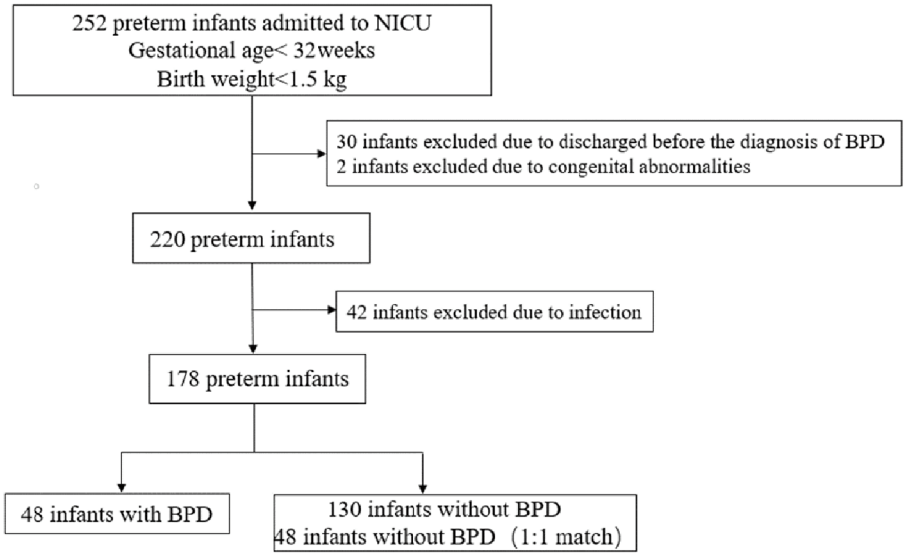

FIGURE 1 | Flowchart of case selection and analysis.

estimated as previously described (14). Briefly, samples were passed through a syringe filter holder (Millipore, Ireland) containing a polycarbonate membrane with an aperture of 5 μm at 37°C and then washed with 2 ml of saline. After the removal of the membrane, it was dried quickly and slightly with a heater and was left overnight at room temperature.

CD62P and CD63 Expressions

CD62P and CD63 were estimated by flow cytometry (FACSCalibur, Becton-Dickinson, San Jose, CA, USA) with the procedure details as previously described (14). In short, 40 μl of whole blood was taken at room temperature and stained with the monoclonal antibody at a saturated concentration for 30 min in dark. FITC-conjugated CD61 is regarded as a platelet-specific monoclonal antibody, and anti-cd62p and anti-cd63 combined with PE in dichroism analysis were used as platelet activation markers. After incubation, 1 ml of PBS containing 1% paraformaldehyde was added to each tube. The samples were fixed at 4°C for 24 h for flow cytometry detection. CD62P and CD63 were detected in 20,000 platelets. All antibodies were purchased from Abcam.

Plasma Thrombopoietin Concentration

TPO levels were measured using a commercially available ELISA (R&D Systems Quantikine Human TPO ELISA kit, Minneapolis, MN, USA), with a lower limit of detection of 15 pg/ml.

Statistical Analysis

Statistical analyses between the two groups were performed using two-tailed Student's *t*-test. One-way analysis of variance was performed to compare the relationship between TPO concentration and platelet count at each time point in BPD group. A value of $p < 0.05$ was considered statistically significant. All values were expressed as mean (SEM) unless otherwise stated. All statistical analyses were done using SPSS 20.0.

RESULTS

Demography Characteristics

A total of 252 eligible premature infants were admitted to our NICU during the study period, after applying exclusion criteria, 178 premature infants were included, in which 48 premature infants diagnosed with BPD, 134 premature infants without BPD, and 48 premature infants in the control group were matched 1:1 according to gestational age, birth weight, and admission diagnosis at their age of postnatal day 28 (**Figure 1**).

The demographic characteristics of the study infants are shown in **Table 1**.

We studied 48 infants in the BPD group (female: 27; male: 21) and 48 infants in the control group (female: 24; male: 24). The infants in the BPD group and control group were similar in their demographic characteristics including gestational age and birth weight. However, the infants with BPD had been exposed to a significantly higher FiO_2 and had a significantly longer ventilation duration (**Table 1**). Among the infants with BPD, 30 infants had a peripheral platelet count $<150 \times 10^9$/L, while none of the infants in the control group had a platelet count $<150 \times 10^9$/L. Infants in both groups received similar conventional treatment according to the unit protocol.

Thirty thrombocytopenic infants in the BPD group were studied serially at postnatal age of day 28, day 35, and day 42, respectively. The platelet count in all these infants returned to normal by the age of day 42.

Peripheral Platelet Count

Peripheral platelet count in the BPD group was significantly lower than that in the control group [BPD vs. controls: 180.3

TABLE 1 | Demographic characteristics of infants with BPD.

Variable	BPD ($n = 48$)	Control ($n = 48$)	p-Value
Gestation (weeks)	28.5 (0.5)	29.7 (0.43)	0.17
Birth weight (g)	1,040 (60)	1,220 (60)	0.14
Gender			
Female	27	24	0.23
Male	21	14	0.25
Maternal disease			
PIH	20	16	0.32
IUGR	4	2	0.25
PROM	6	4	0.30
Oligohydramnios	3	1	0.22
Twin–twin transfusion	1	1	0.5
APH	3	4	0.36
Nil	4	2	0.42
Apgar score			
At 1 min	7	7	0.55
At 5 min	8	9	0.45
Admission diagnosis			
Prematurity	48	48	
RDS	48	44	
Hemoglobin (g/ml)	11.0 (0.3)	10.4 (0.4)	0.18
White cell count ($x10^5$/L)	10.5 (0.3)	11.8 (1.5)	0.55
Platelet count ($x10^9$/L)	170.1 (15.4)	343.1 (23.4)	<0.001
Ventilation duration (days)			
IPPV	20 (0.8)	9 (0.4)	<0.001
CPAP	29 (1.7)	15 (0.7)	<0.001
HFOV	12 (1.3)	7 (0.4)	0.08
Blood gas			
PH	7.37 (0.04)	7.39 (0.03)	0.25
PaO_2	6.31 (0.4)	5.7 (0.4)	0.34
$PaCO_2$	5.0 (0.4)	5.1 (0.3)	0.83
FiO_2	0.27 (0.03)	0.21 (0.3)	<0.001

PIH, pregnancy-induced hypertension; IUGR, intra-uterine growth retardation; PROM, prolonged rupture of membrane; SLE, systemic lupus erythematosus; IPPV, intermittent positive pressure ventilation; CPAP, continuous positive airway pressure; HFOV, high-frequency oscillatory ventilation; BPD, bronchopulmonary dysplasia.

(24.2) $\times$ 10^9/L vs. 345.6 (28.5) $\times$ 10^9/L, $p = 0.001$], as shown in **Figure 2**.

Circulating Megakaryocyte Count

Circulating MK count in the BPD group was significantly more abundant than that in the control group [BPD vs. controls: 30.7 (4.5)/ml vs. 13.3 (2.6)/ml, $p = 0.025$], as shown in **Figure 3**.

CD62P and CD63 Expressions on Platelets

When compared with the controls, premature infants with BPD had significantly greater expressions of CD62P [BPD vs. controls: 29.70 (3.1%) platelets vs. 14.5 (2.5%) platelets, $p = 0.023$] and CD63 [BPD vs. controls: 15.4 (2.0%) platelets vs. 5.8 (1.7%) platelets, $p = 0.015$)], as shown in **Figures 4–6**.

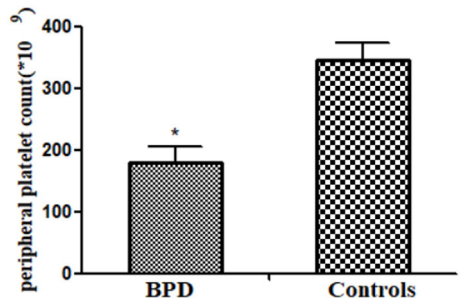

FIGURE 2 | Peripheral platelet counts in infants of bronchopulmonary dysplasia (BPD) and control groups ($p = 0.001$). *$p < 0.05$.

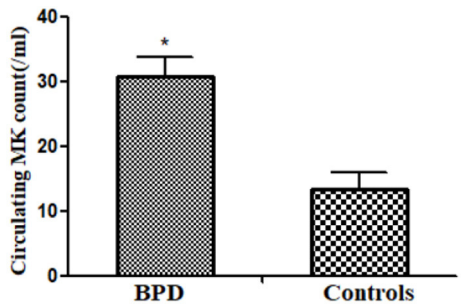

FIGURE 3 | Peripheral megakaryocyte (MK) counts in infants of BPD and control groups ($p = 0.025$). *$p < 0.05$.

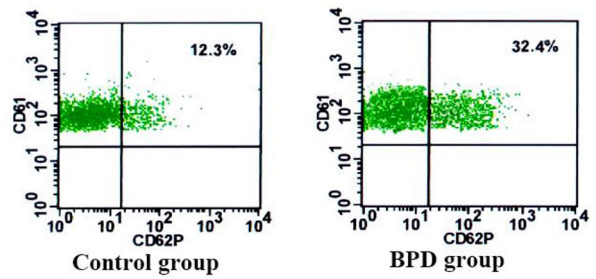

FIGURE 4 | The percentage of CD61+CD62P+ in the control group and BPD group.

Plasma Thrombopoietin Concentration

Circulating MK count in the BPD group was significantly higher than that in the control group [BPD vs. controls: 301.4 (25.9) pg/ml vs. 120.4 (14.2) pg/ml, $p = 0.032$], as shown in **Figure 7**.

Plasma Thrombopoietin Response to Thrombocytopenia in Infants With Bronchopulmonary Dysplasia

TPO levels showed an inverse relationship with peripheral platelet count, peaking near the nadir and decreasing as platelet count increased, as shown in **Figure 8**.

DISCUSSION

In this prospective study, we studied the relevant indicators of platelet metabolism in premature infants with BPD and analyzed its relationship with the occurrence of BPD. Our finding in this study was consistent with our observation in the rat model (15).

In previous studies (16, 17), we have known that CD62p and CD63 are sensitive indicators of platelet activation, and we found that CD62p and CD63 were increased in premature infants who developed BPD compared with those who did not, and the platelet count in the BPD group was significantly lower than in the non-BPD group. Our observation suggested that in infants with BPD, platelet consumption was at least partly responsible for the low peripheral platelet count. The new type of BPD is characterized by alveolar and microvascular dysplasia (5), and endothelial cell injury will impair lung vascular and alveolar growth. Previous workers have reported that pulmonary endothelium was the earliest cell damaged by oxygen free radicals (18), which was followed by an influx of inflammatory cells, such as neutrophils. Once endothelial damage occurs, the activated platelets cause inflammation by the migration of central granulocytes, which play a key role in the arrested lung development (19). In addition, the intercellular adhesion molecule-1, one of the markers in estimating neutrophil attachment to endothelial cells, was elevated in infants with BPD (20). Furthermore, the vascular endothelial growth factor, one of the markers in evaluating the growth and repair of vascular endothelial cell, was lower in infants with BPD than those without BPD (21). In addition, activated polymorphonuclear leukocytes can cause lung tissue injury by the release of toxic oxygen radicals, all of which can further damage the endothelium and increase platelet

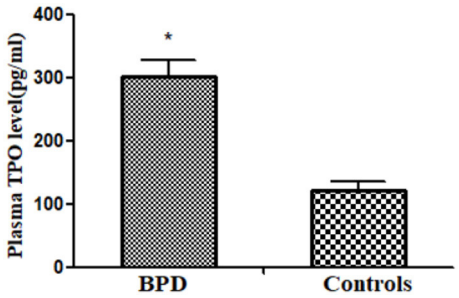

FIGURE 7 | Plasma thrombopoietin (TPO) level in infants of BPD and control groups ($p = 0.032$). *$p < 0.05$.

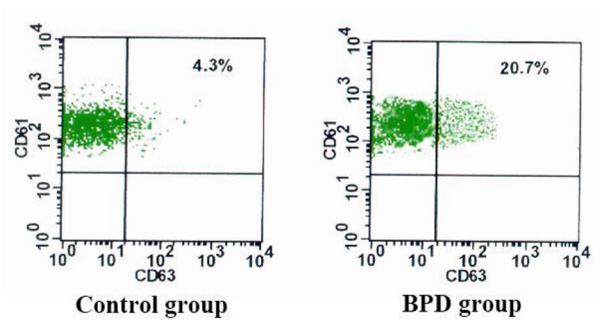

FIGURE 5 | The percentage of CD61 + CD63 in the control group and BPD group.

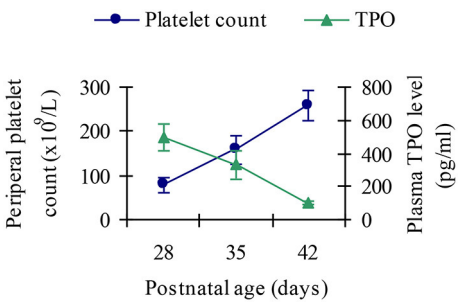

	Day 28	Day 35	Day 42
Platelet count ($\times 10^9$/L)	78.4 (15.2)	155.8 (26.4)	259.3 (36.5)
TPO (pg/ml)	497.3 (35.4)	335.6 (32.1)	94.3 (27.2)

FIGURE 8 | Response of plasma TPO to thrombocytopenia in infants with BPD.

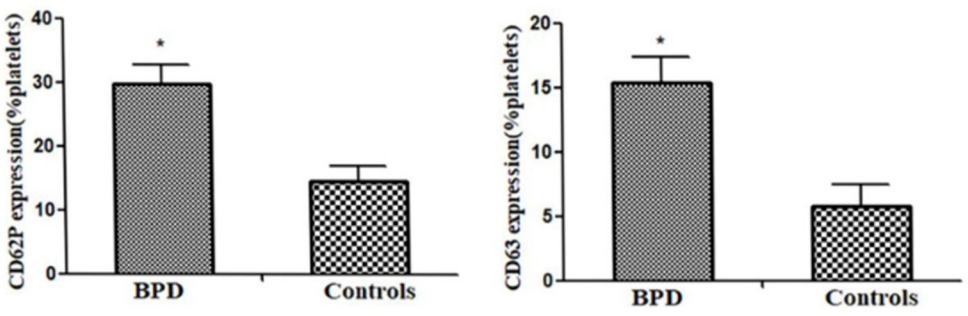

FIGURE 6 | CD62P and CD63 expression in infants of BPD and control groups (all $p < 0.05$). *$p < 0.05$.

activation (22). These observations, together with ours, indicated that pulmonary endothelial damage in infants with BPD may lead to platelet activation and, most likely, increased platelet consumption, resulting in the reduction of peripheral platelet count. Therefore, inhibition of platelet activation may improve the occurrence of BPD.

Our previous study (15) confirmed that the lung is an important site for MK fragmentation and platelet release by comparing the MK and platelet counts between the pre-pulmonary and post-pulmonary blood in rats. Using state-of-the-art intravital microscopy, Lefracais et al. (23) observed the dynamic release of platelets by intravascular megakaryocytes in the lung microcirculation of mice, and intravascular lung megakaryocytes account for about 50% of total platelet production. In this study, as the central arterial and venous catheters were rarely simultaneously available in infants at their postnatal 28 days, we were not able to estimate the platelet and MK count at the pre-pulmonary and post-pulmonary circulation. Thus, we cannot confirm the effect of lung damage in BPD on platelet production. However, it is possible that in infants with BPD, there were lots of pulmonary capillary beds or the damaged endothelium was unable to retain MK for platelet release. On the other hand, mechanical ventilation may damage the pulmonary blood–gas barrier, which causes leakage of fluid, protein, and blood cells into tissue and air spaces. This leakage may result in leakage of MK cells into the alveoli and impairment of MK fragmentation into platelets due to functional impairment of the filtration and sequestration functions of pulmonary capillaries. In this experiment, we found that circulating MK count in the preterm with BPD was higher than that without BPD. The circulating MK, reflecting the MK progenitor in bone marrow, suggests that thrombocytopenia may initiate a feedback mechanism to stimulate the generation of bone marrow megakaryocytes, to increase the number of megakaryocytes in circulation.

Thrombocytopenia is the common complication of newborns in NICU. To our knowledge, TPO is a major regulator of platelet production. So far, there are no reports on plasma TPO level in infants with BPD or its relationship with platelet count. Therefore, in our study, serial TPO and platelet count measurements were obtained in some subjects. Platelet count in infants with BPD showed significantly increased plasma TPO level when compared with the infants in the control group. Our finding that TPO showed a decrease at the time of resolution of thrombocytopenia has also been observed in both adults and children (24, 25). The mechanism might be that plasma TPO concentration is dependent on circulating platelet mass (26). Elevated platelet levels lead to increased binding of cytokines to platelet receptors, which increases the activity of antiplatelet antibodies and reduces plasma concentration. Conversely, lower platelet levels lead to decreased absorption and catabolic metabolism, which leads to higher plasma TPO concentrations. This theory supports our findings.

In conclusion, platelets may play an important role in the formation and development of pulmonary microvascularization in premature infants with BPD. The mechanism may be related to platelet activation and TPO regulation. However, the specific mechanism of TPO-regulating platelets in infants with BPD needs to be further studied, which provides a new idea for the study of BPD.

DATA AVAILABILITY STATEMENT

The original contributions presented in the study are included in the article/supplementary material, further inquiries can be directed to the corresponding authors/s.

ETHICS STATEMENT

The studies involving human participants were reviewed and approved by Guangdong Women and Children Hospital Ethics Committee. Written informed consent to participate in this study was provided by the participant's legal guardian/next of kin.

AUTHOR CONTRIBUTIONS

LYan and ZR conceived and coordinated the study, and wrote the paper. LYan, JW, XX, and LYang performed the experiments. FX and WG collected and analyzed the data. JM collected the references. JY edited the manuscript and provided guidance. All authors reviewed the results and approved the final version of the manuscript.

FUNDING

This work was supported by the Guangdong Natural Found project (2020A1515010266) and the National Natural Science Foundation of China (81873847). The funders of the study had no role in study design, data collection or analysis, decision to publish, or preparation of the manuscript. The corresponding author had full access to all the data in the study and had final responsibility for the decision to submit it for publication.

REFERENCES

1. Stoll BJ, Hansen NI, Bell EF, Walsh MC, Carlo WA, Shankaran S, et al. Trends in care practices, morbidity, and mortality of extremely preterm neonates, 1993-2012. *JAMA*. (2015) 314:1039–51. doi: 10.1001/jama.2015.10244
2. Postma DS, Bush A, van den Berge M. Risk factors and early origins of chronic obstructive pulmonary disease. *Lancet*. (2015) 385:899–909. doi: 10.1016/S0140-6736(14)60446-3
3. Moschino L, Carraro S, Baraldi E. Early-life origin and prevention of chronic obstructive pulmonary diseases. *Pediatr Allergy Immunol*. (2020) 31:16–8. doi: 10.1111/pai.13157
4. Islam JY, Keller RL, Aschner JL, Hartert TV, Moore PE. Understanding the short- and long-term respiratory outcomes of prematurity and bronchopulmonary dysplasia. *Am J Respir Crit Care Med*. (2015) 192:134–56. doi: 10.1164/rccm.201412-2142PP

5. Thébaud B, Goss KN, Laughon M, Whitsett JA, Abman SH, Steinhorn RH, et al. Bronchopulmonary dysplasia. *Nat Rev Dis Primers.* (2019) 5:78–131. doi: 10.1038/s41572-019-0127-7
6. Jiménez J, Richter J, Nagatomo T, Salaets T, Quarck R, Wagennar A, et al. Progressive vascular functional and structural damage in a bronchopulmonary dysplasia model in preterm rabbits exposed to hyperoxia. *Int J Mol Sci.* (2016) 17:e1776. doi: 10.3390/ijms17101776
7. Kroll MH, Afshar-Kharghan V. Platelets in pulmonary vascular physiology and pathology. *Plum Circ.* (2012) 2:291–308. doi: 10.4103/2045-8932.101398
8. Bolouki MK, Zarkesh M, Kamali A, Dalili S, Heidarzadeh A, Rad AH. The association of mean platelet volume with intra ventricular hemorrhage and broncho pulmonary dysplasia in preterm infants. *J Pediat Hematol Onc.* (2015) 15:227–32.
9. Dani C, Poggi C, Barp J, Berti E, Fontanelli G. Mean platelet volume and risk of bronchopulmonary dysplasia and intraventricular hemorrhage in extremely preterm infants. *Am J Perinatol.* (2011) 28:551–7. doi: 10.1055/s-0031-1274503
10. Chen X, Li H, Qiu X, Yang CZ, Walther FJ. Neonatal hematological parameters and the risk of moderate-severe bronchopulmonary dysplasia in extremely premature infants. *BMC Pediatr.* (2019) 19:138–44. doi: 10.1186/s12887-019-1515-6
11. Curley A, Stanworth SJ, Willoughby K, Fustolo-Gunnink SF, Venkatesh V, Hudson C, et al. Randomized trial of platelet-transfusion thresholds in neonates. *N Engl J Med.* (2019) 3:242–51. doi: 10.1056/NEJMoa1807320
12. Ehrenkranz RA, Walsh MC, Vohr BR, Jobe AH, Wright LL, Fanaroff AA. et al. *Validation of the National Institutes of Health consensus definition of bronchopulmonary dysplasia[J]Pediatrics.* (2005) 116:1353–60. doi: 10.1542/peds.2005-0249
13. Gomella T, Cummingham M, Fabien E. *Neonatology*. 6th ed. New York, NY: Lange (2009).
14. Yang J, Zhang HC, Niu JM, Mu XP, Zhang XL, Ying Liu Y, et al. Impact of preeclampsia on megakaryocytopoesis and platelet homeostasis of preterm infants. *Platelets.* (2016) 27:123–7. doi: 10.3109/09537104.2015.1048213
15. Yang J, Yang M, Xu F, Li K, Lee SKM, Ng PC, et al. Effects of oxygen-induced lung damage on megakaryocytopoiesis and platelet homeostasis in a rat model. *Pediatr Res.* (2003) 54:344–52. doi: 10.1203/01.PDR.0000079186.86219.29
16. Ergelen M, Uyarel H. Plateletcrit: a novel prognostic marker for acute coronary syndrome. *Int J Cardiol.* (2014) 177:161. doi: 10.1016/j.ijcard.2014.09.054
17. Taylor ML, Misso NL, Stewart GA, Thompson PJ. differential expression of platelet activation markers CD62P and CD63 following stimulation with PAF, arachidonic acid and collagen. *Platelets.* (2009) 6:394–401. doi: 10.3109/09537109509078478
18. Mittal M, Siddiqui MR, Tran K, Reddy SP, Malik AB. Reactive oxygen species in inflammation and tissue injury. *Antioxid Redox Signal.* (2014) 20:1126–67. doi: 10.1089/ars.2012.5149
19. Bui CB, Pang MA, Sehgal A, Theda C, Lao JC, Berger PJ, et al. Pulmonary hypertension associated with bronchopulmonary dysplasia in preterm infants. *J Reprod Immunol.* (2017) 124:21–9. doi: 10.1016/j.jri.2017.09.013
20. Wang XH, Jia HL, Deng L, Huang WM. Astragalus polysaccharides mediated preventive effects on bronchopulmonary dysplasia in rats. *Pediatr Res.* (2014) 76:347–54. doi: 10.1038/pr.2014.107
21. Baker CD, Abman SH. Impaired pulmonary vascular development in bronchopulmonary dysplasia. *Neonatology.* (2015) 107:344–51. doi: 10.1159/000381129
22. Middleton EA, Rondina MT, Schwertz H, Zimmerman GA. Amicus or adversary revisited: platelets in acute lung injury and acute respiratory distress syndrome. *Am J Respir Cell Mol Biol.* (2018) 59:18–35. doi: 10.1165/rcmb.2017-0420TR
23. Lefrancais E, Ortiz-Munoz G, Caudrillier A, Mallavia B, Liu FC, Sayah DM, et al. The lung is a site of platelet biogenesis and a reservoir for haematopoietic progenitors. *Nature.* (2017) 544:105–9. doi: 10.1038/nature21706
24. Temel T, Cansu DU, Temel HE, Ozakyol AH. Serum thrombopoietin levels and its relationship with thrombocytopenia in patients with cirrhosis. *Hepat Mon.* (2014) 14:e18556–9. doi: 10.5812/hepatmon.18556
25. Del Vecchio GC, Giordano P, Tesse R, Piacente L, Altomare M. De Mattia, D. Clinical significance of serum cytokine levels and thrombopoietic markers in childhood idiopathic thrombocytopenic purpura. *Blood Transfus.* (2012) 10:194–9. doi: 10.2450/2011.0055-11
26. de Graaf CA, Kauppi M, Baldwin T, Hyland CD, Metcalf D, Willson TA, et al. Regulation of hematopoietic stem cells by their mature progeny. *Proc Natl Acad Sci U S A.* (2010) 107:21689–94. doi: 10.1073/pnas.1016166108

Conflict of Interest: The authors declare that the research was conducted in the absence of any commercial or financial relationships that could be construed as a potential conflict of interest.

Publisher's Note: All claims expressed in this article are solely those of the authors and do not necessarily represent those of their affiliated organizations, or those of the publisher, the editors and the reviewers. Any product that may be evaluated in this article, or claim that may be made by its manufacturer, is not guaranteed or endorsed by the publisher.

Copyright © 2021 Yan, Ren, Wang, Xia, Yang, Miao, Xu, Gao and Yang. This is an open-access article distributed under the terms of the Creative Commons Attribution License (CC BY). The use, distribution or reproduction in other forums is permitted, provided the original author(s) and the copyright owner(s) are credited and that the original publication in this journal is cited, in accordance with accepted academic practice. No use, distribution or reproduction is permitted which does not comply with these terms.

frontiers in Pediatrics

ORIGINAL RESEARCH
published: 06 December 2021
doi: 10.3389/fped.2021.709160

Roles of Lung Ultrasound Score in the Extubation Failure From Mechanical Ventilation Among Premature Infants With Neonatal Respiratory Distress Syndrome

Zhenyu Liang[1], Qiong Meng[1], Chuming You[1]*, Bijun Wu[2], Xia Li[1] and Qianmei Wu[1]*

[1] Department of Neonatology, Guangdong Second Provincial General Hospital, Guangzhou, China, [2] Ultrasonic Department, Guangdong Second Provincial General Hospital, Guangzhou, China

Objective: To investigate the predictive value of lung ultrasound score (LUS) in the extubation failure from mechanical ventilation (MV) among premature infants with neonatal respiratory distress syndrome (RDS).

Methods: The retrospective cohort study was conducted with a total of 314 RDS newborns who received MV support for over 24 h. After extubation from MV, infants were divided into extubation success and extubation failure groups. Extubation failure was defined as re-intubation within 48 h after extubation. Univariate and multivariate logistic regression analyses were used to identify the predictors of the extubation failure. The predictive effectiveness of the combined model and LUS in the extubation failure was assessed by receiver operating characteristic curve, area under curve (AUC), and internal validation.

Results: 106 infants failed extubation from MV. The combined model for predicting the extubation failure was performed according to the predictors of gestational age, body length, birth weight, and LUS. The AUC of this combined model was 0.871 (sensitivity: 86.67%, specificity: 74.31%). The AUC of LUS was 0.858 (sensitivity: 84.00%, specificity: 80.69%), and the cutoff value was 18. There was no statistical difference in the predictive power between the combined model and LUS ($Z = 0.880$, $P = 0.379$). The internal validation result showed that the AUC of LUS was 0.855.

Conclusions: LUS presented a good ability in predicting the extubation failure among RDS newborns after MV.

Keywords: lung ultrasound score, premature infants, neonatal respiratory distress syndrome, mechanical ventilation, pulmonary

OPEN ACCESS

Edited by:
Deb Strickland, University of Western Australia, Australia

Reviewed by:
Kelechi Benjamin Ugonna, Sheffield Children's Hospital, United Kingdom
Paolo Bottau, Local Health Authority of Imola, Italy

***Correspondence:**
Chuming You
cmyou_gzdoc@163.com
Qiong Meng
mengqiong1969@163.com

Specialty section:
This article was submitted to Pediatric Pulmonology, a section of the journal Frontiers in Pediatrics

Received: *13 May 2021*
Accepted: *02 November 2021*
Published: *06 December 2021*

Citation:
Liang Z, Meng Q, You C, Wu B, Li X and Wu Q (2021) Roles of Lung Ultrasound Score in the Extubation Failure From Mechanical Ventilation Among Premature Infants With Neonatal Respiratory Distress Syndrome. Front. Pediatr. 9:709160. doi: 10.3389/fped.2021.709160

INTRODUCTION

Neonatal respiratory distress syndrome (RDS), a common respiratory disease, is a leading cause of early morbidity and mortality among infants and children (1, 2). It is characterized by diffuse lesions of the pulmonary capillaries and increased permeability (3). Pieces of evidence showed that premature deaths caused by neonatal RDS accounted for 50–70% of all premature deaths,

and survivors seemed more likely to suffer from severe sequelae (4, 5). Mechanical ventilation (MV) is frequently applied in a neonatal intensive care unit (6) and can efficiently relieve the clinical symptoms of premature infants undergoing severe RDS (7), whereas long-term MV may be associated with the risk of ventilator-relevant lung injury, bronchopulmonary dysplasia, and infection (8, 9). Of note, the ultimate aim of treatment is to help patients weaning from MV support, not to provide MV support (9).

The extubation success of MV has been gradually attracted attention in the treatment of respiratory support in recent years. Studies reported that the extubation of MV is associated with chronic obstructive airway disease, heart failure, decompensation of cardiopulmonary function, positive fluid balance, pneumonia, and diaphragmatic dysfunction (10, 11). A common reason for the weaning failure is the imbalance between ventilation demand and the capacity of spontaneous breathing, such as respiratory pump failure (12). To the best of our knowledge, pulmonary function is an important factor affecting the extubation success from MV in RDS infants. At present, lung ultrasound score (LUS), a reliable measuring method for the bedside evaluation of pulmonary ventilation, is widely used for critically ill patients, especially for neonatal RDS (13, 14). Early researches mentioned that LUS could predict the use of surfactants under continuous positive airway pressure in premature babies (15, 16). Furthermore, LUS and the area of lung consolidation are closely related to the severity of neonatal RDS, which has also been confirmed in several studies (17). However, the application of LUS in the extubation of MV in babies with RDS has not yet been concluded, and further researches are needed to explore.

Herein, we observed the pulmonary ultrasound performance of neonatal RDS and measured the LUS in premature infants, thereby further assessing the reliability and accuracy of LUS in predicting the extubation failure, which may provide guidance for the extubation of MV.

METHODS

Patients

This was a retrospective cohort study. A total of 314 eligible infants who received MV support within 72 h after birth were enrolled consecutively between January 1, 2019, and June 30, 2020. After extubation from MV, infants were divided into extubation success and extubation failure groups. This study was approved by the Institutional Review Board of Guangdong Second Provincial General Hospital (approval number: No.20191101-01-YXKXYJ-SYX), and the written informed consent was obtained from the parents or guardians of the minors.

Eligibility

Inclusion criteria were (1) gestational age <37 weeks, (2) infants with RDS, and (3) MV support for ≥24 h.

Exclusion criteria were (1) congenital diseases, such as congenital heart disease, respiratory malformation, and chromosome abnormality; (2) a history of pneumothorax, air leak, or meconium aspiration syndrome; (3) arrhythmias and hemodynamic instability; (4) >stage III intracranial hemorrhage; (5) taking other experimental drugs or participating in other clinical trials within 1 month before the inclusion in this study; (6) respiratory distress caused by other diseases; and (7) incomplete clinical data.

The definition of neonatal RDS based on the *Practice of Neonatology* (5th edition) (3) were as follows: (1) infants with progressive dyspnea within 6 h after birth accompanied by cyanosis, expiratory groan or inspiratory three concave sign; (2) cases with decreased transparency of bilateral lungs, air bronchogram, indistinct heart, and septal margins, or white lung based on chest X-rays.

Clinical Data

All eligible infants were examined by chest radiograph, lung ultrasound, cardiac color ultrasound, and blood gas analysis within 1 h before the extubation.

General Data

The characteristics of RDS infants were recorded at admission, including gestational age (weeks), sex, nationality, weight (kilogram), and body length (centimeter).

Echocardiographic Indicators

The echocardiographic indicators were recorded including left ventricular end-diastolic diameter (LVEDD), left ventricular end-systolic diameter, aortic dimension, pulmonary valve, aortic valve, tricuspid valve, bicuspid valve, descending aorta, and left ventricular ejection fraction.

Lung Ultrasound Examination

The lung ultrasound examination was performed using the Doppler ultrasound diagnostic instrument (Philips CX50), with a probe frequency of 8–12 MHz. The 12-region method was conducted to examine the anterior, lateral, and posterior walls on both sides of the lung (18). The scoring standard of lung ultrasound is as follows: (1) normal aeration (score = 0); (2) moderate loss of aeration (interstitial syndrome, defined by multiple spaced B lines, or localized pulmonary edema, defined by coalescent B lines in <50% of the intercostal space examined in the transversal plane, or subpleural consolidations) (score = 1); (3) severe loss of aeration (alveolar edema, defined by diffused coalescent B lines occupying the whole intercostal space) (score = 2); and (4) complete loss of lung aeration (lung consolidation defined as a tissue pattern with or without air bronchogram) (score = 3). The images of lung ultrasound examination are shown in **Figure 1**. LUS is calculated as the sum of the 12 regional scores, ranging from 0 to 36; LUS = 0 is normal, and LUS > 0 is abnormal. The observation point was before the extubation of MV. The lung ultrasound was conducted by pediatricians who had participated in the training courses of neonatal pulmonary ultrasound in China. The images stored by two pediatricians were reviewed and controlled for quality by a sonographer (chief physician) with proficient skills in pulmonary ultrasound.

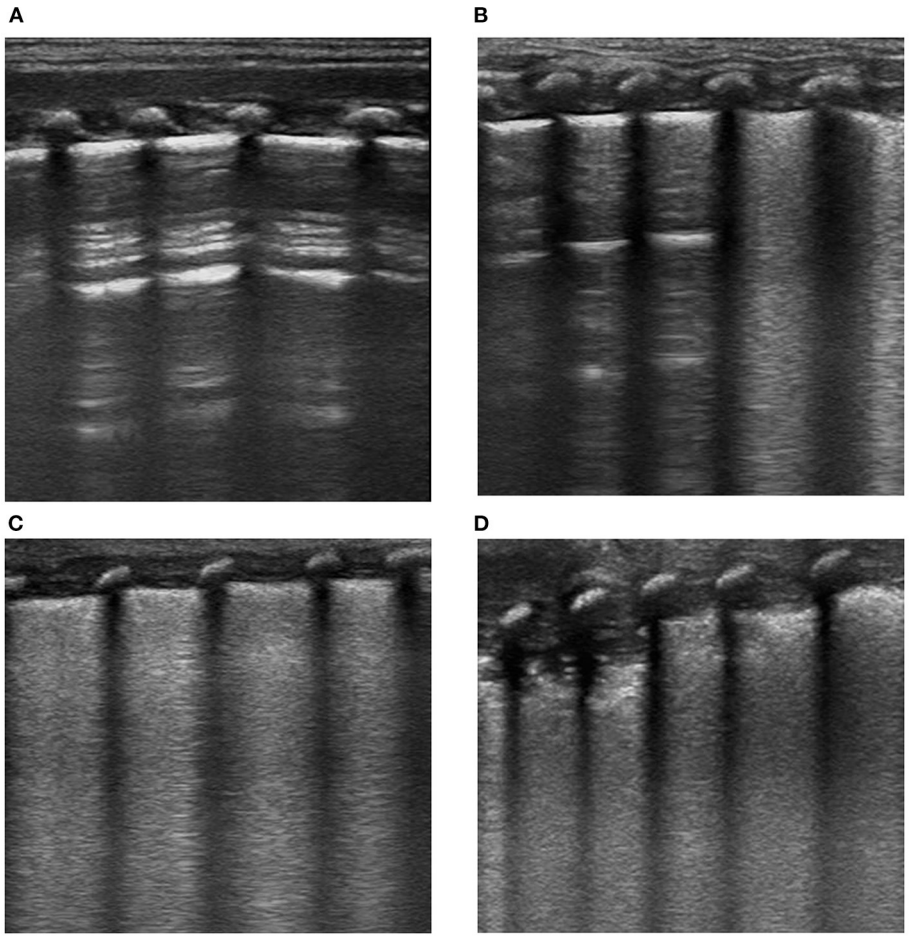

FIGURE 1 | Imaging examination of lung ultrasound in newborns with RDS. **(A)** Score = 0, **(B)** score = 1, **(C)** score = 2, and **(D)** score = 3.

Arterial Blood Gas Analysis

The parameters were analyzed, including oxygenation index (OI), arterial partial pressure of carbon dioxide ($PaCO_2$), and rapid shallow breathing index (RSBI). OI is the ratio of arterial partial pressure of oxygen and fraction of inspired oxygen, which can reflect the severity of acute diseases. RSBI is a ratio of respiratory rate (beats/min) and tidal volume (liter).

Extubation From Mechanical Ventilation

The extubation of ventilators was based on: (1) when fraction of inspired oxygen $\leq$0.4, peak inspiratory pressure = 10–15 cm H_2O, positive end-expiratory pressure) <2–4 cm H_2O, and frequency $\leq$ 10 beats/min; (2) normal arterial blood gas; (3) acid-base electrolyte balance; (4) recovery of spontaneous breathing and sufficient effective ventilation; (5) control or improvement of the primary disease; and (6) reduced secretion and good tolerance of sputum suction. After the extubation, respiratory insufficiency occurred in the infants, which could not be relieved after treatments with oxygen inhalation, nebulization inhaled corticosteroids, or β-receptor agonists. If babies were re-ventilated with endotracheal intubation within 48 h after extubation, the extubation was deemed as failure; otherwise, it was successful (19).

Statistical Analysis

Statistical analysis was performed using SAS 9.4 (SAS Institute Inc.). The normality of data was examined by the Shapiro–Wilk test (W test). Measurement data with normal distribution were presented as mean ± standard deviation ($\bar{x} \pm s$) using *t*-test and, with skewed distribution, were presented as median and quartile [$M(Q_{25}, Q_{75})$] by Mann–Whitney *U*-test. Enumeration data were presented as n (%) with chi-squared [χ^2 (total n $\geq$ 40 and all T $\geq$ 5)] or Fisher (total $n < 40$ and all T < 5) tests. Ranked data were presented as n (%) utilizing the Mann–Whitney U test. $P < 0.05$ was considered statistically significant.

All eligible newborns in this study were randomly divided into the training group ($n = 220$) and testing group ($n = 94$) with a ratio of 7:3. A prediction model was established using the data of the training group. Univariate and multivariable logistic regression analyses were used to identify the predictors of the extubation failure from MV in RDS newborns. A combined model for predicting the extubation failure was established

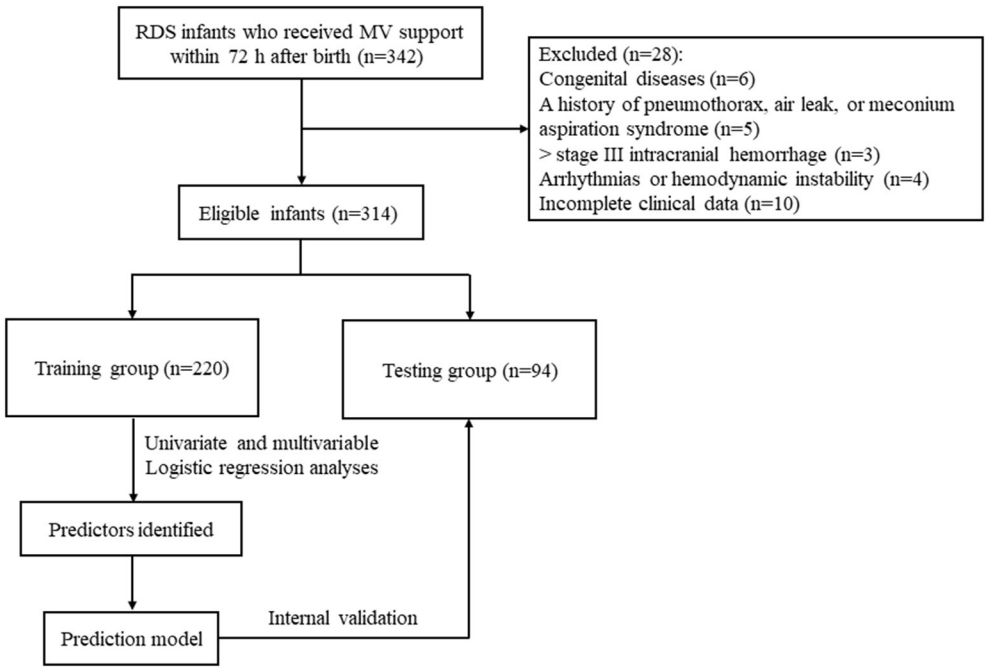

FIGURE 2 | Flow chart of included infants with RDS.

based on the predictors. Then, the predictive power between the combined model and LUS was compared. The predictive performance of LUS for the extubation failure was evaluated using the testing group (as the internal validation). Variance inflation factor (VIF) was used to assess the collinearity of independent variables. The power analysis was performed using SPSS 15.0 (SPSS, Inc., Chicago, IL). The power of the AUC of the combined model was 1.00, and the power of the AUC of LUS was 1.00.

RESULTS

Baseline Data of Premature Infants With Neonatal Respiratory Distress Syndrome

In the current study, a total of 342 premature infants with neonatal RDS who received MV for ≥24 h in the intensive care unit were enrolled in this study. After excluding newborns with congenital diseases ($n = 6$), a history of pneumothorax, air leak, or meconium aspiration syndrome ($n = 5$), > stage III intracranial hemorrhage ($n = 3$), arrhythmias or hemodynamic instability ($n = 4$), and incomplete clinical data ($n = 10$), 314 were finally included. The flow chart of the included patients has been added in our manuscript; please see revised **Figure 2**. One hundred six cases failed extubation from MV. Of the total, 66.88% were males ($n = 210$), and 33.12% ($n = 104$) were females, with the mean gestational age of (32.94 ± 3.44) weeks, the median birth weight of 1.26 (1.01, 1.80) kg, and the mean body length of (40.02 ± 5.38) cm.

Difference Analysis Between the Training and Testing Groups

Of the total 314 newborns, 220 were classified into the training group, and 94 were in the testing group. There were no statistical differences in all included variables regarding gestational age, sex, nationality, body length, birth weight, breathing, OI, arterial partial pressure of oxygen, $PaCO_2$, RSBI, duration of MV, LVEDD, left ventricular end-systolic diameter, aortic dimension, pulmonary valve, tricuspid valve, bicuspid valve, descending aorta, left ventricular ejection fraction, pulmonary artery systolic pressure, LUS, patent foramen ovale, and artery bypass from left to right horizontally, with all $P > 0.05$ (**Table 1**).

Univariate Logistic Regression Analysis for the Extubation Failure

The results of the unavailable analysis in the training set are shown in **Table 2**. Gestational age (31.65 *vs.* 33.60, $t = 4.04$), body length (36.27 *vs.* 42.26, $t = 9.84$), and birth weight (0.99 *vs.* 1.58, $Z = -8.699$) in the extubation failure group were lower than those in the extubation success group, with all $P < 0.001$. $PaCO_2$ (43.04 *vs.* 39.64, $t = 2.61$), LVEDD (13.32 *vs.* 12.53, $t = 2.30$), aortic aorta (0.95 *vs.* 0.89, $t = 2.19$), and LUS (20.72 *vs.* 19.06, $t = -2.92$) in the extubation failure group were higher in comparison with those in the extubation success group, with all $P < 0.05$.

Collinearity Analysis of Independent Variables

The collinear assessment of independent variables is shown in **Table 3**. The VIF values of gestational age, body length, birth

TABLE 1 | Difference analysis between the training and testing groups.

Variables	Testing group ($n = 94$)	Training group ($n = 220$)	Statistics	P
Gestational age, weeks, $\bar{x} \pm s$	32.95 ± 3.32	32.93 ± 3.50	$t = 0.03$	0.972
Sex, n (%), $\bar{x} \pm s$			$\chi^2 = 1.807$	0.179
Male	68 (72.34)	142 (64.55)		
Female	26 (27.66)	78 (35.45)		
Nationalities, n (%)			–	1.000
Han	94 (100.00)	218 (99.09)		
Uyghur	0 (0.00)	2 (0.91)		
Body length, cm, $\bar{x} \pm s$	39.56 ± 5.35	40.22 ± 5.39	$t = -0.99$	0.322
Birth weight, kg, M(Q_{25}, Q_{75})	1.25 (1.04, 1.72)	1.27 (1.01, 1.80)	$Z = -0.219$	0.826
Breathing, beats/min, $\bar{x} \pm s$	49.15 ± 6.79	50.15 ± 5.30	$t = -1.28$	0.203
OI, $\bar{x} \pm s$	4.20 (2.75, 5.96)	3.74 (2.82, 5.15)	$Z = 0.704$	0.482
PaO_2, mmHg, $\bar{x} \pm s$	78.21 ± 23.07	79.57 ± 20.13	$t = -0.52$	0.601
$PaCO_2$, mmHg, $\bar{x} \pm s$	41.98 ± 10.31	40.80 ± 9.25	$t = 1.00$	0.320
RSBI, $\bar{x} \pm s$	87.87 ± 5.24	88.13 ± 5.14	$t = -0.41$	0.682
Duration of MV, h, M(Q_{25}, Q_{75})	102.00 (61.00, 176.00)	128.00 (79.00, 200.00)	$Z = -1.330$	0.184
LVEDD, $\bar{x} \pm s$	13.06 ± 2.27	12.80 ± 2.73	$t = 0.87$	0.385
LVESD, $\bar{x} \pm s$	8.56 ± 1.54	8.24 ± 1.79	$t = 1.52$	0.130
Aortic dimension, $\bar{x} \pm s$	6.47 ± 0.75	6.51 ± 1.08	$t = -0.42$	0.676
Pulmonary valve, $\bar{x} \pm s$	0.80 (0.70, 1.00)	0.80 (0.70, 1.00)	$Z = -1.054$	0.292
Aortic valve, $\bar{x} \pm s$	0.92 ± 0.22	0.91 ± 0.21	$t = 0.27$	0.784
Tricuspid valve, $\bar{x} \pm s$	0.61 ± 0.20	0.64 ± 0.14	$t = -1.06$	0.293
Bicuspid valve, $\bar{x} \pm s$	0.71 ± 0.17	0.71 ± 0.17	$t = -0.11$	0.912
Descending aorta, $\bar{x} \pm s$	1.09 ± 0.23	1.09 ± 0.21	$t = -0.30$	0.762
LVEF, $\bar{x} \pm s$	67.03 ± 4.58	67.15 ± 4.20	$t = -0.22$	0.823
PASP, $\bar{x} \pm s$	38.40 ± 9.78	38.69 ± 12.32	$t = -0.19$	0.850
LUS, $\bar{x} \pm s$	18.78 ± 3.44	19.62 ± 4.08	$t = -1.76$	0.079
PDA, n (%)			$\chi^2 = 0.268$	0.604
No	50 (53.19)	110 (50.00)		
Yes	44 (46.81)	110 (50.00)		
PFO, n (%)			–	1.000
No	3 (3.19)	7 (3.18)		
Yes	91 (96.81)	213 (96.82)		
Artery bypass from left to right horizontally, n (%)			$\chi^2 = 3.192$	0.074
No	69 (73.40)	181 (82.27)		
Yes	25 (26.60)	39 (17.73)		

–, Using Fisher test.

OI, oxygenation index; RSBI, rapid shallow breathing index; PaO_2, arterial partial pressure of oxygen; $PaCO_2$, arterial partial pressure of carbon dioxide; MV, mechanical ventilation; LVEDD, left ventricular end-diastolic dimension; LVESD, left ventricular end-systolic diameter; LVEF, left ventricular ejection fraction; PASP, pulmonary artery systolic pressure; LUS, lung ultrasound score; PDA, patent ductus arteriosus; PFO, patent foramen ovale.

weight, $PaCO_2$, LVEDD, and LUS were 2.020, 3.129, 3.676, 1.025, 1.082, and 1.036, respectively. All VIF values were ≤10, and all tolerance values were <1, indicating no collinearity among the independent variables.

Multivariate Logistic Regression Analysis for the Extubation Failure

The stepwise logistic regression was used to evaluate the predictive factors of the extubation failure among newborns with RDS (**Table 4**). The findings showed that gestational age, body length, birth weight, and LUS were predictive factors of extubation failure. The risk of the extubation failure decreased by 0.149 [95% confidence interval (CI): 0.967–0.990, $P = 0.037$] and 0.181 times (95% CI: 0.705–0.950, $P = 0.009$) for every 1-week increase in gestational age and every 1-cm increase in body length, respectively. When the birth weight gained 1 kg each time, the extubation failure risk reduced by 0.905-folds (95% CI: 0.018–0.504, $P = 0.006$). In addition, a 0.116–fold (95% CI: 1.012–1.231, $P = 0.028$) increase was exhibited in the risk of the extubation failure with per 1 unit increase in LUS (details in **Table 4**).

Prediction for the Extubation Failure From Mechanical Ventilation in Newborns With Respiratory Distress Syndrome

The combined model for predicting the extubation failure among infants with neonatal RDS was carried out according to the

TABLE 2 | Univariate logistic regression analysis for the extubation failure.

Variables	Extubation success ($n = 145$)	Extubation failure ($n = 75$)	Statistics	P
Gestational age, weeks, $\bar{x} \pm s$	33.60 ± 3.57	31.65 ± 2.99	$t = 4.04$	<0.001
Gender, *n* (%), $\bar{x} \pm s$			$\chi^2 = 0.224$	0.636
Male	92 (63.45)	50 (66.67)		
Female	53 (36.55)	25 (33.33)		
Nationalities, *n* (%)			–	0.115
Han	145 (100.00)	73 (97.33)		
Uyghur	0 (0.00)	2 (2.67)		
Body length, cm, $\bar{x} \pm s$	42.26 ± 4.91	36.27 ± 3.91	$t = 9.84$	<0.001
Birth weight, kg, M(Q_{25}, Q_{75})	1.58 (1.24, 2.00)	0.99 (0.92, 1.19)	$Z = -8.699$	<0.001
Breathing, beats/min, $\bar{x} \pm s$	49.94 ± 5.27	50.57 ± 5.38	$t = -0.84$	0.401
OI, $\bar{x} \pm s$	3.76 (2.81, 4.90)	3.65 (2.91, 5.57)	$Z = 0.782$	0.434
PaO_2, mmHg, $\bar{x} \pm s$	80.57 ± 19.89	77.64 ± 20.59	$t = 1.02$	0.307
$PaCO_2$, mmHg, $\bar{x} \pm s$	39.64 ± 9.01	43.04 ± 9.38	$t = -2.61$	0.010
RSBI, $\bar{x} \pm s$	87.92 ± 5.27	88.54 ± 4.87	$t = -0.85$	0.397
Duration of MV, h, M(Q_{25}, Q_{75})	122.0 (66.0, 183.0)	165.0 (81.0, 255.0)	$Z = 1.865$	0.062
LVEDD, $\bar{x} \pm s$	12.53 ± 3.00	13.32 ± 2.02	$t = -2.30$	0.023
LVESD, $\bar{x} \pm s$	8.09 ± 1.97	8.51 ± 1.37	$t = -1.84$	0.067
Aortic dimension, $\bar{x} \pm s$	6.45 ± 1.17	6.63 ± 0.89	$t = -1.23$	0.220
Pulmonary valve, $\bar{x} \pm s$	0.80 (0.70, 1.00)	0.80 (0.80, 1.00)	$Z = 1.527$	0.127
Aortic valve, $\bar{x} \pm s$	0.89 ± 0.23	0.95 ± 0.15	$t = -2.19$	0.030
Tricuspid valve, $\bar{x} \pm s$	0.63 ± 0.14	0.65 ± 0.14	$t = -0.88$	0.377
Bicuspid valve, $\bar{x} \pm s$	0.71 ± 0.19	0.72 ± 0.15	$t = -0.54$	0.593
Descending aorta, $\bar{x} \pm s$	1.08 ± 0.23	1.12 ± 0.17	$t = -1.54$	0.126
LVEF, $\bar{x} \pm s$	67.04 ± 4.32	67.36 ± 3.97	$t = -0.54$	0.593
PASP, $\bar{x} \pm s$	37.0 (35.0, 45.0)	36.0 (35.0, 41.0)	$Z = -1.384$	0.166
LUS, $\bar{x} \pm s$	19.06 ± 3.94	20.72 ± 4.16	$t = -2.92$	0.004
PDA, *n* (%)			$\chi^2 = 0.506$	0.477
No	75 (51.72)	35 (46.67)		
Yes	70 (48.28)	40 (53.33)		
PFO, *n* (%)			–	0.427
No	6 (4.14)	1 (1.33)		
Yes	139 (95.86)	74 (98.67)		
Artery bypass from left to right horizontally, *n* (%)			$\chi^2 = 0.233$	0.629
No	118 (81.38)	63 (84.00)		
Yes	27 (18.62)	12 (16.00)		

–, Using Fisher test.

OI, oxygenation index; RSBI, rapid shallow breathing index; PaO_2, arterial partial pressure of oxygen; $PaCO_2$, arterial partial pressure of carbon dioxide; MV, mechanical ventilation; LVEDD, left ventricular end-diastolic dimension; LVESD, left ventricular end-systolic diameter; LVEF, left ventricular ejection fraction; PASP, pulmonary artery systolic pressure; LUS, lung ultrasound score; PDA, patent ductus arteriosus; PFO, patent foramen ovale.

predictive factors in the training group, i.e., LUS, gestational age, body length, and birth weight. The AUC of this combined model was 0.871 (95% CI: 0.819–0.922) with a sensitivity of 86.67% (95% CI: 77.80–93.40) and a specificity of 74.31% (95% CI: 66.40–81.20). The AUC of LUS was 0.858 (95% CI: 0.804–0.911) with a sensitivity of 84.00% (95% CI: 73.70–91.40) and a specificity of 80.69% (95% CI: 73.30–86.80). There was no statistical difference in the predictive power between the combined model and LUS ($Z = 0.880$, $P = 0.379$) (**Table 5** and **Figure 3A**). The cutoff value of LUS was 18, suggesting LUS > 18 may be associated with the extubation failure in neonatal RDS. The AUC of LUS for predicting the extubation failure was superior to the AUCs of gestational age, body length, and birth weight. The cutoff values of gestational age, body length, and birth weight were 29 weeks, 37 cm, and 1.19 kg, respectively. The calibration curve of the predictive effectiveness of LUS is shown in **Figure 4A** based on the training group. The internal validation using the testing set was carried out as shown in **Table 5** and **Figure 3B**. The AUC of LUS was 0.855 (95% CI: 0.817–0.954). It was indicated that LUS had the predictive ability for extubation failure from MV among newborns with RDS. The fitting effect of the calibration curve is listed in **Figure 4B**, which suggests that the predictive effectiveness of LUS was good.

TABLE 3 | Collinear assessment of independent variables.

Variables	VIF	Tolerance
Gestational age	2.020	0.495
Body length	3.129	0.320
Birth weight	3.676	0.272
$PaCO_2$	1.025	0.976
LVEDD	1.082	0.924
LUS	1.036	0.956

VIF, variance inflation factor; $PaCO_2$, arterial partial pressure of carbon dioxide; LVEDD, left ventricular end-diastolic diameter; LUS, lung ultrasound score.

DISCUSSION

Neonatal RDS is manifested by respiratory dysfunction resulting from the collapse and sharp reduction of residual gas in the alveolar due to the lack of sufficient active substances on the surface of newborn lungs, and it mainly occurs in premature and low birth weight infants. Imaging examination is a common diagnostic technique among newborns with RDS, including chest X-ray, CT, and lung ultrasound (20). Of these, X-ray is a basic diagnostic method for pulmonary lesions, with simple operation and low examination cost, but it is easy to be affected by the overlapping of internal organs in the chest, resulting in insufficient image clarity and unclear display of tiny lung lesions, which is prone to missed diagnosis and misdiagnosis. Both chest X-ray and CT have relatively large radiation damage, which may have a certain adverse effect on the development of neonates (21, 22). Moreover, the poor cooperation of most families made it impossible to perform real-time dynamic detection and repeated scanning on critically ill infants, which affects the diagnostic results. As a non-invasive, dynamic, and real-time imaging technique, ultrasound has been gradually applied in the diagnosis of neonatal pulmonary diseases, such as neonatal RDS, transient tachypnea of new-born, pneumonia, meconium aspiration syndrome, and pneumothorax (20, 23).

Previous studies reported that LUS has good diagnostic accuracy and specificity in comparison with chest X-ray, especially for the quantitative diagnosis of neonatal RDS (24, 25). To date, LUS-related studies focused on the predictive values of LUS in need for surfactants and the severity of neonatal RDS (15, 26). Nonetheless, few studies assessed the role of LUS in the weaning off from MV among babies with RDS. In the current study, a total of 314 infants who underwent MV support were included, with 208 of the extubation success and 106 of the extubation failure. The purpose was to investigate the predictive power of LUS among RDS neonates who failed extubation from MV. The results suggested that gestational age, body length, birth weight, and LUS were the predictive factors of the extubation failure, and a predictive model was conducted to evaluate the risk of extubation failure on the basis of these variables in newborns with RDS. Then, the comparison of predictive effectiveness between the model and LUS was carried out, and no significant difference was observed. The AUC of LUS was 0.858, with a sensitivity of 84.00%, a specificity of 80.69%, and a cutoff value of 18, which was similar to the results of the internal validation. It was indicated that LUS performed the predictive ability for the extubation failure from MV among RDS newborns. When LUS was over 18, the risk of extubation failure from MV may increase in RDS newborns.

The alteration in acoustic patterns is determined by the dynamic change between air and fluids in the lung parenchyma, which is easy to measure (27). LUS can be applied to detect vertical hyperechoic comet-tail B-lines artifacts (BLA) (28), and BLA is commonly considered to be associated with lung aeration and extravascular lung water (EVLW) (29). The change of pulmonary condition can be evaluated by the number of B-lines because B-lines increase with loss of lung aeration and increased EVLW (30). According to Anile et al. (31), the presence of >3 positive lung quadrants was considered a good index to identify EVLW. In Brat et al. (32), the LUS was closely related to the oxygenation status of preterm newborns, and it may be highly reliable to predict the administration of surfactants in preterm infants. What's more, Pang et al. (17) demonstrated that LUS and consolidation areas can be used to grade neonatal RDS and to discriminate neonatal RDS from non-neonatal RDS and can also predict the outcome of applying MV. Tenza-Lozano et al. (33) also mentioned that the feasibility of MV weaning could be assessed by LUS, similar to our findings. It was indicated that LUS is a good predictive tool for the weaning off from MV, and it may be useful for clinicians to intervene early to avoid the extubation failure from MV.

In the present study, we assessed the predictive value of LUS in the extubation failure among RDS infants, which was rarely explored. We discovered that the effectiveness of LUS was similar to that of the combined model in predicting the extubation failure from MV. Given that the operation of LUS was not complicated, the interpretation of LUS diagnosis results has high interobserver agreement even among interpreters with varying levels of experience (34), indicating that LUS may be an effective prediction tool for the extubation outcomes after MV. In addition, some limitations should be warranted caution for interpreting the findings. First, a retrospective cohort study with an internal validation was conducted to assess the effectiveness of LUS in predicting extubation failure among newborns with RDS. Second, LUS is a semiquantitative measurement. The reproducibility of B-line between transducers and between raters was of concern, which depended on the transducer used and interpretation of the raters (35, 36). Third, two pediatricians stored the pulmonary ultrasound images, and the consistency between operators was not evaluated. Further studies with multiple centers, large samples, and perspective designs are needed to explore.

In this study, we found gestational age, body length, birth weight, and LUS were the predictive factors of the extubation failure from MV. The AUC of LUS was 0.858, with a sensitivity of 84.00%, a specificity of 80.69%, and a cutoff value of 18, indicating LUS performed the predictive ability in the extubation failure from MV among newborns with RDS, which may guide pediatricians to conduct early interventions and treatments.

TABLE 4 | Multivariate Logistic regression analysis for the extubation failure.

Variables	*β*	*S. E*	Wald	*P*	*OR*	95% CI	
						Lower	Upper
Gestational age	−0.161	0.077	4.344	0.037	0.851	0.967	0.990
Body length	−0.200	0.076	6.902	0.009	0.819	0.705	0.950
Birth weigh	−2.351	0.849	7.658	0.006	0.095	0.018	0.504
LUS	0.110	0.050	4.811	0.028	1.116	1.012	1.231

OR, odds ratio; CI, confidence interval; LUS, lung ultrasound score.

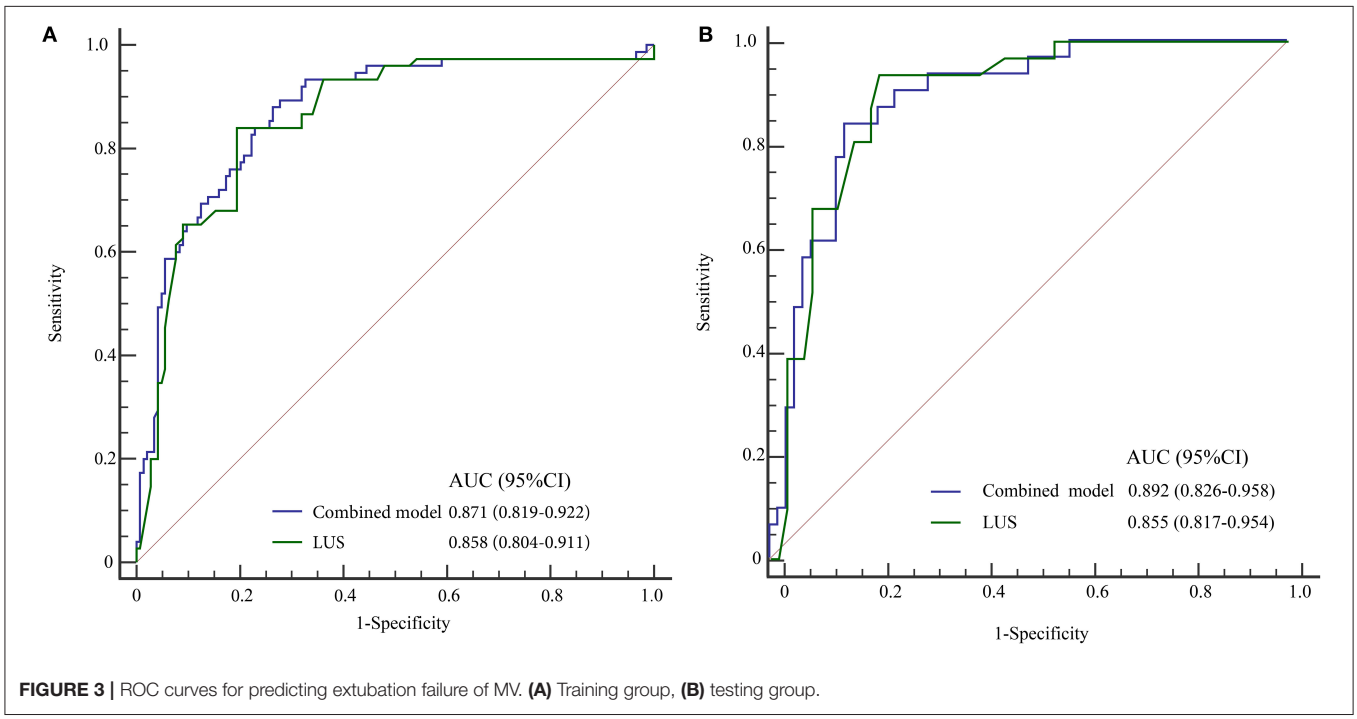

FIGURE 3 | ROC curves for predicting extubation failure of MV. **(A)** Training group, **(B)** testing group.

TABLE 5 | The prediction for the extubation failure in RDS infants.

Variables	AUC	Sensitivity (95% CI)	Specificity (95% CI)	Cut-off	*Z*	*P*
Training group						
Combined model	0.871 (0.819–0.922)	86.67 (76.80–93.40)	74.31 (66.40–81.20)	0.306		
LUS	0.858 (0.804–0.911)	84.00 (73.70–91.40)	80.69 (73.30–86.80)	18	0.880	0.379
Gestational age	0.655 (0.588–0.717)	38.67 (27.60–50.60)	88.89 (82.63–93.50)	29	5.365	<0.001
Body length	0.739 (0.710–0.767)	80.94 (75.20–86.60)	56.82 (55.32–58.25)	37	4.345	<0.001
Birth weigh	0.635 (0.567–0.698)	70.67 (59.02–80.60)	49.66 (41.30–58.10)	1.19	5.732	<0.001
Internal validation						
Combined model	0.892 (0.826–0.958)	93.55 (78.60–99.20)	79.37 (67.30–88.50)	0.306		
LUS	0.855 (0.817–0.954)	83.87 (66.30–94.50)	85.48 (74.20–93.10)	18	0.248	0.804
Gestational age	0.648 (0.553–0.744)	72.92 (61.53–84.26)	30.34 (19.20–41.43)	29	4.134	<0.001
Body length	0.412 (0.206–0.617)	64.31 (39.20–89.42)	19.00 (2.36–35.80)	37	4.349	<0.001
Birth weigh	0.652 (0.458–0.847)	67.70 (51.30–84.20)	0.649 (52.56–77.32)	1.19	2.296	0.022

RDS, respiratory distress syndrome; AUC, area under curve; CI, confidence interval; LUS, lung ultrasound score.

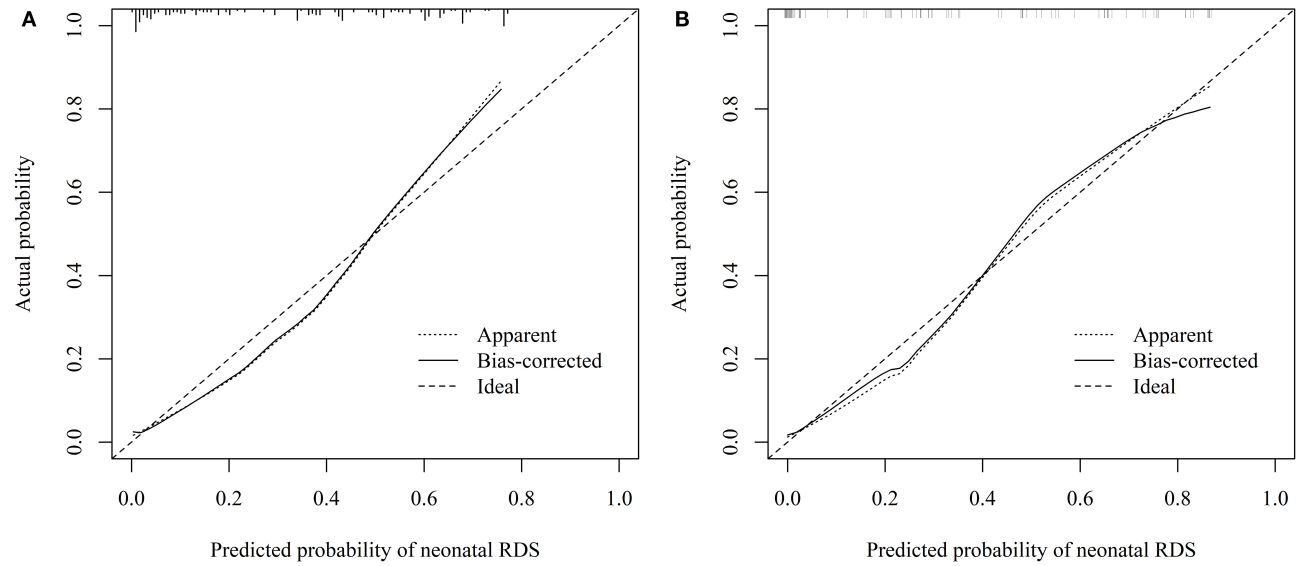

FIGURE 4 | Calibration curves for prediction of LUS. **(A)** training group, **(B)** testing group.

DATA AVAILABILITY STATEMENT

The raw data supporting the conclusions of this article will be made available by the authors, without undue reservation.

ETHICS STATEMENT

The studies involving human participants were reviewed and approved by the Institutional Review Board (IRB) of Guangdong Second Provincial General Hospital. Written informed consent to participate in this study was provided by the participants' legal guardian/next of kin.

AUTHOR CONTRIBUTIONS

ZL, CY, and QM designed the study. ZL wrote the manuscript. QM, BW, XL, and QW collected, analyzed, and interpreted the data. CY critically reviewed, edited, and approved the manuscript. All authors read and approved the final manuscript.

FUNDING

This study was supported by the Medical Research Fund of Guangdong Province (A2020064). The funding body did not play a role in designing the study, or collecting, analyzing, or interpreting data, or writing the manuscript.

REFERENCES

1. Rahtu M, Frerichs I, Waldmann AD, Strodthoff C, Becher T, Bayford R, et al. Early recognition of pneumothorax in neonatal respiratory distress syndrome with electrical impedance tomography. *Am J Respir Crit Care Med.* (2019) 200:1060–1. doi: 10.1164/rccm.201810-1999IM
2. Sweet LR, Keech C, Klein NP, Marshall HS, Tagbo BN, Quine D, et al. Respiratory distress in the neonate: Case definition & guidelines for data collection, analysis, and presentation of maternal immunization safety data. *Vaccine.* (2017) 35:6506–17. doi: 10.1016/j.vaccine.2017.01.046
3. Shao XM, Ye HM, Qiu XS. *Practice of Neonatology (5th edition)*. Beijing: People's Medical Publishing House (China) (2012).
4. Stoll BJ, Hansen NI, Bell EF, Shankaran S, Laptook AR, Walsh MC, et al. Neonatal outcomes of extremely preterm infants from the NICHD Neonatal Research Network. *Pediatrics.* (2010) 126:443–56. doi: 10.1542/peds.2009-2959
5. Parkash A, Haider N, Khoso ZA, Shaikh AS. Frequency, causes and outcome of neonates with respiratory distress admitted to Neonatal Intensive Care Unit, National Institute of Child Health, Karachi. *J Pak Med Assoc.* (2015) 65:771–5.
6. Smallwood CD, Davis MD. Year in review 2018: pediatric mechanical ventilation. *Respir Care.* (2019) 64:855–63. doi: 10.4187/respcare.07029
7. Ding F, Zhang J, Zhang W, Zhao Q, Cheng Z, Wang Y, et al. Clinical study of different modes of non-invasive ventilation treatment in preterm infants with respiratory distress syndrome after extubation. *Front Pediatr.* (2020) 25:63. doi: 10.3389/fped.2020.00063
8. Abdel Rahman DA, Saber S, El-Maghraby A. Diaphragm and lung ultrasound indices in prediction of outcome of weaning from mechanical ventilation in Pediatric Intensive Care Unit. *Indian J Pediatr.* (2020) 87:413–20. doi: 10.1007/s12098-019-03177-y
9. Xue Y, Zhang Z, Sheng CQ, Li YM, Jia FY. The predictive value of diaphragm ultrasound for weaning outcomes in critically ill children. *BMC Pulm Med.* (2019) 19:270. doi: 10.1186/s12890-019-1034-0
10. Glenski JA, Crawford M, Rehder K. High-frequency, small-volume ventilation during thoracic surgery. *Anesthesiology.* (1986) 64:211–4. doi: 10.1097/00000542-198602000-00014
11. Ko DR, Beom J, Lee HS, You JS, Chung HS, Chung SP. Benefits of high-flow nasal cannula therapy for acute pulmonary edema in patients with heart failure in the emergency department: a prospective multi-center randomized controlled trial. *J Clin Med.* (2020) 9:1937. doi: 10.3390/jcm9061937

12. Fadila M, Rajasurya V, Regunath H. *Ventilator Weaning*. Treasure Island, FL: StatPearls Publishing Copyright © 2020 (2020).
13. Szymański P, Kruczek P, Hozejowski R, Wais P. Modified lung ultrasound score predicts ventilation requirements in neonatal respiratory distress syndrome. *BMC Pediatr.* (2021) 21:17. doi: 10.1186/s12887-020-02485-z
14. Sawires HK, Abdel Ghany EA, Hussein NF, Seif HM. Use of lung ultrasound in detection of complications of respiratory distress syndrome. *Ultrasound Med Biol.* (2015) 41:2319–25. doi: 10.1016/j.ultrasmedbio.2015.04.024
15. De Martino L, Yousef N, Ben-Ammar R, Raimondi F, Shankar-Aguilera S, De Luca D. Lung ultrasound score predicts surfactant need in extremely preterm neonates. *Pediatrics.* (2018) 142:463. doi: 10.1542/peds.2018-0463
16. Vento G, Ventura ML, Pastorino R, Kaam A, Carnielli V, Cools F, et al. Lung recruitment before surfactant administration in extremely preterm neonates with respiratory distress syndrome (IN-REC-SUR-E): a randomised, unblinded, controlled trial. *Lancet Respir Med.* (2020) 9:159–66. doi: 10.1016/S2213-2600(20)30179-X
17. Pang H, Zhang B, Shi J, Zang J, Qiu L. Diagnostic value of lung ultrasound in evaluating the severity of neonatal respiratory distress syndrome. *Eur J Radiol.* (2019) 116:186–91. doi: 10.1016/j.ejrad.2019.05.004
18. Rouby JJ, Arbelot C, Gao Y, Zhang M, Lv J, An Y, et al. Training for lung ultrasound score measurement in critically ill patients. *Am J Respir Crit Care Med.* (2018) 198:398–401. doi: 10.1164/rccm.201802-0227LE
19. Moschietto S, Doyen D, Grech L, Dellamonica J, Hyvernat H, Bernardin GJC. Transthoracic echocardiography with Doppler tissue imaging predicts weaning failure from mechanical ventilation: evolution of the left ventricle relaxation rate during a spontaneous breathing trial is the key factor in weaning outcome. *Crit Care.* (2012) 16:R81. doi: 10.1186/cc11339
20. Gregorio-Hernandez R, Arriaga-Redondo M, Perez-Perez A, Ramos-Navarro C, Sanchez-Luna M. Lung ultrasound in preterm infants with respiratory distress: experience in a neonatal intensive care unit. *Eur J Pediatr.* (2020) 179:81–9. doi: 10.1007/s00431-019-03470-0
21. Ait-Ali L, Andreassi MG, Foffa I, Spadoni I, Vano E, Picano E. Cumulative patient effective dose and acute radiation-induced chromosomal DNA damage in children with congenital heart disease. *Heart.* (2010) 96:269–74. doi: 10.1136/hrt.2008.160309
22. Kleinerman RA. Cancer risks following diagnostic and therapeutic radiation exposure in children. *Pediatr Radiol.* (2006) 36(Suppl. 2):121–5. doi: 10.1007/s00247-006-0191-5
23. Liu J, Liu F, Liu Y, Wang HW, Feng ZC. Lung ultrasonography for the diagnosis of severe neonatal pneumonia. *Chest.* (2014) 146:383–8. doi: 10.1378/chest.13-2852
24. Smolarova S, Kocvarova L, Matasova K, Zibolen M, Calkovska A. Impact of updated European Consensus Guidelines on the management of neonatal respiratory distress syndrome on clinical outcome of preterm infants. *Adv Exp Med Biol.* (2015) 835:61–6. doi: 10.1007/5584_2014_39
25. Barillari A, Fioretti M. Lung ultrasound: a new tool for the emergency physician. *Intern Emerg Med.* (2010) 5:335–40. doi: 10.1007/s11739-010-0381-x
26. Vardar G, Karadag N, Karatekin G. The role of lung ultrasound as an early diagnostic tool for need of surfactant therapy in preterm infants with respiratory distress syndrome. *Am J Perinatol.* (2020). 38, 1547–1556. doi: 10.1055/s-0040-1714207
27. Chen SW, Zhang MY, Liu J. Application of lung ultrasonography in the diagnosis of childhood lung diseases. *Chin Med J.* (2015) 128:2672–8. doi: 10.4103/0366-6999.166035
28. Volpicelli G, Elbarbary M, Blaivas M, Lichtenstein DA, Mathis G, Kirkpatrick AW, et al. International evidence-based recommendations for point-of-care lung ultrasound. *Intensive Care Med.* (2012) 38:577–91. doi: 10.1007/s00134-012-2513-4
29. Lichtenstein DA. Ultrasound in the management of thoracic disease. *Crit Care Med.* (2007) 35:S250–61. doi: 10.1097/01.CCM.0000260674.60761.85
30. Bouhemad B, Brisson H, Le-Guen M, Arbelot C, Lu Q, Rouby JJ. Bedside ultrasound assessment of positive end-expiratory pressure-induced lung recruitment. *Am J Respir Crit Care Med.* (2011) 183:341–7. doi: 10.1164/rccm.201003-0369OC
31. Anile A, Russo J, Castiglione G, Volpicelli G. A simplified lung ultrasound approach to detect increased extravascular lung water in critically ill patients. *Crit Ultrasound J.* (2017) 9:13. doi: 10.1186/s13089-017-0068-x
32. Brat R, Yousef N, Klifa R, Reynaud S, Shankar Aguilera S, De Luca D. Lung ultrasonography score to evaluate oxygenation and surfactant need in neonates treated with continuous positive airway pressure. *JAMA Pediatr.* (2015) 169:e151797. doi: 10.1001/jamapediatrics.2015.1797
33. Tenza-Lozano E, Llamas-Alvarez A, Jaimez-Navarro E, Fernández-Sánchez J. Lung and diaphragm ultrasound as predictors of success in weaning from mechanical ventilation. *Crit Ultrasound J.* (2018) 10:12. doi: 10.1186/s13089-018-0094-3
34. Brusa G, Savoia M, Vergine M, Bon A, Copetti R, Cattarossi L. Neonatal lung sonography: interobserver agreement between physician interpreters with varying levels of experience. *J Ultrasound Med.* (2015) 34:1549–54. doi: 10.7863/ultra.15.14.08016
35. Corradi F, Via G, Forfori F, Brusasco C, Tavazzi G. Lung ultrasound and B-lines quantification inaccuracy: B sure to have the right solution. *Intensive Care Med.* (2020) 46:1081–3. doi: 10.1007/s00134-020-06005-6
36. Haaksma ME, Smit JM, Heldeweg MLA, Pisani L, Elbers P, Tuinman PR. Lung ultrasound and B-lines: B careful! *Intensive Care Med.* (2020) 46:544–5. doi: 10.1007/s00134-019-05911-8

Conflict of Interest: The authors declare that the research was conducted in the absence of any commercial or financial relationships that could be construed as a potential conflict of interest.

Publisher's Note: All claims expressed in this article are solely those of the authors and do not necessarily represent those of their affiliated organizations, or those of the publisher, the editors and the reviewers. Any product that may be evaluated in this article, or claim that may be made by its manufacturer, is not guaranteed or endorsed by the publisher.

Copyright © 2021 Liang, Meng, You, Wu, Li and Wu. This is an open-access article distributed under the terms of the Creative Commons Attribution License (CC BY). The use, distribution or reproduction in other forums is permitted, provided the original author(s) and the copyright owner(s) are credited and that the original publication in this journal is cited, in accordance with accepted academic practice. No use, distribution or reproduction is permitted which does not comply with these terms.

frontiers in Pediatrics

ORIGINAL RESEARCH
published: 11 January 2022
doi: 10.3389/fped.2021.792160

Non-invasive High-Frequency Oscillatory Ventilation as Initial Respiratory Support for Preterm Infants With Respiratory Distress Syndrome

Shu-Hua Lai [1,2], Ying-Ling Xie [1,2], Zhi-Qing Chen [1,2], Rong Chen [1,2], Wen-Hong Cai [1,2], Luo-Cheng Wu [1,2], Yun-Feng Lin [1,2,3,4] and Yi-Rong Zheng [1,2,3,4]**

[1] Department of Neonatology, Fujian Maternity and Child Health Hospital, Affiliated Hospital of Fujian Medical University, Fuzhou, China, [2] Fujian Key Laboratory of Women and Children's Critical Diseases Research, Fujian Maternity and Child Health Hospital, Fuzhou, China, [3] Fujian Branch of Shanghai Children's Medical Center, Fuzhou, China, [4] Fujian Children's Hospital, Fuzhou, China

OPEN ACCESS

Edited by:
Deb Strickland,
University of Western Australia, Australia

Reviewed by:
Daniel Klotz,
University of Freiburg, Germany
Gianluca Lista,
Ospedale dei Bambini Vittore Buzzi, Italy

***Correspondence:**
Yun-Feng Lin
linyf2003@qq.com
Yi-Rong Zheng
zhengyirong2020@163.com

Specialty section:
This article was submitted to Neonatology, a section of the journal Frontiers in Pediatrics

Received: 09 October 2021
Accepted: 17 December 2021
Published: 11 January 2022

Citation:
Lai SH, Xie YL, Chen ZQ, Chen R, Cai WH, Wu LC, Lin YF and Zheng YR (2022) Non-invasive High-Frequency Oscillatory Ventilation as Initial Respiratory Support for Preterm Infants With Respiratory Distress Syndrome. Front. Pediatr. 9:792160. doi: 10.3389/fped.2021.792160

Objectives: The aim of this study was to investigate the safety and feasibility of nHFOV as initial respiratory support in preterm infants with RDS.

Methods: This study retrospectively analyzed the clinical data of 244 premature infants with RDS who were treated in our hospital from January 2016 to January 2019 and divided into the nHFOV group ($n = 115$) and the BiPAP group ($n = 129$) based on the initial respiratory support method.

Results: Respiratory outcomes showed that the rate of NIV failure during the first 72 hours of life in the nHFOV group was significantly lower than that in the BiPAP group. The time of NIV in the nHFOV group was significantly shorter than that in the BiPAP group. The time of supplemental oxygen in the nHFOV group was significantly shorter than that in the BiPAP group. The incidence of air leakage syndrome in the nHFOV group was significantly lower than that in the BiPAP group, and the length of hospital stay of the nHFOV group was also significantly shorter than that in the BiPAP group. Although the rate of infants diagnosed with BPD was similar between the two groups, the rate of severe BPD in the nHFOV group was significantly lower than that in the BiPAP group.

Conclusion: This study showed that nHFOV as initial respiratory support for preterm infants with RDS was feasible and safe compared to BiPAP. Furthermore, nHFOV can reduce the need for IMV and reduce the incidence of severe BPD and air leak syndrome.

Keywords: non-invasive high-frequency oscillatory ventilation, biphasic positive airway pressure, preterm infants, respiratory distress syndrome, non-invasive ventilation

INTRODUCTION

Respiratory distress syndrome (RDS) is one of the most common complications in preterm infants and the most common reason for premature death. A large proportion of preterm infants with RDS require invasive mechanical ventilation (IMV) at an early stage of life. Although ventilation is usually life-saving, it can also cause many complications, such as air leak syndrome, lung injury,

and neurodevelopmental impairment (1–3). Neonatologists are increasingly using non-invasive ventilation (NIV) in the neonatal intensive care unit (NICU) to reduce these adverse effects of IMV; among them, biphasic positive airway pressure (BiPAP) is the classic non-invasive ventilation mode. Reports have shown that NIV is feasible in clinical practice and is associated with reducing the need for intubation and decreasing ventilator-related lung injury and other complications (2, 4). Non-invasive high-frequency oscillatory ventilation (nHFOV) is a promising new mode of NIV that can reduce the risk and complications of IMV (5, 6). However, there are few reports on the application of nHFOV for the treatment of premature infants with RDS. We hypothesized that nHFOV was safe and effective as an initial respiratory support for preterm infants with RDS and had more advantages than BiPAP. We conducted a retrospective controlled study to evaluate the efficacy, safety and advantages of nHFOV for the treatment of premature infants with RDS.

METHODS

The present study was approved by the ethics committee of our hospital and adhered to the tenets of the Declaration of Helsinki. Additionally, all parents of the patients signed the consent form before participating in the study.

Patients

Our hospital started using nHFOV in January 2018, and then RDS initial respiratory support was gradually transitioned from the previous BiPAP to nHFOV. Therefore, BiPAP respiratory support was also used in some patients from 2018 and 2019. From January 2016 to January 2019, there was no change in other treatment except respiratory support. This study retrospectively analyzed the clinical data of 244 premature infants with RDS who were treated in our hospital from January 2016 to January 2019 and were divided into two groups based on the initial respiratory support methods. The nHFOV group had 115 premature infants who received nHFOV as initial respiratory support, and the BiPAP group had 129 premature infants who received BiPAP as initial respiratory support (**Figure 1**). All the patients were definitely diagnosed with RDS based on the diagnostic criteria. The diagnostic criteria of RDS are as follows (6): (1) High-risk factors: maternal diabetes during pregnancy, intrauterine infection, premature delivery, premature rupture of membranes for more than 24 h, intrauterine distress, asphyxia during delivery, etc. (2) Clinical symptoms: progressive aggravation of tachypnea within 6 h after birth (>60 times/min); cyanosis, three depressions in inhalation and obvious expiratory moans, irregular breathing, and apnoea; and decreased respiratory sounds in both lungs were detected on auscultation. (3) Typical chest X-ray features.

The inclusion criteria were as follows: (1) premature infants with gestational age of 25–34 weeks; (2) diagnosed with RDS within 24 h of birth and received nHFVO or BiPAP as initial respiratory support. The exclusion criteria were as follows: (1) complications involving severe congenital structural malformations such as congenital heart disease, congenital diaphragmatic hernia, respiratory tract malformation, and severe digestive tract malformation; (2) incomplete data; and (3) the parents of the infants refused to participate in this study.

Management in the Delivery Room

Drying, maintaining warmth and treating the umbilical cord immediately after birth were performed in the delivery room. Then, based on the breathing condition of the premature baby, we started respiratory support in the delivery room with nasal continuous positive airway pressure support or intermittent positive pressure ventilation after intubation. The initial management in the delivery room for all the babies in the two groups was the same.

Respiratory Management

Daily care was performed as needed for preterm infants in the NICU, along with continuous monitoring of pulse oxygen saturation, respiratory rate, and heart rate. nHFOV or BiPAP was started within 24 h of life with clinical signs of respiratory distress. Short binasal prongs (Infant Flow, CareFusion, California, USA) were used as the interface for the two NIV devices. The orogastric tube was kept open to decompress the stomach and to facilitate feeding. All of the preterm infants were given prophylactic caffeine on the first day of life. Caffeine was administered at a loading dose of 20 mg/kg caffeine citrate, and then a daily maintenance dose of 5–10 mg/kg coffee citrate was given. Our unit did not implement preventive use of surfactants. Surfactant requirements were assessed for all preterm infants. Porcine surfactant (Curosurf, Chiesi Farmaceutici, Parma, Italy) was administered as a rescue therapy *via* the intubation, surfactant therapy, extubation (INSURE) method if the infant required $\geq$ 0.40 fraction of inspired oxygen (FiO2) to maintain the target oxygen saturation level of 90–95%. The first dose of surfactant therapy was 200 mg/kg. Additional surfactant doses of 100 mg/kg were administered if the infants still required $\geq$ 0.40 FiO2 to maintain the target oxygen saturation.

In the nHFOV group, a neonatal non-invasive high-frequency ventilator from Medin CNO (Medical Innovations GmbH, Puchheim, Germany) with an output oxygen concentration range of 21 to 100% was used. The initial parameters were as follows: average airway pressure (MAP) was 8 cmH_2O, frequency was 9 Hz, amplitude was adjusted to achieve sufficient chest oscillation at rest, and FiO2 was 0.4. Based on blood gas analysis and transcutaneous oxygen saturation (SpO2) adjustment parameters, FiO2 was adjusted by 0.05, MAP was adjusted by 1 cmH_2O, and frequency was adjusted by 1 Hz each time.

For infants in the BiPAP group, a baseline PEEP of 5 cmH_2O was established, with a high PEEP of 9 cmH_2O, a

Abbreviations: RDS, Respiratory distress syndrome; IMV, Invasive mechanical ventilation; NIV, Non-invasive ventilation; NICU, Neonatal intensive care unit; BiPAP, Biphasic positive airway pressure; nHFOV, Non-invasive high-frequency oscillatory ventilation; FiO2, Inspired oxygen; MAP, Average airway pressure; NCPAP, Nasal continuous positive airway pressure; BPD, Bronchopulmonary dysplasia.

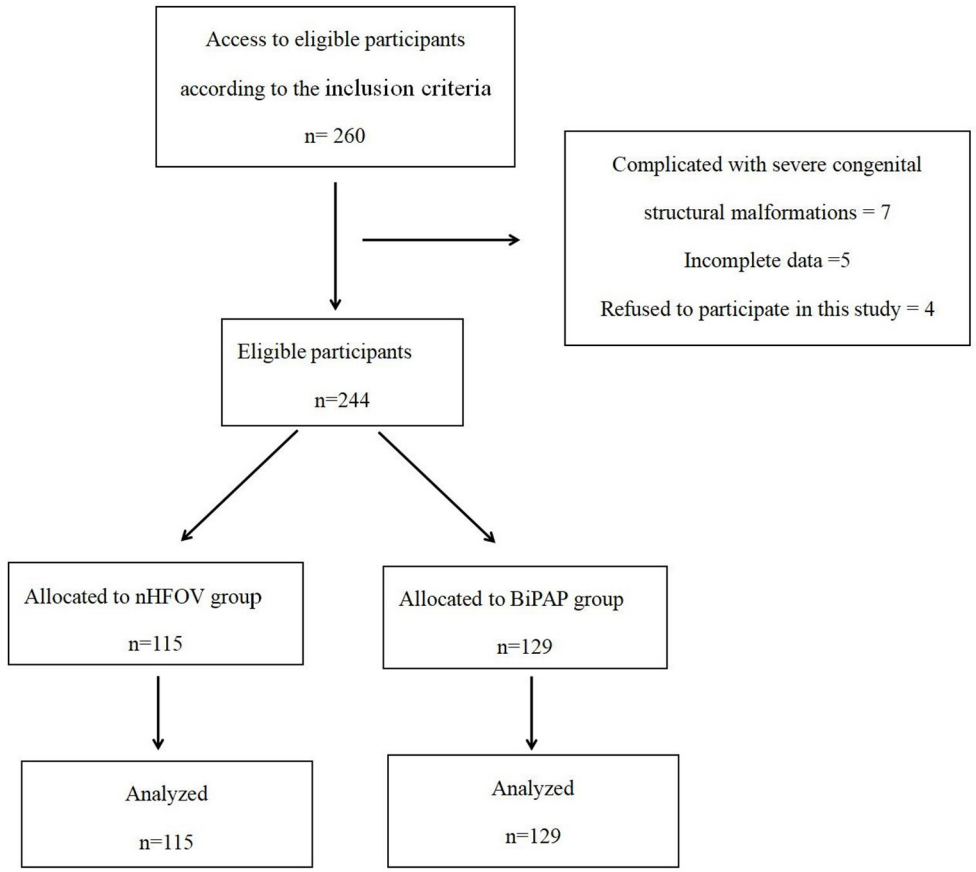

FIGURE 1 | The patient flow diagram of the study.

respiratory rate of 30/min, and an initial inspiratory time of 0.5 s (CareFusion, California, USA). The baseline PEEP was adjusted to 4–7 cmH_2O, and the high PEEP was adjusted to 7–10 cmH_2O.

If the infant remained clinically stable at minimum respiratory parameters with nHFOV (MAP: 6 cmH2O; FiO2: 0.30) and BiPAP (cycle rate: 15 times/min, lower CPAP: 3 cmH_2O; higher CPAP: 5 cmH_2O; FiO2: 0.30), good respiratory effort and maintenance of an oxygen saturation level of 90–95%, conditions were switched to a heated humidified high-flow nasal cannula or nasal continuous positive airway pressure (NCPAP). If the infant under NCPAP had a CPAP level of 3 cmH_2O and FiO2 < 0.25 and tolerated the treatment well for at least 24 h with no evidence of apnoea, the infant was weaned to supplemental oxygen or room air.

Failure of NIV was defined as at least one of the following (7): severe respiratory acidosis (pH $\leq$ 7.20 and PaCO2 $\geq$ 60 mmHg); hypoxemia (PaO_2 $\leq$ 50 mmHg and FiO2 $\geq$ 0.6); recurrent apnoea associated with bradycardia $\geq$ 3 times/hour; or a single episode of apnoea that required bag-and-mask ventilation, pneumothorax or intestinal perforation, severe respiratory distress, or pulmonary hemorrhage.

The definition of bronchopulmonary dysplasia (BPD) was any oxygen dependence ($FiO_2 > 21\%$) of the newborn lasting more than 28 days. Based on the judgement of oxygen dependence and different types of respiratory support measures, BPD can be categorized into three degrees: mild, moderate and severe. Preterm infants with a gestational age less than 32 weeks were assessed at 36 weeks postmenstrual or discharge, and preterm infants with a gestational age more than 32 weeks were assessed at 56 days after birth or discharge. BPD was considered (1) mild for patients without oxygen inhalation; (2) moderate for those requiring oxygen inhalation and FiO2 was $< 30\%$; and (3) severe for those requiring oxygen inhalation, FiO2 was $\geq 30\%$ or positive pressure ventilation was needed (8).

Statistical Analysis

SPSS 25.0 was used for statistical analysis. Continuous data are presented as the mean $\pm$ standard deviation and range. With all continuous data, the normality of the distribution was tested, and they followed a normal distribution. Clinical parameters between the two groups were compared with independent samples *t* tests. $\chi 2$ tests were used to categorize the variables. A *p* value of <0.05 was defined as significant.

TABLE 1 | Comparison of general data between the two groups.

	nHFOV group	BiPAP group	*P*-value
Number	115	129	
Gestational age (weeks)	29.1 ± 1.8	28.9 ± 1.6	0.457
Birthweight (kg)	1.1 ± 0.220	1.2 ± 0.242	0.198
Male/female	59/56	68/61	0.826
Multiple births	14 (12.1%)	17 (13.2%)	0.814
Apgar score at 5 min	8.2 ± 2.1	8.3 ± 2.0	0.979
Intra uterine growth retardation	21 (18.3%)	26 (20.2%)	0.708
Ante-natal steroids (incomplete and full course)	61 (53.0%)	78 (60.4%)	0.242
Cesarean section	55 (47.8%)	74 (57.4%)	0.136
Gestational diabetes mellitus	35 (30.4%)	46 (35.7%)	0.387
Pre-eclampsia	24 (20.9%)	29 (22.5%)	0.763
Maternal age (years)	29.2± 3.0	29.3 ± 2.5	0.744
Prolonged premature rupture of membranes > 18 h	26 (22.6%)	22 (17.1%)	0.276
Chorioamnionitis	13 (11.3%)	10 (7.8%)	0.343

BiPAP, biphasic positive airway pressure; nHFOV, non-invasive high-frequency oscillatory ventilation.

RESULTS

The general data, birth situation and perinatal data of the participants in the two groups are shown in **Table 1**; there were no statistically significant differences between the two groups, which indicated that the baseline characteristics between the two groups were similar (**Table 1**).

The respiratory outcomes showed that the rate of NIV failure in the first 72 h of life was significantly lower in the nHFOV group than in the BiPAP group (9 vs. 23, $P = 0.021$). The time of NIV in the nHFOV group was shorter than that in the BiPAP group (10.5 ± 4.3 vs. 12.7 ± 5.6, $P = 0.032$). Among infants with NIV failure, the time of first intubation in the BiPAP group was significantly earlier than that in the nHFOV group (2.0 ± 1.6 vs. 3.5 ± 2.3, $P = 0.048$), and the time of invasive ventilation in the nHFOV group was significantly shorter than that in the BiPAP group (3.2 ± 1.8 vs. 5.4 ± 2.0, $P = 0.036$). The time of supplemental oxygen in the nHFOV group was shorter than that in the BiPAP group (7.2 ± 4.8 vs. 8.5 ± 5.6, $P = 0.040$). The rate of the required surfactant was similar between the two groups (**Table 2**).

A comparison of the complications between the two groups showed that the incidence of air leakage syndrome in the nHFOV group was significantly lower than that in the BiPAP group (2 vs. 10, $P = 0.038$), and the length of hospital stay was also significantly shorter in the nHFOV group than in the BiPAP group (44.0 ± 10.9 vs. 47.3 ± 12.8, $P = 0.033$). Although the rate of infants diagnosed with BPD was similar between the two groups, the rate of severe BPD in the nHFOV group was significantly lower than that in the BiPAP group (1 vs. 7, $P = 0.046$). The incidence of nasal injury, retinopathy of prematurity requiring laser treatment, necrotizing enterocolitis, and mortality were similar between the two groups (**Table 3**).

DISCUSSION

Various forms of NIV are increasingly being used by neonatologists because of the potential adverse consequences of IMV, particularly ventilator-induced lung injury, and this restricted use of IMV in preterm infants might decrease lung inflammation and reduce the incidence of BPD and death (9). The most commonly used NIV method is BiPAP, and BiPAP is an effective therapy in the early management of RDS in preterm infants (10). nHFOV, as a novel mode of non-invasive ventilation, can improve the removal of carbon dioxide with the advantages of high-frequency ventilation and NIV (11).

Studies have shown that nHFOV can reduce the need for IMV compared to other NIV techniques (12–14). In this study, we found that compared to BiPAP, nHFOV as initial respiratory support reduced the need for IMV within the first 72 h of life. We also found that nHFOV decreased the rate of intubation, shortened the duration of IMV and postponed the first intubation. Compared with other forms of NIV, nHFOV retains a non-invasive interface and maintains continuous airway pressure, and it can also increase functional residual volume, maintain the opening of the upper airway, and prevent alveolar collapse, which can improve ventilation and oxygenation (15). Mukerji et al. used a lung model to compare nHFOV with other forms of NIV, and the results showed that nHFOV could remove carbon dioxide more effectively, promote alveolar revascularization and reduce the rate of tracheal intubation compared with other forms of NIV (16). We suggested that the higher NIV failure rate in the BiPAP group than in the nHFOV group might also be due to BiPAP offering synchronized nasal intermittent positive pressure ventilation using an abdominal capsule, which may be difficult to synchronize with infant breathing and does not result in larger tidal volumes (17). However, with nHFOV, there is no need for synchronization. nHFOV may improve ventilation by enhancing alveolar recruitment by applying higher MAP, and the functional residual capacity was increased (18). On the other hand, despite restricting the use of MAP on nHFOV to 10 cmH_2O, this was still higher than BiPAP for the corresponding FiO_2 levels. Binmanee et al. (19) proved that the use of high NIV (MAP $\geq$ 10 cmH_2O) resulted in the avoidance of intubation in the majority of cases,

TABLE 2 | Comparison of respiratory status between the two groups.

	nHFOV group	BiPAP group	*P*-value
Number	115	129	
NIV failure in the first 72 hours of life	9 (7.8%)	23 (17.8%)	0.021
Required surfactant	46 (40.0%)	59 (45.7%)	0.366
Required ≥ 2 doses of surfactant	10 (8.7%)	17 (13.1%)	0.265
Time at first intubation (days)	3.5 ± 2.3	2.0 ± 1.6	0.048
Duration of NIV (days)	10.5 ± 4.3	12.7 ± 5.6	0.032
Duration of IMV (days)	3.2 ± 1.8	5.4 ± 2.0	0.036
Duration of supplemental oxygen (days)	7.2 ± 4.8	8.5 ± 5.6	0.040

BiPAP, Biphasic positive airway pressure; nHFOV, non-invasive high-frequency oscillatory ventilation; IMV, invasive mechanical ventilation; NIV, Non-invasive ventilation.

TABLE 3 | Comparison of complications between the two groups.

	nHFOV group	BiPAP group	*P*-value
Number	115	129	
Nasal injury	5 (4.3%)	4 (3.1%)	0.738
Air leak syndrome	2 (1.7%)	10 (7.8%)	0.038
Retinopathy of prematurity required laser treatment	4 (3.5%)	9 (7.0%)	0.225
Necrotizing enterocolitis	8 (7.0%)	15 (11.6%)	0.213
BPD	17 (14.8%)	27 (20.9%)	0.212
Mild BPD	10 (8.7%)	11 (8.5%)	0.963
Moderate BPD	6 (5.2%)	9 (7.0%)	0.568
Severe BPD	1 (0.9%)	7 (5.4%)	0.046
Duration of hospitalization (days)	44.0± 10.9	47.3 ±12.8	0.033
Mortality	7 (6.1%)	8 (6.2%)	0.970

BiPAP, biphasic positive airway pressure; nHFOV, non-invasive high-frequency oscillatory ventilation; BPD, bronchopulmonary dysplasia.

without adverse effects. Yaser et al. (20) also found a higher MAP in the successful group than in the failure group as a prophylactic or rescue mode of NIV following extubation. Therefore, these differences may be due to the airway pressure itself rather than the pressure waveform generated from the two NIV modes.

The nHFOV group had a lower rate of air leak syndrome than the BiPAP group, and we suspected that this may be due to the small tidal volumes used, which results in less pressure-and-volume trauma from nHFOV (21). High-frequency oscillation ventilation is a type of oscillation with a high frequency of air flow. Through a diffusion mechanism, a small amount of gas was sent into or out of the airway ventilation method, and there was no synchronization and no man-machine confrontation (22). However, BiPAP offers synchronized nasal intermittent positive pressure ventilation using an abdominal capsule, which may be difficult to synchronize with infant breathing. This situation makes it very easy to create man-machine confrontation; even if the MAP was lower, air leak syndrome was more likely to occur.

BPD is a common and serious complication in premature infants (23). Studies have shown that IMV and high oxygen exposure are high-risk factors for BPD (24, 25). Although the rate of infants diagnosed with BPD was similar between the two groups, the rate of severe BPD in the nHFOV group was significantly lower than that in the BiPAP group. This difference may have resulted from the facilitation of gas exchange in neonates treated with nHFOV, and nHFOV was able to sustain oxygenation and ventilation while leading to improved alveolar or lung development (6, 26–28). These effects on lung development raise the possibility that nHFOV may reduce neonatal chronic lung disease. nHFOV reduces the duration of supplemental oxygen and the use of IMV, which can also help reduce the incidence of severe BPD.

nHFOV reduced the duration of supplemental oxygen and hospitalization, which may have benefitted from the reduction in airway inflammation, lung injury, and incidence of severe BPD by nHFOV. Of concern was the decrease in NEC and retinopathy of prematurity requiring laser treatment in the nHFOV group, which may have been due to nHFOV reducing the duration of supplemental oxygen and IMV and the fluctuations in blood oxygen saturation, although there were no statistically significant differences.

Our study had some limitations, which may affect the validity of our findings. First, it was a retrospective study, and it was not a prospective randomized controlled study, and therefore, the study's objectivity was somewhat limited. Second, it was a single-center study with a small sample size. Third, the follow-up time was not long enough. Fourth, the study infants were not stratified by birth weight or gestational

age, and there was a lack of infants at less than 25-weeks of gestation.

CONCLUSION

This study showed that nHFOV as initial respiratory support in preterm infants with RDS was feasible and safe compared to BiPAP. Furthermore, nHFOV can reduce the need for IMV and reduce the incidence of severe BPD and air leak syndrome.

DATA AVAILABILITY STATEMENT

The data analyzed in this study is subject to the following licenses/restrictions: The data that support the findings of this study are available on request from the corresponding author. The data are not publicly available due to privacy or ethical restrictions. Requests to access these datasets should be directed to Shu-Hua Lai, laishuhua2014@163.com.

AUTHOR CONTRIBUTIONS

S-HL, Y-FL, and Y-RZ designed the study, collected the clinical data, performed the statistical analysis, participated in the operation, and drafted the manuscript. Y-LX , Z-QC, RC, W-HC, and L-CW participated in the operation and revised the article. All authors read and approved the final manuscript.

ACKNOWLEDGMENTS

We appreciated all doctors in our center for fruitful advice and discussions.

REFERENCES

1. Miller JD, Carlo WA. Pulmonary complications of mechanical ventilation in neonates. *Clin Perinatol.* (2008) 35:273–81. doi: 10.1016/j.clp.2007.11.004
2. Sweet DG, Carnielli V, Greisen G, Hallman M, Ozek E, Te Pas A, et al. European consensus guidelines on the management of respiratory distress syndrome - 2019 update. *Neonatology*. (2019) 115:432–50. doi: 10.1159/000499361
3. Walsh MC, Morris BH, Wrage LA, Vohr BR, Poole WK, Tyson JE, et al. Extremely low birth weight neonates with protracted ventilation: mortality and 18-month neurodevelopmental outcomes. *J Pediatr*. (2005) 146:798–804. doi: 10.1016/j.jpeds.2005.01.047
4. Vendettuoli V, Bellu R, Zanini R, Mosca F, Gagliardi L. Italian Neonatal Network: Changes in ventilator strategies and outcomes in preterm infants. *Arch Dis Child Fetal Neonatal Ed.* (2014) 99:F321–4. doi: 10.1136/archdischild-2013-305165
5. Zhu XW, Zhao JN, Tang SF, Yan J, Shi Y. Noninvasive high-frequency oscillatory ventilation versus nasal continuous positive airway pressure in preterm infants with moderate-severe respiratory distress syndrome: a preliminary report. *Pediatr Pulmonol.* (2017) 52:1038–42. doi: 10.1002/ppul.23755
6. Null DM, Alvord J, Leavitt W, Wint A, Dahl MJ, Presson AP, et al. High-frequency nasal ventilation for 21 d maintains gas exchange with lower respiratory pressures and promotes alveolarization in preterm lambs. *Pediatr Res.* (2014) 75:507–16. doi: 10.1038/pr.2013.254
7. Shi Y, De Luca D. Continuous positive airway pressure (CPAP) vs noninvasive positive pressure ventilation (NIPPV) vs noninvasive high frequency oscillation ventilation (NHFOV) as post-extubation support in preterm neonates: protocol for an assessor-blinded, multicenter, randomized controlled trial. *BMC Pediatr*. (2019) 19:256. doi: 10.1186/s12887-019-1625-1
8. Jobe AH, Bancalari E. Bronchopulmonary dysplasia. *Am J Respir Crit Care Med.* (2001) 163:1723–9. doi: 10.1164/ajrccm.163.7.2011060
9. Vliegenthart RJS, Onland W, van Wassenaer-Leemhuis AG et al. Restricted ventilation associated with reduced neurodevelopmental impairment in preterm infants. *Neonatology.* (2017) 112:172–9. doi: 10.1159/000471841
10. Buyuktiryaki M, Okur N, Sari FN, Bekmez BO, Bezirganoglu H, Cakir U, et al. Comparison of three different noninvasive ventilation strategies as initial respiratory support in very low birth weight infants with respiratory distress syndrome: a retrospective study. *Arch Pediatr*. (2020) 27:322–7. doi: 10.1016/j.arcped.2020.06.002
11. Bottino R, Pontiggia F, Ricci C, Gambacorta A, Paladini A, Chijenas V, et al. Nasal high-frequency oscillatory ventilation and CO2 removal: a randomized controlled crossover trial. *Pediatr Pulmonol*. (2018) 53:1245–51. doi: 10.1002/ppul.24120
12. Mukerji A, Singh B, Helou SE, Fusch C, Dunn M, Belik J. et al. Use of noninvasive high-frequency ventilation in the neonatal intensive care unit: a retrospective review. *Am J Perinatol.* (2015) 30:171–6. doi: 10.1055/s-0034-1381317
13. Ali YAH, Seshia MM, Ali E, Alvaro R. Noninvasive High- Frequency Oscillatory Ventilation: A Retrospective Chart Review. *Am J Perinatol.* (2020). doi: 10.1055/s-0040-1718738. [Epub ahead of print].
14. Cao H, Li H, Zhu X, Wang L, Yi M, Li C, Chen L, Shi Y. Three non-invasive ventilation strategies for preterm infants with respiratory distress syndrome: a propensity score analysis. *Arch Med Sci.* (2020) 16:1319–26. doi: 10.5114/aoms.2020.93541
15. Haidar Shehadeh AM. Non-invasive high flow oscillatory ventilation in comparison with nasal continuous positive pressure ventilation for respiratory distress syndrome, a literature review. *J Matern Fetal Neonatal Med.* (2021) 34:2900–9. doi: 10.1080/14767058.2019.1671332
16. Mukerji A, Finelli M, Belik J. Nasal high-frequency oscillation for lung carbon dioxide clearance in the newborn. *Neonatology.* (2013) 103:161–5. doi: 10.1159/000345613
17. Owen LS, Morley CJ, Davis PG. Effects of synchronization during SiPAP-generated nasal intermittent positive pressure ventilation (NIPPV) in preterm infants. *Arch Dis Child Fetal Neonatal Ed.* (2015) 100:F24–30. doi: 10.1136/archdischild-2013-305830
18. De Luca D, Dell'Orto V. Non-invasive high-frequency oscillatory ventilation in neonates: review of physiology, biology, and clinical data. *Arch Dis Child Fetal Neonatal Ed.* (2016) 101:F565–70. doi: 10.1136/archdischild-2016-310664
19. Binmanee A, El Helou S, Shivananda S, Fusch C, Mukerji A. Use of high noninvasive respiratory support pressures in preterm neonates: a single-center experience. *J Matern Fetal Neonatal Med.* (2017) 30:2838–43. doi: 10.1080/14767058.2016.1265931
20. Mukerji A, Sarmiento K, Lee B, Hassall K, Shah V. Non-invasive high-frequency ventilation versus bi-phasic continuous positive airway pressure (BP-CPAP) following CPAP failure in infants <1250 g: a pilot randomized controlled trial. *J Perinatol.* (2017) 37:49–53. doi: 10.1038/jp.2016.172
21. Gaertner VD, Waldmann AD, Davis PG, Bassler D, Springer L, Thomson J, et al. Transmission of oscillatory volumes into the preterm lung during noninvasive high-frequency ventilation. *Am J Respir Crit Care Med.* (2021) 203:998–1005. doi: 10.1164/rccm.202007-2701OC
22. Courtney SE, Asselin JM. High-frequency jet and oscillatory ventilation for neonates: which strategy and when? *Respir Care Clin N Am.* (2006) 12:453–67. doi: 10.1016/j.rcc.2006.06.005
23. Horbar JD, Carpenter JH, Badger GJ, Kenny MJ, Soll RF, Morrow KA, et al. Mortality and neonatal morbidity among infants 501 to 1500 grams from 2000 to 2009. *Pediatrics.* (2012) 129:1019–26. doi: 10.1542/peds.2011-3028

24. Keszler M, Sant'Anna G. Mechanical ventilation and bronchopulmonary dysplasia. *Clin Perinatol.* (2015) 42:781–96. doi: 10.1016/j.clp.2015.08.006
25. Kapadia VS, Chalak LF, Sparks JE, Allen JR, Savani RC, Wyckoff MH. Resuscitation of preterm neonates with limited versus high oxygen strategy. *Pediatrics.* (2013) 132:e1488–96. doi: 10.1542/peds.2013-0978
26. Reyburn B, Li M, Metcalfe DB, Kroll NJ, Alvord J, Wint A, et al. Nasal ventilation alters mesenchymal cell turnover and improves alveolarization in preterm lambs. *Am J Respir Crit Care Med.* (2008) 178:407–18 doi: 10.1164/rccm.200802-359OC
27. Sahni M, Bhandari V. Recent advances in understanding and management of bronchopulmonary dysplasia. *F1000Res.* (2020) 9:F1000. doi: 10.12688/f1000research.25338.1
28. Li Y, Wei Q, Zhao D, Mo Y, Yao L, Li L, et al. Non-invasive high-frequency oscillatory ventilation in preterm infants after extubation: a randomized, controlled trial. *J Int Med Res.* (2021) 49:300060520984915. doi: 10.1177/0300060520984915

Conflict of Interest: The authors declare that the research was conducted in the absence of any commercial or financial relationships that could be construed as a potential conflict of interest.

Publisher's Note: All claims expressed in this article are solely those of the authors and do not necessarily represent those of their affiliated organizations, or those of the publisher, the editors and the reviewers. Any product that may be evaluated in this article, or claim that may be made by its manufacturer, is not guaranteed or endorsed by the publisher.

Copyright © 2022 Lai, Xie, Chen, Chen, Cai, Wu, Lin and Zheng. This is an open-access article distributed under the terms of the Creative Commons Attribution License (CC BY). The use, distribution or reproduction in other forums is permitted, provided the original author(s) and the copyright owner(s) are credited and that the original publication in this journal is cited, in accordance with accepted academic practice. No use, distribution or reproduction is permitted which does not comply with these terms.

Frontiers in Pediatrics

Addresses ongoing challenges in child health and patient care

Explores research that meets ongoing challenges in pediatric patient care and child health, from neonatal screening to adolescent development.

Discover the latest Research Topics

See more →

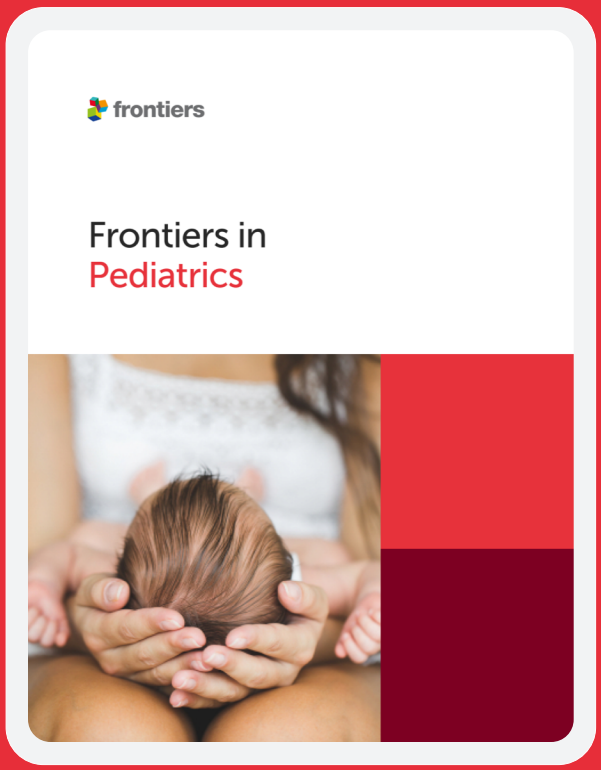

Frontiers

Avenue du Tribunal-Fédéral 34
1005 Lausanne, Switzerland
frontiersin.org

Contact us

+41 (0)21 510 17 00
frontiersin.org/about/contact